The Synthesis and Surface Studies of β-Amino Acids & β-Peptides

---

A thesis submitted

in the partial fulfilment

of the requirements for the degree

of

Doctor of Philosophy in Chemistry

by

Kelly Helen Anderson

University of Canterbury

2007

Work in this thesis has appeared in the following publications:

Brooksby, P. A.; Anderson, K. H.; Downard, A. J.; Abell, A. D., *Langmuir* **2006**, 22, (22), 9304-9312.

Gardiner, J.; Anderson, K. H.; Downard, A.; Abell, A. D., *Journal of Organic Chemistry* **2004**, 69, (10), 3375-3382.

Table of Contents

Abstract ..... **iii**
Abbreviations ..... **vi**
Acknowledgements ..... **ix**
Chapter 1 Introduction **1**
1.1 Electron Transfer in Proteins 2
1.2 Conformation of Peptides 4
1.3 Research Described in This Thesis 15
1.4 References 16
Chapter 2 Electron Transfer and Surface Studies of Immobilised *β*-Peptides **18**
2.1 Introduction 19
2.2 Preparation and Electrochemical Analysis of β-peptide SAMs 35
2.3 Discussion of Electrochemical Analysis of β-Peptide SAMs 58
2.4 Conclusions and Future Work 67
2.5 References 69
Chapter 3 Cross Metathesis on Gold **71**
3.1 Introduction 72
3.2 Synthesis of Olefins 77
3.3 Cross Metathesis Reactions on a Gold Electrode 81
3.4 Electrochemical Analysis 83
3.5 Conclusions and Future Work 90
3.6 References 91
Chapter 4 Synthesis of Compounds Suitable for Surface Immobilisation **93**
4.1 Functionalised β-peptides 94
4.2 Peptide Design and Retrosynthetic Analysis 103
4.3 Synthesis of Model Compounds 105
4.4 Synthesis of β-Peptides 116
4.5 Elucidation of Secondary Structure 130
4.6 Conclusions and Future Work 143
4.7 References 145
Chapter 5 Conformationally Constrained β-Amino Acids **147**
5.1 Introduction 148
5.2 Synthesis of Fluorinated β-Amino Acids 154
5.3 Synthesis of Cyclic β-Amino Acids using Organozinc Reagents 162
5.4 Synthesis of Cyclic β-Amino Acids from Allylglycine 170
5.5 Conclusion and Future Work 180
5.6 References for Chapter Five 181
Chapter 6 Experimental **184**
6.1 General Methods and Procedures 185
6.2 General Synthetic Methods 191
6.3 Experimental Work Described in Chapter 2 194
6.4 Experimental Work Described in Chapter 3 195
6.5 Experimental Work Described in Chapter 4 201
6.6 Experimental Work Described in Chapter 5 246
6.7 References for Chapter Six 267
Appendix A Electroanalytical Methods **269**

A.1 The Potentiostat 269
A.2 Electron Transfer Mechanisms at the Electrode 270
A.3 The Cyclic Voltammetry Technique 271
A.4 Cyclic Voltammetry Theory 274
A.5 The Chronoamperometry Technique 277
A.6 Chronoamperometry Theory 278
Appendix B 281
Appendix C Crystallographic Data 282
C.1 Crystallographic data for cycloheptene-based β-amino acid 5.63 282
C.2 Crystallographic data for conjugate addition/fluorination product 5.43a 287
C.3 References for the Appendix 296

Abstract

This thesis examines the synthesis of conformationally constrained β-amino acids and β-peptides, and the electron transfer properties of the latter when immobilised on gold. Additionally, cross metathesis on gold was investigated as a method for surface functionalisation.

Chapter One introduces the concepts of electron transfer in nature, how it is facilitated by the secondary structure in α-peptides, and why β-peptides might be useful for studying electron transfer. This is followed by a discussion of the properties of β-peptides, including the enhanced stability and variety of helical secondary structures and the greater potential for functionalisation of the peptide backbone when compared to α-peptides. Finally, the conformational constraints of ring-systems on cyclic amino acids is discussed, with reference to the stabilising effect of these compounds on peptide secondary structures.

Chapter Two describes the electrochemical analysis of β-hexapeptides immobilised on gold. The chapter is prefaced by a discussion of the important electron transfer mechanisms for peptides, the fabrication of peptide-gold self-assembled monolayer (SAM) interfaces, and the electron transfer in helical α-peptides. β-Peptides containing an electroactive ferrocene moeity were immobilised on gold and studied using cyclic voltammetry and chronoamperometry. The latter method was used to examine the dependence of the electron transfer rate on overpotential, thereby determining the likely mode of electron transfer through the β-peptides **SSβ_6Fc**, **Fcβ_6SS** and **SC$_{15}\beta_6$Fc**. These peptides exhibited very weak dependence on overpotential, characteristic of electron transfer behaviour of an electron hopping mechanism (which is also thought to occur in helical α-peptides). Both the dipole moment of the peptides and the structure of the sulfur-linker group were found to be important in determining the rate of electron transfer. Conversely, the equivalent α-peptide **SSα_6Fc** exhibited electron transfer behaviour characteristic of the less efficient tunnelling mechanism, which is thought to operate in strand-like peptides.

Chapter Three examines the application of cross metathesis, using a Grubbs' second generation catalyst, as a means to functionalise olefin-terminated self-assembled monolayers on gold.

Firstly, an introduction into the limited published research on cross metathesis on both planar surfaces and nanoparticles is given. Olefin-terminated thiol **3.18**, suitable for immobilisation on gold, and solution phase olefin-terminated ferrocene **3.10** were synthesised as reactants for cross metathesis studies. An analytical methodology was developed involving the cross metathesis of surface-immobilised **3.18** with ferrocene **3.10** in dichloromethane, whereby the concentration of electroactive cross metathesis product **3.22** was monitored electrochemically as a function of time. The concentration of surface-immobilised product **3.22** was determined by integration of the oxidation peak area and found to be highly dependent on both the concentration of immobilised olefin reactant **3.18** and reaction time. Furthermore, the surface concentration of ferrocenyl model disulfide **3.21** and thiol **2.18** decayed markedly upon addition of Grubb's catalyst, as revealed by the decrease in the oxidation peak area, which suggested that catalyst-mediated desorption was occurring.

Chapter Four details the solution-phase synthesis of ferrocene- and thiol-functionalised *β*-hexapeptides used in both the electron transfer studies described in chapter two, and in the determination of secondary structure using circular dichroism and NMR techniques. The synthesis of simple model compounds **4.14**, **4.16** and **4.18** established the incompatibility of the deprotection of methyl and benzyl ester protecting groups with protected-thiol and disulfide linkers, leading to the use of *N*-hydroxysuccinmide-activated sulfur-linkers **4.20** and **4.22** in further synthesis. A number of *β*-hexapeptides were synthesised by amide coupling of *β*-tripeptides functionalised at the *N*- and *C*-termini. Structural studies of the methanol soluble *β*-hexapeptide **4.60** suggested that the covalent attachment of ferrocene moeity to the *C*-terminus of a *β*-peptide did not disrupt the formation of a 14-helix in solution. *β*-peptides containing functionality at both the *C*- and *N*-termini (such as **SSβ_6Fc**, **SSβ_6Et** and acetyl-protected **SC$_{15}\beta_6$Fc**) were not suitable for solution phase structural studies; however, molecular modelling suggested that helical conformations are the most stable these *β*-peptides in solution phase.

Chapter Five outlines the synthesis of novel cyclic *β*-amino acids by two different general synthetic routes. The first uses an efficient conjugate addition/fluorination reaction of *α*,*β*-unsaturated esters with lithiated chiral secondary amines to prepare the novel cyclopentyl- and cyclohexyl-based fluorinated *β*-amino acids **2.43a** and **2.43b**. The high diastereoselectivity of this reaction, which introduces two stereocentres into the achiral unsaturated esters, is directed by the configuration of the attacking amine. The second methodology utilizes the versatile ring-closing metathesis reaction in the synthesis of novel cyclic *β*-amino acids. A stereoselective

trans-alkylation of olefinic *β*-amino acids gave the required *β*-dienes **5.62** and **5.77**. Optimised cyclisation yields were achieved with a Grubb's 2nd generation catalyst for diene **5.62** and Grubb's 1st generation catalyst for diene **5.77**, to give the *trans*-cycloheptyl- and cyclooctyl-based *β*-amino acids **5.63** and **5.78**, respectively. The attempted synthesis of cyclononyl-based *β*-amino acid **5.87** using both catalysts yielded only cyclic dimer products **5.88** and **5.89**. The *trans* configuration of the **5.62** diene was confirmed by x-ray crystallography.

Chapter Six is an experimental chapter and outlines the electrochemical setup and analysis, and the synthesis, purification and characterisation of compounds described in this thesis.

Abbreviations

α	(1) designates an amino acid of the general structure $NH_2CR_2CO_2H$ (2) the activity coefficient
β	(1) designates an amino acid of the general structure $NH_2CR_2CR_2CO_2H$ (2) tunnelling parameter ($Å^{-1}$)
η	overpotential
Γ	surface coverage
δ	NMR chemical shift
Ac	acetyl 
Ala	alanine
Bn	benzyl
Boc	*tert*-butoxy
br s	broad singlet (in NMR)
CA	chronoamperometry
CD	circular dichroism
CM	cross metathesis
CV	cyclic voltammetry
d	doublet (in NMR)
DCC	*N,N'*-dicyclohexylcarbodiimide
DCM	dichloromethane
DIPEA	*N,N*-diisopropylethylamine
DMAP	4-(dimethylamino)pyridine
DMSO	Dimethylsulfoxide
EDCI	1-ethyl-3-(3-dimethylaminopropyl) carbodiimide hydrochloride

ET	electron transfer
Et_3N	triethylamine
EtOAc	ethyl acetate
f	F/RT where F, R, and T are the Faraday and gas constants, and absolute temperature, respectively
Fc	ferrocene
HATU	*O*-(7-azabenzotriazol-1-yl)-*N,N,N′,N′*-tetramethyluronium hexafluorophosphate
HOBT	*N*-hydroxybenzotriazole
HRMS	high resolution mass spectrometry
Hz	hertz (in NMR)
J	coupling constant (in NMR)
i_0	initial current
k_{et}	electron transfer rate (s^{-1})
k_{et}^0	standard electron transfer rate (s^{-1})
k_0	kinetic prefactor
Leu	leucine
m	multiplet (in NMR)
min	minute(s)
mp	melting point
n	the number of electrons transferred
NHS	*N*-hydroxysuccinimide
NMR	nuclear magnetic resonance
Ph	phenyl
ppm	parts per million
q	quartet (in NMR)
R_1	distance between hopping sites
RCM	ring closing metathesis

R_{DA}	donor-acceptor centre-to-centre distance
ROESY	rotational nuclear overhauser effect spectroscopy
rt	room temperature
s	singlet (in NMR)
SAM(s)	self-assembled monolayer(s)
SCE	saturated calomel electrode
t	time
t	triplet (in NMR)
TFA	trifluoroacetic acid
TFE	2,2,2-trifluoroethanol
THF	tetrahydrofuran
TLC	thin layer chromotography
Val	valine

Acknowledgements

Firstly, I would like to thank my supervisor Professor Andrew Abell for his guidance and support over the last four years. I really appreciated the freedom to direct my own PhD. I would also like to thank my co-supervisor Dr Alison Downard for her assistance during my studies and helpful suggestions regarding thesis.

Thanks to Paula Brooksby for introducing me to (and helping me with) the wonderful world of electrochemistry – it would have been overwhelmingly difficult without your help! I would also like to thank all of the staff in the department that made all of this work possible, especially Bruce Clark and Rob Stainthorpe (mass spectroscopy), Professor John Blunt and Rewi Thompson (NMR), Professor Ward Robinson (x-ray crystallography), and Blair Stewart (molecular modelling). Thank you to the Foundation for Research, Science and Technology for the financial support during my PhD.

I would like to thank Dr Peter Duggan for letting me spend some time in his lab at CSIRO, Melbourne. It was a great experience to 'see how the other half lives' in the commercial/industrial world of science.

Thanks to all the students for making it a fun department to work in, especially to the Abell group, and Andrea, Anna Mc and Janna (R.I.P. dessert day). Thanks also to Anna Brady for being a great friend and not hassling me for being a perpetual student!

I would especially like to thank my parents Grada and Brian for looking after me when the going got tough and letting me move home again, after they thought they were free of the kids! I would also like to thank my sisters Tracy and Julia for their support over the last few years.

Finally, thank you so much to Florian for your love, support, endless encouragement and for listening to all my moaning and groaning about how I was 'never going to finish'. I still think you are the best result I obtained from my PhD!

Chapter 1 Introduction

1.1 Electron Transfer in Proteins

Electron-transfer reactions are integral in photosynthesis, respiration, drug metabolism and many other important biological processes. These reactions are catalysed by a diverse range of hundreds of oxidoreductase enzymes (enzymes that catalyse the transfer of electrons between molecules), which are classified into 22 subclasses (some of which are shown in Table 1.1). These enzymes catalyze single- or multi-electron reduction/oxidation reactions of organic and protein substrates, in conjuction with the oxidation/reduction of a natural redox partner such as an electron transfer protein (e.g. cytochrome, ferredoxin, flavoprotein) or small molecule co-substrates (e.g. NAD(P)H, dioxygen). Oxidoreductase enzymes can be substrate-specific such as alcohol dehydrogenase, or promiscuous such as cytochrome P450.

Table 1.1 Some of the 22 subclasses of oxidoreductase enzymes that oxidise or reduce the indicated substrate type, with specific examples indicated.

Oxidoreductase Class	Substrate Type	Example
EC 1.1	CH-OH group	alcohol dehydrogenase
EC 1.2	aldehyde or oxo group	acetaldehyde dehydrogenase
EC 1.3	CH-CH	5-alpha reductase
EC 1.4	CH-NH_2	glutamate dehydrogenase
EC 1.5	CH-NH	sarcosine oxidase
EC 1.6	NADH or NADPH	NADH dehydrogenase
EC 1.7	other nitrogenous compounds	urate oxidase
EC 1.8	sulfur group	glutathione reductase
EC 1.9	heme group	cytochrome c oxidase
EC 1.10	diphenols and related substances	catechol oxidase
EC 1.11	peroxide as an acceptor (peroxidases)	cytochrome c peroxidase
EC 1.13	single donors with incorporation of molecular oxygen (oxygenases)	cysteine dioxygenase
EC 1.14	paired donors with incorporation of molecular oxygen	cytochrome P450
EC 1.15	superoxide radicals	superoxide dismutase
EC 1.16	metal ions	protoporphyrinogen oxidase

1.1.1 Relationship Between Peptide Structure and Function

Electron transfer reactions of oxidoreductase enzymes generally occur between protein-bound coenzymes (non-amino acid prosthetic groups) that are often separated by large molecular distances (10 Å or more).[1] As electron transfer through space (rather than through bonded orbitals) is very inefficient, and does not fit the observed experimental rate data for biological redox processes, another conductive medium was sought. Almost sixty years ago, Michaelis addressed the problem of oxidoreductase protein design, noting that the amino acids must serve as molecular wires to connect the redox centres. In his words, "the task of the protein may be to establish geometric configurations between different prosthetic groups and aid in the formation and stabilization of free radicals".[2] Indeed, we now know, from the structural resolution of many oxidoreductases, that polypeptide chains have been optimised by nature to guide electron transfer along a sequential array of redox moieties.[3-5]

A key realisation was that the rate of electron transfer decay across a hydrogen bond is approximately equal to that across two covalent bonds.[1] Therefore, the hydrogen-bonded network that bridges the amide groups in many common secondary structures may act as a molecular 'shortcut' for electron transfer in proteins. The α-helix (which is stabilised by hydrogen bonding interactions) is found in high concentration in oxidoreductase enzymes, and is therefore considered to play an important role in the electron-transfer process.[1] For example, the oxidoreductase enzyme flavocytochrome B2, which possesses three redox centres, contains a large number of α-helices (Figure 1.1).

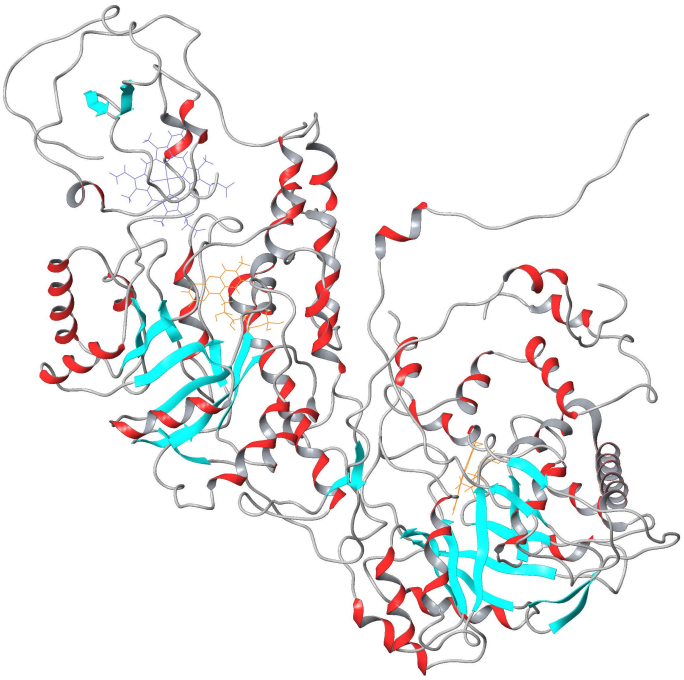

Figure 1.1 The crystal structure of oxidoreductase enzyme, Flavocytochrome B_2. The enzyme contains two flavin mononucleotides redox centres, and one photoporphyrine IX redox centre.[6]

Therefore, it is possible that the hydrogen bonding networks of secondary structures, such as helices, may be important for electron transfer in biological systems. However, understanding the exact nature of electron transfer in peptides has proved challenging, and has yet to be fully unravelled. The importance of primary and secondary structure for electron transfer in biological systems remains controversial. If we are to study or utilise the process of electron transfer, we need to understand the structure/function relationships of amino acids and peptides. The key to understanding what governs the three-dimensional assembly of peptides and proteins lies in a better understanding of the how individual amino acids (in the primary structure), and short sequences of amino acids (in the secondary structure) influence the overall peptide structure. What follows is a discussion of the factors that govern the conformational restriction imposed on peptides when folded into secondary structures.

1.2 Conformation of Peptides

1.2.1 Conformational Restriction in *α*-Peptides

Peptides are highly flexible molecules and as such adopt many random conformations. However, it is often just a few well-defined conformations that give a peptide its biological activity, while the other extended or disordered arrangements generally possess little or no

biological activity. The amino acid sequence of a peptide determines the conformation and spacing of the structural features, and therefore the biological function of the peptide or enzyme. Just as amino acids have conformational flexibility, so too can the overall peptide structure. Consequently the side-chain groups of the constituent amino acids are important in defining the conformational freedom of the peptide. If the peptide is to adopt a desired, discrete conformation, then amino acids that conformationally restrict the peptide become important.

There are many different types of bonding interactions in folded polypeptides that rigidify specific conformations. These interactions, which include disulfide bonds, hydrogen bonding of side chains groups and the peptide backbone, hydrophobic interactions, and ionic bonds from side chain groups transform a non-functional flexible peptide into a well-defined structure (Figure 1.2). The hydrogen bonding interactions of secondary structures are one of the most important contacts in determining the local molecular architecture of a peptide sequence and therefore the ability for a sequence to participate in electron transfer.

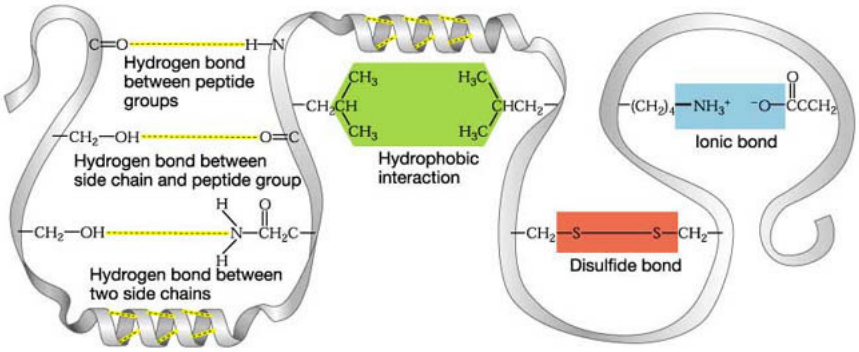

Figure 1.2 Modes of conformation restriction found in endogenous α-peptides (Reproduced from Ref. 7).

Amino acid sequences have the ability to fold into well-defined structural motifs, collectively known as secondary structures. These conformations, which are stabilised by hydrogen bonding interactions between backbone NH and CO groups, include the α-helix, β-sheet and β-turn.

The α-helix is a rigid rod-like structure composed of a tightly coiled polypeptide chain (Figure 1.3). The backbone of the polypeptide lines the helix, while the side chains extend outwards in a right-handed helical array. Hydrogen bonding interactions between CO and NH groups from amino acids four residues apart stabilise the secondary structure. The α-helix can act as a purely structural unit, such as in catalytic enzymes, however it is also thought to promote long-range

electron transfer between redox groups in oxidoreductase enzymes, through the network of hydrogen bonds along the helix backbone.[8]

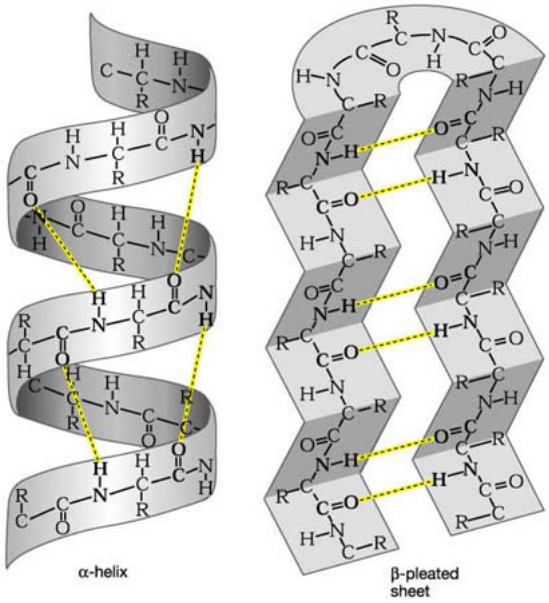

Figure 1.3 Secondary structures found in α-peptides: α-helix (left) and β-pleated sheet (right). (Reproduced from Ref. 7)

The β pleated sheet,* is a structural motif that has an extended sheet-like conformation (Figure 1.3). The β sheet is stabilised by hydrogen bonding interactions between NH and CO backbone groups in polypeptide chains. These sheets can lie in the same direction (parallel β sheet) or opposite direction (antiparallel β sheet). Silk fibroin (the fibres that make up silk) consists almost entirely of stacks of antiparallel β sheets.[9]

The globular shape of many proteins is largely due to the many turns found within the peptide structure. Bends containing hydrogen bond stabilisation between amide bonds from amino acids three residues apart are known as β-turns.

Despite the current level of understanding of peptide secondary structures, it is still often difficult to predict the overall (tertiary) structure and the secondary structure elements of a given primary peptide sequence. For example, the molecular modelling of an α-peptide (peptides comprising α-amino acids) into its three-dimensional protein structure only agrees with known structural data, such as X-ray crystal structures, approximately 60% of the time.[8] Specific

* …so named because it was the second structure elucidated by Pauling and Corey, the α-helix being the first.

sequences of α-amino acids that are known to form an α-helix in one protein, can form a β-strand in another, and in others exhibit no secondary structure at all.

This difficulty in predicting α-peptide conformations is due in part to the large number of possible interactions and backbone conformations that can occur. Specifically designed peptides with compact *predictable* conformations are often designated "foldamers". An important new class of foldamers are the β-peptides (oligomers comprising β-amino acids). Similar to α-peptides, β-peptides can form helical and sheet-like secondary structures, but with increased proteolytic and structural stability. These properties make β-peptides ideal models for studying the structural and biological properties of α-peptide equivalents.

1.2.2 Conformational Restriction in β-Peptides

β-Amino acids are analogues of α-amino acids that possess the same general structure, but contain an extra backbone carbon (Figure 1.4a,b). The increased backbone length of β-amino acids allows a more complex substitution pattern and therefore different nomenclature applies. When β-amino acids possess the same side chains as α-amino acids, the naming is kept consistent. The substitution is denoted by specifying the attachment position along the backbone (eg, substitution at the '3' position gives a β^3 amino acid), so that β-amino acids can be unambiguously identified (Figure 1.4 b,c).*

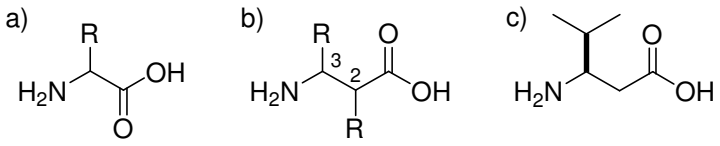

Figure 1.4 Structures of a) an α-amino acid, b) a β-amino acid and c) β^3hVal.

The realisation that β-peptides (polymers of β-amino acids) adopt stable and well-defined conformations in solution, even with as few as four residues†, is unprecedented in α-peptides.[10,11] Such findings have led to much interest in these analogues as tools for comparing and contrasting the structural behaviour of natural α-peptides.[12,13] The study of β-peptides in place of α-peptides is advantageous for many reasons, such as the increased stability and diversity of

* For further detail on naming β-amino acids, see Section 6.1.
† in the case of cyclic *trans*-$\beta^{2,3}$ amino acids, see Figure 1.12

secondary structures and the greater potential for heteroatom substitution along the peptide backbone.[13]

Previously it was assumed that β-peptides would have a larger number of conformations compared to the α-peptide equivalents due to the additional tetrahedral carbon centre (Figure 1.4).[13] While it is true that β-peptides can adopt a larger number of conformations, for substituted β-peptides, the conformers differ significantly in their stability. This is due to the additional sp^3 centre introducing a higher barrier to rotation about the β-amino acid backbone sp^3-sp^3 bond compared to that of the sp^3-sp^2 bonds in the α-amino acid backbone. As a result of this restricted rotation, β-peptides actually have less conformational freedom than α-peptides and this is reflected in their ability to readily adopt secondary structures.

In the case of β-peptides comprising only β^3 residues, there are a number of possible conformations about the backbone sp^3-sp^3 bond (Figure 1.5). Sterically unfavourable conformers occur when bulky groups (such as sidechain groups) are held close in space to other non-hydrogen groups, such as in the (-)-*synclinal (sc)* or *antiperiplanar (ap)* conformations. The energetically most favourable conformer for β^3-peptides that are derived from L-α-amino acids* is (+)-*sc,* which positions the sidechain group distant to the other non-hydrogen groups.[13]

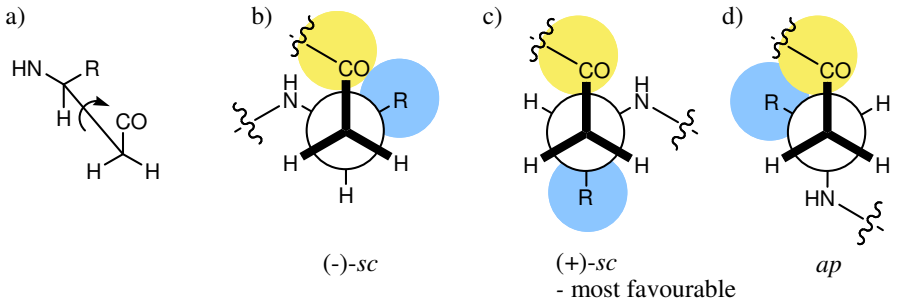

Figure 1.5 β^3-peptide conformers shown as: (a) a sawhorse projection; and as Newman projections (b) and (c) of both synclinal conformations and (d) the anti-periplanar conformation (adapted from Seebach, 2004).[13]

This energy difference means that the secondary structure of the resulting peptide is effectively locked in the most stable conformation and therefore has greater stability compared with an α-peptide equivalent. A β^2 or β^3-peptide consisting of only six residues shows helicity, a

* β-amino acids derived from natural α-amino acids can have the stereodescriptor (*R*) or (*S*), due to the change in priority caused by the insertion of an extra methylene group into the amino acid backbone.

phenomenon not observed in α-peptides of comparable size (except those containing unnatural helix-inducing Aib* residues). Molecular modelling of small β-peptides can quickly (within 200 ns), reveal the most stable peptide conformation.[14] Modelling of α-peptides of a similar size to obtain a low energy structure requires much longer times (except where Aib is present).

β-Peptides with different substitution patterns have other lowest energy conformations. For example, $\beta^{2,3}$ amino acids with (*S,S*)- or (*R,R*) disubstitution (*l*)† sterically favour a (+)-*sc* conformation over a (-)-*sc* or *ap* conformation (Figure 1.6). Conversely a $\beta^{2,3}$ amino acid containing one (R) and one (S) stereocenter (*u*) favours an *ap* conformation. This results in a β-peptide pleated sheet.

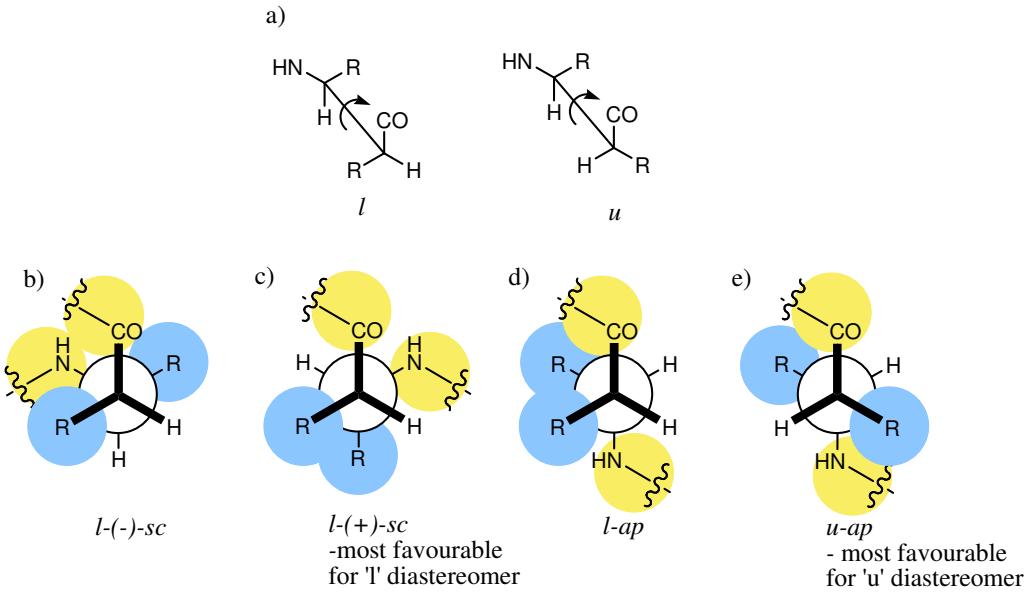

Figure 1.6 *l* and *u* $\beta^{2,3}$-peptide conformers shown as the: (a) sawhorse projections and the Newman projections (b) and (c) of the two syn-clinal conformations and (d) and (e) the two anti-periplanar conformation (adapted from Seebach, 2004).[13]

Types of β-Helix

Over the last ten years the study of β-peptides, particularly by Gellman and Seebach, has resulted in the discovery of five new types of helix.[12,13,15] The conformation that predominates for any given β-peptide is largely dependent on the side chains and the substitution positions. There are

* Aib = $H_2NC(CH_3)_2CO_2H$
† Also denoted '*l*' for 'like', used to describe the relationship between two stereocentres in a diastereomer when both have an (*S*) or (*R*) configuration. Conversely, the stereodescriptor '*u*' for 'unlike' is used to describe a molecule containing an (*S*) and an (*R*) stereocenter.

five known helices, each characterised by the number of atoms between (and including) the hydrogen bonding atoms: the 8-helix, 10-helix, 12-helix, 14-helix and 10/12 helix (Figure 1.7).

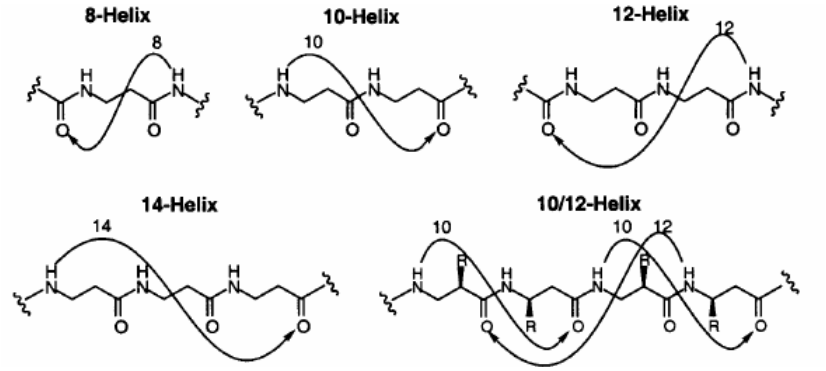

Figure 1.7 Different hydrogen bonding interactions possible in β-peptides (Reproduced from Cheng, 2001).[12]

The 14-helix* is the most common for β-peptides composed of single enantiomers of β^3 or β^2 amino acids. The 10/12-helix, which has an overlapping hydrogen bonding network, occurs in β-peptides where the residues alternate between β^2 and β^3 amino acids.[16,17] The 12-helix is favoured with some cyclic *trans*-$\beta^{2,3}$ β-amino acids, such as *trans*-2-aminocyclopentane carboxylic acid.[18] The 8- and 10- helices are found in β-peptides comprised of β^2-cyclopropyl- and $\beta^{2,3}$-oxetane ring-† residues, respectively.[19,20]

* The 14-helix and 10/12 helix are also known as the 3_{14}-helix and $2.7_{10,12}$ helix, respectively.
† A four-membered cyclic ether.

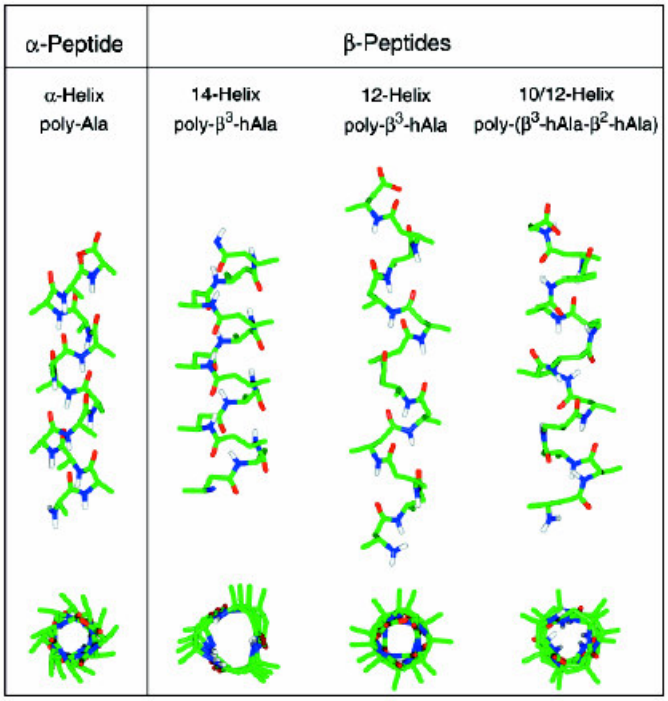

Characteristic	α-Helix	12-Helix	14-Helix
radius (Å)	2.2	2.3	2.7
residues/turn	3.6	2.5	3.0
rise/residue (Å)	1.5	2.1	1.56
dipole moment	N +⟶ C	C +⟶ N	N +⟶ C

Figure 1.8 (a) Structures of the α-helix, 14-helix, 12-helix and 10/12 helix. Carbon atoms are shown in green, oxygen in red and nitrogen in blue. Most hydrogen atoms are omitted for clarity, except amide nitrogens, in white (Reproduced from Cheng, 2001)[12] (b) Helical parameters for α- and β-helices. (Redrawn from Cheng, 2001)[12]

The helix radius, the number of residues per helix turn, the rise per turn and the peptide polarity are unique to each β-peptide (Figure 1.8). The 14-helix has approximately three residues per helix turn, which positions the side chains in a stacked arrangement along the axis of the helix. The radius of the 14-helix is larger than the α-helix, while the rise per residue is very similar. Additionally, the carbonyl groups in a 14-helix point in the opposite direction to those of an α-helix, to reverse the dipole moment. The 10/12-helix lacks a dipole moment, because equal numbers of the carbonyl groups point in both directions along the helix backbone. The 12-helix has an extended conformation with only 2.5 residues per turn and a rise per residue of 2.1 Å. Both the radius and the dipole moment of the 12-helix are same as the α-helix.

1.2.3 Cyclic Amino Acids

Cyclic amino acids and other constrained mimics also play an important role in the stabilisation of secondary structures because of their ability to constrain the bond rotation about the peptide backbone. Cyclic amino acids can induce or terminate secondary structural features such as turns or helices or pre-arrange a peptide in its bioactive conformation.[21]

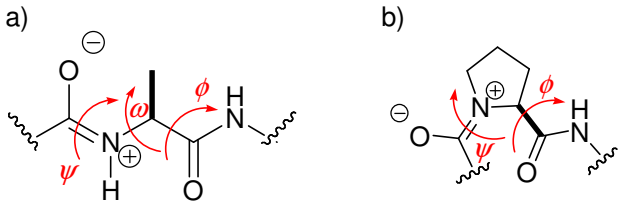

Figure 1.9 Flexibility of α-amino acids along the backbone: (a) (*S*)-Ala and (b) (*S*)-Pro .

With the exception of proline, all of the proteinogenic α-amino acids, (Figure 1.9a, b), have three flexible bonds along their backbone.* Proline is constrained by a ring system, which prevents rotation about the N-C_α bond, leaving only two flexible bonds. Proline is a very important amino acid in biological systems because of its ability to induce or terminate helical secondary structures. As a result, proline is found in many assemblies in biological systems that possess regular and well-defined structural motifs, such as collagen (Figure 1.10).

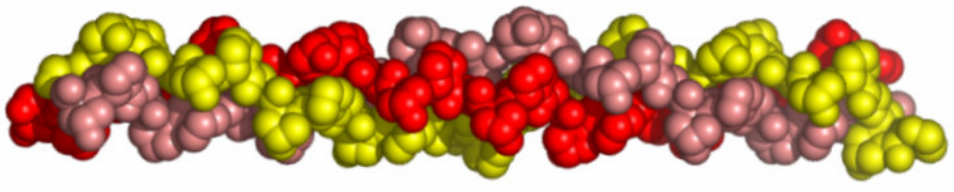

Figure 1.10 Structure of triple-stranded collagen helix (shown as ribbons). (Reproduced from Ref. 22).

Cyclic β-amino acids, a class of compounds that mimic proline, have been used as starting materials for the synthesis of different heterocycles and natural products or mimetics, and as building blocks in β-peptides.[23] Interest in cyclic β-amino acids stems from the constrained nature of these molecules and the rigidifying effects they afford when incorporated into peptide

* One of these bonds, depicted in Figure 1.9 with the symbol ψ , has reduced flexibility due to its partial double-bond nature but can adopt a *cis* or *trans* orientation.

structures. Cyclic *trans* $\beta^{2,3}$ amino acids have fewer available conformations about the peptide backbone than acyclic analogues. This is because certain conformers are not permitted as they would incur a prohibitively large ring strain (such as (-)-*sc* shown in Figure 1.11). The two possible conformations for *trans*-2-amino-cyclohexane carboxylic acid (ACHC) are (+)-*sc* and *ap* (Figure 1.11) Furthermore, these two conformations differ enormously in energy: the *ap* conformer which has diequatorial NH and CO is 11 kcal/mol more stable than the diaxial *ap* conformer.[13]

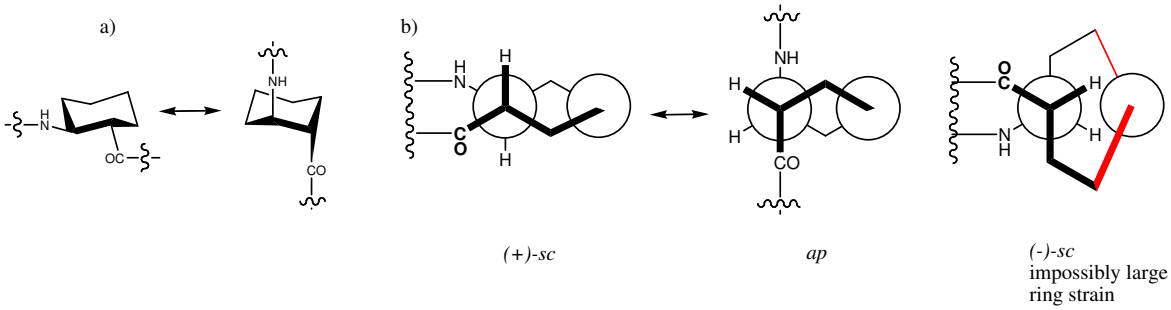

Figure 1.11 *trans*-2-Aminocyclopentanecarboxylic acid $\beta^{2,3}$-peptides can only adopt one conformation. a) Diequatorial (left) is favoured over diaxial (right). b) Synclinal (left) is favoured over anti-periplanar (right). (Adapted from Seebach, 2004)[13]

Gellman *et al* have studied the stabilising effects of cyclic β-amino acids on the helical structure of β-peptides.[12] It was shown that β-peptides comprising only *trans*-cyclic β-amino acids adopt exceptionally stable β-helices, due to the restricted rotation about the peptide backbone. In particular, a tetramer of *trans*-2-aminocyclohexanecarboxylic acid, shown in Figure 1.12, adopts a 14-helix conformation.[24] In contrast, β-*tetra*peptides consisting of *acyclic* β-amino acid residues cannot stabilise a helix.

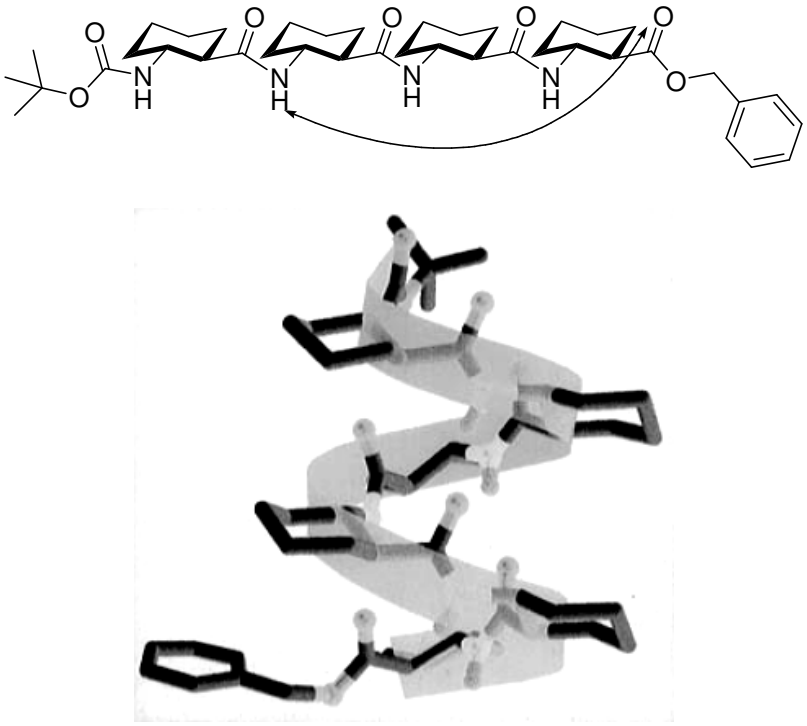

Figure 1.12 A β-peptide comprising *trans*-2-aminocyclohexanecarboxylic acid residues possesses a 14-helix structure.

Cyclic β-amino acids have also been used as building blocks for the preparation of peptidomimetics (analogues of biologically active peptides). The replacement of an α-amino acid with a cyclic β-amino acid in a naturally-occurring biologically active peptide modifies the activity and/or specificity. The effect is due largely to the cycle constraining the peptide backbone dihedral torsion angle, thereby stabilising a particular conformation. Furthermore, the stability of the natural peptide is increased since the β-peptides are resistant to enzymatic degradation.[25] One example (of many) is the use of cyclic β-amino acids to prepare synthetic analogues of the natural peptide Ac-Tyr(SO_3H)-Met-Gly-Trp-Met-Asp-Phe-NH_2, which is released by the brain as a response to nutrient digestion, to treat obesity. Tilley *et al* replaced the adjacent Met and Gly residues with the β-amino acid *trans*-2-aminocyclopentanecarboxylic acid (the *trans* analog of cispentacin).[26] This peptidomimetic proved highly effective in enzyme binding studies and as an appetite suppressant.

1.3 Research Described in This Thesis

Unravelling the relationships between structure and function of biological molecules is a major challenge. Rather than studying the complex biological systems, it is advantageous to work with smaller molecules that are carefully designed to model key aspects of biological molecules. In an attempt to unravel the process of electron transfer in peptides, simplified peptide-redox conjugates have been studied (as described in Chapter Two). In particular, helical α-peptides immobilised on conductive surfaces have provided much insight into the electron transfer mechanisms operating in hydrogen-bonded peptide structures.[3,27] Understanding the electron transfer processes in peptides is important in advancing new fields such as molecular electronics and nanoscale devices.[5]

The work described in this thesis centres around the use of β-amino acids and β-peptides as mimics of the natural amino acids and peptides. The stable and diverse structural properties of β-peptides (as discussed above) makes them particularly suited for the study through electron transfer of peptides and as potential nanoscale devices (such as nanowires). Furthermore, conformationally constrained cyclic β-amino acids are suited to rigidifying the peptide backbone, and thereby stabilising specific secondary structures. This thesis presents both the synthesis and study of electron transfer of surface-immobilised β-peptides, the use of cross-metathesis to functionalise gold surfaces and the synthesis of novel conformationally constrained β-amino acid monomers, as described below:

Chapter two explores the electron transfer through a range of β-hexapeptides on gold using electrochemical techniques. The effect of different groups that link the β-peptides to the surface, and the electron transfer through an analogous α-peptide are compared.

Chapter three details the development of a method of surface modification on gold using a ruthenium-catalysed cross metathesis reaction. The cross-metathesis of a ferrocene-terminated olefin with an olefin-terminated thiol (immobilised on a gold surface) is presented, along with a study of the compatibility and stability of the products and catalyst.

Chapter four describes the synthesis of *β*-peptides (analysed in chapter two) which are suitable for surface immobilisation on gold. The choice of suitable sulphur linkers and compatible protecting groups and redox probe is discussed, followed by the synthesis of *β*-hexapeptides. The characterisation of the secondary structure of some of these peptides by circular dichroism and 2D NMR spectroscopy is also presented.

Chapter five details the synthesis of novel cyclic *β*-amino acids using two approaches. Firstly, the synthesis of cyclic fluorinated *cis β*-amino acids using conjugate addition will be presented. Additionally, the cyclisation using ring-closing metathesis to generate trans *β*-amino acids of seven and eight membered carbocycles is described. The attempted synthesis of a nine-membered cyclic analogue is also discussed.

1.4 References

1. Beratan, D. N.; Onuchic, J. N.; Winkler, J. R.; Gray, H. B., Electron-Tunneling Pathways in Proteins. *Science* **1992,** 258, (5089), 1740-1741.
2. Michaelis, L., In *The Enzymes, Chemistry and Mechanism of Action*, Sumner, J. B.; Myrback, K., Eds. Academic: New York, 1951; pp 1-54.
3. Watanabe, J.; Morita, T.; Kimura, S., Effects of dipole moment, linkers, and chromophores at side chains on long-range electron transfer through helical peptides. *Journal of Physical Chemistry B* **2005,** 109, (30), 14416-14425.
4. Page, C. C.; Moser, C. C.; Chen, X. X.; Dutton, P. L., Natural engineering principles of electron tunnelling in biological oxidation-reduction. *Nature* **1999,** 402, (6757), 47-52.
5. Long, Y. T.; Abu-Rhayem, E.; Kraatz, H. B., Peptide electron transfer: More questions than answers. *Chemistry-a European Journal* **2005,** 11, (18), 5186-5194.
6. Xia, Z. X.; Mathews, F. S., Molecular-Structure of Flavocytochrome-B2 at 2.4 a Resolution. *Journal of Molecular Biology* **1990,** 212, (4), 837-863.
7. Proteins: Function and Structure. In *11*, October, Ed. 2006, n.d.; Vol. http://fig.cox.miami.edu/~cmallery/150/protein/proteinsb.htm.
8. Stryer, L., *Biochemistry*. 3rd ed.; W. H. Freeman and Company: New York, 1988; p 1089.
9. Garret, R. H.; Grisham, C. M., *Biochemistry*. 2nd ed.; Saunders College Publishing: New York, 1999.
10. Seebach, D.; Overhand, M.; Kuehnle, F. N. M.; Martinoni, B., b-Peptides. Synthesis by Arndt-Eistert homologation with concomitant peptide coupling. Structure determination by NMR and CD spectroscopy and by x-ray crystallography. Helical secondary structure of a b-hexapeptide in solution and its stability towards pepsin. *Helvetica Chimica Acta* **1996,** 79, (4), 913-941.
11. Seebach, D.; Ciceri, P. E.; Overhand, M.; Jaun, B.; Rigo, D.; Oberer, L.; Hommel, U.; Amstutz, R.; Widmer, H., Probing the helical secondary structure of short-chain beta-peptides. *Helvetica Chimica Acta* **1996,** 79, (8), 2043-2066.
12. Cheng, R. P.; Gellman, S. H.; DeGrado, W. F., β-peptides: From structure to function. *Chemical Reviews* **2001,** 101, (10), 3219-3232.

13. Seebach, D.; Beck, A. K.; Bierbaum, D. J., The world of beta- and gamma-peptides comprised of homologated proteinogenic amino acids and other components. *Chemistry & Biodiversity* **2004,** 1, (8), 1111-1239.
14. van Gunsteren, W. F.; Burgi, R.; Peter, C.; Daura, X., The key to solving the protein-folding problem lies in an accurate description of the denatured state. *Angewandte Chemie-International Edition* **2001,** 40, (2), 351-355.
15. Gellman, S. H., Foldamers: A manifesto. *Accounts of Chemical Research* **1998,** 31, (4), 173-180.
16. Seebach, D.; Abele, S.; Gademann, K.; Guichard, G.; Hintermann, T.; Jaun, B.; Matthews, J. L.; Schreiber, J. V., beta(2)- and beta(3)-peptides with proteinaceous side chains: Synthesis and solution structures of constitutional isomers, a novel helical secondary structure and the influence of solvation and hydrophobic interactions on folding. *Helvetica Chimica Acta* **1998,** 81, (5), 932-982.
17. Seebach, D.; Gademann, K.; Schreiber, J. V.; Matthews, J. L.; Hintermann, T.; Jaun, B.; Oberer, L.; Hommel, U.; Widmer, H., 'Mixed' beta-peptides: A unique helical secondary structure in solution. *Helvetica Chimica Acta* **1997,** 80, (7), 2033-2038.
18. Appella, D. H.; Christianson, L. A.; Klein, D. A.; Powell, D. R.; Huang, X. L.; Barchi, J. J.; Gellman, S. H., Residue-based control of helix shape in beta-peptide oligomers. *Nature* **1997,** 387, (6631), 381-384.
19. Abele, S.; Seiler, P.; Seebach, D., Synthesis, crystal structures, and modelling of beta-oligopeptides consisting of 1-(aminomethyl)cyclopropanecarboxylic acid: Ribbon-type arrangement of eight-membered H-bonded rings. *Helvetica Chimica Acta* **1999,** 82, (10), 1559-1571.
20. Claridge, T. D. W.; Goodman, J. M.; Moreno, A.; Angus, D.; Barker, S. F.; Taillefumier, C.; Watterson, M. P.; Fleet, G. W. J., 10-Helical conformations in oxetane beta-amino acid hexamers. *Tetrahedron Letters* **2001,** 42, (25), 4251-4255.
21. Labudda-Dawidowska, O.; Wierzba, T. H.; Prahl, A.; Kowalczyk, W.; Gawinski, L.; Plackova, M.; Slaninova, J.; Lammek, B., New bradykinin analogues modified in the C-terminal part with sterically restricted 1-aminocyclohexane-1-carboxylic acid. *Journal of Medicinal Chemistry* **2005,** 48, (25), 8055-8059.
22. Harrison, K., Collagen. In *11*, October, Ed. Chemistry, Structures & 3D Molecules @ 3Dchem.com: 2006, 2005-2006; Vol. http://www.3dchem.com/molecules.asp?ID=195.
23. Fulop, F., The chemistry of 2-aminocycloalkanecarboxylic acids. *Chemical Reviews* **2001,** 101, (7), 2181-2204.
24. Barchi, J. J.; Huang, X. L.; Appella, D. H.; Christianson, L. A.; Durell, S. R.; Gellman, S. H., Solution conformations of helix-forming beta-amino acid homooligomers. *Journal of the American Chemical Society* **2000,** 122, (12), 2711-2718.
25. Gademann, K.; Hintermann, T.; Schreiber, J. V., beta-peptides: Twisting and turning. *Current Medicinal Chemistry* **1999,** 6, (10), 905-925.
26. Tilley, J. W.; Danho, W.; Shiuey, S. J.; Kulesha, I.; Swistok, J.; Makofske, R.; Michalewsky, J.; Triscari, J.; Nelson, D.; Weatherford, S.; Madison, V.; Fry, D.; Cook, C., Analogs of Ac-Cck-7 Incorporating Dipeptide Mimics in Place of Met28-Gly29. *Journal of Medicinal Chemistry* **1992,** 35, (21), 3774-3783.
27. Morita, T.; Kimura, S., Long-range electron transfer over 4 nm governed by an inelastic hopping mechanism in self-assembled monolayers of helical peptides. *Journal of the American Chemical Society* **2003,** 125, (29), 8732-8733.

Chapter 2 Electron Transfer and Surface Studies of Immobilised β-Peptides

2.1 Introduction

While there is continued uncertainty about charge transfer through DNA, charge transfer within proteins is evident.[1] Understanding the exact nature of charge transfer (either electron transfer or hole transfer)* in peptides is of fundamental importance for the elucidation of essential biological processes, and the development of nanoscale devices (functional structures with dimensions ranging 0.1 to 100 nm).† Research in this area is divided into two parts: the study of the electron transfer characteristics of in proteins,[2] and the study of smaller peptide model systems[1] in order to gain insight to the electron transfer of proteins.

As described earlier, the 3D molecular architecture of proteins is determined largely by secondary structures, such as helices, sheets and turns, that rigidify sections of the peptide chain. An understanding of how secondary structure facilitates electron transfer is vital in understanding the overall charge transfer process in proteins. A large body of work exists on the study of electron transfer in α-helices, which are an important secondary structural motif in electron transfer proteins. However, understanding in this area is far from complete and there is continued debate about the exact nature of electron transfer in α-peptides. For example, it is unknown whether electron transfer in peptides is dependent mainly on the primary structure (instead of secondary structure), or whether electron transfer occurs along amide bonds or specific side-chains that can accommodate charge (such as tryptophan and tyrosine) independent of primary and secondary structure.[1]

β-Peptides, which are structurally the closest analogs to α-peptides, demonstrate predictable and discrete folding into stable secondary structures including helices and sheets (as described in chapter one). However, despite the enhanced stability of β-peptide secondary structures, to the best of our knowledge, there are no reported studies on electron transfer. The introduction to this chapter will focus on the theory and methods behind the electron transfer in α-helices as a background for the study of electron transfer in β-peptides presented here.

* For simplicity, only the term 'electron transfer' is used throughout, to represent both electron and hole transfer.
† The area of nanoscale devices is beyond the scope of this thesis. For a review see, Kriplani, U.; Kay, B. K., *Current Opinion in Biotechnology* **2005**, 16, (4), 470-475, and references therein.

2.1.1 Electron Transfer Mechanisms

Electron tunnelling superexchange (elastic) and electron hopping (inelastic) are two of the mechanisms, that are currently proposed to describe electron transfer between a donor and an acceptor group through peptides. Figure 2.1 shows a schematic representation of the hopping mechanism for electron transfer through a helical peptide on gold. The relationship between the acceptor and donor (in this case, gold and ferrocene) distance with respect to electron transfer via electron tunnelling and hopping is described by the equations, $k_{et} = k_0 \exp(-\beta R_{DA})$ and $k_{et} \propto (R_{DA}/R_1)^{-\eta}$, respectively, where k_{et} is the electron transfer rate, k_0 is the kinetic prefactor, β is the tunnelling factor (described later), R_{DA} is the distance between the donor and acceptor, R_1 is the distance between nearest-neighbour hopping sites and η ($1 \leq \eta \leq 2$) is the power parameter which describes bias of electron transfer toward the acceptor.[3,4]

The rate of electron transfer via the hopping mechanism exhibits a linear decay dependence on distance which allows electron transfer to occur efficiently over a longer distance than the tunnelling mechanism.[5] It is thought that this mechanism allows electrons to 'hop' between sites that are electronically coupled (such as via hydrogen bonds).[6,7] The electron hopping mechanism is more efficient than the tunnelling mechanism because of ohmic behaviour when the molecular length is increased.[8] This mechanism is also thought to operate in electron transfer along double-stranded DNA.[9,10]

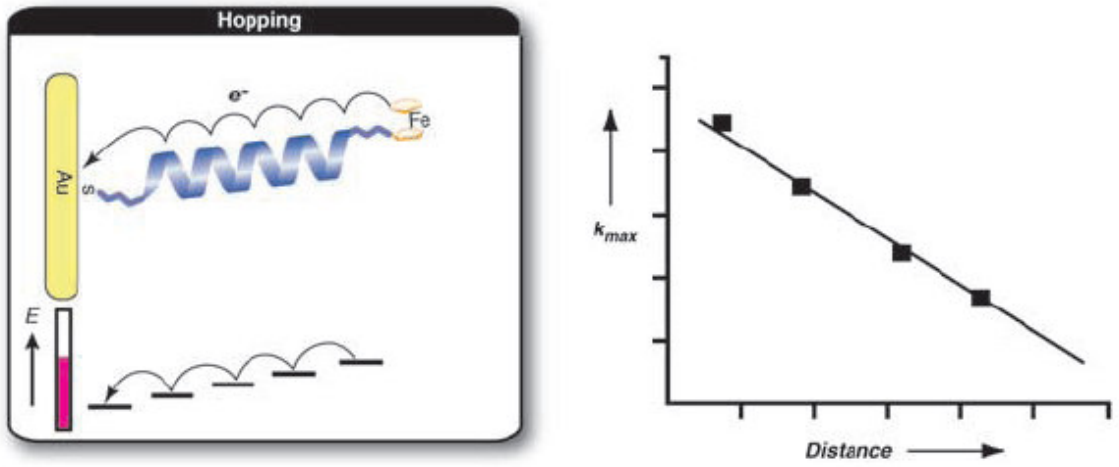

Figure 2.1 Schematic representations of the hopping mechanisms operating in peptides immobilised on Au. The graph shows the decrease in electron transfer rate (k_{et}) with increasing distance between the electrode and the redox centre. (Reproduced from Ref. 1)

Electron tunnelling typically occurs under a large driving force, such as that generated by photoexcitation. As shown in Figure 2.2, the rate of electron tunnelling decays exponentially with increased distance between the donor and acceptor. Therefore, electron tunnelling is not effective for long-range electron transfer (over 4 nm).[11] This distance-dependant decay has been shown to occur on gold surfaces though self-assembled monolayers (SAMs) of alkanethiols that possess an electron donor at the terminal end.[12]

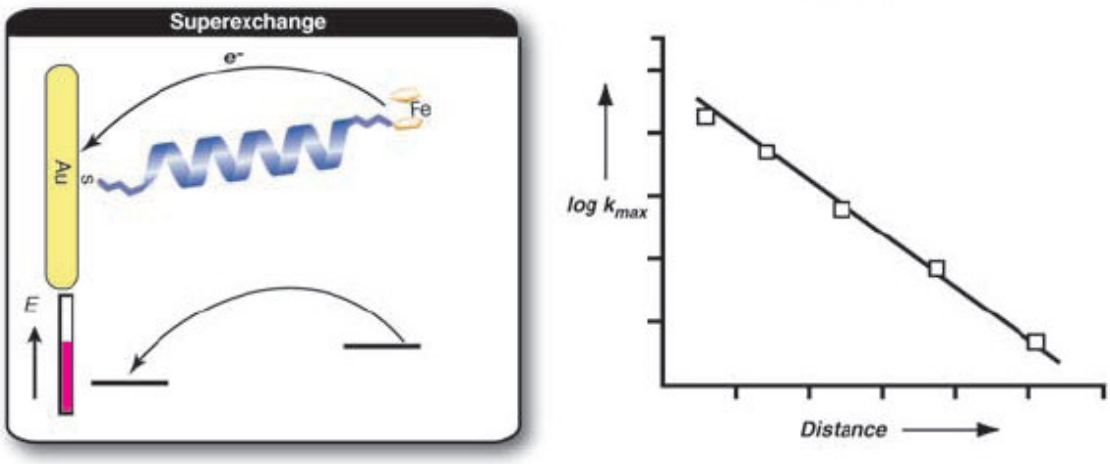

Figure 2.2 Schematic representations of the tunnelling (superexchange) mechanisms operating in peptides immobilised on Au. The graph shows the decrease in electron transfer rate (k) with increasing distance between the electrode and the redox centre. (Reproduced from Ref. 1)

2.1.2 Electron Transfer Studies using Peptides Immobilised on Surfaces

Electron transfer in peptides has been studied in the solution phase, and after immobilisation on a (usually metallic) surface. Electron transfer studies of solution phase peptides requires a redox active species at each terminus, one to act as the donor, the other an acceptor, and a method to initiate the electron transfer (such as ultraviolet irradiation). Immobilised peptides only require one redox probe, which acts as both the donor and the acceptor, with the electrons passing to or from the conductive surface controlled by an applied voltage. The overall structure of redox-functionalised surface peptides leads to a simpler synthetic route. Furthermore, the conformational freedom of the immobilised peptide is minimised by the (quasicrystalline) 2D surface arrangement. Peptides can be assembled in a well-ordered monolayer on surfaces using an appropriate functionality. Thiol or disulfide containing molecules are frequently used as they spontaneously assemble on gold to form a monolayer (known as a self-assembled monolayer or

SAM). Therefore, electrochemical studies using surfaces has become a practical method for the study of electron transfer in peptides, and is the method used in the study presented here.

The electrochemistry of an immobilised species is a powerful analytical tool for determining the ease of reduction and oxidation of the species, organization on the surface, reversibility of the redox process and the rate of electron transfer. The study of peptide electrochemistry on surfaces has led to an increased understanding of how peptide structure facilitates electron transfer. It has become evident that the electron transfer through a peptide is influenced by complex array of variables. Some of these include the separation between the electron acceptor and the donor, the nature of the peptide backbone, the amino acid sequence and the flexibility of the peptide.[13-17]

Aside from electrochemistry, a surface can be characterised by a number of other methods such as atomic force microscopy (AFM), used to measure the surface morphology, reflectance-absorbance fourier transform infrared (FTIR) spectroscopy to look at tilt angle with respect to the surface, and surface plasmon resonance (SPR) to measure biorecognition events.

2.1.3 Immobilising Sulfur-containing Molecules on Gold Surfaces

The study of electron transfer in species immobilised on a surface requires a reproducible and well-defined surface morphology. There are many methods for immobilisation of molecules on surfaces, such as inclusion, coordination, physisorption and covalent immobilization (chemisorption). Proteins are capable of adsorbing on surfaces via physisorbtion, which is an attractive van der Waals force that is non-specific and non-covalent. However, this mode of adsorption leads to an ill-defined surface morphology, and it not desirable for studying specific interactions. Chemisorption to form self-assembled monolayers is favourable because the orientation of the surface species is stable and usually well-defined.

SAMs on a gold surface are typically prepared using sulfur-containing molecules. The adsorption of sulfur on to gold occurs spontaneously, and is thought to form stable covalent Au-S bonds.[18,*] Thioalkanes, thiolipids, modified oligonucleotides, polypeptides, and proteins, or combinations of these, have all been immobilised on surfaces using Au-S bonds. [19-21]

[*] Alkanethiol-metal interactions are not fully understood. X-ray photoemission spectroscopy (XPS) and high resolution studies of SAMS on Au(111) have shown that S-atom bonded to the metal surface exhibits the chemical properties of an alkanethiolate.

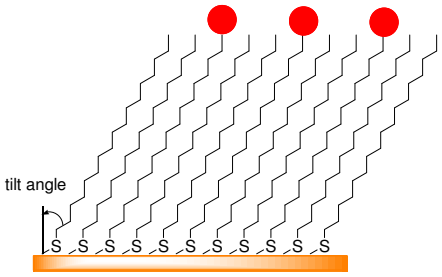

Figure 2.3 Thiols assemble spontaneously on gold, to form an Au-S bond. Terminal redox active groups on alkanethiols are shown with red spheres. Alkane thiols that contain no redox active groups are used to separate those that do, and are known as diluents.

SAMs are constructed by immersing the gold surface in a solution containing a thiol or disulfide-terminated species. Gold-sulfur bond formation is a reversible process. Furthermore, increased temperature, various organic solvents (such as DCM), strongly acidic solutions and oxidation/reduction events can degrade the surface.

Alkane thiols with a chain length of 10 or greater are known to form very highly ordered SAMs (Figure 2.3).[22] The density of alkane thiol molecules on the surface is limited not by the width of the alkyl chain, but by the diameter of the gold atoms. Because the diameter of a single gold atom is larger than that of the alkyl chains, the monolayer tilts to form a more closely packed structure (Figure 2.4). In general, a small surface tilt suggests a well ordered monolayer. This is also true for other cylindrical molecules such as helices and linear polymers. The Van der Waals forces between the alkyl chains strengthen and stabilise the overall monolayer. Longer alkyl chains form more stable monolayers than shorter ones. Destabilising interactions, such as the repulsion of closely spaced, identically charged groups, lead to a poorly ordered monolayer.

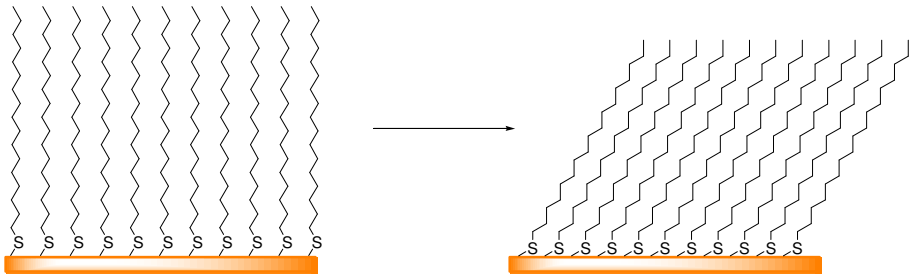

Figure 2.4 The monolayer of cylindrical molecules tilts to form a closest packed structure on the surface.

A redox probe is required to measure electron transfer from the gold surface through the monolayer. The redox probe can be covalently attached to the immobilised species (as shown in Figure 2.3 and Figure 2.6), or can exist as a diffusing solution species (Figure 2.5). The latter is

problematic because if the surface morphology is not uniform, or if there are holes in the monolayer, the diffusing redox moiety can transfer electrons through a shorter route (Figure 2.5b), instead of the desired pathway (Figure 2.5a). Therefore, in this thesis the redox probe was covalently attached to the immobilised peptides and model compounds.

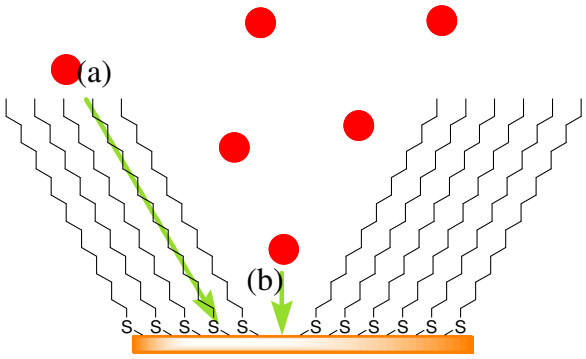

Figure 2.5 Electron transfer in solution phase species (shown as red circles) can occur at defect sites (b) as well as the intended route (a) though the monolayer.

The rate of electron transfer from the surface to the covalently attached probe must be the same for each molecule on the surface in order to obtain adequate electrochemical data. However, a mixture of redox environments occurs if some of the redox groups are in contact with other neighbouring groups, resulting in an undesirable spread of possible oxidation or reduction states, and redox potentials (Figure 2.6a). Furthermore, redox groups that are close in space may be able to pass electrons between each other, affecting the rate of electron transfer in the monolayer. Surfaces of this type are unsuitable for detailed analysis because the observed electron transfer rate is the result of different electron transfer events. Non-redox active thiols (known as diluents) are used to space the redox groups on the surface, as shown in Figure 2.3. Larger molecules that have diameters sufficient to separate the redox group from neighbouring groups do not require diluents (Figure 2.6b).[11]

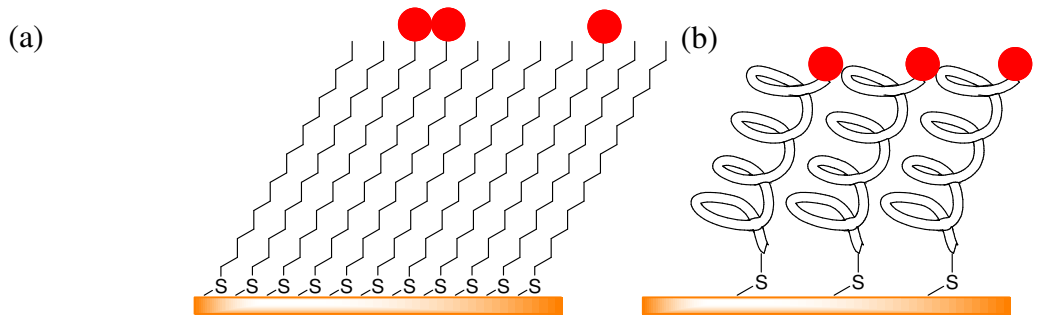

Figure 2.6 SAMs with redox centres (shown as red circles). (a) An inhomogeneous alkyl thiol monolayer and (b) a helical peptide monolayer.

The morphology of SAMs composed of peptides is more complex. The ability to form tightly packed monolayers depends on the length of the peptides, the amino acid composition, and the ability to form intramolecular hydrogen bonds. Short peptides form loosely packed monolayers that show a large degree of disorder and that have up to 15% vacant gold sites. By contrast, longer peptides with stable secondary structure, such as α-helices, form well-ordered monolayers. [1,23] α-Helical peptides, which are stabilised by hydrogen-bonding interactions, have been widely studied as potential molecular wires, and as a means to understand electron transfer in biological systems.

2.1.4 Electron Transfer within Surface Immobilised α-Helical Peptides

The α-helix has a number of physical properties that make it amenable to study electron transfer on gold. Firstly, the secondary structure of the α-helix backbone is cylindrical, stabilised by hydrogen bonds between the backbone amide groups. This network of hydrogen bonds is capable of conducting charge. Secondly, the α-helix possesses a dipole moment (due to the polarity of the amide bonds which all point in the same direction) which reduces the energy barrier for electron transfer.[24] Finally, the α-helix frequently associates with other helices to form self-assembled helix-bundle structures in solution and at the air-water interface.[25]

β, also known as the 'tunnelling parameter'(introduced on page 20), is a factor that depends largely on the nature of the molecule separating the donor and acceptor in an electron transfer reaction, and is a measure of the ability of a molecule to conduct electrons.[8] Table 2.1 gives the experimentally determined tunnelling parameter values for α-helical peptides and a variety of other molecules. A small β value, typically less than 0.6 $Å^{-1}$, indicates that a molecule is a good electron conductor.

Table 2.1 Reported tunnelling parameters of some common synthetic and naturally occurring molecules.

Type of Molecule	Electron Transfer Ability[1] β (Å-1)
Alkyl chains	~1
Linear peptide (no secondary structure)	~1
DNA	0.2 - 0.9
α-Helical peptide	0.6617
Polyolefin	0.2-0.6
oligo (p-phenylene vinylene)	~0.01

The *β* value of alkyl chains and linear peptides is ~1, while the *β* value of *α*-helical peptides is 0.66 $Å^{-1}$. Therefore, these helical peptides are better mediators of electron transfer than alkyl chains and linear (strand) peptides, and of comparable ability to the DNA and π-conjugated polyolefin systems (Table 2.1).[11] This electron transfer ability is not thought to be solely due to the partial double bond character of the peptide bond in the *α*-helix backbone. Rather, the electronic coupling of the hydrogen bonds along the backbone combined with the large dipole moment of helical *α*-peptides is thought to facilitate the movement of electrons. This suggests that helical peptides are suitable as molecular wires.

Surface Orientation of α-Helical Peptides

Assembly of helical peptides on a surface can occur in various ways: normal (perpendicular) to the surface; at a tilt angle (as discussed earlier); or as a disordered layer on the surface (Figure 2.7).[26,27] The 'surface normal' orientation rarely occurs (Figure 2.7a); instead, helical peptides normally have a tilt associated with the monolayer (Figure 2.7b). The cylindrical nature of helical peptides enables the formation of tightly packed SAMs, thereby resulting in small tilt angles. A parallel assembly mode (Figure 2.7c) occurs when there are multiple attachment points along the peptide axis, or with a highly disordered monolayer.

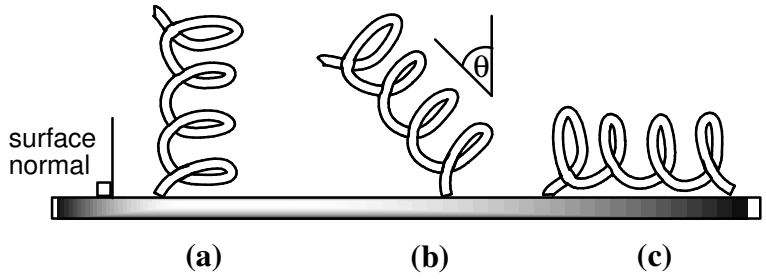

Figure 2.7 α-Helical peptide represented as a spring, can adopt different conformations on the surface: (a) 'surface normal' orientation, (b) tilted orientation and (c) disordered or parallel orientation.

The orientation of the SAMs can be experimentally determined using Fourier transform infrared reflection reflection-absorption spectroscopy (FTIR-RAS) measurements of amide I and II bands at 1675 and 1545 cm^{-1}.[28] A high ratio of amide I to amide II absorbance indicates that the peptide is bound close to 'surface normal' (perpendicular to the surface).

Until 1993, helical peptides received little attention as functional surface species because of the lack of understanding of the principles behind the formation of well-ordered SAMs. One attempt to solve this problem was developed by Whitesell and Chang, who formed helical peptides on a surface using chain polymerisation techniques.[29] A tripodal amino trithiol group was adsorbed to gold which occupied a surface coverage large enough to allow peptide formation. Treatment of the subsequent monolayer with the *N*-carboxyanhydride of alanine gave a substantial layer of polyalanine (Figure 2.8). However the peptide layer had an apparently random orientation,

deduced from FTIR absorption spectroscopy.* Worler *et al* had similar problems with a SAM of poly (γ-benzyl-L-glutamate) formed under an electric field.[26]

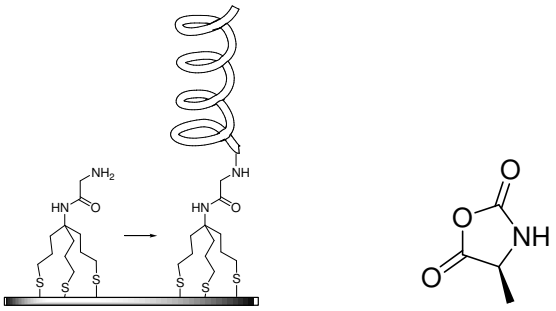

(a) (b)

Figure 2.8 a) Schematic representation of polyalanine (spring) on a monolayer of aminotrithiol. (b) Structure of the *N*-carboxyanhydride of alanine. (Adapted from Ref. 29)

Miura and Kimura formed the first uniform SAM using helical peptides with terminal crown ether groups (Figure 2.9).[27] These peptides were orientated on the surface through coordination of a SAM of amine-terminated thiols and the crown ether groups on the peptides. The tilt angle of the helix from surface normal was found to be 28 °, suggesting the peptides formed a well-ordered surface arrangement.

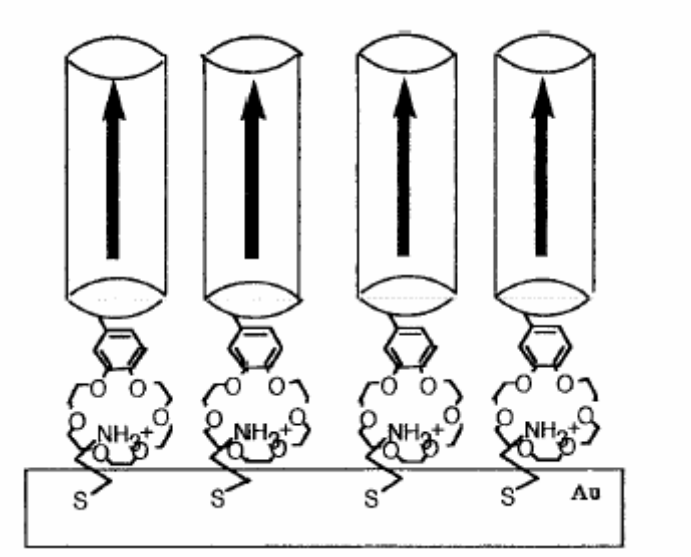

Figure 2.9 Helical α-peptides aligned on the surface using an interaction between crown ether and surface amide groups. (Reproduced from Ref. 27)

* At this early stage of research, exact tilt angles could not be calculated.

As this area has advanced, systematic studies of the physical structure of SAMs of helical peptides on gold have determined the factors that effect the tilt angle of helical peptides on surfaces. Using peptides **2.1**-**2.4,** Miura *et al* showed that peptide length, amino acid composition, and adsorption conditions all had an effect on the tilt angle of SAMs (Table 2.2).[28] These peptides, possessing an Aib-Ala motif (Aib = $NH_2C(CH_3)_2CO_2H$), are known to adopt an α-helical structure in solution. The longest peptide, 24 mer **2.3**, was the closest to surface normal. This better defined self-assembling quality is associated with the larger Van der Waals interaction between neighbouring peptides, which promotes tighter packing. Peptide **2.4**, which contains γ-OBn-Glu residues instead of Ala, had increased tilt angle compared with **2.2**. Peptide self-assembly and surface packing is disrupted by the steric effects of the bulky γ-OBn-Glu residues. It was found that the solvent system used in the preparation of the SAM can also disrupt the self-assembling properties of the peptide. Peptide **2.2**, adsorbed from ethanol, gave a lower tilt angle (and therefore better self-assembly) than from dimethylformamide, a solvent which disrupts peptide intramolecular hydrogen bonding.

Table 2.2 Comparison of the tilt angles various α-peptide SAMS.[28]

α-Peptide		Tilt Angle[28]
	2.1 (n=6)	48 º
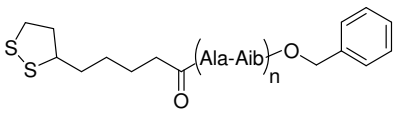	**2.2** (n=8)	36 º (EtOH) 63 º (DMF)
	2.3 (n=12)	30 º
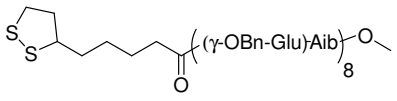	**2.4**	55 º

A similar study using much larger peptides showed that increasing the peptide length could have a destabilising effect.[30] Poly (γ- benzyl-L-glutamate) peptides of 10 and 27 kDa (~ 5 and 14 times longer than **2.3**, respectively), were prepared by solution-phase polymerisation and then adsorbed onto gold. It was found that the larger peptide had a greater surface tilt than the smaller

10 kDa peptide, and that, counterintuitively, an increased surface assembly time led to both a greater tilt angle and a decrease in surface coverage.

Other methods for the controlled introduction of helical groups to surfaces include dip-pen nanolithography, a method whereby a small radius tip (~10 nm) is inked with peptide and stamped on the surface using atomic force microscopy. This method has been used to place both collagen[31] and DNA in 30 nm line bands on the surface. This "direct write" capability, which preserves the structure and functionality of the biomolecules, is important for the development of biological devices and proteomic arrays. Enander *et al* designed a series of charged synthetic polypeptides which could assemble into four-helix bundles on a gold surface.[32] Negatively charged helix-loop-helix motifs were immobilised onto the surface as random coils and positively charged analogues were introduced inducing heterodimersation to give a helical secondary structure.

In summary, the most accessible method for the formation of well-ordered SAMs of α-helical peptides (at present) is by the immersion of a gold surface in an ethanolic solution of thiol-terminated peptides.[28] Furthermore, the incorporation of amino acid residues with large side chains groups (such as Glu) should be avoided, as they have a sterically destabilizing effect on the SAM (Table 2.2). Therefore, in this thesis β-peptides comprising β-amino acids with short alkyl side chains, dissolved in 2,2,2-trifluoroethanol were used to prepare SAMs on gold (as discussed later).

Rate of Electron Transfer in α-Helical Peptides

The rate constant of electron transfer (k_{et}) from a redox group to the surface through a peptide film can be measured electrochemically with cyclic voltammetry and chronoamperometry techniques (as described in Appendix A). The dependence of k_{et} on both the peptide length and overpotential (defined here as a voltage step to a value larger than the standard redox potential, applied in the chronoamperometry technique) are weak for systems where electron hopping is the dominating process. Concurrently, the theoretical electron transfer rate constant for the superexchange electron tunnelling mechanism of the system can be calculated.[33] If the experimentally determined standard rate constant (k_{et}^0) is much faster than the calculated superexchange rate, it is likely that another mode of electron transfer (such as electron hopping) is the dominating process.

The rate of electron transfer in SAMs of helical (Xaa-Aib)$_n$-based α-peptides (without diluents) containing ferrocene (**2.5**-**2.10**) were determined by Kimura *et al* (Table 2.3).[5,11] It was found that the use of diluents had no effect on the experimentally determined k_{et} values. This is because the large diameter of the α-helical peptides effectively isolated the ferrocene probes.

Kimura *et al* found that electron transfer in helical α-peptides was independent of overpotential and was faster than theoretically calculated electron tunnelling rates.[5,11] These results suggest that electron tunnelling does not contribute significantly to electron transfer in these helices, and therefore electron hopping may be the dominating mechanism. As a helical peptide has a network of hydrogen bonds extending from one end of the chain to the other, this result is not surprising.[29] Watanabe *et al* proposed that the electron transfer pathway involves the hydrogen bonded amide groups (discussed later, in section 2.3.2).[11]

Table 2.3 Comparison of the experimentally observed standard rate constant (k_{et}^{0}) of electron transfer for various peptide SAMs, with the calculated superexchange rate.[5,11]

α-Peptide	Experimentally determined k_{et}^{0} (s^{-1})	Calc. Superexchange rate constant (s^{-1})
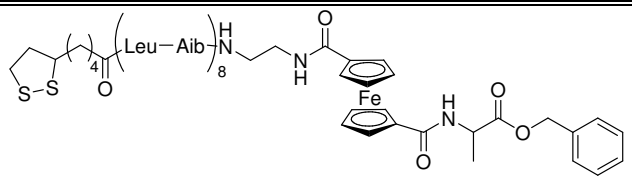 **2.5**	2.0	0.003
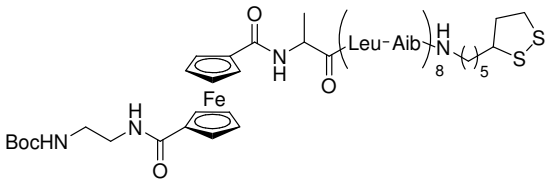 **2.6**	0.68	0.003
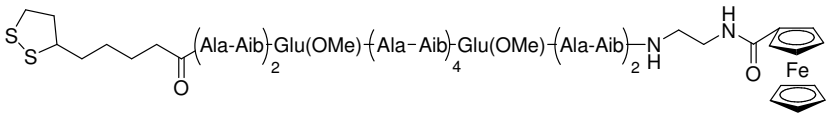 **2.7**	42	0.0005
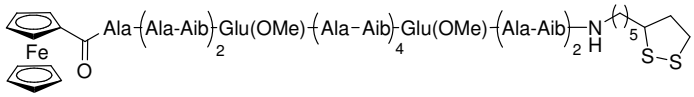 **2.8**	28	0.0005
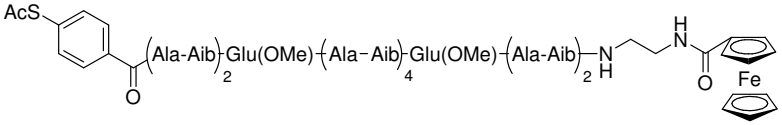 **2.9**	257	0.06
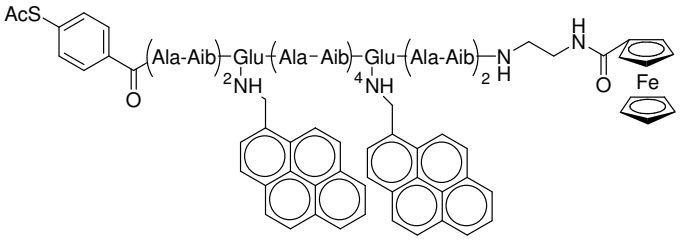 **2.10**	229	0.06

It was found that altering the peptide length, direction of polarity and choice of sulfur linker all had an affect on electron transfer rates. For example, the shorter hexadecapeptides **2.5** and **2.6** had a much lower k_{et} compared to the octadecapeptides **2.7**-**2.10**. Reversing the polarity of the peptides with respect to the surface by attaching the sulfur linker to the *N*-terminus instead of the

C-terminus of the peptide (**2.5** and **2.6**; **2.7** and **2.8**) increased the electron transfer rate. Miura *et al* suggested that the accelerated electron transfer rate of peptides **2.5** and **2.7** is due to the partial positive charge of the *N*-terminus of α-helical peptides, which lowers the energy barrier between the gold surface and the peptide layer (this discussed further in section 2.3.2).[5] Furthermore, the choice of sulfur linker had an effect on electron transfer: the lipoic acid linker on peptide **2.7** greatly slowed the rate of electron transfer compared with the thiobenzoic acid linker on peptide **2.9**. This k_{et} data suggests that electron transfer along the lipoic acid linker is slow compared to electron transfer through the conductive π-orbitals of the thiobenzoate linker.

Electron Transfer in Non Hydrogen-Bonded Helical Peptides

The study of electron transfer in both hydrogen-bonded helical peptides and strand peptides allows one to understand the overall nature of electron transfer in proteins. Electron transfer in strand peptides is thought to occur via the tunnelling mechanism, as outlined earlier in Figure 2.2. This mode of electron transfer is inefficient, and therefore the magnitude of k_{et} is both smaller than and exponentially dependent on peptide length. Some non-hydrogen-bonded examples are discussed below.

Oligoprolines are helical peptides, that do not form a tightly coiled α-helix, but rather a more open type II trans helix, that has a rise per residue distance of 3.12 Å (compared to 1.5 Å in an α-helix) (Chapter One, Figure 1.10). Instead of stabilisation by hydrogen bonding, this helix is stabilised by steric repulsion of the pyrrolidone rings of the proline residues.[13] Therefore, like strand peptides, electron transfer in oligoprolines should *not* occur via electron hopping. Galka *et al*, studied the electron transfer rate in SAMs of oligoprolines ranging from zero to six residues.[16] The rate of electron transfer was both small and dependent on the peptide length, which is characteristic of the electron tunnelling mechanism (Figure 2.10). However, the tunnelling parameter (β) was 0.12 $Å^{-1}$, indicating that these peptides are very good molecular wires. This finding is inconsistent with non-hydrogen bonded secondary structure and the β value for strand peptides of 0.9-1.2 $Å^{-1}$. It was postulated that electron transfer through strained systems, such as oligoprolines, is faster due to favourable electronic effects, which effectively reduces the donor-acceptor distance.

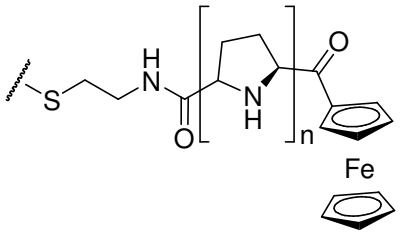

Number of Pro (n)	k_{et} x 10^{-3} (s^{-1})
0	8.3
1	11.2
2	7.5
3	5.2
4	3.6
5	2.5
6	1.8

Figure 2.10 Electron transfer rate constants for the peptide shown with varied number of proline residues.[13]

Another approach to measuring electron transfer in non-helical peptides is through the use of a molecular junction, as shown in Figure 2.11.[34] Xiao *et al* monitored the current decay of the peptide as the gold contacts were moved apart, breaking the gold-sulfur bond to one gold contact. This decay gave a measure of electron transfer (as conductance) of the peptides. Again, as expected for a strand peptide, the rate of electron transfer was found to be highly dependent on the chain length of the peptide, suggesting a superexchange mechanism was prevailing.

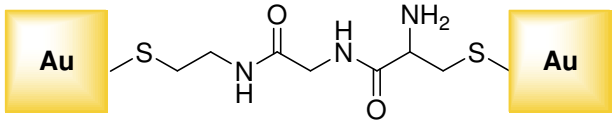

Figure 2.11 Schematic representation of the molecular junction, connected with a disulfide peptide.

Both of these examples indicate that peptides without a hydrogen-bonding network exhibit electron transfer that is characteristic of the superexchange mechanism. Therefore, the peptide secondary structure is important in determining the mode of electron transfer on the surface.

2.1.5 Research Described in This Chapter

β-Peptides are ideal models for studying the physical and biological properties of α-peptides as they possess a diverse range of secondary structures, similar to those found in α-peptides, but with greater conformational stability and the possibility to modify the peptide backbone by introduction of other atoms (e.g. fluorine). As there remains uncertainty about the role of primary and secondary structure in the electron transfer in α-peptides, it is possible that the study of electron transfer in β-peptides could provide valuable information to understanding how (and if) peptide conformation is important for electron transfer. Presented here is a preliminary study into the electron transfer of immobilised β-hexapeptides using electrochemical techniques. Furthermore, these results are compared with electron transfer through an α-peptide analogue.

2.2 Preparation and Electrochemical Analysis of β-peptide SAMs

2.2.1 Composition of β-Peptide SAMs

A surface species must possess three important structural functionalities in order to study the electron transfer by immobilisation on a gold surface (Figure 2.12):

- A sulfur-containing linker group, for covalent attachment of the molecule to the gold surface.
- The spacer component which facilitates electron transfer between the gold and the redox probe. It is the electron transfer though a β-peptide spacer that is of interest in this thesis.
- A redox-active probe to measure electron transfer. The redox probe allows for electrochemical analysis by acting as electron donor or acceptor. The rate of oxidation or reduction of the redox probe by electrons from the gold surface is defined by the spacer component.

-

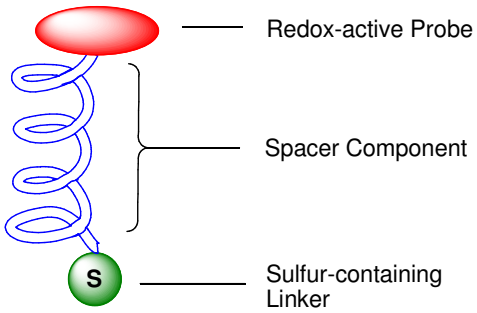

Figure 2.12 Schematic of the important functionality for studying electron transfer on a gold surface.

There are many possibilities for both the redox probe and sulfur linker, but for reasons discussed in chapter three, the sulfur linkers lipoic acid (**3.19**), lipoamine (**4.8**), acetyl-protected hexadecane thiol (**3.16**), and the redox probe ferrocene (Fc), were chosen. The Fc/Fc^+ half-wave potential in aqueous solution is typically observed between 0.2 and 0.5 V (SCE). The exact standard electrode potential value is dependent on other functionalities at the SAM interface, concentration of ferrocene groups on the surface, and identity and concentration of the solution electrolyte.[35]

Five hexapeptides (**2.12**-**2.16**) and one tripeptide (**2.11**) were synthesised with a thiol or disulfide end group as the sulfur linker (**Table 2.4**). The synthesis and structural studies of these peptides are outlined in Chapter Four.

Table 2.4 α and β-peptides synthesised for analysis on gold.

Peptide Structures for SAM Studies	**Code***
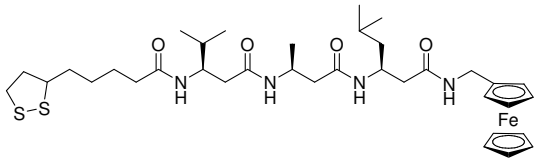	**SSβ_3Fc** (**2.11**)
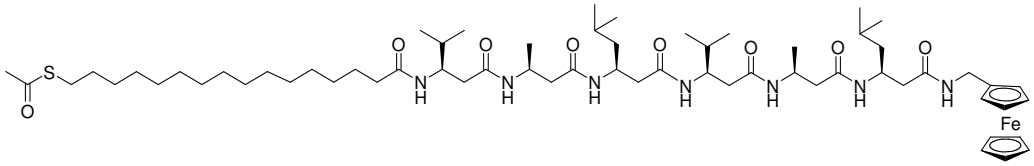	**SC$_{15}\beta_6$Fc** (**2.12**)
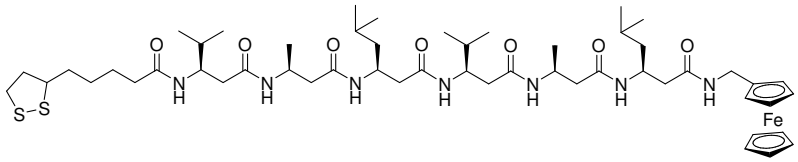	**SSβ_6Fc** (**2.13**)
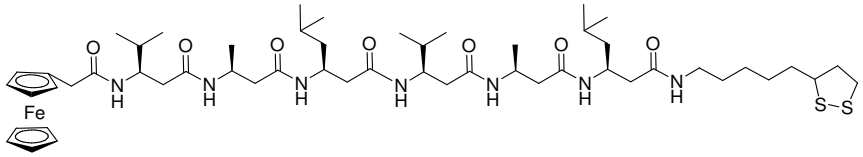	**Fcβ_6SS** (**2.14**)
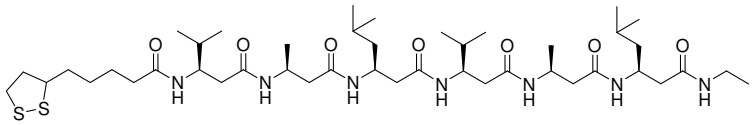	**SSβ_6Et** (**2.15**)
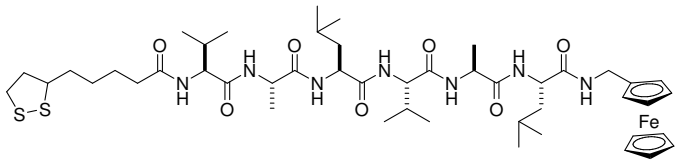	**SSα_6Fc** (**2.16**)

Four of the peptides (**SC$_{15}\beta_6$Fc**, **SSβ_6Fc**, **Fcβ_6SS, SSβ_6Et**) contain a core-structure consisting of two repeat units of β^3hVal-β^3hAla-β^3hLeu. The core structure is based on the β-peptide **2.17**, shown in Figure 2.13, which adopts a 3_{14} helical structure in solution (the 3_{14}-helix is shown in **Figure 1.8**).[36] However it should be noted that a 3_{14} helical structure was not observed for the

* Compound codes are used in this chapter to abbreviate the structures of the peptides. SC_{15} refers to the alkylthiol linker **2.3;** SS is the disulfide-based linker lipoic acid or lipoamine; α indicates the peptide is composed of α-amino acids; β indicated the peptide is composed of β-amino acids; Fc is ferrocene; and Et is an ethyl group in place of ferrocene.

functionalised β-peptides **2.12**-**2.15** in solution (as described in detail in Chapter 4). Furthermore, it is difficult to demonstrate that the secondary structure (helical or strand like) of a species in solution is retained when immobilised on the surface. Therefore the surface phase secondary structure of the peptide SAMs presented here is unknown. It is postulated in the literature that a hydrophobic environment (such as that in a lipid bilayer) may induce intramolecular hydrogen bonding not seen in solution.[37] A SAM containing uncharged molecules (such as the peptides used in this study) is also hydrophobic and which could favour helix formation.

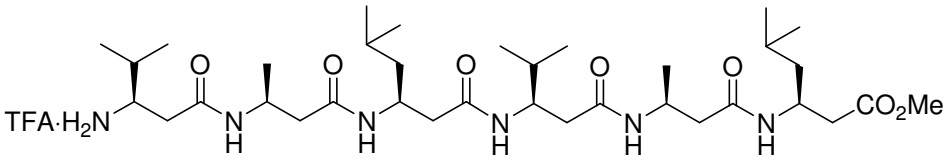

2.17

Figure 2.13 β-hexapeptide **2.17** which possess a 3_{14}-helical structure in solution.

Peptide **2.17** possesses a dipole moment due to the orientation of the carbonyl groups in the helical conformation (see Section 1.2.2) which renders the electrostatic potential at the *C*-terminus partially positive and the *N*-terminus partially negative. The peptides, **Fcβ_6SS** and **SSβ_6Fc,** were synthesised to explore the effect of the polarity on the electron transfer rates (assuming the peptides adopt a helical structure when immobilised on the surface). This was achieved by coupling the positive pole at the *C*-terminus of the β-peptide to either the sulfur linker (as in **Fcβ_6Fc**), or to the ferrocene group (as in **SSβ_6Fc**). Therefore, peptides **Fcβ_6SS** and **SSβ_6Fc** possess opposite polarity with respect to the gold surface.

Similarly, by varying the sulfur-containing linker unit (**SC$_{15}\beta_6$Fc** compared with **SSβ_6Et**) the effect of structural changes on the rate of electron transfer was observed. Furthermore, two control peptides are included: a β-peptide (**SSβ_6Et**) that lacks a redox active ferrocene group, and an analogous α-peptide. The α-hexapeptide **SSα_6Fc**, containing two repeat units of Val-Ala-Leu, and the β-tripeptide **SSβ_3Fc**, containing the β^3hVal-β^3hAla-β^3hLeu unit, have been shown *not* to adopt any stable secondary structure in solution.[38] Therefore, the structure of these peptides is described as 'strand-like' (ie. they have an absence of defined secondary structure). If this strand like conformation is retained when the peptides are immobilised on a surface (and intermolecular

hydrogen bonding is negligible), SAMs of these peptides may exhibit electron transfer via the less efficient tunnelling mechanism.

2.2.2 β-Peptide SAM Preparation and Experimental Conditions

If the reader is unfamiliar with the theoretical and practical details of cyclic voltammetry and chronoamperometry, it is recommended that Appendix A is read first.

Preparation of SAMs and Electrochemical Cell Setup

All peptide SAMs were prepared on the flat face of a gold single-crystal electrode (the working electrode), possessing a gold (111) structure (Figure 2.14). Before forming a SAM, the working electrode was stripped of organic impurities using piranha solution (conc. sulfuric acid/hydrogen peroxide (30 % v/v); 2:1), and electrochemically cleaned by cycling in 0.01 M $HClO_4$ solution.

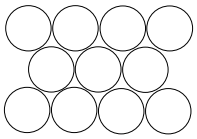

Figure 2.14 The closest-packed arrangement of gold atoms on a (111) surface. A surface of this type can be polished to give very smooth and uniform topography.

SAMs of the hexapeptides were prepared on the gold (111) electrode by immersion in trifluoroethanol solutions of the peptides for 16 hours. A three-electrode cell containing an aqueous solution of 0.1 M $NaClO_4$ was used for voltammetry and chronoamperometry measurements. The working electrode was the Au (111) electrode containing the SAM. A platinum auxiliary electrode and saturated calomel electrode (SCE) reference electrode were also used.

Voltammetry Parameters

Voltammetry was performed over a potential range of 0 to 0.55 V or 0 to 0.6 V, depending on the redox peak positions and widths. This potential range was chosen so that only the ferrocene moiety was oxidised and reduced (and not other functional groups), the thiol was electrochemically stable and gold oxides were not formed. The scan rate was varied from 20 to 500 mVs^{-1}.

Assessing the SAMs

A SAM with uniform, well spaced ferrocene centres was required for voltammetry and chronoamperometry analysis. Surfaces that contain two or more anodic peaks, such as that shown in Figure 2.15 for a SAM of **$SC_{15}\beta_6Fc$**, are unsuitable because some redox centres are in different environments, or too close to each other. The two major peaks, indicated with arrows, are from ferrocene groups that exist in two different environments on the surface. Because these two species have different E^0 values, and therefore different $k_{et}{}^0$ values, the chronoamperometry data will be difficult to interpret quantitatively. Inhomogeneous surfaces, like the one shown, were obtained occasionally. However, only surfaces with single anodic and cathodic peaks were considered suitable for voltammetry and chronoamperometry in this thesis.

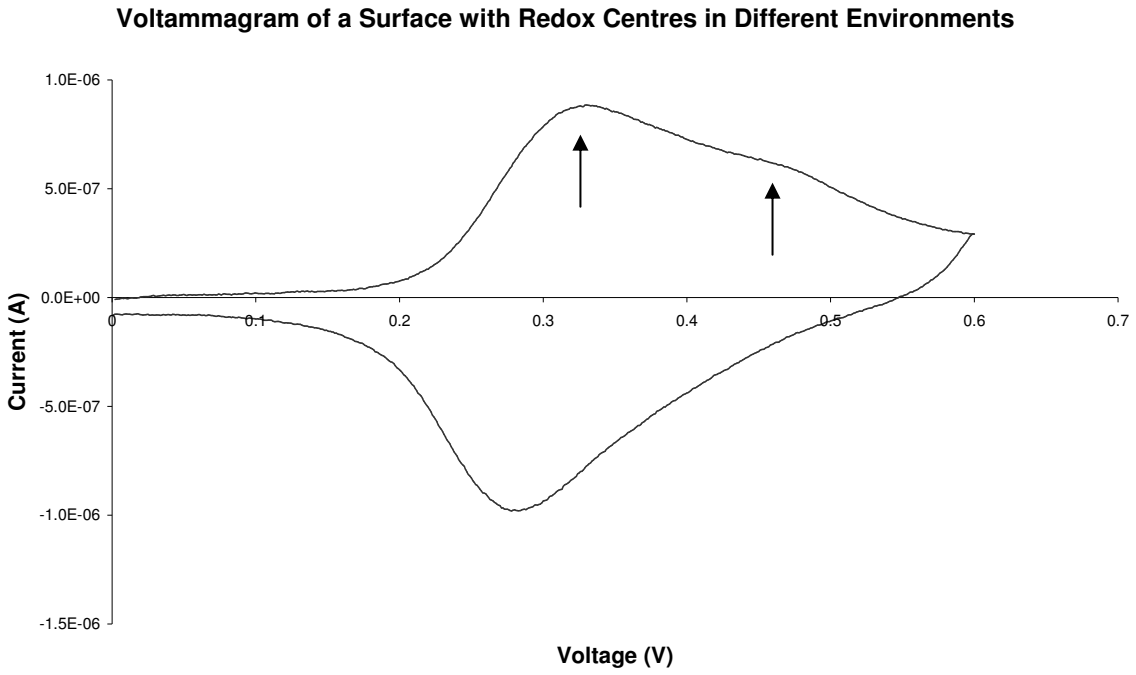

Figure 2.15 A surface of **$SC_{15}\beta_6Fc$** which has redox groups in different environments, as shown by the presence two anodic peaks (indicated with arrows).

2.2.3 Voltammetric Analysis of β-Peptide SAMs

Model Compound $SC_{15}Fc$ (2.18)

The cyclic voltammagrams of ferrocenyl thiol **$SC_{15}Fc$** (**2.18**) contain oxidation and reduction peaks for the one electron transfer process Fc/Fc^+, with an $E_{½}$ of 0.34 V (Figure 2.16). Both of the peaks are broad*, indicating inhomogeneity of the ferrocene environments on the surface. The double layer capacitance of the monolayer is small, as evidenced by the offset of the baseline from zero current in the regions outside the peaks (< 0.2 V and > 0.6 V). This suggests that **$SC_{15}Fc$** forms a well-ordered and tightly packed monolayer that prevents permeation of charged molecules from solution. The oxidation peak area of this model compound was useful for comparison with that of the peptide SAMs, as discussed later.

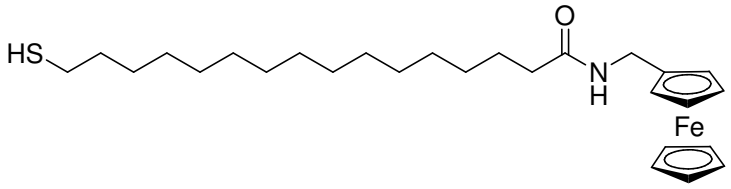

$SC_{15}Fc$ (2.18)

The presence of a prepeak (indicated with an arrow in Figure 2.16) implies that chronoamperometry cannot be performed on monolayers consisting solely of **$SC_{15}Fc$**, presumably because the ferrocenyl groups are in very different environments on the surface, with different electron transfer rates. A diluent would be required to obtain adequate rate data however, as the study of electron transfer in alkylthiols has been well detailed in the literature[12,39,40] and is not the objective in this study, the formation of mixed monolayers was not investigated.

In the voltammagrams of **$SC_{15}Fc$** the oxidation and reduction peak currents do not lie at the same potential values (a situation known as peak splitting) (Figure 2.16). This is evident in all ferrocene-containing SAMs discussed here and is due to the reorganisation energy of the solvent sphere around the ferrocene group when it becomes charged through oxidation to Fc^+.

* Oxidation and reduction peaks are generally described as broad if the peak at half height is wider than 0.1 V.

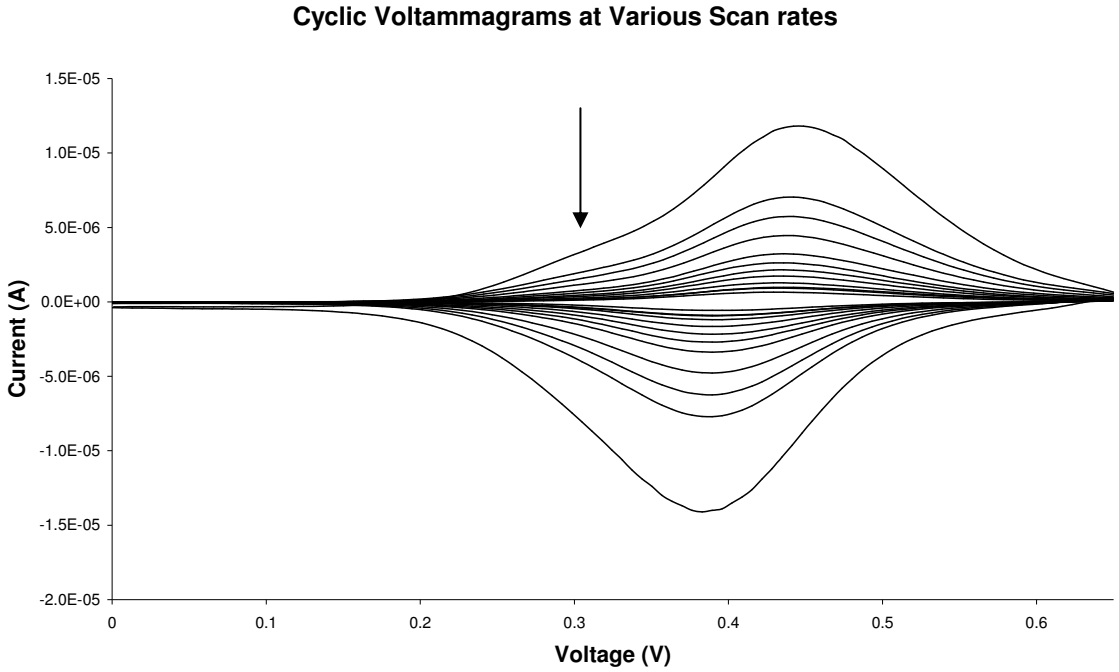

Figure 2.16 Cyclic voltammagrams of **$SC_{15}Fc$** in a 0.1 M $NaClO_4$ aqueous solution at 20 (innermost scan), 35, 50, 65, 85, 100, 125, 150, 200, 250, 300, and 500 (outermost scan) mVs^{-1}.

α-Hexapeptide $SS\alpha_6Fc$ (2.16)

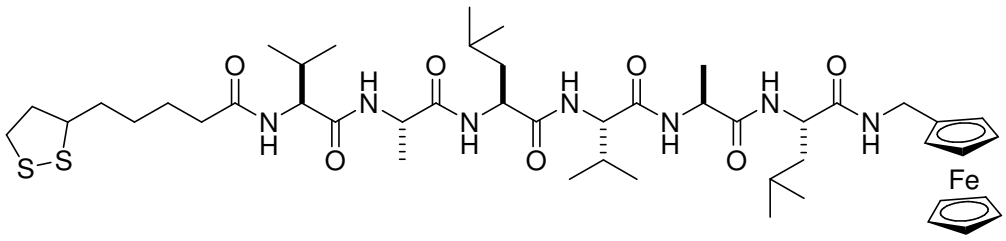

$SS\alpha_6Fc$ (2.16)

The cyclic voltammagrams of α-hexapeptide **SSα6Fc** contain well-defined oxidation and reduction peaks for the one electron redox process Fc/Fc^+ (Figure 2.17a). The oxidation and reduction peaks are broad suggesting that the surface contains a number of similar (but not identical) ferrocene environments. However, this inhomogeneity at the surface did not prevent adequate chronoamperometry data from being collected (as described later). The double-layer capacitance is moderate as evidenced by the offset of the baseline from zero current, particularly after the oxidation peak on the forward scan (the top curve), and the reduction peak of the reverse scan (the bottom curve). The half-wave potential ($E_{½}$) of the ferrocene group in peptide

SSα_6Fc is ~0.33 mV. This potential is consistent with the literature values for monosubstituted ferrocene species.[41]

The voltammagrams reveal a number of important features of the SAM. Firstly, the ferrocene groups of the peptide molecules are likely to be in similar environments on the gold surface, as evidenced by the lack of distinct satellite peaks or peak shoulders. The increase in double-layer capacitance with oxidation of the monolayer suggests that ion penetration is occurring either by film distortion or at surface defects, and suggests the monolayer is not tightly packed. Curve-fitting* of the reduction and oxidation components of the voltammagram gave a reduction peak area 25% smaller than the oxidation peak area (Figure 2.17b). This is not attributed to a physical characteristic, but rather the difficulty in consistent curve-fitting of the peaks because of the double-layer charging. The linear relationship between the peak area and scan rate suggests that electron transfer occurs between the surface-bound ferrocene and gold (rather than from a diffusing solution species) (Figure 2.17b).[5]

Figure 2.17c shows that both the oxidation and reduction peaks shift to less positive potentials as the scan rate increases. The shift of the reduction peak is typical of cyclic voltammagrams for which the rate of electron transfer is slow relative to the timescale of the measurement. If the electron transfer kinetics are relatively slow then the Nernstian concentrations of oxidised and reduced species cannot be maintained at the surface during faster scans (as described in Appendix A, Section **A.4**). However, the behaviour of the oxidation peak is not consistent with such a situation and at present it is unclear why the peak potential decreases (instead of increases) with increasing scan rate.

* The creation of a curved line (based on a nonlinear regression model) that best represents the baseline of the peak thereby removing the double-layer capacitance contribution.

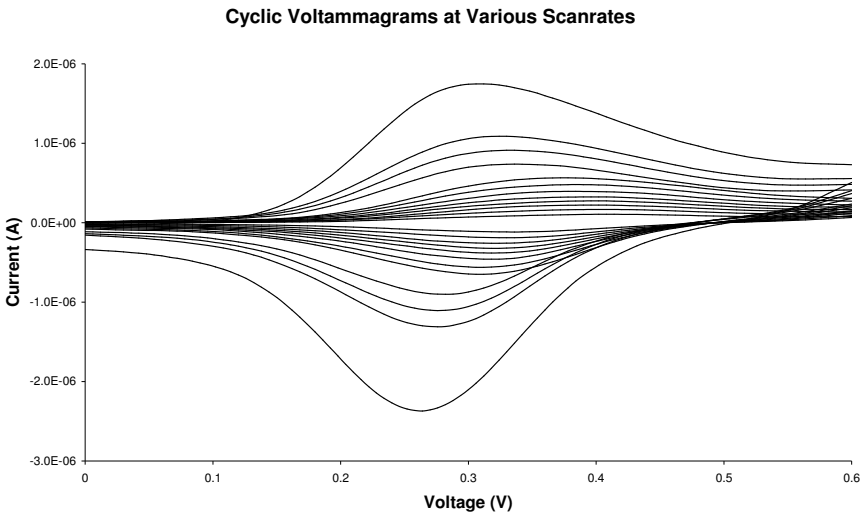

(a)

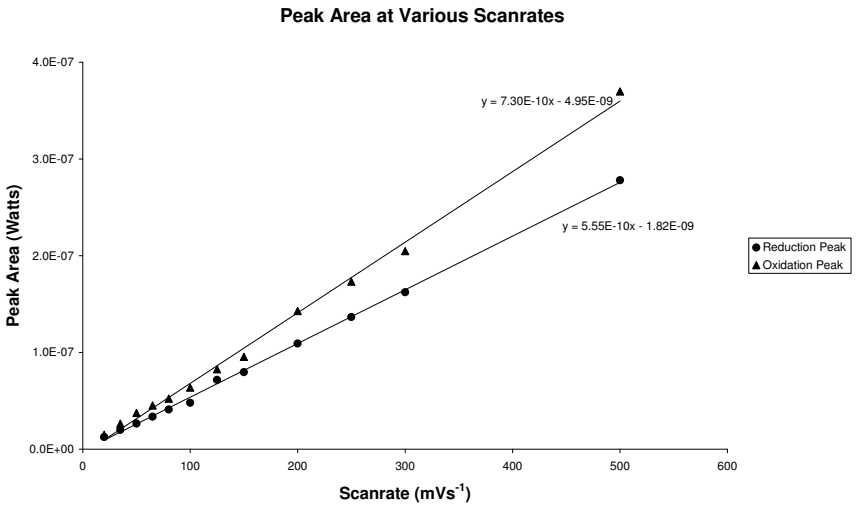

(b)

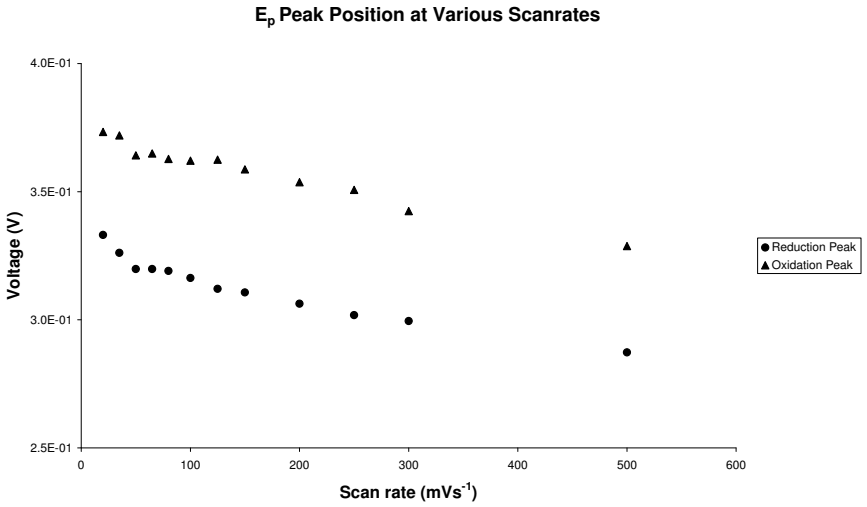

(c)

Figure 2.17.

Results for the SAM of **SSα_6Fc:** (a) Cyclic voltammagrams in a 0.1 M $NaClO_4$ aqueous solution at 20 (innermost scan), 35, 50, 65, 85, 100, 125, 150, 200, 250, 300, and 500 (outermost scan) mVs^{-1}. (b) Plot of peak area against scan rate for reduction and oxidation peaks shown in (a). (c) Plot of peak potential against scan rate for reduction and oxidation peaks shown in (a).

β-Tripeptide SSβ$_3$Fc (2.11)

The cyclic voltammagrams of tripeptide **SSβ_3Fc** show very similar trends to those presented for **SSα_6Fc**. Symmetrical oxidation and reduction peaks for the one electron redox process Fc/Fc$^+$ (Figure 2.18a) are present. The half-wave potential of the ferrocene group in peptide **SSβ_3Fc**, is ~0.33 mV.

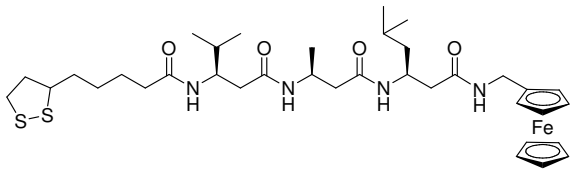

SSβ_3Fc (2.11)

The ferrocene groups of the peptide molecules appear similar in environment on the gold surface, as evidenced by the lack of satellite peaks or peak asymmetry (however suitable chronoamperometry data could not be obtained, as explained later). The double-layer capacitance is moderate as evidenced by the offset of the baseline from zero current, particularly after the oxidation peak on the forward scan (the top curve), and the reduction peak of the reverse scan (the bottom curve). The increase in double-layer capacitance with oxidation of the monolayer suggests that ion penetration is occurring either by film distortion or at surface defects, and suggests the monolayer is not tightly packed.

The linear relationship between the peak area and scan rate suggests that electron transfer occurs between the surface-bound ferrocene and gold (rather than from a diffusing solution species) (Figure 2.17b).[5]

Furthermore, Figure 2.18c shows that both the oxidation and reduction peaks shift to less positive potentials as the scan rate increases, similar to **SSα_6Fc**) (Figure 2.18c). Again, the behaviour of the reduction peak is consistent with slow electron transfer on the timescale of measurement. However, as with peptide **SSα_6Fc**, the behaviour of the oxidation peak is not consistent with this behaviour.

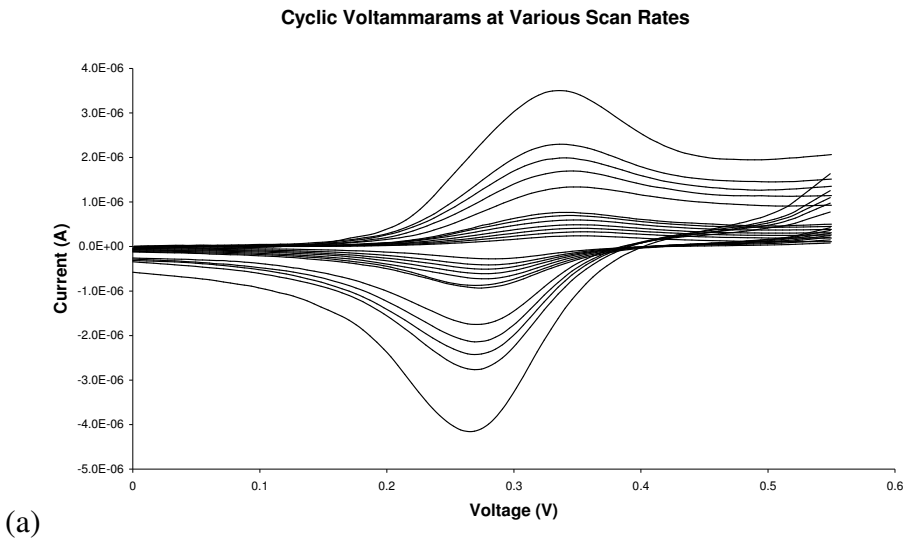

(a)

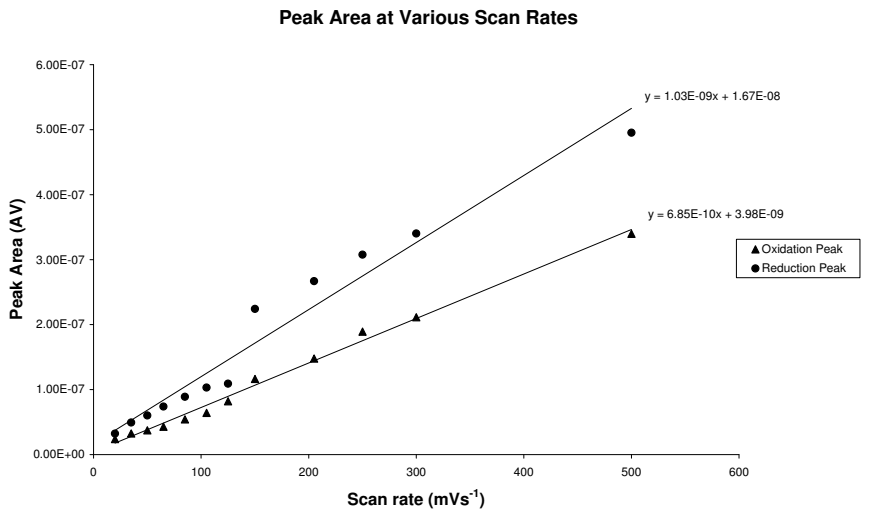

(b)

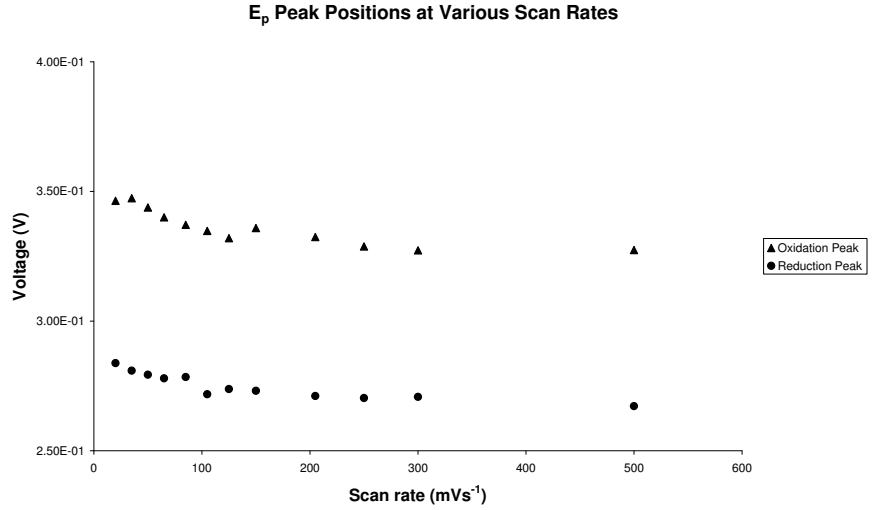

(c)

Figure 2.18

Results for the SAM of **SSβ_3Fc**: (a) Cyclic voltammagrams in a 0.1 M $NaClO_4$ aqueous solution at 20 (innermost scan), 35, 50, 65, 85, 100, 125, 150, 200, 250, 300, and 500 (outermost scan) mVs^{-1}. (b) Plot of peak area against scan rate for reduction and oxidation peaks shown in (a). (c) Plot of peak potential against scan rate for reduction and oxidation peaks shown in (a).

β-Hexapeptides SSβ$_6$Fc (2.12), Fcβ$_6$SS (2.13) and SC$_{15}$β$_6$Fc (2.14)

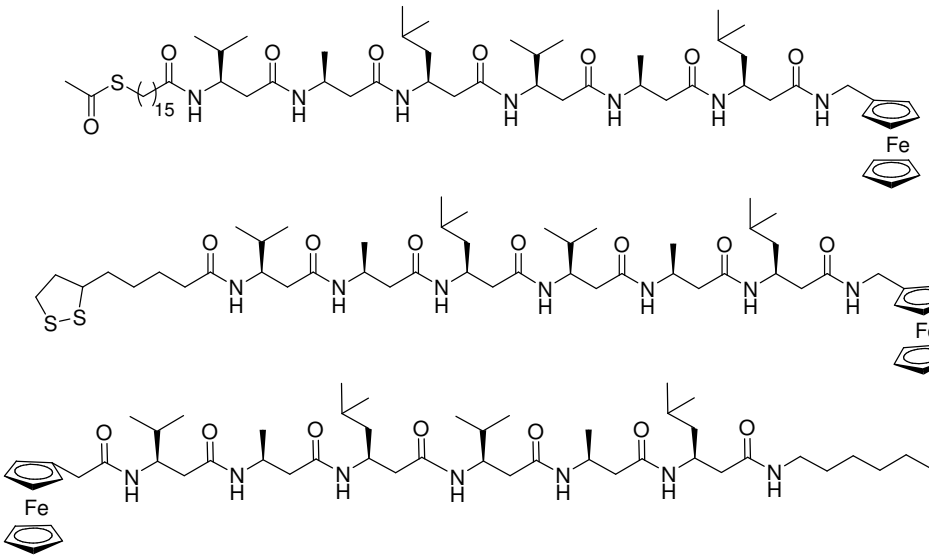

SC$_{15}$β$_6$Fc (**2.12**)

SSβ$_6$Fc (**2.13**)

Fcβ$_6$SS (**2.14**)

As for the peptides **SSα$_6$Fc** and **SSβ$_3$Fc**, voltammetry of β-peptides **SSβ$_6$Fc**, **Fcβ$_6$SS** and **SC$_{15}$βFc** reveals reversible one electron redox chemistry, as evidenced by the presence of symmetrical oxidation and reduction peaks (Figure 2.19a - Figure 2.21a). While the peaks were broad, adequate chronoamperometry data could be obtained (as described later), suggesting that the inhomogeneity of the surface film was not significant.

Each peptide was covalently bound to the gold surface, as indicated by the linear relationship between peak area and scan rate (Figure 2.19b-Figure 2.21b). The half-wave potential of all three species was ~0.33 V. The double-layer capacitance for SAMs of **Fcβ$_6$SS** and **SSβ$_6$Fc** increased after oxidation of the ferrocene group (Figure 2.19a and Figure 2.21a). This occurred to a lesser extent with the **SC$_{15}$β$_6$Fc** SAM (Figure 2.20a). The larger double-layer capacitance of the SAMs of **Fcβ$_6$SS** and **SSβ$_6$Fc** suggests that the monolayers are not densely or regularly packed, and that ions can penetrate into the layer. In comparison, **SC$_{15}$β$_6$Fc**, which contains the C_{15} alkylchain linker, has a smaller contribution of double-layer charging, indicating a more ordered monolayer.

Unlike peptide **SSα6Fc**, the peak potentials of the β-hexapeptides showed little dependence on scan rate, between 20 and 500 mVs^{-1} (Figure 2.19c-Figure 2.21c). The lack of dependence of peak position on scan rate suggests that the electron transfer rate between the gold surface and the ferrocene group for the β-peptides was fast relative to the timescale of measurement.

Therefore, this result suggests that electron transfer through the β-peptide SAMs of **Fcβ_6SS**, **SSβ_6Fc** and **SC$_{15}$$\beta_6$Fc** was faster than through the α-peptide SAM of **SSα_6Fc** and the β-tripeptide **SSβ_3Fc** (which both showed a dependence of peak potential on scan rate over the same range).

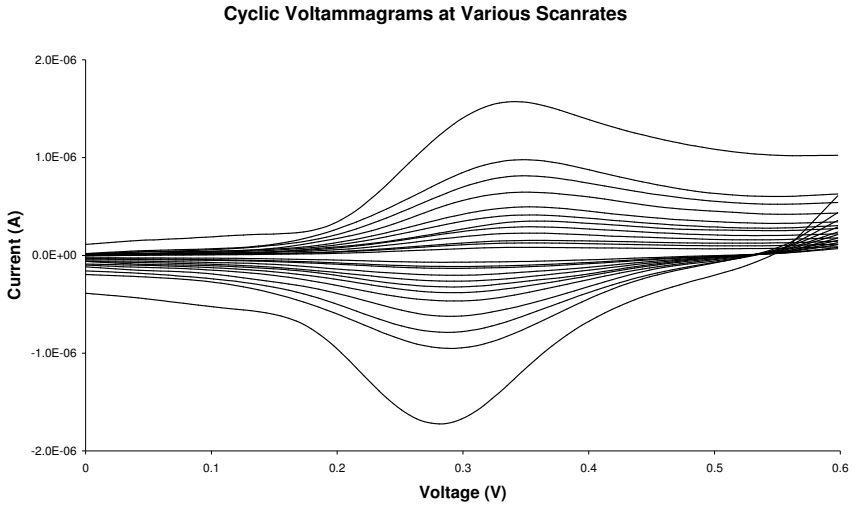

(a)

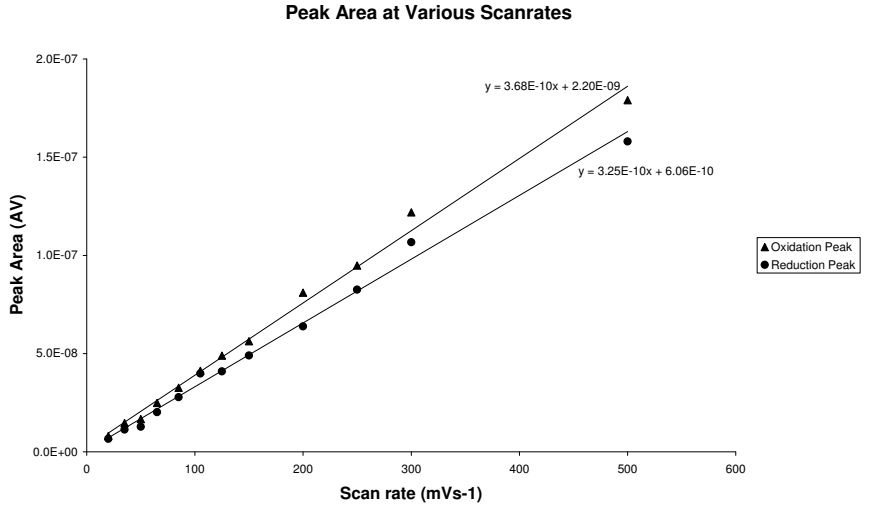

(b)

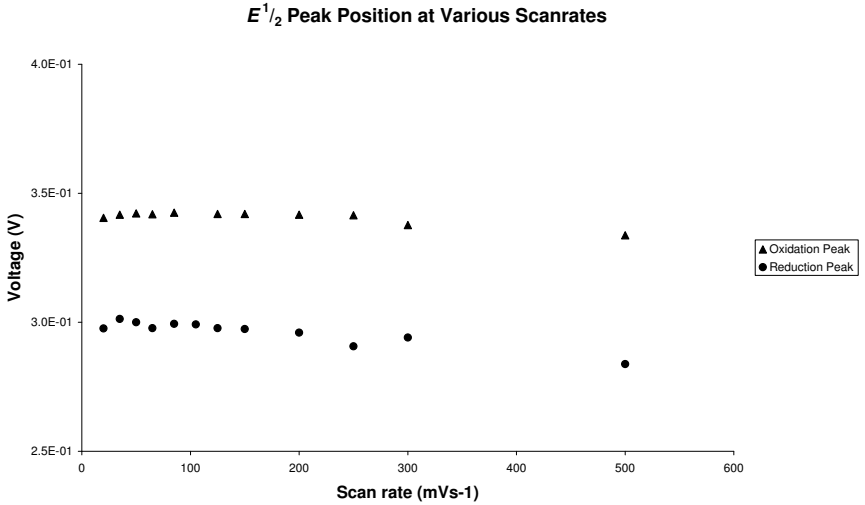

(c)

Figure 2.19.

Results for the SAM of **SSβ_6Fc**: (a) Cyclic voltammagrams in a 0.1 M $NaClO_4$ aqueous solution at 20 (innermost scan), 35, 50, 65, 85, 100, 125, 150, 200, 250, 300, and 500 (outermost scan) mVs^{-1}. (b) Plot of peak area against scan rate for reduction and oxidation peaks shown in (a). (c) Plot of peak potential against scan rate for reduction and oxidation peaks shown in (a).

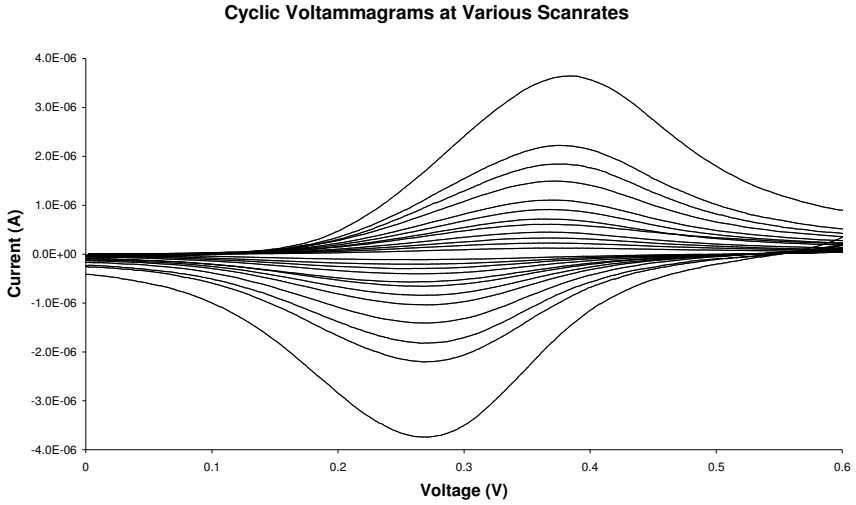

(a)

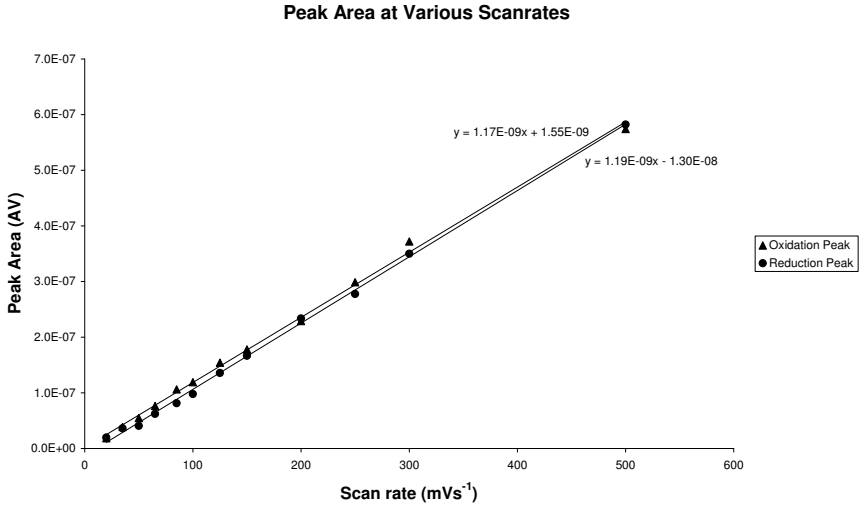

(b)

Figure 2.20.

Results for the SAM of **$SC_{15}\beta_6Fc$**: (a) Cyclic voltammagrams in a 0.1 M $NaClO_4$ aqueous solution at 20 (innermost scan), 35, 50, 65, 85, 100, 125, 150, 200, 250, 300, and 500 (outermost scan) mVs^{-1}. (b) Plot of peak area against scan rate for reduction and oxidation peaks shown in (a). (c) Plot of peak potential against scan rate for reduction and oxidation peaks shown in (a).

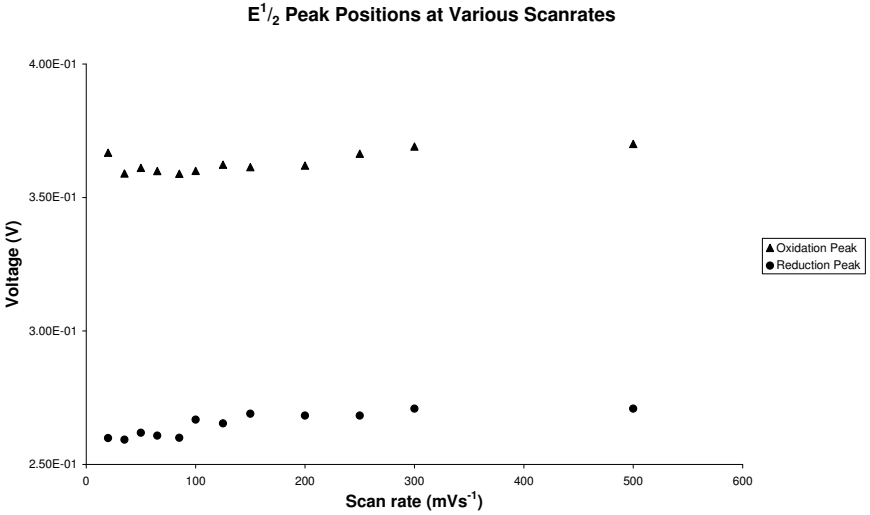

(c)

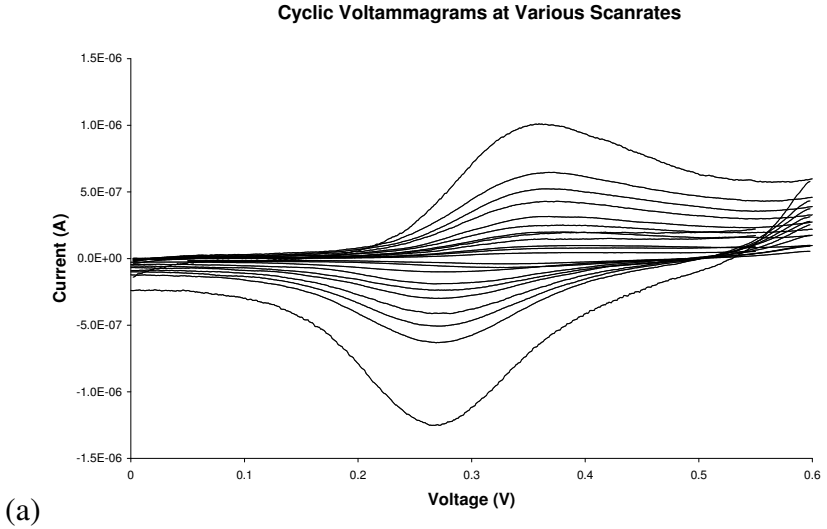

(a)

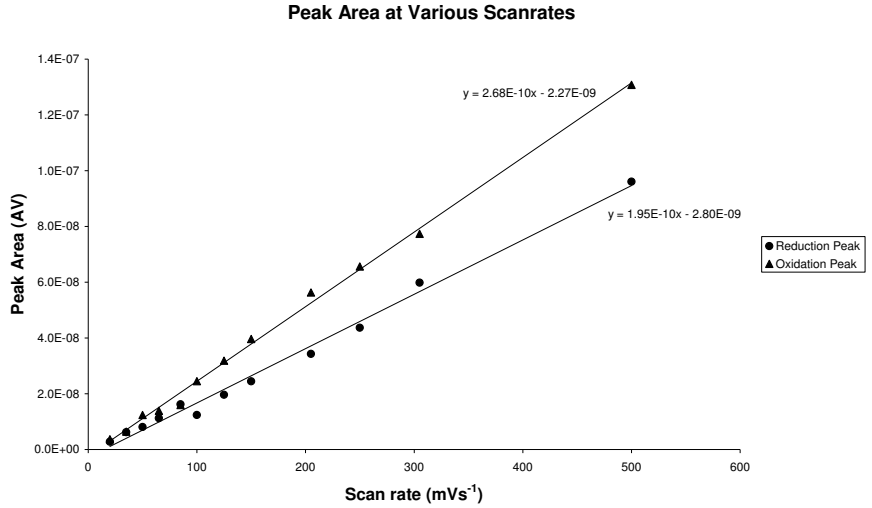

(b)

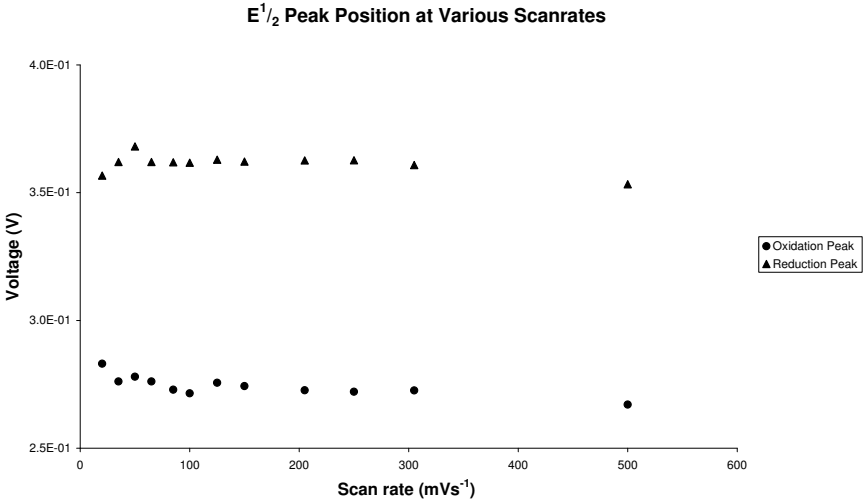

(c)

Figure 2.21.

Results for the SAM of **Fcβ_6SS**: (a) Cyclic voltammagrams in a 0.1 M $NaClO_4$ aqueous solution at 20 (innermost scan), 35, 50, 65, 85, 100, 125, 150, 200, 250, 300, and 500 (outermost scan) mVs^{-1}. (b) Plot of peak area against scan rate for reduction and oxidation peaks shown in (a). (c) Plot of peak potential against scan rate for reduction and oxidation peaks shown in (a).

Non-redox Active Peptide SSβ_6Et

The cyclic voltammogram of **SSβ_6Et**, which contains an ethyl amide group in place of a ferrocene methyl amide, showed no redox activity over the voltage range. As expected, this result confirms that all redox activity in ferrocene-containing peptides is due solely to the ferrocene moiety. The double layer charging capacitance is smaller in the SAM of **SSβ_6Et**, compared to the ferrocenyl analog **SSβ_6Fc** (Figure 2.22). The implications of the cyclic voltammetry results for all of the SAMs, together with chronoamperometry data of the peptides SAMs, will be presented in the discussion (Section 2.3).

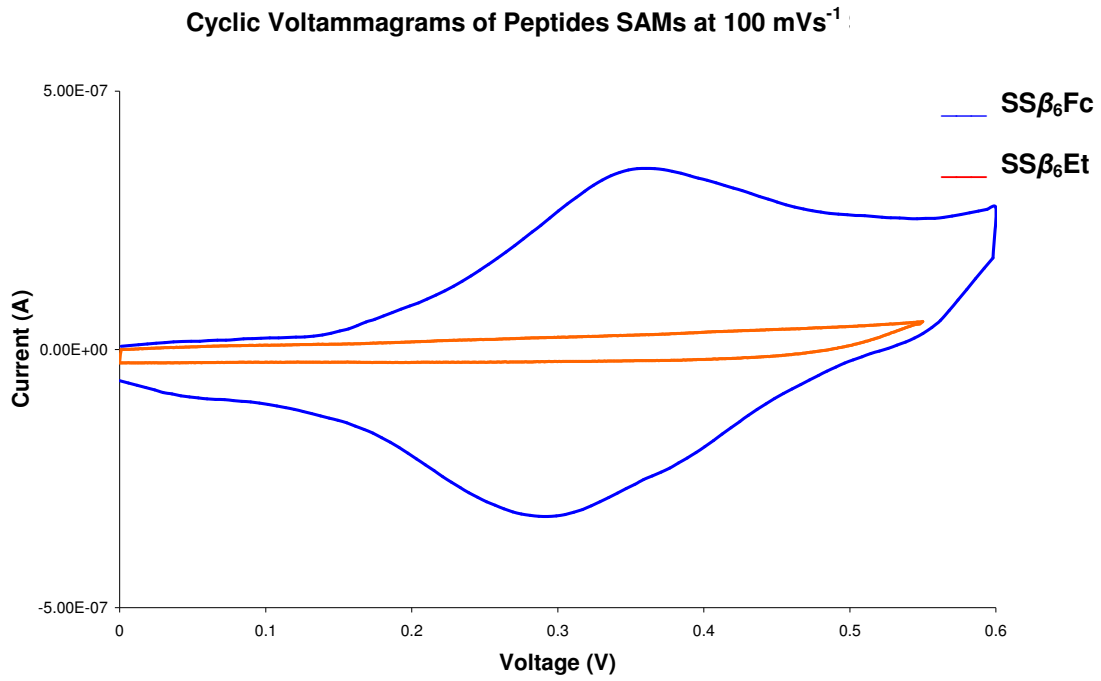

Figure 2.22 Cyclic voltammograms of SAMS of **SSβ_6Fc** and **SSβ_6Et** at a scan rate of 100 mVs^{-1}.

2.2.4 Chronoamperometry of *β*-Peptide SAMs

Chronoamperometic determination of the standard electron transfer rate (k_{et}^0) between the gold surface and the ferrocene group through the functionalised peptides is expressed by the general equation $k_{et} = k_{et}^0 \exp(-\alpha n f \eta)$, where α is the activity coefficient, n is the number of electrons transferred and f is equal to F/RT where F, R, and T are the Faraday and gas constants, and absolute temperature, respectively, and η is the overpotential.[42] Extrapolation of k_{et} data, plotted against overpotential, to $\eta=0$ gives k_{et}^0 (as described in the Appendix, Section **A.6**). Experimentally determined k_{et} values are obtained by plotting the current decay data as the natural log of current against time as described by the equation $i = i_0 \exp(-k_{et} t)$, where i_0, k_{et} and t represent the initial current at $t = 0$, the electron transfer rate constant, and time, respectively.[12] This equation describes the interfacial electron transfer that occurs between the metal and surface-bound redox groups.

For potential steps examining the electron transfer from ferrocene to gold, the initial potential is 0.1 V, and the step potential, E_{step} is E^o plus the overpotential where η = 0 to 0.19 V. For the reverse electron transfer from gold to ferrocenium, the initial potential is ~ 0.56 V (depending on the position of E^o), and the step potential E_{step} is E^o minus the overpotential where η = 0 to 0.19 V. Chronoamperometry measurements were repeated in duplicate for each peptide at 24 different overpotential values.

The current decay against time (*i*-*t*) plots recorded at an overpotential of 0.05 V, for electron transfer from ferrocene to gold for peptides **SC$_{15}$*β*$_6$Fc**, **SS*β*6Et**, **Fc*β*$_6$SS** and **SS*β*$_6$Fc** are shown in Figure 2.23a. As expected, peptides **SC$_{15}$*β*$_6$Fc**, **Fc*β*$_6$SS** and **Fc*β*$_6$SS** display an initial capacitive response between 0-1 ms, after which time a Faradaic response (exponential decay) is observed (Figure 2.23a). The control, peptide **SS*β*$_6$Et**, which does not contain a redox probe, and therefore has no electron transfer along the peptide, shows only a capacitive current response.

The semilog ln(*i*)-*t* plot of the chronoamperometry data gives k_{et} as the gradient in the linear region of the plot, between approximately 2 and 8 ms (Figure 2.23b). Positive overpotentials indicate electron transfer from ferrocene to gold, while negative values indicate electron transfer from gold to ferrocenium. The k_{et} data was analysed by plotting the k_{et} data against overpotential

(Figure 2.24). Extrapolation of the k_{et} data to zero overpotential gives k_{et}^0 for the peptide SAMs. Typically, a large k_{et}^0 value is obtained for SAMs with fast electron transfer.[11] Note that the initial data points are excluded from the trendline, because at low overpotential values (which are close to $E_{½}$), the surface may contain species in both the oxidised and reduced states.

The chronoamperometry semilog ln(i)-t plots for tripeptide **SSβ_3Fc** did not exhibit linearity, indicating that more than one ferrocene environment was present on the surface. Therefore, these results were not analysed to obtain k_{et}^0 data.

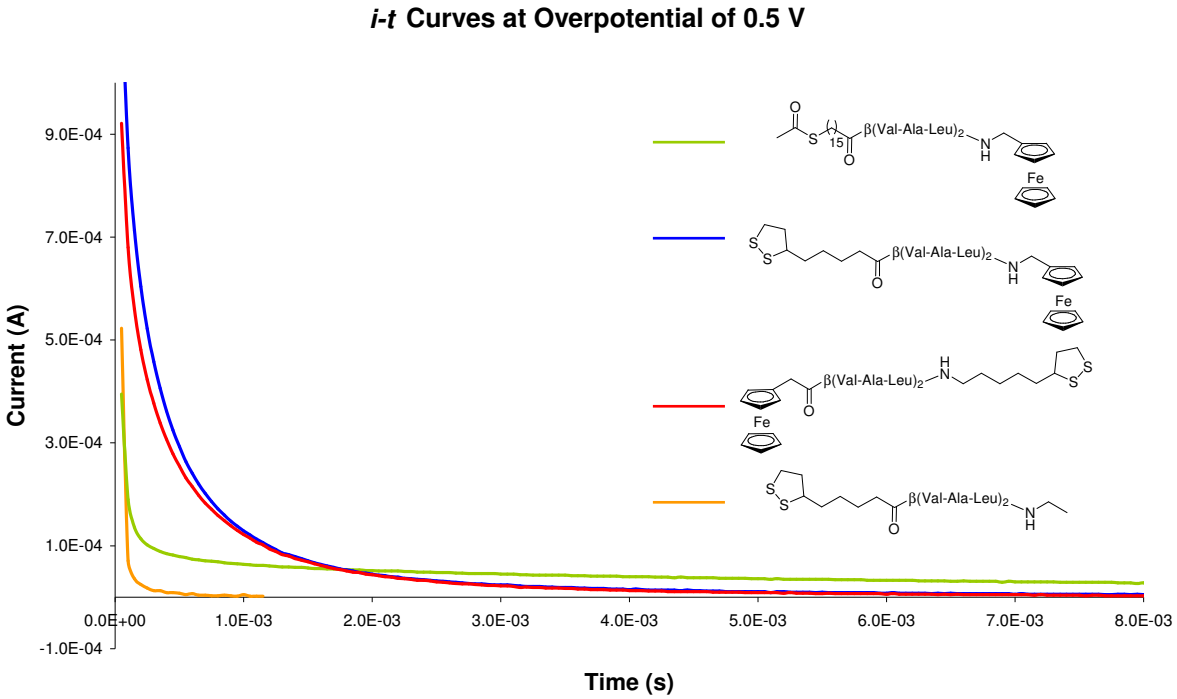

(a)

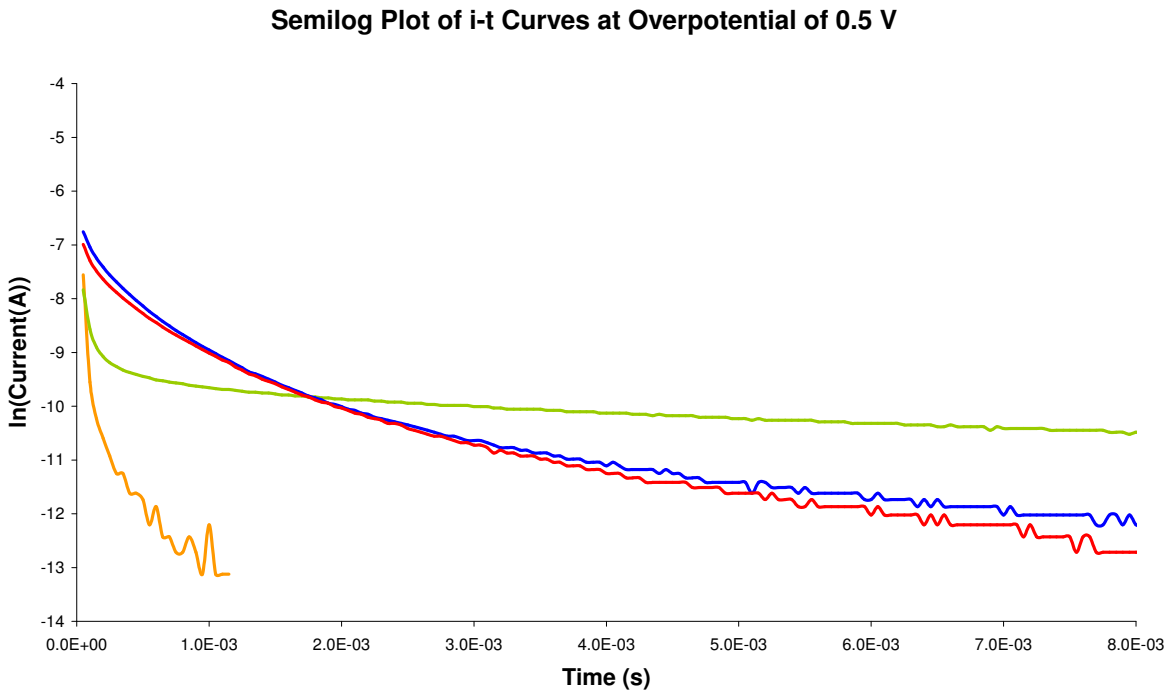

(b)

Figure 2.23 Results in chronoamperometry of the SAMs: (a) *i-t* curves of the peptide SAMs at an overpotential of 0.05 V, (b) its semilog plots for the electron transfer between the ferrocene moiety and gold in the peptide SAMs.

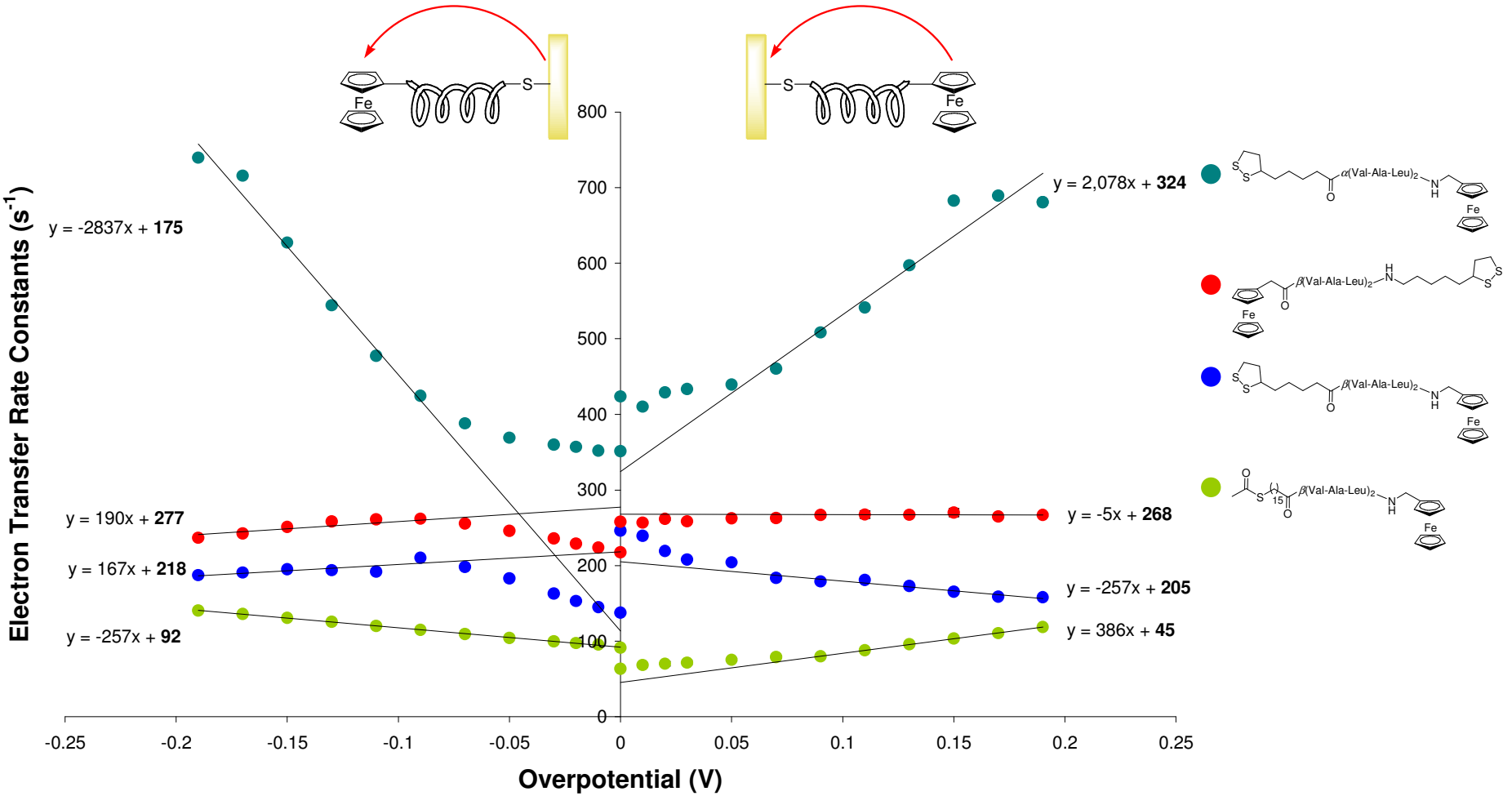

Figure 2.24 Plot showing the dependence of electron transfer rate constants on overpotential. The left-hand side of the graph shows k_{et} values for electron transfer from gold to ferrocenium, and the right-hand side shows k_{et} values for electron transfer from ferrocene to gold. The k_{et}^{0} values are shown in bold as the y-intercept values on the trendline equations.

The plot of k_{et} against overpotential of peptide **SSα_6Fc** exhibits the largest dependence on overpotential, while the other peptides composed of β-amino acids show little dependence. The implications of overpotential dependence and a comparison of the standard k_{et}^0 values will be addressed in the discussion (Section 2.3).

The plot of k_{et} against overpotential of the β-peptide SAMs show a linear relationship between overpotential and k_{et} values. The k_{et}^0 values for the electron transfer from ferrocene to gold for peptides **SC$_{15}\beta_6$Fc**, **SSβ_6Fc** and **Fcβ_6SS** are 45, 205 and 270 s^{-1}, respectively. The k_{et}^0 values for the reverse electron transfer (gold to ferrocenium) are all slightly higher than the previous values, with 90, 220 and 280 s^{-1} for **SC$_{15}\beta_6$Fc**, **SSβ_6Fc** and **Fcβ_6SS**.

The plot of k_{et} against overpotential of the α-peptide **SSα_6Fc**, does not exhibit the same linearity with respect to overpotential as the β-peptide SAMs, especially at negative overpotential values. When a linear trendline is fitted to the larger overpotential values, the k_{et}^0 value for electron transfer from ferrocene to gold is (tentatively) determined to be 320 s^{-1} and from gold to ferrocenium is 175 s^{-1}. However, just as equally, an exponential trendline could be fitted to the same data sets.

When surface species exhibits a tunnelling mode of electron transfer (such as in alkyl chains), the data is plotted as $\ln(k_{et})$ against overpotential.[40] A plot of $\ln(k_{et})$ against overpotential for **SSα_6Fc** gives an expected linear relationship (Figure 2.25). Extrapolation of the trendlines to zero overpotential give k_{et}^0 values of 260 s^{-1} and 380 s^{-1} for electron transfer from gold to ferrocenium and ferrocene to gold, respectively. The magnitude of these values is discussed in section 2.3.2.

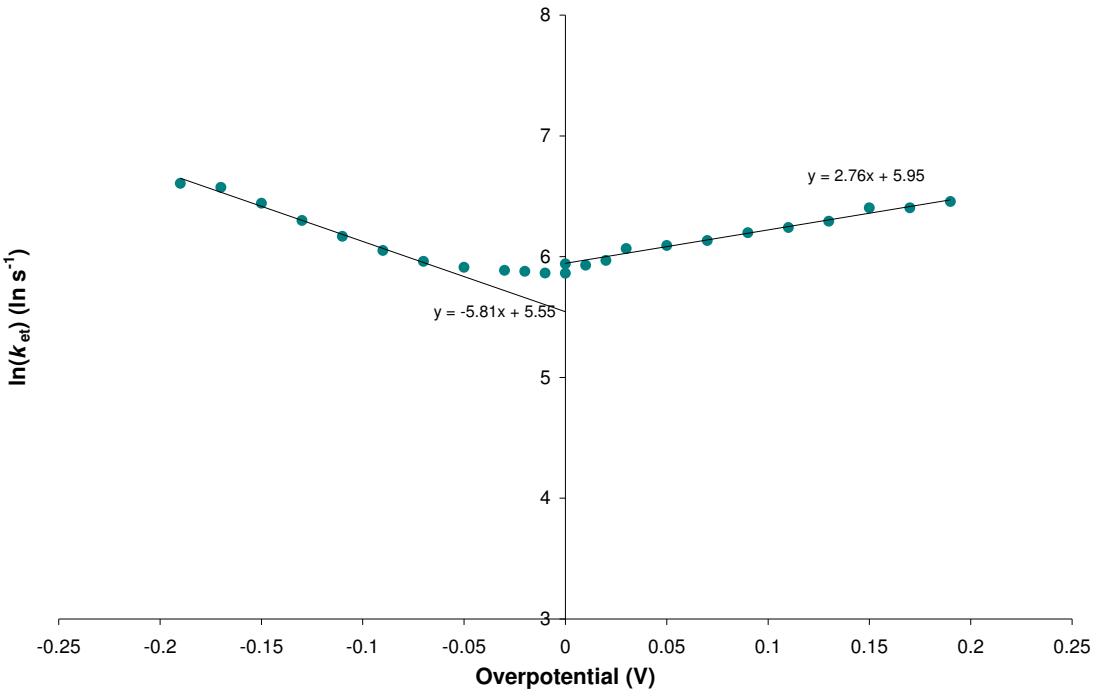

Figure 2.25 Plot of ln(k_{et}) against overpotential for data from peptide **SSα_6Fc**.

2.3 Discussion of Electrochemical Analysis of β-Peptide SAMs

2.3.1 Voltammetric Analysis

Voltammetry of the SAMs of the ferrocene-containing peptides (**SSα_6Fc**, **SSβ_3Fc**, **Fcβ_6SS**, **SSβ_6Fc** and **SC$_{15}\beta_6$Fc**) showed reversible redox chemistry on a gold surface. Predictably, **SSβ_6Et** (without ferrocene) did not show redox chemistry over the same voltage range.

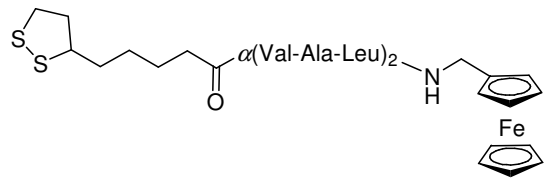

SSα_6Fc

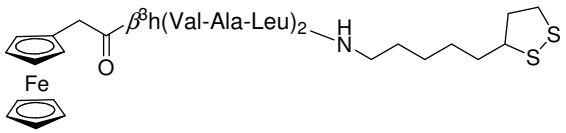

Fcβ_6SS

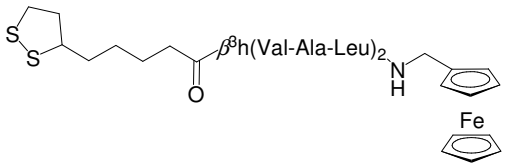

SSβ_6Fc

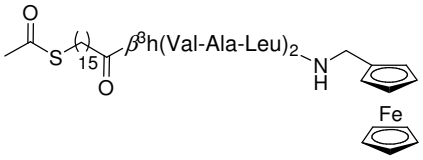

SC$_{15}\beta_6$Fc

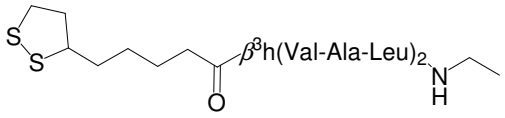

SSβ_6Et

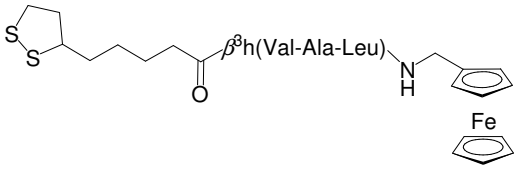

SSβ_3Fc

The peak potentials of ferrocene in the β-hexapeptides were not affected by changing scan rate, while the the reduction peaks of α-peptide **SSα_6Fc** and the β-tripeptide **SSβ_3Fc** showed a weak dependence. As both the α- and β-peptide SAMs were studied over the same scan rate range, this suggests that electron transfer in the α-peptide and β-tripeptide SAMs is slower than that in the β-hexapeptide SAMs. The through-bond distance between gold and ferrocene in the SAMs of **SSα$_6$Fc** and **SSβ$_3$Fc** is shorter than those of the β-hexapeptides. Therefore, if electron tunnelling is the predominating mode of electron transfer, then it would be expected that electron transfer through the β-peptides SAMs is slower, due to the increased distance between donor and acceptor. One possible explanation for this result is that the β-peptides **SSβ_6Fc**, **SC$_{15}\beta_6$Fc** and **Fcβ_6SS** adopt a helical secondary structure which facilitates fast electron transfer along the hydrogen-bonded network of the peptide backbone.[7,43] Electron transfer in **SSα_6Fc** and **SSβ_3Fc** (which should not form any defined secondary structure on the surface) could occur via the slower electron tunnelling mechanism.

The extent of double layer capacitance from ion-penetration into the SAM, indicates the level of organisation in the monolayer. The amount of double layer capacitance in all four ferrocene-containing peptides is moderate, but is significantly reduced in peptide **SSβ_6Et**. This suggests

that the presence of ferrocene increases ion permeation of the monolayer. The ferrocene group is oxidised ($Fc \rightarrow Fc^+$) during the forward scan, losing an electron to become positively charged. This charge may promote further ion permeation into the monolayer. The double-layer capacitance of **$SC_{15}\beta_6Fc$** is smaller than the other ferrocene-containing peptides, indicating a more ordered monolayer.

The SAM of **$SC_{15}\beta_6Fc$** has the largest oxidation peak area, while SAMs of **$Fc\beta_6SS$** and **$SS\beta_6Fc$** form monolayers with approximately one third of the peak area, indicating that only a third as many molecules are attached to the surface. A comparison of the oxidation peak areas of a SAM of the simple alkyl thiol **$SC_{15}Fc$** with the oxidation peak area of the peptide monolayers demonstrates that all of the peptides have a much smaller peak area (6 to 27 %), and therefore less redox centres on the surface than a monolayer of **$SC_{15}Fc$** (Table 2.5). This result is expected because the smaller diameter of **$SC_{15}Fc$** enables more molecules to pack onto the surface. The four peptides, **$SS\beta_3Fc$**, **$SS\alpha_6Fc$**, **$SS\beta_6Fc$** and **$Fc\beta_6SS$**, which contain a lipoic acid linker, have a smaller oxidation peak area than **$SC_{15}\beta_6Fc$**. Furthermore, the α-amino acid containing peptide, **$SS\alpha_6Fc$**, and the β-tripeptide **$SS\beta_3Fc$** both have approximately twice the oxidation peak area of β-peptides **$SS\beta_6Fc$** and **$Fc\beta_6SS$**.

Table 2.5 Area of the oxidation peaks of the peptide SAMs relative to **$SC_{15}Fc$**

Peptide	Oxidation peak area relative to **$SC_{15}Fc$** (%)
$SS\alpha_6Fc$	17
$SS\beta_6Fc$	9
$SC_{15}\beta_6Fc$	27
$Fc\beta_6SS$	6
$SS\beta_3Fc$	19

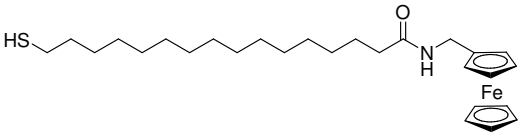

$SC_{15}Fc$

The oxidation peak area of the ferrocene-containing peptides indicates a variable level of organisation on the surface (Table 2.5). **$SC_{15}\beta_6Fc$** had the greatest surface coverage, at approximately double the peak area value of peptides **$SS\beta_6Fc$**, **$SS\alpha_6Fc$** and **$Fc\beta_6SS$**. Therefore, it seems that the sulfur-linker is important in determining the surface organisation of the peptides. Longer straight-chain alkanethiols ($>HSC_{10}H_{21}$) are known to pack in a well-defined close-packed arrangement on gold, regardless of whether the gold surface is a single crystal or

polycrystalline.[44] A packing distance of 0.5 nm between neighbouring molecules, and a surface tilt of 30º are typical for these alkanethiols. However, the widest diameter in peptide **SC$_{15}$$\beta_6$Fc** is across the β-peptide component due to the side chains groups, therefore it seems unlikely that the alkylthiol linker can also form a close-packed arrangement on gold. Indeed, the oxidation peak area of **SC$_{15}$$\beta_6$Fc** in comparison with a monolayer of the simple alkyl thiol **SSC$_{15}$$\beta_6$Fc** is 73% lower.

Lipoic acid, the disulfide linker on peptides **SSβ_6Fc**, **SSα_6Fc** and **Fcβ_6SS**, is thought to bind to gold through two gold-sulfur bonds (in mixed sulfur oxidation states), therefore requiring more surface area for binding. Again, this required area is expected to be smaller than the diameter of the β-peptide component, so the linker-binding area should not be the limiting factor that influences the concentration of the peptide on the surface. However, lipoic acid forms a more disordered monolayer on gold than alkanethiols do,[45] which could result from poor surface-packing and therefore a lower peptide concentration on the surface.

The likely surface concentrations of the peptides **SSα_6Fc** and **SSβ_3Fc** are approximately twice as large as **SSβ_6Fc** and **Fcβ_6SS**, despite containing the same lipoic acid linker. This result suggests that the β-hexapeptides occupy more space on the gold surface than the α-peptide does, and again could suggest that the β-hexapeptides adopt a secondary structure (such as a helical conformation) when immobilised on gold.

2.3.2 Chronoamperometry Analysis

The k_{et}^0 values for the electron transfer across the SAMs, as deduced from plots shown in Figure 2.24 and Figure 2.25 (for **SSα_6Fc**), are summarised in Table 2.6.

Table 2.6 k_{et}^{0} values for electron transfer from the ferrocene to gold.

Peptide	A.1 k_{et}^{0} (s^{-1}) Fc → Au	k_{et}^{0} (s^{-1}) Au → Fc^{+}
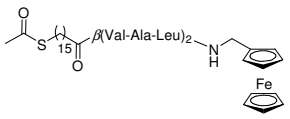 **$SC_{15}\beta_6Fc$**	45	90
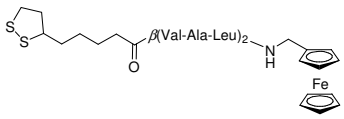 **$SS\beta_6Fc$**	205	220
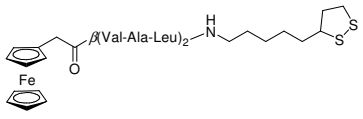 **$Fc\beta_6SS$**	270	280
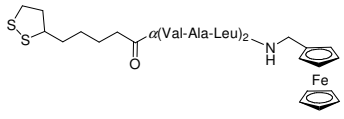 **$SS\alpha_6Fc$**	380	260

As described earlier, it is proposed that the dependence of k_{et} on overpotential is indicative of the mode of electron transfer. For example, the hopping mechanism is thought to have little dependence on overpotential, while the tunnelling mechanism shows a large dependence.[5,11] Because the dependence on distance between donor and acceptor is more important for the tunnelling mechanism, than for the hopping mechanism, the driving force of electron transfer (in this case overpotential) has a greater effect on k_{et}. Therefore, for the tunnelling mechanism, larger overpotential values give significantly faster electron transfer (higher k_{et} values) than smaller overpotential values.

SAMs composed of simple alkane thiols and helical α-peptides, both with terminal redox groups, have been previously studied. In alkyl chains, the likely mode of electron transfer is via a tunnelling mechanism through the chain, because π-orbitals or hydrogen-bonding networks do not extend along the molecule. The dependence of electron transfer rate on overpotential in these systems is very large, spanning a k_{et} range of 10^{7} s^{-1} for overpotentials from 0 to 0.5V.[12,33]

Conversely, the k_{et} values of α-helical peptides, have been shown to exhibit weak dependence on overpotential, with k_{et} values spanning over a range of only ~ 100 s^{-1}, for overpotentials from 0 to 0.2V.[5,11] The postulated mode of electron transfer for α-helical peptides is predominantly via an electron hopping mechanism.[5,11]

The k_{et} values of β-peptides **SSβ_6Fc**, **Fcβ_6SS** and **SC$_{15}$$\beta_6$Fc** show little dependence on overpotential (Figure 2.24). Conversely, the **SSα6Fc** peptide shows a moderate dependence on overpotential, and does not show a linear relationship between overpotential and k_{et}. These results suggest that the mode of electron transfer operating in the β-peptide SAMs is predominantly electron hopping and electron tunnelling for the **SSα6Fc** SAM.

The k_{et}^0 values for electron transfer through **SSα_6Fc** are higher than expected when compared to that of the β-peptides **SSβ_6Fc** and **Fcβ_6SS**, which have the same sulfur-linker group. However, the high k_{et}^0 may be due to other factors, such as:

- a disordered monolayer which could place the ferrocene group close in space to the gold or the amide groups in adjacent peptides, shortening the distance of electron transfer to the gold
- electron transfer between ferrocene moieties (because the strand-like structure does not adequately separate the ferrocene groups, compared to a helical peptide) indicating that a diluent was necessary
- the length of α-peptide backbone, which is six carbons shorter* than that of the β-peptide.

The study of electron transfer in peptides longer than those used here may show greater difference in k_{et}^0, as the effect of distance is greater for peptides in which tunnelling is the predominate mechanism.

Nevertheless, the comparison between the electron transfer properties of the analogous α and β peptides clearly shows a difference in self-assembly properties on the surface. The β-peptides have electron transfer characteristics that are similar to those seen in helical α-peptides, which adopt a helical structure on the surface.

* due to β-amino acids having three backbone carbon atoms, while α-amino acids only have two.

The k_{et}^0 values of the *β*-peptides (obtained here) show similar trends to the literature values for helical *α*-peptides. In particular, the results obtained by Watanabe *et al* on helical *α*-peptides (presented in Table 2.3), are the most comparable to this work.[11] The observed k_{et}^0 values of 40 and 30 s^{-1} for peptides **2.7** and **2.8** containing a lipoic acid linker; and 260 and 230 s^{-1} for peptides **2.9** and **2.10** containing a thiobenzoic acid linker are of the same order of magnitude to the values presented here (Table 2.3). However, the *β*-peptides used in this study are shorter (by six residues) than the *α*-helical peptides (12 residues) so an absolute comparison of rate data cannot be made.

The slowest electron transfer occurred in the SAM of **SC$_{15}$*β*$_6$Fc**, with a k_{et}^0 of only 45 s^{-1} for electron transfer from ferrocene to gold, and 90 s^{-1} for electron transfer from gold and ferrocenium. This peptide contains the longest alkyl component (the C_{15} linker group) of any of the peptides studied here. Electron tunnelling is the likely mechanism of electron transfer operating through the alkyl chain section of the linker and is much slower than the electron hopping mechanism which may occur in the *β*-peptide component. Therefore, electron transfer from the linker/peptide amide bond to the gold seems to be the rate-limiting step in the overall electron transfer process. This assumption is consistent with the data obtained for the other peptides. For example, compared to **SC$_{15}$*β*$_6$Fc**, peptide **SS*β*$_6$Fc** which has a much shorter pentyl moiety between the disulfide group and the peptide and therefore a faster rate of electron transfer, has larger k_{et}^0 values of 205 s^{-1} (Fc→Au) and 220 s^{-1} (Au→Fc^+). This finding is consistent with that of Watanabe *et al* who showed that electron transfer in the *α*-helical peptide group containing a lipoic acid group **2.7** is slower than with an sp^2-hydridised thiobenzoic acid group **2.9** (Table 2.3).

The reversed peptide, **Fc*β*$_6$SS**, has k_{et}^0 values of 270 s^{-1} (Fc→Au) and 280 s^{-1} (Au→Fc^+), which is significantly larger than those of **SS*β*$_6$Fc**. The only difference between these two peptides is the polarity of the *β*-peptide unit with respect to the gold surface if the peptide were to adopt a 3_{14}-helix, and one extra methylene group in the linker of peptide **Fc*β*$_6$SS** (the latter of which should theoretically decrease the value k_{et}^0). The possible dipole moment, running from the *C*-terminus to the *N*-terminus of the *β*-peptide is the opposite orientation to the dipole moment in the *α*-helix (Figure 2.26). Watanabe *et al* showed that the k_{et}^0 values for *α*-helical peptides are higher when the positive pole of the peptide is closest to the gold surface.[5,11] This is consistent with the results presented here in which **Fc*β*$_6$SS**, which has the *C*-terminus (positive pole) closest to the gold surface, has a higher k_{et}^0 value.

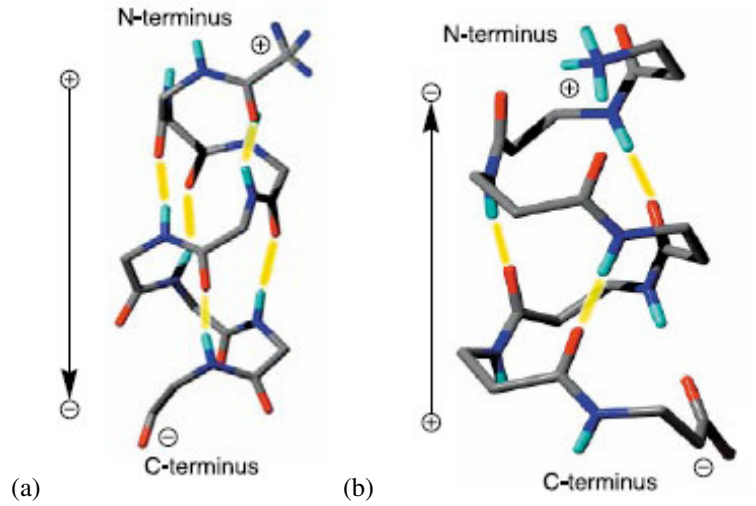

Figure 2.26 (a) The α-helix and (b) the β 14-helix have opposite polarity to each other, because of the opposite direction of the amide bonds. Hydrogen bonds are shown in yellow, N in dark blue, O in red, H in light blue. (Reproduced from Ref. 46)

Watanabe *et al* proposed an energy level diagram for electron transfer along helical α-peptides, which is useful in explaining the observed k_{et}^{0} values obtained here (Figure 2.27).[11] Watanabe's model suggests that electron transfer occurs from the ferrocene highest occupied molecular orbital (HOMO), through to the Fermi level* of gold, via an electron 'hole' because the LUMO energy levels are inaccessibly high. Electron transfer is favourable from the ferrocene HOMO to the lower energy amide HOMO levels. Electron hopping then readily occurs along the amide HOMO levels of the peptide, which have similar energy values. This model suggests that the electron transfer from the amide HOMO to the higher energy sulfur energy level is the rate-limiting step in the overall electron transfer from ferrocene to gold. Therefore, it follows that the rate-limiting step for electron transfer in the reverse direction (from gold to the ferrocenium group) is between the peptide amide HOMO and the ferrocene HOMO energy levels.

* defined as the highest occupied orbital when the temperature is 0 K

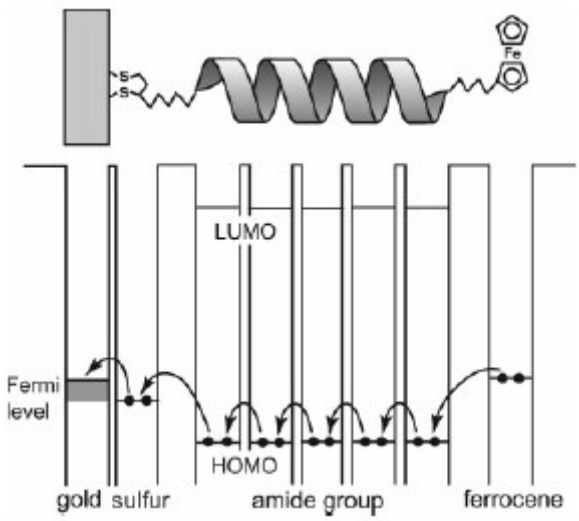

Figure 2.27 Energy diagram for the electron transfer from the ferrocene moiety to gold through a helical α-peptide, via a hopping mechanism. (Reproduced from Ref. 11)

This proposed model only partially agrees with both the results obtained here, and in Watanabe's reported data. The k_{et} values for the electron transfer from ferrocene to gold are determined primarily by the nature of the linker group (**SC$_{15}$$\beta_6$Fc** compared with **SS$\beta_6$Fc** and **Fc$\beta_6$SS**). Furthermore, changing the polarity of the peptide in relation to the ferrocene and linker group would change the energy difference between the sulfur HOMO level and the adjacent peptide amide HOMO level. This explains the difference in k_{et}^0 between peptides **Fcβ_6SS** and **SSβ_6Fc**, assuming they adopt a helical conformation on the surface. However, the reverse electron transfer between gold and ferrocene, if dependent on the difference in energy levels of the peptide amide and ferrocene HOMO should be the same for the **SC$_{15}$$\beta_6$Fc** and **SS$\beta_6$Fc** SAMs, which is not the case. It seems more likely that a combination of factors, such as the chain length of the alkyl component in the linkers, the peptide polarity and the oxidation state of the ferrocene determine the rate of electron transfer rather than only the energy level transitions shown in Figure 2.27.

2.4 Conclusions and Future Work

The results presented here comprise the first study of electron transfer in β-peptides. Significantly, the results of the chronoamperometry studies suggest that the likely mechanism of electron transfer in these β-peptides is a hopping mechanism. Furthermore, the magnitude of the k_{et}^{0} values are comparable with a similar study of electron transfer in α-helical peptides.[11]

The choice of sulfur linker and the polarity of the β-peptide in relation to the surface are both important factors for determining the overall rate of electron transfer. A linker with a longer alkyl component lowers the overall electron transfer rate (such as that in **SC$_{15}$$\beta_6$Fc**). Conversely, **Fc$\beta_6$SS** exhibits faster electron transfer than the reversed dipole analogue **SSβ_6Fc** due to the difference in the energy of the sulfur linker and peptide amide hopping sites. These factors influence electron transfer rate in the same way as for helical α-peptides.

Chronoamperometry studies of the analogous α-strand peptide (**SSα_6Fc**) indicate a tunnelling-type mechanism predominates and suggests that the mode of electron transfer in strand-like α-peptides is different to the mechanism operating in β-peptides.

The results presented here are important for two reasons:

- Electron transfer analysis of surface immobilised β-peptides can be used to determine the likely mechanism of electron transfer. As the mechanism of electron is related to peptide structure, the results tentatively suggest that the β-peptides adopt secondary structure on the surface, which facilitates electron hopping along a hydrogen bonded system. Therefore, electrochemical studies could then act as a method for determining whether secondary structure is present when peptides are immobilised on surfaces.

- It has been suggested that electron transfer in peptides could be independent of primary and secondary structure.[1] Here it has been shown that peptides which may adopt a stable secondary structure on the surface (**SSβ_6Fc**) exhibit different electron transfer characteristics to peptides which are unlikely to form stable regular secondary structure

(**SSα6Fc**). The use of analogous α- and β-peptides eliminates any influence of sidechain groups in determining or affecting the mode of electron transfer.

Future work in this area would benefit from surface infrared (FTIR) studies to determine the orientation, likely secondary structure and uniformity of the α-peptides and *β*-peptides on the surface. Furthermore, the analysis of longer *α*- and *β*-peptides may give a clearer distinction between the k_{et}^{0} values for electron transfer by the slower tunnelling mechanism and the faster hopping mechanism. Studying the effect of peptide length on the rate of electron transfer would also allow for the determination of the tunnelling parameter '*β*' of *β*-peptides, thereby determining their usefulness as nanoscale wires. Electrochemical analysis of *β*-peptides that adopt different helical structures (such as the 12-helix or the 10/12 helix) would provide further insight into the effect of secondary structure on electron transfer in hydrogen-bonded systems.

2.5 References

1. Long, Y. T.; Abu-Rhayem, E.; Kraatz, H. B., *Chemistry-a European Journal* **2005,** 11, (18), 5186-5194.
2. Mutz, M. W.; McLendon, G. L.; Wishart, J. F.; Gaillard, E. R.; Corin, A. F., *Proceedings of the National Academy of Sciences of the United States of America* **1996,** 93, (18), 9521-9526.
3. Bixon, M.; Giese, B.; Wessely, S.; Langenbacher, T.; Michel-Beyerle, M. E.; Jortner, J., *Proceedings of the National Academy of Sciences of the United States of America* **1999,** 96, (21), 11713-11716.
4. Jortner, J.; Bixon, M.; Langenbacher, T.; Michel-Beyerle, M. E., *Proceedings of the National Academy of Sciences of the United States of America* **1998,** 95, (22), 12759-12765.
5. Morita, T.; Kimura, S., *Journal of the American Chemical Society* **2003,** 125, (29), 8732-8733.
6. Petrov, E. G.; May, V.; Hanggi, P., *Chemical Physics* **2002,** 281, (2-3), 211-224.
7. Petrov, E. G.; Shevchenko, Y. V.; Teslenko, V. I.; May, V., *Journal of Chemical Physics* **2001,** 115, (15), 7107-7122.
8. Davis, W. B.; Svec, W. A.; Ratner, M. A.; Wasielewski, M. R., *Nature* **1998,** 396, (6706), 60-63.
9. Berlin, Y. A.; Burin, A. L.; Ratner, M. A., *Journal of the American Chemical Society* **2001,** 123, (2), 260-268.
10. Bixon, M.; Jortner, J., *Journal of Physical Chemistry B* **2000,** 104, (16), 3906-3913.
11. Watanabe, J.; Morita, T.; Kimura, S., *Journal of Physical Chemistry B* **2005,** 109, (30), 14416-14425.
12. Finklea, H. O.; Hanshew, D. D., *Journal of the American Chemical Society* **1992,** 114, (9), 3173-3181.
13. Galka, M. M.; Kraatz, H. B., *Chemphyschem* **2002,** 3, (4), 356-+.
14. Zheng, Y. J.; Case, M. A.; Wishart, J. F.; McLendon, G. L., *Journal of Physical Chemistry B* **2003,** 107, (30), 7288-7292.
15. Isied, S. S.; Ogawa, M. Y.; Wishart, J. F., *Chemical Reviews* **1992,** 92, (3), 381-394.
16. Mishra, A. K.; Chandrasekar, R.; Faraggi, M.; Klapper, M. H., *Journal of the American Chemical Society* **1994,** 116, (4), 1414-1422.
17. Sisido, M.; Hoshino, S.; Kusano, H.; Kuragaki, M.; Makino, M.; Sasaki, H.; Smith, T. A.; Ghiggino, K. P., *Journal of Physical Chemistry B* **2001,** 105, (42), 10407-10415.
18. Vericat, C.; Vela, M. E.; Andreasen, G.; Salvarezza, R. C.; Vazquez, L.; Martin-Gago, J. A., *Langmuir* **2001,** 17, (16), 4919-4924.
19. Lang, H.; Duschl, C.; Vogel, H., *Langmuir* **1994,** 10, (1), 197-210.
20. Mrksich, M.; Whitesides, G. M., *Annual Review of Biophysics and Biomolecular Structure* **1996,** 25, 55-78.
21. Steinem, C.; Janshoff, A.; Ulrich, W. P.; Sieber, M.; Galla, H. J., *Biochimica Et Biophysica Acta-Biomembranes* **1996,** 1279, (2), 169-180.
22. Ulman, A., *Chemical Reviews* **1996,** 96, (4), 1533-1554.
23. Bediako-Amoa, I.; Sutherland, T. C.; Li, C. Z.; Silerova, R.; Kraatz, H. B., *Journal of Physical Chemistry B* **2004,** 108, (2), 704-714.
24. Wada, A., *Advances in Biophysics* **1976,** 9, 1-63.

25. Otoda, K.; Kimura, S.; Imanishi, Y., *Journal of the Chemical Society-Perkin Transactions 1* **1993**, (23), 3011-3016.
26. Worley, C. G.; Linton, R. W.; Samulski, E. T., *Langmuir* **1995,** 11, (10), 3805-3810.
27. Miura, Y.; Kimura, S.; Imanishi, Y.; Umemura, J., *Langmuir* **1998,** 14, (10), 2761-2767.
28. Miura, Y.; Kimura, S.; Imanishi, Y.; Umemura, J., *Langmuir* **1998,** 14, (24), 6935-6940.
29. Whitesell, J. K.; Chang, H. K., *Science* **1993,** 261, (5117), 73-76.
30. Williams, A. J.; Gupta, V. K., *Journal of Physical Chemistry B* **2001,** 105, (22), 5223-5230.
31. Wilson, D. L.; Martin, R.; Hong, S.; Cronin-Golomb, M.; Mirkin, C. A.; Kaplan, D. L., *Proceedings of the National Academy of Sciences of the United States of America* **2001,** 98, (24), 13660-13664.
32. Enander, K.; Aili, D.; Baltzer, L.; Lundstrom, I.; Liedberg, B., *Langmuir* **2005,** 21, (6), 2480-2487.
33. Sek, S.; Palys, B.; Bilewicz, R., *Journal of Physical Chemistry B* **2002,** 106, (23), 5907-5914.
34. Xiao, S. J.; Brunner, S.; Wieland, M., *Journal of Physical Chemistry B* **2004,** 108, (42), 16508-16517.
35. Rowe, G. K.; Creager, S. E., *Langmuir* **1991,** 7, (10), 2307-2312.
36. Seebach, D.; Abele, S.; Gademann, K.; Guichard, G.; Hintermann, T.; Jaun, B.; Matthews, J. L.; Schreiber, J. V., *Helvetica Chimica Acta* **1998,** 81, (5), 932-982.
37. Gardiner, J.; Thomae, A. V.; Mathad, Raveendra I.; Seebach, D.; Kramer, S. D., *Chemistry & Biodiversity* **2006,** 3, 1181-1200.
38. Seebach, D.; Overhand, M.; Kuehnle, F. N. M.; Martinoni, B., *Helvetica Chimica Acta* **1996,** 79, (4), 913-941.
39. Finklea, H. O.; Avery, S.; Lynch, M.; Furtsch, T., *Langmuir* **1987,** 3, (3), 409-413.
40. Chidsey, C. E. D.; Bertozzi, C. R.; Putvinski, T. M.; Mujsce, A. M., *Journal of the American Chemical Society* **1990,** 112, (11), 4301-4306.
41. Brooksby, P. A.; Anderson, K. H.; Downard, A. J.; Abell, A. D., *Langmuir* **2006,** 22, (22), 9304-9312.
42. Bard, A. J.; Faulkner, L. R., *Electrochemical methods : fundamentals and applications* 1st ed.; Wiley: New York, 1980; p 718.
43. Petrov, E. G.; Shevchenko, Y. V.; May, V., *Chemical Physics* **2003,** 288, (2-3), 269-279.
44. Butt, H. J.; Seifert, K.; Bamberg, E., *Journal of Physical Chemistry* **1993,** 97, (28), 7316-7320.
45. Dijksma, M.; Boukamp, B. A.; Kamp, B.; van Bennekom, W. P., *Langmuir* **2002,** 18, (8), 3105-3112.
46. Seebach, D.; Beck, A. K.; Bierbaum, D. J., *Chemistry & Biodiversity* **2004,** 1, (8), 1111-1239.

Chapter 3 Cross Metathesis on Gold

3.1 Introduction

The two general methods of introducing functionality into a monolayer are by synthesising a functional molecule that contains all components for surface attachment and then immobilising this by self-assembly (as described in Chapter Two), or through direct chemical modification of an intermediate monolayer.

Solution phase synthesis of functional molecules, allows the incorporation of a wide variety of functional groups and components. However, this method often requires difficult syntheses and incurs numerous problems through functional group incompatibility.[1] For example, the incompatibility of ferrocene or sulfur with many reaction conditions and common catalysts produces significant challenges for the synthetic chemist (as described in Chapter Four). Furthermore, the synthesis of large molecules, which often possess very poor solubility profiles, is difficult in solution phase.

The introduction of functionality through the direct chemical modification of SAMs to date has focussed largely on substitution of functionalised carboxylic acids,[2] amines,[3] azides,[4] or via Diels Alder[5], or more recently 'click' chemistry[6] such as cycloaddition and ring-opening reactions[7]. The advantage in fabricating a universal interface of this type is that it can be locally modified to generate an array of desirable functionality. However, this approach presents some potential problems including Au-S bond rupture and subsequent desorption under potentially harsh reaction conditions, and steric hindrance at the interface that can slow reaction rates or change mechanistic pathways.

Transition-metal-catalyzed cross metathesis is widely used in solution chemistry to couple two terminal olefin groups with the release of ethene.[8,9] Cross metathesis between an olefin-terminated SAM and a solution phase olefin is known to proceed under relatively mild reaction conditions.[1,10] Thus, surface solution cross metathesis provides a potentially versatile methodology with which to build functionality on monolayer-protected gold nanoparticles and flat surfaces. A detailed fundamental analysis of cross metathesis on gold surfaces is discussed here.

3.1.1 Cross Metathesis Chemistry

A general mechanism for the cross metathesis reaction of two olefin-terminated molecules is shown is Figure 3.1. The first step in the catalytic cycle is a [2+2] cycloaddition reaction of transition metal catalyst carbene **A** with olefin **B** to give a metallocyclobutane **C**. This intermediate collapses releasing ethene gas (**D**), and a new transition metal carbene **E**, containing the alkylidene fragment $\mathbf{R_2}$. Cycloaddition of another olefin, **F**, gives the cyclic intermediate **G**, which collapses to give the cross metathesis product **H**.

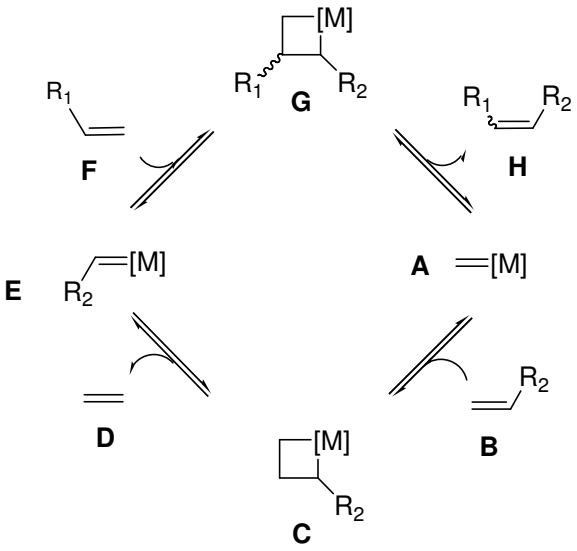

Figure 3.1 The mechanism of cross metathesis for olefin terminated molecules

Other cross metathesis products (not shown) can include homodimers of both olefins **B** and **F**. Homodimerisation generally poses no problems because the homodimers can re-enter the catalytic cycle, and form the desired product. Additionally, homodimersation can be minimised by coupling sterically hindered or electron deficient alkenes.[8] Depending on the reaction conditions used, E, Z, or both isomers are obtained. The preference for heterodimerisation over homodimerisation is determined by the relative thermodynamic stability of the products, because the cross metathesis reaction is reversible.

There are many examples of cross metathesis catalysts containing transition metals centres such as Mo, W and Ru. Two ruthenium catalysts, known as Grubbs' 1st and 2nd Generation (**3.1** and **3.2**, respectively), have emerged as the preferred catalysts because of their tolerance to many functional groups, and stability of these catalysts to air and at increased temperatures.[11,12]

Catalyst **3.2** has better functional group tolerance than **3.1**, particularly toward sulfur-containing molecules.

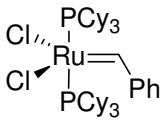

3.1

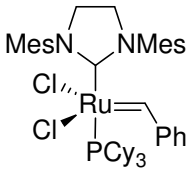

3.2

3.1.2 Literature Examples of Cross Metathesis of SAMs

Only recently has cross metathesis been explored as a mild method to functionalise SAMs, both on flat surfaces and particles. The earliest examples involved encapsulation of gold nanoparticles by the cross metathesis of self-assembled olefins to form cage-like structures. The use of gold nanoparticles allowed for analysis of the reactivity and stability of the cross metathesis products using what are typically solution phase methods, such as NMR spectroscopy and mass spectrometry.[13-16]

Wu *et al* functionalised gold particles with a SAM of an alkylthiolate ligand possessing three terminal olefinic groups.[16] These groups were cross-linked using catalyst **3.1**, and the gold core removed by etching, to form a hollow polymeric capsule.

Another study monitored the rate of cross metathesis of SAMs of olefin-terminated surfactants on gold nanoclusters (small gold particles), by ^{1}H NMR spectroscopy.[14] The encapsulated products were stable to gel permeation chromatography, which is unprecedented for non-crosslinked SAMs on gold particles or surfaces. A similar study demonstrated the cross metathesis of olefin functionalised porphyrin molecules around a gold cluster (Figure 3.2).[13] Mass spectral analysis confirmed that a discrete encased nanoparticle was formed.

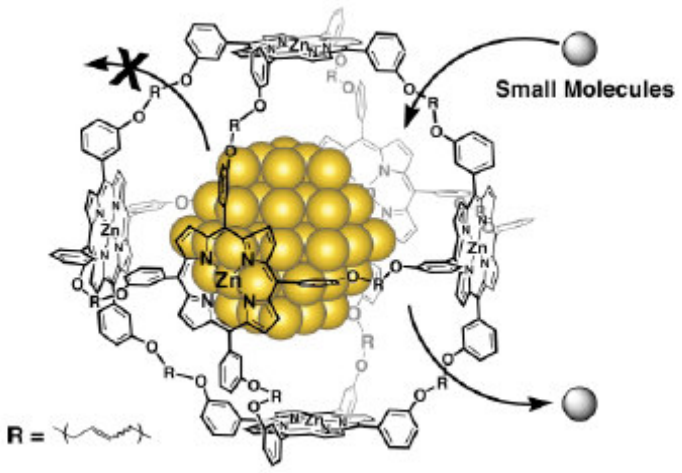

Figure 3.2 Schematic representation of the porphyrin cage confining a Au_{55} cluster. (Reproduced from Ref. 13)

Samanta *et al* functionalized olefin-coated particles with synthetically-useful groups such as a Fischer carbene complex and *N*-hydroxysuccinimide, using cross metathesis.[15] Both of these groups readily react with amines, allowing further functionalisation. Cross metathesis of a ferrocene group to the particles allowed electrochemical detection of the product, thus validating the method.

There were only two literature reports of cross metathesis on planar gold surfaces[1,10] prior to our publication in this area[17]. The first involved coupling various carbonyl functionalities to olefin-terminated SAMs. The functionalized surfaces were characterised by infrared and x-ray photoelectron spectroscopy (XPS) techniques.[1] The second study involved ring opening metathesis polymerisation (ROMP) to build up polymeric chains on gold (Figure 3.3).[10] The ROMP of norbornene was catalysed by **3.1**, and the surface height measured using AFM. Incorporation of a ferrocene-functionalised norbornene group allowed electrochemical detection of the polymeric product.

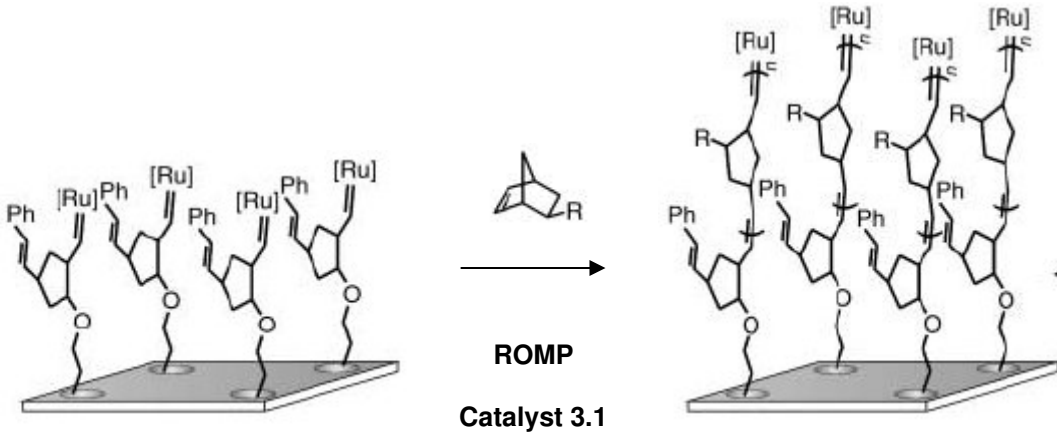

Figure 3.3 Schematic representation of ROMP on gold. (Reproduced from Ref. 10)

While there are three detailed studies of cross metathesis on silicon surfaces, which include SAM stability data and kinetic data at intervals on minute and hourly timescales,[18-20] it is clear that current understanding of cross metathesis at monolayers adsorbed onto gold surfaces is inadequate. Details relating to the appropriate reaction time, surface concentration of the olefin, and monolayer stability remain unknown. Much of the literature on surface cross metathesis reactions and gold relates to nanoparticle interfaces, which have only partial applicability to planar surfaces. Studies on planar gold surfaces are predominantly concerned with examining the final surface structure rather than identifying intermediates.

3.1.3 Research Described in This Chapter and Experimental Design

Specific electrochemical studies of Grubbs'-catalyzed cross metathesis reactions at SAMs over time are limited to two studies noting the appearance of a ferrocenyl peak at the conclusion of a metathesis procedure.[15,18] Our aim was to develop a methodology to measure the amount of cross metathesis product at regular time intervals to establish the optimum reaction conditions, without adversely disturbing the SAM.

Electrochemistry is a simpler, faster technique for analysing surface composition when compared to other methods such as AFM, IR and XPS, provided that the species of interest is electroactive. In order to measure the reaction progress over time with electrochemistry, the product needs to possess a different electrochemical property to the starting species. Coupling a solution phase redox probe, such as ferrocene, to a surface immobilised olefin would allow for

reliable electrochemical quantification of the product with cyclic voltammetry. Ferrocenyl compounds are compatible with metathesis chemistry using Grubbs' catalysts **3.1** and **3.2**.[21,22] The ferrocene group provides reversible one-electron electrochemistry with redox peaks appearing at moderate potentials in aqueous solution, while the current-potential behaviour gives a direct measure of the surface concentration of ferrocene groups (Γ_{Fc}) in the monolayer. Therefore, an olefin-terminated thiol and an olefin-terminated ferrocene derivative were required to study cross metathesis reactions on gold over time and as a function of monolayer composition.

It was expected that on a planar surface, a SAM consisting solely of one compound would hinder cross metathesis because of steric congestion, preventing coordination of the catalyst to the olefin. Dilution of the olefin-terminated thiols, with shorter alkanethiols (diluents) to form a mixed monolayer would make the terminal olefin groups accessible to the catalyst. The commercially available pentanethiol (**C5**) and decanethiol (**C10**) are diluents of suitable length, allowing for the efficient cross metathesis of an olefin-terminated thiol longer than ten carbon units (Figure 3.4).

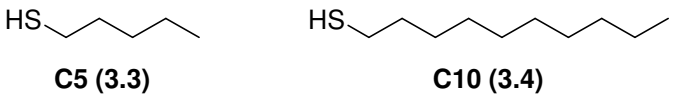

C5 (3.3) **C10 (3.4)**

Figure 3.4 Commercially available alkane thiols suitable as diluents.

3.2 Synthesis of Olefins

3.2.1 Olefin-functionalised Ferrocene Compounds

The initial target, ferrocene ester **3.6**, incorporated an alkene-terminated alcohol tethered through an ester linkage to ferrocene acetic acid. The moderately long alcohol 5-hexen-1-ol was selected in order to separate the two functionalities as cross metathesis is slowed when the olefin is positioned close to a bulky group. Coupling of the acid **3.5** and 5-hexen-1-ol with EDCI and DMAP gave the desired product as a brown oil in yields between 49 and 77% (Scheme 3.1). However, compound **3.6** degraded over several days to give an unidentified brown solid. The

incompatibility of the alkene group with ferrocene was not likely because of the large number of literature compounds possessing both functionalities.[21,22] The ester **3.6** was soluble in dichloromethane (as ferrocene is lipophilic), but the degradation product was not, suggesting a charged species had formed.

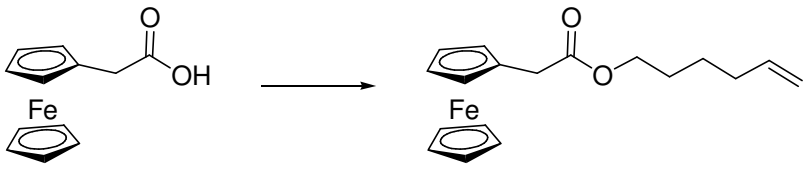

3.5 **3.6**

Scheme 3.1 *Reagents and conditions:* EDCI, DMAP, 5-Hexen-1-ol, DMF, 4 h, 77% yield.

A new target **3.10** was designed, replacing the ester functionality of **3.6** with a more stable amide bond. Ferrocene methyl amides are stable, and are often used as protecting groups for primary amines.[23] Homoallylamine* (**3.13)** was chosen as the nucleophile in the coupling reaction with ferroceneacetic acid **3.5**, because the resulting homoallylamide is more reactive to metathesis with Grubbs's catalyst than allylamide (formed from commercially available allylamine). The electronic and steric effects of the amide are reduced in homoallylamine compared to the shorter allyamine.[24,25]

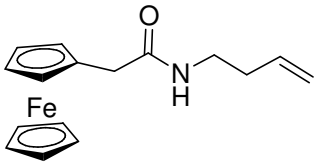

3.10

Homoallylamine was synthesised according to a literature procedure, from 4-bromo-1-butene **3.11** (Scheme 3.2).[25] **3.11** was reacted with sodium phthalimide, in a substitution reaction, to give the corresponding homoallylphthalimide (**3.12**) as a yellow solid. Deprotection of the phthlamide group with an Ing-Manske exchange procedure using an excess of hydrazine monohydrate gave the desired amine **3.13** as the hydrochloride salt, in 78 % overall yield.

* IUPAC name: but-3-en-1-amine

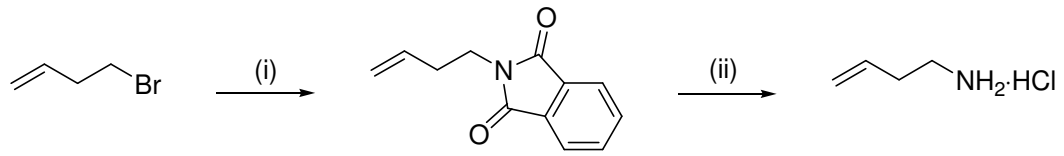

3.11 **3.12** **3.13**

Scheme 3.2 *Reagents and conditions:* (i) sodium phthalimide, DMF, 110 ºC, 12 h, (ii) hydrazine monohydrate, ethanol, 50 ºC, 2 h, 78% overall yield.

A HATU mediated coupling of ferroceneacetic acid and homoallylamine gave the ferrocenemethyl amide **3.10** as a brown crystalline solid in 65 % yield (Scheme 3.3). The amide proved more stable than the ester, with no observed degradation. This suggests that greater electronic withdrawing effects of the ester group, coupled with the electron donating ability of the ferrocene group were important for degradation of compound **3.6**.

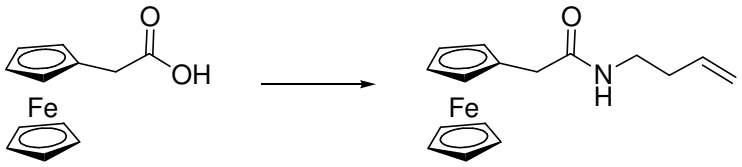

3.5 **3.10**

Scheme 3.3 *Reagents and conditions:* HATU, DIPEA, but-3-en-1-amine, DMF, 2 h, 65% yield.

3.2.2 Olefin-functionalised Surface Linkers

The synthetic route used to introduce a terminal olefin moiety into a sulfur-containing molecule suitable for self-assembly on gold is shown in Scheme 3.4. Commercially available 16-mercaptohexadecanoic acid **3.15** was chosen as the starting material because it contains a requisite thiol group, an acid group for functionalization and possesses a long chain length to extend above the **C5** and **C10** diluent layer on gold. Due to the high nucleophilicity of sulfur, the thiol group of **3.15** first required protection to avoid intra- and intermolecular thioesterification during the later amide-coupling step. Reduction of the contaminant disulfide and subsequent acetylation was carried out in a one-pot reaction using zinc and acetyl chloride, to give the thioacylated acid **3.16** in 92% yield. Amide coupling of **3.16** and homoallylamine **3.13** with HATU afforded the olefin **3.17** in 91% yield. Deprotection of the thioacetyl group with sodium thiomethoxide under N_2 gave the free thiol **3.18** as a white solid, in 83% yield.

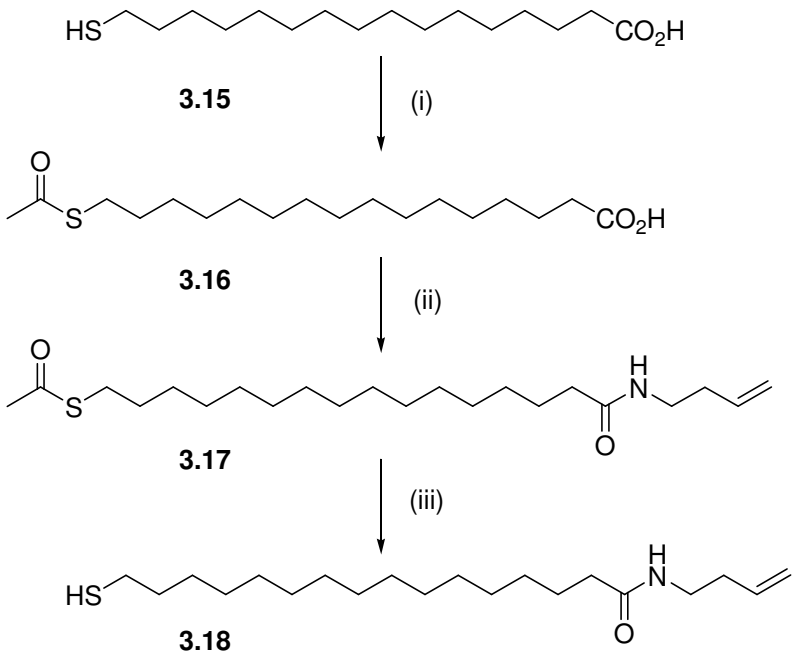

Scheme 3.4 *Reagents and conditions:* (i) Zinc powder, acetic acid, DCM, rt, 15 min, then acetyl chloride, 0 ºC, 10 min, 83% yield, (ii) HATU, but-3-en-1-amine, DIPEA, DMF, rt, 16 h, 91% yield (iii) sodium thiomethoxide, DCM, methanol, N_2, 30 min, 83% yield.

A second olefin was prepared using lipoic acid **3.19**, a useful surface linker because it readily forms SAMs through the spontaneous rupture of the disulfide bond in the presence of gold (Scheme 3.5). The disulfide group is stable to many reaction conditions and requires no protection/deprotection steps. Linker **3.19** was esterified with a commercially available alcohol, 9-decen-1-ol, using HATU, to give **3.20** as a pale yellow oil in 74% yield.

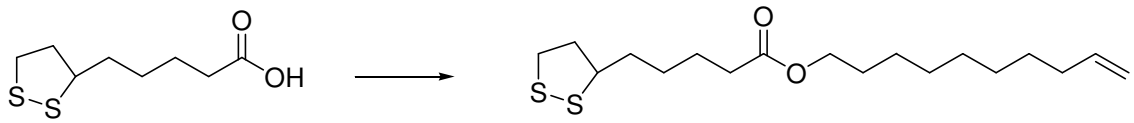

3.19 **3.20**

Scheme 3.5 *Reagents and conditions:* 9-decen-1-ol, DMF, HATU, DIPEA, rt, 16 h, 74% yield.

3.2.3 Model Ferrocene Compounds

Model compounds **3.21** and **2.18**, both containing ferrocene and sulfur groups (the same sulfur linkers in compounds **3.20** and **3.18**) were also synthesised (described in Chapter Four). These compounds were required for estimating the maximum surface coverage of the linkers on gold electrodes, and as a measure of linker stability towards the cross metathesis conditions.

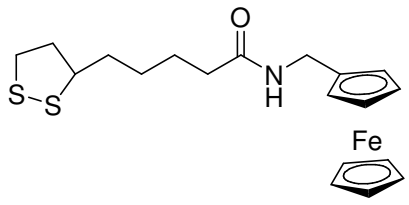

3.21

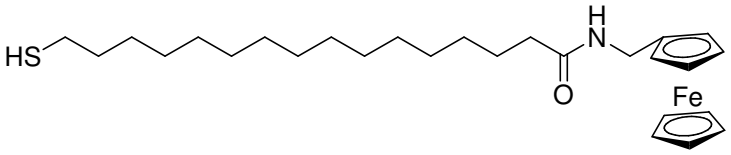

2.18

3.3 Cross Metathesis Reactions on a Gold Electrode[*]

3.3.1 Preparation of the Electrode

The gold (111) surface was polished and annealed using a hydrogen flame prior to electrochemical cleaning. The electrode was cycled (20-50 mV s^{-1}) between potentials of -0.2 and 1.45 V (SCE) in a solution of aqueous 0.01 M $HClO_4$ for 3 hours or until successive cycles for 10 min were substantially unchanged. A polycrystalline gold surface was used for thiol desorption experiments and prepared in the same way as the Au (111) electrode.

3.3.2 Formation of Mixed Monolayers

Au-S bond formation is reversible and therefore surface immobilised thiols are able to undergo exchange with solution phase thiols. A number of factors govern the ability for a thiol to exchange with another, for example, larger chain length thiols easily replace those of a shorter

[*] This work was performed in collaboration with Dr Paula Brooksby, University of Canterbury.

chain length. This principle can be applied to form mixed monolayers by assembling the diluent and olefin species onto the Au (111) electrode in two stages. The diluent monolayer **C5** or **C10** was adsorbed for up to 3 days, rinsed and briefly sonicated in ethanol to remove excess and weakly bound diluent, and finally dried with nitrogen gas. The surface was then immersed into the olefin-terminated thiol **3.18** for between 15 and 90 min, displacing diluent thiols to create a mixed monolayer. The resulting monolayer for a dodecanethiol diluent is represented on the left side of Scheme 3.6.

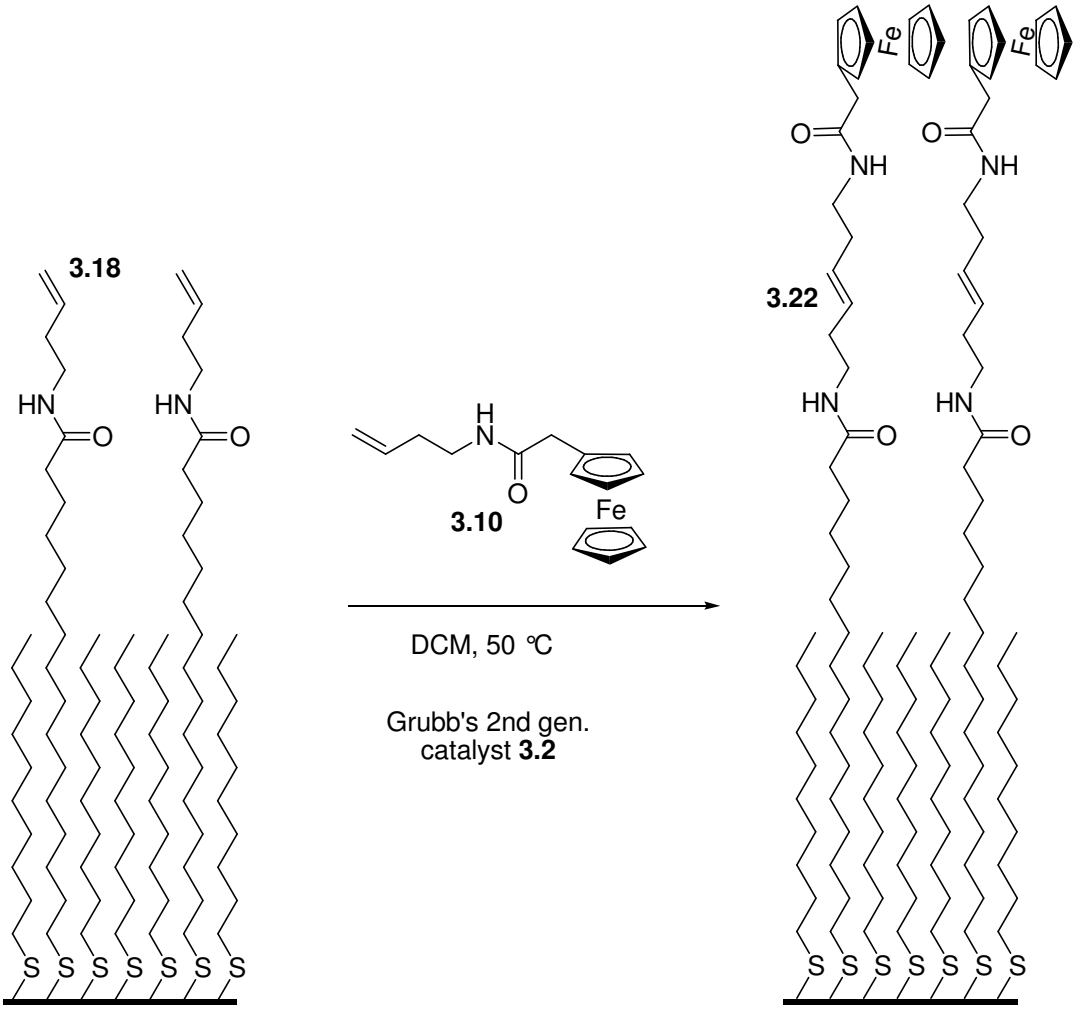

Scheme 3.6 Schematic representation of a mixed monolayer for the cross metathesis reaction between the surface bound olefin **3.18** and a solution olefin **3.10**, giving the immobilised ferrocenyl product, **3.22**.

3.3.3 Cross Metathesis Reactions

The gold electrode, with the attached mixed monolayer, was suspended in a dichloromethane solution containing Grubbs' catalyst **3.2** and the olefin-terminated ferrocenyl species **3.10**, and the mixture was heated at reflux under N_2 (Scheme 3.6). The reaction was typically allowed to proceed for up to 6 hours. At known reaction time intervals (*t*) the gold electrode was briefly removed from the dichloromethane solution, placed into an electrochemical cell and a cyclic voltammogram of the surface was recorded.

3.4 Electrochemical Analysis[*]

3.4.1 Analysis of Cross-Metathesis Product 3.22

Voltammetry was performed over a potential range of 0 to 0.65 V, typically at a scan rate of 100 mVs^{-1}. A representative voltammogram of the redox active cross metathesis product **3.22** in aqueous 0.1 M $NaClO_4$ is shown in Figure 3.5 (solid line). For comparison, a second voltammogram of the model compound **2.18** (dashed line) shows a typical ferrocene response from an undiluted monolayer of a long-chain alkanethiol containing an amide linked ferrocene group.

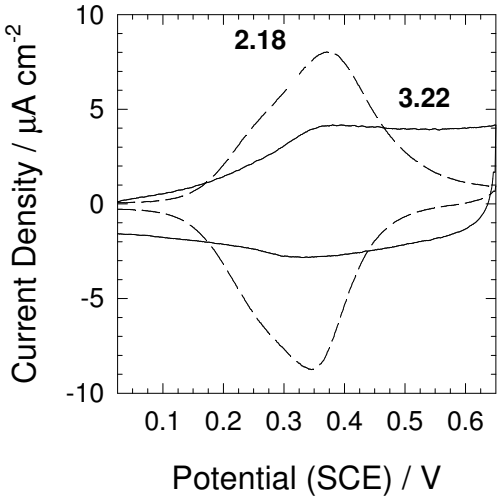

Figure 3.5 Cyclic voltammograms of the cross metathesis product, **3.22**, at 150 min with a **C10** diluent (solid line) and a monolayer of **2.18** (dashed line) at a scan rate of 100 mV s^{-1}.

[*] This work was performed by Dr Paula Brooksby, University of Canterbury.

The voltammogram of **2.18** has two distinctive features. The first is peak asymmetry probably due to neighbouring ferrocene groups experiencing electrostatic destabilization with progressive oxidation. Second, the measured background current, before and after ferrocene oxidation, is not the same. A small increase in the capacitance current following oxidation is attributed to some ion penetration into the SAM either by film distortion or at points where there are film defects. The ferrocene peak potentials for **3.22** (at t = 150 min) are near those of **2.18**, but the capacitive current is much larger both before and after ferrocene oxidation. This background current contributes to the apparent smaller reduction peak. Peak fitting of the oxidation and reduction components of the voltammogram gave a reduction peak area that was approximately 5% smaller than the oxidation peak. However, the reduction peak is much more difficult to fit with confidence; hence, the oxidation peak areas were used for all peak analyses.

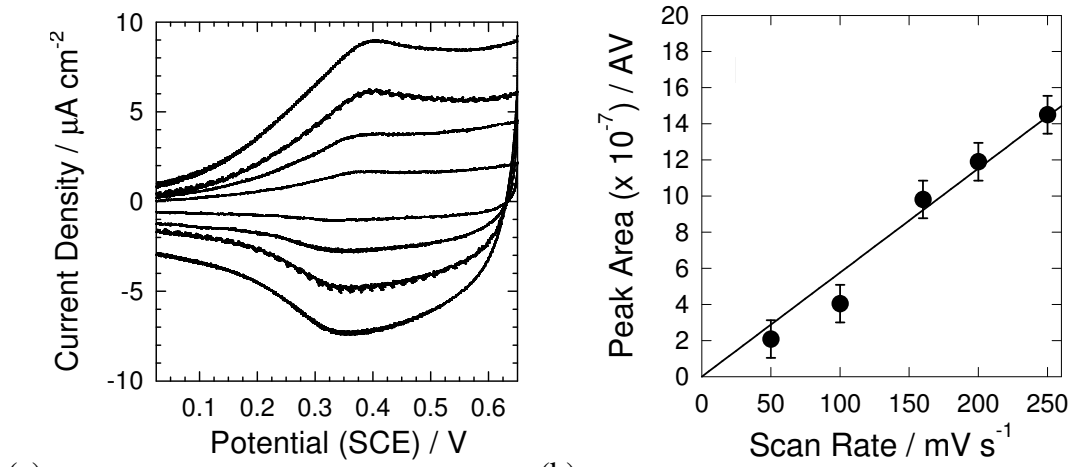

Figure 3.6 (a) Cyclic voltammagrams of surface species **3.22** at t = 75 min. The scan rates are 50 (inner), 100, 160, 200 and 250 (outer) mVs^{-1}. (b) Plot of the oxidation peak areas of **3.22** shown in (a) against scan rate.

Voltammograms were recorded at a range of scan rates to confirm that the response of **3.22** was due to a surface confined species. Figure 3.6a depicts the voltammograms for scan rates from 50 to 250 mV s^{-1} for the cross metathesis product **3.22** at t = 75 min, and Figure 3.6b shows a plot of oxidation peak areas, expressed as the product of current and potential, against scan rate. The plot of peak area versus scan rate is linear and passes through zero with the exception of the point at 100 mV s^{-1}, which lies outside the error estimates. This result confirms that ferrocene is bound to the SAM, rather than diffusing into solution.

3.4.2 Cross Metathesis Reaction Kinetics

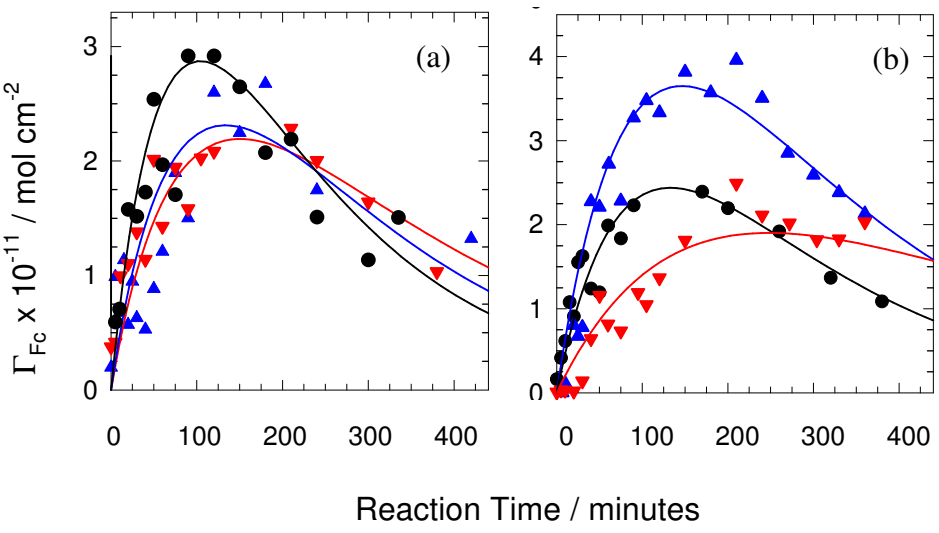

Figure 3.7 Plot showing the surface concentration (Γ_{Fc}) of **3.22** with time during the cross metathesis reaction. (a) Diluent is **C5**, and the olefin **3.18** adsorption times are (●) 15, (▲) 30, and (▼) 60 min. (b) Diluent is **C10**, and the olefin **3.18** adsorption times are (●) 30, (▲) 60, and (▼) 90 min. The fitted lines for each data set are the simulated results from the kinetic model for each surface.

A plot of the surface concentration (Γ_{Fc}) of the cross metathesis product **3.22** over reaction time, *t*, is shown in Figure 3.7a for a **C5** diluent, and Figure 3.7b for a **C10** diluent. Each data series represents a different adsorption time for olefin **3.18** on the gold surface. The adsorption times for olefin **3.18** with the **C5** diluent are 15, 30, and 60 min and for the **C10** diluent are 30, 60, and 90 min. Figure 3.7 clearly shows that for each monolayer a maximum surface concentration of ferrocene is reached, after which there is a rapid decline in the amount of ferrocene remaining on the surface with increasing reaction time. Furthermore, the initial concentration of **3.18** in the SAM, as controlled by the adsorption time, dictates the maximum value of surface concentration of **3.22** (Γ_{Fc}) measured during cross metathesis. The maximum Γ_{Fc} for **3.22** with the **C5** diluent was 2.9 x 10^{-11} mol cm^{-2} at an olefin (**2.6**) adsorption time of 15 min. In contrast, the maximum Γ_{Fc} for **3.22** with the **C10** diluent was 4.0 x 10^{-11} mol cm^{-2} at an adsorption time of 60 min. Furthermore, the initial slopes of the plots and the reaction time required to give the maximum yield of cross metathesis product is a function of the adsorption time: increasing the adsorption time increases the optimum reaction time and decreases the initial slope of the plots.

A mixed monolayer composed of a significantly longer chain diluent (**C15**) with olefin **3.18** adsorption times up to 2 hours did not give a measurable ferrocene response for the CM reaction (up to 6 hours) with the olefin-terminated ferrocene. The length of the olefin **3.18** is not

appreciably longer than that of the **C15** alkyl chain. Likewise, the reaction of a full monolayer of **3.18** (without diluent) and ferrocenyl olefin **3.10** did not give a measurable cross metathesis product **3.22** after 6 hours reaction time. These two results demonstrate that terminal olefin groups congested on the surface are unavailable for cross metathesis, presumably since the Grubbs' catalyst is unable to bind effectively.

Models were developed to explain the observed surface concentrations of product **3.22**, in relation to the distance between immobilised olefin **3.18** on the surface, and the contribution of self-cross metathesis (Figure 3.8a). These models assume that longer olefin adsorption times lead to a greater concentration of **3.18** on the surface.

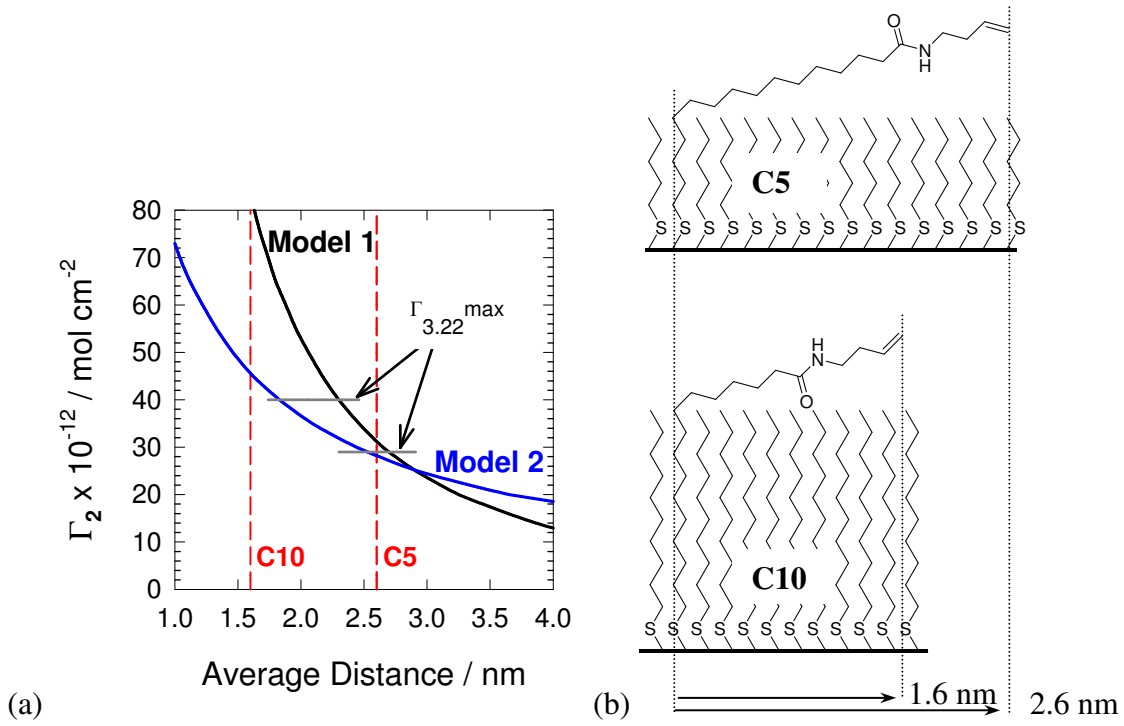

Figure 3.8 (a) Graph showing the calculated average distance between terminal olefin groups in a monolayer as a function of surface concentration (solid lines). Model 1 is for an idealized surface configuration, and Model 2 assumes adsorption of **3.18** at diluent defects only. The two vertical dashed lines represent the average separation distance for **3.18** above which cross metathesis between surface olefin groups is assumed negligible for the pentanethiol (**C5**) and decanethiol (**C10**) diluents. The two short horizontal lines are the maximum measured values for cross metathesis product using pentanethiol and decanethiol diluents. (b) Illustration showing the effect of diluent length on the distance olefin (**3.18**) can tilt over the surface. If the average distances between olefin **3.18** is less than double the tilt length, then self-cross metathesis competes with surface solution cross metathesis.

In the first model (**model 1**), the average distance between each olefin **3.18** was calculated as a function of surface concentration, assuming each molecule is attached to the surface in an idealized adsorption pattern (evenly spaced on the surface). A plot of Γ_{Fc} against average distance (= {2}/{$\sqrt{\pi N_A \Gamma}$}), where N_A is Avogadro's constant, is shown as the solid line in

Figure 3.8a . Here the idealized adsorption pattern is based on a spherical area surrounding the centrally located olefin. A more realistic model (**model 2**) assumes that adsorption of a second thiol (the diluent being the first) to a SAM surface typically occurs by place exchange at defect sites, such as domain boundaries or plane steps, followed by much slower exchange inside the domains.[26] The average distance between olefin **3.18** (=$\{L\}/\{AN_A\Gamma\}$) is shown in Figure 3.8a as a blue line. For model 2, the total length (L) of defects per surface area (A) is based on a survey of **C10** SAM images published in the literature, and a value for L/A of 0.44 nm^{-1} is used. In addition, Figure 3.8a shows two short horizontal lines labeled $\Gamma_{3.22}^{max}$ (the largest maximum measured value of Γ_{Fc} for **3.22** with both diluents) and two vertical dashed lines (**C5** and **C10**) whose origins are described below.

The lengths of the **C5** and **C10** diluents were calculated using Spartan to be 0.91 and 1.54 nm, respectively, and the total length of olefin **3.18** is 2.5 nm. The difference between the length of the diluent and **3.18** determined the maximum distance that the immobilised form of **3.18** can extend over the surface, where the shorter the diluent the greater the distance the olefin extends (Figure 3.8b). The average distance between the olefinic groups must be greater than twice the tilt distance permitted by the diluent in order to avoid self-cross metathesis on the surface between molecules of **3.18**, otherwise known as 'biting back'. Self-cross metathesis of olefin **3.18** competes with surface solution cross metathesis reaction between **3.18** and ferrocenyl olefin **3.10** when the surface olefins are less than twice the tilt distance. The vertical dashed lines in Figure 3.8a at 1.6 and 2.6 nm represent an estimate of the maximum average distance between each olefin **3.18** for a given diluent (**C5** or **C10**, respectively), about which either self-cross metathesis or surface solution cross metathesis predominates. Long adsorption times result in high surface concentrations of **3.18** such that the average distance between surface olefins becomes less than 0.8 (**C5**) or 1.3 nm (**C10**). Self-cross metathesis then competes effectively with surface solution cross metathesis to olefin **3.10**. Moreover, the observed decrease in the initial slopes of the plots in Figure 3.7, with longer olefin adsorption times, suggests there is a reaction rate change associated with the interfacial chemistry as the concentration of **3.18** increases. Hence, there is a concurrent increase in the optimum reaction time as the concentration of **3.18** increases.

While these models rationalise the dependence of the surface cross metathesis product concentration on thiol adsorption time, they cannot explain the decrease in surface product concentration during the course of each reaction. The decline in product **3.22** with time could be

due to a number of factors: the product **3.22** re-entering the catalytic cycle to form dimers, or desorption of the SAM over time. Cross metathesis is a reversible reaction favouring the thermodynamically most stable product. Therefore, it is possible that **3.22** could be recycled by the catalyst to form surface olefin or solution ferrocene dimers. However, there is no straightforward way to determine if this is occurring. The second important factor to consider is desorption of the thiols from the surface. This is detailed in the next section.

3.4.3 Thiol Stability and Desorption

SAMs of the ferrocene disulfide **3.21** and the ferrocene thiol **2.18** (without diluents) on a gold polycrystalline electrode* were used to investigate thiol stability under cross metathesis reaction conditions. SAMs of **3.21** and **2.18** were suspended in refluxing dichloromethane without catalyst. Periodically, the electrodes were removed and the surface concentration of the ferrocene species was determined by cyclic voltammetry. At t = 150 min, Grubbs' catalyst **3.2** was added to the refluxing solution and electrochemical monitoring of the ferrocene signal continued. Additionally, the disulfide monolayer **3.21** was examined for two different adsorption protocols: a 16 hour and a 3-day adsorption period.

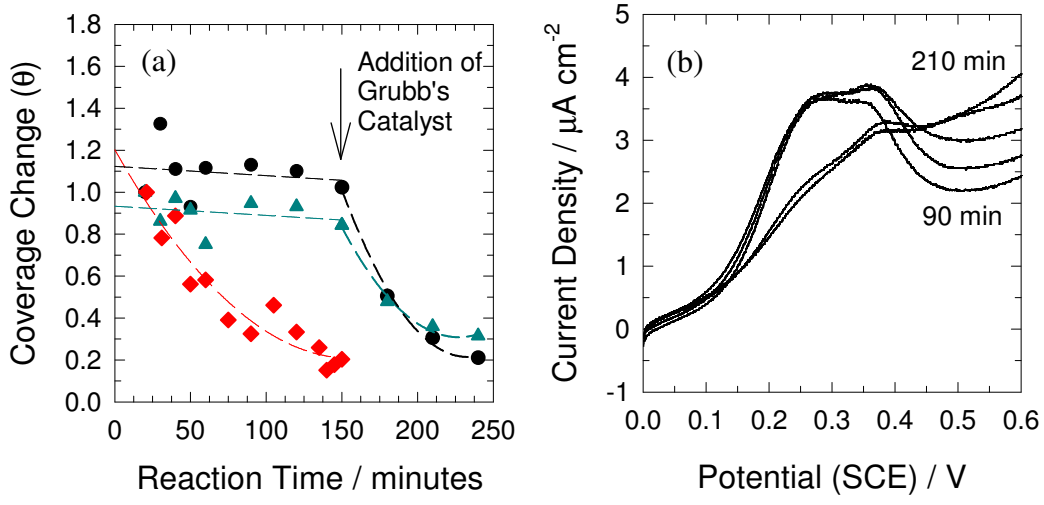

Figure 3.9 (a) Plot showing the relative stability of SAMs over time in refluxing dichloromethane: **3.21** adsorbed for 16 hours (◆), **3.21** adsorbed for 3 days (▲), **2.18** adsorbed for 3 days(●). Arrow indicated the time (150 min) when Grubbs' catalyst **3.2** was added to the dichloromethane. (b) Oxidation scan for **3.21** after a 3 day adsorption, refluxing in dichloromethane for t = 90, 120, 150, 180 and 210 min, with Grubbs' catalyst **3.2** added at 150 min.

* A polycrystalline electrode was used for convenience because it had a greater surface area than the Au (111) electrode.

Figure 3.9a shows a plot of the ferrocene oxidation peak area for **3.21** and **2.18** refluxing in dichloromethane up to t = 250 min. A monolayer of **3.21** that had a shortened adsorption step of 16 hours (compared to the 3 days for the other two monolayers) is represented by the diamonds in Figure 3.9a. Since a significant loss of ferrocene had occurred up to 150 min, there was no addition of Grubbs' catalyst to the refluxing dichloromethane. The triangles and circles represent monolayers of **3.21** and **2.18** generated from a 3 day adsorption step, respectively. These films are relatively stable in refluxing solvent, but upon addition of Grubbs' catalyst **3.2**, a significant decrease in the ferrocene current is apparent.

Figure 3.9b shows oxidation peaks for **3.21** taken from Figure 3.9b at t = 90, 120, 150, 180, and 210 min. A large reduction in the ferrocene peak area was observed upon addition of the catalyst **3.2**. Concurrently, a continual increase in the capacitance current was observed during this time, presumably due to desorption of the film (cleavage of the Au-S bond) rather than degradation of the ferrocene terminus. An increase in the background capacitance caused by pinholes in the film is consistent with desorption of a monolayer. Nevertheless, it is not clear if desorption is influenced by the nature of the terminal groups, that is, whether desorption of the diluent and the olefin are equally affected. However, desorption of **3.22** is the most likely the origin of the decline in ferrocene concentration as shown earlier in the cross metathesis kinetic studies in Figure 3.7.

A recent AFM study showed that the force required to rupture a gold-sulfur bond is lower for a cyclic disulfide than for an alkanethiol.[27] This is because the Au-S bond rupture is accompanied by simultaneous intramolecular S-S bond reformation. On planar gold and in a dichloromethane solution, we speculate that pairs of sulfur groups (olefins or diluents) in close proximity would desorb 'two at a time' to form S-S linkages rather than as a negatively charged thiolate ion. This proposed mechanism is consistent with the desorption results of this study, which have clearly demonstrated that the Au-S bond is not stable under the mild experimental conditions in the presence of Grubbs' catalyst.

There are two methods for addressing the gold-thiolate instability: the first using multiple attachment points as with cross-linked nanoparticle monolayers and second with Si substrates that contain Si-C linkages.[18-20] A study of the cross metathesis of terminal olefins on Si substrates, using Grubbs' first-generation catalyst, clearly demonstrated the monolayer stability

in similar experimental conditions.[20] However, the results showed complete product formation required more that 24 hours. The optimal cross metathesis reaction time of approximately 150 min observed in this study is determined at the time for the maximum ferrocene signal. It does not take into account that thiol desorption is continuously occurring and that unreacted olefin, **3.18**, will also be desorbing. Therefore, in the absence of thiol desorption, both the maximum cross metathesis product and the optimum time would be greater, although by an unknown amount. Further studies on stable monolayers are required to compare the two types of catalysts, but certainly, gold-thiol-based monolayer chemistry would benefit from using the catalyst giving faster metathesis to avoid desorption problems. It is important to note that while addition of Grubbs' catalyst accelerated thiol desorption (Figure 3.9), the cause of this effect is unknown at this time.

3.5 Conclusions and Future Work

Cyclic voltammetry has been used to monitor the cross metathesis of a ferrocenyl redox probe to an olefin-terminated SAM on gold. Cross metathesis between the solution phase ferrocenyl olefin **3.10** and olefin terminated thiol **3.18** in a mixed-monolayer with short diluent species proceeded readily in refluxing dichloromethane. Self cross metathesis competes with surface solution cross metathesis when the olefins of the monolayer are spatially close. Thus, the adsorption time for the olefin must be considered an important parameter when fabricating the initial mixed monolayer surface. A model is presented that relates the average surface concentration of olefin to the maximum possible (heterodimer) cross metathesis product. A high concentration of surface olefin leads to spatial congestion and mixed-cross metathesis products that also include homodimers. These factors need to be considered when using cross metathesis to construct surface architecture. Cross metathesis products were not observed for diluents with length near that of the olefin or indeed if no diluent is used, that is, steric congestion at the interface impedes cross metathesis.

A further significant outcome of this study is the observation of an adverse effect of the catalyst-solvent system on the gold thiolate bond. Strong experimental and model evidence is presented for alkanethiol and cyclic thiol desorption from the gold surface in the presence of the catalyst, but little is known about the fate of each component (olefin and diluent) in the mixed monolayers. Further investigation is required before this route to surface architecture on gold

can be fully exploited. Studies of cross-linked monolayers on gold nanoparticles from cross metathesis reactions show that the Au-S bond is relatively stable on these types of interfaces and that significant thiol losses are not observed, presumably because there are multiple attachment points between the monolayer and the gold surface. Hence, multiple thiol bonding sites on planar gold surfaces should afford greater stability than was observed in this study.

The work presented here has important implications to a number of factors of monolayer chemistry, such as olefin cross metathesis and product distributions, optimal reaction times, adsorption time, thermal stability of SAMs, and desorption with Grubbs' catalyst. An electrochemistry-based method has been developed to monitor cross metathesis reactions, and this has been used to determine the optimum reaction time to give the maximum yield. This is especially important for gold surfaces that are unable to withstand long periods of time in heated solvents. The apparent optimum reaction time for cross metathesis product formation was found to be approximately 150 minutes for planar gold surfaces, which is significantly shorter than the 24 hours typically reported for cross metathesis using Grubbs' first-generation catalyst on Si.[20] However, the observed optimum reaction time is dependent on the rate of thiol desorption and needs to be taken into account when using cross metathesis and gold-thiol systems. The customary practice of allowing cross metathesis reactions at gold-thiol SAMs to continue for greater than 24 hours is apparently excessive (in the presence of Grubbs' second generation catalyst) and should be avoided with adsorbates of short chain length. Similar time-dependent studies with the first-generation catalyst would also benefit future cross metathesis applications on gold-thiol-based monolayers.

3.6 References

1. Lee, J. K.; Lee, K. B.; Kim, D. J.; Choi, I. S., *Langmuir* **2003,** 19, (20), 8141-8143.
2. Fabre, B.; Hauquier, F., *Journal of Physical Chemistry B* **2006,** 110, (13), 6848-6855.
3. Sabapathy, R. C.; Crooks, R. M., *Langmuir* **2000,** 16, (20), 7783-7788.
4. Collman, J. P.; Devaraj, N. K.; Eberspacher, T. P. A.; Chidsey, C. E. D., *Langmuir* **2006,** 22, (6), 2457-2464.
5. Yousaf, M. N.; Chan, E. W. L.; Mrksich, M., *Angewandte Chemie-International Edition* **2000,** 39, (11), 1943.
6. Hartmuth C. Kolb, M. G. F. K. B. S., *Angewandte Chemie International Edition* **2001,** 40, (11), 2004-2021.
7. Collman, J. P.; Devaraj, N. K.; Chidsey, C. E. D., *Langmuir* **2004,** 20, (4), 1051-1053.

8. Connon, S. J.; Blechert, S., *Angewandte Chemie-International Edition* **2003,** 42, (17), 1900-1923.
9. Vernall, A. J.; Abell, A. D., *Aldrichimica Acta* **2003,** 36, (3), 93-105.
10. Li, X. M.; Huskens, J.; Reinhoudt, D. N., *Nanotechnology* **2003,** 14, (10), 1064-1070.
11. Schwab, P.; Grubbs, R. H.; Ziller, J. W., *Journal of the American Chemical Society* **1996,** 118, (1), 100-110.
12. Scholl, M.; Ding, S.; Lee, C. W.; Grubbs, R. H., *Organic Letters* **1999,** 1, (6), 953-956.
13. Inomata, T.; Konishi, K., *Chemical Communications* **2003**, (11), 1282-1283.
14. Pusztay, S. V.; Wei, A.; Stavens, K. B.; Andres, R. P., *Supramolecular Chemistry* **2002,** 14, (2-3), 291-294.
15. Samanta, D.; Faure, N.; Rondelez, F.; Sarkar, A., *Chemical Communications* **2003**, (10), 1186-1187.
16. Wu, M. L.; O'Neill, S. A.; Brousseau, L. C.; McConnell, W. P.; Shultz, D. A.; Linderman, R. J.; Feldheim, D. L., *Chemical Communications* **2000**, (9), 775-776.
17. Brooksby, P. A.; Anderson, K. H.; Downard, A. J.; Abell, A. D., *Langmuir* **2006,** 22, (22), 9304-9312.
18. Liu, X. G.; Guo, S. W.; Mirkin, C. A., *Angewandte Chemie-International Edition* **2003,** 42, (39), 4785-4789.
19. Perring, M.; Dutta, S.; Arafat, S.; Mitchell, M.; Kenis, P. J. A.; Bowden, N. B., *Langmuir* **2005,** 21, (23), 10537-10544.
20. Dutta, S.; Perring, M.; Barrett, S.; Mitchell, M.; Kenis, P. J. A.; Bowden, N. B., *Langmuir* **2006,** 22, (5), 2146-2155.
21. Seshadri, H.; Lovely, C. J., *Organic Letters* **2000,** 2, (3), 327-330.
22. Martinez, V.; Blais, J. C.; Bravic, G.; Astruc, D., *Organometallics* **2004,** 23, (4), 861-874.
23. Eckert, H.; Forster, B.; Seidel, C., *Zeitschrift fuer Naturforschung, B: Chemical Sciences* **1991,** 46, (3), 339-52.
24. Aitken, S. G. Design, synthesis and testing of β-strand mimics as protease inhibitors. Ph.D, University of Canterbury, Christchurch, 2006.
25. McNaughton, B. R.; Bucholtz, K. M.; Camaano-Moure, A.; Miller, B. L., *Organic Letters* **2005,** 7, (4), 733-736.
26. Baralia, G. G.; Duwez, A.-S.; Nysten, B.; Jonas, A. M., *Langmuir* **2005**, (21), 6825.
27. Langry, K. C.; Ratto, T. V.; Rudd, R. E.; McElfresh, M. W., *Langmuir* **2005,** 21, (26), 12064-12067.

Chapter 4 Synthesis of Compounds Suitable for Surface Immobilisation

4.1 Functionalised β-peptides

The syntheses of the functionalised peptides studied in Chapter Two are presented here. The design of *β*-peptides for immobilisation onto gold required careful thought with regards to structural features that govern the stability of the peptide helix and the formation of a well-ordered SAM. It was also necessary that the *β*-peptides could be functionalised with a sulfur group (for chemisorption on gold) and a redox active probe (such as ferrocene) without disrupting the helical structure.

The introduction to this chapter includes a discussion of the factors that stabilise the 14-helix and literature examples of functionalised *β*-peptides. Analytical methods, such as the 2D-NMR spectroscopy experiments NOESY and ROESY, circular dichroism (CD) spectroscopy and x-ray crystallography are the favoured techniques for determining secondary structure in *β*-peptides, and these methods are summarised in Section 4.1.3. Following the introduction, the syntheses of model compounds (in order to determine the compatibility of various functional groups with sulfur chemistry), and functionalised peptides for immobilisation on gold are presented.

4.1.1 Stabilisation of the 14-helix

Both the order and structure of the different constituent *β*-amino acid residues greatly affects the ability of a *β*-peptide to form stable secondary structures. This is similar to the effect that different *α*-amino acid residues have in *α*-peptides; while some can stabilise, others may have no effect or may disrupt, sheets and turns. However, many of the factors that stabilise *α*-helices in *α*-peptides, destabilise *β*-helices and *vice versa*. For example, it has been observed that while β^3hVal and other aliphatic β^3amino acids with *α*-branched sidechain groups stabilise a 14-helix structure in solution, the corresponding *α*-amino acids are known to destabilize *α*-helices.[1] Similarly, the 1-hydroxyethyl side chain of threonine stabilises the helical structure of *β*-peptides, but destabilises *α*-peptides.

Seebach *et al* reported that pairs of oppositely charged residues in adjacent positions (*i*, *i* +3) along the helix backbone stabilise the 14-helix through ionic interactions (Figure 4.1).[2]

Furthermore, Gellman *et al* reported that cyclohexylamine carboxylic acid (ACHC) residues induce the stabilisation of the 14-helix (as described in Chapter One, Section 1.2.3).[3] A comprehensive list of stabilizing and destabilizing effects are summarised in Table 4.1.

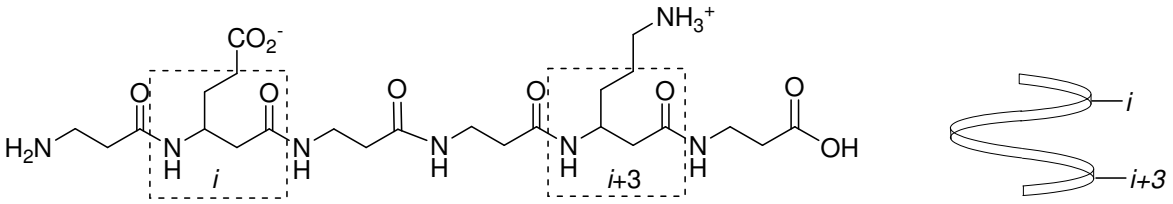

Figure 4.1 Sidechain groups at positions *i* and *i*+3 lie adjacent in the 3_{14}-helix.

Table 4.1 Some of the destabilising and stabilising effects of *β*-amino acids on the 14-helix.

Destabilising Effects	Stabilising Effects
- *β*-Amino acid residues with inverse absolute configuration[4,5]	- Disubstituted (*S*,*S*)-$\beta^{2,3}$-amino acid building blocks[6]
- Side chains of the same charge in the *i* and the *i* + 3 positions[4]	- Incorporation of (*S*,*S*)-2-aminocyclohexane carboxylic acid[7]
- Lack of *α*-branched side chains[8]	- Complexation of metal ions,[5] disulfide bonds[9] or salt bridges[2] between *i* and *i* + 3 positions
	- Fluorine in an axial (*Re*) position at the β^2 backbone carbon[10]

4.1.2 Literature Examples of Functionalised *β*-Peptides

β-Peptides can be derivatized (in a similar fashion to *α*-peptides) at either the sidechain groups or at the *N* and *C*-termini to create functional molecules that are useful for biological or structural studies. However, there exist very few examples of functionalised *β*-peptides, especially those with modified (non-peptidic) terminal groups. One such example, by Gellman *et al*, is the use of functionalised *β*-peptides with *N*-terminal fluorescent labels to study the uptake of *β*-peptides in cells (Figure 4.2a).[11] The *β*-peptides were designed to adopt either 14-helix conformation

(peptides **1**, **2** and **5**) or a strand-like conformation (no secondary structure; peptides **3** and **4**). These peptides were synthesised on resin, and labelled with flurorescein (Figure 4.2b; a non-toxic dye that fluoresces at 460 nm). Circular dichroism (CD) spectroscopy * showed that the *N*-terminal functionalisation did not disrupt the 14-helical structure of *β*-peptides **1**, **2** and **5**, as evidenced by the presence of a minimum at ~215 nm (Figure 4.2c). Peptide **3** contains a *β*hGly residue, which is flexible and therefore reduces 14-helical propensity, while peptide **4** contains a cyclic residue of inverse absolute configuration (*R*,*R*) (instead of (*S*,*S*) as in peptide **1**) which should disrupt helix formation entirely.

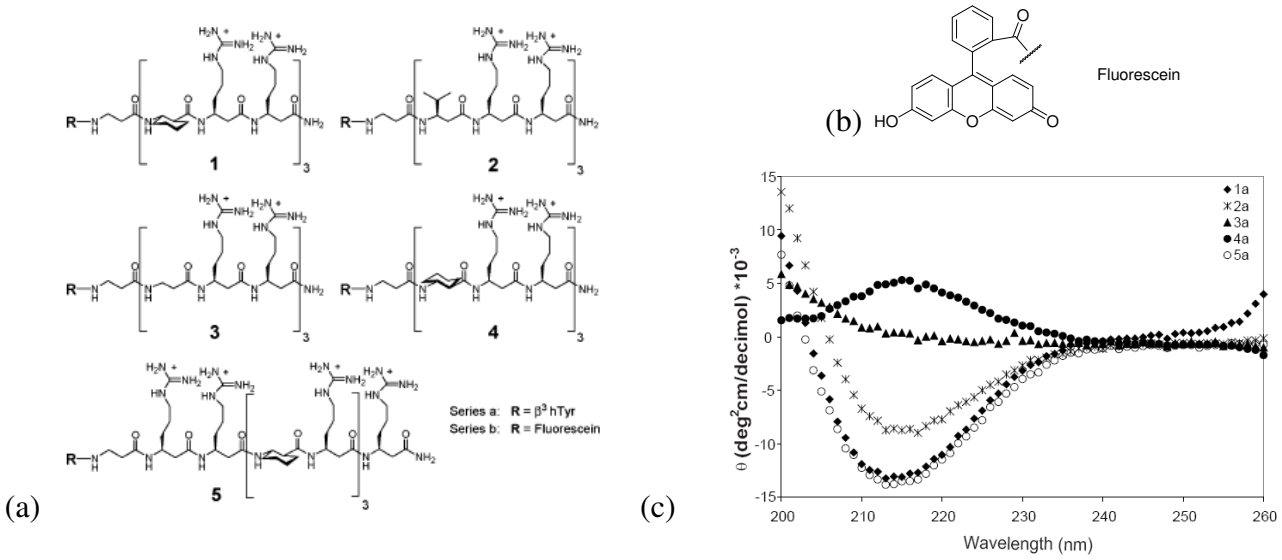

Figure 4.2 (a) Structures of the fluorescein-labelled *β*-peptides 1-5; (b) fluorscein; and (c) CD spectra of fluorescein-labelled peptides 1-5. (Reproduced from Ref. 11)

The modification of amino acid backbone and sidechain groups constitutes the remainder of the literature on the synthesis of functionalized *β*-peptide structures. Prominent examples are the synthesis of glycopeptides (carbohydrate-containing peptides) [12] and nucleopeptides (nucleobase-containing peptides).

The modification of peptides with sugar residues allows the construction of highly diverse glycopeptide libraries with structure that can mimic carbohydrate-protein interactions. Ziegler *et al* synthesised a *β*-peptide containing glucopyranose residues attached at the β^3 position using short alkyl tethers, via a solid-phase approach (Figure 4.3a).[12-15] Sharma *et al* synthesised *β*-peptides with furanose substitution at the β^3 position (Figure 4.3b). These novel *β*-peptides

* This method is described in section 4.1.3.

which consist of alternating substituted (S) and (R)-β^3amino acids residues[13,14] demonstrated CD spectra characteristic of 10/12 helices.

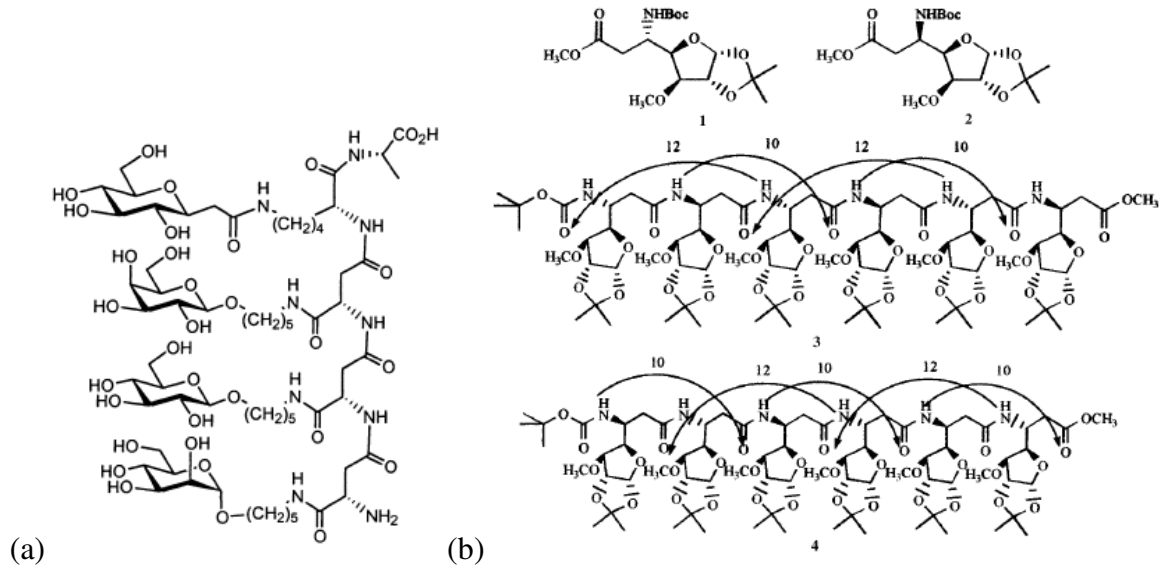

Figure 4.3 (a) A β-peptide containing glucopyranose residues attached at the β^3 position using short alkyl tethers. (b) A β-peptides with furanose substitution at the β^3 position. The arrows show the hydrogen-bonding interactions that stabilise the 10/12 helix. Reproduced from ref. 14.

In another approach, Suhara *et al* synthesised β-amino acid monomers in which the backbone was incorporated into a sugar-like cyclic structure (known as glycamino acids) (Figure 4.4).[15] A hexapeptide synthesised from these cyclic monomers possessed 14-helix structure in solution.

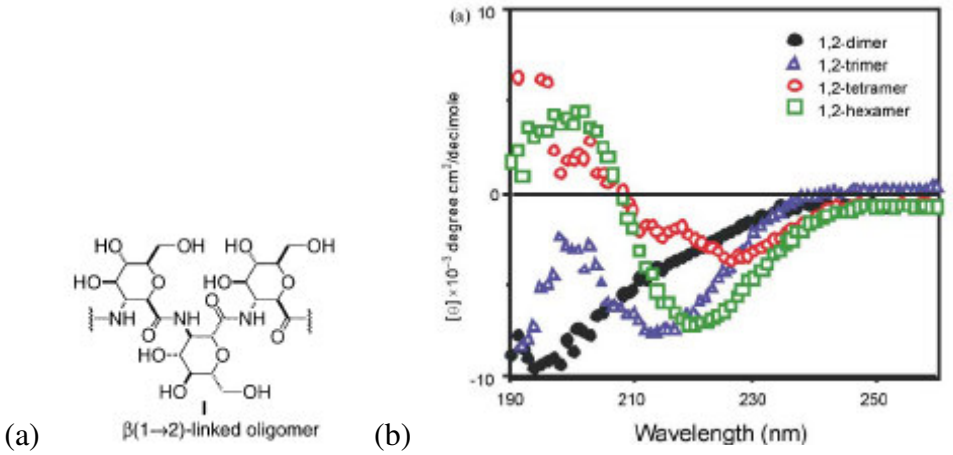

Figure 4.4 (a) Structure and (b) CD spectra of β-glycamino acid peptides. Reproduced from ref 15

Chakraborty and Diederichsen synthesised β-peptides that adopted a 14-helix and contained complementary nucleobase pairs.[16] The nucleobases were positioned at *i* and *i*+3 intervals along the peptide backbone allowing them to stack upon each other, and form hydrogen bonding interactions with a complementary strand. The helix stability and base pairing were confirmed

by circular dichroism and temperature-dependent UV spectroscopy (to observe the 'melting' of the nucleobase hydrogen bonds).

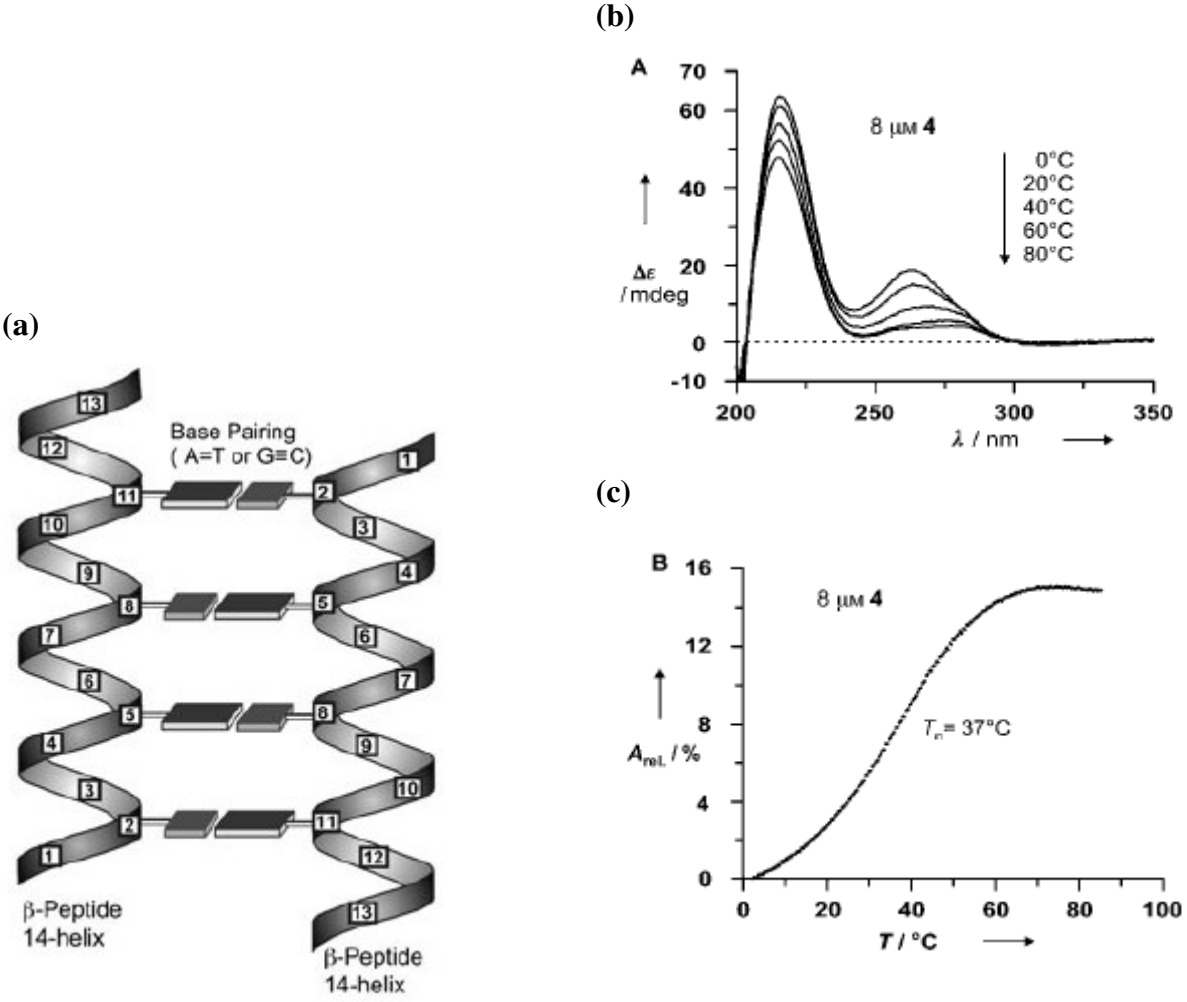

Figure 4.5 (a) Model of the antiparallel *β*-peptide helix association mediated by nucleobase pairing; (b) circular dichroism spectra of the *β*-peptides, with increasing temperature; (c) temperature dependent UV spectrum of the base paired *β*-peptide.

In summary, the limited evidence currently available seems to suggest that functionalisation of the *β*-peptides, especially at the *N*-terminal position (as shown in Figure 4.2), does not prevent the formation of a helical structure in solution. However, there are no reported surface-immobilisation studies of *β*-peptides, and therefore no indication as to whether they retain helicity on the surface (excluding the findings presented in Chapter Two). However, it has been illustrated with functionalised α-peptides (that are helical in solution) that self-assembly on gold leads to the formation of well-ordered monolayers (Table 2.2). This suggests that the helical structure of short peptides is maintained on the surface.

4.1.3 Determining Peptide Secondary Structure

Various spectroscopic and crystallographic techniques are used to characterise and determine the stability of secondary structures. The most important techniques are described below.

4.1.3.1 Circular Dichroism

Circular dichroism (CD) refers to the differential absorption of left handed and right handed circularly polarised light. If the left and right handed circularly polarised light are not absorbed to equal extents then the sample possesses elliptical polarisation. A CD spectrum is obtained when the elipticity is measured as a function of wavelength.

The most useful region for looking at secondary structure is between 180 and 240 nm. The absorption in this region is principally due to the amide bond, in particular the weak $n \rightarrow \pi^*$ transition around 200 nm and the more intense $\pi \rightarrow \pi^*$ transition around 190 nm. When the circularly polarised light is passed through a solution containing peptides or proteins, the amide bonds in the secondary structure motifs absorb light differently to those in a strand-like conformation (those not in a hydrogen-bonded or regular, repeating secondary structure).

The 'fingerprint' spectra for various types of secondary structure in both α- and β-peptides is shown in Figure 4.6. Generally, different secondary structural features can be identified from a CD spectrum based on the minimum and maximum wavelength positions. This technique is especially important for large proteins, as the ratio of helices to β-turns and β-sheets can be determined, whereas such information can be difficult to obtain from the analysis of NMR spectroscopy or X-ray data.

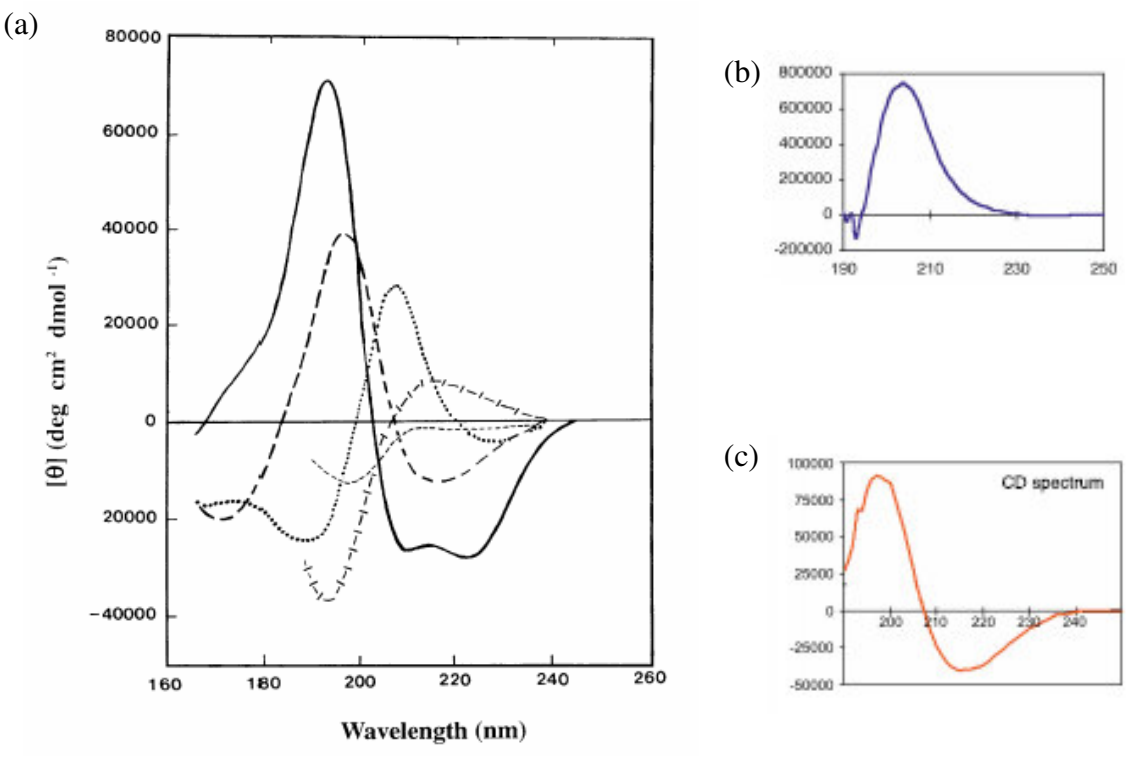

Figure 4.6 Far UV CD spectra associated with different types of secondary structure. (a) Solid line, α-helix; long dashed line, anti-parallel β-sheet; dotted line, type I β-turn; cross dashed line, extended (poly(Pro)) helix; short dashed line, irregular structure; (Reproduced from [17]); (b) a β-peptide 10/12 helix; and (c) a β-peptide 14-helix.

CD is generally useful is determining the type of helix present in β-peptides, albeit with a level of caution. Occasionally CD spectra do not agree with solution phase NMR data and X-ray data. Examples exist of peptides that have CD spectra that suggest secondary structures that are sterically impossible or implausable.[18]

4.1.3.2 Nuclear Magnetic Resonance

Nuclear magnetic resonance (NMR) is a powerful tool for the study of peptide secondary structure in solution or solid-state. Information about which residues are hydrogen bonded, the arrangement of atoms in space and the denaturing effects of temperature can all be gathered from 1 and 2D NMR techniques.

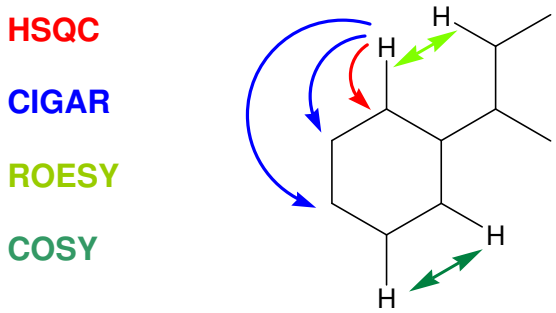

Figure 4.7 2D-NMR experiments: ^{1}H to ^{13}C correlations seen by HSQC and CIGAR; ^{1}H to ^{1}H correlations seen by COSY and ROESY.

Various 2D NMR techniques can deconvolute 'crowded' proton and carbon spectra into individual carbon and proton chemical shifts. The correlation types of 2D-techniques used in this study are shown in Figure 4.7. The through-bond ^{1}H coupling experiment, COSY, shows correlations between protons attached to adjacent atoms. This technique is often used in conjunction with through-bond proton to carbon coupling experiments HSQC and CIGAR, which allow the chemical shifts of each proton and carbon atom to be assigned. HSQC shows correlations between a proton and the directly attached carbon, while CIGAR shows correlations between protons and carbons two or three bonds away.

NOE experiments, which include the 1D and 2D NOESY and ROESY*, measure the correlations between protons or other nucleii, through space. These techniques, in theory, can be used to calculate distances between the nuclei, because the falloff of correlation intensity through space occurs with a power of r^{-6} (where r is radius). The NOE experiments reveal correlations between protons within 5 Å distance of each other through space (rather than through bonds). Therefore, NOE is one of the most valuable measurements for identifying the close contacts that occur as a result of hydrogen bonding, and therefore helps to assign the secondary structure of peptides.

However, NOE correlations that are very weak are not always observed, allowing conformations that are in low abundance to disappear, while those with stronger NOE correlations are overrepresented. Another limitation of NMR studies is that only an "average" conformation is obtained because data is collected over a longer time span (10^{-7} s), compared with the rate of conformational change (10^{-12} s).[19]

* (which differs from the NOESY by using a rotating frame pulse sequence, and is more useful for obtaining data for compounds of molecular weights ranging between 700 and 1200 $gmol^{-1}$)

4.1.3.3 X-ray Analysis

X-ray crystallography provides the 3D structural "image" of a molecule by looking at the diffraction pattern caused by the scattering of X-rays by electrons. It affords such information as atom connectivity, relative* stereochemistry and hydrogen bonding of a peptide captured in one solid-phase conformation. However, this technique does not give any information about the stability of the particular conformation, the number of other possible solid phase conformations, or the peptide conformation(s) in solution phase.

In smaller peptides, the secondary structure is largely dependant on environmental factors such as the solvent used in crystallization, or interactions with other peptide molecules. Despite the remarkable stability of the secondary structure of β-peptides, the only crystal structures to date are of those that comprise cyclic β-amino acids.

4.1.3.4 Other analyses

Fourier transform infrared (FTIR) analysis can give qualitative information on the type of NH bonding present in a peptide in solution phase. Intramolecular hydrogen bonding NH groups have a lower energy band than non-hydrogen bonded groups.[20] More recently, the immobilisation of peptides on surfaces has been used to study secondary structures of peptides comprising α-amino acids (see Chapter Two). When a peptide is immobilised on a surface, highly sensitive methods, such as atomic force microscopy (AFM), surface IR and electrochemistry can be used to study both the chemical and electrical properties, as well as biorecognition events (the binding of a biological substrate with its target).

* or absolute in the presence of a 'heavy atom'

4.2 Peptide Design and Retrosynthetic Analysis

4.2.1 Synthetic Methods

The key requirement for the synthesis of a β-peptide suitable for studying electron transfer on a gold surface was the ability to introduce a sulfur linker and a ferrocene group to opposing termini. The synthesis of most longer peptide chains (of six or more residues) is achieved via a solid-phase approach. This technique avoids peptide solubility problems and the purification of intermediates. Solid-phase is particularly useful for the synthesis of β-peptides, which have much lower solubility in organic solvents when compared to the corresponding α-peptides. Unfortunately, the solid-phase approach was deemed not suitable for the synthesis of the functionalized peptides required in this work, because of the incompatibility of certain reagents with the ferrocene moiety and sulfur linkers. In particular, trifluoroacetic acid (TFA), which is often used to cleave peptides from the solid-phase resin, is not compatible with ferrocene methyl amine or disulfides, both of which are required in this work. Therefore, a solution phase method was necessary for the synthesis of suitable β-peptides.

4.2.2 Choice of a Suitable *β*-Peptide

While peptides with charged residues (e.g. Arg) have favourable solubility properties (such as good solubility in water and methanol)[21] even when protected at both ends, the charges have a destabilising effect on peptide SAMs, as illustrated by Miura *et al* with α-helical peptides (see Chapter Two, Table 2.2).[22] Amino acids with bulky or long side chains have the same negative effect towards the formation of an ordered SAM. Therefore, a β-peptide structure comprising only aliphatic side chains was required. One such peptide (**2.17**, shown below), developed and studied by Seebach *et al* is composed of two repeated units of β^3hVal-β^3hAla-β^3hLeu.[6,18] This hexapeptide forms a very stable 3_{14} helix in solution, as elucidated by 2D-NMR techniques and CD.[6] The branched side-chain groups of Val and Leu stabilise a 3_{14}-helix, and increase its solubility in organic solvents (compared to, for example, a hexapeptide solely of β-Ala).[18] Furthermore, peptide **2.17** can be synthesized in solution phase using conventional protecting

groups and standard coupling agents.[6] Therefore, functionalized β-peptides, based around the peptide **2.17** core structure were deemed as suitable synthetic targets for immobilisation on gold.

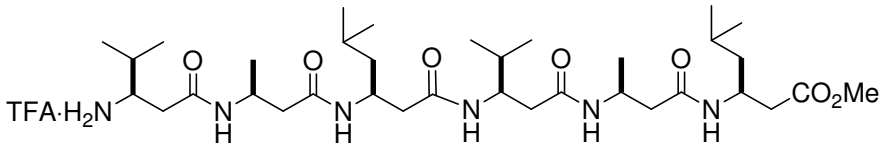

2.17

Once β-peptides with protecting groups at both termini reach a certain length (of four or more amide bonds) solubility in common organic solvents, such as dichloromethane, tetrahydrofuran, methanol and dimethylformamide, is greatly diminished. This poor solubility is due to the intramolecular hydrogen bonding that occurs, rendering lone pairs or suitable protons on the peptide unavailable for hydrogen bonding with the solvent molecules. Solubility problems would be encountered if the peptide is synthesised one amino acid residue at a time, especially when attempting to deprotect or purify intermediates for further coupling. Functionalisation of the hexapeptide at both the *C* and *N* terminus with a sulfur linker and a ferrocene group, would require seven amide bonds. This poses a potential problem for the envisaged solution phase synthesis.

A strategy was devised whereby the β-tripeptide, β^3hVal-β^3hAla-β^3hLeu, is functionalised at the *N* or *C* terminus with either the sulfur linker or the redox active group (Figure 4.8). Subsequent coupling of the two β-tripeptides, gives the fully functionalised hexapeptide. The resulting hexapeptide is insoluble in methanol, unlike the deprotected tripeptides and coupling reagents, allowing for efficient purification.

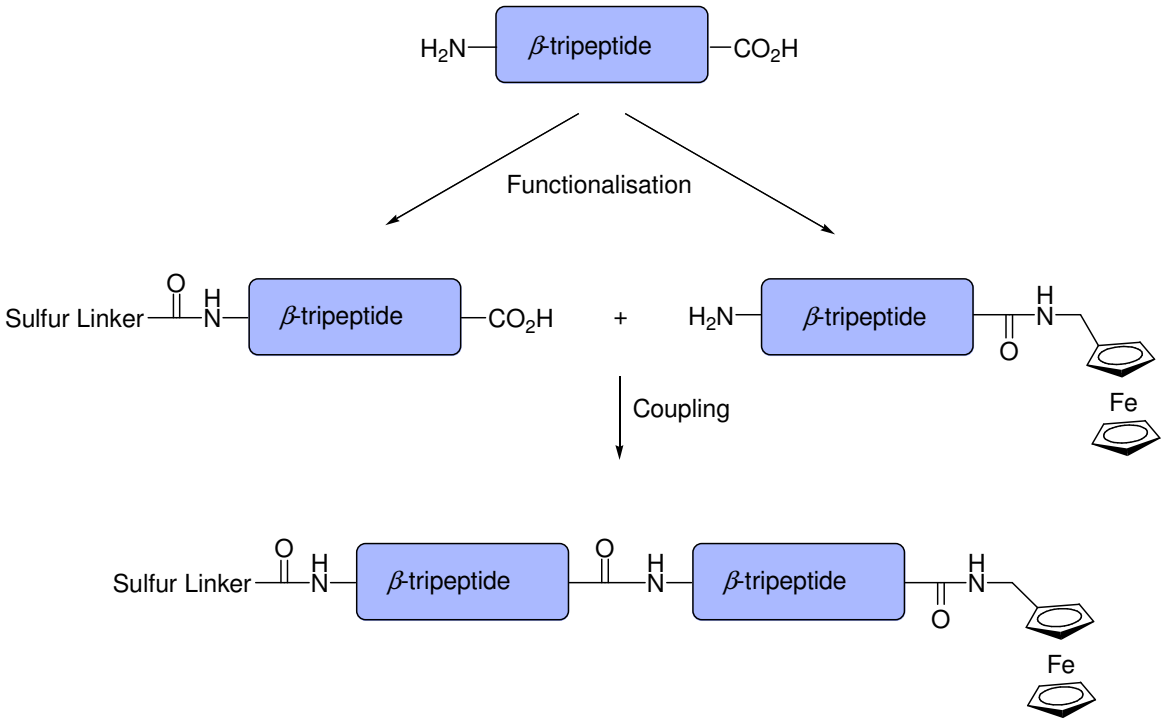

Figure 4.8 Schematic representation of functionalised β-tripeptide units that can be coupled together to form the β-hexapeptide.

This approach enables the synthesis of a range of functionalised hexapeptides by coupling together different combinations of functionalised tripeptides.

4.3 Synthesis of Model Compounds

The compatibility of various sulfur linkers and ferrocene with different protecting groups and conditions was first assessed by synthesising several model compounds. These studies are outline below.

4.3.1 Sulfur-containing Linker Molecules

A sulfur-containing linker is required to immobilise the β-peptide onto a gold surface. The linker acts as the molecular 'alligator clip', connecting the molecule to gold and allowing current to pass through it. There are many possible linkers capable of spontaneous immobilisation on gold, each with different synthetic compatibility. Some of the more common carboxylic acid linkers are shown in Figure 4.9. The simplest linkers *p*-mercaptobenzoic acid (**4.1**) and alkanethiol (**4.2**) (the latter commercially available in a range of different lengths) each contain a thiol group. The use of *p*-mercaptobenzoic acid (**4.1**) instead of alkanethiol (**4.2**) has benefits

because it is a better electron conductor, and has a rigid structure, both of which are useful properties for surface species. Thiol groups, which are nucleophilic, require additional protection and deprotection steps to mask the reactivity.

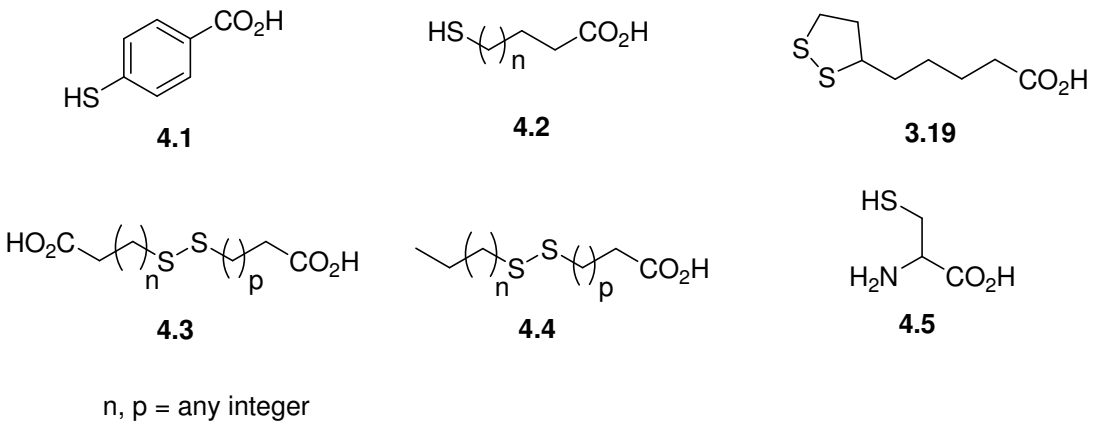

Figure 4.9 Sulfur-containing species suitable for spontaneous immobilisation on gold.

Disulfides (**3.19**, **4.3** and **4.4**) are commonly used as linkers because the disulfide bond spontaneously ruptures on contact with gold to form two adjacent gold-sulfur bonds. Furthermore, disulfides do not require the same protection/deprotection steps necessary with thiols. Disulfides include homodisulfides **4.3**, mixed disulfides **4.4** and lipoic acid (**3.19**). The homodisulfides, when assembled on gold, position both sulfur groups adjacent on the surface. This is undesirable for work described in this thesis, because it may lead to inadequate folding of the β-peptide (which would be attached the carboxylic acid group) or electron transfer between two closely assembled peptides due to surface crowding. Mixed disulfides such as **4.4** often contain a diluent such as an alkanethiol, and a carboxylic acid (or other group) for functionalization. However, the synthesis of mixed thiols is difficult as it results in a mixture of homo- and heterodisulfides. Lipoic acid (**3.19**) is a convenient linker because it contains an intramolecular disulfide, and therefore can immobilise on gold independent of other molecules, allowing for a more evenly spaced SAM.

Sulfur-containing amino acids, such as cysteine **4.5**, which may be already present in the peptide structure or can be inserted with only minimal structural effects, are convenient linkers for the immobilisation of very large peptides and proteins. However, immobilisation of helical peptides with cysteine is unlikely to result in a structure that is bound normal to the surface, because the thiol side chains lies perpendicular to the helix axis.

Linkers of the type **4.1**, **4.2** (**3.15**, where n = 13) and **3.19** were deemed most suitable for surface attachment of β-peptides in this research project (Figure 4.10). The use of a range of different linkers, coupled to the peptide through the *N*-terminus, allows for a comparison of the surface packing effects of the different species and the effect of the linker length on the rate of electron transfer (as described in Chapter Two).

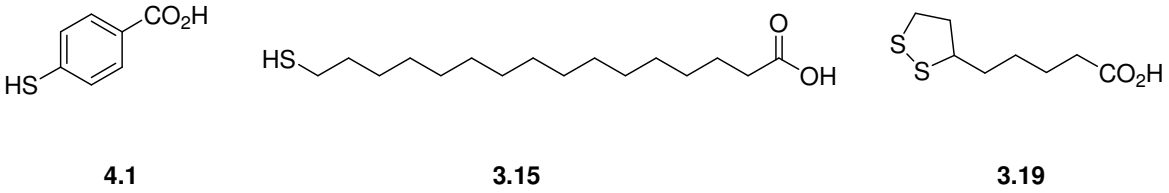

4.1 **3.15** **3.19**

Figure 4.10 Linkers considered suitable for the surface attachment of β-peptides to gold.

The sulfur linkers **3.15** and **4.1** were protected as the acetylthiol analogues **3.16** and **4.9** to mask the reactivity of the thiol group (Scheme 4.1). Protection of the thiol group prevents formation of thioesters, disulfides and other side products during the subsequent coupling steps.

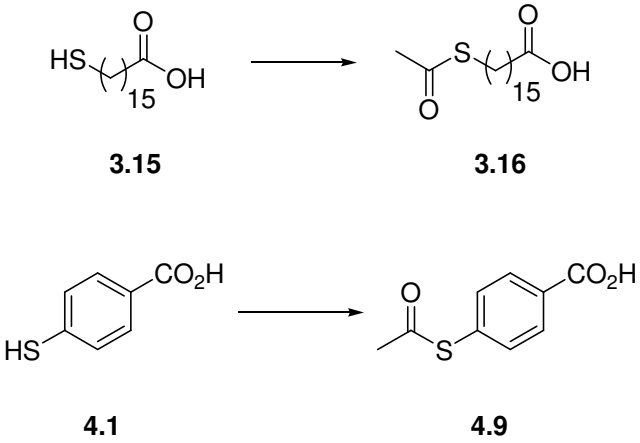

3.15 **3.16**

4.1 **4.9**

Scheme 4.1 *Reagents and conditions*: Zinc powder, acetic acid, DCM, rt, 15 min, then acetyl chloride, 0 ºC, 10 min, (**3.16**: 83% yield; **4.9**: 89% yield).

4.3.2 Synthesis of Amine-Terminated Linker 4.8

The β-hexapeptide **2.17** adopts a 3_{14}-helix, a secondary structure which possesses a dipole moment (Chapter One, Figure 1.8).[18] Watanabe *et al* showed that the dipole moment of α-helical peptides is important in determining the rate of electron transfer (Chapter Two, Table 2.3). Attachment of the sulfur linker to *C*-terminus (rather than the *N*-terminus) of the peptide changes the direction of the dipole with regard to the surface. Therefore, an amine-terminated linker **4.8** was synthesized for covalent attachment to the peptide, to probe the effect of the β-peptide dipole orientation on electron transfer (as discussed in Chapter Two).

The amine linker was synthesized in a two-step procedure from racemic lipoic acid **3.19** (Scheme 4.2). Reaction of the carboxylic acid group with ethyl chloroformate gave an activated ester which was treated with ammonia solution to give lipoamide (**4.6**) as a light yellow solid, in 82% yield. This was reacted with $LiAlH_4$, which reduced both the amide and disulfide groups to give compound **4.7**. Oxidation of the sulfhydryl groups to the disulfide by stirring in mildly acidic solution with atmospheric O_2 for 24 h gave the lipoamine (**4.8**) as a pale yellow solid in 28% yield over two steps.

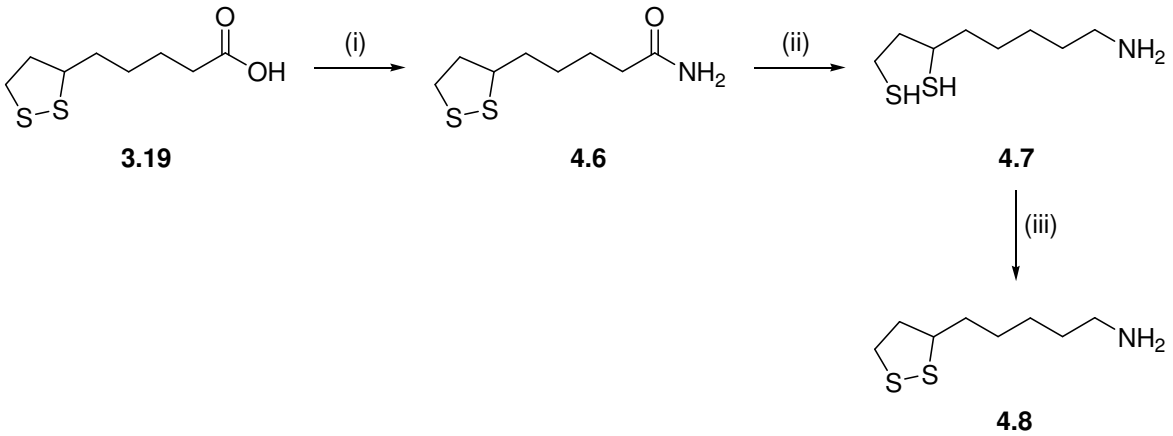

3.19 **4.6** **4.7** **4.8**

Scheme 4.2 *Reagents and conditions:* (i) Ethyl chloroformate, triethylamine, THF, 0 ºC, 30 min, then NH_4OH, rt, 1 h, 82% yield, (ii) $LiAlH_4$, THF, 70 ºC, 16 h, then H_2O, 0 ºC, 30 min, (iii) pH 6.5 (HCl), H_2O, air, rt, 24 h, 28% yield (steps (ii) and (ii)).

4.3.3 Incompatibility of the Sulfur Linkers with Carboxylic Acid Protecting Groups

A particular difficulty in synthesizing sulfur-containing compounds is the undesirable reactivity of the sulfur group towards many standard reaction conditions. The deprotection steps of peptide carboxylic acid protecting groups, the methyl and benzyl esters, proved incompatible with the sulfur-containing linkers **4.9**, **3.16** and **3.19**.

Coupling of the linker **3.16** with tripeptide **4.10** to give the functionalised tripeptide **4.11** required both the thiol group of the linker and the *C*-terminus of the peptide to be protected to avoid the formation of undesired side products. However, the cleavage of the methyl ester protecting group of the functionalised tripeptide **4.11** during the attempted synthesis of **AcSC$_{15}$$\beta_6$Fc** (**2.12**) proved to be problematic (Scheme 4.3). Hydrolysis of the methyl ester of **4.11** to give free acid **4.12** (for a subsequent coupling reaction) under basic conditions resulted in the partial cleavage of both the methyl ester and acylated thiol. This gave a mixture of protected and deprotected acetyl thiols and disulfides.

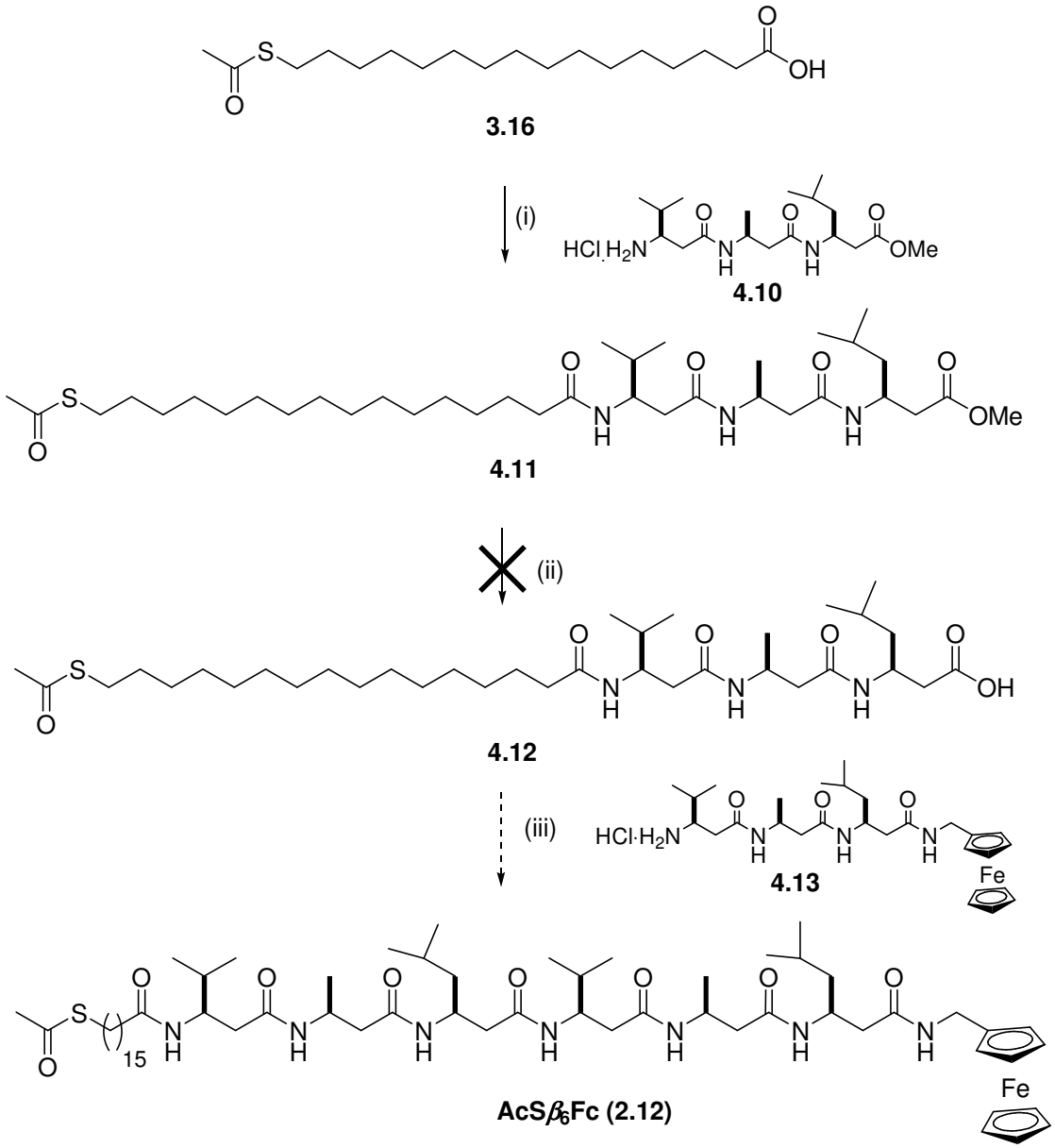

Scheme 4.3 *Reagents and conditions:* (i) HATU, DIPEA, DMF, rt, 16 h, 76% yield, (ii) LiOH, THF, H_2O, rt, 2 h.

The difficulties involved in the deprotection of the methyl esters of **4.11** led to the attempted use of a benzyl ester protecting group, which does not require cleavage under basic conditions. Coupling of acetyl thiol **4.9** and TFA·β^3hAla-OBn using HATU gave the amide **4.14** (Scheme 4.4). However, subsequent attempted benzyl ester deprotection with H_2 and Pd/C returned only starting material **4.14** (instead of free acid **4.15**). It is reported that sulfur species act as poisons to many hydrogenation catalysts, so it seems likely that the acetyl-protected sulfur group is incompatible with the Pd catalyst.[23]

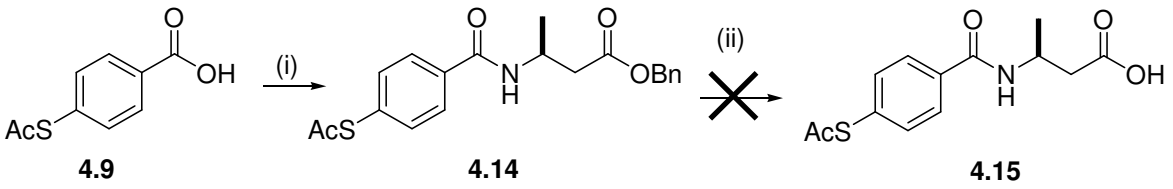

4.9 **4.14** **4.15**

Scheme 4.4 *Reagents and conditions:* (i) TFA·β^3hAlaOBn, HATU, DIPEA, DMF, rt, 16 h, 82% yield, (ii) Pd/C, H_2, MeOH, rt, 16 h.

Similar problems were encountered with disulfide linker **3.19**. Hydrolysis of methyl ester **4.16** under basic conditions with LiOH gave the carboxylic acid **4.17** in only 11% yield (Scheme 4.5). Hydroxide ions can oxidatively cleave disulfide bonds, giving an unstable sulfenic acid group and a thiol; this free thiol can then react to form a disulfide bond with another thiol, giving undesirable by-products.

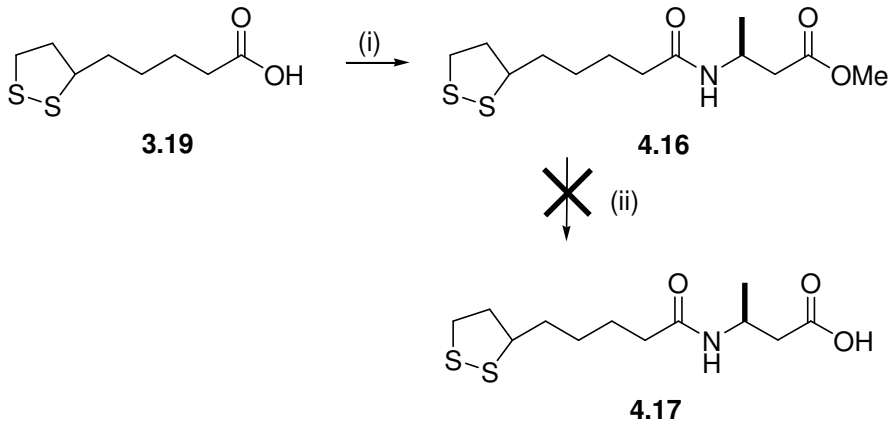

3.19 **4.16** **4.17**

Scheme 4.5 *Reagents and conditions:* (i) TFA·β^3hAlaOMe, HATU, DIPEA, DMF, 16 h, 79% yield, (ii) LiOH, THF, H_2O, 16 h, 11% yield.

Similarly, hydrogenation of a benzyl ester with Pd/C is not compatible with a disulfide group (Scheme 4.6). Coupling lipoic acid (**3.19**) and TFA·β^3hAlaOBn gave benzyl ester **4.18** in 95% yield. However, hydrogenation of **4.18** with Pd/C under H_2 gave an intractable mixture, instead of deprotected product **4.19**. Again, it was assumed that the disulfide bond was acting as a catalyst poison.

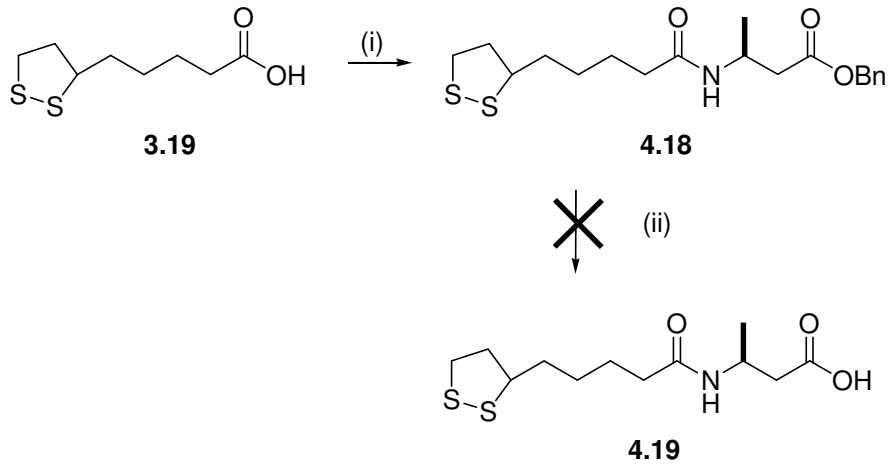

Scheme 4.6 *Reagents and conditions:* (i) TFA·β^3hAlaOBn, HATU, DIPEA, DMF, 16 h, 95% yield, (ii) Pd/C, H_2, MeOH, 16 h.

4.3.4 Synthesis and Reactions of Succinimide-Activated Linkers 4.20 and 4.22

A method involving the pre-activation of the acid terminus with *N*-hydroxysuccinimide was used in order to avoid the problematic deprotection step at the *C*-terminus of the tripeptide. The resulting succinimide ester intermediate only reacts with the *N*-terminus of a fully-deprotected amino acid or peptide (Scheme 4.7). Furthermore, succinimide esters are stable enough to isolate and purify using standard chromatography techniques. Using this methodology, lipoic acid (**3.19**) was coupled with *N*-hydroxysuccinimide, using EDCI and HOBT, to give the succinimide-activated ester **4.20**. Subsequent nucleophilic substitution with HCl·Ala-OH in mildly basic (pH 8-9) conditions gave the amide **4.21** in 77% yield.

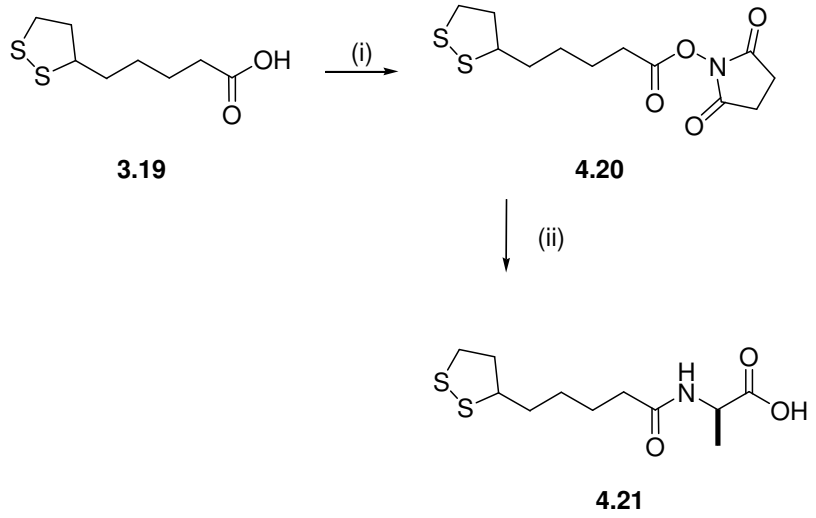

Scheme 4.7 *Reagents and conditions:* (i) *N*-hydroxysuccinimide, EDCI, HOBT, DIPEA, THF, rt, 24 h, 89% yield, (ii) HCl·AlaOH, Et_3N, THF, H_2O, rt, 16 h, 77% yield.

The same methodology was applied to the acetyl thiol **3.16** to give the succinimide-activated ester **4.22** (Scheme 4.8). This approach was mild enough to successfully prepare the functionalised tripeptide **4.12** from the linker **4.22** and *β*-tripeptide **4.23**, without cleavage of the acetyl group.

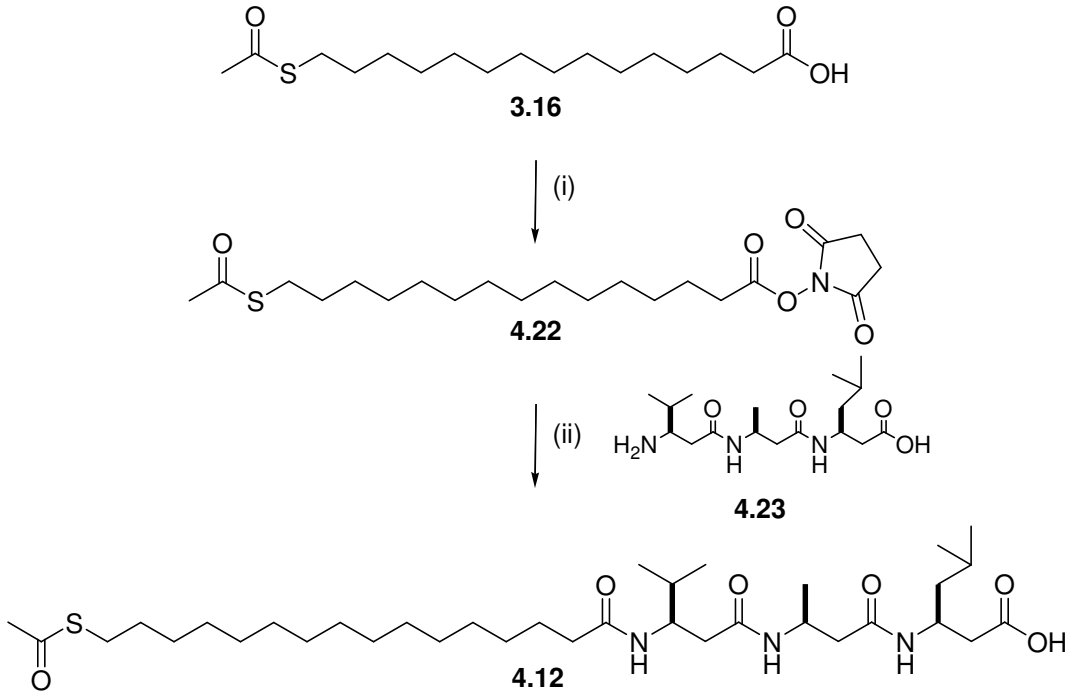

Scheme 4.8 *Reagents and conditions:* (i) NHS, EDCI, DCM, rt, 16 h, 87% yield, (ii) Et_3N, THF, H_2O, rt, 16 h, 45% yield.

4.3.5 Ferrocene-containing Compounds

Ferrocene groups were used as redox probes for electrochemical analysis of the peptides (see Chapter Two). Commercially available ferrocene acetic acid and ferrocene carboxylic acid (**3.5** and **4.24**, respectively) were suitable for coupling to the *N*- terminus of the peptides, through an amide linkage. Because the ferrocene complex is electron donating, and therefore deactivates an adjacent carbonyl centre, the acetic acid **3.5** was chosen over the carboxylic acid **4.24**.

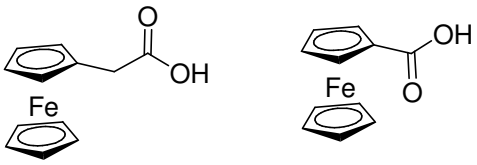

3.5 **4.24**

Ferrocene methyl amine (**4.27**) was identified as a suitable compound for coupling to the acid terminus of the peptide. The amine **4.27** was synthesized from ferrocene carboxadehyde (**4.25**) in two steps (Scheme 4.9) beginning with the condensation reaction of the aldehyde with hydroxylamine hydrochloride gave the aldoxime **4.26** as a brown solid, in 97% yield. Subsequent reduction of the oxime using LiH in THF afforded the desired amine **4.27** as a brown oil, in 78 % yield.

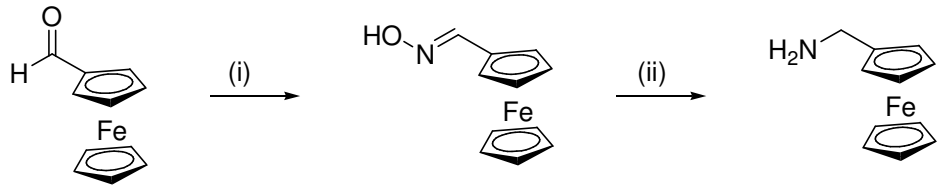

4.25 **4.26** **4.27**

Scheme 4.9 *Reagents and conditions:* (i) hydroxylamine hydrochloride, sodium acetate, H_2O, ethanol, N_2, Δ, 3 h, 97% yield, (ii) LiH, THF, N_2, 14 h, 76% yield.

4.3.6 Synthesis of Linker-Ferrocene Model Compounds 3.21 and 2.18

The 16-mercaptohexadecanoic acid (**3.16**), lipoic acid (**3.19**) and *p*-mercaptobenzoic acid (**4.9**) linkers were coupled with ferrocene amine **4.27** (Scheme 4.10-Scheme 4.12) to determine the compatibility of the sulfur groups with ferrocene, and to produce model compounds for electroanalysis (see Chapter Two and Three).

The acetyl-protected mercaptohexadecanoic acid **3.16** was coupled with ferrocene methyl amine (**4.27**) using HATU to give the ferrocenyl amide **4.28** in 82 % yield (Scheme 4.10). Deprotection of the acetyl group with sodium thiomethoxide under basic, O_2 free conditions gave the free thiol **2.18** in 87 % yield.

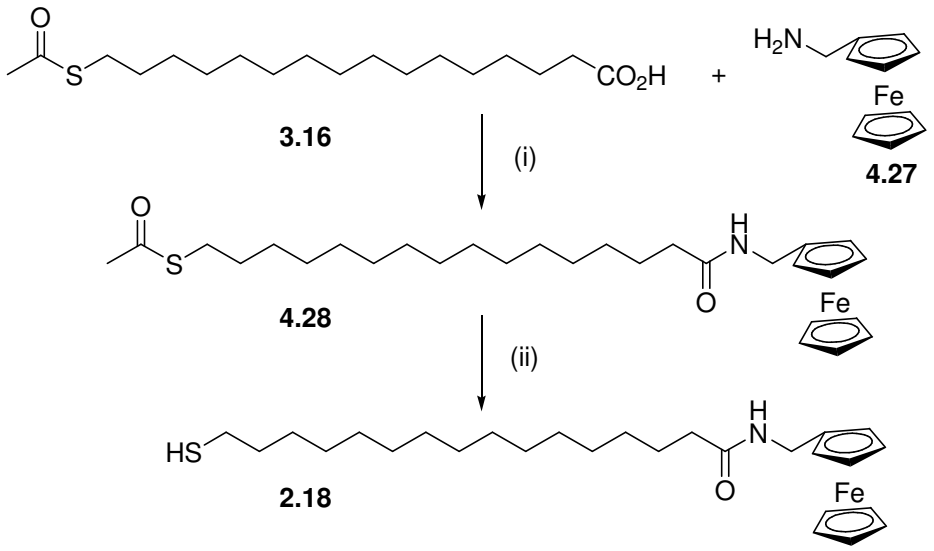

Scheme 4.10 *Reagents and conditions:* (i) **4.27**, HATU, DIPEA, DMF, rt, 16 h, 80% yield, (ii) sodium thiomethoxide, methanol, DCM, N_2, 30 min, 87% yield.

Similarly, coupling racemic lipoic acid (**3.19**) with ferrocene methyl amine (**4.27**) using HATU gave the ferrocene amide **3.21** in 56 % yield (Scheme 4.11). Despite the presence of both the reducing ferrocene group and the oxidising disulfide group, **3.21** was stable at room temperature.

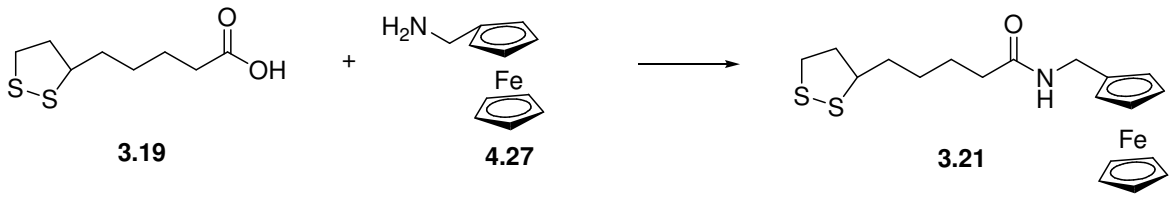

Scheme 4.11 *Reagents and conditions:* Ferrocene methyl amine, HATU, DIPEA, DMF, rt, 16 h, 56% yield.

The attempted synthesis of a ferrocenyl derivative of *p*-mercaptobenzoic acid (**4.29**) is shown in Scheme 4.12. The coupling of linker **4.9** with ferrocene methyl amine (**4.27**) using HATU failed to give the desired amide **4.29**. Instead, the moderate basicity of the ferrocene methylamine cleaved the acetyl protecting group to give the free thiol, which dimerised to give disulfide **4.30**. The increased reactivity of the acetyl group of the benzoic acid linker to cleavage, compared to the alkyl linker **3.16**, is due to the electronic withdrawing effects and resonance stabilisation of the aromatic ring. Unfortunately the incompatibility of linker **4.9** with amines precluded its further use.

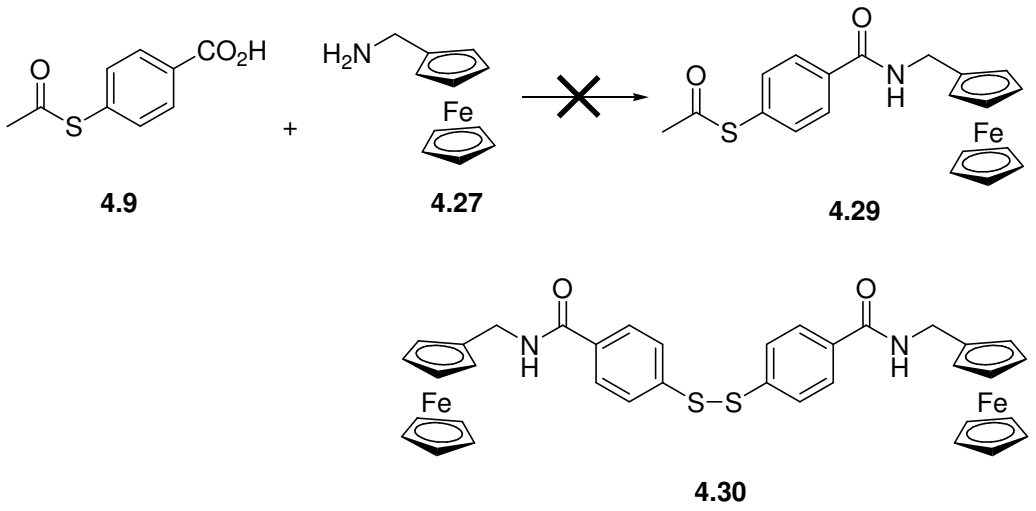

4.9 **4.27** **4.29**

4.30

Scheme 4.12 *Reagents and conditions:* **4.27**, HATU, DIPEA, DMF, rt, 16 h.

4.4 Synthesis of β-Peptides

4.4.1 Synthesis of β^3-Amino Acid Monomers

β^3-Amino acids are readily prepared from the α-amino acid precursors by *Arndt-Eistert* homologation. This method leaves the stereocenter at the α-carbon intact and formally inserts a CH_2 group into the amino acid backbone. Boc-(*S*)-β^3hAla-OMe, Boc-(*R*)-β^3hVal-OMe* and Boc-(*S*)-β^3hLeu-OMe were prepared in this way from α-amino acids Boc-(*S*)-Val-OH, Boc-(*S*)-Ala-OH and Boc-(*S*)-Leu-OH (Scheme 4.13). The α-amino acids **4.31a-c** were reacted with ethyl chloroformate to give the activated esters. The subsequent nucleophilic attack of diazomethane (added as an ethereal solution) at the activated carbonyl centres, afforded the diazoketones **4.32a-c**. The silver benzoate catalysed Wolff rearrangement of the diazoketones in MeOH, driven by the loss of N_2, gave the β-amino esters **4.33a**, **4.33b** and **4.33c**.

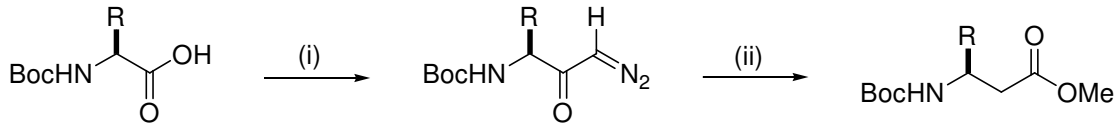

4.31a R= CH_3	**4.32a** 70% yield	**4.33a** 72% yield
4.31b R=$CH(CH_3)_2$	**4.32b** 56% yield	**4.33b** 78% yield
4.31c R=$CH_2CH(CH_3)_2$	**4.32c** 73% yield	**4.33c** 87% yield

Scheme 4.13 *Reagents and conditions:* (i) Ethyl chloroformate, Et_3N, THF, 30 min, -30 ºC, then CH_2N_2 in Et_2O, rt, 3 h, (ii) silver benzoate, methanol, Et_3N, THF, -15 ºC - rt, 3 h.

* Note that the change in stereochemical assignment from (S) to (R) occurs only in β^3Val as a result of the change in priority of the groups around the stereocentre.

4.4.2 Synthesis of β-Tripeptide 4.39

Peptide coupling of the β^3hVal, β^3hAla and β^3hLeu monomers gave the Boc-(*R*)-β^3hVal-(*S*)-β^3hAla-(*S*)-β^3Leu-OMe tripeptide (**4.39**), used in later functionalisation and synthesis of a range of hexapeptides. Synthesis of the β^3-tripeptide began with the hydrolysis of the methyl ester of Boc-(*R*)-β^3hVal-OMe **4.33b** under basic conditions with LiOH to give the free acid **4.34** in quantitative yield (Scheme 4.14). Concurrently, deprotection of the Boc protecting group of Boc-(*S*)-β^3hAla-OMe (**4.33a**) with trifluoroacetic (TFA) acid gave the free amine **4.35** as the TFA salt, in quantitative yield. Coupling of the deprotected acid and amine groups with HATU afforded the β-dipeptide **4.36** in 82% yield.

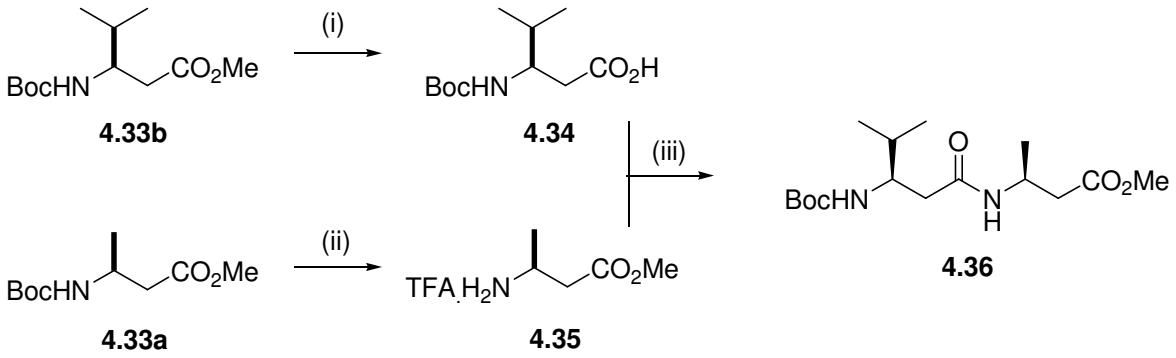

Scheme 4.14 *Reagents and conditions:* (i) LiOH, THF, H_2O, 16 h, 98% yield, (ii), TFA, DCM, 16 h, quant. yield, (iii) HATU, DIPEA, DMF, 16 h, 83% yield.

Hydrolysis of the dipeptide **4.36** under basic conditions gave the free acid **4.37**. Removal of the Boc group from **4.33c** with TFA gave the free amine **4.38** as the TFA salt (Scheme 4.15). Coupling the deprotected intermediates with HATU afforded the β-tripeptide **4.39** in 93% yield.

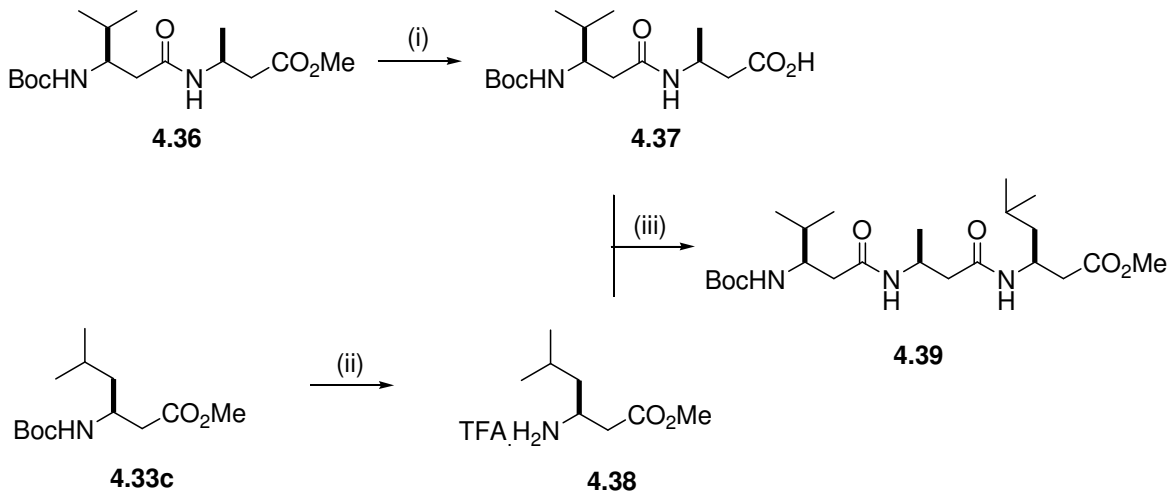

Scheme 4.15 *Reagents and conditions:* (i) LiOH, THF, H_2O, rt, 16 h, 75% yield, (ii) TFA, DCM, rt, 16 h, quant. yield, (iii) HATU, DIPEA, DMF, rt, 16 h, 93% yield.

4.4.3 Synthesis of the β-Hexapeptide 2.17

The literature hexapeptide HCl·[(*R*)-β^3hVal-(*S*)-β^3hAla-(*S*)-β^3Leu]$_2$-OMe **2.17** was synthesized according to Scheme 4.16. The CD spectrum and NMR studies of peptide **2.17** are published in the literature.[6] Peptide **2.17** was used both to compare and to validate the CD spectra and 2D NMR studies of the linker- and ferrocene-functionalized β-peptides, as described in section 4.5.

The β-tripeptide **4.39** was deprotected at either the N- or C-terminus to give free amine **4.10** and free acid **4.40**. Coupling of the two tripeptides using HATU afforded the protected β-hexapeptide **4.41** in 68% yield.

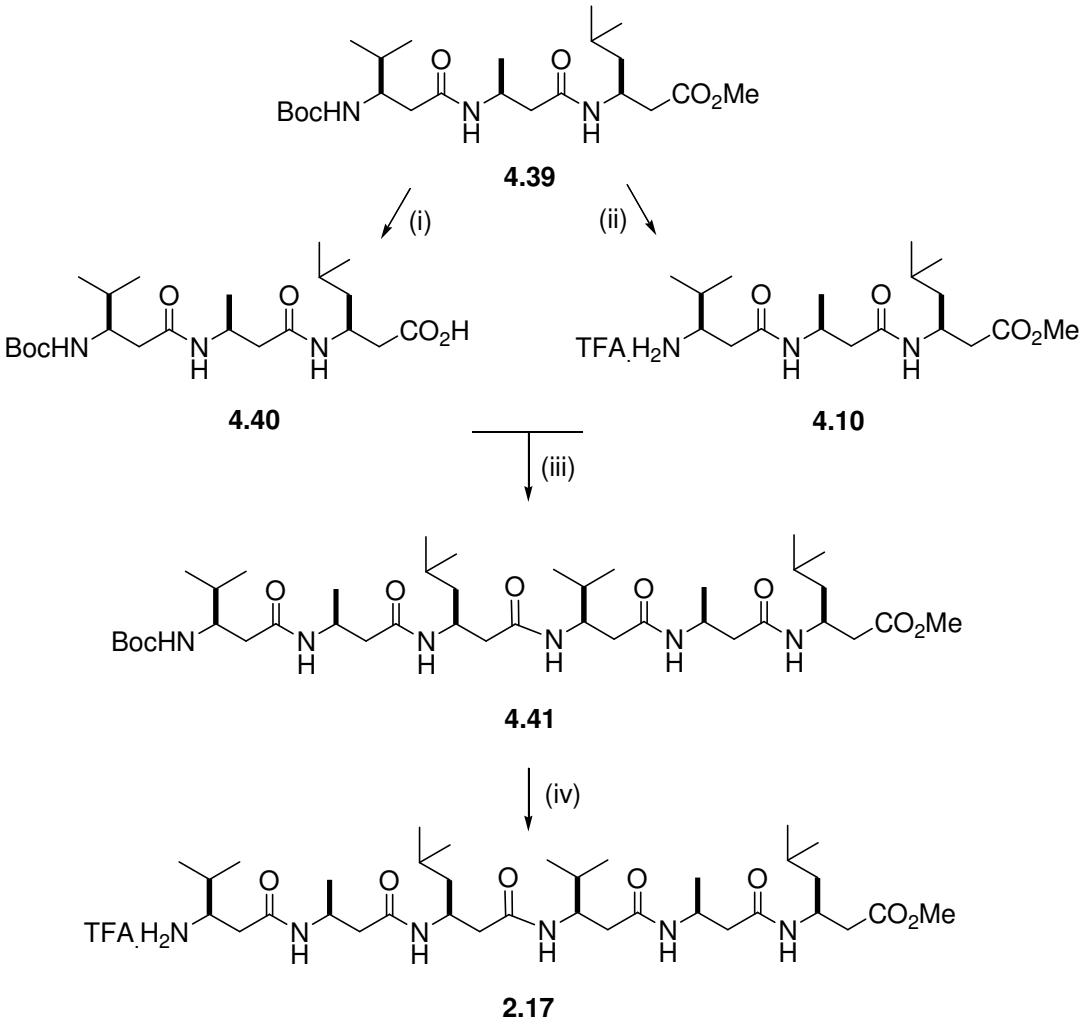

Scheme 4.16 *Reagents and conditions:* (i) LiOH, THF, H_2O, rt, 16 h, quant. yield, (ii) TFA, DCM, rt, 16 h, quant. yield, (iii) HATU, DIPEA, DMF, rt, 16 h, 93% yield, (iv) TFA, rt, 2 h, quant. yield.

The solubility properties of the hexapeptide **4.41** differed markedly from the deprotected tripeptides **4.10** and **4.40**. This allowed for an efficient purification of the product **4.41** by filtration, after first removing the solvents *in vacuo*, and sonicating the resulting residue in methanol. The coupling reagents, by-products and unreacted tripeptides were all soluble in the methanol, while the hexapeptide was not. The hexapeptide was solubilised in 2,2,2-trifluoroethanol. Deprotection of the Boc group with TFA gave the methanol-soluble amine salt **2.17**.

4.4.4 Synthesis of Functionalised Tripeptides

Functionalisation at the N-terminus

Scheme 4.17 shows the synthesis of sulfur-linker terminated *β*-tripeptides **4.12** and **4.42** for incorporation into hexapeptides such as **SSβ_6Fc** and **SC$_{15}\beta_6$Fc** (presented in Chapter Two). The sulfur linker was coupled using the methodology described in section 4.3.3, whereby the linker was first activated with *N*-hydroxysuccinimide to give the succinimidyl ester, which was then displaced by a free amine group. The tripeptide free-acid **4.40** was deprotected using trifluoroacetic acid to give the fully-deprotected peptide **4.23**. Reaction of this compound with succinimide-activated linkers **4.20** and **4.22** in a THF/water mixture gave **4.42** and **4.12** in 75 and 81% yield, respectively.

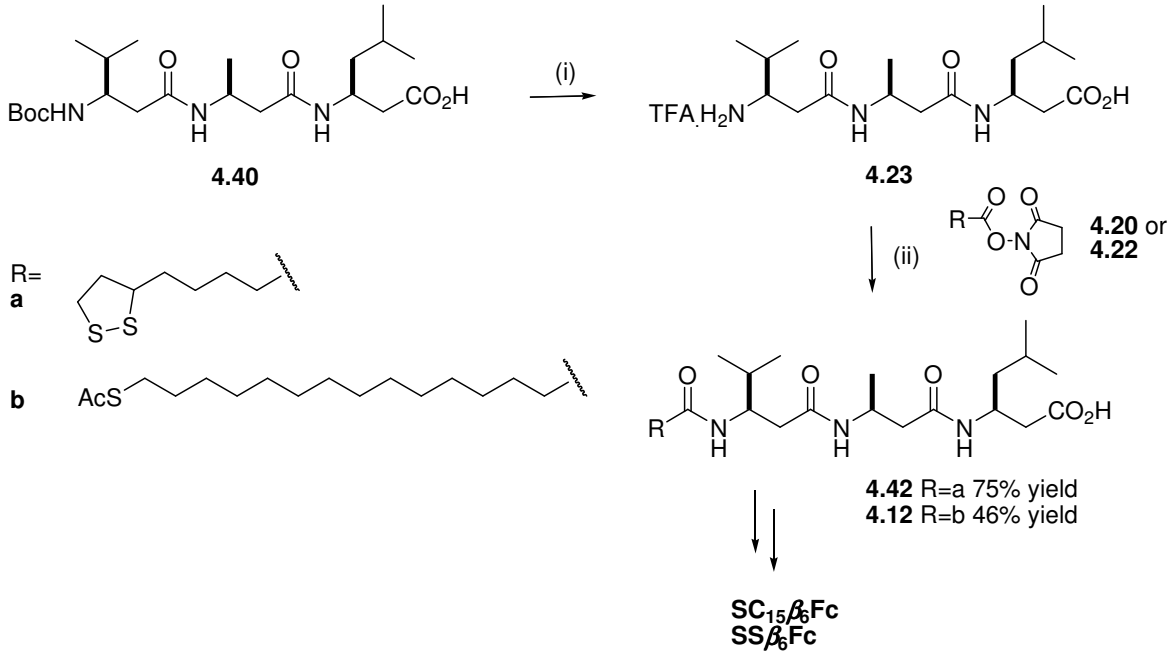

Scheme 4.17 *Reagents and conditions:* (i) TFA, DCM, rt, 16 h, quant.yield, (ii) **4.20** or **4.22** ; Et_3N, THF, H_2O, rt, 16 h.

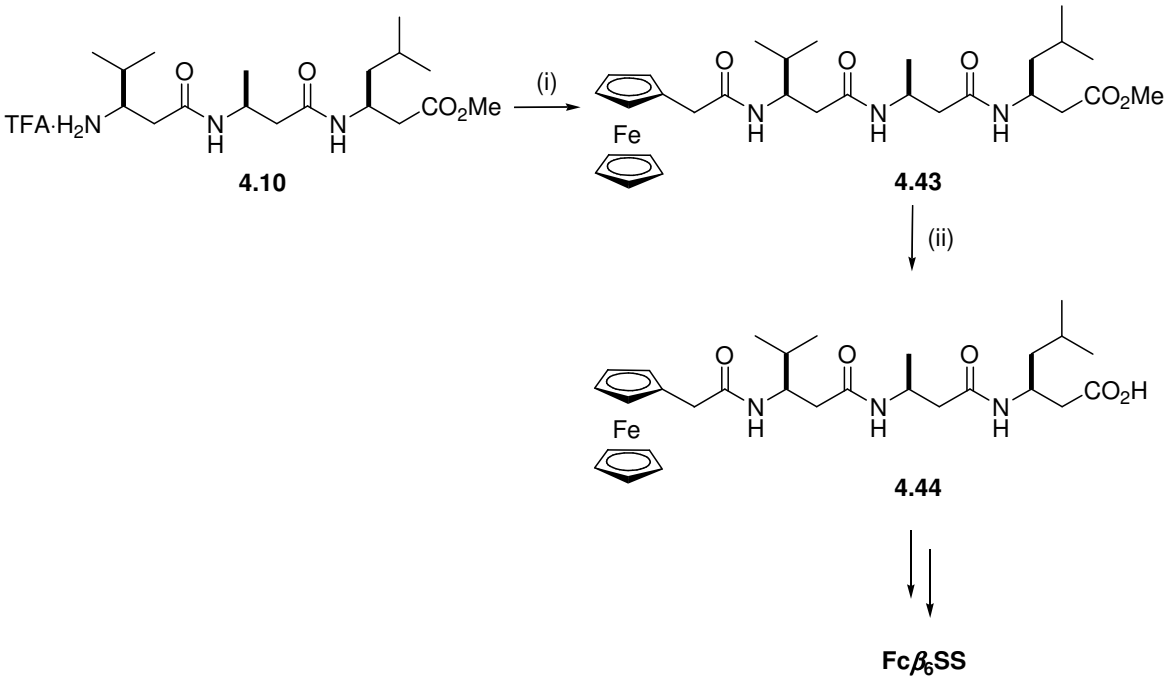

Scheme 4.18 *Reagents and conditions:* (i) ferroceneacetic acid, HATU, DIPEA, DMF, rt, 16 h, 71% yield, (ii) LiOH, THF, H_2O, rt, 4 h, 89% yield.

The synthesis of the ferrocene-*N*-terminated tripeptide **4.44** is shown in Scheme 4.18. This tripeptide (which has the ferrocene group attached to the N-terminus of the peptide) was synthesized for incorporation in the 'reversed dipole' hexapeptide **Fcβ_6SS**, (see chapter two). Coupling of the deprotected tripeptide **4.10** and ferrocene acetic acid with HATU gave the ferrocenyl peptide **4.43** in 71% yield. Hydrolysis of the methyl ester under basic conditions with LiOH gave the free acid **4.44** in quantitative yield.

Functionalisation at the C-terminus

The partially deprotected tripeptide **4.40**, was coupled with the relevant nucleophile to give a series of *C*-terminus functionalised peptides (Scheme 4.19). The coupling of redox active ferrocene methylamine (**4.27**) with tripeptide **4.40** afforded the ferrocenyl amide **4.45**, in 49% yield. Additionally, ethyl amine and 9-decen-1-ol groups were coupled to tripeptide **4.40** to give the ethyl amide **4.46** and the ester **4.47**. The ethyl amide **4.46** was synthesized for incorporation into the hexapeptide **SSβ_6Et** (a model compound without a redox active moiety, Chapter Two). The ester **4.47** was synthesized for incorporation into a hexapeptide as a possible surface-immobilised olefin suitable for cross metathesis (CM) (see Chapter Three). Finally, lipoamine (**4.8**) was coupled to tripeptide **4.40** to give amide **4.48**, used in the synthesis of the reversed-dipole hexapeptide **Fcβ_6SS**.

Deprotection of the ethyl amide **4.46** with trifluoroacetic acid gave the free amine **4.50** in quantitative yield. However, ferrocene, disulfide groups and some alkenes are not stable in the presence of trifluoroacetic acid, due to its moderate oxidising ability. Accordingly, compounds **4.45, 4.47** and **4.48**, were deprotected using 4 M hydrogen chloride in dioxane. The ferrocene group of tripeptide **4.45** was protonated the acidic deprotection, giving a green compound. The compound, dissolved in methanol, was passed through an alumina plug, to deprotonate the ferrocene species, giving the desired compound **4.49** as a yellow solid.

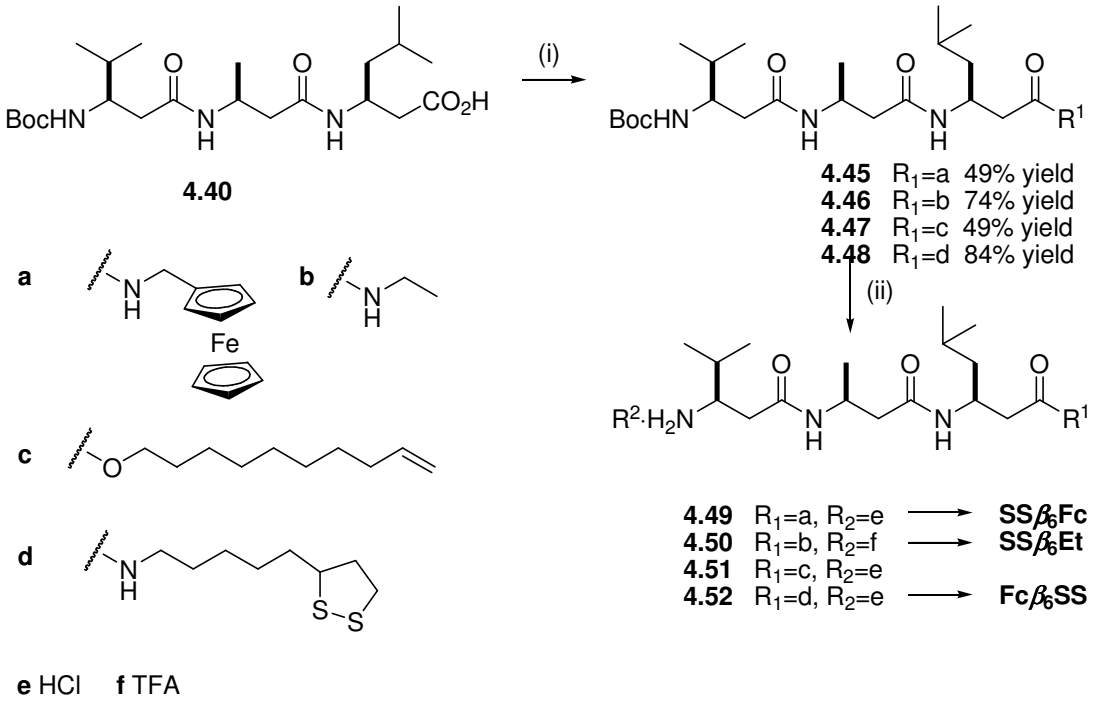

Scheme 4.19 *Reagents and conditions:* **4.8**, **4.27**, ethylamine hydrochloride, or 9-decen-1-ol; HATU, DIPEA, DMF, rt, 16 h, (ii) 4 M HCl, dioxane, TFE, 10 min, or TFA, DCM, 16 h.

Functionalisation at Both Termini

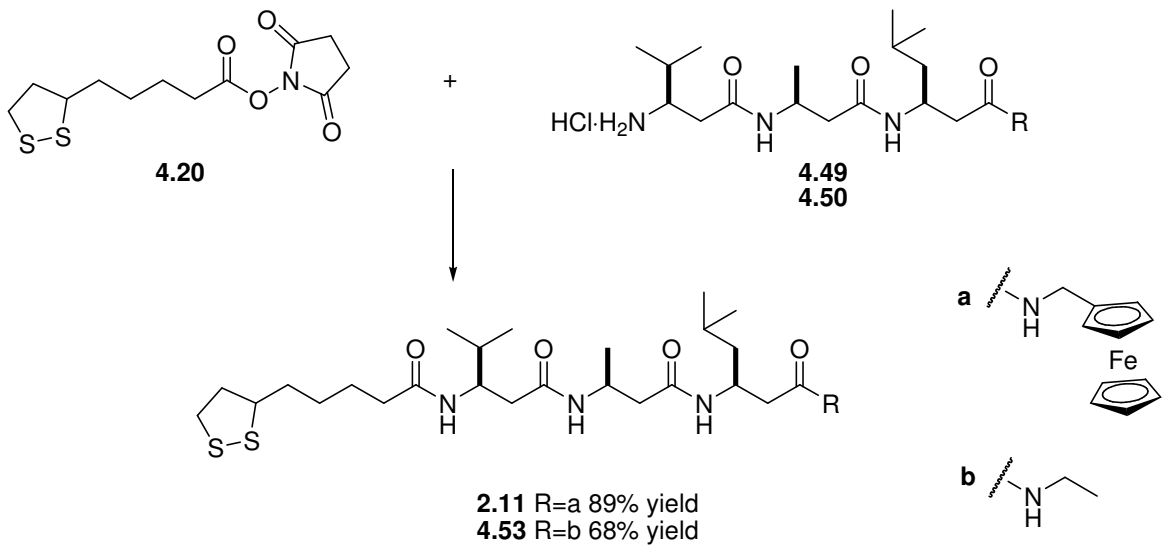

Scheme 4.20 *Reagents and conditions*: Et_3N, DMF, rt, 16 h.

A functionalised tripeptide **SSβ_3Fc** (**2.11**) was synthesised for electron transfer studies (as outlined in Chapter Two). An ethyl amide terminated analogue **4.53** was also synthesised, as a possible diluent for **2.11** in future electrochemical studies. The two functionalised tripeptides were synthesised by coupling *N*-hydroxysuccinimide-activated lipoic acid (**4.20**) with deprotected tripeptides **4.49** and **4.50** in the presence of triethylamine.

4.4.5 Synthesis of Functionalised Hexapeptides

Eight functionalised hexapeptides were synthesized with a sulfur linker, ferrocene group or both, by coupling different combinations of *N* and *C*-functionalised tripeptides. Eight β-hexapeptides were synthesized by coupling two appropriately deprotected tripeptides with HATU (Scheme 4.21), four of which (**2.13** (**SSβ_6Fc**), **2.15** (**SSβ_6Et**) **4.57** (the acetyl protected analogue of **SC$_{15}\beta_6$Fc**) and **Fcβ_6SS** (**2.14**)) were used in electrochemical studies described in Chapter Two. The peptides were not soluble in H_2O, acetonitrile or MeOH, which precluded purification by HPLC. However, adequate purification was achieved by filtration from methanol (as described for the synthesis of peptide **4.41**), followed by chromatography on lipophilic Sephadex resin, eluting with gradients of methanol/2,2,2-trifluoroethanol.

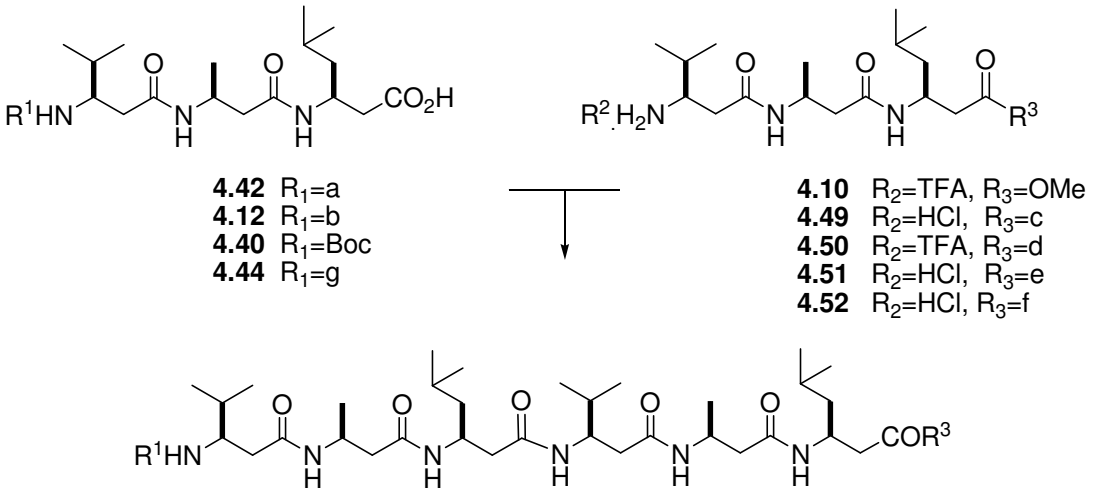

Scheme 4.21 *Reagents and conditions:* HATU, DIPEA, DMF, rt, 16 h.

Hexapeptide	R^1	R^3	Yield (%)
2.15 (**SSβ_6Et**)	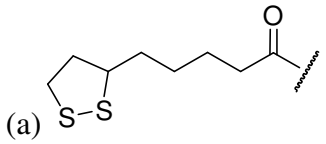 (a)	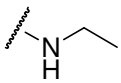 (d)	41
4.54		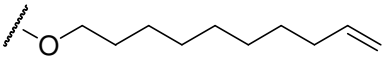 (e)	66
4.55		OMe	79
2.13 (**SSβ_6Fc**)		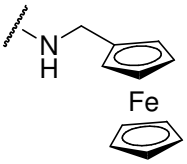 (c)	71
4.56	Boc		85
4.57	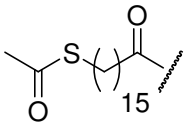 (b)		74
4.58		OMe	63
2.14 (**Fcβ_6SS**)	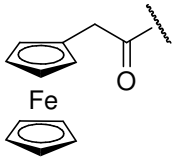 (g)	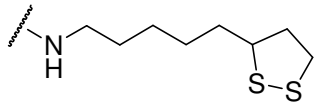 (f)	64

The four hexapeptides which contained the disulfide linker **3.19**, were synthesized with a variety of C-terminal groups:

(1) Hexapeptide **2.13** (**SSβ_6Fc**) contained the redox active ferrocene moiety;
(2) Hexapeptide **2.15** (**SSβ_6Et**) has a terminal ethyl amide group for use as a possible diluent of **2.13**, and as a comparison of electron transfer in peptides with and without ferrocene groups (see chapter two);
(3) Hexapeptide **4.54**, containing an olefin-terminated ester group, for functionalisation using cross metathesis (see chapter three);
(4) And hexapeptide **4.55**, a methyl ester terminated peptide for structural studies.

Two hexapeptides (**4.57**, the acetyl protected analogue of **SC$_{15}\beta_6$Fc**; and **4.58**) containing the acetyl protected hexadecanethiol linker **3.16** were synthesized. Peptide **4.57** contained a terminal ferrocene moiety, and peptide **4.58** had a methyl ester group at the *C*-terminus as possible diluent. Peptide **4.56** had no sulfur linker, instead it was protected at the N terminus with a Boc group, and contained a ferrocene group at the C terminus. This peptide was used to probe the secondary structural effects of ferrocene on the β-peptides (described in section 4.5).

Finally, hexapeptide **Fcβ_6SS** (**2.14**) was synthesized with reversed linker and ferrocene connectivity compared with the other redox active peptides (see Chapter Two). This variation was included to compare the effect of β-peptide dipole on electron transfer.

Deprotection of Peptide 4.57

The insolubility of peptide **4.57** precluded deprotection of the acetyl group using sodium thiomethoxide in methanol, as shown earlier (Scheme 4.10). Furthermore, isolation and purification of the resulting free thiol would be difficult due to the poor solubility of the peptide in most solvents, which would not greatly improve upon deprotection. The most efficient method was to deprotect the peptide in the presence of the gold surface, where it would rapidly become immobilised to form a SAM (Scheme 4.22). This was achieved by dissolving peptide **4.57** in 2,2,2-trifluoroethanol containing aqueous ammonia solution under a nitrogen atmosphere (to prevent disulfide formation) in the same vessel as a gold electrode. The free thiol spontaneously formed a peptide monolayer, removing the need for purification.

Electrochemical analysis of the resulting monolayer is presented in Chapter Two.

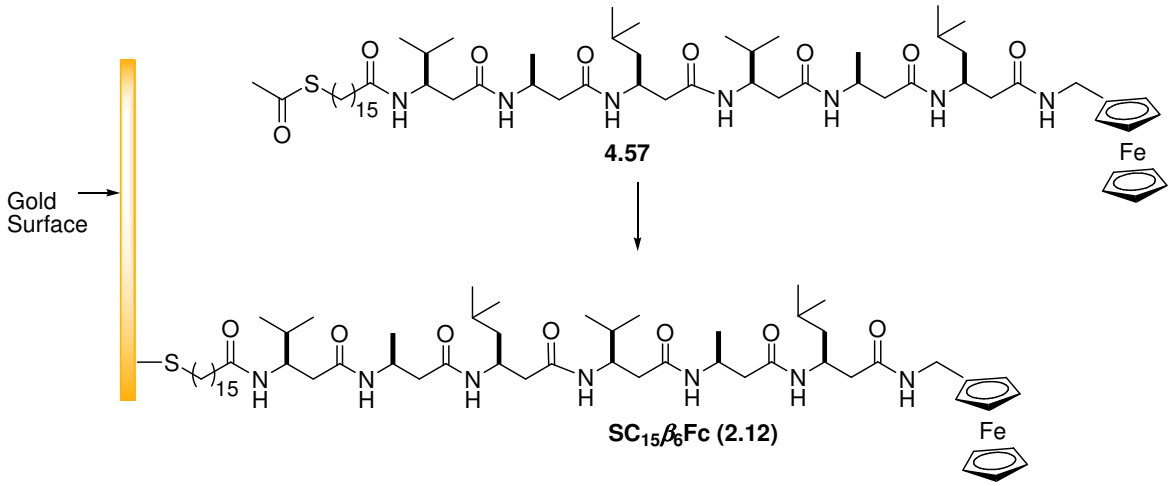

Scheme 4.22 *Reagents and conditions:* NH_3 (aq), 2,2,2-trifluoroethanol, gold surface, N_2, 16 h.

Deprotection and Purification of Peptide 4.56

As most 2D NMR and CD studies of β-peptides are performed in methanol, a methanol-soluble peptide was required. Fully functionalised peptides (such as those in Scheme 4.21) are not soluble in methanol. The ferrocenyl peptide **4.56** was synthesized to study the effects of the ferrocene moiety on the helical secondary structure of the β-peptides, as it is easily converted into the methanol-soluble hexapeptide **4.60**. Cleavage of the Boc group of **4.56** with 4 M HCl/dioxane in 2,2,2-trifluoroethanol gave the protonated ferrocenyl peptide **4.59** as a green solid. The ferrocene group was deprotonated by passing the peptide through alumina, yielding **4.60** as a yellow solid. Peptide **4.60** was soluble in methanol, and therefore suitable for further purification and structural analysis.

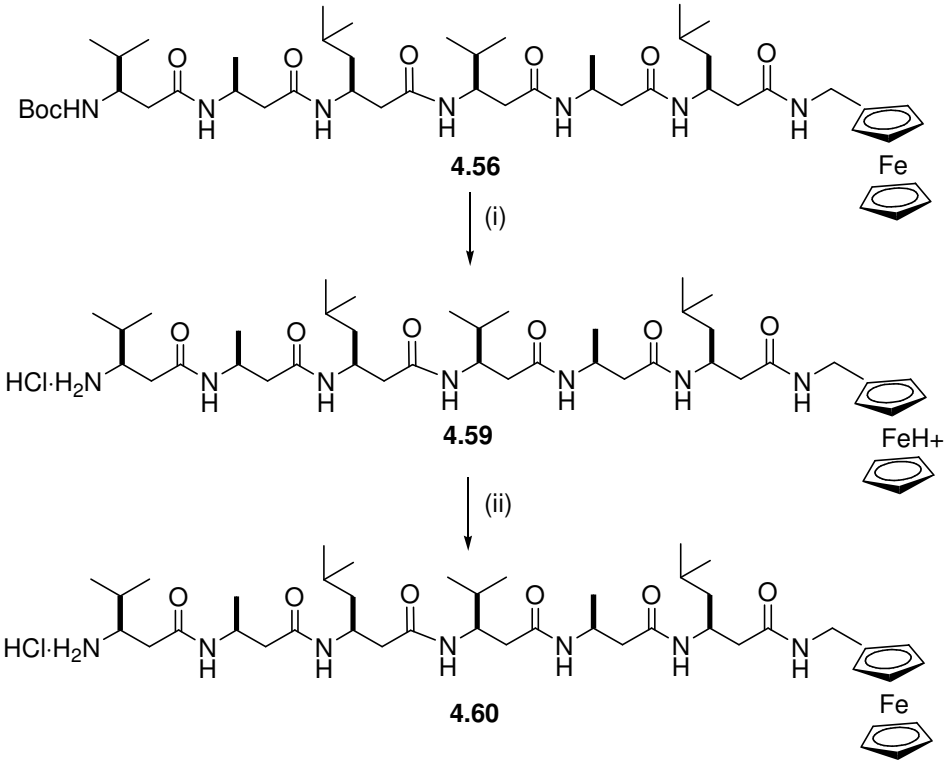

Scheme 4.23 *Reagents and conditions:* (i) 4 M HCl, dioxane, TFE, 10 min, (ii) alumina plug, methanol; chromatography (C_{18}-coated silica), 95% overall yield.

The peptide was purified using column chromatography on C_{18}-coated silica gel, eluting with gradients of water and methanol. HPLC analysis of the purified peptide showed that there were no significant contaminants (Figure 4.11).

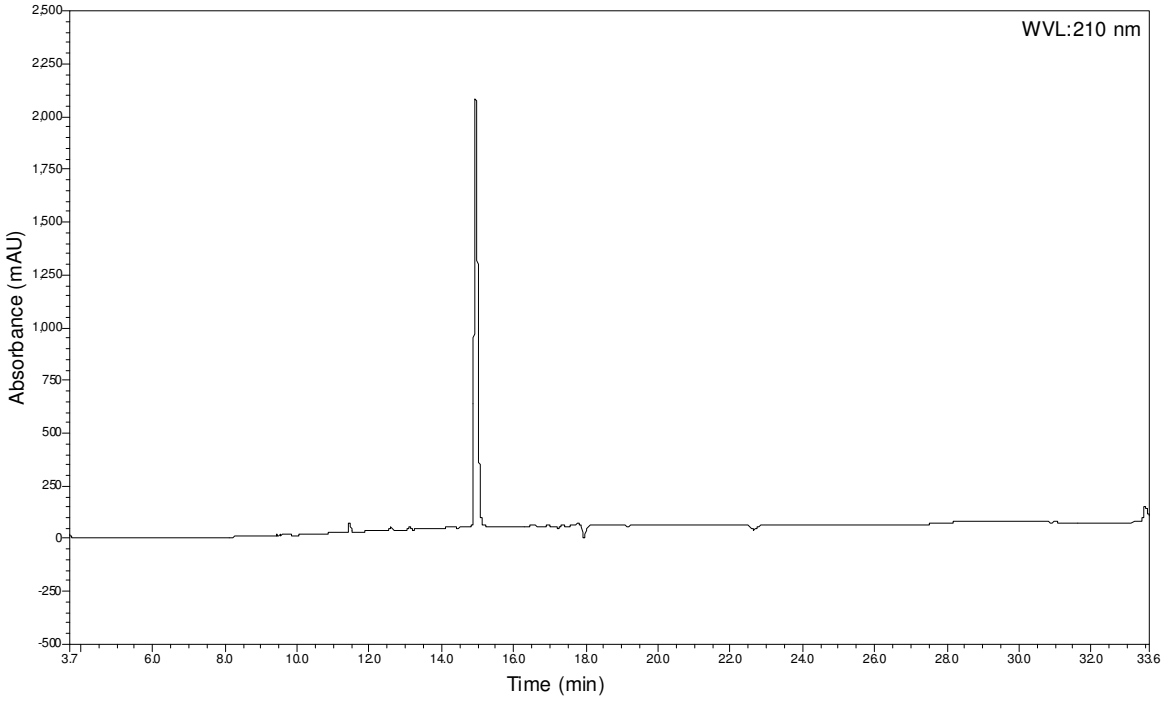

Figure 4.11 HPLC analysis of hexapeptide **4.60** at an absorbance of 210 nm.

4.4.6 Synthesis of *α*-Hexapeptide 2.16

Synthesis of the functionalized α-peptide **SS*α*6Fc** (**2.16**) enabled the comparison of the rate and mode of electron transfer between α- and β-peptides (as presented in Chapter Two). Peptide **2.16** was synthesized from analogous α-amino acids residues, and contained a disulfide linker and ferrocene moiety. The [(*S*)-Val-(*S*)-Ala-(*S*)-Leu]$_2$ peptide core was previously synthesized by Seebach *et al* and showed no helicity in solution.[24]

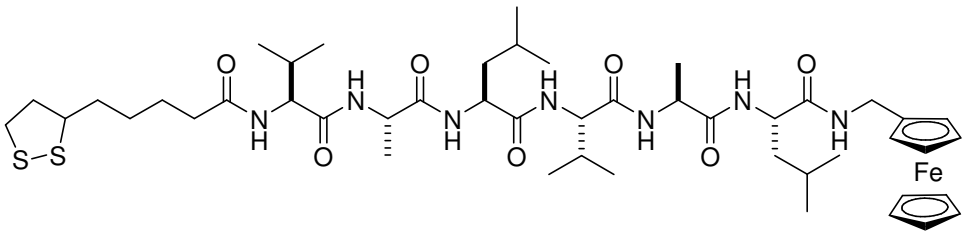

SSα_6Fc (2.16)

Synthesis of the α-tripeptide **4.65** from α-amino acids is shown in Scheme 4.24. Coupling of Boc-(*S*)-Val-OH (**4.61**) and HCl·(*S*)-Ala-OMe (**4.62**) using HATU gave dipeptide **4.63** in 82% yield. Subsequent hydrolysis under basic conditions to give free acid **4.64**, followed by coupling with HCl·(*S*)-Leu-OMe using HATU afforded the tripeptide **4.65** in 89% yield.

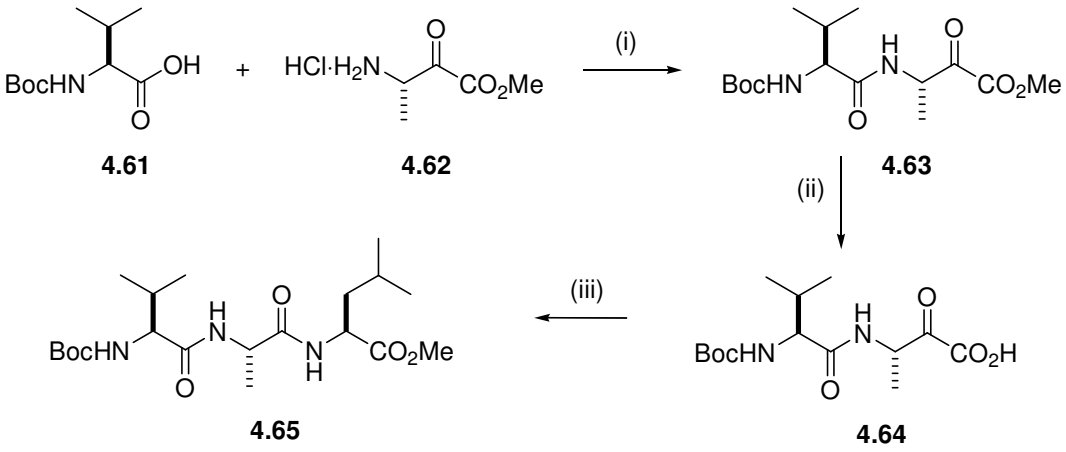

4.61 **4.62** **4.63** **4.64** **4.65**

Scheme 4.24 *Reagents and conditions:* (i) HATU, DIPEA, DMF, rt, 16 h, 82% yield, (ii) LiOH, THF, H_2O, 0 ºC to rt, 2 h, quant. yield, (iii) (*S*)-Val-OMe, HATU, DIPEA, DMF, rt, 16 h, 89% yield.

The separate deprotection of tripeptide **4.65** at the *N*-and *C*-terminus, gave free amine **4.66** and at the *C*-terminus only gave acid **4.67**, respectively. Tripeptide **4.66** was coupled with lipoic acid using HATU to afford lipoamide **4.68**. Tripeptide **4.67** was coupled with ferrocene methyl amine (**4.27**) to give ferrocenyl peptide **4.69**. Boc-deprotection of tripeptide **4.69** with 4M HCl/dioxane, and coupling with lipoamide **4.68** using HATU afforded the functionalised α-peptide **2.16** in 80% yield. The peptide was purified by sonicating the crude reaction mixture in methanol and collecting the precipitated solid by filtration.

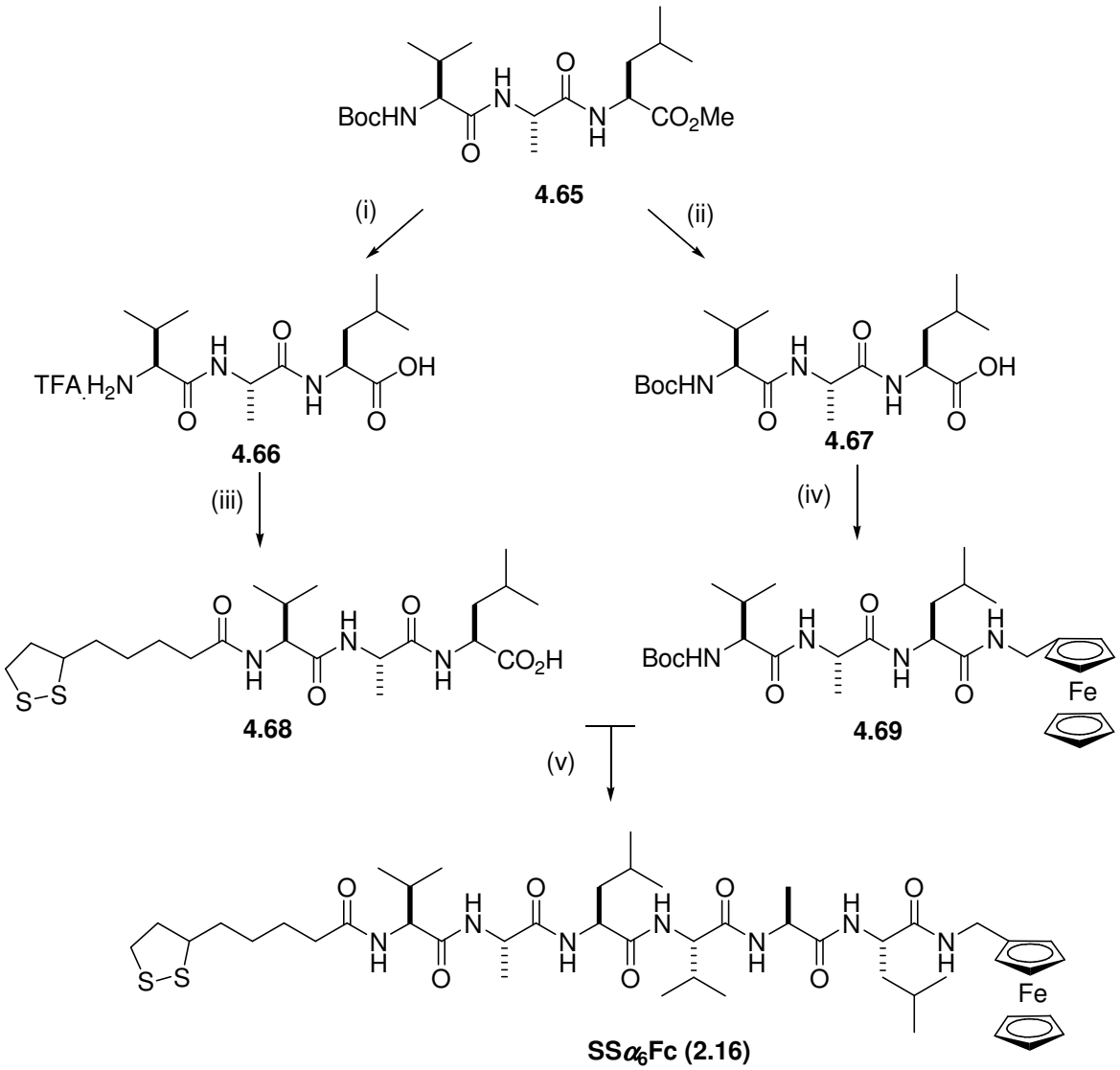

Scheme 4.25 *Reagents and conditions:* (i) LiOH, THF, H_2O, 0 ºC- rt, 2 h; TFA, DCM, 1 h, 97% yield, (ii) LiOH, THF, H_2O, 0 ºC – rt, 2 h, 97% yield, (iii) **4.20**, THF, H_2O, Et_3N, rt, 16 h, 62% yield, (iv) **4.27**, HATU, DIPEA, DMF, rt, 16 h, 64% yield, (v) (**4.69** first treated with TFA, DCM, rt, 1 h), HATU, DIPEA, DMF, rt, 16 h, 88% yield.

4.5 Elucidation of Secondary Structure

4.5.1 CD Studies

The CD spectrum of methanol-soluble hexapeptide **4.60,** which contains a *C*-terminal ferrocene group, was compared with that of literature hexapeptide **2.17**, which is known to form a 3_{14}-helix in methanol.[25] In agreement with the literature, the CD spectrum of hexapeptide **2.17** displayed a strong characteristic *Cotton* effect (a CD response from secondary structure), with a distinctive minimum at ~215 nm, and a sharp rise to a maximum at ~200 nm (Figure 4.12).[18] Ferrocene terminated peptide **4.60** showed a similar absorbance between 215 and 260 nm but had a minimum at ~208 nm, instead of at the characteristic 215 nm. This difference may be explained by the strong absorbance of the ferrocene moiety in the lower wavelength region of the spectrum (see Appendix B). However, based on this result it could not be established that compound **4.60** also adopts a 3_{14}-helix in solution, and that the ferrocene moiety does not destabilize the secondary structure of the peptide.

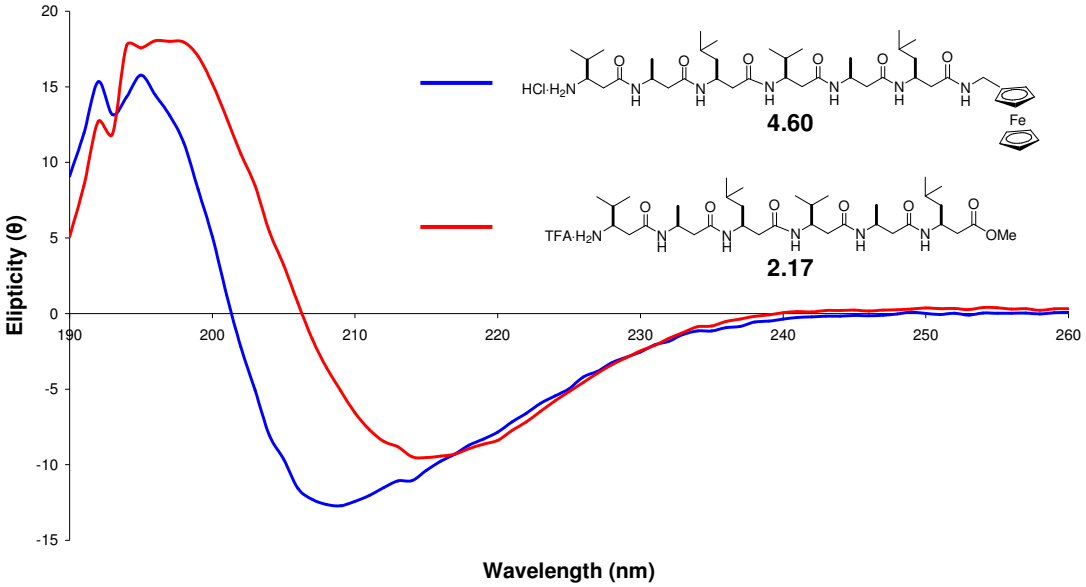

Figure 4.12 The CD spectra of **2.17** (red) and **4.60** (blue) (0.2 mM in methanol).

The CD spectra of peptides **2.12**-**2.15** and **4.54**-**4.58** (structures given on page 124), were measured in 2,2,2-trifluoroethanol, as these peptides are not soluble in methanol. The peptides, which contain substitution at both the *N*- and *C*-termini, exhibited nearly identical CD spectra but which differed significantly from the spectra of the peptides **2.17** and **4.60**. A representative

CD trace, of the peptide **4.57**, is shown in Figure 4.13. The characteristic minimum at 215 nm was entirely absent from all spectra. The spectrum appears to show an absorbance similar to that of a 10/12-helix (see Figure 4.6c), although this type of helix is not favoured by peptides consisting only of β^3 residues and is therefore unlikely. These results imply that the peptides do not adopt a 14-helix secondary structure in 2,2,2-trifluoroethanol.

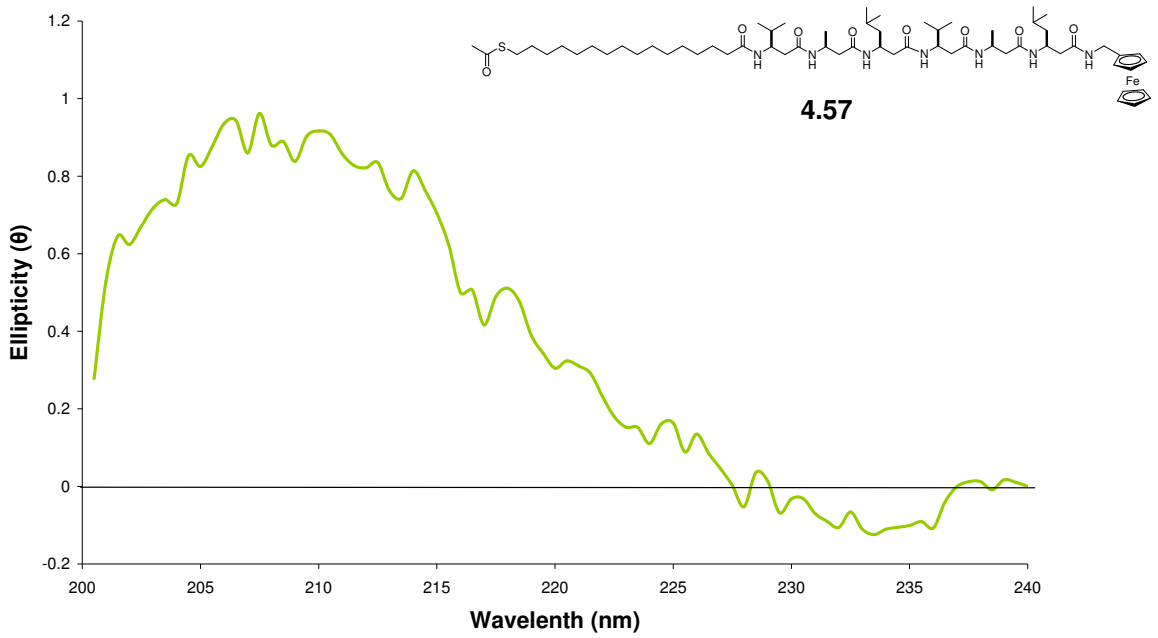

Figure 4.13 CD spectrum of **4.57** (0.2 mM in TFE).

Similar observations were reported by Gardiner *et al*[26] who synthesized the pyridine-2,6-dicarboxylic acid **4.70**, used to study the membrane permeation of β-peptides. It was found that peptide **4.70** exhibited only a very weak characteristic *Cotton* effect in methanol, and no defined structure in 2D-NMR studies. Some *N*-protecting groups (e.g. Boc groups)[18] are known to have a destabilizing effect on β-peptides in solution, however other *N*-terminal groups, such as polyethylene glycol units or fluorescein (Figure 4.2), have been shown to have no detrimental effect on β-peptide helicity.[11,27]

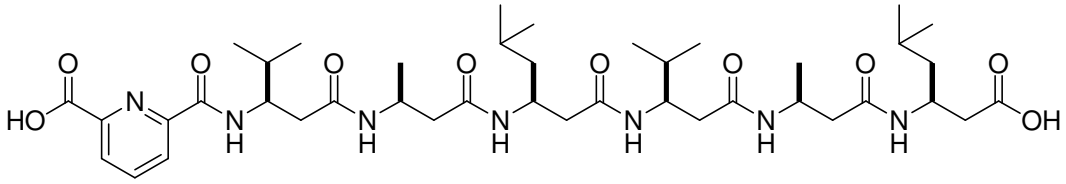

4.70

It is well established that CD spectroscopy cannot always be used to reliably characterise the secondary structure of β-peptides. Numerous examples exist where the CD signal shows a

response characteristic of a secondary structure that is sterically unfavoured or impossible.[18] Unfortunately, the theory behind CD cannot explain specific spectral features. Seebach, who has studied β-peptides extensively over the last ten years, notes:

"Despite a multitude of measured CD spectra in published and unpublished investigations … it has not been possible to assign the obtained 'fingerprints' clearly and unambiguously to certain secondary structures." – Dieter Seebach[18]

Therefore, the only conclusion from the CD spectra of β-peptides **2.12**-**2.15** and **4.54**-**4.58** is that the characteristic CD curve for the 3_{14}-helix in 2,2,2-trifluoroethanol is absent. However, this finding does not discount the fact that such secondary structures could exist either in solution, or when immobilised on a surface. The CD spectrum of peptide **4.60** appears consistent with that of a 14-helix, which is confirmed by 2D NMR studies and direct comparison with literature peptide **2.17** (discussed below).

4.5.2 2D NMR Studies

NMR spectroscopy is a valuable tool in the analysis of the secondary structure of peptides in solution. Various NMR experiments that show proton correlations *through space* allow one to build up a picture of the predominant solution phase secondary structure(s). Therefore, where adequate CD data is lacking, NMR spectroscopy can be used to characterise the type of helix or turn.

1D NMR Analysis of 4.60

Ferrocenyl peptide **4.60** was analysed using NMR spectroscopy to confirm that a 3_{14}-helix formed in solution, as predicted by CD spectroscopy. The peptide was sufficiently soluble in deuterated methanol (CD_3OD) to allow characterisation using various NMR spectroscopic techniques. The ^1H NMR spectrum showed a good separation of proton chemical shifts of the same functional groups on different residues (Figure 4.14). For example, the NH, adjacent methine and backbone methylene protons (indicated with red, green bands and blue bands, respectively) each comprise a large chemical shift range. This is important for structural analysis, because individual proton-proton correlations must be unambiguous.

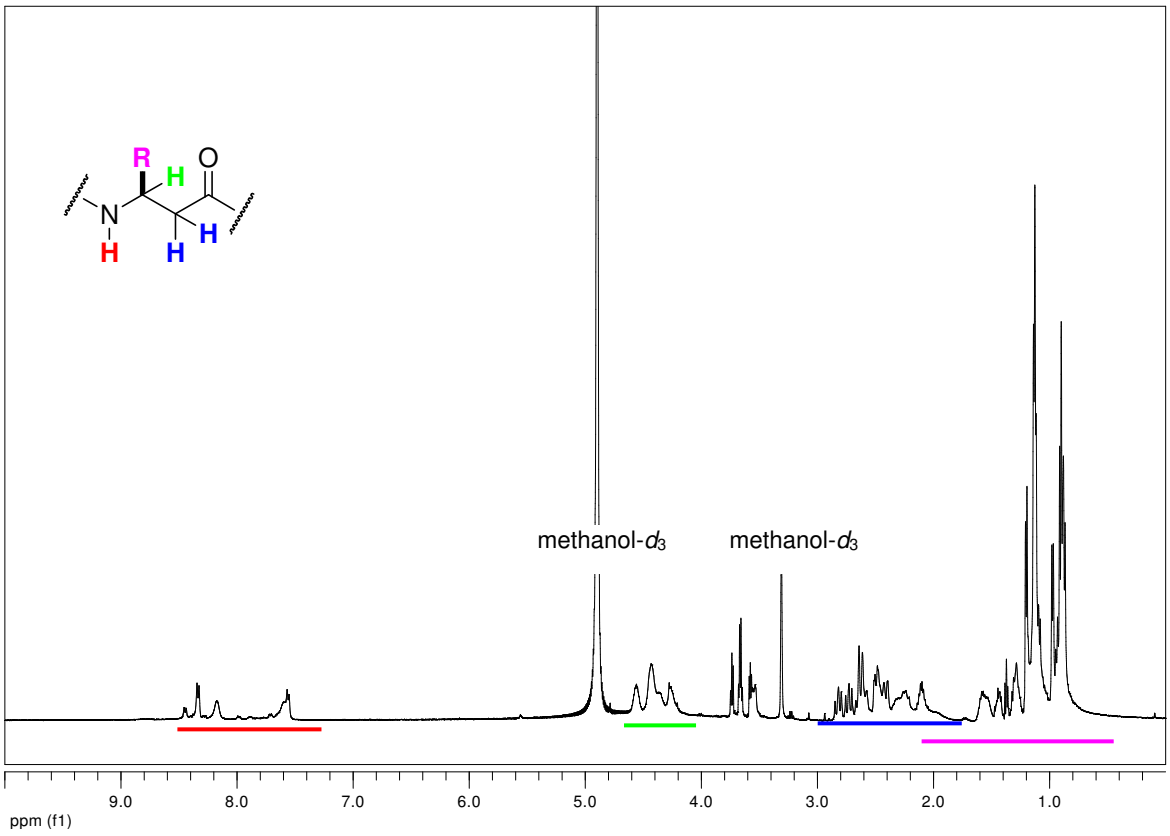

Figure 4.14 ^{1}H NMR spectrum of **4.60** in methanol-d_3. The coloured bands indicate the different proton environments of the peptide.

If peptide **4.60** possesses a 3_{14}-helix in solution, then NH protons will be involved in intramolecular hydrogen bonding. NH protons can rapidly undergo hydrogen exchange with protic solvents (solvents with a dissociable proton(s)). When the solvent is a protic deuterated solvent (such as D_2O, CD_3OD, TFE-d_3), the NH signal is weakened over time, to zero. However, NH protons in hydrogen bonds are held between the lone pairs of the oxygen and nitrogen and are slower to exchange. The chemical shift of these protons is also less effected by the temperature of the solvent than intermolecular hydrogen bonded protons.[28,29] This is because *inter*molecular hydrogen bonds (including those with the solvent) are cleaved with increasing temperature, due to the increased in entropy of the system.

A basic assessment of hydrogen bonding in peptide **4.60** was carried out to determine whether a detailed and time-consuming 2D NMR study of its secondary structure was worthwhile. The effect of temperature on the NH proton chemical shifts of peptide **4.60** in MeOH was measured over a temperature range of 23-45 ºC. Figure 4.15 shows the NH region of spectra measured at 37, 40 and 45 ºC (top to bottom). Two NH peaks, labelled '1' and '2', show a greater upfield

shift with increasing temperature, compared to the change in chemical shift of NH peak '3'. Note also, that the small peak downfield of peak 3 disappears as solvent exchange gives the entirely deuterated form. The change in chemical shift with temperature is an indication of whether hydrogen bonding is intermolecular (with solvent or other molecules) or intramolecular.[28-30] In general, a change in chemical shift gradients of greater than 4 ppbK^{-1} is evidence for intermolecular hydrogen bonding, while those smaller than 3 ppbK^{-1} support intramolecular hydrogen bonding. Protons 1 and 2 both change at greater than 4 ppmK^{-1}, which can be attributed to intermolecular hydrogen bonding. The change in chemical shift of proton 3 is 2.6 ppmK^{-1}, which is within the range that indicates intramolecular hydrogen bonding. This result supported pursuing a more detailed (2D) NMR analysis of peptide **4.60**.

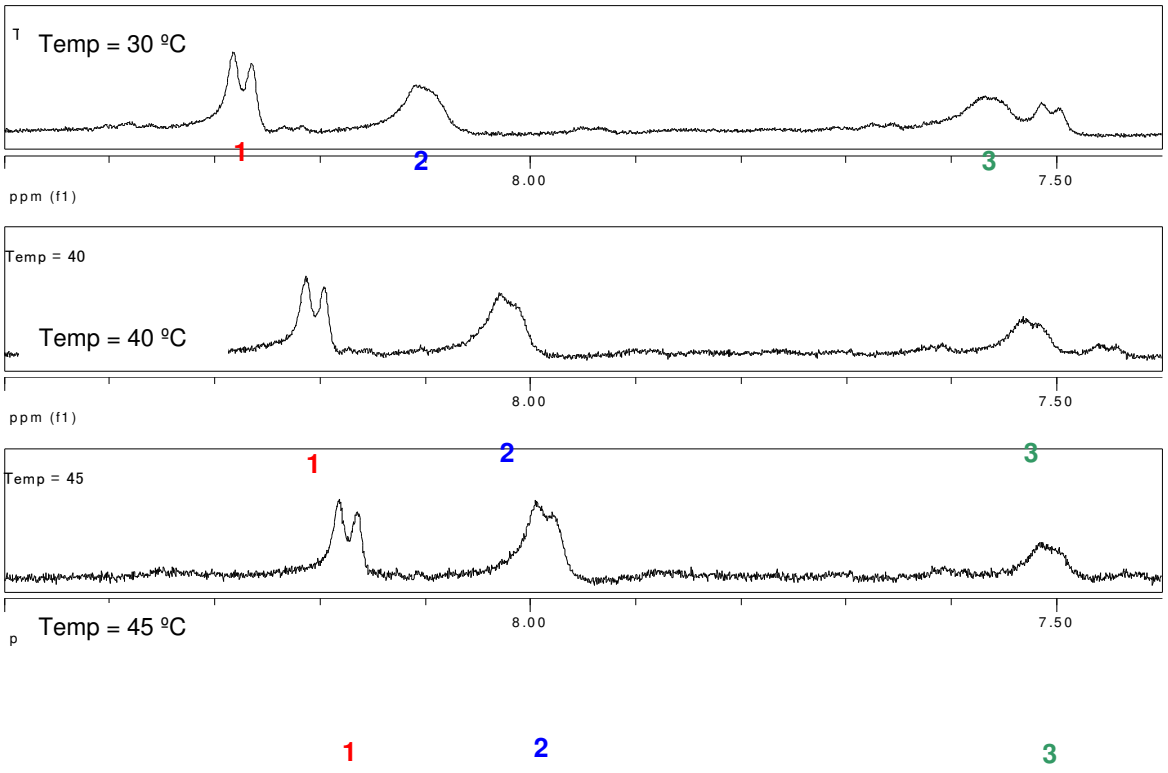

Figure 4.15 ^{1}H NMR spectra of three NH protons on **4.60** in methanol-d_3 at different temperatures: 37, 40 and 45 ºC.

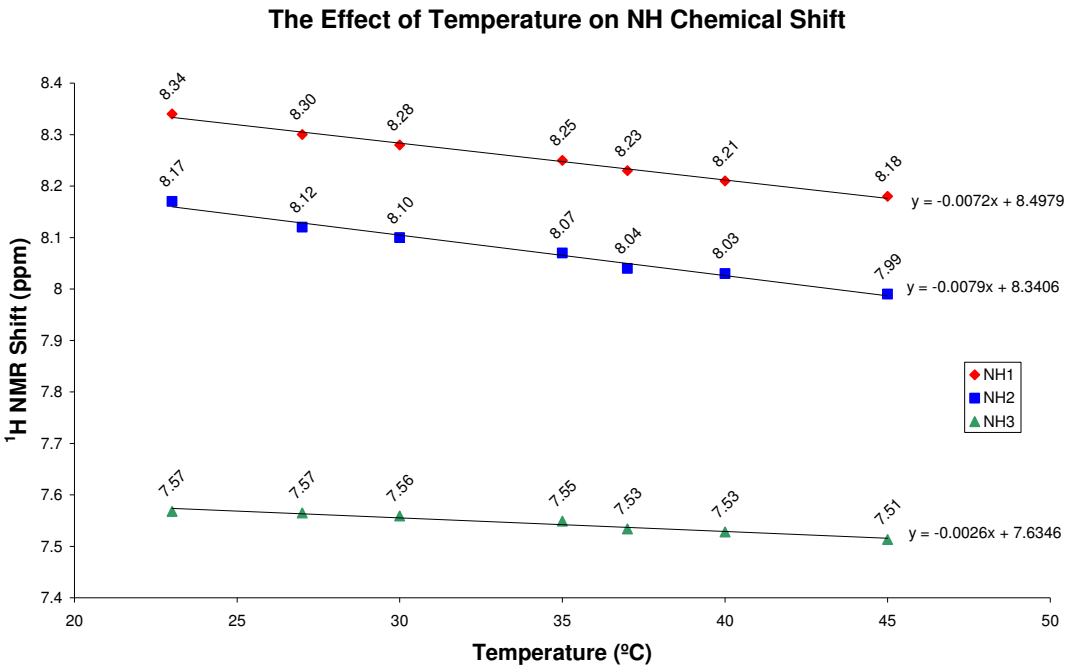

Figure 4.16 Chemical shift (ppm) of three NH protons of **4.60** at different temperatures. NH protons 1, 2 and 3 (as assigned in Figure 4.15) are shown in red, blue and green respectively. The chemical shift values are shown next to the data points.

2D NMR Analysis of 4.60

To determine whether **4.60** forms a helical structure in solution using through-space techniques, each proton resonance was first assigned using a combination of through-bond NMR techniques such as COSY, HSQC and CIGAR. Figure 4.17a shows the proton chemical shifts (in ppm) that could be unambiguously assigned using these techniques. Only the protons in the two β-valine and β-alanine residues could be conclusively assigned in the correct position within the peptide, because the two β-leucine residues had very similar chemical shifts. The same procedure was repeated for the literature peptide **2.17** for comparison (Figure 4.17b).

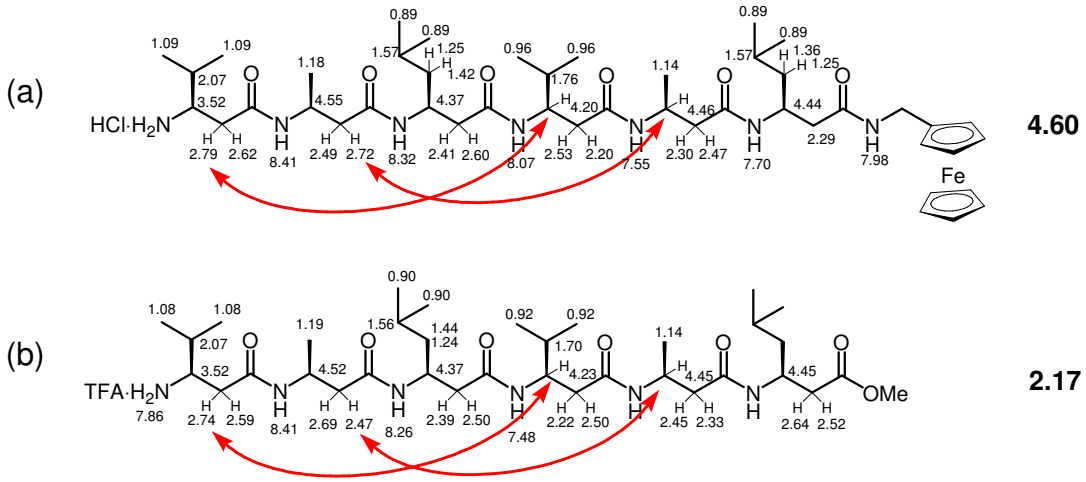

Figure 4.17 The partially assigned structures of **4.60** (a) and **2.17** (b) showing ^{1}H chemical shifts (ppm). The red arrows indicate proton-proton correlations observed in the 2D ROESY spectrum, shown in Figure 4.18.

Once the relevant protons and carbons on the peptide structure were assigned to individual chemical shifts using through-bond correlations, *through-space* correlations were sought. When amide groups in peptides participate in hydrogen bonding (such as in secondary structure), protons that are many bonds apart are brought close together. NMR experiments used to identify these structures, such as NOESY and ROESY, show correlations between protons that are within 3 Å of each other.

The 2D ROESY spectrum of peptide **4.60** is shown in Figure 4.18a. The black regions along the diagonal of the spectrum are due to the chemical shifts of protons in the peptide, while each of the blue areas are from through-space correlations between sets of protons. The *x* and *y* (f(1) and f(2) on the spectrum) coordinates of each correlation correspond to the chemical shifts of the two coupled protons. Many of the through-space correlations shown on the spectrum are (predictably) between different protons on the same *β*-amino acid residue. These correlations confirm the proton assignment in Figure 4.17a. The structurally important correlations are those between protons on different residues that would not be within 3 Å of each if the peptide was in a strand-like conformation. Two unambiguous correlations of this type were found between a β^3 methine proton and a β^2 methylene proton on the different *β*Ala residues, and between a β^3 methine proton and a β^2 methylene proton of the different *β*Val residues. These are shown in red double-headed arrows in Figure 4.17a and with black arrows on the ROESY spectrum in Figure 4.18a

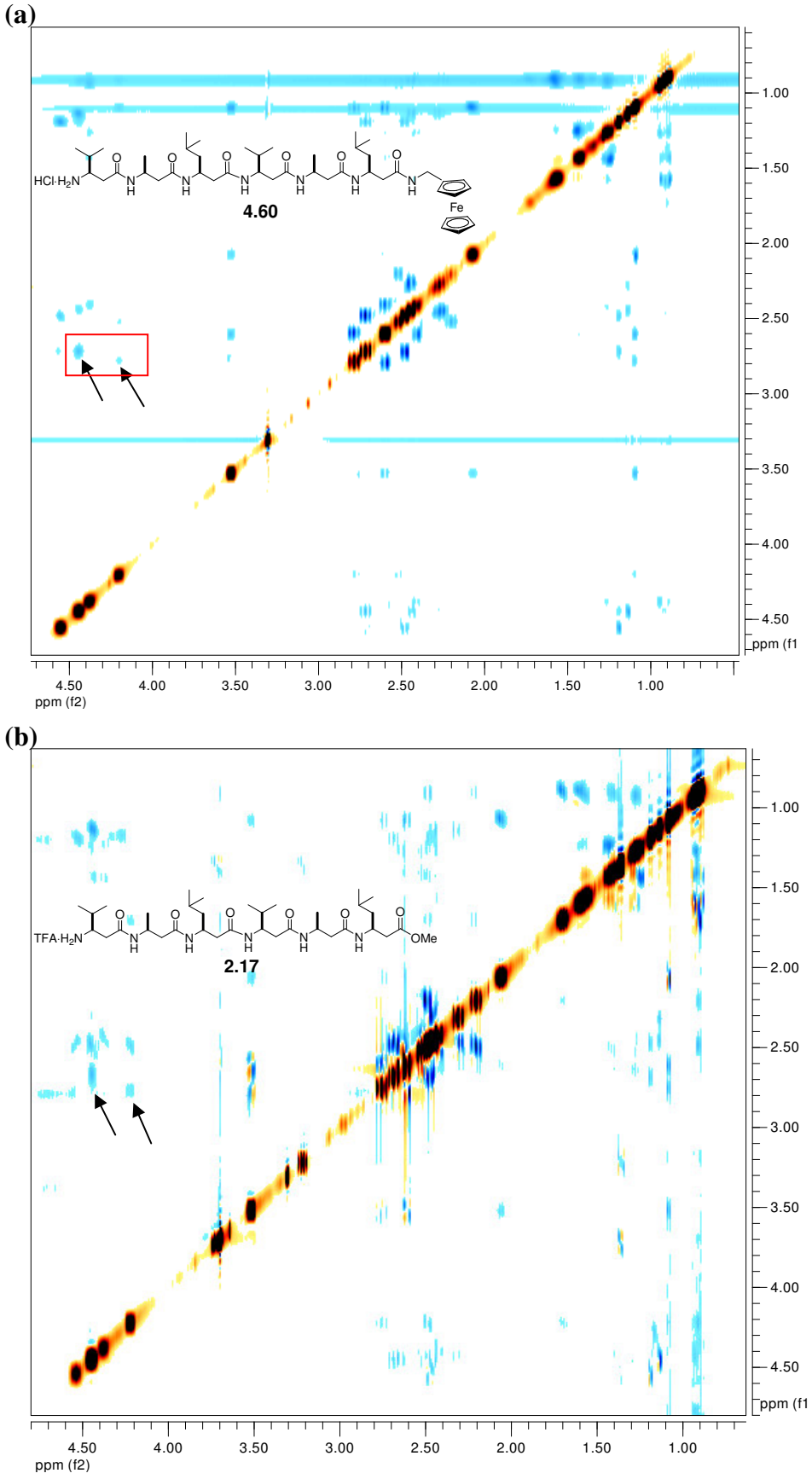

Figure 4.18 2D ROESY spectra of peptides **4.60** (a) and **2.17** (b) showing through space proton-proton correlations. The black arrows indicate the important secondary structural correlations between backbone protons as illustrated with red arrows in Figure 4.17. The red rectangle indicates the expanded area of the contour plot in Figure 4.19.

The correlation intensity in peptide **4.60** is much larger between the two βAla protons compared with the βVal protons (Figure 4.19). ROE intensity is related to the distance between protons with inverse sixth power dependence (r^{-6}). Therefore, the distance between the two alanine protons is smaller than between the valine protons.

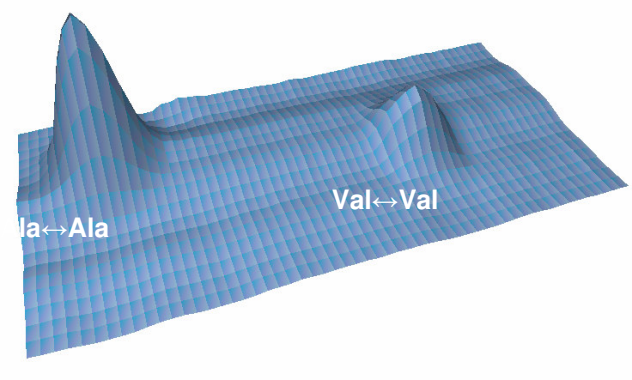

Figure 4.19 Contour plot of an area of the ROESY spectrum of peptide **4.60** indicated with a red rectangle in Figure 4.18a, showing the difference in intensity of the correlations.

The literature peptide **2.17** was analysed using 2D NMR in the same way as ferrocenyl peptide **4.60**. Through-space coupling was observed between a β^3 methine proton and a β^2 methylene proton on the different βAla residues, and between a β^3 methine proton and a β^2 methylene proton of the different βVal residues of literature peptide **2.17**, as indicated in the 2D ROESY spectrum (Figure 4.17b and Figure 4.18b). Furthermore, the correlation intensity between the βAla protons was larger than that between βVal peaks (not shown). Both of these results are identical to the correlations and intensities found in the ferrocenyl peptide **4.60**. Based on these observations, it can be suggested that, in solution, peptide **4.60** adopts a secondary structure that is very similar to that of peptide **2.17**, the latter of which has been shown by Seebach *et al* to adopt a 3_{14}-helical structure in solution.[25] Therefore, this result suggests that the presence of a ferrocenyl terminal group does not disrupt helix formation in β-hexapeptides of this type.

NMR of Peptides 2.12-2.15 and 4.54-4.58

The capped peptides **2.12**-**2.15** and **4.54**-**4.58** were not sufficiently soluble in common deuterated NMR solvents such as CD_3OD or DMSO-d_6, but were moderately soluble in deuterated trifluoroethanol (TFE-d_3). These peptides were pure by ^{1}H NMR spectroscopy, and regions of the spectra could be assigned to various functional groups. However, in TFE-d_3, the backbone

methine and methylene proton signals for all six β-amino acid residues were overlapping, as shown with blue and green bands in Figure 4.20. Also, amino acids of the same type (eg. both βAla residues) had identical chemical shifts. Unfortunately, this precluded any NMR structural studies of the peptides because correlations could not be assigned to individual protons.

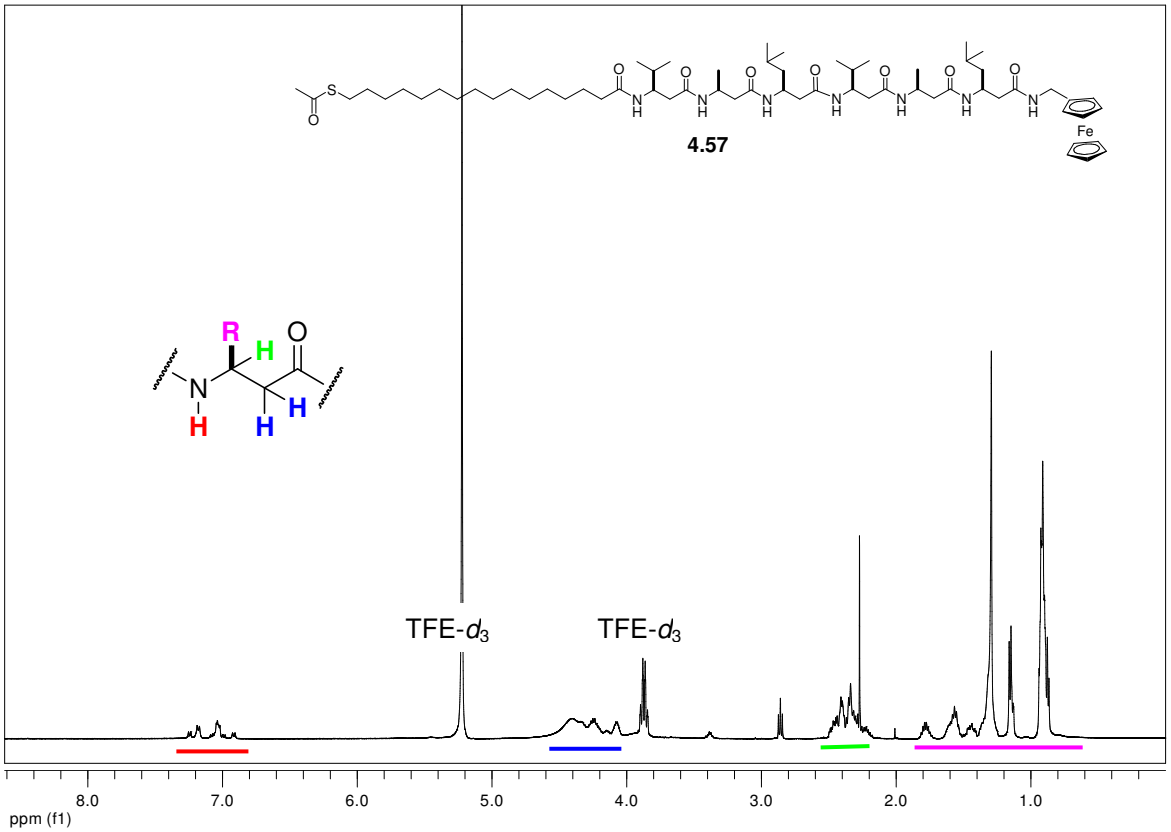

Figure 4.20 ^{1}H NMR of peptide **4.57** in TFE-d_3 (solvent signals indicated). The coloured bands indicate the different proton environments of the peptide.

4.5.3 Molecular Modelling*

Peptide 4.60

Hexapeptide **4.60** was modelled using molecular mechanics calculations on Macromodel software (as described in Chapter Six). Figure 4.21 shows a representative lowest energy structure of **4.60** in two orientations. The top image illustrates a close contact between the methine backbone proton of one β^3hAla residue and a methylene proton of the other β^3hAla residue, with a distance of 2.20 Å. The lower image shows the same correlation, but between the two β^3hVal residues, with a distance of 2.63 Å. These close contacts are within the required 3 Å to be seen with 2D ROESY NMR. Therefore, the modelling supports the two backbone correlations shown in Figure 4.17 and Figure 4.19. The greater intensity of the βAla-βAla coupling compared with the βVal-βVal coupling is consistent with the closer distance between the appropriate protons in the model structure.

The proposed model also shows four hydrogen bonding contacts (not shown) which hold the peptide in a rigid helical structure. The number of atoms between the hydrogen bonds are 14, which is consistent with a 3_{14}-helix. Models of the β-peptide **2.17**,[18] calculated by Seebach *et al* using different software show a different orientation of two carbonyl groups compared to the structures presented here, which is probably due to differences in the modelling parameters and software. Nevertheless, the modelling suggests that **4.60** readily folds into a low-energy, hydrogen-bonded structure. As there are currently no force field parameters developed specifically for β-peptides, and the modelling software limits the solvent choice to chloroform or water (whereas methanol was used for CD and NMR studies), the results shown here are speculative. Furthermore, due to software limitations, the ferrocene moiety could not be included in the model, and is instead represented as a single cyclopentadienyl ring instead. In spite of these modifications, some features of the modelling were consistent with the 2D NMR analysis.

* Molecular modeling was performed by Blair Stewart, University of Canterbury.

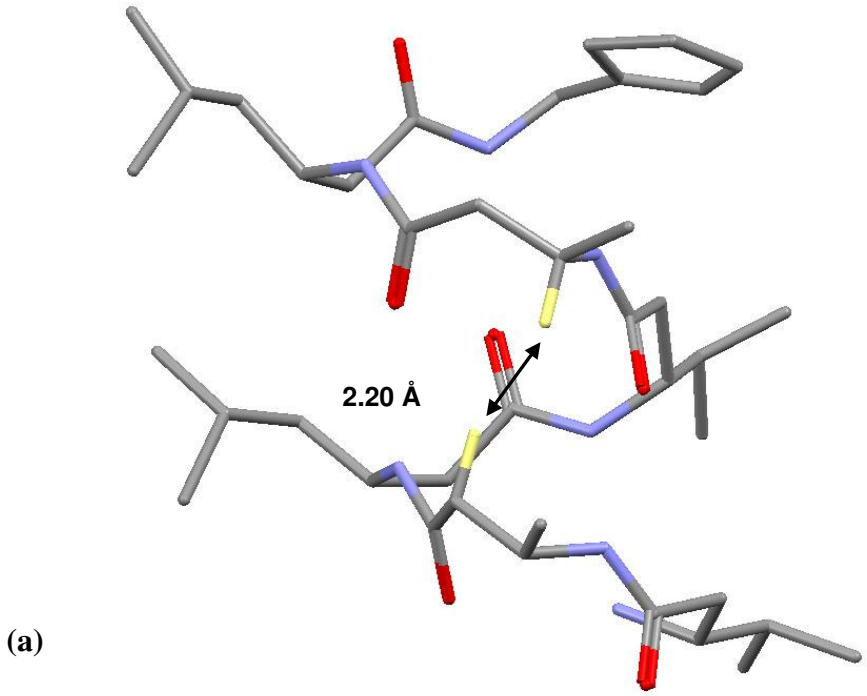

(a)

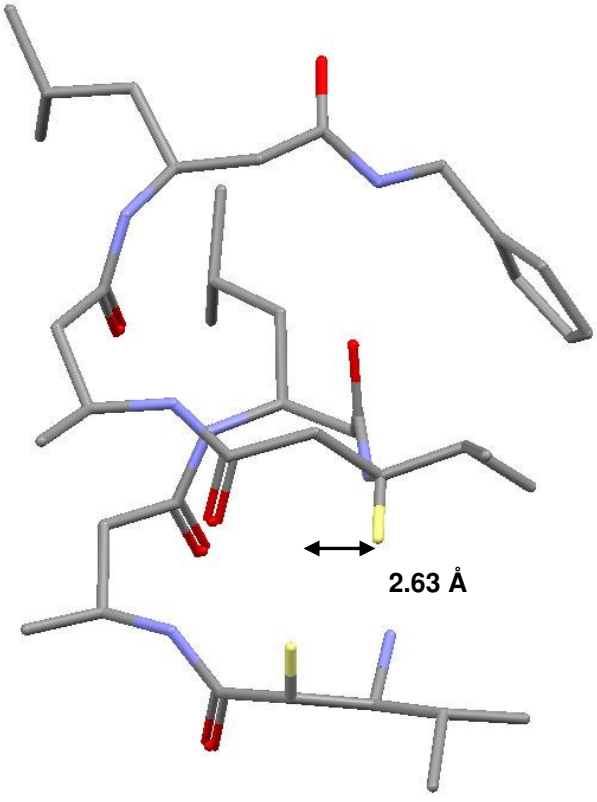

(b)

Figure 4.21 Lowest global energy minimum conformation of **4.60**. The ROESY correlations between (a) βAla-βAla and (b) βVal-βVal are shown with arrows. Carbon = grey, nitrogen = blue, oxygen = red, hydrogen = light yellow. For clarity, only the relevant protons are shown.

Capped Peptides 4.54, 2.13 and 2.15

Capped peptides **4.54**, **2.13**, and **2.15** were modelled using the same parameters as **4.60**. These peptides also readily adopted low-energy helical structures (representative structures are shown in Figure 4.22, viewed down the helix-pore) when modelled in water and chloroform. The structures each contain identical hydrogen-bonding networks along the peptide backbone, similar to that obtained for helical peptide **4.60**. Importantly, in a polar solvent (water) or non-polar solvent (chloroform) the hydrophobic side chains are presented on the surface of the peptide, while the polar amide groups line the helix pore. This conformation is important for the self-assembly of α-helical peptides through Van der Waals interactions between the hydrophobic side chains,[31] and therefore could also facilitate self-assembly in β-peptides. However, as these models cannot be verified by CD or NMR experimental evidence, it can only be tentatively suggested from these results that the capped β-peptides adopt helical structures in solution.

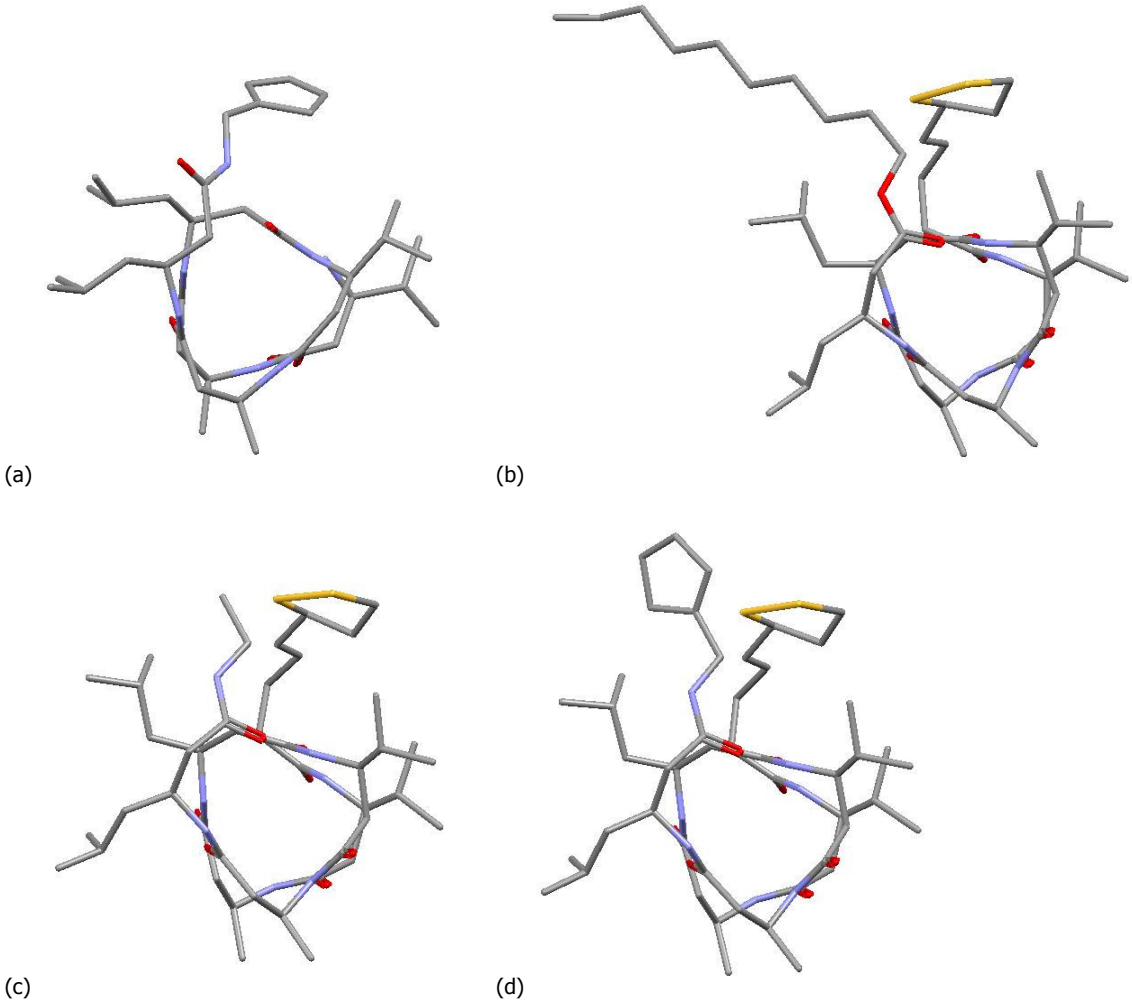

Figure 4.22 Lowest global energy minima conformations of β-peptides, viewed down the helix axis: (a) **4.60**, (b) **4.54**, (c) **2.15** and (d) **2.13** (with ferrocene simulated as a single cyclopentadienyl ring). Carbon = grey, nitrogen = blue, oxygen = red, sulfur = dark yellow. Hydrogens are omitted for clarity.

4.6 Conclusions and Future Work

β-Peptides have been widely studied, with significant contributions having been made by the research groups of Gellman and Seebach.[18,32] Many comparisons have been made between the secondary structure, stability and biological activity of β-peptides and natural α-peptides analogues. However, electron transfer in β-peptides, to our knowledge, has not been investigated despite the recognition that electron transfer in nature occurs readily through helical structures.

Table 4.2 β-Peptides synthesized in this chapter.

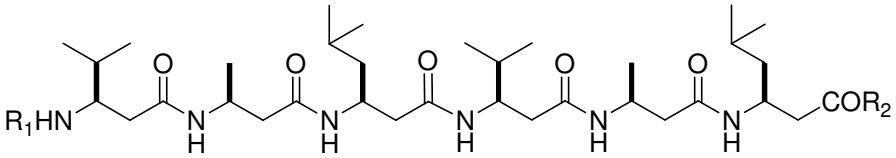

Hexapeptide	R^1	R^2
2.17	H·TFA	OMe
4.55	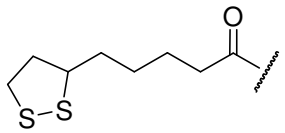	
2.15 (SSβ_6Et)		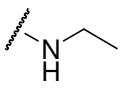
4.54		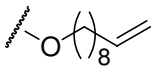
2.13 (SSβ_6Fc)		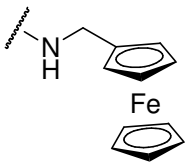
4.56	Boc	
4.60	H·HCl	
4.57	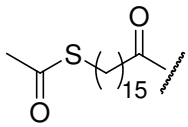	
4.58		OMe
2.14 (Fcβ_6SS)	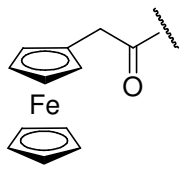	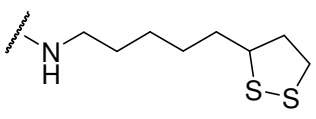

A range of novel β-peptides suitable for immobilisation on a gold surface was synthesized in order to determine the mode of electron transfer though the β-peptide structure. These functionalised peptides were based on the literature peptide **2.17**, which forms a 3_{14}-helix in solution. A synthetic approach was developed involving the coupling of functionalised tripeptides, to avoid peptide solubility problems and to assist in purification. Two of the peptides, **2.12** and **2.13**, both contained a C-terminal ferrocene redox probe necessary for determining the electron transfer rate along the peptide structure, and sulfur linkers for attachment to the gold surface. Two structural analogues, **2.15** and **4.58**, that lack a ferrocene redox probe were synthesized as controls for electron transfer and structural studies. Furthermore, these peptides have the potential to act as diluents to investigate the isolation of ferrocenyl peptides on a gold surface. An olefin terminated peptide **4.54** was synthesized as a possible reactant for cross metathesis on gold (as discussed in Chapter Three). Finally, a ferrocenyl hexapeptide **2.14**, which contains a sulfur linker at the C-terminus (instead of the *N*-terminus as in **2.12** and **2.13**) was synthesised to probe the effect of a reversed dipole moment (with respect to the gold surface) on electron transfer.

β-Hexapeptide **4.56** was synthesized and deprotected to give the ferrocenyl amine **4.60**. This peptide appeared to exhibit a 3_{14}-helix in methanol, verified by the direct comparison of 2D-NMR data and CD with helical literature peptide **2.17**. Importantly, this result suggests the ferrocenyl moiety does not interfere with helix-formation in β-peptides of this type. Furthermore, the molecular modelling of peptide **4.60**, which showed a low energy helical conformation, was validated by the 2D-NMR studies. The secondary structure of the capped peptides **2.12**-**2.15** and **4.54**-**4.58** could not be determined by CD or NMR studies. However, preliminary molecular modelling of the capped peptides using the same parameters as for peptide **4.60** tentatively suggests that a helical conformation (similar to a 3_{14}-helix structure) is stable in solution.

The α-peptide **2.16** was synthesised using α-amino acids, analogous to those used in the β-peptide structures. This peptide was synthesised to compare the mode of electron transfer along α- and β-peptide chains (as discussed in Chapter Two).

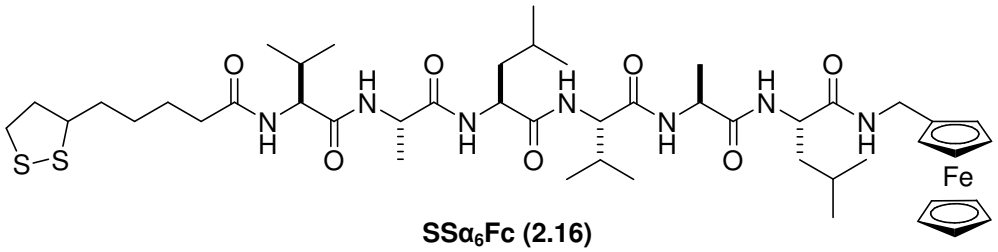

SSα$_6$Fc (2.16)

Future work in this area could include the synthesis of *β*-peptides comprising cyclic *β*-amino acids. There is much evidence to suggest that cyclic *β*-amino acids have a stabilising effect on *β*-helices. Therefore, any destabilising effect due to the presence of the sulfur linker group would be minimised. Furthermore, the synthesis of longer functionalised *β*-peptides would prove interesting both for structural studies (using CD and 2D NMR) and for electrochemical studies (as presented in Chapter Two).

4.7 References

1. Kritzer, J. A.; Tirado-Rives, J.; Hart, S. A.; Lear, J. D.; Jorgensen, W. L.; Schepartz, A., *Journal of the American Chemical Society* **2005,** 127, (1), 167-178.
2. Arvidsson, P. I.; Rueping, M.; Seebach, D., *Chemical Communications* **2001**, (7), 649-650.
3. Appella, D. H.; Christianson, L. A.; Klein, D. A.; Powell, D. R.; Huang, X. L.; Barchi, J. J.; Gellman, S. H., *Nature* **1997,** 387, (6631), 381-384.
4. Seebach, D.; Sifferlen, T.; Mathieu, P. A.; Hane, A. M.; Krell, C. M.; Bierbaum, D. J.; Abele, S., *Helvetica Chimica Acta* **2000,** 83, (11), 2849-2864.
5. Rossi, F.; Lelais, G.; Seebach, D., *Helvetica Chimica Acta* **2003,** 86, (7), 2653-2661.
6. Seebach, D.; Abele, S.; Gademann, K.; Guichard, G.; Hintermann, T.; Jaun, B.; Matthews, J. L.; Schreiber, J. V., *Helvetica Chimica Acta* **1998,** 81, (5), 932-982.
7. Seebach, D.; Jacobi, A.; Rueping, M.; Gademann, K.; Ernst, M.; Jaun, B., *Helvetica Chimica Acta* **2000,** 83, (9), 2115-2140.
8. Glattli, A.; Seebach, D.; van Gunsteren, W. F., *Helvetica Chimica Acta* **2004,** 87, (10), 2487-2506.
9. Jacobi, A.; Seebach, D., *Helvetica Chimica Acta* **1999,** 82, (8), 1150-1172.
10. Gessier, F.; Noti, C.; Rueping, M.; Seebach, D., *Helvetica Chimica Acta* **2003,** 86, (6), 1862-1870.
11. Potocky, T. B.; Menon, A. K.; Gellman, S. H., *Journal of the American Chemical Society* **2005,** 127, (11), 3686-3687.
12. Ziegler, T.; Roseling, D.; Subramanian, L. R., *Tetrahedron-Asymmetry* **2002,** 13, (9), 911-914.
13. Sharma, G. V. M.; Reddy, K. R.; Krishna, P. R.; Sankar, A. R.; Jayaprakash, P.; Jagannadh, B.; Kunwar, A. C., *Angewandte Chemie-International Edition* **2004,** 43, (30), 3961-3965.

14. Sharma, G. V. M.; Reddy, K. R.; Krishna, P. R.; Sankar, A. R.; Narsimulu, K.; Kumar, S. K.; Jayaprakash, P.; Jagannadh, B.; Kunwar, A. C., *Journal of the American Chemical Society* **2003,** 125, (45), 13670-13671.
15. Suhara, Y.; Yamaguchi, Y.; Collins, B.; Schnaar, R. L.; Yanagishita, M.; Hildreth, J. E. K.; Shimada, I.; Ichikawa, Y., *Bioorganic & Medicinal Chemistry* **2002,** 10, (6), 1999-2013.
16. Chakraborty, P.; Diederichsen, U., *Chemistry-a European Journal* **2005,** 11, (11), 3207-3216.
17. Kelly, S. M.; Jess, T. J.; Price, N. C., *Biochimica Et Biophysica Acta-Proteins and Proteomics* **2005,** 1751, (2), 119-139.
18. Seebach, D.; Beck, A. K.; Bierbaum, D. J., *Chemistry & Biodiversity* **2004,** 1, (8), 1111-1239.
19. Seebach, D.; Hook, D. F.; Glattli, A., *Biopolymers* **2006,** 84, (1), 23-37.
20. Dado, G. P.; Gellman, S. H., *Journal of the American Chemical Society* **1994,** 116, (3), 1054-1062.
21. Arvidsson, P. I.; Frackenpohl, J.; Seebach, D., *Helvetica Chimica Acta* **2003,** 86, (5), 1522-1553.
22. Miura, Y.; Kimura, S.; Imanishi, Y.; Umemura, J., *Langmuir* **1998,** 14, (24), 6935-6940.
23. Palinko, I., Effects of Surface Modifiers in the Liquid-Phase Hydrogenation of Olefins over Silica-Supported Pt, Pd and Rh Catalysts .2. Thiophene and Cs2. In *Catalyst Deactivation 1994*, 1994; Vol. 88, pp 603-608.
24. Seebach, D.; Studer, A.; Pfammatter, E.; Widmer, H., *Helvetica Chimica Acta* **1994,** 77, (7), 2035-50.
25. Seebach, D.; Overhand, M.; Kuehnle, F. N. M.; Martinoni, B., *Helvetica Chimica Acta* **1996,** 79, (4), 913-941.
26. Gardiner, J.; Thomae, A. V.; Mathad, Raveendra I.; Seebach, D.; Kramer, S. D., *Chemistry & Biodiversity* **2006,** 3, 1181-1200.
27. Gardiner, J., personal communication. In 2006.
28. Kessler, H., *Angewandte Chemie-International Edition in English* **1982,** 21, (7), 512-523.
29. Daley, M. E.; Graether, S. P.; Sykes, B. D., *Biochemistry* **2004,** 43, (41), 13012-13017.
30. Gademann, K.; Jaun, B.; Seebach, D.; Perozzo, R.; Scapozza, L.; Folkers, G., *Helvetica Chimica Acta* **1999,** 82, (1), 1-11.
31. Otoda, K.; Kimura, S.; Imanishi, Y., *Journal of the Chemical Society-Perkin Transactions 1* **1993**, (23), 3011-3016.
32. Cheng, R. P.; Gellman, S. H.; DeGrado, W. F., *Chemical Reviews* **2001,** 101, (10), 3219-3232.

Chapter 5 Conformationally Constrained β-Amino Acids

5.1 Introduction

Cyclic *β*-amino acids are an important class of constrained compounds, useful for stabilising important secondary structures such as helices and sheets (as described in section 1.2.3). Most literature syntheses of cyclic *β*-amino acids focus on both the *cis* and *trans* isomers 2-aminocyclopentanecarboxylic acid (**5.1**) and 2-aminocyclohexanecarboxylic acid (**5.2**). There exist very few examples of synthetic routes to give larger ring sizes such as cycloheptene, cyclooctene and cyclononene-based amino acids.

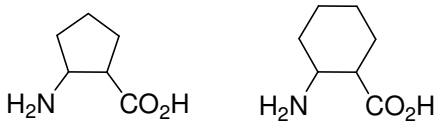

5.1 **5.2**

Outlined below are some key examples of synthetic methodologies, from the early racemic syntheses to those utilising enzymatic resolution, chiral auxiliaries and transition metal catalysts.

Racemic Syntheses

The first synthesis of cyclic *β*-amino acids was completed in 1972. This racemic synthesis, developed by Cannon *et al* occurs via two steps. Firstly, chlorosulfonyl isocyanate was reacted with cycloalkene **5.3**, via 1,2 dipolar cycloaddition, to give the fused *β*-lactams (**5.4**) Scheme 5.1).[1] The second step involved ring opening of the lactams with hydrochloric acid to give the *β*-amino acids (**5.5**). This route was applied to cyclopentene, cyclohexene and bicyclic systems.[2]

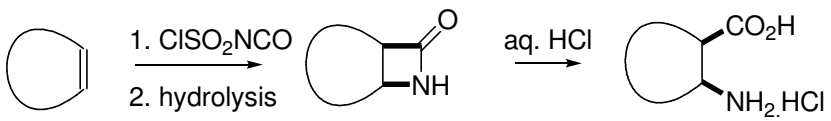

5.3 **(±) 5.4** **(±) 5.5**

Scheme 5.1 Synthesis of *β*-amino acids through 1,2 cycloaddition.

cis- And *trans*-cyclohexane-based *β*-amino acids **5.8** and **5.13**, have also been prepared from the Diels-Alder adduct tetrahydroanthranilic anhydride **5.6** (Scheme 5.2). [3,4 5,6] The *cis*-isomer **5.8** was prepared by ring-opening of this cyclic anhydride **5.6** with aqueous ammonia to give the

monoamide **5.7**. Hoffman degradation of the resulting amide with hypobromite (or hypochlorite if a double bond was present) gave the *β*-amino acid **5.8**.

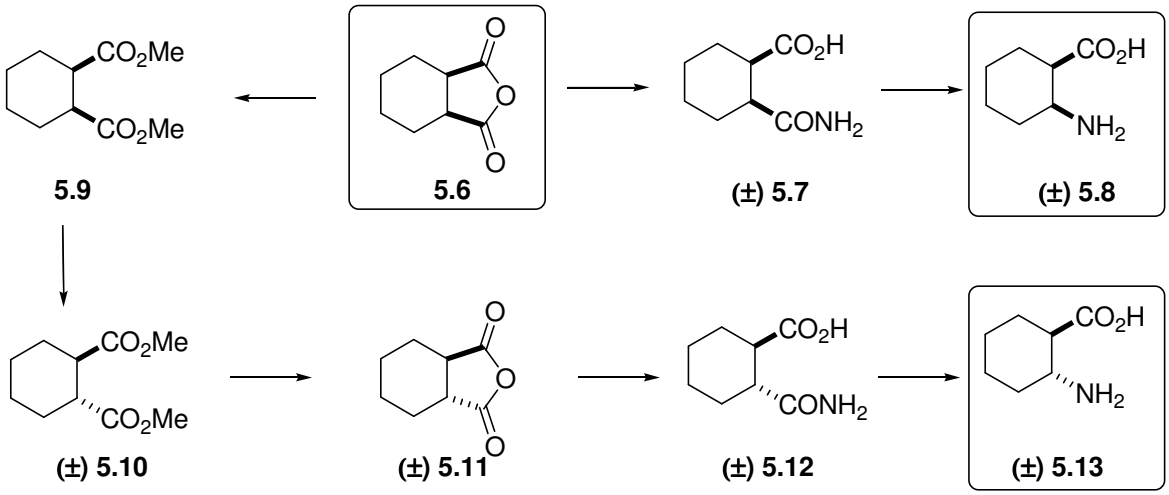

Scheme 5.2 Racemic synthesis of *cis* and *trans* ACHC (**5.8** and **5.13**, respectively).

The synthesis of *trans*-cyclohexane **5.13** required three additional steps. Esterification of anhydride **5.6** gave the *cis*-diester **5.9** and this was epimerised with sodium methoxide to give the *trans*-diester **5.10**. Dehydration of this ester afforded the *trans* anhydride **5.11**, which was reacted to give the amine **5.13** in two steps, as previously described.[7]

Enzymatically-resolved Syntheses

With the realisation that cyclic *β*-amino acids are valuable in the synthesis of constrained mimetics, the availability of enantiomerically pure *β*-amino acid became important. Enantiomerically pure *cis β*-amino acid **5.8** was synthesised from diester **5.9** (Scheme 5.3). This ester was regiospecifically hydrolysed using pig liver esterase to give the monoester **5.14**.[8,9] Reaction of this ester with sodium azide afforded the azide intermediate **5.7**. A subsequent Curtius rearrangement of the azide gave the enantiomerically pure *cis β*-amino acid **5.8**. In a related synthesis, epimerisation of the methyl ester of **5.14** to the *trans*-analogue, gave the enantiomerically pure *trans-β*-amino acid **5.13** (not shown).[10]

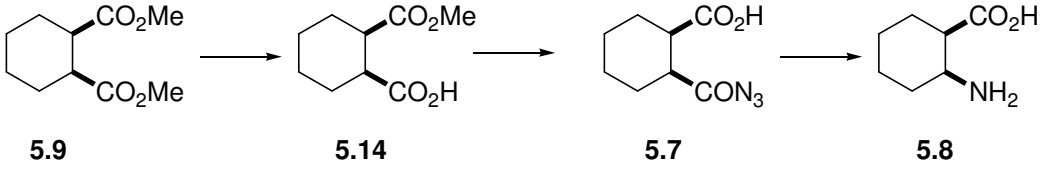

Scheme 5.3 Enantiomeric synthesis of *cis*-ACHC using enzymatic resolution.

More recently, a general enzymatically-catalysed synthesis of cyclic *β*-amino acids was developed by Forro *et al.*[11] The *β*-lactam **(±) 5.15** was enantioselectively hydrolysed with a lipase B enzyme, giving *cis β*-amino acid **5.16**. This resolved the other *β*-lactam enantiomer **5.15**, which could then be hydrolysed non-enzymatically (Scheme 5.4).

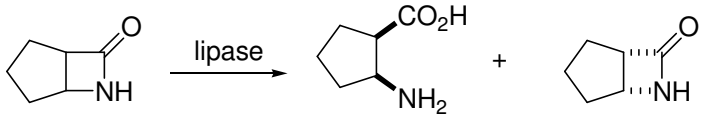

(±) **5.15** **5.16** **5.15**

Scheme 5.4 Enzyme catalysed resolution of a racemic *β*-lactam.

Another reaction sequence which includes an enzymatic resolution step involves the enantioselective acylation of *β*-amino acid **(±) 5.17**, to give the amide **5.18** and resolving the other enantiomer **5.17**. [12,13]

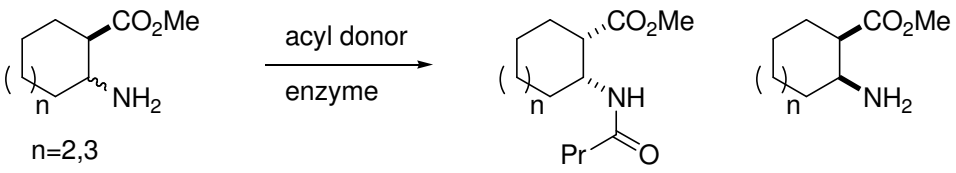

(±) 5.17 **5.18** **(+) 5.17**

Chiral Auxiliaries

The use of chiral auxiliaries to introduce stereocentres into achiral molecules has proven very successful in the synthesis of *β*-amino acids. For example, the racemic ketone **(±) 5.19** was reacted with chiral *α*-methyl benzylamine, to give the enantiomerically pure *β*-enaminoester **5.20** (Scheme 5.5).[14] . This intermediate was reduced at the least hindered face of the double bond using sodium borohydride. This gave *cis β*-amino ester **5.21** as the major stereoisomer. An alternative reduction at the more hindered face of enaminoester **5.20** with sodium cyanoborohydride gave the corresponding *trans β*-amino acid (not shown).[15]

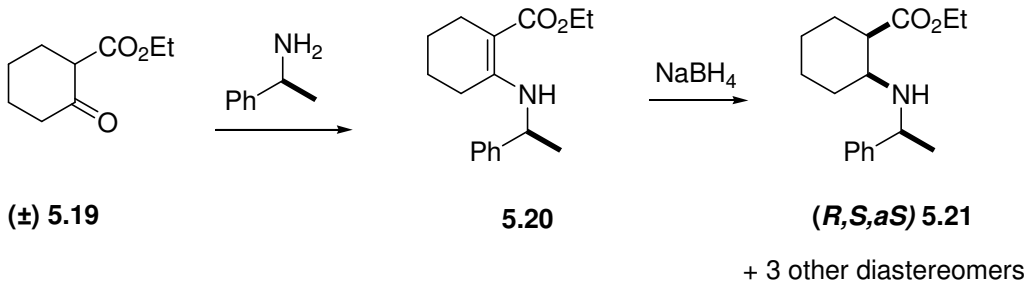

Scheme 5.5 Diastereoselective reduction of a *β*-enaminoester to give a *β*-amino acid.

Davies *et al* synthesised enantiomerically pure cyclic *β*-amino acids in 98% diastereomeric excess (*de*) via conjugate addition of a chiral amine to cyclic *α*,*β*-unsaturated esters (Scheme 5.6).[16,17] Stereoselective addition of the chiral amine, followed by aqueous quenching of the lithium enolate gave the *cis* product **5.23** as the major isomer. The chiral amine moiety was hydrogenated with $Pd(OH)_2$ to give the cyclopentane-based *β*-amino acid **5.15**, (or first epimerised to give the *trans* product **5.25**). This versatile general method was also used to synthesize novel heterocyclic *β*-amino acids (Scheme 5.6).[18]

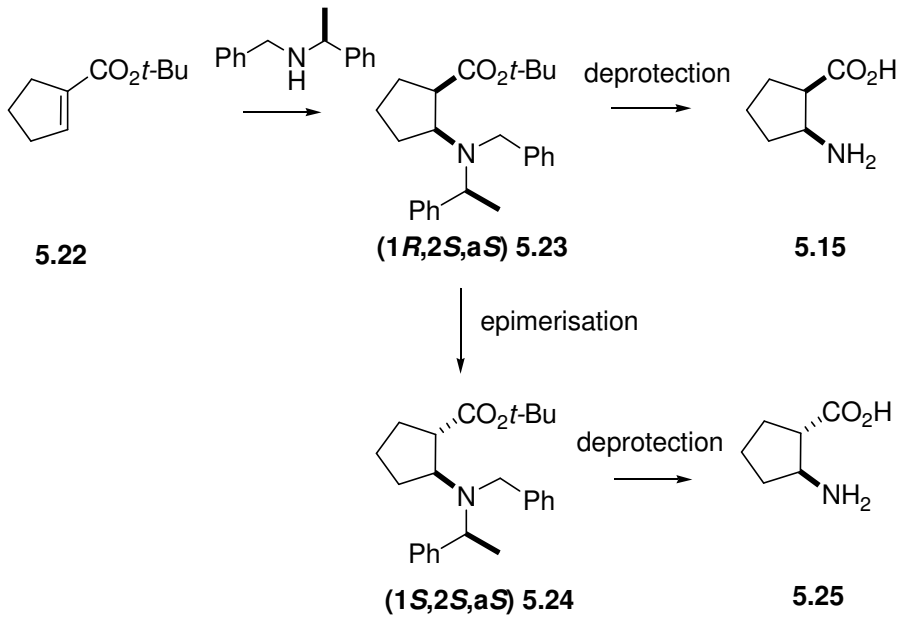

Scheme 5.6 Diastereomeric synthesis of *cispentacin* (**5.15**) and *trans* ACPC (**5.25**) from an *α*,*β*-unsaturated precursor.

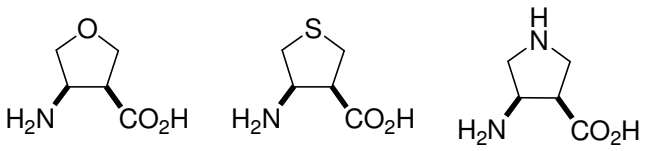

Figure 5.1 Heterocyclic species synthesised by conjugate addition reactions.

Enders *et al* synthesised cycloheptane-based *β*-amino acids using a conjugate addition/alkylation reaction of *α*,*β*-unsaturated ester **5.26** (Scheme 5.7).[19,20] This gave the cyclic intermediate **5.27** in >96% de. This chiral auxiliary was cleaved to give the *β*-amino acid **5.28**.

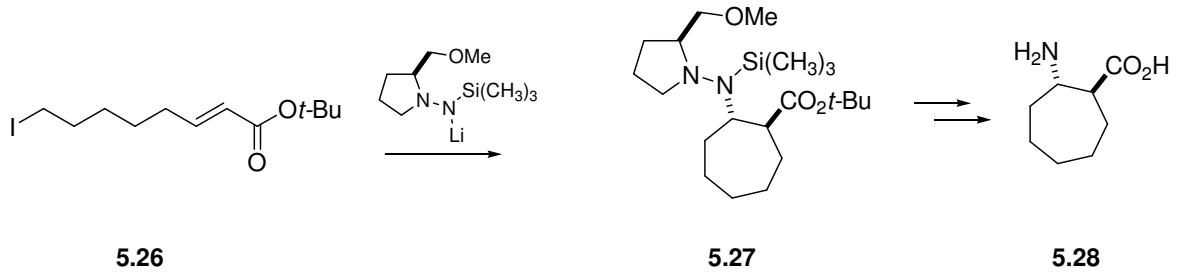

5.26 **5.27** **5.28**

Scheme 5.7 The enantioselective synthesis of *trans*-2-amino-cycloheptane-1-carboxylic acid **5.28** using conjugate addition/alkylation.

Ruthenium Catalysts

More recently, the application of ruthenium catalysts in the synthesis of *β*-amino acids has been explored. Ruthenium catalysts have been employed both in the stereoselective hydrogenation of alkenes, and in the ring-closing metathesis (RCM) of dienes. [21-24]

Enantioselective hydrogenation of the *α*,*β*-unsaturated ester **5.29** using a ruthenium catalyst with chiral ligands gave the *β*-amino ester **5.30**, in up to 99% *de* (Figure 5.2). This reaction proved efficient for the synthesis of cyclopentane and cyclohexane examples. However, hydrogenation of seven- and eight-membered cycles gave lower diastereoselectivity.[22]

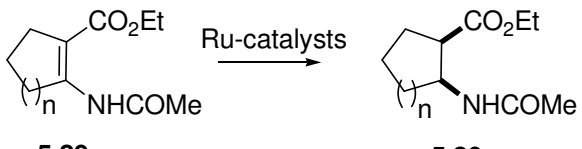

5.29 **5.30**

n	*de* (%)
1	99
2	92
3	80
4	44

Figure 5.2 Ruthenium-catalysed enantioselective hydrogenation.

A versatile method to synthesize *cis* or *trans* *β*-amino acids utilises a RCM approach using Grubb's 1st and 2nd Generation ruthenium catalysts **3.1** and **3.2** (illustrated in Chapter Three, Section 3.1.1). Gardiner *et al* demonstrated the synthesis of cyclic *β*-amino acids (**5.33**) from natural *α*-amino acids using RCM.[23] The generalised scheme is shown in Scheme 5.8. This synthesis involved the conversion of *α*-amino acid side chain to an alkene by various synthetic

methods (not shown), followed by Ardnt-Eistert homologation to give the olefinic β-amino acid (**5.31**). Allylation at the β^2 position gave the *trans*-diene **5.32**, necessary for cyclisation using Grubb's catalyst **3.1** or **3.2**.

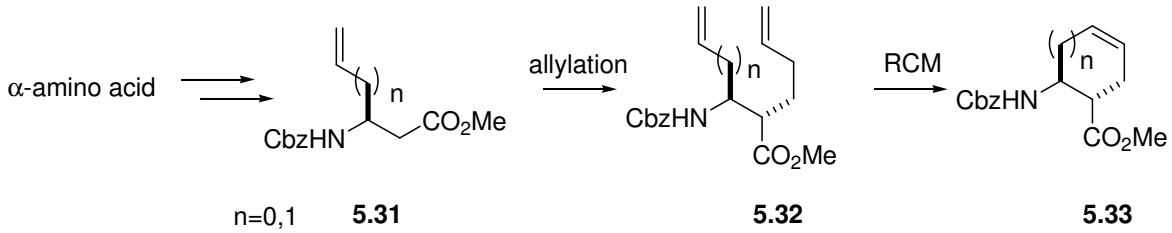

n=0,1 **5.31** **5.32** **5.33**

Scheme 5.8 The generalised scheme for the synthesis of cyclic β-amino acids via RCM.

5.1.1 Research Described in This Chapter

As described in Chapter One, a particular advantage of β-amino acids over the natural α-analogues is the possibility to introduce substitution and conformational constraints (cycles) into the peptide backbone. The synthesis of enantiomerically pure β-amino acids typically requires the use of expensive chiral reagents and catalysts, or natural enzymes. However, Gardiner's RCM metathesis approach is distinctive in that the chirality of the starting material defines the chirality in the overall cyclic β-amino acid.[21,23] Furthermore, the cycloalkene product obtained from RCM can be further modified at the olefin, allowing for greater functionalisation.

Very few syntheses address stereoselective substitution in the cyclic β-amino acid backbone. The conjugate addition approach by Davies *et al* has proven useful for alkylation and hydroxylation, however to date, no halogen substitutions in cyclic β-amino using this methodology have been studied. The research in this chapter addresses the synthesis of two classes of cyclic β-amino acids that were largely unexplored in the literature:

- Cyclic β-amino acids with fluorine substitution along the peptide backbone
- Synthesis of larger (seven, eight and nine-membered) cyclic amino acids using the RCM approach

5.2 Synthesis of Fluorinated β-Amino Acids

5.2.1 Background

As described earlier in this chapter, the conjugate addition of a chiral amine with an *α,β*-unsaturated system is an efficient and stereoselective method to synthesise enantiomerically pure *β*-amino acids. Quenching of the lithium enolate intermediate with a species other than a proton introduces functionality into the β^2 position of the resulting *β*-amino acid (**5.35**) (Scheme 5.9). Various alkylations, to introduce methyl,[25] ethyl,[26] allyl,[27] benzyl,[27] phenyl, substituted phenyl[28] and hydroxyl groups,[29] are described in the literature.

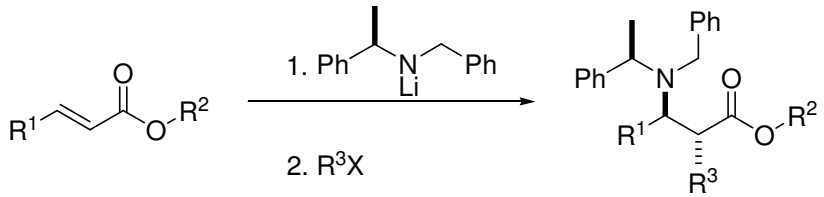

5.34 **5.35**

Scheme 5.9 The tandem conjugate addition/alkylation reaction.

The diastereomeric ratios for alkylations range from 0 to >94 % *de*.[18] The stereochemistry of the reaction is governed by two processes – firstly, the geometry of addition of the chiral amine to the double bond; and secondly, the subsequent attack of the electrophile (R^3X) by the intermediate enolate. These points will be discussed in detail in the next section.

Andrews *et al* established a general procedure to introduce fluorine into the β^2 position of *β*-amino acids.[30] The C-F bond is increasingly important in medicinal chemistry as a replacement for C-O and C-H bonds.[31] Fluorine possesses a small atomic radius, and is sterically the closest substitute for the C-H bond. The high electronegativity of fluorine makes the C-F bond a suitable replacement for the C-O bond, and the high bond strength renders this bond resistant to chemical degradation. It is estimated that 20-25% of all pharmaceuticals under development contain at least one C-F bond.[31]

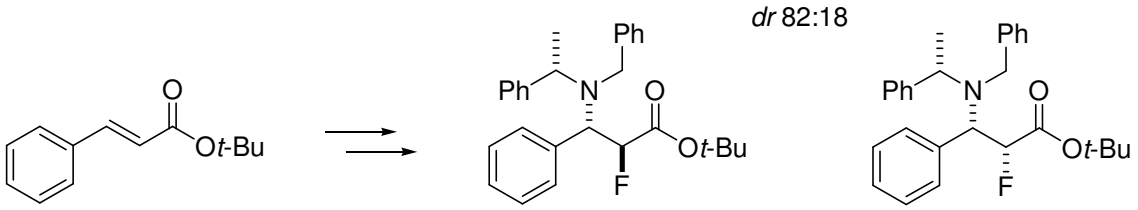

5.36 **5.37** **5.38**

Scheme 5.10 Conjugate addition/fluorination of cinnamic acid to give a β^2-fluorinated amino acid.

Andrews *et al* performed the tandem conjugate addition/fluorination reaction on α,β-unsaturated cinnamic acid (**5.36**), with *N*-fluorobenzenesulfonimide as the electrophilic fluorine source (Scheme 5.10).[30] This gave two diastereromers, **5.37** and **5.38**, in a quantitative overall yield and with a diastereomeric ratio of 82:18 (a diastereomeric excess of 64%). The major diastereoisomer **5.37** was formed by the nucleophilic attack of the enolate from the opposite face with respect to the chiral amine group. The conjugate addition/fluorination reaction of another unsaturated ester, ethyl crotonate ($CH_3CH{=}CHCO_2CH_2CH_3$), gave a diastereomeric ratio of 83:17 (66% diastereomeric excess).[30]

The conjugate addition/fluorination reaction has proven to be very effective for the synthesis of acyclic fluorinated β amino acids. However, there are no other reported syntheses of this type on any other substrates. Given the importance of cyclic amino acids in natural and synthetic peptides, the synthesis of cyclic fluorinated amino acids was an important and obvious synthetic target. Presented here, is the synthesis of cyclic β^2-fluorinated amino acids using a conjugate addition/fluorination reaction.

5.2.2 Synthesis of Novel Cyclic Fluorinated β-Amino Acids 5.43a and 5.43b

Novel five and six-membered cyclic fluorinated β-amino acids were synthesised from cyclopentenyl- and cyclohexenyl-based α,β-unsaturated esters **5.40a** and **5.40b** using the methodology described by Andrews *et al* (Scheme 5.11).[30] The commercially available 1-cycloalkene-1-carboxylic acids **5.39a** and **5.39b** were first protected with bulky *tert*-butyl ester groups. This prevented nucleophilic attack at the carbonyl group by the lithium amide in the

subsequent reaction step. The coupling of *tert*-butyl alcohol with the cyclic acids **5.39a** and **5.39b** using the reagents EDCI/DMAP,[32] EDCI/HOBt[33] and HATU were attempted, however the yields were poor despite the generality of these methods on other substrates. A likely reason is steric hindrance of the bulky coupling agents with the relatively hindered carboxylic acid group of the alkenes. The reaction of the acids **5.39a** and **5.39b** with isobutylene gas and catalytic sulfuric acid in a sealed tube for 48 hours was successful, giving the *tert*-butyl esters **5.40a** and **5.40b** in 92% and 96% yield, respectively.

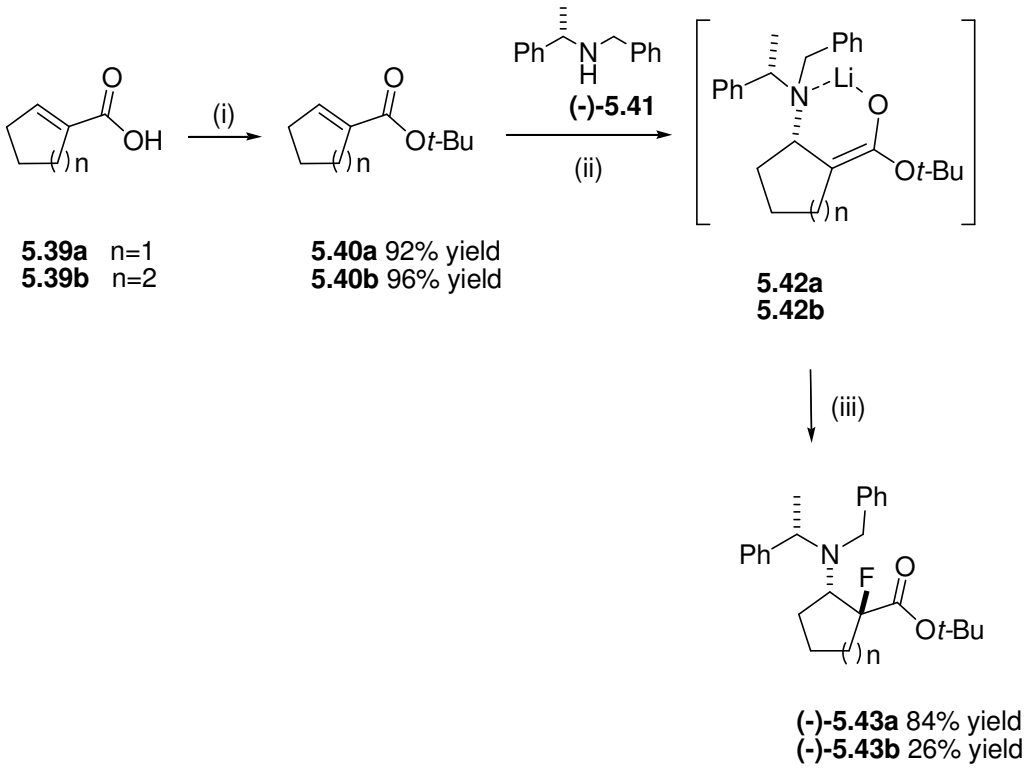

Scheme 5.11 *Reagents and conditions:* (i) isobutylene (g), H_2SO_4 (cat), DCM, sealed tube, 48 h (ii) BuLi, THF, -78 ºC, 30 min, (iii) *N*-fluorobenzenesulfonimide, 3 h, -78 ºC to 0 ºC.

Conjugate addition of the lithiated (*S*)-(-)-*N*-benzyl-*α*-methylbenzylamine salt (formed by reacting butyl lithium with secondary amine **(-)-5.41**), to the esters **5.40a** and **5.40b** at -78 ºC gave the lithium enolate intermediates **5.42a** and **5.42b**. Because of the chirality of the methylbenzylamine group, there is only one favourable alignment of the *α*,*β*-unsaturated ester with the chiral amine. This creates exclusively the (*R*) stereocenter on the intermediates **5.42a** and **5.42b**, as shown in Scheme 5.11. Davies *et al* proposed four possible alignment modes of the chiral amine **5.41** and cinnamic acid (as shown in Figure 5.3 looking from above).[18] The unfavoured alignment modes each encounter a steric hindrance between a proton or methyl group on the chiral amine with the phenyl or proton on the cinnamic acid. The favoured arrangement has no steric clashes.

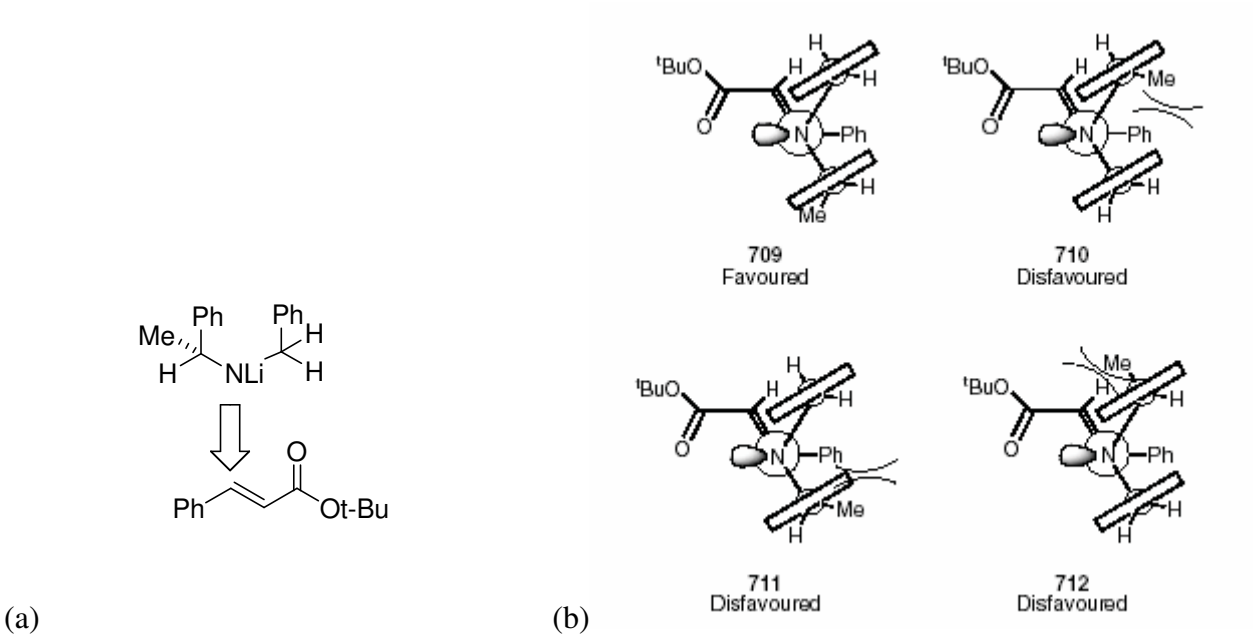

Figure 5.3 (a) The nitrogen group must align with the *α*,*β*-unsaturated ester so nucleophilic attack can occur. (b) The proposed geometries of nucleophilic attack, seen from above. Steric clashes are represented with brackets. The phenyl groups are shown from the top view, as rectangles. (Reproduced from Ref. [18])

The lithium enolate intermediate is stabilised by the coordination of the lithium ion with the oxygen and nitrogen atoms. This also serves to hold the intermediate in a rigid conformation, which makes the subsequent fluorination step stereoselective. The nucleophilic fluorine source could approach either from the top or bottom face (as drawn in Figure 5.4). However, approach from the top face is sterically favoured because of the bulky phenyl amine groups which lie on the lower face. Therefore, attack of the enolate at the nucleophilic fluorine source, *N*-fluorobenzenesulfonimide, gave the *trans*-fluorinated *β*-amino esters at the major isomers (**5.43a** and **5.43b**). The cyclopentyl example **5.43a** was formed in a higher yield than the cyclohexyl analogue **5.43b**, giving 94% and 35% conversion respectively. The greater planarity of the cyclopentyl ring may allow a closer approach of the fluorine source to the reactive enolate centre of **5.42a**.

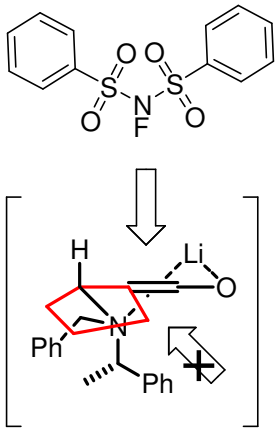

Figure 5.4 Lithium enolate transition state **5.42**a (cyclopentane ring shown in red for clarity). The electrophile is attacked from the less hindered top face.

^{19}F NMR was used to quantify the diastereomeric excess of the major isomers **5.43a** and **5.43b** as it gives sharp, distinct peaks. The spectra of the crude reaction mixtures are shown in Figure 5.5. The major peak at ~-145 ppm in each spectrum corresponds to the major isomer, as shown. The smaller peaks between -130 and -150 ppm are presumably due to diastereoisomers, although this was not confirmed because the quantity of each was too small to isolate.

Integration of the major and minor peaks between ~-130-150 ppm gave a diastereomeric ratio for each of the reaction mixtures. The diastereomeric ratio of the major isomer to the minor isomers in Figure 5.5a was 93:7, and in Figure 5.5b was 97:3. This stereospecificity is much higher than that reported by Andrews *et al* for conjugate addition/fluorination on linear unsaturated esters, and is probably due to the rigidity and steric effects imposed by the ring system. Conjugate addition reactions in the literature show similarly high diastereomeric ratios for other $\beta^{2,3}$-substituted and cyclic $\beta^{2,3}$ amino acids.[18]

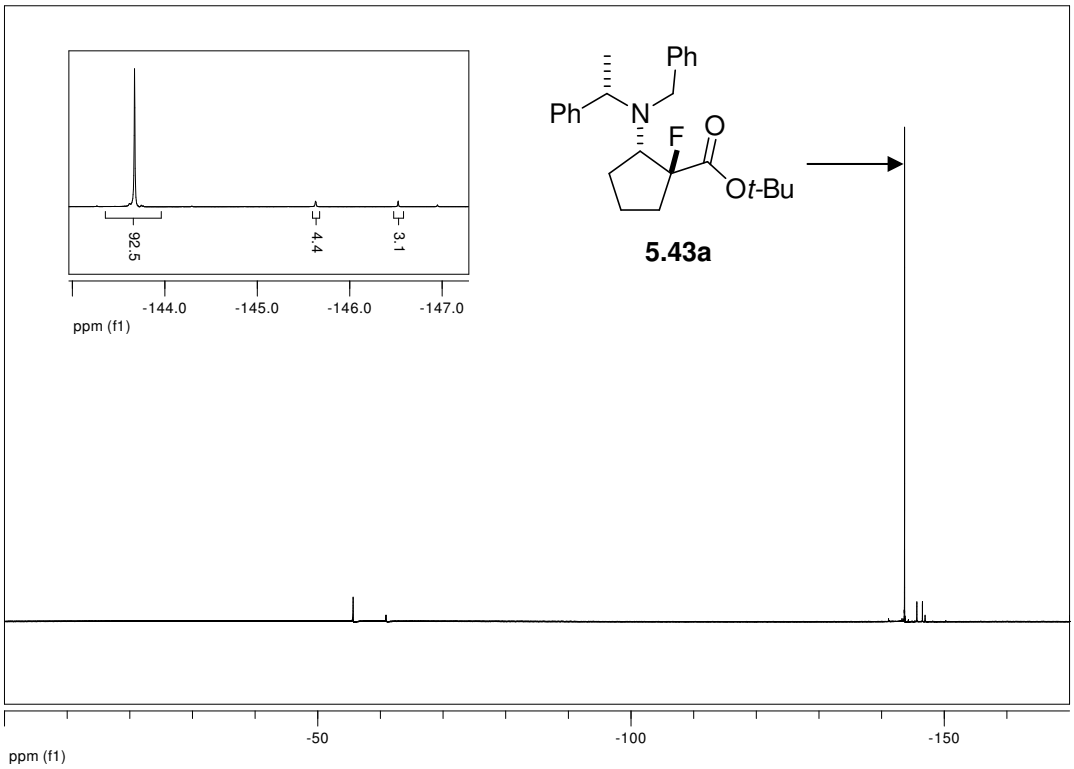

a)

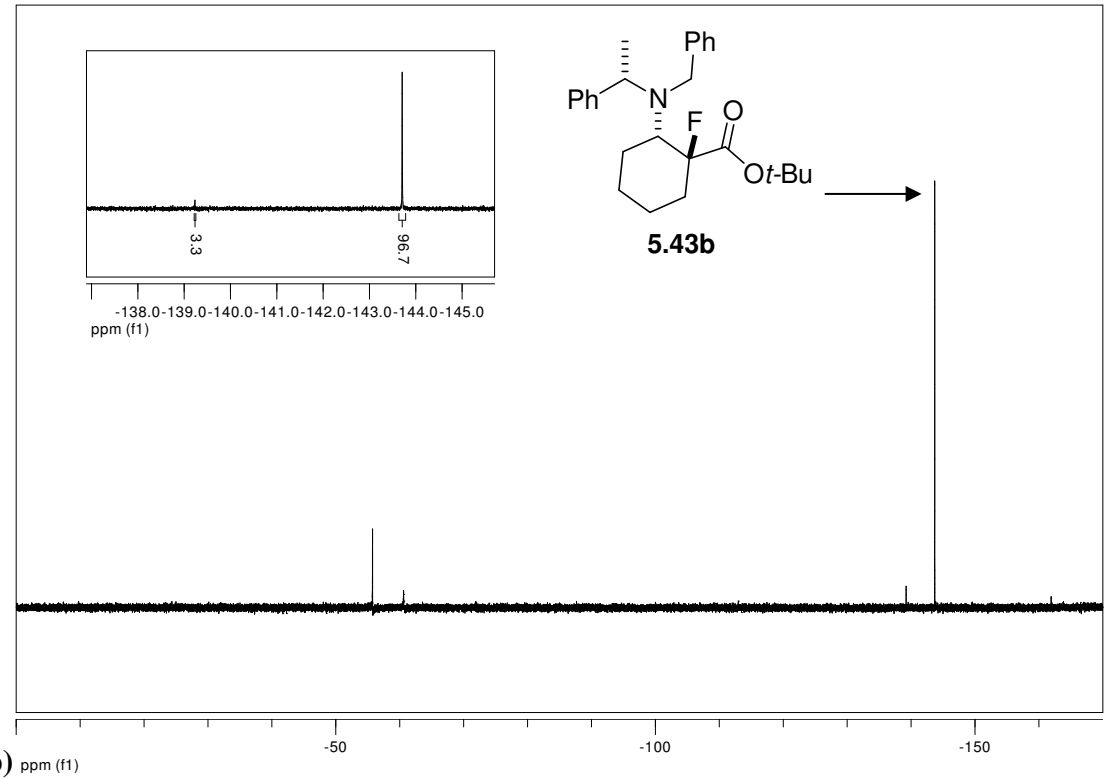

b)

Figure 5.5 ^{19}F NMR of the crude product of conjugate addition/fluorination of a) **5.43a** and b) **5.43b** fluorinated *β*-amino esters. The inset figures show the major isomers and possible other isomers (not isolated).

Typically, the relative stereochemistry at the β^2 and β^3 positions of cyclic *β*-amino acids can be confirmed by the magnitude of the coupling constants between the β^2 and β^3 protons (utilising the Karplus equation). However, confirmation of the absolute stereochemistry of the products

5.43a and **5.43b** is difficult by NMR spectroscopy due to the absence of a proton at the β^2 stereocenter. However, an X-ray crystal structure of compound **5.43a** was obtained, confirming the assigned stereochemistry (Figure 5.6). The stereochemistry of the (*R*)-*α*-methylbenzylamine moiety is known, so (despite the lack of heavy atoms in the molecule) the absolute stereochemistry of the compound could be assigned. It was inferred that conjugate addition/fluorination to give compound **5.43b** (for which no x-ray data was obtained) would result in the same absolute stereochemistry as **5.43a**, because of the structural similarity of the esters **5.40a** and **5.40b**. The asymmetric unit of the crystal of compound **5.43a** contained four molecules, each with a unique conformation. The difference between these conformations was less than 0.5 Å.

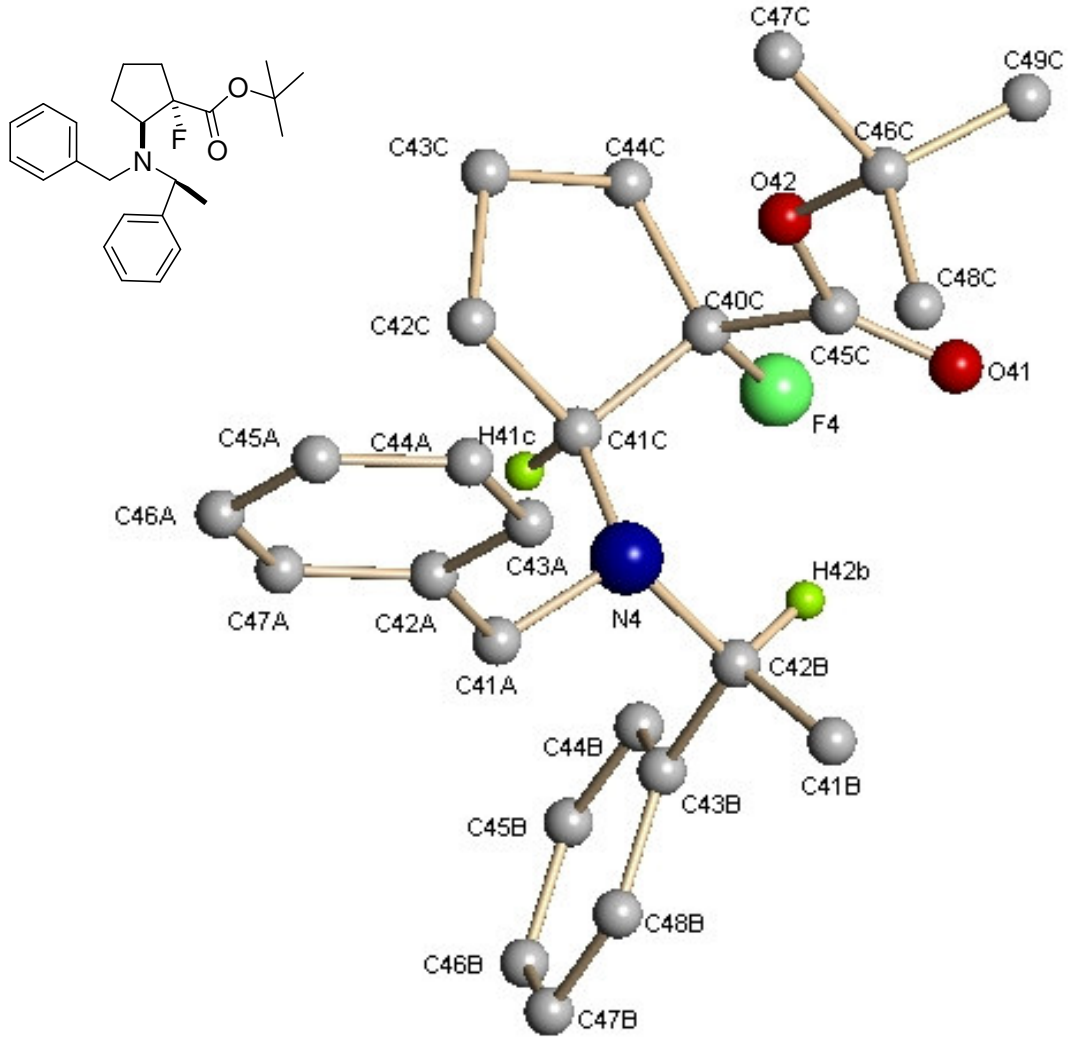

Figure 5.6 X-ray crystal structure of **5.43a** showing one of the four molecules in the asymmetric unit. Atom colours: C, grey; N, blue; O, red, F, green, H, yellow-green. Atom sizes are not to scale and many hydrogens are omitted for clarity.

The same conjugate addition/fluorination reaction with the other enantiomer of the chiral amine, (*R*)-(+)-*N*-Benzyl-*α*-methylbenzylamine **(+)-5.41**, gave **(+)-5.43a** and **(+)-5.43b**, the enantiomers of compounds **(-)-5.43a** and **(-)-5.43b** (Scheme 5.12). Predictably, the optical rotation of these compounds was the reverse polarity of **(-)-5.43a** and **(-)-5.43b**.

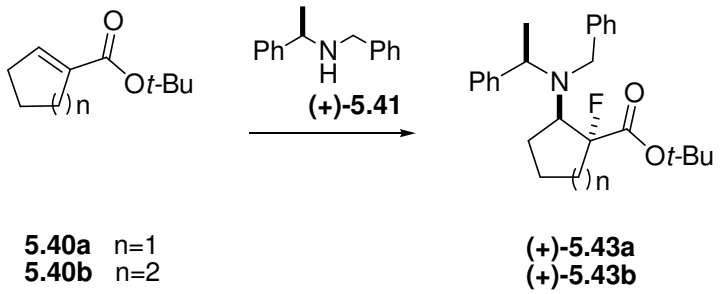

5.40a n=1
5.40b n=2

(+)-5.43a
(+)-5.43b

Scheme 5.12 *Reagents and conditions:* BuLi, THF, -78 ºC, 30 min, then *N*-fluorobenzenesulfonimide, -78-0 ºC.

The removal of the protecting amine and ester groups, to give the cyclic *β*-amino acid, was demonstrated with **5.43a** (Scheme 5.13). The amine was deprotected by hydrogenation of the dibenzyl groups with hydrogen gas and Pearlman's catalyst ($Pd(OH)_2$). A commonly reported hydrogenation method for compounds of this type uses 5 atm of hydrogen gas with methanol and acetic acid or ethyl acetate as the solvent. However, when compound **5.43a** was treated under those conditions, an intractable mixture was obtained. Hydrogenation using only 1 atm of hydrogen gas gave the desired amine **5.44** in 83% yield as a clear oil. Deprotection of the ester group with trifluoroacetic acid gave the *β*-amino acid **5.45** in quantitative yield.

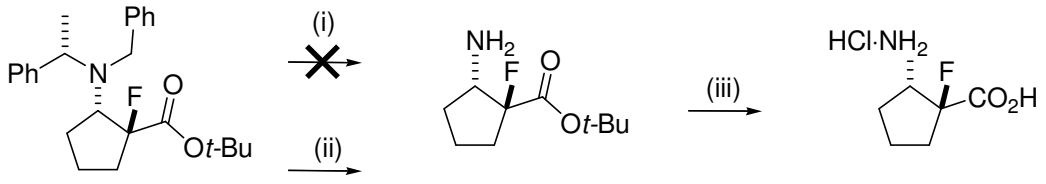

5.43a **5.44** **5.45**

Scheme 5.13 *Reagents and conditions:* (i) $Pd(OH)_2$, MeOH, H_2 (5 atm), rt, 16 h, no product formed, (ii) $Pd(OH)_2$, methanol, H_2 (1 atm), rt, 3 h, 83% yield, (iii) 4 M HCl/dioxane, rt, 30 min, 49% yield.

5.3 Synthesis of Cyclic β-Amino Acids using Organozinc Reagents

5.3.1 The RCM Reaction

RCM is a versatile reaction for the formation of cyclic alkenes from dienes. The reaction is entropically driven, cyclising a diene, and liberating ethene gas (Figure 5.7). Coordination of an alkene from diene **F** leads to intermediate **A** with ruthenium center and gives the key intermediate cyclobutyl-ruthenium species **C**. **C** and **G** collapse to form a new double bond **A** and **D**. The reaction is reversible if ethylene remains in the system, and the product **D** can reform the cyclobutyl intermediate **C** to give the most stable double-bond (*cis* or *trans*). The two most common catalysts for RCM are the Grubb's 1st and 2nd Generation catalysts **3.1** and **3.2**.

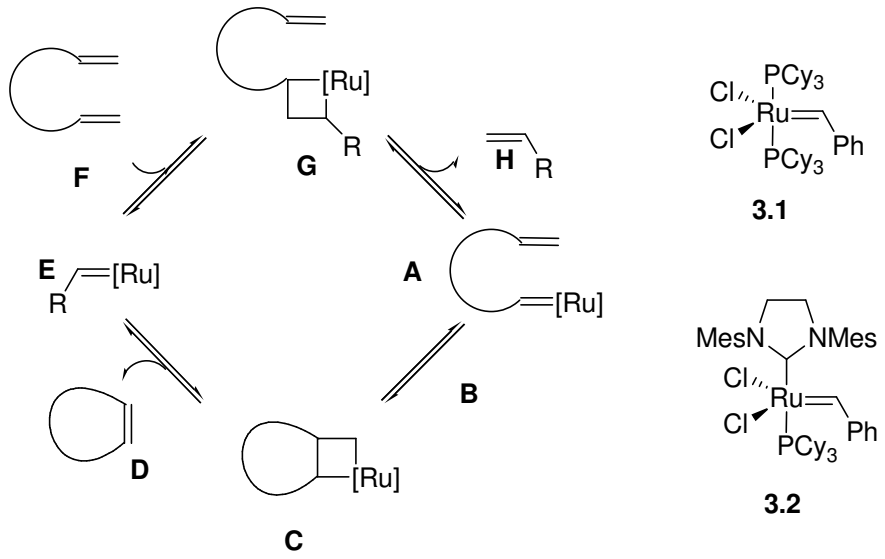

Figure 5.7 Ruthenium-catalysed RCM of a diene using Grubbs' catalyst **3.1** or **3.2**. R = Ph in the first catalytic cycle and H in every cycle thereafter.

The initial sequence in the synthesis of cyclic *β*-amino acids by Gardiner *et al* of the Abell research group, University of Canterbury, involved the multi-step conversion of natural *α*-amino acids into olefinic *β*-amino acids (Scheme 5.8).[21,23] Gardiner *et al* applied this general methodology to the synthesis of cyclopentyl- and cyclohexyl-based *β*-amino acids from enantiomerically pure *α*-amino acids.[21] The success of this methodology towards the synthesis of cyclopentyl- and cyclohexyl-based *trans* cyclic *β*-amino acids warranted an attempt with

larger ring sizes. Presented here is an investigation of the synthesis of seven, eight and nine-membered cyclic β-amino acids using the RCM approach.

5.3.2 Retrosynthetic Analysis of Cycloheptyl and Cyclooctyl-based β-Amino Acids from α-Amino Acids

The retrosynthetic analysis for the synthesis of the seven-membered cyclic β-amino ester **5.51a** and the attempted synthesis of eight-membered β-amino ester **5.51b** is shown in Scheme 5.14. This methodology is based on the synthesis of cyclohexane and cyclopentane-based β-amino acids by Gardiner *et al*, whereby allylation of an olefin-terminated β-amino acid gave the dienes suitable for RCM (Scheme 5.8). The length of the sidechain olefin groups in compounds **5.53a** and **5.53b** would dictate the overall ring size of the cyclic amino acid.

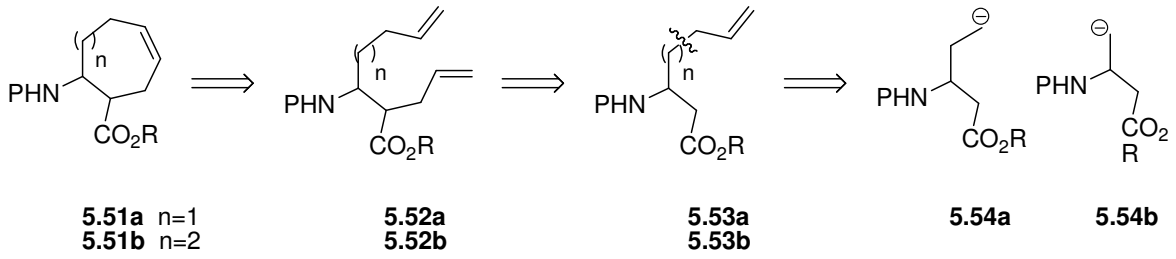

5.51a n=1 **5.51b** n=2 | **5.52a** **5.52b** | **5.53a** **5.53b** | **5.54a** | **5.54b**

Scheme 5.14 Retrosynthetic analysis for the synthesis of seven and eight-membered cyclic β-amino acids.

The alkenes **5.53a** and **5.53b** could not be synthesised via a direct conversion of an α-amino acid side chain. A formal disconnection of a terminal allyl unit from **5.53a** and **5.53b** gave the anionic synthons **5.54a** and **5.54b**, which can be derived from the organozinc compounds **5.55a** and **5.55b** shown in Scheme 5.15. Jackson *et al* allylated the organozinc reagents to give compounds of the type **5.53**.[34-36] It was shown that the organozinc reagents **5.55a** and **5.55b** could be synthesised from the hydroxylated β-amino acids **5.56a**[*] and **5.56b**. These β-amino acids were, in turn, derived from selectively protected aspartic acid **5.57a** and the homologated analogue of *N*-protected homoserine (**5.57b**). The side chain of aspartic acid can function as part of a β-amino acid backbone, leaving the former backbone carboxylic acid group to act as the new side chain.

[*] Note that synthon **5.64a** was also synthesised from the Ardnt-Eister homologation of serine. This work was published by carried out and published concurrently with the aspartic acid approach, in collaboration with Gardiner.

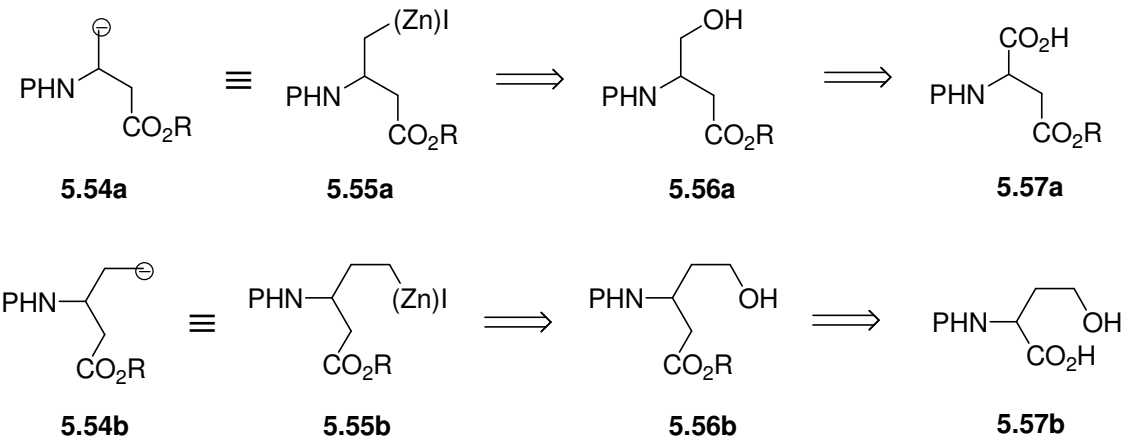

5.54a **5.55a** **5.56a** **5.57a**

5.54b **5.55b** **5.56b** **5.57b**

Scheme 5.15 Retrosynthetic analysis for the synthesis of seven and eight-membered cyclic *β*-amino acids (continued from Scheme 5.14).

The *α*-amino acids aspartic acid and homoserine were ideal starting materials for the synthesis of cyclohexyl and cyclooctyl-based *β*-amino acids. Suitable protecting groups for this reaction scheme were a Boc group for the amine and a methyl ester for the acid terminus. Cleaving Cbz or benzyl ester protecting groups would require hydrogenation, and are therefore are not compatible if the olefin moiety is desired for further functionalisation.

5.3.3 Synthesis of *trans*-7-Aminocyclohept-3-ene-1-carboxylic Acid (5.63)

The synthesis of the cycloheptyl *β*-amino acid **5.63** using RCM, is shown Scheme 5.16. As described in the previous section, aspartic acid **5.58** is a useful starting material because it possesses a *β*-amino acid-like backbone.

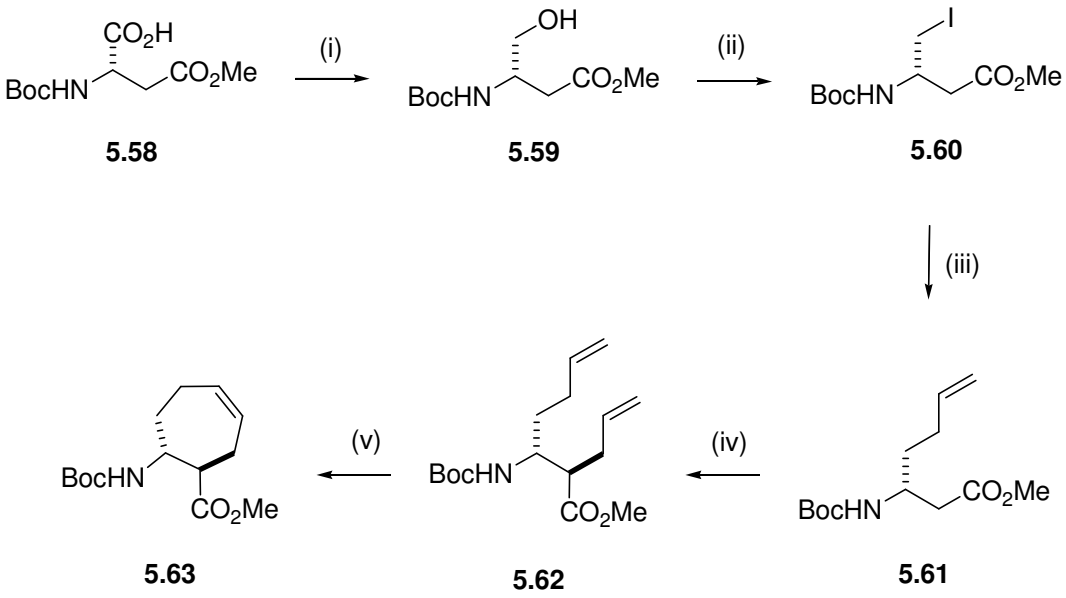

5.58 **5.59** **5.60** **5.61** **5.62** **5.63**

Scheme 5.16 *Reagents and conditions:* (i) *N*-hydroxysuccinimide, DCC, ethyl acetate, rt, 16 h, then $NaBH_4$, THF, H_2O, 0 ºC, 5 min, 50% overall yield, (ii) I_2, PPh_3, imidazole, DCM, rt, 1 h, quant. yield, (iii) Zn, DMF, rt, 30 min, then CuCN.2LiCl, DMF, allyl bromide, -55 ºC – rt, 16 h, 61% yield, (iv) LiCl, THF, LDA, allyl bromide, -78 ºC – rt, 16 h, 42 % yield, (v) 3.2, benzene, rt, 16 h, 70% yield.

The free acid group of the partially protected aspartic acid **5.58** was coupled with *N*-hydroxysuccinimide to give an activated succinimide ester. This was reduced with sodium borohydride to give alcohol **5.59** in 50% yield. The low yield of this reaction was due to the facile intramolecular condensation reaction of **5.59** to give lactone **5.64** (Scheme 5.17).

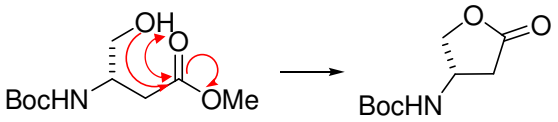

5.59 **5.64**

Scheme 5.17 A facile intramolecular condensation reactions gives lactone **5.64**.

The alcohol **5.59** was reacted with iodine, triphenylphosphine and imidazole to give the iodide **5.60** in quantitative yield. This was reacted with activated zinc metal to afford the nucleophilic organozinc compound **5.64**, followed by a CuCN mediated coupling with allyl bromide gave the olefin **5.60**, in a one-pot reaction in 61% overall yield (Scheme 5.18). Jackson *et al* proposed the dicoordinated species shown in Figure 5.8, to account for the peculiarly high stability of these zinc intermediates.

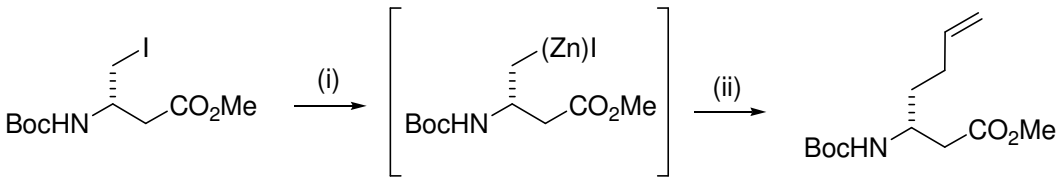

5.60 **5.64** **5.61**

Scheme 5.18 *Reagents and conditions:* (i) Zn, DMF, rt, 30 min, (ii) CuCN.2LiCl, DMF, allyl bromide, -55 ºC – rt, 16 h, 61% yield.

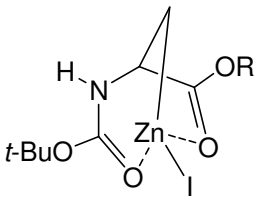

Figure 5.8

The nucleophilicity of organozinc compounds is due to the difference in electronegativity of carbon and zinc. This polarises the electron density of the carbon-zinc bond towards carbon. The synthetic utility of these reactions for the synthesis of amino acids possessing unnatural side-chains was established by Jackson *et al.*[34,35] However, the formation of the intermediate zinc complex **5.64** from zinc metal proved difficult and suffered poor reproducibility. Despite the low cost, safe handling and functional group tolerance of zinc reagents, the unreliability of zinc insertion is evidenced by the lack of industrial processes using this chemistry.[37] The particular difficulty of forming organozinc compounds lies in the activation of the zinc dust, by removal of the oxide layer from the surface. A number of approaches have been published, such as electrochemical cleaning;[38] treatment with TMSCl,[39] 1,2-dibromoethane,[40] or both;[41] and iodine.[42] All of these methods suffer from lack of reproducibility or achieved only partial conversion before the zinc-insertion reaction self-terminated.

Despite these limitations, enough allylated material (**5.61**) was obtained to complete the synthesis. Deprotonation of olefin **5.61** at the β^2-position (adjacent to the carbonyl group) using lithium diisopropylamine (LDA) gave a lithiated enolate intermediate **5.66** (Scheme 5.19). Subsequent nucleophilic attack of allyl bromide gave the diene species **5.62**, in 38% yield. Only the *trans*-isomer was obtained, as evidenced by the lack of the other diastereoisomer in the NMR spectrum (and an x-ray crystal structure, as described later). This stereoselectivity is attributed to the nitrogen-coordinated lithium enolate species **5.66**, as shown in Scheme 5.19. The configuration at the substituted β^3-position, directs attack at the opposite face to the sidechain, giving a *trans*-configuration.

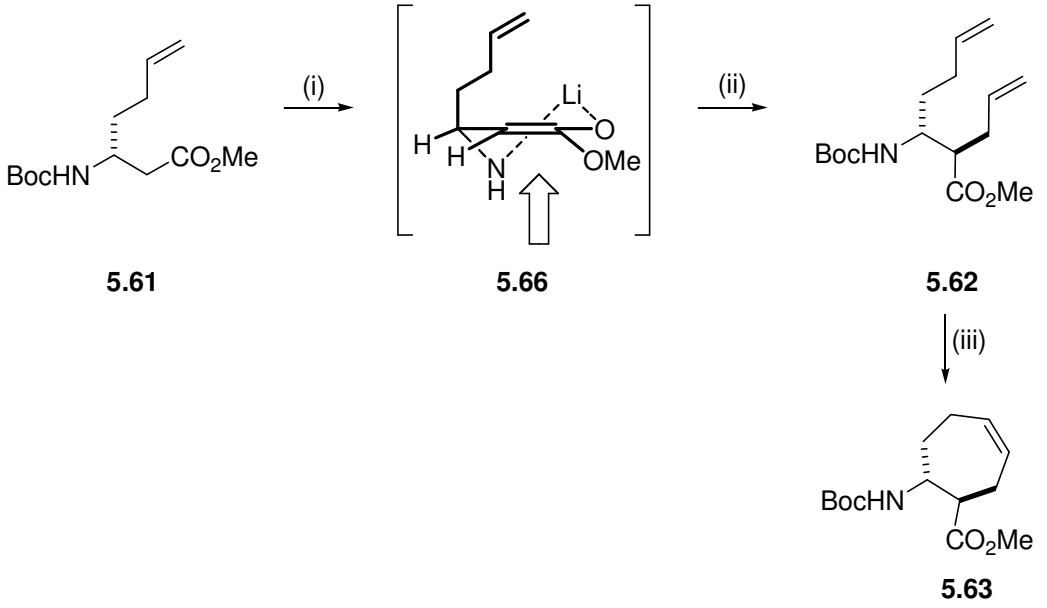

5.61 **5.66** **5.62** **5.63**

Scheme 5.19 The proposed lithiated intermediate, formed by treatment of **5.61** with LDA. The arrow shows the direction of approach of the allyl bromide. *Reagents and conditions*: (i) LiCl, THF, LDA, -78 ºC, 1 h, (ii) allyl bromide, -78 ºC – 0 ºC, 16 h, 42% yield, (iii) Grubbs' 2nd Gen., benzene, rt, 16 h, 70% yield.

RCM of the diene at room temperature with Grubb's catalyst **3.2** gave the cyclic β-amino acid **5.63**, in 70% yield. An X-ray crystal structure confirmed the absolute configuration of **5.63**, where the configuration at the β^3 position is defined by that of the starting material **5.58** (Figure 5.9).

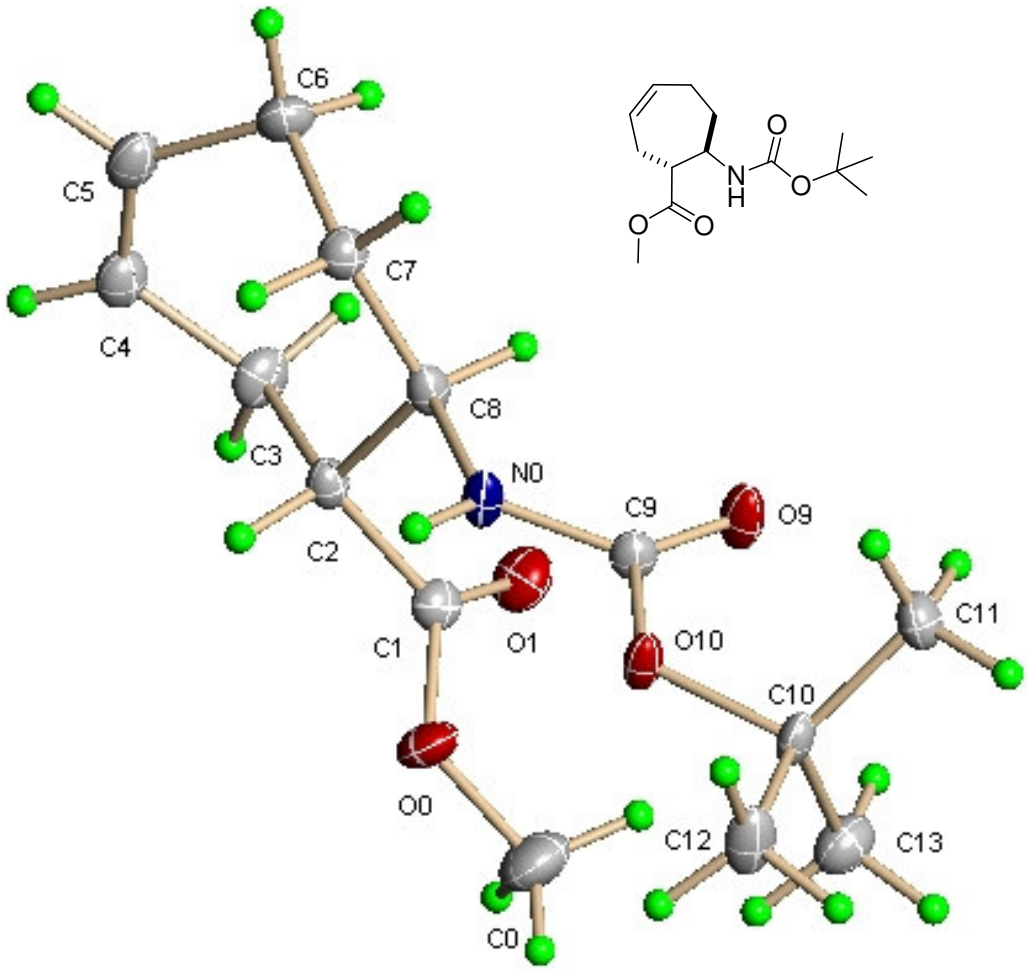

Figure 5.9 X-ray crystal structure of compound **5.63**, showing the absolute configuration at the two chiral centres.

5.3.4 Attempted Synthesis of *trans*-8-Aminocyclooct-3-ene-1-carboxylic Acid (5.71)

Scheme 5.20 outlines the initial strategy for the attempted synthesis of eight-membered cyclic *β*-amino acid (**5.71**). (*S*)-homoserine (**5.64**) was a useful starting material, based on the retrosynthetic analysis described in Scheme 5.15.

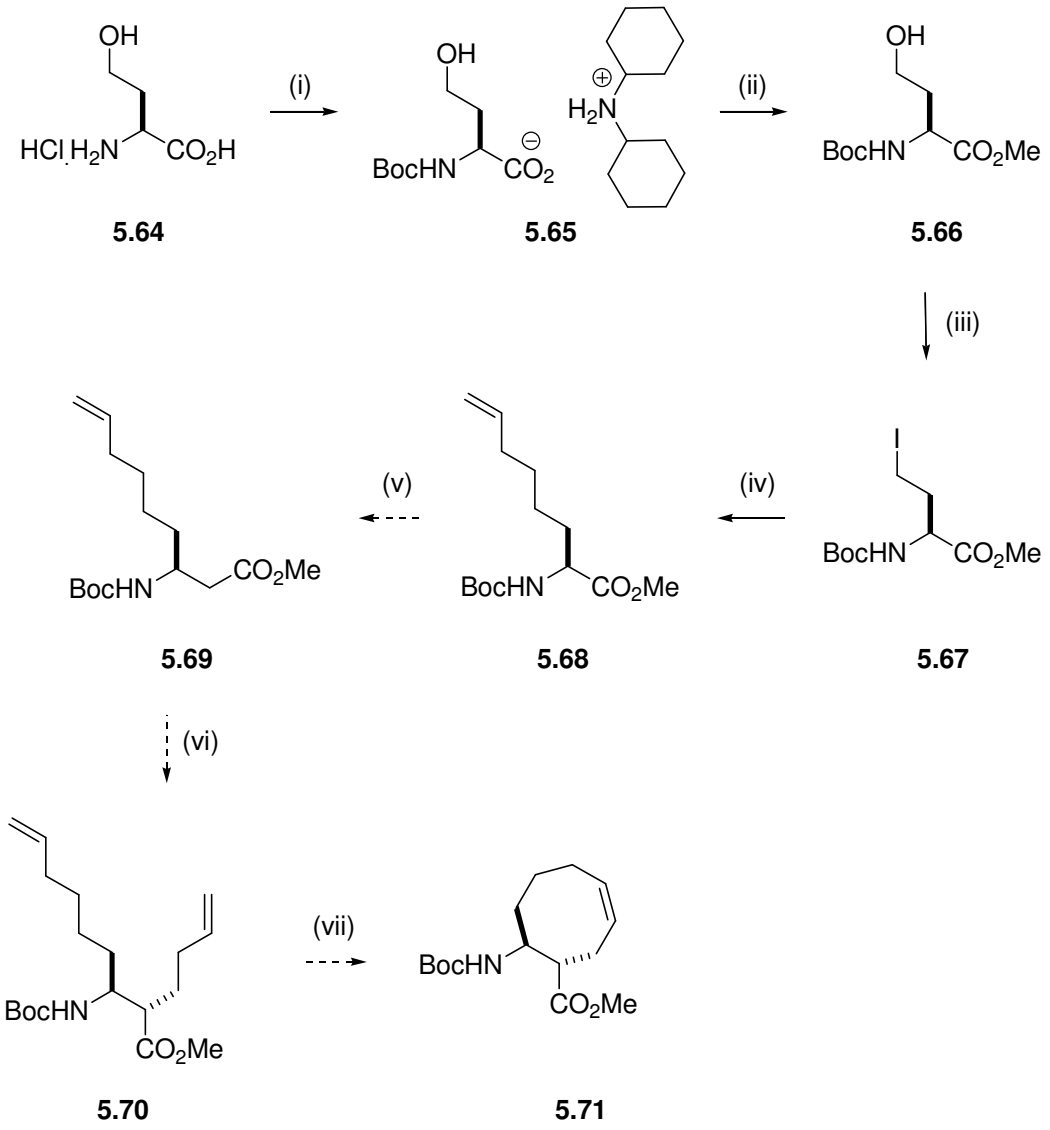

Scheme 5.20 *Reagents and conditions:* (i) $(Boc)_2O$, $NaHCO_3$, dioxane/H_2O, 0 ºC – rt, 16 h, then dicyclohexylamine, ethanol, 96% yield, (ii) MeI, DMF, N_2, rt, 16 h, 66% yield, (iii) I_2, imidazole, PPh_3, DCM, rt, 3 h, 93% yield, (iii) Zn, I_2, 0 ºC – rt, 1 h, $CuBrSMe_2$, allyl chloride, -15 ºC – rt, 16 h, 72% yield.

Homoserine **5.64** was reacted with Boc-anhydride to give *tert*-butyl carbamate in quantitative yield. This was treated with the dicyclohexylamine to give the organic salt **5.65**. The bulky salt prevents lactonisation via nucleophilic attack of the hydroxy group on the carbonyl centre, which would give cyclic ether (as shown in the synthesis of compound **5.59** in Scheme 5.17). The organic salt **5.65** was reacted with methyl iodide to give the methyl ester **5.66** in 98% yield. Reaction of the alcohol with iodine, in the presence of triphenylphosphine and imidazole, gave the iodide **5.67** in 89 % yield.

Again, allylation of the iodide **5.67** using Zn/Cu coupling, as described in the previous section, proved problematic as many attempts returned only starting material. A different copper catalyst, CuBr·DMS, was evaluated, but gave similarly unpredictable results. Only one attempt of many was successful, giving the allylated product **5.68**, in 73% yield. However, not enough material was obtained to complete the synthesis. This sequence was abandoned and another synthetic route was sought.

5.4 Synthesis of Cyclic β-Amino Acids from Allylglycine

5.4.1 Retrosynthetic Analysis of Cycloalkene-based *β*-Amino Acids from *α*-Allylglycine

The problematic Zn/Cu chemistry was avoided by alkylating allylglycine (**5.74**) with longer chain haloalkenes to give the dienes **5.73** (Scheme 5.21). Allylglycine (**5.74**) is a convenient olefinic starting material for the synthesis of cyclic *β*-amino acids, as previously reported by Gardiner *et al.*[21] Homologation of **5.74** to give the *β*-amino acid analog, followed by alkylation with longer chain alkenes (of four or more carbons), gave access to dienes of the type **5.73** which are suitable for RCM.

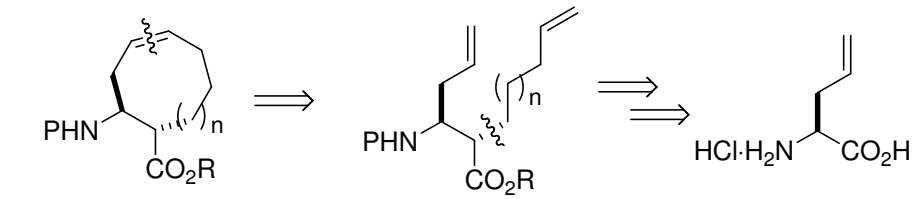

n=1,2 **5.72** **5.73** **5.74**

Scheme 5.21 Retrosynthetic analysis for the synthesis of cyclooctyl and cyclononyl-based *β*-amino acids from allylglycine.

5.4.2 Synthesis of *trans*-2-Aminocyclooct-4-ene-1-carboxylic Acid (5.78)

The synthesis of cyclooctene *β*-amino acid **5.78** from (*S*)-allylglycine **5.74** is outlined in Scheme 5.22. Allylglycine **5.74** was reacted with Boc-anhydride to give the protected amino acid **5.75**. This was homologated, using Arndt-Eistert conditions, to give β^3h-allylglycine **5.76** in 62% yield.[43]

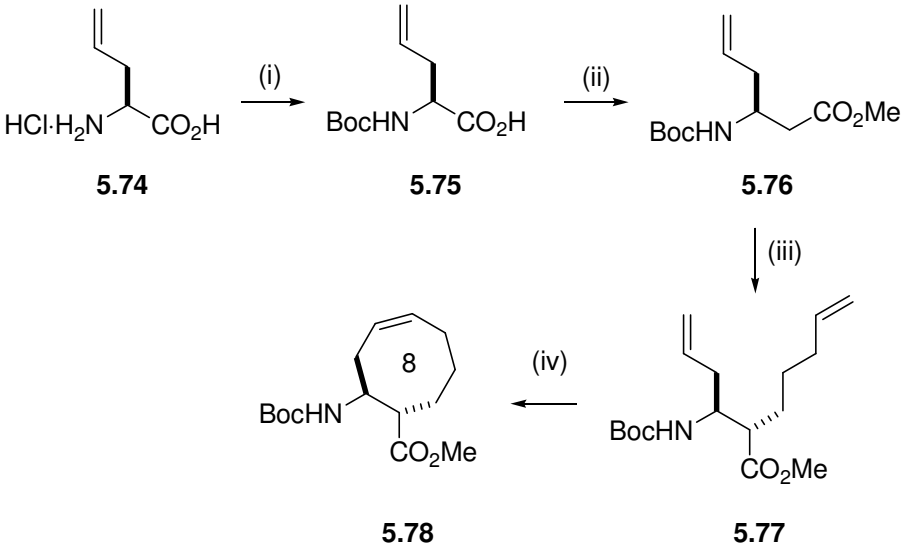

Scheme 5.22 *Reagents and conditions:* (i) Boc_2O, Et_3N, DCM, 0 ºC – rt, 16 h, quant. yield, (ii) ethyl chloroformate, Et_3N, diazomethane, -30 ºC to rt, 3 h, then silver benzoate, methanol, Et_3N, THF, -25 ºC – rt, 3 h, 49% overall yield, (iii) BuLi, HMDS, -40 ºC, 2 h, 5-bromo-1-pentene, NaI, THF, -78 ºC – rt, 16 h, 37% yield, (iv) Grubbs' 1st Gen., DCM, N_2, Δ, 20 h, 82% yield.

The attempted alkylation of the *β*-amino acid **5.76** at the β^2 position with 5-bromo-pent-1-ene and LDA to give diene **5.77** returned only starting material. The alkylation conditions were the as those used for the successful allylation (using allyl bromide) to give diene **5.62**, in the synthesis of the seven membered *β*-amino acid (Scheme 5.19). Therefore the electrophilicity of allyl bromide, compared to 5-bromopent-1-ene, is critical to the success of this alkylation reaction. The relative rate of reaction of an allyl group in an S_N2 reaction is 100 times faster than for a *n*-butyl substituent.[44]

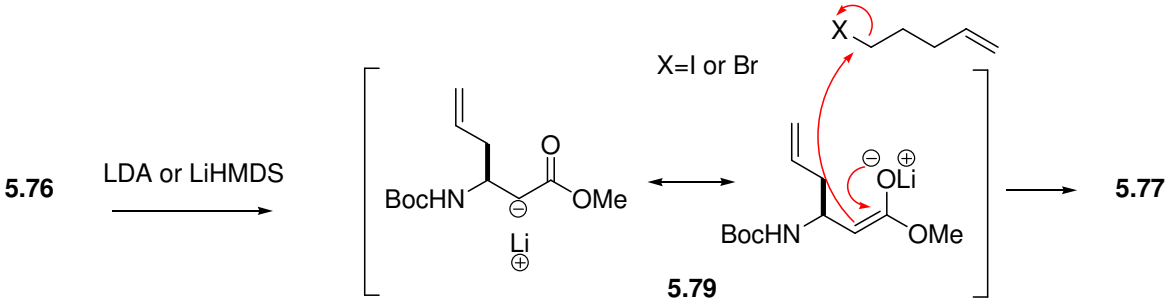

Scheme 5.23 Formation and reaction of enolate **5.79**.

The general alkylation reaction proceeds in two steps: deprotonation at the β^2 position to give the lithium enolate **5.79**, and nucleophilic attack of the haloalkene to give diene **5.77**. The alkylation of *β*-allylglycine with LDA and methyl iodide is reported in the literature in high yields.[21] Consequently, it must be the nucleophilic attack of the enolate intermediate on the electrophile that is problematic.

Better leaving groups, such as iodine and methanesulfonate, were assessed to replace bromine. 5-Bromopent-1-ene (**5.80**) was reacted with sodium iodide, in a Finkelstein substitution to give 5-iodopent-1-ene **5.81** and precipitated sodium bromide (Scheme 5.24). The crude iodide mixture was added directly to the enolate mixture at -78 ºC. 5-Hexen-1-ol (**5.82**) was reacted with methane sulfonyl chloride to give hex-4-en-1-yl methanesulfonate **5.83**, in quantitative yield.

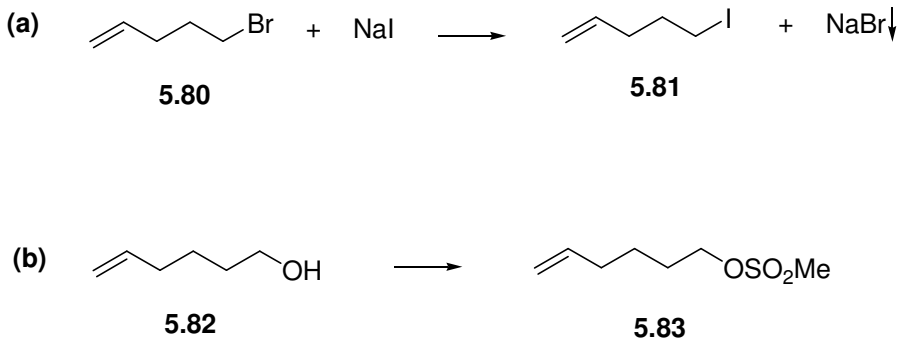

Scheme 5.24 (a) Finkelstein reaction with 1,2-dimethoxyethane (DME) soluble sodium iodide and 5-bromo-pent-1-ene, gave the equivalent iodide and sodium bromide. The latter is insoluble in DME, thereby driving the equilibrium to the right. *Reagents and conditions:* DME, rt, 30 min, (b) *Reagents and conditions:* MsCl, Et_3N, DCM, 1 h, rt, (quant. yield).

Table 5.1 Yield of diene **5.77** for alkylation using different lithium bases and electrophiles.

Electrophile	Base	Yield of **5.77** (%)
5-bromopent-1-ene (**5.80**)	LDA	0
5-bromopent-1-ene	LiHMDS	3
5-iodopent-1-ene (**5.81**)	LDA	0
5-iodopent-1-ene	LiHMDS	37
hex-4-en-1-yl methanesulfonate (**5.83**)	LiHMDS	0

The use of the base lithium hexamethyldisilazide (LiHMDS) to form the enolate **2.66a** in place of LDA was also evaluated. It was found that both the type of lithium base and the halogen played a significant role in successful alkylation at the β^2 position (Table 5.1). Product **5.77** was

not obtained when ester **5.76** was deprotonated (at the β^2 position) with LDA, followed by addition of either 5-bromo- or 5-iodopent-1-ene as the electrophile. Conversely, deprotonation with LiHMDS followed by addition of 5-bromopent-1-ene gave a very low yield (3%), and 5-iodo-pent-1-ene gave a moderate yield (37%) of diene **5.77**. Iodoalkanes are more reactive (accounting for the improved yield) because iodide is a better leaving group than bromide. Methanesulfonate **5.83**, which is a better leaving group than an iodide but more sterically demanding, gave no alkylated product.

The effect of the nature of the lithium base on the product yield obtained in alkylation reactions is described in the literature.[45,46] For some alkylations, LDA gives a very low yield compared with LiHMDS, despite LDA being both a stronger base and sterically less hindered than LiHMDS. The formation of the lithium enolate with LDA or LiHMDS leads to the corresponding amine (diisopropylamine ($NH(i\text{-}Pr)_2$) or hexamethyldisilazane ($NH(Si(Me)_3$), respectively) in solution. The presence of amine is important in determining the mode of complexation of the enolate with the lithium ions.[47] Because stronger bases (those with a higher pKa) are more nucleophilic, a heterodimer-enolate transition state is favoured (as shown in Figure 5.10 for the deprotonation of benzonitrile).[47] Hexamethyldisilazane is much less nucleophilic than diisopropyl amine. Therefore, less heterodimer is present when the enolate is formed with LiHMDS, compared with LDA. In some systems, the presence of heterodimer complex may sterically hinder the approach of the electrophile, preventing the alkylation from occurring.

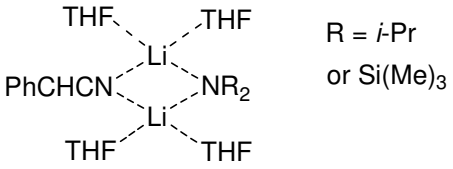

Figure 5.10 Heterodimer formed in THF with the deprotonated benzonitrile anion (PhCHCN-), lithium ions and amine (R') formed by protonation of the lithium base.

The RCM of diene **5.77**, to give the cyclic alkene **5.78** initially proved difficult. Attempted RCM with Grubb's catalyst **3.2** at ~2 mM concentration in benzene (the same conditions used to form cycloheptyl β-amino acid ring **5.63**) gave various dimerised side-products, instead of cyclic product **5.78**. The dimers (which were not fully characterised) were identified by the chemical

shift of the olefinic protons, which were at ~5.3 ppm in the ^{1}H NMR spectrum. These shifts are consistent with those of disubstituted *trans*-olefins, commonly formed during cross metathesis.[48]

Crieghton *et al* demonstrated that both the concentration of the diene and the choice of catalyst were critical in forming 8-membered cycles from dipeptides.[49] It was shown that catalysts **3.1** and **3.2** both gave poor yields of cyclised product (~25 %) at 12, 50 and 100 mM initial diene concentrations. Grubb's catalyst **3.2** gave a larger amount of dimer over cyclic product at all reaction concentrations after 24 hours, compared to catalyst **3.1**. Furthermore, the longer the reaction proceeded, the more dimer by-products formed. Creighton *et al* determined that the optimum RCM conditions to form the 8-membered cycles occurred at 3mM initial diene concentration using Grubb's catalyst **3.1**. Here, the attempted cyclisation of diene **5.77** using these conditions, in benzene at room temperature, gave only ~15% conversion to product. However, cyclisation of the diene **5.77** at the same concentration with **3.1** in refluxing DCM gave the novel cyclic product **5.78** in 82% yield.

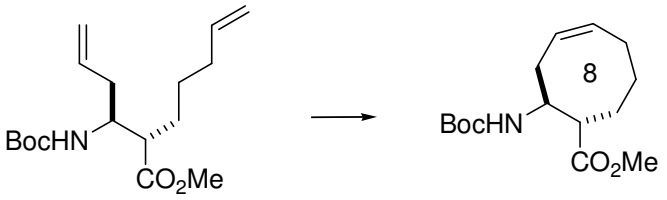

5.77 **5.78**

Scheme 5.25 *Reagents and conditions*: Grubbs' catalyst **3.1**, DCM, Δ, 16 h, 82% yield.

To the best of our knowledge, **5.78** is the first example of an unsaturated cyclooctyl-based *β*-amino acid. The only other reported example of a *trans*-cyclooctyl-based *β*-amino acid utilises a lipase-catalysed enzymatic resolution of a racemic starting compound.[50] Therefore, the methodology presented here provides an efficient non-enzymatic route to such cyclic compounds.

5.4.3 Attempted Synthesis of *trans*-2-Aminocyclonon-4-ene-1-carboxylic Acid (5.87)

The attempted synthesis of a cyclononene β-amino acid **5.87** following a procedure analogous to the synthesis of cyclooctene **5.78** is shown in Scheme 5.26. Examples of cyclononane (or -nonene)-based β-amino acids are unreported in the literature.

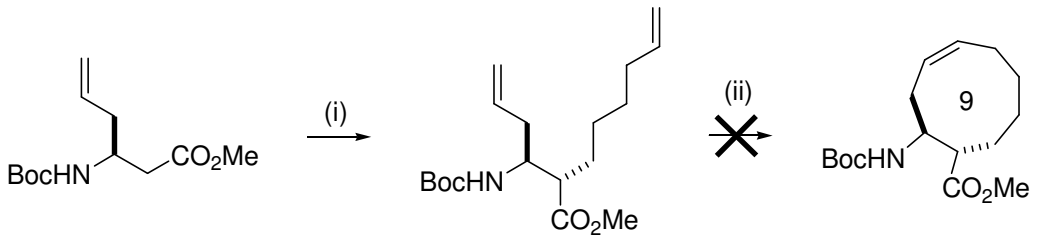

5.77 **5.86** **5.87**

Scheme 5.26 *Reagents and conditions:* (i) lithium bis(trimethylsilyl)amide, THF, -40 ºC, 2 h, 6-iodo-hex-1-ene, -78 ºC – rt, 16 h, 31% yield, (ii) see Table 5.2.

Iodonation of 5-hexen-1-ol (**5.84**) gave the appropriate electrophile, 6-iodo-hex-1-ene (**5.85**) (Scheme 5.27). Alkylation at the β^2-position of olefin **5.77** with 6-iodo hex-1-ene (**5.85**) using LiHMDS gave diene **5.86** in 31% yield.

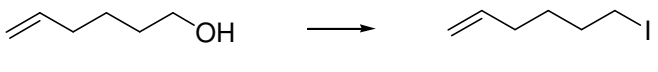

5.82 **5.85**

Scheme 5.27 *Reagents and conditions:* I_2, imidazole, PPh_3, DCM, rt, 3 h, 98% yield

Attempted RCM using the same conditions that gave cyclooctene **5.78** in good yield, failed to give cyclononene product **5.87**. Instead, two different cyclic dimers **5.88** and **5.89**, were formed (Scheme 5.28). Therefore, cross metathesis (CM) must be occurring preferentially over RCM, even at very low (0.3 mM) diene concentrations. Once CM has occurred to form the linear dimer, subsequent RCM gave the 18-membered rings.

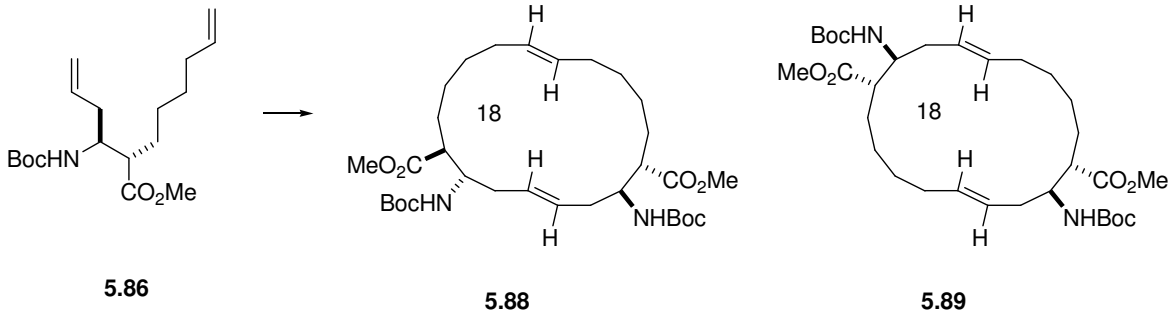

5.86 **5.88** **5.89**

Scheme 5.28 Cyclic dimer products obtained during the attempted RCM reaction of **5.86**.

The two products **5.88** and **5.89** were inseparable by column chromatography. Varying the reaction conditions, as shown in Table 5.2, gave these products in different ratios, as determined from the methine C**H**CO_2 peaks in the ^{1}H NMR spectra of the product mixtures. Conditions A (the conditions used to successfully form cycle **5.78**) using catalyst **3.1** gave a 1.4:1 ratio of products **5.88** to **5.89**. Greater dilution and the use of catalyst **3.2** gave a higher ratio of **5.88** over the other (conditions B), while microwave-assisted RCM using catalyst **3.2** gave almost exclusively product **5.88**. None of the reaction conditions evaluated gave detectable amounts of the desired cyclic product **5.87**.

Table 5.2 Conditions for the attempted synthesis of **5.87**.

Conditions	[diene] mM	Catalyst	Heating	Ratio ($^{5.88}/_{5.89}$)	Yield (%)
A	3	**3.1**	refluxing DCM	1.38	62
B	1	**3.2**	refluxing DCM	1.94	77
C	0.3	**3.2**	microwave DCM	49	70

Dimer **5.88** was favoured under all three reaction conditions, and to the greatest extent with microwave-assisted metathesis. CM between the two hexenyl side-chains probably occurred first, followed by RCM of the allyl groups to give the product. This is because steric factors make the longer alkene chains more accessible (and therefore more reactive) to the catalyst than the shorter allyl group. This steric control has been described the literature, with the greater reactivity of homoallylglycine compared with allylglycine.[51] CM usually gives the thermodynamically more favourable *trans* double bond. However because metathesis is reversible the double bonds within the product can isomerise to give the most

thermodynamically favourable structure.[52] Nevertheless, *trans* double bonds are energetically more favourable in rings containing 11 or more members.[53]

The structures of compounds **5.88** and **5.89** were assigned on the basis of ^{1}H NMR, mass spectroscopy and hydrogenation (as described below). There were seven possible structures that the two products could take: compound **5.88** could have a *cis-cis, cis-trans, trans-cis* or *trans-trans* geometry about the two double bonds; while compound **5.89** could have a *cis-cis, cis-trans* or *trans-trans* geometry about the two double bonds. Because of the rotational symmetry in compound **5.89**, there is only one *cis-trans* isomer. Hydrogenation of the product mixture did not result in a single product, therefore two different structures, of the type **5.88** and **5.89**, were present.

The ^{1}H NMR spectra of the product mixtures showed a total of three NH, β^2 and β^3 protons for each isomer, instead of six. Therefore, both **5.88** and **5.89** had an element of symmetry, rendering each proton identical in chemical shift to another proton within the same molecule. The proton NMR spectra of the product mixtures showed the olefinic protons lie between 5.1 and 5.4 ppm in $CDCl_3$. These shifts are typical for *trans* double bond protons (Figure 5.11a,b,c). In contrast, the olefinic protons of cyclic β-amino ester **5.78** occur between 5.6 and 5.9 ppm (Figure 5.11d), which is typical of protons in *cis* double bonds.

The product mixtures contained only two NH peaks, with integrals consistent with the ratios of **5.88** to **5.89**. Furthermore, all four double bond protons of **5.88** had identical chemical shifts, while the olefinic protons on the **5.89** have two different chemical shifts (~5.35 and 5.20 ppm in $CDCl_3$). The symmetry in compound **5.88** renders both ends of the double bond in the same environment, therefore only giving a single alkene peak in the ^{1}H NMR. Based on these observations the most-likely structure for each of the two products are the *trans-trans* isomers **5.88** and **5.89**. Both of these structures have an element of symmetry leading to the simplified NMR spectra: **5.88** has an axis of rotational symmetry, running through the double bonds, while **5.89** has an axis of rotational symmetry perpendicular to the plane of the ring, and situated in the middle of the ring (directly out of the page).

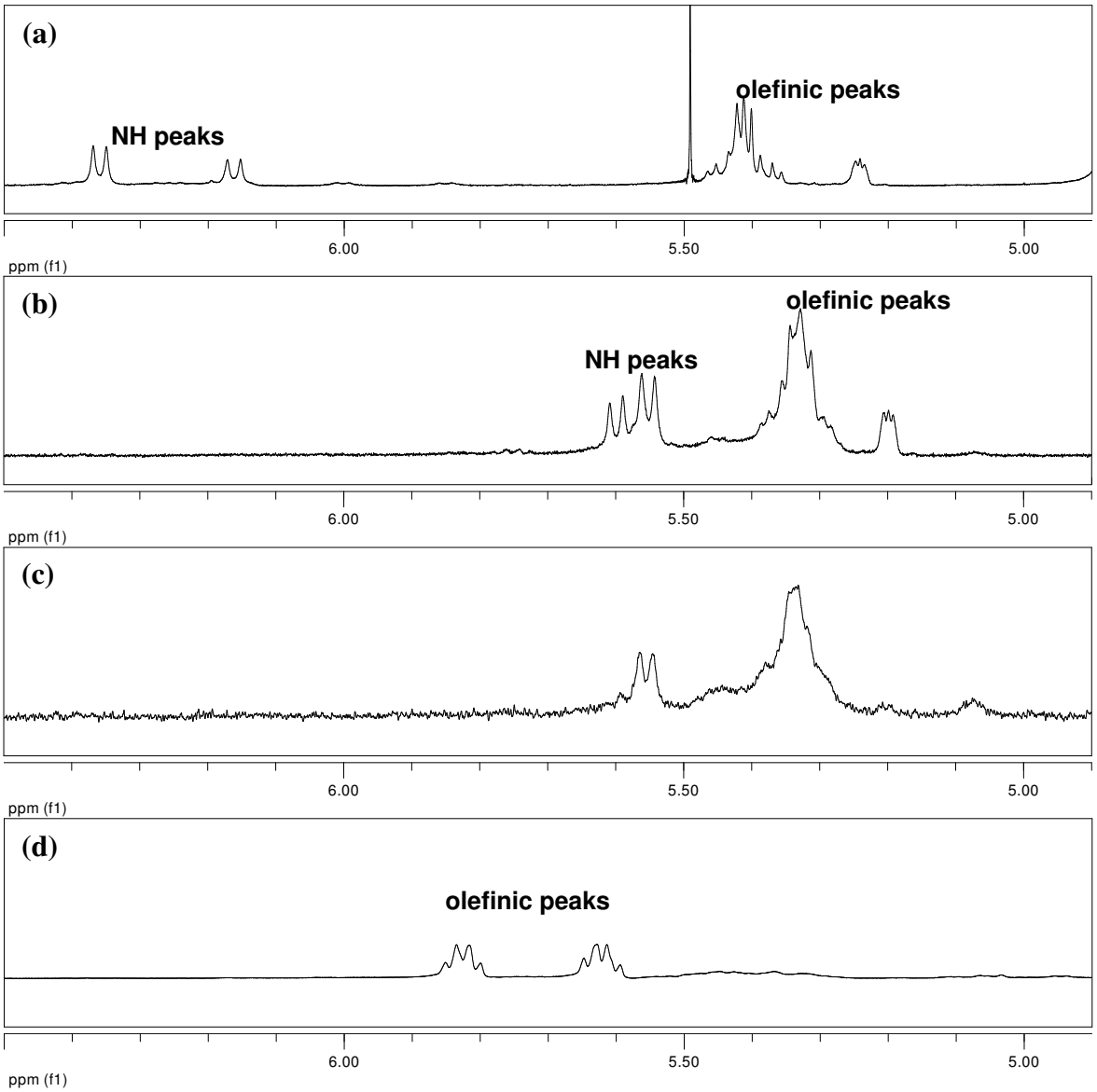

Figure 5.11 ^{1}H NMR spectra showing the olefinic protons of the product mixtures from reaction conditions shown in Table 5.2. (a) Conditions A in CD_3OD; (b) conditions B in $CDCl_3$; (c) conditions C in $CDCl_3$; (d) cyclic alkene **5.78** in $CDCl_3$.

Despite the high dilution of the alkene **5.86** under all of the reaction conditions (shown in Table 5.2), no nine-membered ring product formed. This is consistent with both the lack of nine-membered carbocycles formed by metathesis in the literature, and reports of failed syntheses.[54,55] The only successful examples of metathesis to form nine-membered cycles are those with heteroatoms, such as nitrogen or oxygen, in the ring. [54,56,57]

It was apparent from the synthesis of seven and eight and attempted synthesis of nine -membered carbocycles, that the larger the ring size over this range, the more difficult it was to obtain the desired product. This is consistent with modelling and experimental data on the properties of

different cycloalkenes.[53] The deviation of the C-C=C-C bond dihedral angle of cycloheptene to cyclodecene rings from the ideal of value of zero degrees, is shown in Figure 5.12.

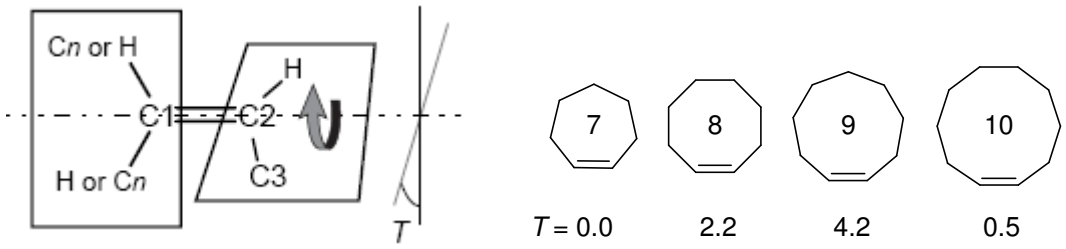

Figure 5.12 The degree of twisting (*T,* in degrees) from ideal value of 0, for cycloheptene to cyclodecene ring sizes.[53]

The ring strain causes the double-bond to twist, by an angle (*T*). This twisting effect reduces the *p*-orbital overlap at the double bonds. Cyclooctene and cyclononene both have twist angles that are larger than zero, which could explain the increased difficulty in cyclising the cyclooctyl-based amino acid and the inability to cyclise the cyclononene-based amino acid. When the catalyst has coordinated with one of the olefinic groups of the diene (see Figure 5.7, **A**), good orbital overlap is needed with the other olefinic group to form the cyclobutyl intermediate. If this intermediate cannot form with an olefin on the same molecule, it will react with another olefin (in a CM reaction). This result was seen in the attempted synthesis of cyclononene *β*-amino ester **5.78**.

The cyclodecene ring has lower twist angle than cyclooctene or cyclonone. Ten-membered carbocyclic structures formed by RCM in good yield using Grubb's catalyst **3.2** are reported in the literature.[58] This supports the theory presented here that the dihedral angle about the double bond is important in determining whether RCM can occur.

5.5 Conclusion and Future Work

Cyclic *β*-amino acids are an important class of constrained amino acids that restrict conformational freedom when incorporated into peptide structures. The synthesis of cyclic *β*-amino acids has evolved from the early racemic syntheses to the use of enzymatic resolution and stereoselective addition and alkylation reactions, to afford the enantiomerically pure *cis* and *trans* compounds. Presented in this chapter is the synthesis of novel constrained *β*-amino acids with ring sizes of five, six, seven and eight-members.

The novel fluorinated *β*-amino acids **5.43a** and **5.43b** were synthesised using a recently developed conjugate addition/fluorination reaction. The stereoselectivity of the reaction was very high, providing an excellent route to cyclic fluorinated *cis*-*β*-amino acids. Synthesis of the six membered analog **5.43b** was lower yielding, but also gave very high stereospecificity. The absolute configuration was determined by X-ray crystallography of **5.43a**.

Future work in the area of cyclic fluorinated *β*-amino acids the would involve investigation of the *trans* analogs of **5.43a** and **5.43b**. *Trans*-cyclic *β*-amino acids polymers stabilise helices while the *cis* analogs adopt *β*-sheets. Davies *et al* illustrated that substitution of the *α*,*β*-unsaturated ester starting material with bulky groups (such as *tert*-buty and isopropyl) can direct proton quenching of the lithiated intermediate. This has yet to be explored in conjuction with the conjugate addition/fluorination reaction methodology, but may give access to *trans*-fluorinated analogs of **5.43a** and **5.43b**.

RCM is a facile and efficient method to generate constrained carbocyclic *β*-amino acids, while retaining the integrity of the amino acid stereocenters. The novel carbocyclic *β*-*trans*-amino esters **5.63** and **5.78** were synthesised using a key RCM step of chiral dienes. These seven and eight membered carbocycles, along with the attempted synthesis of cyclononene based **5.87** provides a useful insight into the effects of ring size on RCM.

Future work in this area would involve the incorporation of the cycloheptene and cyclooctene-based *β*-amino acids into peptide chains. Gellman *et al* showed that polymers of cyclopentane-based *β*-amino acids form different helical structures to those of cyclohexane-based analogs.[59] It

would be of interest to investigate the type of helices adopted by *β*-peptides containing cyclic *β*-amino acids of larger ring sizes, such as cycloheptane and cyclooctane.

5.6 References

1. Nativ, E.; Rona, P., *Israel Journal of Chemistry* **1972,** 10, (1), 55-58.
2. Fulop, F., *Chemical Reviews* **2001,** 101, (7), 2181-2204.
3. Bernath, G.; Kovacs, K.; Lang, K. L., *Acta Chimica Academiae Scientarium Hungaricae* **1970,** 64, (2), 183.
4. Plieninger, H.; Schneider, K., *Chemische Berichte-Recueil* **1959,** 92, (7), 1594-1599.
5. Bernath, G.; Gondos, G.; Kovacs, K.; Sohar, P., *Tetrahedron* **1973,** 29, (7), 981-4.
6. Bernath, G.; Gera, L.; Gondos, G.; Panovics, I.; Ecsery, Z., *Acta Chimica Academiae Scientiarum Hungaricae* **1976,** 89, (1), 61-84.
7. Bernath, G.; Stajer, G.; Szabo, A. E.; Fulop, F.; Sohar, P., *Tetrahedron* **1985,** 41, (7), 1353-1365.
8. Kurihara, M. A.; Kamiyama, K.; Kobayashi, S.; Ohno, M., *Tetrahedron Letters* **1985,** 26, (47), 5831-5834.
9. Kaga, H.; Kobayashi, S.; Ohno, M., *Tetrahedron Letters* **1988,** 29, (9), 1057-1060.
10. Kobayashi, S.; Kamiyama, K.; Ohno, M., *Chemical & Pharmaceutical Bulletin* **1990,** 38, (2), 350-354.
11. Forro, E.; Fulop, F., *Organic Letters* **2003,** 5, (8), 1209-1212.
12. Gyarmati, Z. C.; Liljeblad, A.; Rintola, M.; Bernath, G.; Kanerva, L. T., *Tetrahedron: Asymmetry* **2003,** 14, (23), 3805-3814.
13. Forro, E.; Arva, J.; Fulop, F., *Tetrahedron: Asymmetry* **2001,** 12, (4), 643-649.
14. Xu, D. Q.; Prasad, K.; Repic, O.; Blacklock, T. J., *Tetrahedron-Asymmetry* **1997,** 8, (9), 1445-1451.
15. LePlae, P. R.; Umezawa, N.; Lee, H. S.; Gellman, S. H., *Journal of Organic Chemistry* **2001,** 66, (16), 5629-5632.
16. Davies, S. G.; Ichihara, O.; Walters, I. A. S., *Synlett* **1993**, (7), 461-462.
17. Davies, S. G.; Ichihara, O.; Lenoir, I.; Walters, I. A. S., *Journal of the Chemical Society-Perkin Transactions 1* **1994**, (11), 1411-1415.
18. Davies, S. G.; Smith, A. D.; Price, P. D., *Tetrahedron-Asymmetry* **2005,** 16, (17), 2833-2891.
19. Enders, D.; Wiedemann, J.; Bettray, W., *Synlett* **1995**, (4), 369-71.
20. Enders, D.; Wiedemann, J., *Liebigs Annalen/Recueil* **1997**, (4), 699-706.
21. Abell, A. D.; Gardiner, J., *Organic Letters* **2002,** 4, (21), 3663-3666.
22. Tang, W. J.; Wu, S. L.; Zhang, X. M., *Journal of the American Chemical Society* **2003,** 125, (32), 9570-9571.
23. Gardiner, J.; Anderson, K. H.; Downard, A.; Abell, A. D., *Journal of Organic Chemistry* **2004,** 69, (10), 3375-3382.
24. Tang, W.; Wu, S.; Zhang, X., *Journal of the American Chemical Society* **2003,** 125, (32), 9570-9571.
25. Davies, S. G.; Garrido, N. M.; Ichihara, O.; Walters, I. A. S., *Journal of the Chemical Society-Chemical Communications* **1993**, (14), 1153-1155.

26. Jarvest, R. L.; Berge, J. M.; Brown, P.; Houge-Frydrych, C. S. V.; O'Hanlon, P. J.; McNair, D. J.; Pope, A. J.; Rittenhouse, S., *Bioorganic & Medicinal Chemistry Letters* **2003,** 13, (7), 1265-1268.
27. Davies, S. G.; Walters, I. A. S., *Journal of the Chemical Society-Perkin Transactions 1* **1994**, (9), 1129-1139.
28. Langenhan, J. M.; Gellman, S. H., *Journal of Organic Chemistry* **2003,** 68, (16), 6440-6443.
29. Bunnage, M. E.; Chernega, A. N.; Davies, S. G.; Goodwin, C. J., *Journal of the Chemical Society-Perkin Transactions 1* **1994**, (17), 2373-2384.
30. Andrews, P. C.; Bhaskar, V.; Bromfield, K. M.; Dodd, A. M.; Duggan, P. J.; Duggan, S. A. M.; McCarthy, T. D., *Synlett* **2004**, (5), 791-794.
31. Isanbor, C.; O'Hagan, D., *Journal of Fluorine Chemistry* **2006,** 127, (3), 303-319.
32. Shimizu, K.; Kawase, A.; Haneishi, T.; Kato, Y.; Kinoshita, K.; Ohmori, M.; Furuta, Y.; Emura, T.; Kato, N.; Mitsui, T.; Yamaguchi, K.; Morita, K.; Sekiguchi, N.; Yamamoto, T.; Matsushita, T.; Shimaoka, S.; Sugita, A.; Morikawa, K., *Bioorganic & Medicinal Chemistry Letters* **2006,** 16, (12), 3323-3329.
33. Arasappan, A.; Njoroge, F. G.; Chen, K. X.; Venkatraman, S.; Parekh, T. N.; Gu, H. N.; Pichardo, J.; Butkiewicz, N.; Prongay, A.; Madison, V.; Girijavallabhan, V., *Bioorganic & Medicinal Chemistry Letters* **2006,** 16, (15), 3960-3965.
34. Jackson, R. F. W.; Wishart, N.; Wood, A.; James, K.; Wythes, M. J., *Journal of Organic Chemistry* **1992,** 57, (12), 3397-3404.
35. Jackson, R. F. W.; Moore, R. J.; Dexter, C. S.; Elliot, J.; Mowbray, C. E., *Journal of Organic Chemistry* **1998,** 63, (22), 7875-7884.
36. Dexter, C. S.; Jackson, R. F. W.; Elliott, J., *Journal of Organic Chemistry* **1999,** 64, (20), 7579-7585.
37. Kimura, M.; Seki, M., *Tetrahedron Letters* **2004,** 45, (8), 1635-1637.
38. Zylber, N.; Zylber, J.; Rollin, Y.; Dunach, E.; Perichon, J., *Journal of Organometallic Chemistry* **1993,** 444, (1-2), 1-4.
39. Gawronski, J. K., *Tetrahedron Letters* **1984,** 25, (24), 2605-2608.
40. Knochel, P.; Normant, J. F., *Tetrahedron Letters* **1984,** 25, (14), 1475-1478.
41. Knochel, P.; Yeh, M. C. P.; Berk, S. C.; Talbert, J., *Journal of Organic Chemistry* **1988,** 53, (10), 2390-2392.
42. Huo, S. Q., *Organic Letters* **2003,** 5, (4), 423-425.
43. Seebach, D.; Overhand, M.; Kuehnle, F. N. M.; Martinoni, B., *Helvetica Chimica Acta* **1996,** 79, (4), 913-941.
44. March, J., *Advanced Organic Chemistry*. 4th ed.; Wiley-Interscience: New York, 1992.
45. Rychnovsky, S. D.; Swenson, S. S., *Journal of Organic Chemistry* **1997,** 62, (5), 1333-1340.
46. Godbert, N.; Bryce, M. R.; Dahaoui, S.; Batsanov, A. S.; Howard, J. A. K.; Hazendonk, P., *European Journal of Organic Chemistry* **2001**, (4), 749-757.
47. Corset, J.; Castella-Ventura, M.; Froment, F.; Strzalko, T.; Wartski, L., *Journal of Organic Chemistry* **2003,** 68, (10), 3902-3911.
48. Vernall, A. J. Cross metathesis and ring-closing methathesis reactions of modified amino acids and peptides. Ph.D., University of Canterbury, Christchurch, 2005.
49. Creighton, C. J.; Leo, G. C.; Du, Y.; Reitz, A. B., *Bioorganic & Medicinal Chemistry* **2004,** 12, (16), 4375-4385.
50. Kiss, L.; Forro, E.; Bernath, G.; Fueloep, F., *Synthesis* **2005**, (8), 1265-1268.
51. Vernall, A. J.; Abell, A. D., *Aldrichimica Acta* **2003,** 36, (3), 93-105.
52. Aitken, S. G.; Abell, A. D., *Australian Journal of Chemistry* **2005,** 58, (1), 3-13.
53. Barrows, S. E.; Eberlein, T. H., *Journal of Chemical Education* **2005,** 82, (9), 1334-1339.

54. Holt, D. J.; Barker, W. D.; Jenkins, P. R.; Panda, J.; Ghosh, S., *Journal of Organic Chemistry* **2000,** 65, (2), 482-493.
55. Hok, S.; Schore, N. E., *Journal of Organic Chemistry* **2006,** 71, (4), 1736-1738.
56. Kaul, R.; Surprenant, S.; Lubell, W. D., *Journal of Organic Chemistry* **2005,** 70, (12), 4901-4902.
57. Kaul, R.; Surprenant, S.; Lubell, W. D., *Journal of Organic Chemistry* **2005,** 70, (10), 3838-3844.
58. Beumer, R.; Bayon, P.; Bugada, P.; Ducki, S.; Mongelli, N.; Sirtori, F. R.; Telser, J.; Gennari, C., *Tetrahedron* **2003,** 59, (44), 8803-8820.
59. Cheng, R. P.; Gellman, S. H.; DeGrado, W. F., *Chemical Reviews* **2001,** 101, (10), 3219-3232.

Chapter 6 Experimental

6.1 General Methods and Procedures

6.1.1 General Practise

β-Amino Acid Nomenclature

The naming of β-amino acids used in this thesis is based on nomenclature developed by Seebach.[1] β^3-Amino acids (and peptides) that contain a side chain at the '3' position of the carbon backbone (from a formal insertion of CH_2) are designated H-β^3hXaa-OH, were Xaa is the name of the parent α-amino acid. Similarly, β^2 amino acids, which have a side chain at the '2' position take the form of Hβ^2hXaa.

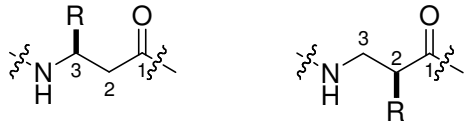

β3-homo-amino acids
H-β3hXaa-OH

β2-homo-amino acids
H-β2hXaa-OH

Confusion arises with earlier nomenclature based on a formal exchange of the α-NH_2 group and a β-H atom of an α-amino acid. For example, βhGly has been referred to as β-Ala, because it is a structural isomer of α-Ala, yet it does not contain a methyl side chain associated with alanine. The use of the name 'β-Iso-amino acid' and the use of the abbreviation 'H-βiXaa-OH' has been proposed to clarify this point.[1]

X-Ray Crystallography

All measurements were made with a Siemens CCD area detector using graphite-monochromatized Mo Kα (λ 0.71073 Å) radiation at 92 F. The data reduction was performed using SAINT.[2] Intensities were corrected for Lorentz and polarization effects and for absorption using SADABS. Space groups were determined from systematic absenses and checked for higher symmetry. The structures were solved by direct methods using *SHELXS*[3] and refined on F^2 using all data by full-matrix least squares procedures with *SHELXL-97*.[4] All non-hydrogen atoms were refined with anisotropic displacement parameters. All hydrogen atoms were fixed in

idealised positions. In all cases, final Fourier syntheses showed no significant residual electron density in chemically sensible positions.

Molecular Modelling

All molecular modelling was carried out by Blair Stewart, University of Canterbury. Molecular mechanics calculations were carried out on a SGI IRIX 6.5 workstation, using MacroModel (v6.5) molecular modelling software, OPLS_01 force field and the implicit H_2O/chloroform GB/SA solvation system. Monte Carlo conformational searches were carried out without imposition of any constraint and with inclusion of amide bonds in the rotatable bonds. 5000 structures were generated and minimized until the gradient was less than 0.05 kJ/Å mol by the TNCG gradient implemented in MacroModel. All conformers with energy 12 kcal/mol above the global minimum conformer were discarded.

Circular Dichroism

Circular dichroism was carried out at the University of Otago, Dunedin. The samples were dissolved in trifluoroethanol or methanol at 0.2 mM concentration at 22 ± 2 °C and analysed using a J-Y monochromater (France) fitted with a Glanz-Thompson polarizer. The photo multiplier tube signal was converted with an analog to digital converter and the data was processed with GlobalWorks software.

Melting Points

All melting points were obtained on an Electrothermal apparatus and are uncalibrated. Melting points are not reported for diastereomeric mixtures.

Cooled Solutions

Cooled solutions comprised the following: -78 ºC using $CO_{2(s)}$ and acetone; -30 ºC, -25 ºC and -15 ºC using CO_2(*S*) and methanol/water mixtures.

Sonication

Solutions were sonicated in a water trough at rt for a specified time using a Branson 2510 sonicator.

NMR Spectroscopy

NMR spectra of all compounds except **5.40a**, **5.40b**, **5.43a**, and **5.43b** were obtained as described below.

Proton spectra were obtained on a Varian Inova spectrometer operating at 500 MHz or a Varian Unity spectrometer, operating at 300 MHz. Carbon NMR spectra were obtained on a Varian Unity 300 spectrometer operating at 75 MHz, with a delay of (D_1) of 1 second. Fluorine NMR spectra were obtained on a Varian Unity 300 spectrometer operating at 282 MHz. All spectra were obtained at 23° C unless specified. Chemical shifts are reported in parts per million (ppm) on the δ scale (in which trimethylsilane (TMS) is referenced to 0.00 ppm). Solvents used in NMR analysis (reference peak listed) included $CDCl_3$ ($C\mathbf{H}Cl_3$ at δ_H 7.26 ppm, $\mathbf{C}DCl_3$ at δ_C 77.0 ppm); CD_3OD ($C\mathbf{H}D_2OD$ at δ_H 3.31 ppm, $\mathbf{C}D_3OD$ at δ_C 49.05 ppm); $(CD_3)_2SO$ ($(C\mathbf{H}D_2)_2SO$ at δ_H 2.50 ppm, $(\mathbf{C}D_3)_2SO$ at δ_C 49.43 ppm); CF_3CD_2OH ($CF_3C\mathbf{H}DOH$ at δ_H 3.88 ppm, $\mathbf{C}F_3CD_2OH$ at δ_C 61.5 ppm); D_2O (containing 1% *tert*-butanol) ($D\mathbf{H}O$ at δ_H 4.80 ppm, $(C\mathbf{H_3})_3OH$ at δ_C 30.83 ppm). Two-dimensional NMR experiments included COSY, HSQC, CIGAR and ROESY. All were obtained on the Varian Inova spectrometer operating at 500 MHz. The HSQC and CIGAR experiments were all obtained with a delay of (D_1) of 1s. ROESY spectra were obtained with mixing time of 300 ms.

NMR spectra for compounds **5.40a**, **5.40b**, **5.43a** and **5.43b** were obtained on a Bruker Av400 spectrometer at CSIRO, Clayton, Australia. Proton spectra were obtained at 400 MHz, carbon spectra at 100 MHz and fluorine spectra at 188 MHz.

Infrared Spectroscopy

Infrared spectra were obtained using a Shimadzu 9201PC series FTIR interfaced with an Intel 486 PC operating Shimadzu's HyperIR software. Diffuse reflectance spectra were obtained using a solid KBr matrix.

Small Molecule Mass Spectrometry

Electron impact (EI) mass spectra were obtained on a Kratos MS80 RFA mass spectrometer operating at 4000V (accelerating potential) and 70 eV (ionization energy). The source temperature was 200-250° C. Electrospray ionization (ESI) mass spectra were obtained on a micromass LCT TOF mass spectrometer, with a probe voltage of 3200V, temperature of 150° C and a source temperature of 80° C. Direct ionization used 10μL of a 10μg mL^{-1} solution, using a

carrier solvent of 50% acetonitrile/water at a flow rate of 20µL min^{-1}. Ionization was assisted by the addition of 0.5% formic acid.

Optical Rotation

Optical rotations were measured on a Perkin-Elmer 341 polarimeter, with a 1.0 dm cell length. Measurements were performed at 22 ± 2 ºC in HPLC-grade solvents. $[\alpha]_D$ values are given in $deg.mL.g^{-1}.dm^{-1}$ and samples concentration values quoted in this thesis are in 10^1 $mg.mL^{-1}$.

High Pressure Liquid Chromatography (HPLC)

Analytical HPLC was carried out on a Dionex liquid chromatograph equipped with a UVD 340U diode array detector, and connected to an Alltech ELSD 800. For reversed phase HPLC, a Phenomenex Prodigy C_{18} μ S3 column (5 μ, 250 x 4.6 mm) was used. A standard flow rate of 1 $mL.min^{-1}$ was used with variable concentrations of methanol (HPLC grade) in water (milli-Q). The gradient consisted of a 36 min run with the following steps – 4 min of 40% methanol in water, followed by a linear gradient to 100% methanol over 12 min which was maintained for 10 min before returning to 40% methanol over 2 min, which was maintained for 8 min to allow the column time to re-equilibrate.

Elemental Analysis

Microanalysis was performed for carbon, nitrogen and hydrogen at the University of Otago Microanalytical Laboratory. All reported values are within ± 0.5% of the calculated value.

Glassware

Oven-dried glassware was used in all reactions performed under an inert atmosphere (either anhydrous nitrogen or argon).

Concentrating *in vacuo*

Concentration *in vacuo* refers to the removal of solvents and volatiles under reduced pressure by rotary evaporation (low vacuum pump), followed by application of high vacuum (oil pump) for a minimum of thirty minutes.

Thin-layer Chromatography

Analytical thin layer chromatography (TLC) was performed on plastic-backed Merck Kieselgel $KG60F_{254}$ silica plates. Traces were visualised using short wave UV light or a suitable dip, including basic potassium permanganate (general), vanillin (general) or $PdCl_2$ (sulfur).

Flash and Column Chromatography

Flash chromatography (postitive pressure of anhydrous nitrogen) and column chromatography (atmospheric pressure) was performed using 230-400 mesh Merck Silica gel 60, Fluka Silica gel 100 C_{18}-reversed phase (fully endcapped) or lipophilic sephadex (Aldrich). In this text, 'silica' refers to Silica gel 60 and 'C_{18}-coated silica' refers to the other. The eluting solvents petroleum ether 50/70*, ethyl acetate and dichloromethane were distilled in bulk from calcium hydride chips and methanol (HPLC grade) was used as received.

Reagents and Solvents

Tetrahydrofuran and diethyl ether were distilled from sodium benzophenone ketyl under an inert atmosphere immediately prior to use. Dichloromethane, 1,2-dichloroethane, benzene, toluene, triethylamine and 1,1,2-trichloroethane were distilled from calcium hydride under an inert atmosphere. Merck Alumina 70-290 mesh, anhydrous dimethylformamide and 2,2,2-trifluoroethanol were obtained from commercial sources.

Ultraviolet-Visible Spectroscopy

Ultraviolet-visible spectroscopy was performed on a GBC UV/Vis 918 spectrometer running the default GBC Scientific v2.01 software package.

Flashmaster™ Chromotography

Automated chromatography was performed on the Argonaut Technologies FlashMaster II flash chromatography system. The FlashMaster II system controlled the gradient solvent mixing, flow control, peak detection and peak fraction collection through factory-packed, disposable silica ISOLUTE® column cartridges.

* A mixture of hexanes with a boiling point range between 50 and 70 ºC.

6.1.2 General Electrochemical Methods

Electrochemical Measurements

All electrochemical measurements were performed using a computer-controlled EG&G PAR model 273A instrument. A standard glass three-electrode electrochemical cell that allowed for continuous gas purging was used. A gold (111) working electrode was purchased from Metal Crystals & Oxides Ltd. (U.K.) and treated as described below. The working electrode was suspended in the electrochemical cell using the hanging meniscus method. This allows the front electrode surface to be in contact with the solution but without requiring the sides of the electrode to be insulated. A large area gold wire was used for the secondary electrode, and a saturated calomel electrode (SCE) was used for the reference electrode. Prior to making electrochemical measurements, the electrolyte solutions were degassed with N_2 for 30 minutes, and the working electrode containing the SAM was potential cycled ten times at 50 mVs^{-1} between 0 and 0.55 V. All measurements were made at 22 ± 2 °C under N_2. Cyclic voltammetry and chronoamperometry experiments were performed according to the method described in individual chapters (Chapter 2, Section 2.2.2 and Section 2.2.4, and Chapter 3, Section 3.4.1). Voltammetric peak analysis was performed by integration of the peaks.[5]

Gold Working Electrode Surface Preparation

To clean the gold working electrode and determine the microscopic area, the surface was polished using 0.05 μm alumina and a microcloth initially, followed by sonication in ethanol and water, then H_2 flame annealed and cooling. The electrode was cycled (20-50 mV s^{-1}) between -0.2 and 1.45 V (SCE) in aqueous 0.01 M $HClO_4$ for 3 h or until successive cycles for 10 min were substantially unchanged. The area of the electrode was calculated from the total charge required to reduce a monolayer of gold oxide and compared to the calculated charge required for gold (111) taken as 222 μC cm^{-2} and determined to be 0.20 cm^2.

Reagents and Solvents

$NaClO_4 \cdot H_2O$ (Scharlau Chemie®, S. A.), $HClO_4$ (70%, AnalaR®) and 2,2,2-trifluoroethanol (99.5%, Aldrich®) were used as received. Milli-Q water, >18 MΩ cm^{-1}, was used for all aqueous solutions.

6.2 General Synthetic Methods

General Method A: Coupling with HATU

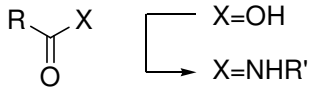

Primary amine (1.0 equiv) and carboxylic acid (1.0 equiv) were dissolved in dimethylformamide at rt, under N_2. First diisopropylethylamine (4.0 equiv) and then HATU (1.0 equiv) were added, and the reaction stirred for 16 h at rt. The reaction mixture was diluted with ethyl acetate, washed with saturated aqueous NH_4Cl, $NaHCO_3$, and NaCl, dried ($MgSO_4$), and the solvent removed *in vacuo*. The crude mixture was purified by column chromatography, as specified for each compound.

Modified General Method A: Coupling with HATU (dimethylformamide-insoluble product)

Primary amine (1.0 equiv) and carboxylic acid (1.0 equiv) were dissolved in dimethylformamide at rt, under N_2. First diisopropylethylamine (4 equiv), and then HATU (1 equiv) were added, and the reaction stirred for 16 h. The solvent was removed *in vacuo* (high vacuum rotary evaporator), and the residue was sonicated in methanol for 10 min. The insoluble material was filtered, and washed with methanol and methanol/water (1:1) redissolved in 2,2,2-trifluoroethanol (to remove from the glass frit filter), and the solvent removed *in vacuo.* If necessary, the crude mixture was purified by column chromatography on lipophilic sephadex, as specified for each compound.

General Method B: Aqueous coupling to succinimide esters

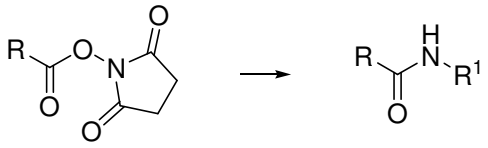

N-Hydroxysuccinimide-ester (1.0 equiv) and primary amine (1.1 equiv) were dissolved in a water/tetrahydrofuran mixture at rt. Triethylamine or diisopropylamine (~2 equiv) was added keeping the pH below 8.5 (universal indicator paper) and the reaction mixture was stirred for 16 h. The pH was adjusted to 3 (universal indicator paper) with 1 M aqueous citric acid and extracted twice with ethyl acetate. The organic layers were combined, washed with water, dried ($MgSO_4$) and the solvent removed *in vacuo*. The crude mixture was purified by column chromatography, as specified for each compound.

General Method C: Synthesis of diazoketones

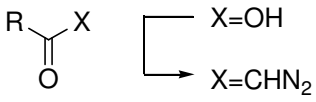

The acid was dissolved in anhydrous tetrahydrofuran and the solution was cooled to -30 ºC. Triethylamine (1.0 equiv) and ethyl chloroformate (1.0 equiv) were added and the reaction mixture stirred for 15 min at this temperature, before warming on an ice-bath. A solution of CH_2N_2* in diethylether (~ 2 equiv) was added until a yellow colour persisted, and stirring continued for a further 3 h at rt. The excess diazomethane was quenched with acetic acid, diluted with ethyl acetate, washed with saturated aqueous NH_4Cl, $NaHCO_3$ and NaCl and dried ($MgSO_4$). The solvent was removed *in vacuo* to give the crude diazoketone. The crude mixture was purified by column chromatography, as specified for each compound.

* ***Highly explosive*** – avoid contact with ground or unsmooth glass, and keep cold. Prepared according to Vogel, A. I.;Furniss, B. S., Vogel's Textbook of practical organic chemistry. 5th ed.; Longman Scientific & Technical London, 1989; p 1514.

General Method D: Wolff rearrangement

The diazoketone (1.0 equiv) was dissolved in anhydrous methanol under N_2 at -25 ºC, with the exclusion of light.* Silver benzoate (0.11 equiv), dissolved in triethylamine (2.9 equiv), was added and the reaction mixture was allowed to warm to rt over 3 h. The solvent was removed *in vacuo* and the residue was taken up in ethyl acetate. The organic layer was extracted with saturated aqueous NH_4Cl, $NaHCO_3$ and NaCl, dried ($MgSO_4$) and the solvent removed *in vacuo*. The crude mixture was purified by column chromatography, as specified for each compound.

General Method E: Methyl ester hydrolysis

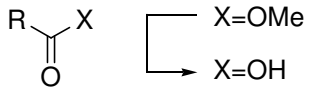

LiOH (0.2 M aqueous, 2.0 equiv) was added to a solution of carboxylic acid ester (1 equiv), dissolved in tetrahydrofuran cooled over an ice-bath. The reaction mixture was warmed to rt and stirred for 2 h, before adjusting the pH to 3 (universal indicator paper) with 1 M aqueous citric acid. The aqueous layer was extracted twice with ethyl acetate and the combined organic extracts were dried ($MgSO_4$) and evaporated to give the crude carboxylic acid. The crude product was used without further purification.

General Method F: Boc-deprotection with trifluoroacetic acid

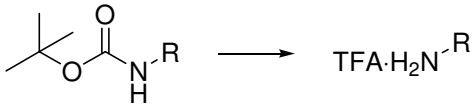

The Boc-protected amine was dissolved in 1:1 trifluoroacetic acid/dichloromethane and stirred for 2 h at rt. The solvent was removed *in vacuo*, twice co-evaporated *in vacuo* with

* Light was excluded by wrapping the reaction vessel in black polythene.

dichloromethane, and co-evaporated *in vacuo* with methanol to give the deprotected amine as a TFA salt. The crude product was used without further purification.

General Method G: Boc-deprotection with HCl/dioxane

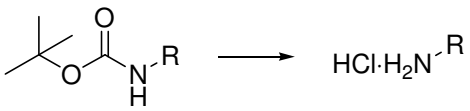

The Boc-protected amine was dissolved in 4 M HCl/dioxane (Aldrich$^{(R)}$) and stirred for 2 h at rt. The solvent was removed *in vacuo* to give the deprotected amine as a hydrochloride salt. The crude product was used without further purification.

Modified General Method G: Boc-deprotection with HCl/dioxane of ferrocene species

The Boc-protected amine was dissolved in 4 M HCl/dioxane (Aldrich$^{(R)}$) and stirred for 10-15 min at rt. The solvent was removed *in vacuo* to give the deprotected amine as a green residue (due to FcH^+). The residue was dissolved in methanol, passed through an alumina plug (to deprotonate the ferrocene), and the solvent removed *in vacuo* to give a yellow hydrochloride salt. Unless specified otherwise, the crude product was used without further purification.

6.3 Experimental Work Described in Chapter 2

Formation of SAMs

SAMs of hexapeptides were prepared by immersing the gold electrode into a solution of 2,2,2-trifluoroethanol (99.5%, Aldrich, used as received) containing ~ 1 $mg.mL^{-1}$ of thiol or disulfide. Peptides were adsorbed for 16 h using a hanging meniscus method. Prior to adsorption, **4.57** was deprotected in-situ by adding of NH_3 (aq) (0.1 mL) to the trifluoroethanol (2 mL), to give the free thiol **SC15β_6Fc** (**2.12**).

Data Analysis

Voltammetric peak analysis was performed by integration of the peaks using Linkfit.[5] Polynomial baselines (correlating to the double layer charging currents) were solved for and subtracted from the voltammogram prior to the integration.

Chronoamperometry analysis was performed in Microsoft Excel by obtaining the natural logarithmic data for the absolute value of the observed current and plotting this against time. The gradient of the graph in the linear region (2 ms to 8 ms) was obtained using a linear trendline to give the k_{et} values. The k_{et} values were plotted against overpotential. Error bars show one standard deviation of the obtained data. The chronoamperometry analysis of each peptide was measured either in duplicate (for good agreement) or triplicate.

6.4 Experimental Work Described in Chapter 3

6.4.1 Electrochemical Methods

Cross Metathesis Reactions

SAMs were prepared by immersing the gold electrode into an ethanolic solution containing ~1 $mg.mL^{-1}$ of the thiol. The adsorption times were dependent on the desired surface composition. Typically, diluents were adsorbed from 16 to 72 h and the olefin from a few min up to several h. Exact adsorption times are detailed in Chapter 3, Sections 3.3 and 3.4.

Cross metathesis was carried out in dichloromethane (50 mL) at reflux containing the olefin-terminated ferrocene (**3.10**) (10 mg, 33.7 μmol) and Grubbs' catalyst **3.2** (5 mg) with constant stirring under N_2. The gold electrode, with attached olefin-terminated SAM (**3.18**), and diluent (**C5**, **C10** or hexadecanethiol) was suspended in this solution. At known reaction time intervals (t), the electrode was removed, rinsed with dichloromethane, then water, dried with N_2, and placed into the electrochemical cell for voltammetry. Following the electrochemical analysis, the electrode was again rinsed, dried, and replaced into the cross metathesis solution.

Thiol Stability Tests

SAMs were prepared by immersing the gold electrode into an ethanolic solution containing ~1 $mg.mL^{-1}$ of the thiol. The adsorption times were dependent on the desired surface composition: the thiols were adsorbed for 16 h (**3.21**) or 36 h (**2.18, 3.21**) (both without diluents).

Thiol stability tests were carried out in dichloromethane (50 mL) at reflux with constant stirring under N_2. The gold (111) electrode, with attached ferrocene-terminated SAM (**2.18** or **3.21**), was suspended in this solution. After the electrode was suspended in the refluxing DCM for known time intervals (*t*) (detailed in Chapter 3, Section 3.4), the electrode was removed, rinsed with dichloromethane, then water, dried with N_2, and placed into the electrochemical cell for voltammetry. Following the electrochemical analysis, the electrode was rinsed, dried, and replaced into the refluxing DCM. At 150 min, Grubbs' catalyst **3.2** was added and electrochemical analysis continued until an insufficient redox signal was seen (~6 hrs).

6.4.2 Synthesis of Olefins

Hex-5-en-1-yl ferrocenylacetate (3.6)

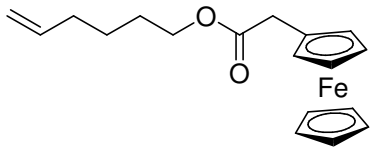

Ferrocene acetic acid (50 mg, 0.20 mmol), DMAP (50 mg, 0.41 mmol) and EDCI (79 mg, 0.41 mmol) were added to anhydrous dimethylformamide (20 mL). 5-Hexen-1-ol (29 μL, 0.41 mmol) was added and the reaction mixture stirred under N_2 for 4 h at rt. The reaction mixture was diluted with ethyl acetate (50 mL), and the organic layer washed with saturated aqueous NH_4Cl, $NaHCO_3$ and NaCl. The organic layer was separated and dried ($MgSO_4$), and the solvent removed *in vacuo* to give a dark brown oil. The crude mixture was purified by column chromatography (silica; 1:9 ethyl acetate, petroleum ether) to give the product as a brown oil (52 mg, 77%).

^{1}H NMR ($CDCl_3$) δ: 5.79 (tdd, 1H, C**H**=CH_2, *J*=16.9, 10.2, 6.7 Hz), 4.99 (m, 2H, CH=C**H$_2$**), 4.23 (br s, 2H, Fc), 4.14 (br s, 7H, Fc), 4.10 (t, 2H, OC**H$_2$**, *J*=6.7 Hz), 3.31 (br s, 2H, FcC**H$_2$**), 2.08 (q, 2H, C**H$_2$**CH=CH_2, *J*=7.2 Hz), 1.66 (m, 2H, OCH_2C**H$_2$**), 1.46 (m, 2H, OCH_2CH_2C**H$_2$**).
^{13}C NMR ($CDCl_3$) δ: 171.1, 138.2, 114.8, 80.4, 68.7, 68.6, 67.7, 64.4, 35.4, 33.2, 27.9, 25.1.
FTIR (KBr, cm^{-1}) 2923.9, 1732.0, 1639.4.
HRMS calc for $C_{18}H_{23}O_2Fe$ (MH^+) 327.1047; found 327.1062.

***N*-But-3-en-1-yl-2-ferrocenylacetamide (3.10)**

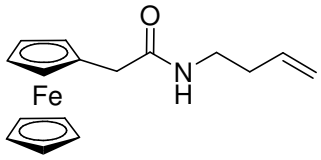

Ferrocene acetic acid (118 mg, 0.48 mmol) and 3-buten-1-amine hydrochloride (52 mg, 0.48 mmol) were coupled in dimethylformamide (50 mL) using HATU (184 mg, 0.48 mmol) and diisopropylethylamine (338 μL, 1.9 mmol) according to general method A. The reaction mixture was purified by column chromatography (silica; ethyl acetate/petroleum ether 1:1) to give the product as a brown crystalline solid (95 mg, 65% yield).

mp = 66-68 ºC
^{1}H NMR (300 MHz, $CDCl_3$) δ: 5.64 (m, 2H, N**H**, C**H**=CH_2), 4.98 (m, 2H, CH=C**H$_2$**), 4.13 (m, 9H, Fc), 3.30 (m, 2H, FcC**H$_2$**), 3.23 (q, 2H, NHC**H$_2$**, *J*=6.3 Hz), 2.16 (q, 2H, $NHCH_2$C**H$_2$**, *J*=6.8 Hz).
^{13}C NMR ($CDCl_3$:CD_3OD, 3:1) δ: 170.8, 134.9, 117.2, 80.7, 69.1, 68.8, 68.3, 38.1, 37.8, 33.5.
Microanalysis cald for $C_{16}H_{20}FeNO$: C, 64.67; H, 6.44; N, 4.71; found C, 64.41; H, 6.36; N, 4.63.
FTIR (KBr, diffuse reflection method, cm^{-1}): 3076.2, 2904.6, 1635.5, 1558.4, 999.1, 918.1, 709.8.
HRMS calcd for $C_{16}H_{20}FeNO$ (MH^+) 298.0894; found 298.0909.

3-Buten-1-amine hydrochloride (3.13)[6]

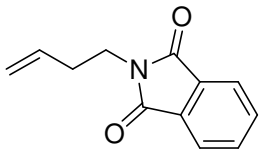

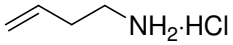

4-Bromo-1-butene (1.01 mL, 10 mmol) and potassium phthalimide (2.78 g, 15 mmol) were dissolved in anhydrous dimethylformamide (50 mL). The reaction mixture was stirred at 110 ºC for 16 h under N_2, cooled to rt and diluted with ethyl acetate (100 mL). The organic layer was washed with saturated aqueous NH_4Cl, $NaHCO_3$, dried ($MgSO_4$) and the solvent removed *in vacuo*. The crude mixture was purified by flash chromatrography (silica; 1:4 ethyl acetate, petroleum ether) to give the phthalimide product as a white solid.

The phthalimide (1.00 g, 5.0 mmol) was dissolved in ethanol (25 mL) and the solution heated to 50 ºC. Hydrazine monohydrate (~0.60 g, ~19 mmol) was added and the reaction mixture was stirred under N_2 until no starting material remained (monitored by TLC). The reaction was quenched with 1 M hydrochloric acid (added until no white precipitate remained). The resulting solution was stirred for 10 min, followed by removal of the solvents *in vacuo*, to give the product as a yellow solid (0.84 g, 78% over two steps).

Spectral properties are in agreement with those in the literature.[7]

mp 176 ºC (lit.[7] 178-180 ºC)
^{1}H NMR (CD_3OD) δ: 5.82 (m, 1H, CH_2=C**H**), 5.22 (m, 2H, C**H$_2$**=CH), 3.00 (t, 2H, C**H$_2$**NH, *J*=6.8 Hz), 2.43 (q, 2H, C**H$_2$**CH_2NH, *J*=6.3 Hz).

16-(Acetylthio)hexadecanoic acid (3.16)

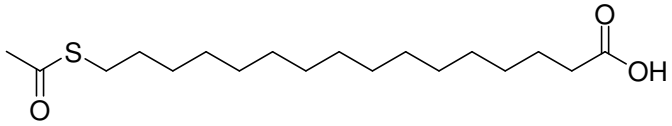

16-Mercaptohexanedecanoic acid (50 mg, 0.17 mmol) was dissolved in dichloromethane (0.6 mL) and acetic acid (0.6 mL). Zinc dust (0.1 g) was added and the mixture stirred for 15 min, to give a clear solution. The mixture was cooled on an ice-bath, acetyl chloride (0.24 mL) was added, and when evolution of hydrogen gas ceased, the solution was allowed to warm to rt. After a further 10 min, the zinc was removed by filtration through a bed of celite, and the filtrate washed twice with ice cold aqueous 0.2 M hydrochloric acid (25 mL). The solvent was removed *in vacuo* to give the product as a white solid, which required no purification (48 mg, 83%).

Spectral properties agreed with the literature.[8]

mp = 79-80 ºC (no literature mp)
^{1}H NMR ($CDCl_3$) δ: 2.85 (t, 2H, AcSC**H$_2$**, *J*=7.4 Hz), 2.34 (t, 2H, C**H$_2$**CO, *J*=7.5 Hz), 2.32 (s, 3H, C**H$_3$**COS), 1.66-1.61 (m, 2H), 1.58-1.52 (m, 2H), 1.35-1.24 (m, 22H).

***S*-[16-(But-3-en-1-ylamino)-16-oxohexadecyl]ethanethioate (3.17)**

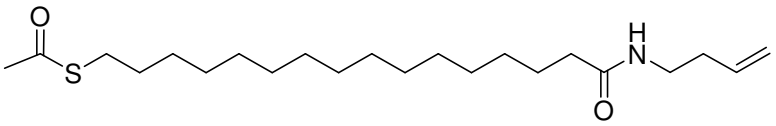

16-(Acetylthio)hexadecanoic acid (**3.16**) (162 mg, 0.49 mmol) and 3-buten-1-amine hydrochloride (52 mg, 0.49 mmol) were coupled in dimethylformamide (50 mL) using HATU (186 mg, 0.49 mmol) and diisopropylethylamine (341 μL, 2.0 mmol) according to general method A. The crude mixture was purified by column chromatography (silica; 1:1, ethyl acetate, petroleum ether) to give the product as a white solid (171 mg, 91%).

mp = 80-81 ºC

^{1}H NMR ($CDCl_3$) δ: 5.76 (m, 1H, C**H**=CH_2), 5.41 (m, N**H**), 5.09 (m, 2H, CH=C**H$_2$**) , 3.33 (q, 2H, NHC**H$_2$**, *J*=6.4 Hz), 2.86 (t, 2H, SC**H$_2$**, *J*=7.4 Hz), 2.32 (s, 3H, C**H$_3$**COS), 2.26 (m, 2H, $NHCH_2$C**H$_2$**), 2.14 (t, 2H, COC**H$_2$**, *J*=7.7 Hz), 1.57 (m, 4H), 1.35-1.24 (m, 22H).

^{13}C NMR ($CDCl_3$:CD_3OD, 3:1) δ: 195.8, 173.0, 135.2, 116.7, 38.2, 36.6, 33.6, 30.4, 29.4, 29.4, 29.3, 29.2, 29.1, 28.9, 28.6, 25.6.

Microanalysis calcd for $C_{22}H_{41}NO_2S$: C, 68.88; H, 10.77; N, 3.65; found C, 68.90; H, 10.56; N, 3.91.

HRMS calcd for $C_{22}H_{42}NO_2S$ (MH^+) 384.2936; found 384.2924.

_N_-But-3-en-1-yl-16-mercaptohexadecanamide (3.18)

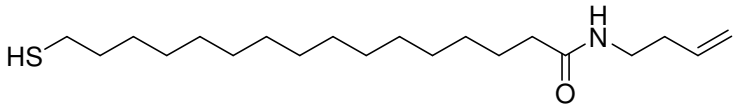

S-[16-(But-3-en-1-ylamino)-16-oxohexadecyl]ethanethioate (**3.17**) (58 mg, 0.15 mmol) was stirred in a mixture of dichloromethane (5 mL) and methanol (1.5 mL) under N_2. Sodium thiomethoxide (10 mg, 0.15 mmol) dissolved in methanol (450 μL) was added and the mixture stirred for 30 min at rt. The reaction mixture was diluted with dichloromethane (10 mL), and the organic layer washed successively with 0.3 M aqueous hydrochloric acid, saturated aqueous NaCl and dried ($MgSO_4$). The solvent was removed *in vacuo* and the crude mixture purified by column chromatography (silica; 1:1 ethyl acetate, petroleum ether) to give the product as a white solid (43 mg, 83%).

mp = 61-63 ºC

^{1}H NMR ($CDCl_3$) δ: 5.75 (m, 1H, C**H**=CH_2), 5.52 (br s, 1H, N**H**), 5.08 (m, 2H, CH=C**H$_2$**), 3.32 (dd, 2H, NHC**H$_2$**, *J*=12.5, 6.7 Hz), 2.51 (dd, 2H, SC**H$_2$**, *J*=14.7, 7.5 Hz), 2.25 (m, 2H, $NHCH_2$C**H$_2$**), 2.13 (t, 2H, C**H$_2$**CO, *J*=7.6 Hz), 1.59 (m, 4H), 1.35-1.23 (m, 22 H).

^{13}C NMR ($CDCl_3$) δ: 173.1, 135.3, 117.0, 38.2, 36.8, 34.0, 33.8, 29.6, 29.4, 29.3, 29.2, 29.0, 28.3, 25.7, 24.6.

HRMS calcd for $C_{20}H_{40}NOS$ (MH^+) 342.2831; found 342.2842.

FTIR (KBr, cm^{-1}) 3309.6, 2920.0, 2850.6, 1635.5, 1554.5, 1469.7.

Dec-5-en-1-yl 5-(1,2-dithiolan-(3*S*/*R*)-3-yl) pentanoate (3.20)

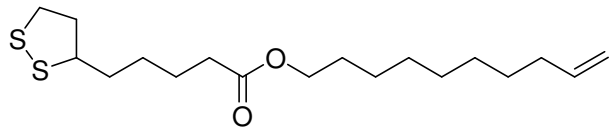

Racemic lipoic acid (**3.19**) (100 mg, 0.49 mmol) and 9-decen-1-ol (200 μL, 1.1 mmol) were coupled in dimethylformamide (50 mL) using HATU (185 mg, 0.49 mmol) and diisopropylethylamine (338 μL, 1.9 mmol) according to general method A. The crude mixture was purified by column chromatography (silica; 1:9 ethyl acetate, petroleum ether), to give the product as a light yellow oil (124 mg, 74%).

^{1}H NMR ($CDCl_3$) δ: 5.80 (m, 1H, C**H**=CH_2), 4.95 (m, 2H, CH=C**H$_2$**), 4.05 (t, 2H, OC**H$_2$**, *J*=6.7 Hz), 3.56 (m, 1H, SC**H**), 3.14 (m, 2H, SC**H$_2$**), 2.46 (m, 1H, SCH_2C**H**H), 2.31 (t, 2H, C**H$_2$**CO, *J*=7.4 Hz), 2.03 (q, 2H, *J*=6.8 Hz), 1.90 (m, 1H, SCH_2CH**H**), 1.72-1.58 (m, 6H), 1.46 (m, 2H, $CHCH_2$C**H$_2$**CH_2), 1.38-1.25 (m, 10H).
^{13}C NMR ($CDCl_3$) δ: 173.5, 139.1, 114.1, 64.4, 56.3, 40.2, 38.4, 34.6, 34.1, 33.7, 29.3, 29.1, 29.0, 28.8, 28.7, 28.6, 25.9, 24.7.
FTIR (KBr, cm^{-1}) 1735.8, 1639.4, 995.2, 910.3.
HRMS calcd for $C_{18}H_{33}O_2S_2$ (MH^+) 345.1922; found 345.1945.

6.5 Experimental Work Described in Chapter 4

6.5.1 Synthesis of Model Compounds

5-(1,2-Dithiolan-(3*S*/*R*)-3-yl)pentanamide (4.6)

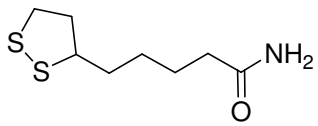

Racemic lipoic acid (**3.19**) (0.50 g, 2.4 mmol) and triethylamine (338 μL, 2.4 mmol) were dissolved in anhydrous tetrahydrofuran (10 mL) and the reaction mixture was cooled on an ice-

bath. Ethylchloroformate (230 μL, 2.4 mmol) was added and the reaction mixture was stirred for 30 min before being poured onto a mixture of aqueous ammonium hydroxide (1.7 mL, 28% in water) and tetrahydrofuran (10 mL). The reaction mixture was stirred for 1 h at rt and then diluted with water (50 mL) and ethyl acetate (50 mL). The organic layer was separated, washed with water and saturated aqueous NaCl, dried ($MgSO_4$) and the solvent removed *in vacuo*. The crude mixture was purified by column chromatography (silica; 1:9 methanol, ethyl acetate), to give the product as a light yellow solid (0.41 g, 82%).

Spectral and physical properties are in agreement with those in the literature. [9]

mp = 125-126 ºC (lit.[9] 126-129 ºC)
^{1}H NMR ($CDCl_3$) δ: 5.81 (s, 1H, N**H**), 5.53 (s, 1H, N**H**), 3.56 (dd, 1H, SC**H**, *J*=8.0, 6.6 Hz), 3.13 (m, 2H, SC**H$_2$**), 2.45 (dd, 1H, SCHC**H**H, *J*=12.7, 6.4 Hz), 2.23 (t, 2H, C**H$_2$**CO, *J*=7.5, 7.5 Hz), 1.90 (dd, 1H, SCHCH**H**, *J*=13.1, 6.6 Hz,), 1.67 (m, 4H, CHC**H$_2$**CH_2C**H$_2$**), 1.47 (ddd, 2H, CHCH_2C**H$_2$**, *J*=9.4, 7.7, 2.8 Hz).

5-(1,2-Dithiolan-(3*S*/*R*)-3-yl)pentan-1-amine (4.8)

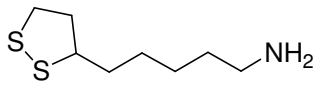

α-Lipoamide (**4.6**) (0.40 g, 2.0 mmol) was dissolved in anhydrous tetrahydrofuran (50 mL). Lithium aluminium hydride (9.5 mL of 1 M solution in tetrahydrofuran, 9.5 mmol) was added and the reaction mixture was heated at reflux for 16 h. The reaction mixture was cooled on an ice-bath, distilled water (4 mL) was added and stirred for 30 min. After evaporation of the solvent, methanol was added and the insoluble solid removed by filtration. The supernatant was evaporated and an aliquot of distilled water (50 mL) added. The pH of the solution was adjusted to 6.5 (universal indicator paper) with 1 M aqueous hydrochloric acid and stirring continued at rt for 24 h. The product was extracted with 1-butanol and the organic phases washed with 1 M aqueous sodium hydroxide and 1 M aqueous hydrochloric acid. The solvent was removed *in vacuo* to give the product as pale-yellow solid (106 mg, 28%).

Spectral properties are in agreement with those in the literature.[10]

^{1}H NMR (CD_3OD) δ: 3.58 (m, 1H, SC**H**), 3.14 (m, 2H, SC**H$_2$**), 2.92 (m, 2H, C**H$_2$**NH_2), 2.47 (dt, 1H, SCH_2C**H**H, *J*=12.4, 12.3, 6.7 Hz), 1.89 (dt, 1H, SCH_2CH**H**, *J*=13.5, 13.5, 6.9 Hz), 1.68 (m, 4H, CHC**H$_2$**CH_2CH_2C**H$_2$**), 1.47 (m, 4H, $CHCH_2$C**H$_2$**C**H$_2$**CH_2).

4-(Acetylthio)benzoic acid (4.9)

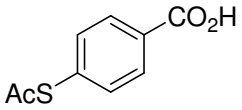

4-Mercaptobenzoic acid (**4.1**) (81 mg, 0.52 mmol) was dissolved in dichloromethane (2 mL) and acetic acid (2 mL). Zinc dust (0.3 g) was added and stirred for 15 min, to give a clear solution, and then cooled on an ice-bath. Acetyl chloride (0.75 mL) was added, and when evolution of hydrogen gas ceased, the reaction mixture was allowed to warm to rt. After 10 min, the zinc was removed by filtration through celite and the filtrate washed twice with ice-cold 0.2 M aqueous hydrochloric acid. The solvent was removed *in vacuo* to give a crude mixture, which was recrystallised from methanol to give the product as a white solid (91 mg, 89%).

Spectral properties are in agreement with those in the literature.[11]

mp = 182-190 ºC

^{1}H NMR (acetone-d_6) δ: 8.13 (d, 2H, Ar-2, *J*=8.5 Hz), 7.54 (d, 2H, Ar-3, *J*=8.5 Hz), 2.46 (s, 3H, C**H$_3$**).

^{13}C NMR (DMSO-d_6) δ: 192.5, 166.6, 134.1, 132.9, 131.4, 129.9, 30.3.

1-[16-(Acetylthio)hexadecanoyl]-(*R*)-β^3hVal-(*S*)-β^3hAla-(*S*)-β^3hLeu methyl ester (4.11)

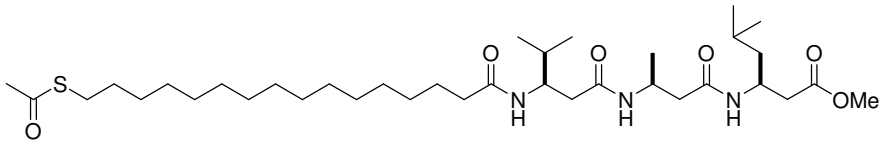

HCl·β^3hVal-β^3hAla-β^3hLeu methyl ester (**4.10**) (86 mg, 0.22 mmol) and 16-(acetylthio)hexadecanoic acid (**3.16**) (72 mg, 0.22 mmol) were coupled in dimethylformamide (20 mL) using HATU (83 mg, 0.22 mmol) and diisopropylethylamine (15 μL, 0.87 mmol) according to general method A. The crude mixture was purified with column chromatography (silica; 1:20 methanol, dichloromethane) to give the product as a white solid (112 mg, 76%).

^{1}H NMR (CD_3OD) δ: 7.93 (d, 1H, N**H**, *J*=9.3 Hz), 7.78 (d, 1H, N**H**, *J*=7.7 Hz), 7.68 (d, 1H, N**H**, *J*=9.0 Hz), 4.30 (m, 1H, NHC**H**CH_2) 4.22-4.08 (m, 2H, NHC**H**CH, NHC**H**CH_3), 3.65 (s, 3H, OC**H$_3$**), 2.86 (t, 2H, AcSC**H$_2$**, *J*=7.3 Hz,), 2.51-2.38 (m, 4H, CH_2CHC**H$_2$**CO, CHCHC**H**HCO, CH_3CHC**H**HCO), 2.30 (s, 3H, SCOC**H$_3$**), 2.24-2.14 (m, 4H, C**H$_2$**CO, CHCHCH**H**CO, CH_3CHCH**H**CO), 1.79 (m, 1H, NHCHC**H**), 1.65-1.52 (m, 5H, NHCHCH_2C**H**), 1.45 (m, 1H, NHCHC**H**H), 1.378-1.29 (m, 23H, NHCHCH**H**), 1.13 (d, 3H, CHC**H$_3$**, *J*=6.7 Hz), 0.92 (m, 12H, C(C**H$_3$**)$_2$).

^{13}C NMR ($CDCl_3$:CD_3OD, 3:1) δ: 197.7, 175.5, 173.1, 172.5, 172.2, 53.0, 52.2, 45.6, 44.3, 43.3, 40.8, 39.7, 37.2, 33.0, 30.7, 30.5-30.4 (m, 8 CH_2), 30.3, 30.2, 30.2, 30.0, 29.8, 29.6, 27.0, 25.8, 23.6, 22.2, 20.0, 19.6, 18.6.

HRMS calcd for $C_{36}H_{68}N_3O_6S$ (MH^+) 670.4829; found 670.4833.

4-(Acetylthio)benzoic acid (*S*)-β^3hAla benzyl ester (4.14)

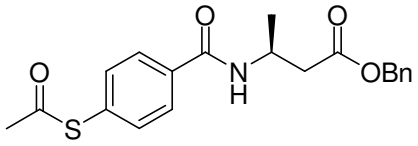

4-(Acetylthio)benzoic acid (**4.9**) (27 mg, 0.14 mmol) and TFA·β^3hAla-OBn (39 mg, 0.14 mmol) were coupled in dimethylformamide (5 mL) with HATU (67 mg, 0.17 mmol) and diisopropylethylamine (120 μL, 0.70 mmol) according to general method A. The solvent was removed *in vacuo* to give the product as a white solid (40 mg, 82%).

mp = 114-115 ºC

^{1}H NMR ($CDCl_3$) δ: 7.73 (d, 2H, Ar-2, *J*=8.3 Hz), 7.44 (d, 2H, Ar-3, *J*=8.3 Hz), 7.35 (br s, 5H, OCH_2**Ph**), 6.93 (d, 1H, N**H**, *J*=8.0 Hz), 5.15 (br s, 2H, $OC\mathbf{H_2}Ph$), 4.56 (m, 1H, NHC**H**), 2.72 (dd, 1H, NHCHC**H**H, *J*=15.8, 5.2 Hz), 2.64 (dd, 1H, NHCHC**H**H, *J*=15.8, 4.8 Hz), 2.44 (s, 3H, $COC\mathbf{H_3}$), 1.32 (d, 3H, $CHC\mathbf{H_3}$, *J*=6.8 Hz).

^{13}C NMR ($CDCl_3$) 193.0, 171.7, 165.6, 135.4, 135.2, 134.3, 131.6, 128.7, 128.5, 128.4, 127.6, 66.7, 42.4, 39.8, 30.4, 20.0.

HRMS calcd for $C_{20}H_{22}NO_4S$ (MH^+) 372.1263; found 372.1270.

5-[1,2]Dithiolan-(3*S*/*R*)-3-yl-pentanoyl-(*S*)-β^3hAla methyl ester (4.16)

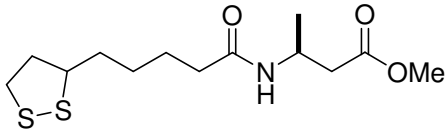

Racemic lipoic acid (**3.19**) (114 mg, 0.55 mmol) and TFA·β^3hAla methyl ester (**4.35**) (99 mg, 0.46 mmol) were coupled in dimethylformamide (5 mL) with HATU (210 mg, 0.55 mmol) and diisopropylethylamine (383 μL, 2.2 mmol), according to general method A. The crude mixture was purified by column chromatrography (silica; 1:1 ethyl acetate, petroleum ether), to give the product as a clear oil (111 mg, 79% yield).

^{1}H NMR ($CDCl_3$) δ: 7.93 (d, 1H, N**H**, *J*=7.1 Hz), 4.26 (m, 1H, NHC**H**), 3.65 (s, 3H, OC**H$_3$**), 3.57 (m, 1H, SC**H**), 3.17-3.10 (m, 2H, SC**H$_2$**), 2.54-2.44 (m, 3H, CHC**H$_2$**CO, SCH_2C**H**H), 2.16 (t, 2H, CH_2C**H$_2$**CO, *J*=7.3 Hz), 1.89 (m, 1H, SCH_2CH**H**), 1.76-1.60 (m, 4H, C**H$_2$**CH_2C**H$_2$**CH_2CO), 1.45 (m, 2H, $SCHCH_2$C**H$_2$**CH_2), 1.18 (d, 3H, CHC**H$_3$**, *J*=6.7 Hz).

^{13}C NMR (CD3OD) δ: 175.2, 173.3, 57.6, 52.2, 43.7, 41.5, 41.3, 39.4, 36.9, (36.93, 36.91)*, (35.77, 35.75), (29.83, 29.81), (26.77, 26.75), 20.5.

HRMS calcd for $C_{13}H_{24}NO_3S_2$ (MH^+) 306.1198; found 306.1182.

5-[1,2]Dithiolan-(3*S*/*R*)-3-yl-pentanoyl-(*S*)-*β*^{3}hAla benzyl ester (4.18)

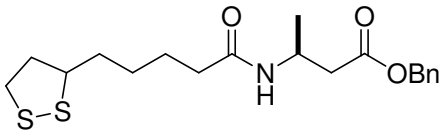

Racemic lipoic acid (**3.19**) (188 mg, 0.61 mmol) and the TFA·*β*^{3}hAlaOBn (188 mg, 0.62 mmol) were coupled in dimethylformamide (5 mL) with HATU (233 mg, 0.61 mmol) and diisopropylethylamine (430 μL, 2.5 mmol) according to general method A. The crude mixture was purified by column chromatography (silica; 1:1 ethyl acetate, petroleum ether) to give the product as a clear oil (223 g, 95%).

^{1}H NMR ($CDCl_3$) δ: 7.37-7.31 (m, 5H, OCH_2**Ph**), 6.06 (d, N**H**, *J*=7.6 Hz), 5.11 (s, 2H, OC**H$_2$**), 4.35 (m, 1H, NHC**H**), 3.53 (m, 1H, SC**H**), 3.18-3.06 (m, 2H, SC**H$_2$**), 2.59-2.51 (m, 2H, CHC**H$_2$**CO), 2.43 (m, 1H, SCH_2C**H**H), 2.09 (t, 2H, CH_2C**H$_2$**CO *J*=7.4 Hz), 1.88 (m, 1H, SCH_2CH**H**), 1.70-1.56 (m, 4H, C**H$_2$**CH_2C**H$_2$**CH_2CO), 1.42 (m, 2H, CH_2C**H$_2$**CH_2CH_2CO), 1.20 (d, 3H, C**H$_3$**, *J*=6.7 Hz).

^{13}C NMR ($CDCl_3$) δ: 171.8, 171.4, 135.4, 128.5, 128.2, 128.1, 66.3, 56.2, 41.8, 40.1, 39.9, 38.3, 36.3, 34.4, 28.7, 25.2, 19.9.

HRMS calcd for $C_{19}H_{28}NO_3S_2$ (MH^+) 382.1511; found 382.2509.

* Resonances for (SCHC**H$_2$**C**H$_2$**C**H$_2$**C**H$_2$**) are doubled due to the presence of an epimer. The doubled resonances were assigned using HSQC correlations.

1-{[5-(1,2-dithiolan-(3*S*/*R*)-3-yl)pentanoyl]oxy}pyrrolidine-2,5-dione (4.20)

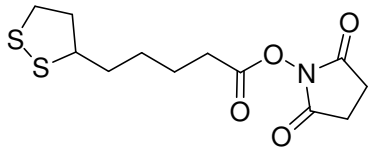

N-Hydroxysuccinimide (0.16 g, 1.3 mmol) and racemic lipoic acid (**3.19**) (200 mg, 0.97 mmol) were coupled in tetrahydrofuran (50 mL) using HOBt (0.20 g, 1.5 mmol), EDCI (0.24 g, 1.3 mmol) and diisopropylethylamine (0.68 mL, 3.9 mmol). The reaction mixture was stirred for 24 h at rt at which time the solvent was removed *in vacuo*. The residue was partitioned between ethyl acetate and water. the organic layer separated, washed with saturated aqueous $NaHCO_3$, NH_4Cl and NaCl and dried ($MgSO_4$). Flash chromatography (silica, 1:1 ethyl acetate, petroleum ether) gave the product as a yellow solid (0.26 g, 89%).

Spectral properties are in agreement with those in the literature.[12]

mp = 85-87 ºC

^{1}H NMR ($CDCl_3$) δ: 3.58 (m, 1H, SC**H**), 3.21-3.10 (m, 2H, SC**H$_2$**), 2.84 (m, 4H, CO(C**H$_2$**)$_2$CO), 2.63 (t, 2H, C**H$_2$**CON, *J*=7.4 Hz), 2.47 (dt, 1H, SCH_2C**H**H, *J*=6.6 Hz, *J*=12.5 Hz), 1.93 (m, 1H, SCH_2C**H**H), 1.82-1.69 (m, 4H, CHC**H$_2$**CH_2C**H$_2$**), 1.62-1.52 (m, 2H, $CHCH_2C$**H$_2$**CH_2).

5-[1,2]Dithiolan-(3*S*/*R*)-3-yl-pentanoyl-(*S*)-Ala-OH (4.21)

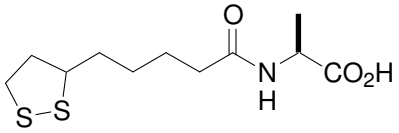

HCl·(*S*)-Ala-OH (15 mg, 0.17 mmol) and *N*-hydroxysuccinimide-activated lipoic acid (**4.20**) (50 mg, 0.17 mmol) were coupled in a mixture of tetrahydrofuran (5 mL), water (5 mL) and diisopropylethylamine (115 μL, 0.66 mmol) according to general method B. The crude mixture was purified by column chromatography (silica; 1:4 methanol, dichloromethane) to give the product as a light yellow oil (36 mg, 77%).

^{1}H NMR (CD_3OD) δ: 4.27 (m, 1H, NHC**H**), 3.57 (m, 1H, SC**H**) 3.19-3.07 (m, 2H, SC**H$_2$**), 2.46 (m, 1H, SCH_2C**H**H), 2.24 (t, 3H, COC**H$_2$** *J*=7.4 Hz), 1.89 (m, 1H, SCH_2C**H**H), 1.74-1.61 (m, 4H, CHC**H$_2$**CH_2C**H$_2$**), 1.48 (m, 2H, $CHCH_2$C**H$_2$**CH_2), 1.36 (d, 3H, CHC**H$_3$**, *J*=7.2 Hz).
^{13}C NMR (CD_3OD) δ: 178.9, 175.5, 57.6, 50.8, 41.3, 39.4, (36.79, 36.72)*, (35.83, 35.78), (29.93, 29.88), (26.67, 26.63), 18.4.
HRMS calcd for $C_{11}H_{21}NO_3S_2$ (MH^+) 279.0963; found 279.0953.

S-{16-[(2,5-Dioxopyrrolidin-1-yl)oxy]-16-oxohexadecyl}ethanethioate (4.22)

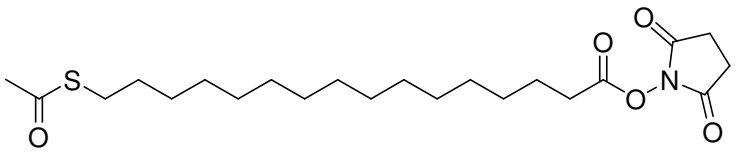

16-(Acetylthio)hexadecanoic acid (**3.16**) (0.20 g, 0.62 mmol) and *N*-hydroxysuccinimide (0.28 g, 2.4 mmol) were coupled in anhydrous dichloromethane (20 mL) using EDCI (0.48 g, 2.4 mmol), over 16 h. The reaction mixture was diluted with dichloromethane (20 mL), washed with water, dried ($MgSO_4$) and concentrated *in vacuo*. The crude mixture was purified by flash chromatographed (silica, 4:1 →2:1 ethyl acetate, petroleum ether) to give the product as a white solid (0.14 g, 87%).

Spectral properties are in agreement with those in the literature.[13]

mp = 71-73 ºC (no literature mp)
^{1}H NMR ($CDCl_3$) δ: 2.86 (m, 6H, C**H$_2$**SAc, COC**H$_2$**C**H$_2$**CO), 2.60 (t, 2H, C**H$_2$**COON, *J*=7.5 Hz), 2.32 (s, 3H, C**H$_3$**CO), 1.74 (td, 2H, C**H$_2$**CH_2CO, *J*=7.4 Hz, *J*=15.1 Hz), 1.56 (m, 2H, C**H$_2$**CH_2S), 1.42-1.25 (m, 22H, CH_2).

* Resonances for (SCHC**H$_2$**C**H$_2$**C**H$_2$**C**H$_2$**) are doubled due to the presence of an epimer. The doubled resonances were assigned using HSQC correlations.

Ferrocenemethylamine (4.27) [14,15]

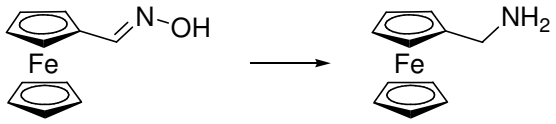

Ferrocenecarboxaldehyde (**4.25**) (1.00 g, 4.7 mmol) was dissolved in ethanol (10 mL) under N_2. A solution of hydroxylamine (0.65 g, 9.3 mmol) in water (3.5 mL) and sodium acetate (1.49 g, 18 mmol) were added and the reaction mixture heated under reflux for 3 h. The solvent was removed *in vacuo*, and dichloromethane (20 mL) was added and stirring continued for 30 min. The resulting light brown precipitate was filtered and the filtrate concentrated *in vacuo* to give the oxime (**4.26**) as a red-brown solid (1.04 g, 97%).

Oxime (**4.26**) (2.25 g, 9.4 mmol) was dissolved in anhydrous tetrahydrofuran (100 mL). Lithium hydride (1.70 g, 49 mmol) was added portionwise *with caution* and the mixture stirred under N_2 for 14 h. Toluene (100 mL) was added to the solution, followed by ethyl acetate *with caution* (15 mL). A few drops of 5 M aqueous NaOH were added until the precipitation of inorganic salts was complete. The mixture was filtered to give a yellow filtrate and a gummy solid residue. The residue was washed with toluene-methanol (80:20) and the combined organic fractions concentrated *in vacuo*. Inorganic impurities were removed by dissolution in dichloromethane (50 mL), followed by filtration. Evaporation of the filtrate *in vacuo*, followed by purification using column chromatography (silica; 95:5 methanol/ammonium hydroxide (28% in water)) gave the product as a brown oil (1.57 g, 76%).

Spectral properties are in agreement with those in the literature.[14]

^{1}H NMR ($CDCl_3$) δ: 4.15 (s, 2H, Fc), 4.13 (s, 5H, Fc), 4.10 (s, 2H, Fc), 3.54 (br s, 2H, FcC**H$_2$**), 1.40 (br s, 2H, N**H$_2$**).

***S*-{16-[(Ferrocenylmethyl)amino]-16-oxo-hexadecyl}ethanethioate (4.28)**

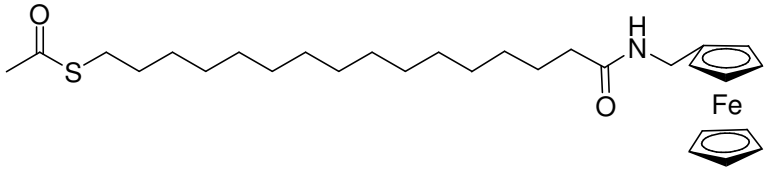

Ferrocene methylamine (**4.27**) (50 mg, 0.23 mmol) and 16-(acetylthio)hexadecanoic acid (**3.16**) (84 mg, 0.25 mmol) were coupled in dimethylformamide (50 ml) using HATU (114 mg, 0.30 mmol) and diisopropylethylamine (80 μL, 0.46 mmol) according to general method A. The crude mixture was purified by column chromatography (silica; 1:3 ethyl acetate, petroleum ether) to give the product as a yellow solid (100 mg, 80%).

mp = 86 ºC

^{1}H NMR ($CDCl_3$) δ: 5.52 (m, 1H, N**H**), 4.21 (m, 9H, Fc), 4.10 (m, 2H, FcC**H$_2$**), 2.86 (t, 2H, AcSC**H$_2$**, *J*=7.4 Hz), 2.31 (s, 3H, C**H$_3$**COS), 2.15 (t, 2H, C**H$_2$**CO, *J*=7.5 Hz), 1.65-1.52 (m, 4H), 1.35-1.24 (m, 22H).

^{13}C NMR ($CDCl_3$) δ: 196.1, 172.4, 84.8, 68.5, 68.2, 68.1, 38.8, 36.8, 30.6, 29.6, 29.6, 29.5, 29.5, 29.3, 29.3, 29.1, 29.1, 28.8, 25.8.

HRMS calcd for $C_{29}H_{46}NO_2SFe$ (MH^+) 528.2599; found 528.2581.

FTIR (KBr, cm^{-1}) 3330.8, 2920.0, 2850.6, 1689.5, 1647.1, 1531.4, 813.9.

Microanalysis calcd. for $C_{29}H_{45}FeNO_2S$: C, 66.02; H, 8.60; N, 2.65; found C, 65.87; H, 8.38; N, 2.65.

***N*-(Ferrocenylmethyl)-16-mercaptohexadecanamide (2.18)**

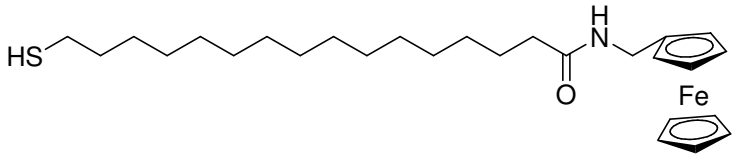

S-{16-[(Ferrocenylmethyl)amino]-16-oxo-hexadecyl}ethanethioate (**4.28**) (26 mg, 43 μmol) was stirred in a mixture of dichloromethane (3 mL) and methanol (1 mL) under N_2. A solution of

sodium thiomethoxide (3 mg, 43 μmol) in methanol (450 μL) was added and stirred for 30 min at rt. The reaction mixture was diluted with dichloromethane (10 mL) and washed with 0.3 M aqueous hydrochloric acid, saturated aqueous NaCl, dried ($MgSO_4$) and the solvent removed *in vacuo*. The crude mixture was purified by column chromatography (silica; 1:3 ethyl acetate, petroleum ether) to give the product as a yellow solid (18 mg, 87%).

mp = 72-74 ºC

^{1}H NMR ($CDCl_3$) δ: 5.60 (m, 1H, N**H**), 4.17-4.13 (m, 11H, **FcCH$_2$**), 2.51 (q, 2H, SC**H$_2$**, *J*=6.8 Hz), 2.16 (t, 2H, C**H$_2$**CO, *J*=7.2 Hz), 1.61 (m, 4H), 1.36-1.24 (m, 22H).

^{13}C NMR ($CDCl_3$) δ: 172.4, 84.8, 68.5, 68.2, 68.1, 38.8, 36.8, 34.0, 29.6, 29.6, 29.5, 29.5, 29.3, 29.3, 29.1, 28.4, 25.8, 24.6.

HRMS calcd for $C_{27}H_{44}NOSFe$ (MH^+) 486.2493; found 486.2503.

FTIR (KBr, cm^{-1}) 2920.0, 2850.6, 1647.1, 1535.2.

5-(1,2-Dithiolan-(3*S*/*R*)-3-yl)-*N*-(ferrocenylmethyl)pentanamide (3.21)

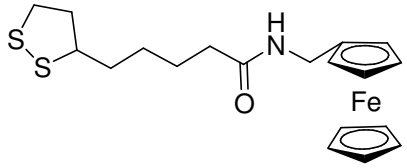

Racemic lipoic acid (**3.19**) (36 mg, 0.17 mmol) and ferrocene methylamine (**4.27**) (38 mg, 0.17 mmol) were coupled in dimethylformamide (10 mL) with HATU (66 mg, 0.17 mmol) and diisopropylethylamine (118 μL, 0.68 mmol) according to general method A. The crude brown oil was purified with column chromatrography (silica; 1:1 ethyl acetate, petroleum ether) to give the product as a yellow-brown oil (39 mg, 56%).

^{1}H NMR ($CDCl_3$) δ: 5.55 (m, 1H, N**H**), 4.20-4.15 (m, 9H, Fc), 4.13 (d, 2H, C**H$_2$**Fc, *J*=4.1 Hz), 3.56 (m, 1H, SC**H**), 3.19-3.08 (m, 2H, SC**H$_2$**), 2.45 (m, 1H, SCH_2CHH), 2.17 (t, 2H, C**H$_2$**CO, *J*=7.3 Hz,), 1.90 (m, 1H, SCH_2CH**H**), 1.72-1.61 (m, 4H, CHC**H$_2$**CH_2C**H$_2$**), 1.50-1.42 (m, 2H, $CHCH_2$C**H$_2$**CH_2).

^{13}C NMR ($CDCl_3$) δ: 171.9, 84.6, 68.5, 68.2, 68.1, 56.4, 40.1, 38.8, 38.4, 36.3, 34.5, 28.8, 25.3.

FTIR (KBr, cm^{-1}) 3298.0, 2927.7, 1643.2, 1546.8.

HRMS calcd for $C_{19}H_{26}NOS_2Fe$ (MH^+) 404.0805; found 404.0786.

6.5.2 Synthesis of β^3-Amino Acid Monomers

Boc-(*S*)-β^3hAla methyl ester (4.33a)

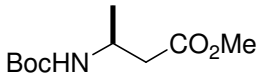

Boc-(*S*)-Ala-OH (**4.31a**) (3.78 g, 20 mmol), ethyl chloroformate (2.02 mL, 20 mmol), triethylamine (2.94 mL, 20 mmol) and diazomethane (~0.40 M in diethyl ether, ~100 mL) were reacted according to general Method C. Puficiation of the crude mixture by column chromatography (silica; 1:4 ethyl acetate, petroleum ether) gave the diazoketone **4.32a** as a yellow oil (3.02 g, 70%).
Selected data: ^{1}H NMR ($CDCl_3$) δ: 5.43 (s, 1H, COC**H**N_2)

Boc-Ala-diazoketone (**4.32a**) (3.02 g, 14 mmol), silver benzoate (0.36 g, 1.6 mmol), methanol (20 mL) and triethylamine (5.72 mL, 41 mmol) were reacted according to general method D. The crude product was purified by column chromatography (silica; 1:9 ethyl acetate, petroleum ether) to give the product as a clear oil (2.22 g, 72%).

Spectra properties are in agreement with those in the literature.[16]

^{1}H NMR ($CDCl_3$) δ: 4.91 (m, 1H, N**H**) 4.03 (m, 1H, C**H**CH_3), 3.68 (s, 3H, OC**H$_3$**), 2.54-2.46 (m, 2H, CHC**H$_2$**), 1.44 (s, 9H, C(C**H$_3$**)$_3$), 1.21 (d, 3H, CHC**H$_3$**, *J*=6.7 Hz).

Boc-(*R*)-β^3hVal methyl ester (4.33b)

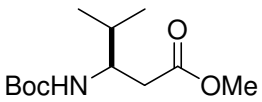

Boc-(*S*)-Val-OH (**4.31b**) (4.34 g, 20 mmol), ethyl chloroformate (1.95 mL, 20 mmol), triethylamine (2.84 mL, 20 mmol) and diazomethane (~0.40 M in diethyl ether, ~100 mL) were reacted according to general Method C. Purification of the crude mixture by column chromatography (silica; 1:4 ethyl acetate, petroleum ether) gave diazoketone **4.32b** as a yellow oil (2.82 g, 58%).

Selected data: ^{1}H NMR ($CDCl_3$) δ: 5.43 (s, 1H, COC**H**N_2)

Boc-Val-diazoketone (**4.32b**) (2.82 g, 12 mmol), silver benzoate (0.30 g, 1.3 mmol), methanol (20 mL) and triethylamine (4.73 mL, 34 mmol) were reacted according to general method D. The crude product was purified by column chromatography (silica; 1:9 ethyl acetate, petroleum ether) to give the product as a clear oil (2.30 g, 78%).

Spectral properties are in agreement with those in the literature.[17]

^{1}H NMR ($CDCl_3$) δ: 4.86 (d, 1H, N**H**, *J*=8.9 Hz), 3.74 (m, 1H, NHC**H**), 3.66 (s, 3H, OC**H**$_3$) 2.48 (m, 2H, COC**H**$_2$), 1.79 (m, 1H, NHCHC**H**), 1.41 (s, 9H, C**H**$(CH_3)_2$), 0.90 (d, 1H, CH$(C\mathbf{H_3})_2$), *J*=6.8 Hz).

Boc-(*S*)-β^3hLeu methyl ester (4.33b)

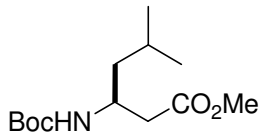

Boc-(*S*)-Leu-OH (**4.31c**) (4.63 g, 20 mmol), ethyl chloroformate (1.95 mL, 20 mmol), triethylamine (2.84 mL, 20 mol) and diazomethane (~0.40 M in diethyl ether, ~100 mL) were reacted according to general Method C. Purification of the crude mixture using column chromatography (silica; 1:4 ethyl acetate, Petroleum Ether) gave diazoketone **4.32c** as a yellow oil (3.69 g, 73%).
Selected data: ^{1}H NMR ($CDCl_3$) δ: 5.44 (s, 1H, COC**H**N_2)

Boc-Leu-diazoketone (**4.32c**) (3.69 g, 14.5 mmol), silver benzoate (0.36 g, 1.59 mmol), methanol (20 mL) and triethylamine (5.84 mL, 41.9 mmol) were reacted according to general method D. The crude product was purified by column chromatography (silica; 1:9 ethyl acetate, petroleum ether) to give the product as a clear oil (3.29 g, 87%).

Spectral properties are in agreement with those in the literature.[16]

^{1}H NMR ($CDCl_3$) δ: 4.84 (m, 1H, NH), 3.98 (m, 1H, NHC**H**), 3.67 (s, 3H, OC**H$_3$**), 2.50 (m, 2H, C**H$_2$**CO), 1.63 (m, 1H, C**H**(CH_3)$_2$), 1.42 (m, 10H, NHCHC**H**H, C(C**H$_3$**)$_3$), 1.26 (m, 1H, NHCHCH**H**), 0.91 (m, 6H, CH(C**H$_3$**)$_2$).

6.5.3 Synthesis of *β*-Tripeptide (4.39)

Boc-(*R*)-*β*^{3}hVal-OH (4.34)

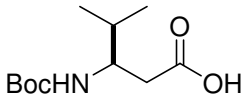

Boc-*β*^{3}hVal methyl ester (**4.33b**) (1.65 g, 6.7 mmol) was dissolved in tetrahydrofuran (50 mL) and hydrolysed with LiOH (0.2 M, 67 mL) according to general method E. The product was obtained as a white solid (1.62 g, 98%) that required no further purification.

Spectral properties are in agreement with those in the literature.[18]

mp = 74-77 ºC (lit.[18] 65-66 ºC)
^{1}H NMR (CD_3OD) δ: 6.50 (d, 1H, N**H**, *J*=9.3 Hz), 3.77 (m, 1H, NHC**H**), 2.48 (dd, CHC**H**H, *J*=15.2, 4.9 Hz), 2.35 (dd, CHCH**H**, *J*=15.2, 8.7 Hz), 1.77 (m, NHCHC**H**), 1.42 (s, 9H, C(C**H$_3$**)$_3$), 0.91 (m, 6H, CH(C**H$_3$**)$_2$).

TFA·(*S*)-*β*^{3}hAla methyl ester (4.35)

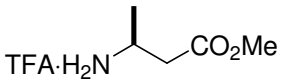

Boc-*β*^{3}hAla methyl ester (**4.33a**) (0.21 g, 0.96 mmol) was deprotected in trifluoroacetic acid (2.5 mL) and dichloromethane (2.5 mL) according to general method F. The free amine was obtained as a light yellow oil (0.22 g, quant).

Spectral properties agreed with those in the literature.[19]

^{1}H NMR (CD_3OD) δ: 3.73 (s, 3H, OC**H$_3$**), 3.65 (m, 1H, NHC**H**), 2.74-2.58 (m, 2H, CHC**H$_2$**), 1.35 (d, 3H, CHC**H$_3$**, *J*=6.7 Hz).

Boc-(*R*)-β^3hVal-(*S*)-β^3hAla methyl ester (4.36)

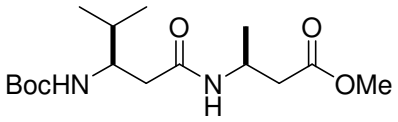

Boc-β^3hVal-OH (**4.34**) (2.36 g, 10 mmol) and TFA·β^3hAla methyl ester (**4.35**) (2.21 g, 10 mmol) were coupled in DMF (70 mL) using HATU (4.11 g, 11 mmol) and diisopropylethylamine (7.5 mL, 43 mmol) according to general method A. The crude mixture was purified by column chromatography (silica; 1:1 ethyl acetate, petroleum ether) to give the product as a white solid (2.74 g, 83%).

Spectral and physical properties are in agreement with those in the literature.[18]

mp = 125-127 ºC (lit.[18] 133-134 ºC)
^{1}H NMR (CD_3OD) δ: 6.40 (d, 1H, N**H**CHCH_3, *J*=6.3 Hz), 5.07 (d, 1H, N**H**CHCH, *J*=9.2 Hz), 4.34 (m, 1H, NHC**H**CH_3), 3.68 (s, 3H, OC**H$_3$**), 3.65 (NHC**H**CH), 2.55-2.26 (m, 4H, 2 x C**H$_2$**CO), 1.78 (m, 1H, NHCHC**H**), 1.42 (s, 9H, C(C**H$_3$**)$_3$), 1.20 (d, 1H, CHC**H$_3$**, *J*=6.8 Hz), 0.90 (d, 1H, CHC(C**H$_3$**)$_2$, *J*=6.7 Hz).

Boc-(*R*)-β^3hVal-(*S*)β^3hAla-OH (4.37)

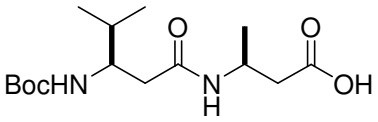

Boc-β^3hVal-β^3hAla methyl ester (**4.36**) (2.74 g, 8.3 mmol) was dissolved in tetrahydrofuran (50 mL) and hydrolysed with LiOH (0.2 M, 83 mL) according to general method E. The product was obtained as a white solid (1.97 g, 75%) that required no further purification.

mp = 161 ºC

^{1}H NMR (CD_3OD) δ: 4.22 (m, 1H, NHC**H**CH_3), 3.73 (m, 1H, NHC**H**CH), 2.56 (dd, 1H, *J*=5.8 Hz, *J*=15.6 Hz, CHC**H$_2$**), 2.36 (m, 2H, CHC**H$_2$**), 2.20 (dd, 2H, CHC**H$_2$**, *J*=9.1 Hz, *J*=14.1 Hz,), 1.73 (m, 1H, C**H**$(CH_3)_2$), 1.43 (s, 9H, CH(C**H$_3$**)$_3$), 1.19 (d, 3H, NHCHC**H$_3$**, *J*=6.7 Hz,), 0.91 (m, 6H, CH(C**H$_3$**)$_2$).

^{13}C NMR (CD_3OD) δ: 174.7, 173.2, 158.0, 80.0, 55.0, 43.7, 41.5, 40.2, 33.7, 28.8, 20.2, 19.7, 18.4.

HRMS calcd for $C_{15}H_{29}N_2O_5$ (MH^+) 317.2076; found 317.2084.

TFA-(*S*)-*β*^{3}hLeu methyl ester (4.38)

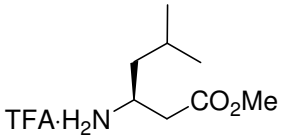

Boc-*β*^{3}hLeu methyl ester (**4.33c**) (0.21 g, 0.81 mmol) was deprotected in trifluoroacetic acid (2.5 mL) and dichloromethane (2.5 mL) according to general method F. The free amine was obtained as a light yellow oil (0.22 g, quant.).

Spectral properties agreed with those in the literature.[20]

^{1}H NMR (CD_3OD) δ: 3.74 (m, 1H, NHC**H**), 3.61 (s, 3H, OC**H$_3$**), 2.79 (dd, 1H, *J*=4.4 Hz, *J*=17.4 Hz, C**H**HCO), 2.61 (dd, 1H, *J*=7.9 Hz, *J*=17.4 Hz, CH**H**CO), 1.71 (m, 1H, C**H**$(CH_3)_2$), 1.51 (m, 2H, C**H$_2$**CH$(CH_3)_2$), 0.97 (m, 6H, CH(C**H$_3$**)$_2$).

Boc-(*R*)-β^3hVal-(*S*)-β^3hAla-(*S*)-β^3hLeu methyl ester (4.39)

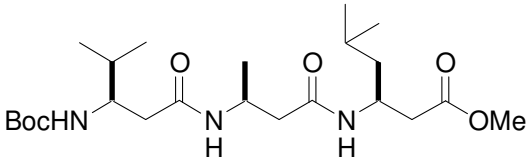

Boc-β^3hVal-β^3hAla-OH (**4.39**) (0.18 g, 0.57 mmol) and TFA·β^3hLeu methyl ester (0.22 g, 0.81 mmol) were coupled in dimethylformamide (10 mL) with HATU (0.28 g, 0.74 mmol) and diisopropylethylamine (0.52 mL, 2.3 mmol) according to general method A. The crude mixture was purified by column chromatrography (silica; 0:1→3:17 methanol, ethyl acetate) to give the product as a white solid (0.24 g, 93%).

Physical and spectral properties are in agreement with those in the literature.[18]

mp = 180-181 ºC (lit.[18] 178-179 ºC)
^{1}H NMR ($CDCl_3$) δ: 6.88 (d, 1H, N**H**, *J*=7.3 Hz), 6.43 (d, 1H, N**H**, *J*=8.6 Hz), 5.11 (d, 1H, N**H**, *J*=9.5 Hz), 4.33 (m, 1H, NHC**H**CH_2), 4.20 (m, 1H, NHC**H**CH_3), 3.72-3.66 (m, 4H, OC**H$_3$**, NHC**H**CH), 2.56-2.24 (m, 6H, 3 x C**H$_2$**CO), 1.77 (m, 1H, CHC**H**$(CH_3)_2$), 1.58 (m, 1H, NHCHCH_2C**H**), 1.51-1.38 (m, 10H, C(C**H$_3$**)$_3$, NHCHC**H**H) 1.30 (m, 1H, NHCHCH**H**), 1.20 (d, 3H, CHC**H$_3$**, *J*=6.7 Hz, 1 H), 0.90 (d, 12H, 2 x CH(C**H$_3$**)$_2$).

6.5.4 Synthesis of the β-Hexapeptide (2.17)

Boc-(*R*)-β^3hVal-(*S*)-β^3hAla-(*S*)-β^3hLeu-OH (4.40)

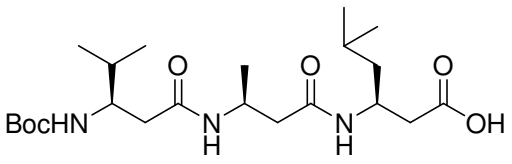

Boc-β^3hVal-β^3hAla-β^3hLeu methyl ester (**4.39**) (0.40 g, 0.87 mmol) in tetrahydrofuran (30 mL) was hydrolysed with LiOH (0.2 M, 8.7 mL) according to general method E. The product was obtained as a white solid (0.39 g, quant.) that required no further purification.

Spectral and physical properties are in agreement with those in the literature.[18]

mp = 188-189 ºC (lit.[18] 190-191 ºC)

^{1}H NMR (CD_3OD) δ: 4.30 (m, 1H, NHC**H**), 4.16 (m, 1H, NHC**H**), 3.75 (m, 1H, NHC**H**CH), 2.47-2.36 (m, 4H, CHC**H$_2$**CO), 2.22-2.16 (m, 2H, CHC**H$_2$**CO), 1.73 (m, 1H, NHCHC**H**), 1.62 (m, 1H, $CHCH_2C$**H**$(CH_3)_2$), 1.47 (m, 1H, CHC**H**HCH$(CH_3)_2$), 1.42 (s, 9H, C(C**H$_3$**)$_3$), 1.31 (m, 1H, CHCH**H**CH$(CH_3)_2$), 1.16 (d, 3H, CHCHC**H$_3$**, *J*=6.7 Hz), 0.93-0.89 (m, 12H, CH(C**H$_3$**)$_2$).

TFA·(*R*)-β^3hVal-(*S*)-β^3hAla-(*S*)-β^3hLeu methyl ester (4.10)

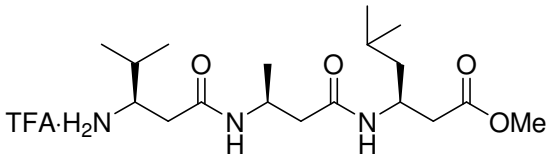

Boc-β^3hVal-β^3hAla-β^3hLeu methyl ester (**4.33c**) (100 mg, 0.22 mmol) was deprotected in trifluoroacetic acid (2.5 mL) and dichloromethane (2.5 mL) according to general method F. The free amine was obtained as a light yellow oil (103 mg, quant.).

^{1}H NMR (CD_3OD, 300 MHz) δ: 4.27 (m, 2H, NHC**H**CH_3, NHC**H**CH_2CH), 3.64 (s, 3H, OC**H$_3$**), 3.32 (m, 1H, NHC**H**CH), 2.65-2.28 (m, 6H, 6 x C**H$_2$**CO), 1.95 (m, 1H, NHCHC**H**), 1.63 (m, 1H, $NHCHCH_2C$**H**), 1.46 (m, 1H, NHCHC**H**HCH), 1.27 (m, 1H, NHCHC**H**HCH), 1.16 (m, 3H, CHC**H$_3$**), 1.03 (m, 6H, CHCH(C**H$_3$**)$_2$), 0.91 (m, 6H, CH_2CH(C**H$_3$**)$_2$.

Boc-(*R*)-β^3hVal-(*S*)-β^3hAla-(*S*)-β^3hLeu-(*R*)-β^3hVal-(*S*)-β^3hAla-(*S*)-β^3hLeu methyl ester (4.41)

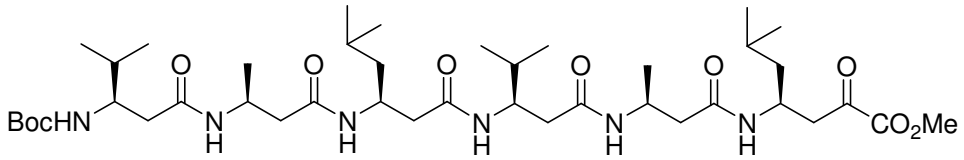

Boc-β^3hVal-β^3hAla-β^3hLeu-OH (**4.39**) (78 mg, 0.18 mmol) and TFA·β^3hVal-β^3hAla-β^3hLeu methyl ester (**4.10**) (83 mg, 0.18 mmol) were coupled in dimethylformamide (10 mL) using HATU (67 mg, 0.18 mmol) and diisopropylethylamine (122 μL, 0.70 mmol), according to modified general method A. The product was obtained as a pale yellow solid that required no further purification (132 mg, 93%).

Physical and spectral properties are in agreement with those in the literature. [18]

mp = 241-243 ºC (lit.[18] 240 ºC)

^{1}H NMR (TFE-d_3) δ: 7.18-7.07 (m, 5H, N**H**) 6.95 (d, 1H, N**H**, *J*=9.1 Hz), 4.37 (m, 1H, NHC**H**CH_2CH), 4.30 (m, 1H, NHC**H**CH_2CH), 4.22 (m, 2H, 2 x NHC**H**CH_3), 4.07 (m, 1H, NHC**H**$CH(CH_3)_2$), 3.69 (m, 1H, BocNHC**H**) 3.68 (s, 3H, OMe), 2.56-2.23 (m, 12H, C**H$_2$**CO), 1.82-1.72 (m, 2H, 2 x CHC**H**$(CH_3)_2$), 1.59 (m, 2H, 2 x NHCHCH_2C**H**), 1.52-1.43 (m, 11H, C(C**H$_3$**)$_3$, 2 x CHC**H**HCH$(CH_3)_2$), 1.31 (m, 2H, 2 x CHCH**H**CH$(CH_3)_2$), 1.18 (t, 6H, NHCHC**H$_3$**, *J*=5.4 Hz), 0.91 (m, 24H, CH(C**H$_3$**)$_2$).

TFA-(*R*)-β^3hVal-(*S*)-β^3hAla-(*S*)-β^3hLeu-(*R*)-β^3hVal-(*S*)-β^3hAla-(*S*)-β^3hLeu methyl ester (2.17)

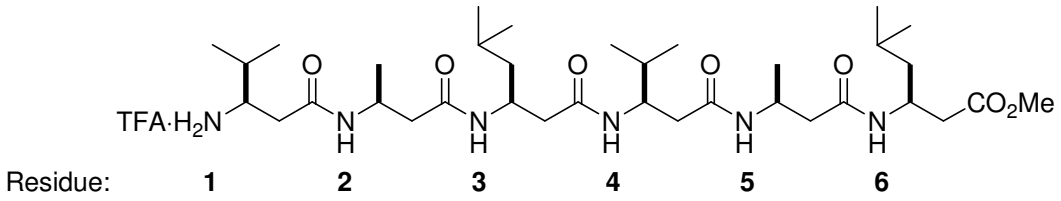

Boc-(β^3hVal-β^3hAla-β^3hLeu)$_2$ methyl ester (**4.41**) (21 mg, 27 μmol) was dissolved in trifluoroacetic acid (2 mL) and stirred for 2 h at rt. The solvent was removed *in vacuo* and the residue resuspended in dichloromethane twice and concentrated *in vacuo*. The residue was redissolved in methanol and concentrated *in vacuo*. The product was obtained as a light brown solid (21 mg, quant.) that required no further purification.

Spectral and physical properties are in agreement with those in the literature.[18]

mp= 214-216 ºC (lit.[18] 220-222 ºC)

Where necessary, the chemical shift data is appended with the residue number indicated in the chemical structure above.

^{1}H NMR (CD_3OD) δ: 8.74 (d, 1H, N**H**, *J*=4.8 Hz), 8.43 (d, 1H, N**H**, *J*=7.7 Hz), 8.39 (d, 1H, N**H**, *J*=9.3 Hz), 8.26 (d, 1H, N**H**, *J*=8.9 Hz), 7.80 (d, 1H, N**H**, *J*=7.0 Hz), 7.48 (d, 1H, N**H**, *J*=9.4 Hz), 4.54 (m, 1H, *2*-NHC**H**CH_3), 4.45 (m, 2H, *5*-NHC**H**CH_3, *6*-NHC**H**CH_2), 4.38 (m, 1H, *3*-NHC**H**CH_2), 4.22 (m, 1H, *4*-NHC**H**CH), 3.70 (s, 3H, OC**H$_3$**), 3.52 (m, *1*-NH_2C**H**CH), 2.76 (dd, 1H, *1*-NH_2CHC**H**H, *J*=15.4, 11.5 Hz), 2.69 (m, 1H, *2*-NHCHC**H**H), 2.64 (m, 1H, *6*-NHCHC**H**HCO), 2.59 (m, 1H, *1*-NHCHCH**H**), 2.52 (m, 1H, *6*-NHCHC**H**HCO), 2.50 (m, 2H, *3*-NHCHC**H**HCO, *4*-NHCHC**H**H), 2.47 (m, 1H, *2*-NHCHCH**H**), 2.45 (m, 1H, *5*-NHCHC**H**H), 2.39 (m, 1H, *3*-NHCHCH**H**CO), 2.33 (dd, 1H, *5*-NHCHCHH, *J*=15.1, 10.8 Hz), 2.22 (dd, 1H, *4*-NHCHCH**H**, *J*=14.7, 11.8 Hz), 2.07 (m, 1H, *1*-NH_2CHC**H**), 1.70 (m, 1H, *4*-NHCHC**H**), 1.56 (m, 2H, *3*,*6*-NHCHCH_2C**H**), 1.42 (m, 2H, *3*,*6*-NHCHC**H**H), 1.24 (m, 2H, *3*,*6*-NHCHC**H**H), 1.20 (d, 3H, *2*-NHCHC**H$_3$**, *J*=6.6 Hz), 1.14 (d, 3H, *5*-NHCHC**H$_3$**, *J*=6.7 Hz), 1.08 (d, 6H, *1*-CHCH(C**H$_3$**)$_2$, *J*=6.9 Hz), 0.92 (m, 12H, *4*-CHCH(C**H$_3$**)$_2$), 0.88 (m, 12H, *3*,*6*-CH_2CH(C**H$_3$**)$_2$).

6.5.5 Synthesis of Functionalised Tripeptides

TFA·β^3hVal-β^3hAla-β^3hLeu-OH (4.23)

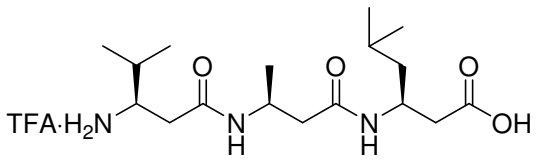

Boc-β^3hVal-β^3hAla-β^3hLeu-OH (**4.39**) (0.48 g, 1.1 mmol) was deprotected in trifluoroacetic acid (10 mL) and dichloromethane (10 mL) according to general method F. The free amine was obtained as a light yellow oil (0.50 g, quant).

Spectral properties are in agreement with those in the literature.[21]

^{1}H NMR (CD_3OD) δ: 4.28 (m, 2H, $NH_2C\mathbf{H}CH_2$, $NHC\mathbf{H}CH_3$), 3.35 (m, 1H, $NHC\mathbf{H}CH$), 2.60 (m, 1H, $NH_2CHC\mathbf{H}H$), 2.48-2.32 (m, 5H, $NH_2CHCH\mathbf{H}$, $CH_3CHC\mathbf{H_2}CO$, $CH_2CHC\mathbf{H_2}CO$), 1.94 (m, 1H, $NH_2CHC\mathbf{H}$), 1.63 (m, 1H, $CH_2C\mathbf{H}(CH_3)_2$), 1.46 (m, 1H, $NHCHC\mathbf{H}H$), 1.31 (m, 1H, $NHCHCH\mathbf{H}$), 1.17 (d, 3H, $NHCHCHC\mathbf{H_3}$) J=5.1 Hz), 1.01 (m, 6H, $CHCH(C\mathbf{H_3})_2$), 0.91 (m, 6H, $CH_2CH(C\mathbf{H_3})_2$).

1-[16-(Acetylthio)hexadecanoyl]-β^3hVal-β^3hAla-β^3hLeu-OH (4.12)

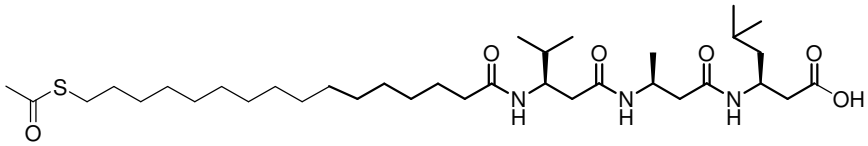

TFA·β^3hVal-β^3hAla-β^3hLeu-OH (**4.23**) (0.48 g, 1.1 mmol) and *N*-hydroxysuccinimate-activated 16-(acetylthio)hexadecanoic acid (**4.22**) (0.56 g, 1.3 mmol) were coupled in a mixture of tetrahydrofuran (30 mL), water (20 mL) and triethylamine (0.30 mL, 4.2 mmol) according to general method B. The crude mixture was purified by column chromatography (silica; 1:9 ethyl acetate, methanol) to give the product as a white solid (0.26 g, 45%).

mp = 184-186 ºC

^{1}H NMR ($CDCl_3$/TFE-d_3 10:1; 300 MHz) δ: 7.03 (d, 1H, N**H**, J=7.9 Hz), 6.64 (d, 1H, N**H**, J=9.3 Hz), 6.41 (d, 1H, N**H**, J=9.7 Hz), 4.29 (m, 1H, $NHC\mathbf{H}CH_2$), 4.09 (m, 1H, $NHC\mathbf{H}CH_3$),

3.95 (m, 1H, NHC**H**CH), 2.84 (t, 2H, SC**H$_2$**, *J*=7.3 Hz), 2.57-2.09 (m, 8H, 4 x C**H$_2$**CO), 2.30 (s, 3H, C**H$_3$**CO), 1.73 (m, 1H, C**H**(CH$_3$)$_2$), 1.60-1.17 (m, 29H, (C**H$_2$**)$_{13}$, NHCHC**H$_2$**C**H**), 1.09 (d, 3H, CHC**H$_3$**, *J*=6.4 Hz), 0.89-0.85 (m, 12H, 2 x CH(C**H$_3$**)$_2$).

^{13}C NMR (CDCl$_3$/TFE-d_3 10:1; 300 MHz) δ: 198.1, 174.9, 174.5, 171.0, 171.3, 52.0, 44.9, 43.4, 43.2, 42.0, 38.8, 36.6, 32.0, 30.5, 29.6-29.5 (m, 8 CH$_2$), 29.4, 29.4, 29.3, 29.2, 29.1, 28.7, 25.9, 24.8, 22.6, 21.7, 19.3, 18.9, 17.9.

HRMS calcd for $C_{35}H_{66}N_3O_6S$ (MH^+) 656.4672; found 656.4702.

5-[1,2]Dithiolan-(3*S*/*R*)-3-yl-pentanoyl-*β*^{3}hVal-*β*^{3}hAla-*β*^{3}hLeu-OH (4.42)

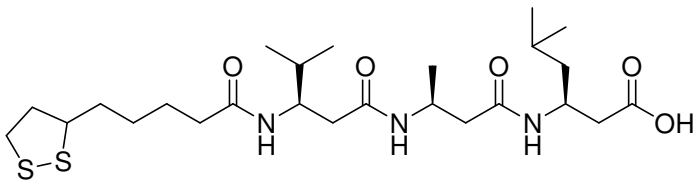

TFA·*β*^{3}hVal-*β*^{3}hAla-*β*^{3}hLeu-OH (**4.23**) (140 mg, 0.31 mmol) and *N*-hydroxysuccinimide-activated lipoic acid (**4.20**) (112 mg, 0.37 mmol) were coupled in a mixture of tetrahydrofuran (30 mL), water (20 mL) and triethylamine (205 μL, 1.5 mmol) according to general method B. The product was obtained as a white solid (122 mg, 75%) that required no further purification.

^{1}H NMR (CD$_3$OD/CDCl$_3$ 2:1) δ: 7.76 (d, 1H, N**H**, *J*=9.4 Hz), 7.64 (d, 1H, N**H**, *J*=8.0 Hz), 7.55 (d, 1H, N**H**, *J*=9.0 Hz), 4.27 (m, 1H, NHC**H**CH$_2$), 4.12 (m, 1H, NHC**H**CH$_3$), 4.03 (m, 1H, NHC**H**CH), 3.54 (m, 1H, SC**H**), 3.18-3.06 (m, 2H, SCH$_2$C**H$_2$**), 2.48-2.36 (m, 5H, SCH$_2$C**H**H, CH$_2$CHC**H$_2$**CO, CHCHC**H**HCO, CH$_3$CHC**H**HCO), 2.24-2.16 (m, 4H, CH$_2$C**H$_2$**CO, CHCHCH**H**CO, CH$_3$CHCH**H**CO), 1.89 (m, 1H, SCH$_2$CH**H**), 1.80-1.57 (m, 6H, NHCHC**H**, NHCH$_2$C**H**, CHC**H$_2$**CH$_2$C**H$_2$**), 1.44 (m, 3H, CHCH$_2$C**H$_2$**CH$_2$, C**H**HCH(CH$_3$)$_2$), 1.30 (m, 1H, CH**H**CH(CH$_3$)$_2$), 1.13 (d, 3H, CHC**H$_3$**, *J*=6.7 Hz), 0.91-0.89 (m, 12H, 2 x C(C**H$_3$**)$_2$).

^{13}C NMR (CD$_3$OD/CDCl$_3$ 2:1) δ: 174.5, 174.2, 172.4, 172.0, 57.2, 52.9, 45.5, 44.1, 43.1, 41.0, 40.6, 39.5, 39.1, 36.9, 36.8, 35.4, 35.4, 32.9, 29.7, 29.6, 26.5, 26.0, 25.7, 23.5, 22.2, 19.9, 19.6, 18.6.

HRMS calcd for $C_{25}H_{46}N_3O_5S_2$ (MH^+) 532.2879; found 532.2870

2-Ferrocenyl-acetamide-β^3hVal- β^3hVal- β^3hVal methyl ester (4.43)

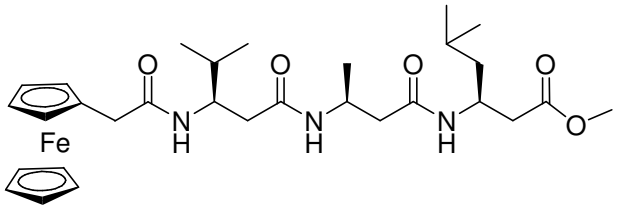

HCl·β^3hVal-β^3hAla-β^3hLeu methyl ester (**4.10**) (86 mg, 0.22 mmol) and ferroceneacetic acid (**3.5**) (80 mg, 0.33 mmol) were coupled in dimethylformamide (30 mL) using HATU (125 mg, 0.33 mmol) and diisopropylethylamine (150 μL, 0.88 mmol), according to general method A. The crude reaction mixture was purified using column chromatography (silica; 0:1→4:96 methanol, ethyl acetate) to give the product as a yellow/brown solid (191 mg, 71%).

mp = 200-208 ºC (dec)

^{1}H NMR (CD_3OD) δ: 7.90 (d, 1H, N**H**, *J*=8.7 Hz), 7.74 (d, 1H, N**H**, *J*=7.7 Hz), 7.50 (d, 1H, N**H**, *J*=9.2 Hz), 4.30 (m, 1H, NHC**H**CH_2), 4.23-4.10 (m, 9H, Fc), 4.11 (m, 1H, NHC**H**CH_3), 4.03 (m, 1H, NHC**H**CH), 3.64 (s, 3H OC**H$_3$**), 3.25 (d, 2H, FcC**H$_2$**), 2.44-2.36 ((m, 4H NHCH(CH$(CH_3)_2$)C**H**H, NHCH(C**H**CH_3)C**H**H, NHCH(C**H**CH_2)C**H$_2$**) 2.22 (dd, 1H, NHCH(CH$(CH_3)_2$)C**H**H, *J*=14.3, 9.2 Hz), 2.14 (dd, 1H, NHCH(C**H**CH_3)C**H**H, *J*=13.7, 7.4 Hz), 1.75 (m, 1H, NHCHC**H**), 1.61 (m, 1H, NHCHCH_2C**H**), 1.46 (m, 1H, NHCHC**H**H), 1.27 (m, 1H, NHCHCH**H**), 1.08 (d, 3H, CHC**H$_3$**, *J*=6.6 Hz), 0.92 (m, 12H, 2 x CH(C**H$_3$**)$_2$).

^{13}C NMR (CD_3OD) δ: 172.9, 172.7, 172.0, 171.8, 69.6, 69.4, 69.4, 68.8, 68.7, 52.7, 52.1, 45.3, 44.0, 43.9, 43.1, 40.4, 39.1, 38.3, 32.5, 25.5, 23.4, 22.1, 19.7, 19.5, 18.5.

HRMS calcd for $C_{30}H_{46}N_3O_5Fe$ (MH^+) 584.2787; found 584.2777.

2-Ferrocenylacetamide-β^3hVal- β^3hVal- β^3hVal-OH (4.44)

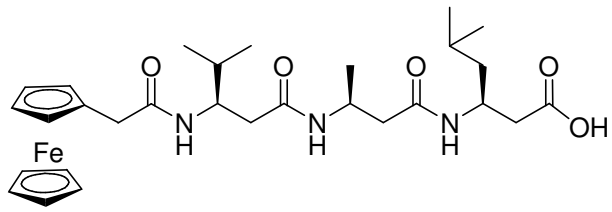

$FcCH_2CONH$-β^3hVal-β^3hAla-β^3hLeu methyl ester (**4.43**) (101 mg, 0.17 mmol) in tetrahydrofuran (30 mL), was hydrolysed with LiOH (0.2 M aqueous, 1.73 mL) according to general method E. The dark brown solid mixture was purified by column chromatography (silica; 1:19 methanol, dichloromethane) to give the product as a pale yellow solid (99 mg, 89%).

mp = 160 ºC (dec)

^{1}H (CD_3OD) δ: 7.90 (d, 1H, N**H**, *J*=8.8 Hz), 7.77 (d, 1H, N**H**, *J*=7.9 Hz), 7.53 (d, 1H, N**H**, *J*=9.3 Hz), 4.32 (m, 1H, NHC**H**CH_2CH), 4.12 (m, 1H, NHC**H**CH_3), 4.25-4.12 (m, 9H, Fc), 4.04 (m, 1H, NHC**H**CH), 3.27 (d, 2H, FcC**H$_2$**, *J*=8.3 Hz), 2.44-2.36 (m, 4H NHCH($CH(CH_3)_2$)C**H**H, NHCH($CHCH_3$)C**H**H, NHCH($CHCH_2$)C**H$_2$**), 2.24 (dd, 1H, NHCH($CH(CH_3)_2$)C**H**H, *J*=14.3, 9.2 Hz), 2.18 (dd, 1H, NHCH($CHCH_3$)C**H**H, *J*=13.7, 7.4 Hz), 1.77 (m, 1H, NHCHC**H**), 1.64 (m, 1H, NHCHCH_2C**H**), 1.49 (m, 1H, NHCHC**H**H), 1.33 (m, 1H, NHCHCH**H**), 1.10 (d, 3H, CHC**H$_3$**, *J*=6.6 Hz), 0.95-0.93 (m, 6H, $CH_2CH(CH_3)_2$), 0.89-0.86 (m, 6H, $CHCH(CH_3)_2$).

^{13}C (CD_3OD) δ: 174.8, 173.6, 172.7, 172.6, 70.1, 70.0, 69.8, 69.0, 53.4, 45.9, 44.6, 43.6, 41.0, 39.7, 38.6, 33.3, 26.1, 23.7, 22.2, 20.1, 19.7, 18.5.

HRMS calcd for $C_{29}H_{44}N_3O_5Fe$ (MH^+) 570.2630; found 570.2634.

Boc-(*R*)-β^3hVal-(*S*)-β^3hAla-(*S*)-β^3hLeu-*N*-ferrocenyl methanamide (4.45)

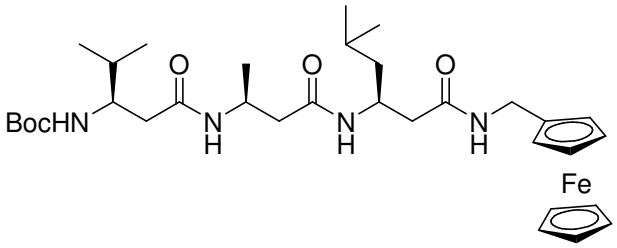

Boc-β^3hVal-β^3hAla-β^3hLeu-OH (**4.40**) (0.33 g, 0.75 mmol) and ferrocene methylamine (**4.27**) (0.24 g, 1.1 mmol) were coupled in dimethylformamide (30 mL) with HATU (0.29 g, 0.76 mmol) and diisopropylethylamine (0.53 mL, 3.0 mmol), according to general method A. The product, upon sitting, precipitated from the ethyl acetate and was filtered to obtain a yellow solid (0.24 g, 49%).

mp = 210 ºC (dec)

^{1}H NMR (TFE-d_3) δ: 7.19 (t, 1H, N**H**CH_2, *J*=4.6 Hz), 7.04 (d, 1H, N**H**, *J*=8.6 Hz,), 6.99 (d, 1H, N**H,** *J*=8.2 Hz), 5.41 (d, 1H, N**H**CHCH**,** *J*=9.6 Hz,), 4.35-4.19 (m, 11H, Fc, Fc**CH_2**), 4.12 (m, 1H, NHC**H**CH_2), 4.06 (m, 1H, NHCHC**H_3**), 3.67 (m, 1H, NHC**H**CH), 2.44-2.31 (m, 4H, $CH(CH_2CH(CH_3)_2)C$**H_2**, $CH(CH(CH_3)_2)CH$**H**, $CH(CH_3)CH$**H**), 2.25-2.19 (m, 2H, $CH(CH(CH_3)_2)C$**H**H, $CH(CH_3)C$**H**H), 1.73 (m, 1H, CHC**H**$(CH_3)_2$), 1.54 (m, 1H, $NHCHCH_2C$**H**), 1.44 (m, 1H, NHCHC**H**H), 1.42 (s, 9H, $C(C$**H_3**$)_3$), 1.28 (m, 1H, NHCHCH**H**), 1.15 (d, 3H, CHC**H_3** *J*=6.4 Hz,), 0.92-0.86 (m, 12H, 2 x $CH(C$**H_3**$)_2$).

^{13}C NMR (TFE-d_3) δ: 174.8, 174.3, 174.0, 159.4, 82.5, 72.3-71.6 (br, Fc), 55.6, 47.6, 45.5, 44.9, 44.3, 43.5, 41.1, 40.9, 34.4, 29.0, 26.5, 23.5, 22.2, 20.4, 19.7, 18.3.

HRMS calcd for $C_{33}H_{53}FeN_4O_5$ (MH^+) 640.3287; found 640.3315.

Boc-(*R*)-β^3hVal-(*S*)-β^3hAla-(*S*)-β^3hLeu-*N*-ethanamide (4.46)

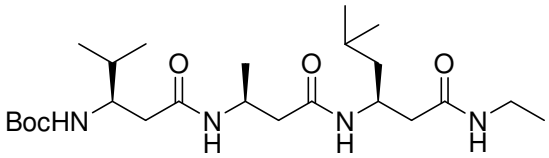

Boc-β^3hVal-β^3hAla-β^3hLeu-OH (**4.40**) (76 mg, 0.17 mmol) and ethylamine hydrochloride (30 mg, 0.37 mmol) were coupled in dimethylformamide (5 mL) with HATU (65 mg, 0.17 mmol) and diisopropylethylamine (120 μL, 0.69 mmol) according to general method A. The crude residue was suspended in ethyl acetate (5 mL), sonicated, and filtered to give the product as a white solid (60 mg, 74%).

mp = 208-210 ºC

^{1}H NMR (TFE-d_3/CD_3OD 1:1) δ: 4.22 (m, 1H, NHC**H**CH_2CH), 4.10 (m, 1H, NHC**H**CH_3), 3.70 (m, 1H, NHC**H**CH), 3.13 (q, 2H, NHC**H$_2$**CH_3, *J*=7.2 Hz), 2.40-2.21 (m, 4H, NHCH($CH(CH_3)_2$C**H**H, NHCH(CH_3)C**H**H, NHCH($CHCH_2(CH_3)_2$C**H$_2$**), 2.17-2.11 (m, 2H, NHCH($CH(CH_3)_2$CH**H**, NHCH(CH_3)CH**H**), 1.68 (m, 1H, NHCHC**H**), 1.55 (m, 1H, $NHCHCH_2$C**H**), 1.39 (m, 1H, NHCHC**H**H), 1.36 (s, 9H, C(C**H$_3$**)$_3$), 1.23 (m, 1H, NHCHCH**H**), 1.11 (d, 3H, NHCHC**H$_3$**, *J*=6.7 Hz), 1.06 (t, 3H, $NHCH_2$C**H$_3$**, *J*=7.3 Hz), 0.85 (m, 12H, 2 x $CH(CH_3)_2$).

^{13}C NMR (TFE-d_3: CD_3OD 1:1) δ: 173.5, 173.3, 172.8, 158.2, 80.3, 55.9, 55.0, 46.7, 44.8, 44.6, 44.1, 43.1, 40.3, 35.3, 33.9, 28.8, 28.7, 26.0, 23.6, 22.0, 20.0, 19.5, 18.3, 14.6.

HRMS calcd for $C_{24}H_{47}N_4O_5$ (MH^+) 471.3546; found 471.3534.

Boc-(*R*)-β^3hVal-(*S*)-β^3hAla-(*S*)-β^3hLeu-dec-9-enyl ester (4.47)

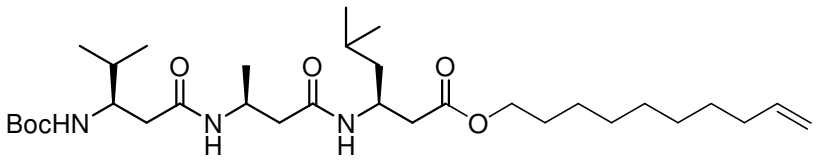

Boc-β^3hVal-β^3hAla-β^3hLeu-OH (**4.40**) (0.39 g, 0.87 mmol) and 9-decen-1-ol were dissolved in dimethylformamide (30 mL) and the reaction mixture was cooled on an ice-bath. EDCI (0.34 g, 0.18 mmol) and DMAP (0.22 g, 0.18 mmol) were added, and the mixture was stirred for 16 h.

The reaction mixture was diluted with ethyl acetate and washed with saturated aqueous $NaHCO_3$, NH_4Cl and NaCl. The organic layer was dried ($MgSO_4$) and the solvent removed *in vacuo*. The crude mixture was purified by column chromatography (silica; 1:9 methanol, ethyl acetate), to give the product as a light brown glassy solid (0.25 g, 49%).

^{1}H NMR ($CDCl_3$) δ: 7.00 (m, 1H, N**H**), 6.58 (m, 1H, N**H**), 5.76 (m, 1H, CH_2=C**H**), 5.22 (m, 1H, N**H**), 4.91 (m, 2H, C**H$_2$**=CH), 4.27 (m, 1H, NHC**H**CH_2), 4.17 (m, 1H, NHC**H**CH_3), 4.01 (m, 2H, OC**H$_2$**), 3.65 (m, 1H, NHC**H**CH), 2.45-2.23 (m, 6H, 3 x C**H$_2$**CO), 1.98 (m, 2H, C**H$_2$**CH=CH_2), 1.74 (m, 1H, NHCHC**H**), 1.56 (m, 3H, OCH_2C**H$_2$**, $CHCH_2$C**H**$(CH_3)_2$)) , 1.47-1.21 (m, 21H, $(OCH_2)_2$(C**H$_2$**)$_5$, C(C**H$_3$**)$_3$, NHCHC**H$_2$**), 1.15 (m, 3H, CHC**H**$_3$), 0.91-0.82 (d, 12H, 2 x CH(C**H**$_3$)$_2$).

^{13}C NMR ($CDCl_3$) δ: 171.5, 170.7, 170.4, 155.9, 138.8, 114.0, 78.5, 64.5, 53.4, 44.3, 42.8, 42.6, 39.6, 39.2, 33.5, 32.3, 29.1, 29.0, 28.8, 28.6, 28.4, 28.3, 28.1, 25.7, 24.8, 22.9, 21.7, 19.5, 19.2, 18.2.

HRMS calc for $C_{32}H_{60}N_3O_6$ (MH^+) 582.4482; found 582.4464.

Boc-(*R*)-*β*^{3}hVal-(*S*)-*β*^{3}hAla-(*S*)-*β*^{3}Val-*N*-(5-[1,2]dithiolan-(3*S*/*R*)-3-yl-pentamide) (4.48)

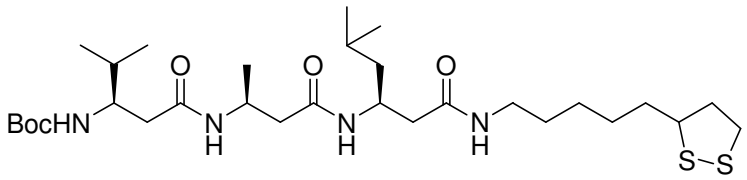

Boc-*β*^{3}hVal-*β*^{3}hAla-*β*^{3}hLeu-OH (**4.40**) (78 mg, 0.18 mmol) and lipoamine (**4.8**) (33 mg, 0.18 mmol) were coupled in dimethylformamide (10 mL) using HATU (66 mg, 0.18 mmol) and diisopropylethylamine (121 μL, 0.70 mmol) according to general method A. The product was precipitated from ethyl acetate (2 mL), sonicated, and filtered, to give a pale yellow solid (91 mg, 84%).

mp = 203-206 ºC

^{1}H NMR (TFE-d_3) δ: 7.07 (m, 3H, 3 x N**H**), 5.41 (d, 1H, N**H**, *J*=10.4 Hz), 4.28 (m, 1H, NHC**H**CH_2), 4.19 (m, 1H, NHC**H**CH_3), 3.70 (m, 1H, NHC**H**CH), 3.60 (m, 1H, SC**H**), 3.18 (m, 2H, SC**H$_2$**), 2.48-2.21 (m, 7H, SCH_2C**H**H, 3 x C**H$_2$**CO), 1.93 (m, 1H, SCH_2CH**H**), 1.76-1.27 (m,

14H, C**H**$_2$C**H**$_2$C**H**$_2$C**H**$_2$C**H**$_2$, NHCHC**H**, NHCHC**H**$_2$C**H**), 1.42 (s, 9H, C(C**H**$_3$)$_3$), 1.18 (d, 3H, CHC**H**$_3$, *J*=6.4 Hz), 0.92-0.89 (m, 12H, 2 x CH(C**H**$_3$)$_2$).

^{13}C NMR (TFE-d$_3$) δ: 174.8, 174.7, 174.2, 159.3, 82.5, 58.6, 55.6, 47.6, 45.6, 44.9, 44.5, 43.6, 42.0, 41.4, 41.2, 39.5, 36.3, 34.4, 30.5, 30.4, 29.1, 28.1, 26.5, 23.7, 22.3, 20.4, 19.8, 18.4.

HRMS calcd for $C_{30}H_{57}N_4O_5S_2$ (MH^+) 617.3770; found 617.3790.

5-[1,2]Dithiolan-(3*S*/*R*)-3-yl-pentanoyl-(*R*)-*β*^{3}hVal-(*S*)-*β*^{3}hAla-(*S*)-*β*^{3}hLeu-*N*-ferrocenylmethanamide (2.11)

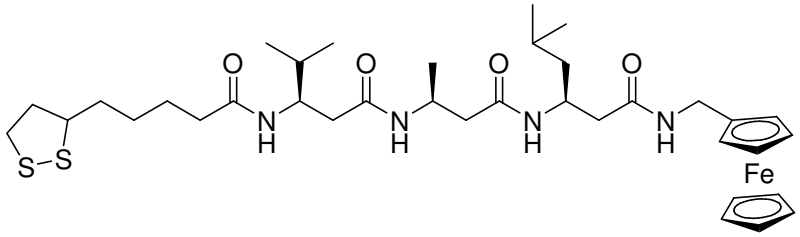

N-hydroxysuccinimide-activated lipoic acid (**4.20**) (26 mg, 86 μmol) and HCl·(*R*)-*β*^{3}hVal-(*S*)-*β*^{3}hAla-(*S*)-*β*^{3}hLeu-*N*-ferrocenyl methanamide (preparation described on page 230) (45 mg, 78 μmol) were dissolved in dimethylformamide (5 mL) followed by the addition of triethylamine (43 μL, 0.31 mmol). The reaction mixture was stirred under N_2 for 16 h, then evaporated in vacuo to remove the solvents. The crude mixture was dried under high-vacuum for 30 min, and sonicated in methanol (10 mL) for 30 min. The suspension was filtered, to give the product as a yellow solid (51 mg, 89%).

mp = 261 ºC (dec)

^{1}H NMR (TFE-*d*$_3$) δ: 7.16 (t, 1H, N**H**CH$_2$, *J*=5.3, 5.3 Hz), 7.07 (d, 1H, N**H**CHCH$_3$, *J*=8.3 Hz), 7.00 (d, 1H, N**H**CHCH$_2$CH(CH$_3$)$_2$, *J*=9.0 Hz), 6.83, (d, `H, N**H**CHCH(CH$_3$)$_2$, *J*=9.5 Hz), 4.25 (m, 1H, C**H**CH$_2$CH(CH$_3$)$_2$), 4.22-4.10 (m, 11H, **Fc**-C**H**$_2$), 4.14 (m, 1H, C**H**CH$_3$), 4.05 (m, 1H, C**H**CH(CH$_3$)$_2$) 3.58 (m, 1H, SC**H**), 3.18-3.06 (m, 2H, SC**H**$_2$), 2.48-2.19 (m, 9H, 3 x C**H**$_2$CO, SCHC**H**H, (CH$_2$)$_3$C**H**$_2$CO), 1.93 (m, 1H, SCHCH**H**), 1.80-1.40 (m, 9H, SCHC**H**$_2$C**H**$_2$C**H**$_2$, CHC**H**(CH$_3$)$_2$, CH**H**C**H**(CH$_3$)$_2$), 1.28 (m, 1H, C**H**HCH(CH$_3$)$_2$), 1.13 (d, 3H, CHC**H**$_3$, *J*=6.6 Hz), 0.93-0.86 (m, 12H, 2 x CH(C**H**$_3$)$_2$).

^{13}C NMR (TFE-*d*$_3$) δ: 177.5, 174.4, 174.2, 174.0, 71.2, 70.4, 58.4, 54.2, 47.5, 45.4, 44.9, 44.0, 43.4, 41.9, 41.0, 40.4, 39.5, 37.9, 35.9, 33.8, 30.4, 27.3, 26.5, 23.5, 22.3, 20.4, 19.8, 18.8.

HRMS calc for $C_{36}H_{57}N_4O_4S_2Fe$ (MH^+) 729.3171; found 726.3161.

5-[1,2]Dithiolan-(3*S*/*R*)-3-yl-pentanoyl-(*R*)-β^3hVal-(*S*)-β^3hAla-(*S*)-β^3hLeu-N-ethanamide (4.53)

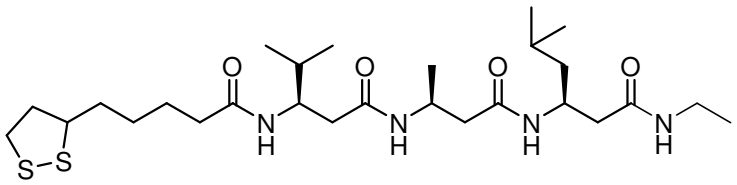

Lipoamide-(*R*)-β^3hVal-(*S*)-β^3hAla-(*S*)-β^3hLeu-OH (**4.42**) (50 mg, 94 μmol) and ethylamine hydrochloride (10 mg, 0.12 mmol) were coupled in dimethylformamide (10 mL) using HATU (36 mg, 95 μmol) and diisopropylethylamine (65 μL, 0.38 mmol). The reaction mixture was stirred for 16 h, at which time the solvent was removed *in vacuo*. The residue was sonicated in ethanol (5 mL) and filtered to give the pure product as an off-white solid (36 mg, 68%).

^{1}H NMR (CD_3OD/TFE-d_3 2:1) δ: 4.25 (m, 1H, C**H**$CH_2CH(CH_3)_2$), 4.13 (m, 1H, C**H**CH_3), 4.07 (m, 1H, C**H**$CH(CH_3)_2$), 3.53 (m, 1H, SC**H**), 3.17-3.06 (m, 4H, SC**H$_2$**, C**H$_2$**CH_3), 2.46-2.17 (m, 9H, 3 x NHCHC**H$_2$**, SCHC**H**H, $(CH_2)_3$C**H$_2$**CO), 1.86 (m, 1H, SCHCH**H**), 1.78-1.44 (m, 9H, SCHC**H$_2$**C**H$_2$**C**H$_2$**, CHC**H**$(CH_3)_2$, CH**H**C**H**$(CH_3)_2$), 1.28 (m, 1H, C**H**HCH$(CH_3)_2$), 1.26 (m, 1H, C**H**HCH$(CH_3)_2$), 1.13-1.07 (m, 6H, CHC**H$_3$**, CH_2C**H$_3$**), 0.91-0.87 (m, 12H, 2 x CH(C**H$_3$**)$_2$).
^{13}C NMR (CD_3OD/TFE-d_3 2:1) δ: 176.9, 174.2, 174.1, 173.7, 58.4, 54.4, 47.6, 45.6, 45.4, 44.4, 43.9, 42.2, 40.8, 40.1, 38.0, 36.5, 36.3, 34.3, 30.8, 27.7, 26.9, 24.3, 22.9, 20.9, 20.3, 19.3, 15.4.
HRMS calc for $C_{27}H_{51}N_4O_4S_2$ (MH^+) 559.3352; found 559.3332.

6.5.6 Synthesis of Functionalised Hexapeptides

5-[1,2]Dithiolan-(3*S*/*R*)-3-ylpentanoyl-(*R*)-β^3hVal-(*S*)-β^3hAla-(*S*)-β^3hLeu-(*R*)-β^3hVal-(*S*)-β^3hAla-(*S*)-β^3hLeu-1-ferrocenylmethanamide (SSβ_6Fc, 2.13)

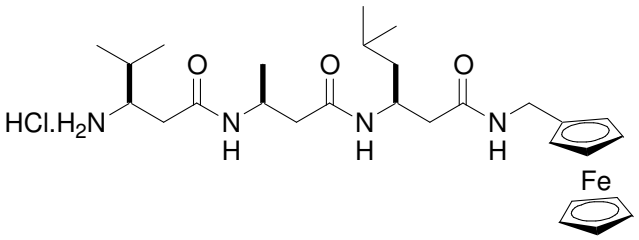

Boc-β^3hVal-β^3hAla-β^3hLeu-NHCH$_2$Fc (**4.49**) (92 mg, 0.14 mmol) was dissolved in trifluoroethanol (5 mL), followed by the addition of HCl (4 M in dioxane, 1 mL) was added. The reaction mixture was stirred for 5 min at rt, then the solvent was removed *in vacuo*. The product (HCl·β^3hVal-β^3hAla-β^3hLeu-NHCH$_2$Fc) was obtained as a glassy yellow solid and used without purification.

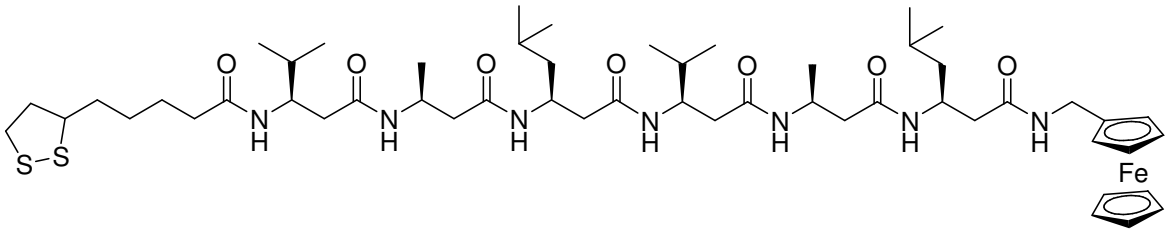

Crude HCl·β^3hVal-β^3hAla-β^3hLeu-NHCH$_2$Fc (see above) (83 mg, 0.14 mmol) and lipoamide-β^3hVal-β^3hAla-β^3hLeu-OH (**4.42**) (76 mg, 0.14 mmol) were coupled in dimethylformamide (5 mL) using HATU (54 mg, 0.14 mmol) and diisopropylethylamine (105 µL, 0.57 mmol) according to modified general method A. Chromatography (lipophilic sephadex; 1:0→1:9→1:1→0:1 methanol, trifluoroethanol) gave the product as a glassy yellow solid (107 mg, 71%).

^{1}H NMR (TFE-d_3) δ: 7.30- 7.01 (m, 6H, N**H**), 6.91 (d, 1H, N**H**, *J*=8.3 Hz), 4.06-4.38 (m, 17H, 6 x NHC**H**, **Fc**C**H$_2$**), 3.59 (m, 1H, SC**H**), 3.18 (m, 1H, SC**H**H), 3.12 (m, 1H, SCH**H**), 2.52-2.21 (m, 15H, 7 x C**H$_2$**CO, SCH$_2$C**H**H), 1.93 (m, 1H, SCH$_2$C**H**H), 1.82-1.52 (m, 8H, 2 x

NHCHC**H**$(CH_3)_2$, 2 x NHCHCH$_2$C**H,** C**H$_2$**CH$_2$C**H$_2$**CH$_2$CO), 1.45 (m, 4H, SCHCH$_2$C**H$_2$**$(CH_2)_2$, 2 x CHC**H**HCH$(CH_3)_2$), 1.29 (m, 2H, 2 x CHCH**H**CH$(CH_3)_2$), 1.15 (m, 6H, 2 x CHC**H$_3$**), 0.98-0.81 (m, 24H, 4 x CH(C**H$_3$**)$_2$).

^{13}C NMR (TFE-d_3) δ: 177.7, 174.5, 174.3, 174.1, 174.0, 173.9, 58.5, 54.4, 47.5, 47.4, 45.4, 44.0, 43.2, 42.0, 39.6, 38.0, 36.1, 34.0, 30.5, 30.5, 27.5, 26.7, 26.6, 23.7, 23.6, 22.7, 22.5, 20.7, 20.6, 19.8, 19.1, 19.0.

HRMS calcd for $C_{53}H_{88}N_7O_7S_2Fe$ (MH^+) 1054.5536; found 1054.5511.

2-Ferrocenylacetamide-(*R*)-β^3hVal-(*S*)-β^3hAla-(*S*)-β^3hLeu-(*R*)-β^3hVal-(*S*)-β^3hAla-(*S*)-β^3hLeu-*N*-(5-[1,2]dithiolan-(3*S*/*R*)-3-yl-pentamide) (Fcβ_6SS, 2.14)

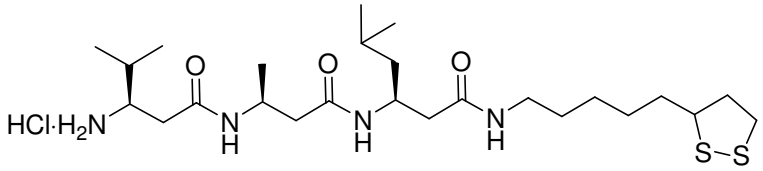

Boc-β^3hVal-β^3hAla-β^3hLeu-lipoamide (**4.48**) (53 mg, 86 μmol) was dissolved in trifluoroethanol (5 mL), followed by HCl (4 M in dioxane, 3 mL). The reaction mixture was stirred for 30 min at rt, and then the solvent was removed *in vacuo*. The product (HCl·β^3hVal-β^3hAla-β^3Leu-lipoamide) was obtained as a glassy off-white solid and was used without further purification.

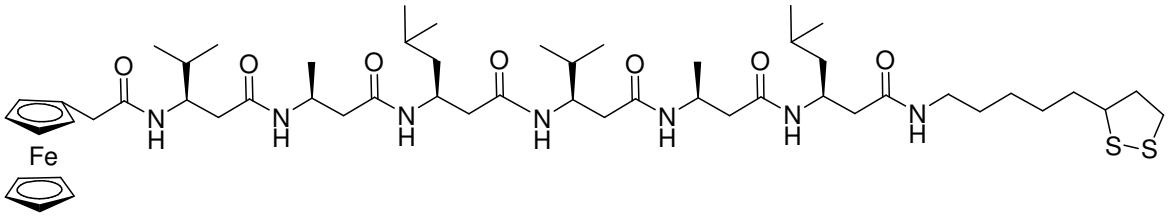

HCl·β^3hVal-β^3hAla-β^3Val-lipoamide (see above) (43 mg, 86 μmol) and FcCH$_2$CO-β^3hVal-β^3hVal-β^3hVal-OH (**4.44**) (49 mg, 86 μmol) were coupled using HATU (33 mg, 86 μmol) and diisopropylethylamine (60 μL, 0.34 mmol) according to modified general method A. The crude residue was purified by column chromatography (lipophilic sephadex; 1:0→1:9→1:1→0:1 methanol, trifluoroethanol) to give the product as a glassy yellow solid (59 mg, 64%).

^{1}H NMR (TFE-d_3) δ: 7.26 (t, 1H, N**H**CH$_2$, *J*=9.1 Hz), 7.12-7.04 (m, 3H, N**H**), 6.91 (d, 1H, N**H**, *J*=8.6 Hz,), 4.40-4.16 (m, 13H, 2 x NHC**H**CH$_2$, 2 x NHC**H**CH$_3$, **Fc**CH$_2$), 4.10-3.96 (m, 2H, 2 x

NHC**H**CH), 3.60 (m, 1H, SC**H**), 3.28-3.10 (m, 4H, SC**H$_2$**, FcC**H$_2$**), 2.60-2.28 (m, 13H, 6 x C**H$_2$**CO, SCH$_2$C**H**H), 1.93 (m, 1H, SCH$_2$CH**H**), 1.82-1.27 (m, 18H, (C**H$_2$**)$_5$, 2 x NHCHC**H**, 2 x NHCHC**H$_2$**C**H**), 1.19 (d, 3H, CHC**H$_3$**, *J*=5.5 Hz), 1.14 (d, 3H, CHC**H$_3$**, *J*=6.3 Hz), 0.99-0.79 (m, 24H, 4 x CH(C**H$_3$**)$_2$).

^{13}C NMR (TFE-d$_3$) δ: 174.8, 174.7, 174.1, 174.0, 173.9, 173.8, 58.6, 57.3, 54.3, 54.0, 47.5, 47.3, 45.3, 45.2, 44.0, 43.3, 42.0, 41.4, 40.2, 39.5, 36.2, 33.8, 33.7, 30.5, 30.4, 28.1, 26.6, 26.5, 23.8, 23.7, 22.6, 22.4, 20.6, 20.5, 19.7, 19.4, 19.0, 18.4.

HRMS calcd for $C_{54}H_{90}N_7O_7S_2$ (MH^+) 1068.5693; found 1068.5747.

5-[1,2]Dithiolan-(3*S*/*R*)-3-yl-pentanoyl-(*R*)-*β*^{3}hVal-(*S*)-*β*^{3}hAla-(*S*)-*β*^{3}hLeu-(*R*)-*β*^{3}hVal-(*S*)-*β*^{3}hAla-(*S*)-*β*^{3}hLeu-ethanamide (SS*β*$_6$Et, 2.15)

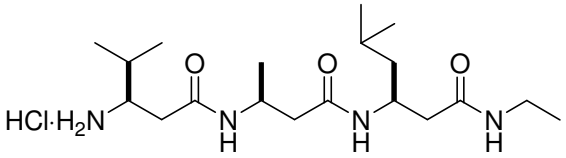

Boc-*β*^{3}hVal-*β*^{3}hAla-*β*^{3}hLeu-NHEt (**4.50**) (49 mg, 0.10 mmol) was deprotected in trifluoroacetic acid (2.5 mL) and dichloromethane (2.5 mL) according to general method F. The product (HCl·*β*^{3}hVal-*β*^{3}hAla-*β*^{3}hLeu-NHEt) was obtained as a light yellow oil (50 mg, quant).

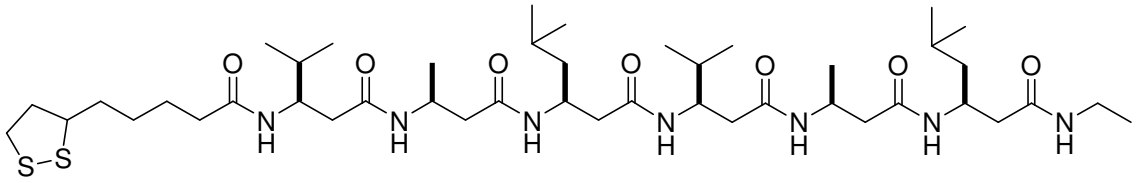

Crude HCl·*β*3hVal-*β*3hAla-*β*3hLeu-NHEt (see above) (34 mg, 70 μmol) and lipoamide-*β*3hVal-*β*3hAla-*β*3hLeu-OH (**4.42**) (37 mg, 70 μmol) were coupled in dimethylformamide (5 mL) using HATU (27 mg, 70 μmol) and diisopropylethylamine (48 μL, 0.28 mmol) according to modified general method A. The product was obtained as an off-white solid (25 mg, 41%). No further purification was required.

mp = 292ºC (dec)

^{1}H NMR (TFE-d_3) δ: 7.24-6.93 (m, 7H, 7 x N**H**), 4.31-4.22 (m, 4H, 4 x NHC**H**), 4.08 (m, 2H, 2 x NHC**H**), 3.59-3.56 (m, 1H, SC**H**), 3.24-3.08 (m, 4H, C**H$_2$**S, NHC**H$_2$**), 2.47-2.30 (m, 15H, 6 x NHCHC**H$_2$**CO, $(CH_2)_3$C**H$_2$**CO, SCH_2C**H**H), 1.94-1.90 (m, 1H, SCH_2CH**H**), 1.81-1.53 (m, 8H, 2 x NHCHC**H**$(CH_3)_2$, 2 x NHCHCH_2C**H,** C**H$_2$**CH_2C**H$_2$**CH_2**CO**), 1.46 (m, 4H, SCHC**H$_2$**C$H_2(CH_2)_2$, 2 x CHC**H**HCH$(CH_3)_2$), 1.31 (m, 2H, 2 x CHCH**H**CH$(CH_3)_2$), 1.17-1.10 (m, 9H, 2 x CHC**H$_3$**, CH_2C**H$_3$**), 0.91- 0.90 (m, 24H, CH(C**H$_3$**)$_2$).

^{13}C NMR (TFE-d_3) δ:178.9, 176.0, 175.6, 175.4, 175.1, 175.0, 175.0, 59.6, 55.5, 48.7, 48.6, 46.5, 46.4, 45.1, 44.6, 44.4, 43.2, 41.4, 40.7, 39.2, 37.6, 37.2, 35.2, 35.1, 31.7, 31.6, 28.7, 27.8, 27.7, 24.9, 24.8, 23.8, 23.6, 21.9, 21.7, 21.0, 20.9, 20.2, 20.2, 15.9.

HRMS calcd for $C_{44}H_{82}N_7O_7S_2$ (MH^+) 884.5717; found 884.5753.

5-[1,2]Dithiolan-(3*S*/*R*)-3-ylpentanoyl-(*R*)-*β*^{3}hVal-(*S*)-*β*^{3}hAla-(*S*)-*β*^{3}hLeu-(*R*)-*β*^{3}hVal-(*S*)-*β*^{3}hAla-(*S*)-*β*^{3}hLeu-dec-9-enyl ester (4.54)

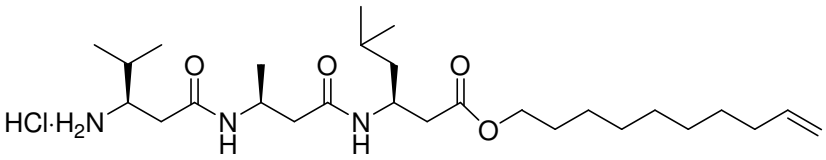

Boc-*β*^{3}hVal-*β*^{3}hAla-*β*^{3}hLeu-decenyl (**4.51**) (73 mg, 0.13 mmol) was dissolved in 5 mL of dichloromethane at rt. HCl (4 M in dioxane, 1 mL) was added and the reaction mixture was stirred for 1.5 h. The solvent was removed *in vacuo* to give the product (HCl·*β*^{3}hVal-*β*^{3}hAla-*β*^{3}hLeu-decenyl) as a clear oil (65 mg, quant.), which was used without further purification.

^{1}H NMR (CD_3OD) δ: 5.80 (tdd, 1H, C**H**=CH_2, *J*=17.0, 10.2, 6.7, 6.7 Hz), 4.99-4.90 (m, 2H, CH=C**H$_2$**), 4.28 (m, 2H, NHC**H**, NHC**H**CH_2), 4.06 (m, 2H, OC**H$_2$**), 3.35 (m, 1H, NHC**H**CH), 2.63-2.30 (m, 6H, 3 x C**H$_2$**CO), 2.04 (q, 2H, C**H$_2$**CH=CH_2, *J*=6.9 Hz), 1.97 (m, 1H, NH_2CHC**H**), 1.62 (m, 3H, NHCHCH_2C**H**, OCH_2C**H$_2$**), 1.48 (m, 1H, NHCHC**H**H), 1.40-1.27 (m, 11H, $(OCH_2)_2$(C**H$_2$**)$_5$, NHCHCH**H**), 1.18 (d, 3H, CHC**H$_3$**, *J*=6.8 Hz), 1.04-1.01 (m, 6H, CH(C**H**$_3)_2$), 0.92 (m, 6H, CH(C**H**$_3)_2$).

^{13}C NMR (CD_3OD) δ: 172.9, 172.7, 171.5, 140.0, 114.8, 65.8, 55.8, 46.1, 44.5, 43.3, 41.2, 35.3, 34.9, 31.7, 30.5, 30.3, 30.1, 30.1, 29.7, 27.1, 26.0, 23.7, 22.2, 20.4, 18.8, 18.3.

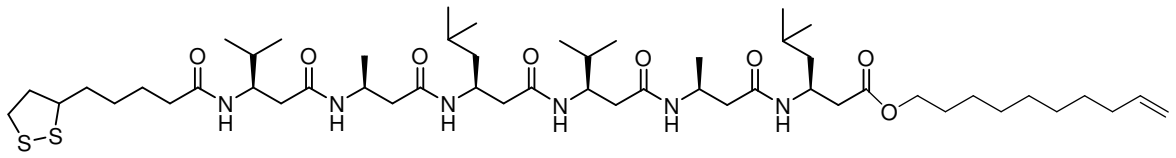

Crude HCl·β^3hVal-β^3hAla-β^3hLeu-decenyl (see above) (65 mg, 0.13 mmol) and SS-β^3hVal-β^3hAla-β^3hLeu-OH (**4.42**) (73 mg, 0.14 mmol) were coupled in dimethylformamide (10 mL) using HATU (53 mg, 0.14 mmol) and diisopropylethylamine (90 μL, 0.56 mmol) according to modified general method A. The crude mixture was purified by column chromatography (lipophilic sephadex; 1:0→1:9→1:1→0:1 methanol, trifluoroethanol) to give the product as an off-white solid (83 mg, 66%).

^{1}H NMR (TFE-d_3) δ: 7.31 (d, 1H, N**H**, *J*=6.9 Hz), 7.25 (d, 1H, N**H**, *J*=8.4 Hz), 7.03 (d, 1H, N**H**, *J*=8.8 Hz), 7.15 (m, 1H, N**H**), 6.90 (m, 1H, N**H**), 6.84 (d, 1H, N**H**, *J*=8.4 Hz), 5.84 (m, 1H, C**H**=CH_2), 5.01-4.91 (m, 2H, CH=C**H$_2$**), 4.41-4.05 (m, 8H, 6 x NHC**H**, OC**H$_2$**), 3.58 (m, 1H, SC**H**), 3.20-3.08 (m, 2H, SC**H$_2$**), 2.55-2.23 (m, 15H, 7 x C**H$_2$**CO, SCH_2C**H**H), 2.05 (m, 2H, C**H$_2$**CH=CH_2), 1.93 (m, 1H, SCH_2C**H**H), 1.82-1.54 (m, 10H, 2 x NHCHC**H**, 2 x NHCHCH_2C**H**, CHC**H$_2$**CH_2C**H$_2$**, OCH_2**CH$_2$**), 1.51-1.26 (m, 16H, $CHCH_2$C**H$_2$**CH_2, 2 x NHCHC**H$_2$**CH, $O(CH_2)_2$(C**H$_2$**)$_5$), 1.17 (m, 6H, CHC**H$_3$**), 0.92 (m, 24H, CH(C**H$_3$**)$_2$).

^{13}C NMR (TFE-d_3) δ: 177.7, 175.4, 174.4, 174.0, 173.9, 173.8, 173.5, 141.3, 115.1, 67.5, 58.4, 54.2, 47.4, 46.8, 45.5, 45.3, 45.1, 43.9, 43.0, 42.0, 41.9, 41.3, 40.1, 39.5, 38.0, 36.0, 35.4, 35.3, 34.0, 30.8, 30.6, 30.5, 30.0, 27.3, 26.6, 23.6, 23.5, 22.7, 22.6, 20.7, 20.5, 19.7, 19.1, 19.0.

HRMS calcd for $C_{52}H_{95}N_6O_8S_2$ (MH^+) 995.6653; found 995.6610.

5-[1,2]Dithiolan-(3*S*/*R*)-3-yl-pentanoyl-(*R*)-β^3hVal-(*S*)-β^3hAla-(*S*)-β^3hLeu-(*R*)-β^3hVal-(*S*)-β^3hAla-(*S*)-β^3hLeu methyl ester (4.55)

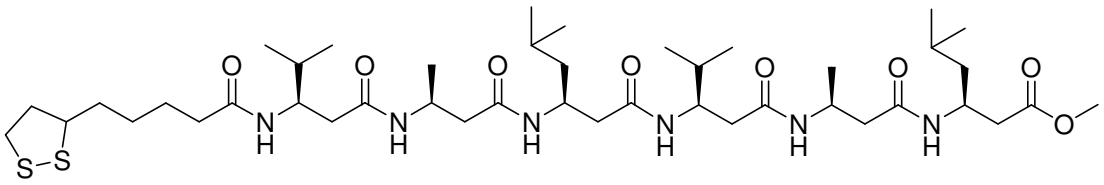

Lipoamide-(*R*)-β^3hVal-(*S*)-β^3hAla-(*S*)-β^3hLeu-OH (**4.42**) (100 mg, 0.19 mmol) and TFA·(*R*)-β^3hVal-(*S*)-β^3hAla-(*S*)-β^3hLeu methyl ester (**4.10**) (89 mg, 0.19 mmol) were coupled in DMF (20 mL) using HATU (72 mg, 0.19 mmol) and DIPEA (130 µL, 0.75 mmol) according to modified general method A. The product was obtained as an off-white glassy solid (129 mg, 79%).

^{1}H NMR (TFE-d_3) δ: 7.34 (m, 1H, N**H**), 7.29 (d, 1H, N**H**, *J*=7.3 Hz), 7.17 (m, 1H, N**H**), 7.04 (d, 1H, N**H**, *J*=9.1 Hz), 6.90 (m, 1H, N**H**), 6.86 (d, 1H, N**H**, *J*=9.0 Hz), 4.35-4.10 (m, 6H, 6 x N**H**), 3.67 (s, 3H, OC**H$_3$**), 3.57 (m, 1H, SC**H**), 3.20-3.07 (m, 2H, C**H$_2$**S), 2.56-2.22 (m, 15H, 6 x CHC**H$_2$**CO, $(CH_2)_3$C**H$_2$**CO, SCH_2C**H**H), 1.92 (m, 1H, SCH_2C**H**H), 1.80-1.56 (m, 8H, 2 x NHCHC**H**$(CH_3)_2$, 2 x $NHCHCH_2$C**H**, C**H$_2$**CH_2C**H$_2$**CH_2CO), 1.46 (m, 4H, $SCHCH_2$C**H$_2$**$(CH_2)_2$, 2 x CHC**H**HCH(CH3)2), 1.36-129 (m, 2H, 2 x CHCH**H**CH$(CH_3)_2$), 1.15 (m, 6H, CHC**H$_3$**), 0.91 (m, 24H, CH(C**H$_3$**)$_2$).

^{13}C NMR (TFE-d_3) δ: 177.7, 175.7, 174.4, 174.0, 173.9, 173.8, 173.4, 58.4, 58.4, 57.3, 54.2, 53.3, 48.9, 47.3, 46.7, 45.5, 45.2, 45.1, 44.9, 43.9, 43.8, 43.0, 41.9, 41.9, 41.0, 40.1, 39.5, 38.0, 36.0, 34.1, 34.0, 30.5, 30.4, 27.4, 26.6, 26.5, 23.6, 23.5, 22.7, 22.6, 20.7, 20.4, 19.7, 19.6, 19.1, 19.0.

HRMS calcd for $C_{43}H_{79}N_6O_8S_2$ (MH^+) 871.5401; found 871.5361.

Boc-(*R*)-β^3hVal-(*S*)-β^3hAla-(*S*)-β^3h-Leu-(*R*)-β^3hVal-(*S*)-β^3hAla-(*S*)-β^3h-Leu-*N*-ferrocenylmethanamide (4.56)

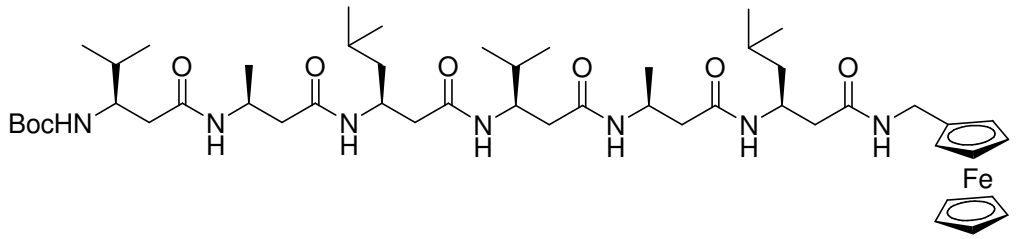

Boc-β^3hVal-β^3hAla-β^3hLeu-OH (**4.40**) (38 mg, 87 μmol) and HCl·β^3hVal-β^3hAla-β^3hLeu-$NHCH_2Fc$ (50 mg, 87 μmol; preparation described on page 230) were coupled in DMF (50 mL) using HATU (33 mg, 87 μmol) and diisopropylethylamine (60 μL, 0.35 mmol) according to modified general method A. The product was obtained as a yellow powder (71 mg, 85%) which did not require further purification.

mp = >250 ºC (dec)

^{1}H NMR (TFE-d_3) δ: 7.17-7.03 (m, 5H, 5 x N**H**), 6.98 (d, 1H, N**H**, *J*=8.7 Hz), 5.46 (d, 1H, N**H**, *J*=9.7 Hz), 4.54-4.12 (m, 15H, C**H$_2$Fc**, 2 x NHC**H**CH$_3$, 2 x NHC**H**CH$_2$), 4.04 (m, 1H, CH$_2$CONHC**H**CH), 3.69 (m, 1H, BocNHC**H**), 2.45-2.21 (m, 12H, 6 x C**H$_2$**CO), 1.80-1.69 (m, 2H, 2 x CHC**H**(CH$_3$)$_2$), 1.56 (m, 2H, 2 x NHCHCH$_2$C**H**), 1.47-1.42 (m, 11H, C(C**H$_3$**)$_3$, 2 x CHC**H**HCH(CH$_3$)$_2$), 1.29 (m, 2H, CHCH**H**CH(CH$_3$)$_2$), 1.18-1.13 (m, 6H, 2 x NHCHC**H$_3$**), 0.91-0.86 (m, 24H, 2 x CH(C**H$_3$**)$_2$).

^{13}C NMR (TFE-d_3) δ: 174.8, 174.2, 174.2, 174.1, 174.0, 173.9, 82.5, 74.4 (10C, Fc), 55.7, 54.4, 47.5, 47.5, 47.5, 47.5, 45.4, 45.4, 45.0, 44.9, 44.3, 44.0, 43.3, 43.3, 43.3, 41.1, 40.2, 40.2, 34.4, 33.6, 29.0, 26.6, 26.5, 23.7, 23.6, 22.4, 22.3, 20.5, 20.5, 19.7, 18.9, 18.4.

HRMS calcd for $C_{50}H_{84}N_7O_8Fe$ (MH^+) 966.5731; found 966.5733.

1-[16-(Acetylthiol)hexadecyl](ferrocenylmethyl)]-β^3hVal-β^3hAla-β^3hLeu-β^3hVal-β^3hAla-β^3hLeu-*N*-ferrocenylmethanamide (4.57)

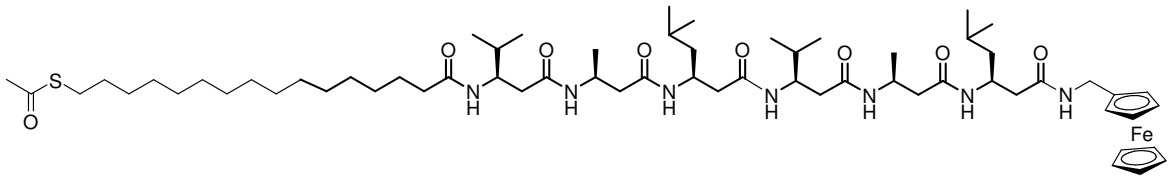

$AcS(CH_2)_{15}CO$-β^3hVal-β^3hAla-β^3hLeu-OH (**4.12**) (172 mg, 0.26 mmol) and HCl·β^3hVal-β^3hAla-β^3hLeu-$NHCH_2Fc$ (168 mg, 0.26 mmol; preparation described on page 230) were coupled in dimethylformamide (50 mL) using HATU (99 mg, 0.26 mmol) and diisopropylethylamine (185 µL, 1.1 mmol) according to modified general method A. Chromatography (lipophilic sephadex; 1:0→1:9→1:1→0:1 methanol, trifluoroethanol) gave the product as a glassy yellow solid (228 mg, 74%).

mp >270 ºC (dec)

^{1}H NMR (TFE-d_3) δ: 7.25 (d, 1H, N**H**, *J*=8.4 Hz), 7.19 (d, 1H, N**H**, *J*=8.1 Hz), 7.09 (d, 1H, N**H**, *J*=8.7 Hz), 7.05 (m, 2H, 2N**H**), 7.00 (d, 1H, N**H**, *J*=8.7 Hz), 6.93 (d, 1H, N**H**, *J*=9.1 Hz), 4.34-4.05 (m, 17H, 6 x NHC**H**, **FcCH_2**), 2.88 (t, 2H, AcSC$\mathbf{H_2}$, *J*=7.3 Hz), 2.50-2.22 (m, 17H, 6 x CHCH_2CO, CH_3COS, CH_2CH_2CO), 1.79 (m, 2H, 2 x CHC**H**$(CH_3)_2$), 1.58 (m, 6H, 2 x CH_2, 2 x NHCHCH_2C**H**), 1.46 (m, 2H, 2 x CHC**H**HCH$(CH_3)_2$), 1.40-1.31 (m, 24H, (C$\mathbf{H_2}$)$_{11}$, 2 x CHCH**H**CH$(CH_3)_2$), 1.16 (m, 6H, 2 x C$\mathbf{H_3}$), 0.94-0.88 (m, 24H, C(CH_3)$_2$).

^{13}C NMR (TFE-d_3) δ: 204.1, 178.3, 174.5, 174.5, 174.3, 174.1, 174.0, 173.9, 75.2-70.9 (10 C, Fc), 54.4, 54.3, 47.7, 47.6, 47.4, 45.5, 45.4, 45.3, 44.9, 44.0, 43.4, 43.2, 40.9, 40.2, 38.4, 34.1, 33.9, 31.2, 31.2, 31.1, 31.0, 30.9, 30.8, 30.6, 30.3, 27.9, 26.7, 26.6, 23.8, 23.7, 22.7, 22.5, 22.4, 20.7, 20.6, 19.8, 19.2, 19.0, 18.9, 18.5.

HRMS calcd for $C_{63}H_{108}N_7O_8S$ (MH^+) 1178.7330; found 1178.7283.

1-[16-(Acetylthio)hexadecanoyl]-(*R*)-β^3hVal-(*S*)-β^3hAla-(*S*)-β^3hLeu-(*R*)-β^3hVal-(*S*)-β^3hAla-(*S*)-β^3hLeu methyl ester (4.58)

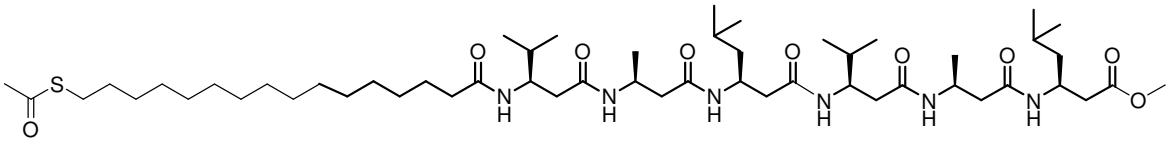

AcS(CH_2)$_{15}$CO-β^3hVal-β^3hAla-β^3hLeu-OH (**4.12**) (93 mg, 0.14 mmol) and TFA·β^3hVal-β^3hAla-β^3hLeu methyl ester (**4.10**) (72 mg, 0.15 mmol) were coupled in DMF (50 mL) using HATU (54 mg, 0.14 mmol) and DIPEA (98 μL, 0.56) according to modified general method A. The crude mixture was purified by column chromatography (lipophilic sephadex; 1:0→1:9→1:1→0:1 methanol, trifluoroethanol) to give the product as a white solid (141 mg, 63%).

mp = 264 ºC (dec)

^{1}H NMR (TFE-d_3) δ: 7.30 (m, 1H, N**H**), 7.22 (m, 1H, N**H**), 7.08 (m, 1H, N**H**), 7.03 (m, 1H, N**H**), 6.92 (d, 1H, N**H**, *J*=7.1 Hz), 6.85 (d, 1H, N**H**, *J*=9.2 Hz), 4.35(m, 2H, 2 x NHC**H**CH_2), 4.24 (m, 2H, 2 x NHC**H**CH_3), 4.08 (m, 2H, 2 x NHC**H**CH), 3.67 (s, 3H, OC**H$_3$**), 2.85 (t, 2H, AcSC**H$_2$**, *J*=7.3 Hz), 2.53-2.21 (m, 17H, 6 x CHC**H$_2$**CO, C**H$_3$**COS, CH_2C**H$_2$**CO), 1.78 (m, 2H, 2 x CHC**H**(CH_3)$_2$), 1.56 (m, 6H, 2 x CH_2, 2 x NHCHCH_2C**H**), 1.45 (m, 2H, 2 x CHC**H**HCH(CH_3)$_2$), 1.39-1.29 (m, 24H, (C**H$_2$**)$_{11}$, 2 x CHCH**H**CH(CH_3)$_2$), 1.16 (m, 6H, 2 x CHC**H$_3$**), 0.92-0.88 (m, 24H, 4 x CH(C**H$_3$**)$_2$).

^{13}C NMR (TFE-d_3) δ: 203.8, 178.2, 175.7, 174.4, 174.1, 173.9, 173.8, 173.5, 54.5, 54.2, 53.3, 47.3, 46.8, 45.4, 45.3, 45.2, 44.9, 43.8, 43.0, 41.1, 40.1, 38.3, 34.0, 33.9, 33.7, 31.1, 31.0, 30.8, 30.5, 30.2, 27.8, 26.5, 23.6, 23.5, 22.7, 22.6, 22.4, 20.6, 20.4, 19.7, 19.0, 18.9, 18.8.

HRMS calcd for $C_{53}H_{99}N_6O_9S$ (MH^+) 995.7194; found 995.7238.

HCl·(*R*)-β^3hVal-(*S*)-β^3hAla-(*S*)-β^3hLeu-(*R*)-β^3hVal-(*S*)-β^3hAla-(*S*)-β^3hLeu-*N*-ferrocenylmethanamide (4.60)

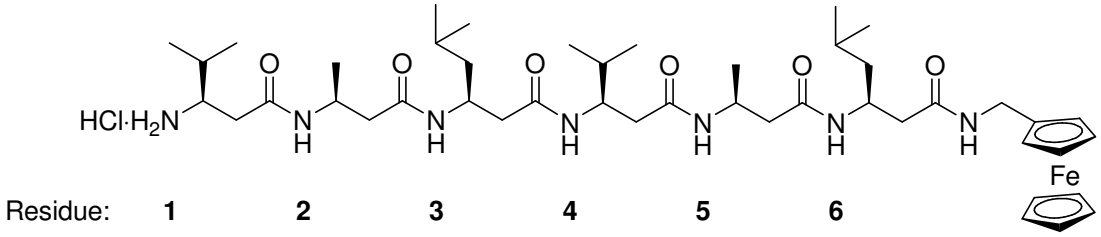

Boc-(β^3hVal-β^3hAla-β^3hLeu)$_2$-NHCH$_2$Fc (**4.56**) (25 mg, 26 μmol) was stirred in 4M HCl/dioxane (0.5 mL) for 10 min at rt. The solvent was removed *in vacuo* and the crude mixture passed through an alumina plug, eluting with methanol. The solvent was removed *in vacuo* and the resulting residue was purified by column chromatography (C_{18}-coated silica; 1:1→0:1 water, methanol) to give the product as a yellow solid (22 mg, 95%).

^{1}H NMR (CD_3OD) δ: 8.41 (d, 1H, *2*-N**H**, *J*=9.5 Hz), 8.32 (d, 1H, *3*-N**H**, *J*=9.1 Hz), 8.27 (d, 1H, N**H**, *J*=9.9 Hz), 8.07 (d, 1H, *4*-N**H**, *J*=9.3 Hz), 7.98 (d, 1H, N**H**CH$_2$Fc, *J*=8.4 Hz), 7.70 (d, 1H, *6*-N**H**, *J*=10.0 Hz), 7.55 (d, 1H, *5*-N**H**, *J*=8.4 Hz) 4.55 (m, 1H, *2*-NHC**H**), 4.46 (m, 1H, *5*-NHC**H**), 4.44 (m, 1H, *6*-NHC**H**), 4.37 (m, 1H, *3*-NHC**H**), 4.26 (m, 2H, C**H$_2$**Fc), 4.20 (m, 1H, *4*-NHC**H**), 3.52 (m, 1H, *1*-NHC**H**), 2.79 (dd, 1H, *1*-C**H**HCO, *J*=15.2, 11.6 Hz), 2.72 (dd, 1H, *2*-C**H**HCO, *J*=14.9, 11.6 Hz), 2.62 (m, 1H, *1*-CH**H**CO), 2.60 (m, 1H, *3*-C**H**HCO), 2.53 (m, 1H, *4*-C**H**HCO), 2.49 (m, 1H, *2*-CH**H**CO), 2.47 (m, 1H, *5*-C**H**HCO), 2.41 (m, 1H, *3*-CH**H**CO), 2.30 (m, 1H, *5*-CH**H**CO), 2.29 (m, 2H, *6*-C**H$_2$**CO), 2.20 (m, 1H, *4*-CH**H**CO), 1.76 (m, 1H, *4*-NHCHC**H**) 1.57 (m, 2H, 2 x NHCHCH$_2$C**H**), 1.42 (m, 1H, *3*-NHCHC**H**H), 1.36 (m, 1H, *6*-NHCHCH**H**), 1.25 (m, 2H, *3*,*6*-NHCHCH**H**), 1.18 (d, 3H, *2*-CHC**H$_3$**, *J*=6.7 Hz), 1.14 (d, 3H, *5*-CHC**H$_3$**, *J*=6.7 Hz), 1.09 (m, 6H, *1*-CH(C**H$_3$**)$_2$), 0.96 (d, 6H, 4-CH(C**H$_3$**)$_2$, *J*=6.5 Hz), 0.89 (m, 12H, *3*,*6*-CH(C**H$_3$**)$_2$).

^{13}C NMR (CD_3OD) δ: 173.2, 172.7, 172.1, 171.9, 171.6, 171.2, 70.4 (10 C, Fc), 56.4, 53.1, 46.5, 46.1, 45.8, 45.4, 43.7, 43.5, 43.3, 43.2, 42.0, 41.8, 39.4, 36.2, 34.5, 32.1, 26.1, 26.0, 26.0, 23.7, 23.4, 23.1, 22.9, 21.2, 20.9, 19.9, 19.8, 19.2, 18.2.

HRMS calcd for $C_{45}H_{76}N_7O_6Fe$ (MH^+) 866.5206; found 866.5200.

$[\alpha]_D$ = -9 (c=0.75, methanol)

6.5.7 Synthesis of *α*-Hexapeptide 2.16

Boc-(*S*)-Val-(*S*)-Ala methyl ester (4.63)

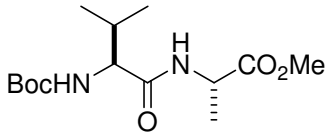

Boc-(*S*)-Val-OH (**4.61**) (1.25 g, 5.8 mmol) and HCl·(*S*)-Ala methyl ester (**4.62**) (0.80 g, 5.8 mmol) were coupled in dimethylformamide (25 mL) using HATU (2.19 g, 5.8 mmol) and diisopropylethylamine (4.01 mL, 23 mmol) according to general method A. The crude product was purified by column chromatography (silica; 1:2 ethyl acetate, petroleum ether) to give the product as a white solid (1.56 g, 82%).

The spectral properties are in agreement with those in the literature.[22] The difference in melting point compared to the literature value may be due to the presence of water in the solid.

mp = 105-107 ºC (lit.[22] 112-116 ºC)
^{1}H NMR (CD_3OD) δ: 6.34 (m, 1H, N**H**), 5.03 (m, 1H, NHC**H**CH_3), 3.91 (m, 1H, NHC**H**CH), 3.75 (s, 3H, OC**H$_3$**), 2.14 (m, 1H, NHCHC**H**), 1.44 (s, 9H, C(C**H$_3$**)$_3$, 1.42 (d, 3H, CHC**H$_3$**, *J*=7.2 Hz, 1 H), 0.97 (d, 3H, CH(C**H$_3$**)CH_3, *J*=6.8 Hz), 0.92 (d, 3H, CH(CH_3)C**H$_3$**, *J*=6.8 Hz).

Boc-(*S*)-Val-(*S*)-Ala-OH (4.64)

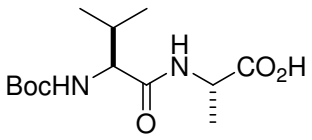

Boc-(*S*)-Val-(*S*)-Ala methyl ester (**4.63**) (1.56 g, 5.2 mmol) was hydrolysed with LiOH (0.2 M, 51.5 mL, 10 mmol) in tetrahydrofuran according to general method E. A white solid was obtained which was used without further purification (1.49 g, quant.).

Physical and spectral properties are in agreement with those in the literature.[23]

mp = (lit.[23] 86 ºC)

^{1}H NMR (CD_3OD) δ: 8.24 (d, 1H, N**H**, *J*=4.9 Hz), 6.55 (d, 1H, N**H**, *J*=8.1 Hz) 4.39 (m, 1H, NHC**H**CH_3), 3.90 (m, 1H, NHC**H**CH), 2.04 (m, 1H, CHC**H**$(CH_3)_2$), 1.44 (s, 9H, C(C**H$_3$**)$_3$), 1.41 (d, 3H, CHC**H$_3$**, *J*=7.0), 0.98 (d, 3H, CH(C**H$_3$**)CH_3, *J*=9.8 Hz), 0.92 (d, 3H, CH(CH_3)C**H$_3$**), *J*=5.9 Hz).

Boc-(*S*)-Val-(*S*)-Ala-(*S*)-Leu methyl ester (4.65)

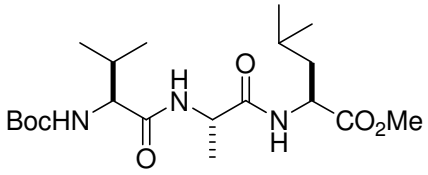

Boc-(*S*)-Val-(*S*)-Ala-OH (**4.64**) (1.33 g, 4.6 mmol) and HCl·(*S*)-Leu methyl ester (0.92 g, 4.9 mmol) were coupled in dimethylformamide (20 mL) using HATU (0.92 g, 4.7 mmol) and diisopropylethylamine (3.22 mL, 19 mmol) according to general method A. The crude mixture was purified by column chromatography (silica; 1:1 ethyl acetate, petroleum ether) to give the product a white solid (1.71 g, 89%).

The physical and spectral properties agreed with those in the literature.[24]

mp = 158-161 ºC (lit.[24] 160 ºC)

^{1}H NMR (CD_3OD) δ: 6.58 (d, 1H, N**H**, *J*=8.3 Hz), 4.46-4.38 (m, 2H, NHC**H**CH_2, NHC**H**CH_3), 3.89 (d, 1H, NHC**H**CH, *J*=6.5 Hz), 3.70 (m, 3H, OC**H$_3$**), 2.03 (m, 1H, NHCHC**H**), 1.70 (m, 1H, NHCHCH_2C**H**), 1.62-1.59 (m, 2H, NHCHC**H$_2$**), 1.44 (s, 9H, C(C**H$_3$**)$_3$), 1.36 (d, 3H, CHC**H$_3$**, *J*=7.1 Hz), 0.95-0.89 (m, 12H, CH(C**H$_3$**)$_3$.

TFA·(*S*)-Val-(*S*)-Ala-(*S*)-Leu-OH (4.66)

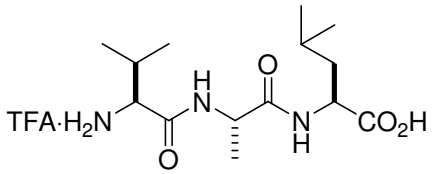

Boc-Val-Ala-Leu-OH (**4.67**) (180 mg, 0.45 mmol) was deprotected in trifluoroacetic acid (2.5 mL) and dichloromethane (2.5 mL) according to general method F. The product was obtained as a light yellow oil (186 mg, quant).

Spectral properties are in agreement with those in the literature.[21]

^{1}H NMR (CD_3OD) δ: 8.53 (d, 1H, N**H**, *J*=6.2 Hz), 8.31 (d, 1H, N**H**, *J*=8.5 Hz), 6.91 (m, 1H, N**H**), 4.45 (m, 2H, NHC**H**CH_2, NHC**H**CH_3), 3.70 (m, 1H, NHC**H**CH), 2.19 (m, 1H, NH_2CHC**H**), 1.78-1.60 (m, 3H, NHCHC**H$_2$**C**H**), 1.39 (d, 1H, NHCHC**H$_3$**, *J*=6.9 Hz), 1.04 (m, 6H, NHCHCH(C**H$_3$**)$_2$), 0.91 (m, 6H, CH_2CH(C**H$_3$**)$_2$).

Boc-(*S*)-Val-(*S*)-Ala-(*S*)-Leu-OH (4.67)

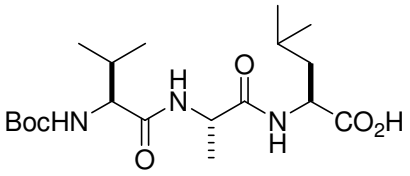

Boc-(*S*)-Val-(*S*)-Ala-(*S*)-Leu methyl ester (**4.65**) (200 mg, 0.48 mmol) was hydrolysed with LiOH (0.2 M, 4.8 mL, 0.96 mmol) in tetrahydrofuran according to general method E. A white solid was obtained, which was used without further purification (187 mg, 97%).

The spectral properties are in agreement with those in the literature.[24]

mp = 91 ºC (no literature melting point)

^{1}H NMR (CD_3OD) δ: 8.20 (d, N**H**, *J*=8.4 Hz), 8.09 (d, N**H**, *J*=7.1 Hz), 6.58 (d, N**H**CHCH, *J*=8.7 Hz), 4.41 (m, 2H, NHC**H**CH_3, NHC**H**CH_2CH), 3.89 (m, 1H, NHC**H**CH), 2.03 (m, 1H, NHCHC**H**), 1.72 (m, 1H, $NHCHCH_2$C**H**) , 1.62 (m, 2H, NHCHC**H$_2$**CH), 1.44 (s, 9H, C(C**H$_3$**)$_3$),

1.36 (d, 3H, CHC**H**$_3$, *J*=7.1 Hz), 0.95 (d, 3H, C(C**H**$_3$)$_2$, *J*=6.6 Hz), 0.91 (d, 3H, C(C**H**$_3$)$_2$, *J*=6.5 Hz).

5-[1,2]Dithiolan-(3*S*/*R*)-3-yl-pentanoyl-(*S*)-Val-(*S*)-Ala-(*S*)-Leu-OH (4.68)

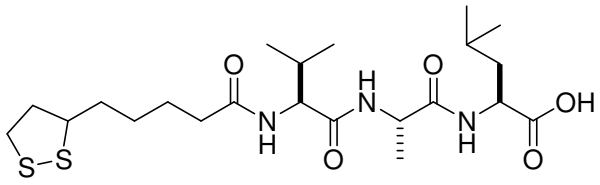

TFA·(*S*)-Val-(*S*)-Ala-(*S*)-Leu-OH (**4.66**) (200 mg, 0.48 mmol) and *N*-hydroxysuccinimide-activated lipoic acid (**4.42**) (218 mg, 0.72 mmol) were coupled in tetrahydrofuran/water (2:1, 50 mL) with triethylamine (134 μL, 0.96 mmol) according to general method B. The product was obtained as a white solid (146 mg, 62%) that required no further purification.

mp = 192 ºC

^{1}H NMR (CD_3OD) δ: 8.20 (m, 2H, N**H**CHCH$_3$, N**H**CHCH$_2$), 7.94 (d, 1H, N**H**CHCH, *J*=8.7 Hz), 4.43 (m, 2H, NHC**H**CH$_3$, NHC**H**CH$_2$), 4.21 (m, 1H, NHC**H**CH), 3.57 (m, 1H, SC**H**), 3.17 (m, 1H, SC**H**H), 3.09 (m, 1H, SCH**H**), 2.46 (m, 1H, SCH$_2$C**H**H), 2.28 (m, 2H, C**H$_2$**CO), 2.05 (qd, 1H, NHCHC**H**, *J*=13.5, 6.8, 6.8, 6.7 Hz), 1.89 (m, 1H, SCH$_2$CH**H**), 1.73 (m, 2H, NHCHCH$_2$C**H**, CHC**H**HCH$_2$CH$_2$), 1.64 (m, 5H, NHCHC**H$_2$**CH, SCHCH**H**CH$_2$C**H$_2$**), 1.46 (m, 2H, SCHCH$_2$C**H$_2$**CH$_2$), 1.35 (d, 3H, CHC**H$_3$**, *J*=7.1 Hz), 0.96-0.90 (m, 12H, 2 x CH(C**H$_3$**)$_2$).

^{13}C NMR (CD_3OD) δ: 176.1, 175.9, 174.7, 173.4, 60.0, 57.6, 52.0, 50.0, 41.7, 41.3, 39.4, (36.7, 36.6)*, (35.8, 35.8), 32.0, (30.0, 29.9), (26.8, 26.7), 25.9, 23.5, 21.9, 19.9, 18.8, 18.2.

HRMS calcd for $C_{22}H_{40}N_3O_5S_2$ (MH^+) 490.2409; found 490.2407.

* Resonances for (SCH**C$_2$**H$_2$**C$_2$**H$_2$**C$_2$**H$_2$) are doubled due to the presence of an epimer. The doubled resonances were assigned using HSQC correlations.

Boc-(*S*)-Val-(*S*)-Ala-(*S*)-Leu-*N*-ferrocenylmethanamide (4.69)

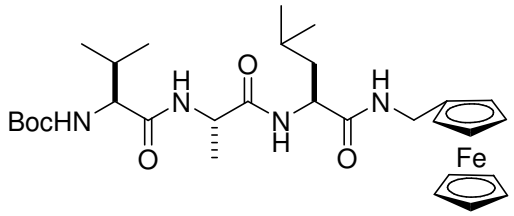

Boc-(*S*)-Val-(*S*)-Ala-(*S*)-Leu-OH (**4.67**) (193 mg, 0.48 mmol) and ferrocene methylamine (**4.27**) (103 mg, 0.48 mmol) were coupled in dimethylformamide (20 mL) using HATU (183 mg, 0.48 mmol) and diisopropylethylamine (335 μL, 1.9 mmol) according to general method A. The crude mixture was dissolved in methanol (5 mL) and the resulting yellow precipitate separated by filtration. The product, obtained as a yellow powder, required no further purification (184 mg, 64%).

mp = 226 ºC (dec)

^{1}H NMR (DMSO-d_6) δ: 8.08 (t, 1H, N**H**CH$_2$Fc, *J*=5.8 Hz), 7.96, (d, N**H**, *J*=8.7 Hz), 7.90 (d, N**H**, *J*=7.0 Hz), 6.75 (d, N**H**CHCH, *J*=8.8 Hz), 4.33 (m, 2H, NHC**H**CH$_3$, NHC**H**CH$_2$CH), 4.16-4.13 (m, 9H, Fc), 3.97 (m, 2H, NHC**H$_2$**Fc), 3.78 (dd, 1H, NHC**H**CH, *J*=8.5, 6.5 Hz), 1.94 (m, 1H, NHCHC**H**), 1.59 (m, 1H, NHCHCH$_2$C**H**), 1.46 (m, 2H, NHCHC**H$_2$**CH), 1.37 (s, 9H, C(C**H$_3$**), 1.18 (d, 3H, CHC**H$_3$**, *J*=7.0 Hz), 0.88-0.79 (m, 12H, 2 x C(C**H$_3$**)$_2$).

^{13}C NMR (DMSO-d_6) δ: 171.7, 171.2, 170.9, 155.5, 86.2, 78.0, 68.3, 67.4, 67.3, 67.1, 67.1, 59.5, 50.8, 47.9, 41.1, 37.3, 30.2, 28.1, 24.1, 23.0, 21.5, 19.1, 18.2, 17.9.

HRMS calcd for $C_{29}H_{46}N_6O_4Fe$ (MH^+) 598.2930; found 598.2933.

Micro. calculated for $C_{29}H_{45}FeNO_2S$. C, 60.20; H, 7.75; N, 9.36; found C, 59.67; H, 7.75; N, 9.36.

$[\alpha]_D$ = -70.4, (c=0.15, 2,2,2-TFE)

5-[1,2]dithiolan-(3*S*/*R*)-3-yl-pentanoyl-(*S*)-Val-(*S*)-Ala-(*S*)-Leu-(*S*)-Val-(*S*)-Ala-(*S*)-Leu-*N*-ferrocenylmethanamide (SSα_6Fc, 2.16)

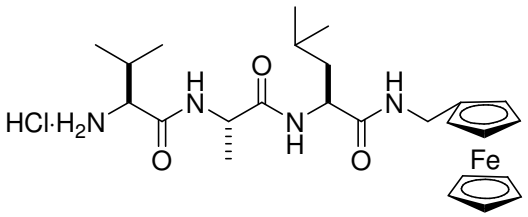

Boc-(*S*)-Val-(*S*)-Ala-(*S*)-Leu-NHCH$_2$Fc (**4.69**) (126 mg, 0.21 mmol) was deprotected with 4 M HCl/dioxane (5 mL) according to modified general method G. The product (HCl·(*S*)-Val-(*S*)-Ala-(*S*)-Leu-NHCH$_2$Fc) was obtained as a yellow residue (112 mg, quant.) and was used without further purification.

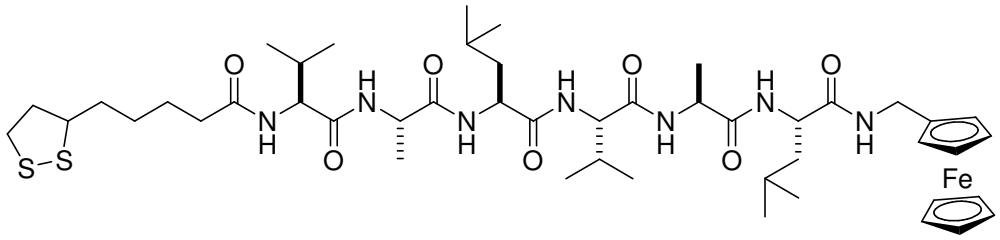

Lipoamide-(*S*)-Val-(*S*)-Ala-(*S*)-Leu-OH (**4.68**) (69 mg, 0.14 mmol) and crude HCl·(*S*)-Val-(*S*)-Ala-(*S*)-Leu-NHCH$_2$Fc (see above) (75 mg, 0.14 mmol) were coupled in dimethylformamide (15 mL) using HATU (53 mg, 0.14 mmol) and diisopropylethylamine (98 µL, 0.56 mmol) according to modified general method A. A yellow solid was obtained (119 mg, 88%) and did not require further purification.

mp = 255 ºC (dec)

^{1}H NMR (DMSO-d_6) δ: 8.03 (m, 3H, 3 x N**H**), 7.98 (d, 1H, N**H**, *J*=8.3 Hz), 7.87 (d, 1H, N**H**, *J*=7.9 Hz) 7.83 (d, 1H, N**H**CHCH, *J*=9.0 Hz), 7.60 (d, 1H, N**H**CHCH, *J*=8.7 Hz) 4.28 (m, 4H, 2 x NHC**H**CH$_3$, 2 x NHC**H**CH$_2$), 4.15 (m, 9H, 2 x NHC**H**CH, Fc), 4.06 (s, 2H, Fc), 3.96 (m, 2H, NHC**H$_2$**Fc), 3.59 (m, 1H, SC**H**), 3.17 (m, 1H, SC**H**H), 3.11 (m, 1H, SC**H**H), 2.40 (m, 1H, SCH$_2$C**H**H), 2.22-2.10 (m, 2H, C**H$_2$**CO), 1.98-1.82 (m, 3H, SCH$_2$CH**H**, 2 x NHCHC**H**), 1.68-1.40 (m, 9H, SCHC**H$_2$**CH$_2$C**H$_2$**, 2 x NHCHC**H$_2$**C**H**), 1.34 (m, 2H, SCHCH$_2$C**H$_2$**CH$_2$), 1.18 (m, 6H, 3 x CHC**H$_3$**), 0.87-0.82 (m, 24H, 4 x CH(C**H$_3$**)$_2$).

^{13}C NMR (TFE-d_3/$CDCl_3$ 2:1) δ selected peaks: 177.8, 176.1, 174.7, 58.4, 58.4, 54.3, 52.2, 42.1, 41.9, 40.8, 39.9, 37.6, 37.4, 36.2, 36.0, 32.2, 31.7, 30.5, 30.4, 27.0, 26.9, 26.7, 26.5, 24.3, 24.0, 22.8, 22.2, 20.3, 20.2, 19.8, 18.4.*

Micro. calculated for ($C_{29}H_{45}FeNO_2S$ + ½ CF_3CH_2OH). C, 56.57; H, 7.47; N, 9.62; found C, 56.65; H, 7.71; N, 9.74.

HRMS calcd for $C_{47}H_{75}N_7O_7S_2Fe$ (MH^+) 969.4519; found 969.4479.

6.6 Experimental Work Described in Chapter 5

6.6.1 Synthesis of Cyclic Fluorinated β-Amino Acids 5.43a and 5.43b

Cyclopent-1-enecarboxylic acid tert-butyl ester (5.40a)

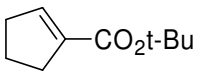

Cyclopentene-1-carboxylic acid (**5.39a**) (0.20 g, 1.8 mmol), H_2SO_4 (conc, 5 drops) and dichloromethane (5 mL) were added to a pressure tube and cooled to -78 ºC (acetone/CO_2(*S*)). 2-methyl propene (5 mL, condensed at -78 ºC into a conical flask) was added and the neck sealed with a metal lid. The reaction mixture was allowed to warm to rt and stirred for 48 h. The pressure tube was cooled to -78 ºC and a needle inserted to release the pressure before removing the lid. The reaction mixture was poured into a separating funnel containing saturated aqueous Na_2CO_3 and diethyl ether. The organic layer was separated, dried ($MgSO_4$) and concentrated *in vacuo*. The crude mixture was purified by column chromatography (silica; 10:1 petroleum ether, diethyl ether) without delay, to give the product as a clear oil (0.28 g, 92%).

Spectral properties are in agreement with those in the literature.[25]

^{1}H NMR ($CDCl_3$) δ: 6.64 (br s, 1H, C**H**=C), 2.52-2.42 (m, 4H, C**H$_2$**CH_2C**H$_2$**), 1.91 (CH_2C**H$_2$**CH_2) 1.46 (s, 9H, C(C**H$_3$**)$_3$.

* The compound was poorly soluble in all available NMR solvents, so a completely resolved carbon spectrum was unobtainable.

Cyclohex-1-enecarboxylic acid tert-butyl ester (5.40b)

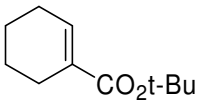

Cyclohexene-1-carboxylic acid (**5.39b**) (0.20 g, 1.6 mmol), H_2SO_4 (conc, 5 drops) and dichloromethane (5 mL) were added to a pressure tube and cooled to -78 ºC (acetone/CO_2(*S*)). 2-methyl propene (5 mL, condensed at -78 ºC into a conical flask) was added and the neck sealed with a metal lid. The reaction mixture allowed to warm to rt and stirred for 20 h. The pressure tube was cooled to -78 ºC and a needle inserted to release the pressure, before removing the lid. The reaction mixture was poured into a separating funnel containing saturated aqueous Na_2CO_3 and diethyl ether. The organic layer was separated dried ($MgSO_4$) and concentrated *in vacuo*. The crude mixture was purified by column chromatography (silica; 10:1 petroleum ether, diethyl ether) without delay, to give the product as a clear oil (0.28 g, 96% yield).

Spectral properties are in agreement with those in the literature.[26]

^{1}H NMR ($CDCl_3$) δ: 6.77 (m, 1H, C**H**=C), 2.14-2.03 (m, 2H, CHC**H$_2$**(CH_2)$_2$C**H$_2$**), 1.54-1.46 (m, 4H, C**H$_2$**C**H$_2$**CH_2CO), 1.39 (s, 9H, C(C**H$_3$**)$_3$).

(1*S*,2*S*,*αS*)-2-[Benzyl-(1-phenyl-ethyl)-amino]-1-fluoro-cyclopentanecarboxylic acid tert-butyl ester (5.43a)

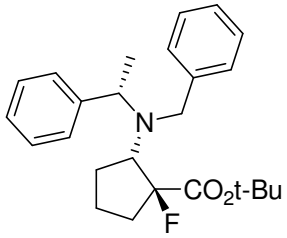

A solution of (*S*)-(-)-*N*-benzyl-*α*-methylbenzy1amine (**(-)-5.41**) (0.38 mL, 1.8 mmol) in anhydrous tetrahydrofuran (5 mL) was stirred under N_2, cooled to – 78 ºC and butyllithium (0.89 mL, 1.8 mmol, 1.5 M in hexane) was added dropwise via syringe. The resultant pink lithium amide solution was stirred for 1 hr before a solution of cyclopent-1-ene carboxylic acid *tert*-butyl ester (**5.40a**) (0.20 g, 1.2 mmol) in anhydrous tetrahydrofuran (2 mL) was added. The resultant yellow enolate solution was stirred for a further 2 h before solid *N*-fluorobenzene sulfonimide (0.57 g, 1.8 mmol) was added. The reaction mixture was warmed to -30 ºC over 2 h, during which time (at approximately -40 ºC) a yellow precipitate formed. The reaction was quenched by the addition of saturated aqueous NH_4Cl and extracted twice with dichloromethane. The combined organic extracts were dried ($MgSO_4$) and concentrated *in vacuo* to give the crude mixture from which the diastereoselectivity of the reaction was assessed (as described in Chapter Five). The crude product mixture was purified by Flashmaster^{TM} chromatography (silica (20 g), λ = 240 nm; 0:1→5:95 ethyl acetate, hexanes) to give the pure product as a clear oil (0.38 g, 84%), a sample of which was crystallised from ethanol.

mp = 65-68 ºC

^{1}H NMR ($CDCl_3$) δ: 7.46-7.19 (m, 10H, 2 x Ph), 4.34 (q, 1H, NC**H**CH_3, *J*=6.9 Hz), 4.00 and 3.42 (AB system, 2H, J_{AB}=15.4, PhC**H$_2$**N), 3.55 (dt, 1H, NC**H**CH_2, *J*=9.0, 9.0, 23.0 Hz), 2.29 (m, 1H, CFC**H**H), 1.97 (m, 1H, CFCH**H**), 1.69 (m, 4H, C**H$_2$**C**H$_2$**CF), 1.59 (s, 9H, *t*-Bu), 1.39 (d, 3H, CHC**H$_3$**, *J*=6.9 Hz).

^{13}C NMR ($CDCl_3$) δ: 170.0 (*J*=28.6 Hz), 142.5, 141.4, 128.7, 128.7, 127.9, 127.9, 127.8, 126.7, 126.3, 104.3 (*J*=193.3 Hz), 82.3, 70.6 (*J*=22.8 Hz), 57.4 (*J*=2.4 Hz), 51.6, 36.16 (*J*=24.5 Hz), 29.87 (*J*=6.3 Hz), 28.2, 20.67 (*J*=3.9 Hz), 17.4.

^{19}F NMR ($CDCl_3$) δ: -143.76.

HRMS calcd for $C_{25}H_{33}NO_2F$ (MH^+) 398.2495; found 398.2505.

$[\alpha]_D$ = -29.7 (c 0.90, $CHCl_3$)

Other enantiomer: is $[\alpha]_D$ = +33.4 (c 0.50, $CHCl_3$)

(1*S*,2*S*,*αS*)-2-[Benzyl-(1-phenyl-ethyl)-amino]-1-fluoro-cyclohexanecarboxylic acid tert-butyl ester (5.43b)

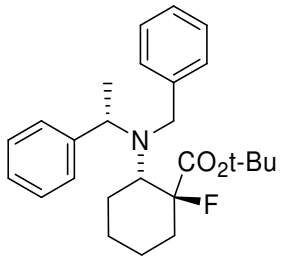

A solution of (*S*)-(-)-*N*-benzyl-*α*-methylbenzy1amine ((**-**)**-5.41**) (0.35 mL, 1.7 mmol) in anhydrous tetrahydrofuran (5 mL) was stirred under N_2, cooled to –78 ºC and butyllithium (0.82 mL, 1.7 mmol, 1.5 M in hexane) was added dropwise via syringe. The resultant pink lithium amide solution was stirred for 1 h whereupon cyclohex-1-ene carboxylic acid *tert*-butyl ester (**5.40b**) (0.20 g, 1.1 mmol) was added as a solution in anhydrous tetrahydrofuran (2 mL). The resultant yellow enolate solution was stirred for a further 2 h before solid *N*-fluorobenzene sulfonimide (0.52 g, 1.7 mmol) was added. The reaction mixture was warmed to -30 ºC over 2 h, during which time (at about -40 ºC) a yellow precipitate formed. The reaction was quenched by the addition of saturated aqueous NH_4Cl and extracted twice with dichloromethane. The combined organic extracts were dried and concentrated *in vacuo* to give the crude mixture from which the diastereoselectivity of the reaction was assessed (as described in Chapter Five). The crude product mixture was purified by Flashmaster^{TM} chromatography (silica (20 g), λ = 240 nm; 0:1→4:96 ethyl acetate, hexanes) to give the pure product as a clear oil (118 mg, 26%).

^{1}H NMR ($CDCl_3$) δ: 7.48-7.17 (m, 10H, 2 x Ph), 4.14 (q, 1H, NC**H**CH_3, *J*=6.7 Hz), 3.95 and 3.84 (AB system, 2H, J_{AB}=14.8 Hz, PhC**H$_2$**N), 2.92 (dt, 1H, NHC**H**CH_2, *J*=12.5, 12.5, 3.7 Hz), 2.14 (dq, 1H, CHC**H**H, *J*=12.9, 2.8 Hz), 1.94 (m, 2H, CHCH**H,** CFC**H**H), 1.80 (m, 1H, $CHCH_2$C**H**H), 1.72 (m, 1H, $CHCH_2CH_2$C**H**H), 1.60 (m, 2H, $CHCH_2CH_2$C**H**H), 1.44 (s, 9H, C(C**H$_3$**)$_3$), 1.39 (m, 1H, CFCH**H**), 1.33 (d, 3H, CHC**H$_3$**, *J*=6.8 Hz), 1.25 (m, 1H, CHC_2CH**H**).

^{13}C NMR ($CDCl_3$) δ: 170.7 (*J*=27.6 Hz), 144.1, 141.8, 128.4, 128.3, 128.0, 127.5, 126.5, 126.3, 94.9 (*J*=191.7), 82.3, 63.2 (*J*=18.4 Hz), 57.5, 50.7, 36.6 (*J*=21.7 Hz), 27.9, 27.7 (*J*=6.9 Hz), 25.5, 22.7 (*J*=10.0 Hz), 15.3.
^{19}F NMR ($CDCl_3$) δ: -143.7.
$[\alpha]_D$ = -50.8 (c 0.50, $CHCl_3$)
HRMS calcd for $C_{26}H_{35}NO_2F$ (MH^+) 411.2566; found 411.2568.

tert-Butyl (1*R*,2*R*)-2-amino-1-fluorocyclopentanecarboxylate (5.44)

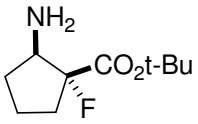

Method 1: $Pd(OH)_2$ on carbon (13 mg) was added to a solution of 2-[benzyl-(1-phenylethyl)-amino]-1-fluorocyclohexanecarboxylic acid *tert*-butyl ester (**5.43a**) (50 mg, 0.13 mmol) in a mixture of degassed methanol/dichloromethane (5:1, 12 mL) and the resultant black suspension stirred under a hydrogen atmosphere (5 atm) for 16 h. The reaction mixture was filtered through a plug of celite (eluent methanol) and concentrated *in vacuo* to give an intractable solid.

Method 2: $Pd(OH)_2$ on carbon (13 mg) was added to a solution of 2-[benzyl-(1-phenylethyl)-amino]-1-fluorocyclohexanecarboxylic acid *tert*-butyl ester (**5.43a**) (50 mg, 0.13 mmol) in a degassed methanol (5 mL). The resultant black suspension was stirred under a hydrogen atmosphere (1 atm) for 3 h. The reaction mixture was filtered through a plug of celite (eluent methanol) and concentrated *in vacuo*. Petroleum ether (2 mL) was added to the crude mixture then decanted off leaving the product as a light yellow oil (22 mg, 83%).

^{1}H NMR (CD_3OD) δ: 3.41 (td, 1H, NHC**H**, *J*=21.8, 7.5, 7.5 Hz), 2.28 (m, 1H, CFC**H**H), 2.13 (m, 1H, CHC**H**H), 1.98 (m, 1H, CFCH**H**), 1.86-1.73 (m, 2H, $CH_2C\mathbf{H_2}CH_2$), 1.55 (m, 1H, CHCH**H**), 1.52 (s, 9H, $C(C\mathbf{H_3})_3$).
^{13}C NMR (CD_3OD) δ: 171.1 (d, *J*=27.2 Hz), 104.9 (*J*=191.9 Hz), 84.1, 62.7 (d, *J*=27.6 Hz), 35.6 (d, *J*=23.6 Hz), 34.7 (d, *J*=3.7 Hz), 28.4, 21.9 (d, *J*=1.5 Hz).
HRMS calcd for $C_{10}H_{19}NO_2F$ (MH^+) 204.1400; found 204.1392.

(1*R*,2*R*)-2-amino-1-fluorocyclopentanecarboxylic acid trifluoroacetate (5.45)

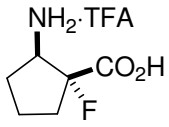

tert-Butyl 2-amino-1-fluorocyclopentanecarboxylate (**5.44**) (20 mg, 99 μmol) was deprotected in trifluoroacetic acid (2.5 mL) and dichloromethane (2.5 mL) according to general method F. The crude residue was dissolved in acetone and ether added until a white precipitate formed. The precipitate was filtered to give the product as a white solid (6 mg, 49%).

^{1}H NMR (CD_3OD) δ: 3.84 (td, 1H, $NH_2C\mathbf{H}$, *J*=20.1, 7.2 Hz), 2.38 (m, 1H, CHC**H**H, 2.25-2.16 (m, 2H, C$\mathbf{H_2}$CF), 1.96-1.81 (CHCH**H**C$\mathbf{H_2}$).

^{13}C NMR (CD_3OD) δ: 174.4, 100.4 (*J*=206.1 Hz) 58.2 (*J*=33.9 Hz), 36.4 (*J*=24.0 Hz), 30.3 (*J*=1.7 Hz), 22.2.

^{19}F NMR (CD_3OD) δ: 149.99

HRMS calcd for $C_6H_{11}NO_2F$ (MH^+) 148.0774; found 148.0779.

$[\alpha]_D$ = +4.7 (c=0.43, CH3OH)

6.6.2 Synthesis of *trans*-7-Aminocyclohept-3-ene-1-carboxylic Acid (5.63)

Methyl (3*S*)-3-[(*tert*-butoxycarbonyl)amino]-4-hydroxybutanoate (5.50)

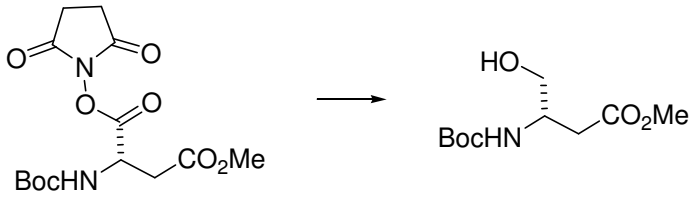

N-Boc aspartic acid *β* methyl ester (**5.58**) (12.7 g, 51 mmol) was dissolved in ethyl acetate (100 mL) and the solution was cooled on an ice-bath. *N*-hydroxysuccinimide (6.29 g, 46 mmol) and a solution of *N*,*N*'-dicyclohexylcarbodiimide (10.7 g, 52 mmol) in ethyl acetate (50 mL) were added. The reaction was warmed to rt and stirred for 16 h. The precipitate of dicyclohexylurea was filtered off and the filtrate washed with saturated aqueous $NaHCO_3$, NaCl, dried ($MgSO_4$) and evaporated *in vacuo* to give crude succinimide ester (17.9 g, 100%) as a white solid.

Sodium borohydride was dissolved in a mixture of water (4 mL) and tetrahydrofuran (30 mL) and the reaction mixture cooled on an ice-bath. A solution of succinimide ester (see above) (3.44 g, 10 mmol) in tetrahydrofuran (30 mL) was added dropwise over 30 s. The reaction was monitored by TLC (1:1 ethyl acetate, petroleum ether) and after approximately 5 min, the reaction was observed to have gone to completion. Saturated aqueous NH_4Cl was added to quench the reaction. The reaction mixture was diluted with ethyl acetate, washed with saturated aqueous NaCl, dried ($MgSO_4$) and the solvent removed *in vacuo*. The crude mixture was purified by column chromatography (silica; 1:1 ethyl acetate, petroleum ether) to give the product as a colourless oil (1.16 g, 50%).

Physical and spectral properties agreed with those in the literature.[27]

^{1}H NMR ($CDCl_3$, 300 MHz) δ: 5.35 (d, 1H, N**H**, *J*=8.4 Hz,), 3.94 (m, 1H, NHC**H**), 3.68 (d, 1H, C$\mathbf{H}_2$OH, *J*=4.3 Hz,), 3.63 (s, 3H, OC$\mathbf{H}_3$), 2.57 (d, 1H, COC$\mathbf{H}_2$, *J*=6.2 Hz), 1.37 (s, 9H, C(C$\mathbf{H}_3$)$_3$).

Methyl (3*S*)-3-[(*tert*-butoxycarbonyl)amino]-4-iodobutanoate (5.60)

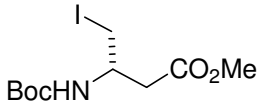

Imidazole (0.58 g, 8.6 mmol) and triphenylphosphine (2.25 g, 8.6 mmol) were dissolved in anhydrous dichloromethane under N_2. Iodine (2.18 g, 8.6 mmol) was added slowly, with vigorous stirring, to give a pale yellow precipitate. The alcohol (**5.50**) (2.00 g, 8.6 mmol) was dissolved in anhydrous dichloromethane (40 mL) under N_2 and transferred to the reaction mixture via syringe. The reaction was monitored by TLC (2:1 ethyl acetate, petroleum ether) and observed to have gone to completion after 1 h. The mixture was filtered before washing with 1 M aqueous sodium thiosulfate, saturated aqueous NaCl, dried ($MgSO_4$), and concentrated *in vacuo*. The crude residue was slurried in diethyl ether and filtered through a bed of silica, eluting with additional ether. The filtrate was concentrated *in vacuo* to give the product as an off-white solid (2.94 g, quant.).

Spectral properties are in agreement with those in the literature.[27]

^{1}H NMR ($CDCl_3$, 300 MHz) δ: 5.11 (m, N**H**), 3.90 (m, 1H, NHC**H**), 3.68 (s, 3H, OC**H**$_3$), 3.40 (m, 2H, C**H**$_2$I), 2.68 (dq, 2H, *J*=5.7 Hz, *J*=16.4 Hz, COC**H**$_2$), 1.42 (s, 9H, C(C**H**$_3$)$_3$).

Methyl (3*R*)-3-[(*tert*-butoxycarbonyl)amino]hept-6-enoate (5.61)

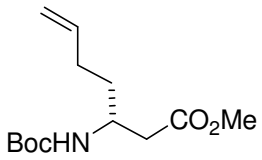

Zinc dust (147 mg, 2.3 mmol) was weighed into a round bottom flask with side arm, repeatedly evacuated (with heating) and finally flushed with N_2. Anhydrous dimethylformamide (0.5 mL) and trimethylsilyl chloride (6 μL, 0.046 mmol) were added, and the resultant mixture stirred for 30 min at rt. The iodide (**5.60**) (264 mg, 0.77 mmol) was dissolved in anhydrous dimethylformamide (0.5 mL) under N_2 and transferred by syringe to the zinc suspension cooled

on an ice-bath. TLC analysis (2:1 ethyl acetate, petroleum ether) showed complete consumption of the iodide within 15 min. The preformed zinc reagent was cooled to -55 ºC. A solution of CuCN·2LiCl, prepared by dissolving copper(I) cyanide (67 mg, 1.5 mmol) in anhydrous dimethylformamide (0.5 mL), was transferred via syringe to the reaction mixture, then allowed to warm on an ice-bath for 5 min. After re-cooling to -55 ºC, allyl chloride (1.00 mmol) was added, the mixture was allowed to warm to rt and stirred for 16 h. Ethyl acetate (30 mL) was added and the organic layer was washed with saturated aqueous NH_4Cl, water, saturated aqueous NaCl, dried ($MgSO_4$) and the solvent removed *in vacuo*. The crude mixture was purified with flash column chromatography (silica; 1:4 ethyl acetate, petroleum ether) to give the product as a clear oil (121 mg, 61%).

Spectral properties are in agreement with those in the literature.[27]

^{1}H NMR ($CDCl_3$) δ: 5.83-5.75 (m, 1H, C**H**=CH_2), 5.05-4.96 (m, 2H, CH=C**H**$_2$), 4.93 (m, 1H, N**H**), 3.92 (m, 1H, NHC**H**), 3.68 (s, 3H, OC**H**$_3$), 2.52 (m, 2H, COC**H**$_2$), 2.10 (m, 2H, C**H**$_2$), 1.58 (m, 2H, C**H**$_2$), 1.43 (s, 9H, C(C**H**$_3$).

Methyl (2*R*,3*R*)-2-allyl-3-[(*tert*-butoxycarbonyl)amino]hept-6-enoate (5.62)

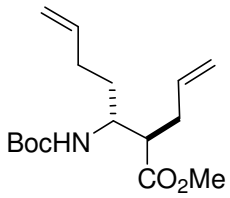

Anhydrous LiCl (0.19 g, 4.5 mmol) and olefin **5.61** (0.40 g, 1.54 mmol) were added to anhydrous tetrahydrofuran (10 mL) and the reaction mixture was cooled to -78 ºC. LDA (1.7 mL (2 M in tetrahydrofuran/hexane, 2.2 equiv) was added and the solution stirred at -78 ºC for 1 h, followed by the addition of allyl bromide (540 μL, 4 equiv). The reaction mixture was stirred at -78 ºC for a further 1 h and then allowed to warm to rt over 16 h. The mixture was quenched with saturated aqueous NH_4Cl, diluted with ethyl acetate, washed successively with saturated aqueous $NaHCO_3$ and NaCl. The organic layer was dried ($MgSO_4$) and the solvent removed *in vacuo*. The crude mixture was purified by column chromatraphy (silica, 1:4 ethyl acetate, petroleum ether) to give the product as a clear oil (192 mg, 42%).

^{1}H NMR ($CDCl_3$, 300 MHz) δ: 5.78 (m, 2H, 2xC**H**=CH_2), 5.22 (d, N**H**, *J*=9 Hz), 5.106-4.94 (m, 4H, 2xCH=C**H**$_2$), 3.83 (m, 1H, NHC**H**), 3.68 (s, 3H, OC**H**$_3$), 2.62 (m, 1H, C**H**), 2.44-2.26 (m, 2H, C**H**$_2$), 2.09 (m, 2H, C**H**$_2$), 1.47 (m, 2H, C**H**$_2$), 1.44 (s, 9H, C(C**H**$_3$)$_3$).

^{13}C NMR ($CDCl_3$, 300 MHz) δ: 175.0, 155.8, 139.0, 134.9, 117.2, 114.2, 79.0, 51.5, 51.0, 48.7, 28.8, 28.7, 28.4, 26.0.

HRMS calcd for $C_{16}H_{27}NO_4Na$ (MNa^+) 320.1838; found 320.1835.

$[\alpha]_D$ = +21.8 (c=0.8, $CHCl_3$)

Methyl (1*R*,7*R*)-7-[(*tert*-butoxycarbonyl)amino]cyclohept-3-ene-1-carboxylate (5.63)

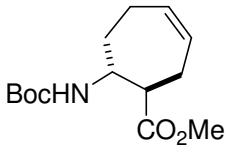

Diene (**5.62**) (28 mg, 96 μmol) was ring-closed in anhydrous benzene (1 mL) under N_2 using Grubbs' 2nd Gen. catalyst (8 mg, 9.6 μmol). The solution was stirred at rt for 16 h at which time the solvent was removed *in vacuo*. The resulting black residue was purified by column chromatography (silica; 1:4 ethyl acetate, petroleum ether) to give the product as a white solid (18 mg, 70% yield).

mp = 74-77 ºC

^{1}H NMR ($CDCl_3$, 300 MHz) δ: 5.82 (m, 1H, CH_2CH_2C**H**=CH), 5.72 (m, 1H, $CHCH_2$C**H**=CH), 4.65 (m, 1H, N**H**), 4.04 (m, 1H, NHC**H**), 3.67 (s, 3H, OC**H**$_3$), 2.45-2.37 (m, 2H, CH=CHC**H**H, COC**H**), 2.27 (dd, 1H, CH=CHC**H**HCH, *J*=7.5, *J*=13.9 Hz), 2.20-2.14 (m, 1H, NHCHCH_2C**H**H), 2.11-1.99 (m, 2H, NHCHC**H**H, NHCHCH_2CH**H**), 1.41 (s, 10H, NHCHCH**H**, C(C**H**$_3$)$_3$).

^{13}C NMR ($CDCl_3$, 300 MHz) δ: 174.3, 154.6, 133.0, 128.8, 79.3, 54.1, 51.8, 49.7, 32.3, 28.3, 27.3, 23.9.

HRMS calcd for $C_{14}H_{24}NO_4$ (MH^+) 270.1705; found 270.1713.

$[\alpha]_D$ = -2.9 º (c=0.45, CH_3OH)

6.6.3 Attempted Synthesis of *trans*-8-Aminocyclooct-3-ene-1-carboyxlic Acid (5.71)

(2*S*)-2-[(*tert*-butoxycarbonyl)amino]-4-hydroxybutanoic acid (5.65)

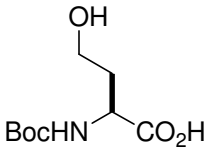

(*S*)-Homoserine (**5.64**) (5.00 g, 42 mmol) and $NaHCO_3$ (8.85 g, 105 mol) were dissolved in dioxane/water (2:1, 120 mL) and cooled on an ice-bath. $(Boc)_2O$ (11.0 g, 50 mmol) was dissolved in dioxane (25 mL) and added dropwise to the reaction mixture, and stirred for 16 h at rt. The solvent was removed *in vacuo* and the residue dissolved in water and washed twice with diethyl ether. The pH of the aqueous solution was adjusted to 2 (universal indicator paper) with 5% aqueous $KHSO_4$ and extracted twice with ethyl acetate. The combined organic layers were dried ($MgSO_4$) and concentrated *in vacuo* to give the product as a clear oil that required no further purification (8.84 g, 96%).

Spectral properties are in agreement with those in the literature.[28]

^{1}H NMR ($CDCl_3$) δ: 5.52 (m, 1H, N**H**), 4.48 (m, 1H, NHC**H**), 3.82-3.70 (m, 2H, C**H$_2$**OH), 2.19 (m, 1H, CHC**H**H), 1.76 (m, 1H, CHCH**H**), 1.44 (s, 3H, C(C**H$_3$**)$_3$).

Methyl (2*S*)-2-[(*tert*-butoxycarbonyl)amino]-4-hydroxybutanoate (5.66)

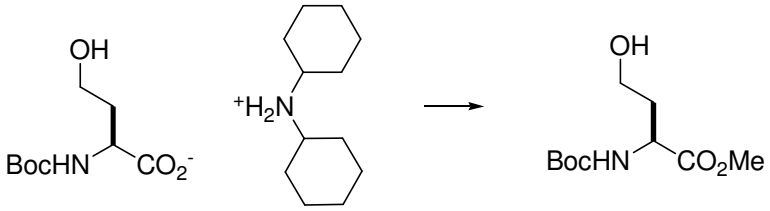

Boc-(*S*)-Homoserine (**5.65**) (1.49 g, 6.8 mmol) was dissolved in methanol (10 mL) and dicyclohexylamine was added dropwise, with stirring, to the solution until it became basic. The

solvent was removed *in vacuo* and the resulting white precipitate was resuspended in diethyl ether. The white solid was collected by suction filtration and dried in a vacuum desiccator over P_2O_5 (2.72 g, quant).

Methyl iodide (320 μL, 5.1 mmol) was added dropwise to a stirred suspension of the dicyclohexylammonium salt of Boc-(*S*)-homoserine (2.72 g, 6.8 mmol) in anhydrous dimethylformamide (30 mL) and stirred at rt for 16 h. The reaction mixture was concentrated *in vacuo* and the residue coevaporated with toluene three times. Water (55 mL) was added to the residue and the resulting aqueous solution extracted twice with ethyl acetate. The combined organic extracts were washed with water, saturated aqueous NaCl, dried ($MgSO_4$) and concentrated *in vacuo*. The crude viscous yellow oil was purified by flash chromatography (silica; diethyl ether) to give the product as a colourless viscous oil (1.05 g, 66%).

Physical and spectral properties agreed with those in the literature.[29]

^{1}H NMR ($CDCl_3$) δ: 5.41 (br d, 1H, N**H**) 4.47 (m, 1H, NHC**H**), 3.75 (s, 3H, OC$\mathbf{H_3}$), 3.70 (m, 2H, HOC$\mathbf{H_2}$), 2.13(m, 1H, CHCH**H**), 1.63 (m, 1H, CHCH**H**), 1.43 (s, 9H, C(C$\mathbf{H_3}$)$_3$).

Methyl (2*S*)-2-[(*tert*-butoxycarbonyl)amino]-4-iodobutanoate (5.67)

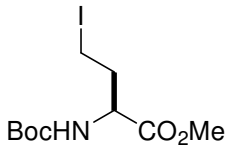

Imidazole (0.31 g, 4.5 mmol) and triphenylphosphine (1.18 g, 4.5 mmol) were dissolved in anhydrous dichloromethane under N_2. Iodine (1.14 g, 4.5 mmol) was added slowly with vigorous stirring, to give a pale yellow precipitate. Boc-(*S*)-homoserine methyl ester (**5.66**) (1.00 g, 4.5 mmol) was dissolved in anhydrous dichloromethane (40 mL) under N_2 and transferred to the reaction mixture via syringe. The reaction was monitored by TLC (2:1, ethyl acetate, petroleum ether) and observed to have gone to completion after 1 h. The mixture was filtered before washing with 1 M aqueous sodium thiosulfate, saturated aqueous NaCl, dried ($MgSO_4$), and concentrated *in vacuo*. The crude residue was slurried in diethyl ether and filtered through a

bed of silica, eluting with additional ether. The filtrate was concentrated *in vacuo* to give the product as an off-white solid (1.43 g, 93%).

mp = 39 ºC

^{1}H NMR ($CDCl_3$) δ: 5.09 (m, N**H**), 4.33 (m, 1H, NHC**H**), 3.74 (s, 3H, OC**H**$_3$), 3.18- 3.15 (t, 2H, IC**H**$_2$, *J*=8.0 Hz), 2.40 (m, 1H, CHC**H**H), 2.17 (m, 1H, CHCH**H**), 1.43 (s, 9H, CH(C**H**$_3$)$_3$).

^{13}C NMR ($CDCl_3$) δ: 171.8, 155.0, 79.7, 54.0, 52.2, 36.4, 28.0.

HRMS calcd for $C_{10}H_{19}NO_4I$ (MH^+) 344.0359; found 344.0363.

Methyl (2*S*)-2-[(tert-butoxycarbonyl)amino]hept-6-enoate (5.68)

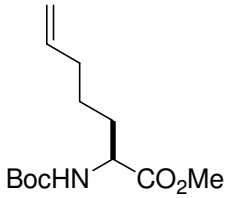

Zinc dust (0.23 g, 3.5 mmol, Aldrich) was weighed into a 25 mL round bottom flask with a side arm. Iodine (50 mg) was added and the flask was heated under vacuum for 10 min, then flushed with N_2 and evacuated a further three times. Iodide **5.67** (0.40 g, 1.2 mmol) dissolved in anhydrous dimethylformamide (5 mL) was added dropwise, *via* syringe, to the activated zinc slurry which was cooled on an ice-bath. The reaction mixture was then allowed to warm to rt and stirred for 1 h to give the organozinc intermediate. The insertion process was monitored by TLC analysis (3:7 ethyl acetate, petroleum ether). CuBr·DMS (31 mg, 0.15 mol) was weighed into a separate flask with a side arm, and dried with a heat gun under vacuum until the appearance changed from a white solid to a light green powder. Anhydrous dimethylformamide (5 mL) was added, followed by allyl chloride (120 μL, 1.5 mmol). The reaction mixture was then cooled to -15 ºC. Once the zinc insertion was judged to have reached completion, stirring of the reaction mixture was ceased to allow the zinc powder to settle. The supernatant was removed via syringe (care being taken to minimise the transfer of zinc) and added dropwise to the solution of electrophile and copper catalyst. The cooling bath was removed and the solution was stirred at rt for 16 h. The reaction mixture was diluted with ethyl acetate and stirred for a further 15 min. The organic phase was washed successively with 1 M $Na_2S_2O_3$, water, saturated aqueous NaCl, dried ($MgSO_4$) and concentrated *in vacuo*. The crude oil was purified by column

chromatography (silica; 1:9 ethyl acetate, petroleum ether) to give the product as a colourless oil (0.22 g, 72%).

Physical and spectral properties are consistent with those in the literature.[30]

^{1}H NMR ($CDCl_3$) δ: 5.80-5.72 (m, 1H, CH_2=C**H**), 5.02-4.95 (m, 2H, NH, CH=C**H**$_2$), 4.29 (m, 1H, HNC**H**), 3.73 (s, 3H, OC**H**$_3$), 2.07 (m, 1H, CHC**H**H), 1.85-1.77 (m, 1H, CHCH**H**), 1.68-1.56 (m, 2H, CH_2C**H**$_2$$CH_2$), 1.44 (s, 9H, CH(C**H**$_3$)$_3$), 0.92 (t, 2H, CH_2=CHC**H**$_2$, *J*=7.0 Hz).
$[\alpha]_D$ = -15.4, (c=1.0, CH_3OH)

6.6.4 Synthesis of *trans*-2-Aminocyclooct-4-ene-1-carboxylic Acid (5.78)

(2*S*)-2-[(tert-butoxycarbonyl)amino]pent-4-enoic acid (5.75)[31]

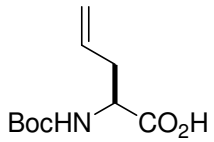

(*S*)-Allyl glycine (**5.74**) (2.0 g, 17 mmol) was stirred (as a suspension) in anhydrous dichloromethane (20 mL) and cooled on an ice-bath. Triethylamine (3.0 mL, 22 mmol) and a solution of di-*tert*-butyl dicarbonate (3.77 g, 17 mmol) in dichloromethane (10 mL) were added and the reaction mixture allowed to warm to rt over 16 h. The progress of the reaction was monitored by TLC (*n*-butanol/water/acetic acid, 4:2:1). The reaction mixture was washed with 1 M hydrochloric acid, dried ($MgSO_4$) and the solvent evaporated to give the product as a clear oil (3.73 g, quant.).

Spectral properties are in agreement with those in the literature.[32]

^{1}H NMR (CD_3OD) δ: 5.79 (m, 1H, C**H**=CH_2), 5.06-5.13 (m, 2H, CH=C**H$_2$**), 4.13 (m, 1H, NHC**H**), 2.53 (m, 1H, NHCHC**H**H), 2.42 (m, 1H, NHCHCH**H**), 1.43 (s, 9H, C(C**H$_3$**)$_3$).
$[\alpha]_D$ = +17.1, (c=0.63, $CDCl_3$); lit.[32] $[\alpha]_D$ +14.5 (c = 0.013, $CDCl_3$)

(3*S*)-methyl 3-[(tert-butoxycarbonyl)amino]hex-5-enoate (5.76)

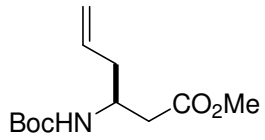

Boc-(*S*)-allylGly-OH (**5.75**) (3.65 g, 17 mmol), ethyl chloroformate (1.62 mL, 17 mmol), triethylamine (2.36 mL, 17 mmol) and diazomethane (~0.40 M in diethyl ether, ~100 mL), were reacted according to general Method C. Purification of the crude mixture using column chromatography (silica; 1:4 ethyl acetate, petroleum ether) gave the diazoketone as a yellow oil (3.00 g, 74% yield).

The diazoketone (3.00 g, 13 mmol), silver benzoate (0.32 g, 1.4 mmol), methanol (20 mL) and triethylamine (5.07 mL, 36 mmol) were reacted according to general method D. The crude product was purified by column chromatography (silica; 1:9 ethyl acetate, petroleum ether) to give the product as a clear oil (2.02 g, 66% yield).

Spectral properties are in agreement with those in the literature.[33]

^{1}H ($CDCl_3$) δ: 5.74 (m, 1H, C**H**=CH_2), 5.09 (m, 2H, CH=C**H$_2$**), 4.95 (br s, 1H, N**H**), 3.98 (m, 1H, NHC**H**), 3.67 (s, 3H, OC**H$_3$**), 2.52 (m, 2H, C**H$_2$**CH=CH_2), 2.30 (m, 2H, C**H$_2$**CO), 1.42 (s, 9H, C(C**H$_3$**)$_3$).
$[\alpha]_D$ = +10.0, (c=0.2, CH_3OH)

Methyl (2*S*)-2-{(1*S*)-1-[(*tert*-butoxycarbonyl)amino]but-3-en-1-yl}hept-6-enoate (5.77)

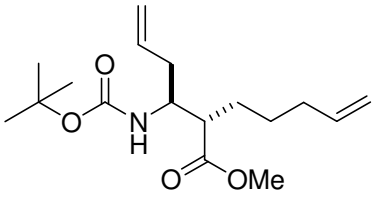

Optimum conditions: BuLi (0.8 M solution in hexanes; 1.21 mL, 0.95 mmol) and 1,1,1,3,3,3-hexamethyldisilazane (LiHMDS) (214 μL, 1.0 mmol) were added to anhydrous tetrahydrofuran (2 mL) and the reaction mixture was cooled on an ice-bath, under N_2. The reaction mixture was stirred for 20 min, then cooled to -40 ºC, and Boc-β^3hAllylglycine methyl ester (**5.76**) (100 mg, 0.41 mmol) dissolved in tetrahydrofuran (1 mL) was added slowly, stirred for 2 h, then cooled to -78 ºC. In a separate flask, sodium iodide (0.31 g, 2.0 mmol) was dissolved in anhydrous 1,2-dimethoxyethane (2 mL) at rt, under N_2. 5-Bromo-1-pentene (243 μL, 2.0 mmol) was added and the reaction mixture was stirred for 30 min to form 5-iodo-1-pentene**.** The iodide was transferred by syringe to the first reaction flask and the reaction mixture was stirred at -78 ºC for 2 h, then allowed to warm to rt over 16 h. The reaction was quenched with saturated aqueous NH_4Cl and diluted with ethyl acetate. The organic layer was separated, washed with saturated aqueous NaCl, dried ($MgSO_4$) and concentrated *in vacuo*. The crude mixture was purified by column chromatography (silica; 0:1-1:9 ethyl acetate, petroleum ether) to give the product as a colourless oil (48 mg, 37%).

Other conditions: Same as above except LiHMDS was replaced with LDA, and the electrophile was either 5-bromopent-1-ene or 5-iodopente-1-ene; or LiHMDS was used but the electrophile was replaced with 5-bromopent-1-ene or hex-4-en-1-yl methanesulfonate (see Table 5.1).

^{1}H NMR ($CDCl_3$) δ: 5.75 (m, 2H, 2 x C**H**=CH_2), 5.32 (d, NH, *J*=10 Hz), 5.08-4.93 (m, 4H, 2 x CH=C**H$_2$**), 3.83 (m, 1H, NHC**H**), 3.69 (s, 3H, OC**H$_3$**), 2.59 (m, 1H, C**H**CO), 2.26 - 2.13 (m, 2H, NHCHC**H$_2$**), 2.04 (m, $COCH(CH_2)_2C\mathbf{H_2}$), 1.68 (m, 1H, COCHC**H**H), 1.55 (m, 1H, COCHCH**H**), 1.48 – 1.30 (m, 4H, $COCHC\mathbf{H_2}C\mathbf{H_2}$), 1.43 (s, 9H, $OC(C\mathbf{H_3})_3$).

^{13}C NMR ($CDCl_3$) δ: 175.6, 155.7, 138.1, 134.2, 117.7, 114.8, 79.0, 51.5, 50.8, 47.5, 38.9, 33.4, 29.3, 28.3, 26.5.

$[\alpha]_D$ = -7.2 (c=1.0, $CHCl_3$)

HRMS calcd for $C_{17}H_{30}NO_4$ (MH^+) 312.2175; found 312.2163.

Methyl (1*S*,2*S*)-2-[(*tert*-butoxycarbonyl)amino]cyclooct-4-ene-1-carboxylate (5.78)

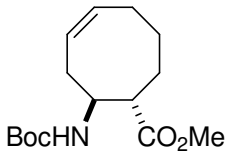

Diene **5.77** (10 mg, 32 μmol) was dissolved in dichloromethane (10.7 mL, 3mM diene concentration) and stirred under N_2. Grubbs' 1st Gen. catalyst (2.5 mg, 3.2 μmol) was added and the reaction mixture heated to reflux for 20 h. The reaction was cooled to rt and concentrated under vacuum to give a black oil. Purification by column chromatography (silica; 1:4 ethyl acetate, petroleum ether) gave the product as a the clear oil (7.5 mg, 82%).

^{1}H NMR ($CDCl_3$) δ: 5.84 (td, 1H, NHCHCH$_2$C**H,** *J*=9.6, 7.8, 7.8 Hz,), 5.63 (dt, 1H, (CH$_2$)$_3$C**H**, *J*=10.0, 9.9, 7.0 Hz,), 4.52 (br s, 1H, N**H**), 4.02 (m, 1H, NHC**H**), 3.65 (s, 3H, OC**H$_3$**), 2.64 (m, 1H, NHCHC**H**H), 2.47 (m, 1H, COC**H**), 2.31 (m, 1H, NHCHCH**H**), 2.16 (m, 2H, COCHC**H$_2$**(CH)$_2$), 1.80-1.66 (m, 3H, COCHCH**H**C**H**H), 1.49-1.42 (m, 10H, C(C**H$_3$**)$_3$ and COCHCH$_2$CH**H**).

^{13}C NMR ($CDCl_3$) δ: 175.9, 154.7, 133.2, 125.9, 79.3, 53.1, 51.8, 49.6, 30.2, 28.62, 28.3, 28.0, 26.3.

HRMS calcd for $C_{15}H_{25}NO_4$ (MH^+) 284.1862; found 284.1858.

$[\alpha]_D$ = +52.0 (c=0.1, CH_3OH)

Hex-4-en-1-yl methanesulfonate (5.83)

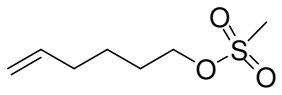

5-Hexen-1-ol (**5.82**) (240 μL, 2.0 mmol) and triethylamine (746 μL, 5.4 mmol) were added to dichloromethane (10 mL) and stirred under N_2 at rt. Methanesulfonyl chloride (170 μL, 2.2 mmol) was added slowly and the reaction mixture was stirred for 1 h. Water (10 mL) was added and the mixture was extracted with twice with dichloromethane. The organic fractions were washed with NaCl, dried ($MgSO_4$) and concentrated *in vacuo* to give the product as a light yellow oil that was used without further purification (0.36 g, quant).

Physical and spectral properties are in agreement with those in the literature.[34]

^{1}H NMR ($CDCl_3$) δ: 5.77 (m, 1H, C**H**=CH_2), 4.99 (m, 2H, CH=C**H$_2$**), 4.22 (t, C**H$_2$**O, 2H, *J*=6.2, 6.2 Hz), 2.99 (s, 3H, SO_2C**H$_3$**), 2.08 (q, 2H, CHC**H$_2$**, *J*=7.0, 7.0, 7.0 Hz), 1.75 (m, 2H, C**H$_2$**CH_2O), 1.50 (m, 2H, $CHCH_2$C**H$_2$**).

6-Iodohex-1-ene (5.85)

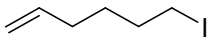

Triphenylphosphine (1.35 g, 5.5 mmol) and imidazole (0.37 g, 5.5 mmol) were dissolved in anhydrous dichloromethane (50 mL) under N_2. Iodine (1.39 g, 5.5 mmol) was added slowly over 5 min resulting in a yellow suspension. 5-Hexen-1-ol (**5.82**) (0.60 mL, 5.0 mmol) was added and the reaction mixture stirred for 1 h. The mixture was filtered before washing with aqueous 1 M aqueous sodium thiosulfate (1 M) and saturated aqueous NaCl (50 mL), dried ($MgSO_4$) and concentrated *in vacuo*. Flash chromatography (silica; 1:9 ethyl acetate/petroleum ether) gave the desired iodide as a colourless, clear liquid (1.03 g, 98%).

Spectral properties are in agreement with those in the literature. [35]

^{1}H NMR ($CDCl_3$) δ: 5.79 (m, 1H, C**H**=CH_2) 5.03-4.95 (m, 2H, CH=C**H$_2$**), 3.19 (t, 1H, C**H$_2$**I, *J*=7.0 Hz), 2.10-2.05 (m, 2H, CH_2=CHC**H$_2$**), 1.86-1.80 (m, 2H, C**H$_2$**CH_2I), 1.53-1.47 (m, 2H, C**H**$_2(CH_2)_2$I).

6.6.5 Attempted Synthesis of *trans*-2-Aminocyclonon-4-ene-1-carboxylic Acid (5.87)

(2*S*)-2-{(1*S*)-1-[(*tert*-butoxycarbonyl)amino]but-3-en-1-yl}oct-6-enoate (5.86)

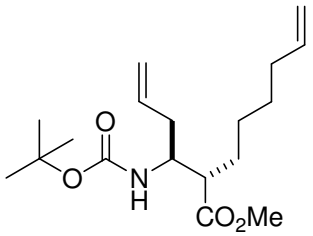

Lithium bis(trimethylsilyl)amide (1.0 M solution in hexanes; 0.99 mL, 0.82 mmol) was added to anhydrous tetrahydrofuran (2 mL) at -40 ºC under N_2. Boc-β^3hAllylglycine methyl ester (**5.77**) (100 mg, 0.41 mmol) dissolved in tetrahydrofuran (1 mL) was added slowly, stirred for 2 h, then cooled to -78 ºC. 6-Iodohex-1-ene (250 μL, 1.8 mmol) was added and the reaction mixture stirred at -78 ºC for 2 h then allowed to warm to rt over 16 h. The reaction was quenched was saturated aqueous NH_4Cl and diluted with ethyl acetate. The organic layer was separated, washed with saturated aqueous NaCl, dried ($MgSO_4$) and concentrated *in vacuo*. The crude mixture was purified by column chromatography (silica; 0:1-1:9 ethyl acetate, petroleum ether) to give the product as a colourless oil (41 mg, 31%).

^{1}H NMR ($CDCl_3$) δ: 5.76 (m, 2H, 2 x C**H**=CH_2), 5.32 (d, 1H, N**H**, *J*=9.8 Hz), 5.07-4.91 (m, 4H, 2 x CH=C**H$_2$**), 3.82 (m, 1H, NHC**H**), 3.68 (s, 3H, OC**H$_3$**), 2.57 (m, 1H, COC**H**), 2.23-2.13 (m, 2H, NHCHC**H$_2$**), 2.02 (m, 2H, $COCH(CH_2)_3$C**H$_2$**), 1.66 (m, 1H, COCHC**H**H), 1.54 (m, 1H, COCHC**H**H), 1.42 (s, 9H, $OC(CH_3)_3$), 1.36 (m, 3H, $COCHCH_2CH$**H**C**H$_2$**), 1.25 (m, 1H, $COCHCH_2$C**H**H).

^{13}C NMR ($CDCl_3$) δ: 175.6, 155.7, 138.6, 134.2, 117.7, 114.4, 79.0, 51.5, 50.9, 47.6, 38.9, 33.4, 29.7, 28.6, 28.3, 26.8.

HRMS calcd for $C_{18}H_{32}NO_4$ (MH^+) 326.2331; found 326.2325.

$[\alpha]_D$ = -6.7 (c = 0.01, $CDCl_3$)

Dimethyl (1*S*,2*S*,7*S*,8*S*)-2,7-bis[(*tert*-butoxycarbonyl)amino]-(4*E*,13*E*)-cyclooctadeca-4,13-diene-1,8-dicarboxylate *and* dimethyl (1*S*,2*S*,10*S*,11*S*)-2,11-bis[(*tert*-butoxycarbonyl)amino]-(4*E*,13*E*)-cyclooctadeca-4,13-diene-1,10-dicarboxylate (5.88 and 5.89)

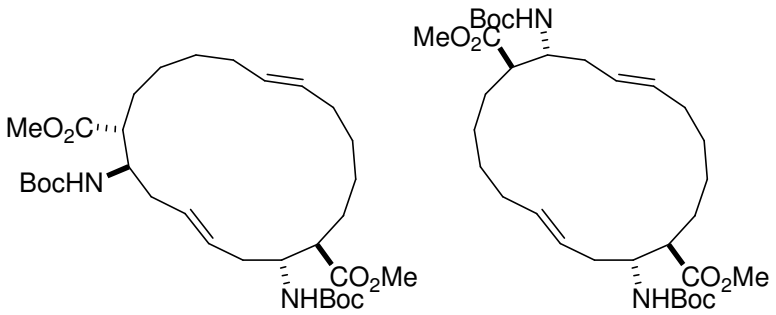

Conditions A: Diene **5.86** (10 mg, 31 μmol) was dissolved in dichloromethane (10.2 mL) and stirred under N_2. Grubbs' 1st Gen. catalyst (2.5 mg, 3.1 mmol) was added and the reaction mixture was refluxed for 36 h. The solvent was removed *in vacuo* and the crude residue was purified by column chromatography (silica; 0:1→1:19→1:9 ethyl acetate, petroleum ether) to give an inseparable mixture of dimer products **5.88** and **5.89** in a ratio of 1.4:1, as a light brown oil (5.5 mg, 62%).

Conditions B: Diene **5.86** (30 mg, 92 μmol) was dissolved in dichloromethane (92 mL) and stirred under N_2. Grubbs' 2nd Gen. catalyst (8 mg, 9.2 mmol) was added and the reaction mixture was refluxed for 36 h. The solvent was removed *in vacuo* and the crude residue was purified by column chromatography (silica; 0:1→1:19→1:9 ethyl acetate, petroleum ether) to give an inseparable mixture of dimer products **5.88** and **5.89** in a ratio 1.9:1, as a light brown oil (21 mg, 77%).

Conditions C: Diene **5.86** (10 mg, 31 μmol) was dissolved in dichloromethane (100 mL) and degassed under N_2. Grubbs' 2nd Gen. catalyst (2.5 mg, 3.1 mmol) was added and the reaction mixture was heated in the microwave reactor for 10 min on 100% power. The solvent was removed *in vacuo* and the crude residue was purified by column chromatography (silica;

0:1→1:19→1:9 ethyl acetate, petroleum ether) to give an inseparable mixture of dimer products **5.88** and **5.89** in a ratio of 49:1, as a light brown oil (6.5 mg, 70%).

Minor isomer **5.89**: ^{1}H NMR (C_6D_6) δ: 5.94 (d, 2 x N**H**, *J*=5.3 Hz), 5.26 (m, 2H, NHCHCH$_2$C**H**=CH), 5.07 (m, 2H, CH(CH$_2$)$_4$C**H**=CH), 4.01 (m, 2H, NHC**H**), 3.19 (s, 6H, OMe), 2.85, (m, 2H, C**H**CO), 2.58 (m, 2H, NHCHC**H**H), 2.02 (m, 2H, COCH(CH$_2$)$_3$C**H**H), 1.89 (m, 2H, NHCHCH**H**), 1.88 (m, 2H, COCHC**H**H), 1.73 (m, 2H, COCH(CH$_2$)$_3$C**H**H), 1.45 (m, 2H, COCHCH**H**).

Major isomer **5.88**: ^{1}H NMR (C_6D_6) δ: 5.92 (d, 2 x N**H**, *J*=5.6 Hz), 5.21 (m, 4H, C**H**=C**H**), 4.07 (m, 2H, NHC**H**), 2.74 (dt, 2H, C**H**CO, *J*=7.5, 7.5, 3.4 Hz), 2.61 (m, 2H, NHCHCH**H**), 2.01 (m, 2H, NHCHC**H**H), 1.82 (m, 4H, COCH(CH$_2$)$_3$C**H$_2$**), 1.64 (m, 4H, C**H$_2$**CHCO), 1.44 (m, 2H, C**H**HCH$_2$CHCO), 1.43 (m, 2H, CH**H**CH$_2$CH$_2$CHCO), 1.23 (m, 2H, C**H**HCH$_2$CH$_2$CHCO), 1.22 (m, 2H, CH**H**CH$_2$CHCO).

^{13}C NMR ($CDCl_3$) δ: selected peaks 134.1, 131.2, 129.8, 126.6, 79.1, 79.1, 51.7, 51.5, 51.2, 46.9, 45.6, 37.7, 32.3, 31.6, 29.6, 29.4, 28.4, 28.0, 27.4, 26.0, 25.9.

HRMS calcd for $C_{32}H_{55}N_2O_8$ (MH^+) 595.3958; found 595.3970.

6.7 References

1. Seebach, D.; Beck, A. K.; Bierbaum, D. J., *Chemistry & Biodiversity* **2004,** 1, (8), 1111-1239.
2. Bruker-AXS, S., **1997-1999**.
3. Sheldrick, G. M., Sect. A. In *Acta Crystallogr.*, 1990; Vol. A46, p 467.
4. Sheldrick, G. M., *SADABS*. University of Gottingen: 1998.
5. Loring, J. S. 2000. Ph.D. Thesis, University of California at Davis.
6. McNaughton, B. R.; Bucholtz, K. M.; Camaano-Moure, A.; Miller, B. L., *Organic Letters* **2005,** 7, (4), 733-736.
7. Koziara, A.; Osowskapacewicka, K.; Zawadzki, S.; Zwierzak, A., *Synthesis-Stuttgart* **1985**, (2), 202-204.
8. Svedhem, S.; Hollander, C.-A.; Shi, J.; Konradsson, P.; Liedberg, B.; Svensson, S. C. T., *Journal of Organic Chemistry* **2001,** 66, (13), 4494-4503.
9. Sigma-Aldrich, (2006). *62330 Fluka* (±)-*α-Lipoamide BioChemika, ≥98.0%* (*HPLC*) Retrieved December 17th, 2006, from Sigma Aldrich New Zealand, http://www.sigmaaldrich.com/catalog/search/ProductDetail/FLUKA/62330.
10. Lin, S.-Y.; Chen, C.-h.; Lin, M.-C.; Hsu, H.-F., *Analytical Chemistry* **2005,** 77, (15), 4821-4828.
11. Gouliaev, A. H.; Ho, J.; Felding, J.; Sams, C.; Pedersen, H.; Jensen, K. B.; Hansen, A. H.; Lundorf, M. D.; Husemoen, G. N.; Franch, T.; Thisted, T. A building block capable of transferring a functional entity in preparation of DNA duplexes. 2003-DK174 (2003078626), 20030314., 2003.
12. Gruzman, A.; Hidmi, A.; Katzhendler, J.; Haj-Yehie, A.; Sasson, S., *Bioorganic & Medicinal Chemistry* **2004,** 12, (5), 1183-1190.
13. Ohlsson, J.; Magnusson, G., *Tetrahedron* **2000,** 56, (51), 9975-9984.
14. Beer, P. D.; Smith, D. K., *Journal of the Chemical Society, Dalton Transactions: Inorganic Chemistry* **1998**, (3), 417-423.
15. Sun, H. W., Qingmin; Huang, Runqiu; Li, Heng; Li, Yonghong., *Journal of Organometallic Chemistry* **2002,** 655, (1-2), 182-185.
16. Johnson, R. L.; Verschoor, K., *Journal of Medicinal Chemistry* **1983,** 26, (10), 1457-1462.
17. Gopi, H. N.; Roy, R. S.; Raghothama, S. R.; Karle, I. L.; Balaram, P., *Helvetica Chimica Acta* **2002,** 85, (10), 3313-3330.
18. Seebach, D.; Overhand, M.; Kuehnle, F. N. M.; Martinoni, B., *Helvetica Chimica Acta* **1996,** 79, (4), 913-941.
19. Dutot, L.; Gaucher, A.; Wright, K.; Wakselman, M.; Mazaleyrat, J.-P.; Oancea, S.; Peggion, C.; Formaggio, F.; Toniolo, C., *Tetrahedron: Asymmetry* **2006,** 17, (3), 363-371.
20. Payne, R. J.; Brown, K. M.; Coxon, J. M.; Morton, J. D.; Lee, H. Y.-Y.; Abell, A. D., *Australian Journal of Chemistry* **2004,** 57, (9), 877-884.
21. Schreiber, J. V.; Frackenpohl, J.; Moser, F.; Fleischmann, T.; Kohler, H.-P. E.; Seebach, D., *ChemBioChem* **2002,** 3, (5), 424-432.
22. Tsuboi, S.; Okada, Y., *Chemical & Pharmaceutical Bulletin* **1989,** 37, (1), 46-9.
23. Voelkert, M.; Koul, S.; Mueller, G. H.; Lehnig, M.; Waldmann, H., *Journal of Organic Chemistry* **2002,** 67, (20), 6902-6910.

24. Seebach, D.; Studer, A.; Pfammatter, E.; Widmer, H., *Helvetica Chimica Acta* **1994,** 77, (7), 2035-50.
25. Erickson, K. L.; Markstein, J.; Kim, K., *Journal of Organic Chemistry* **1971,** 36, (8), 1024-30.
26. Trost, B. M.; Salzmann, T. N.; Hiroi, K., *Journal of the American Chemical Society* **1976,** 98, (16), 4887-902.
27. Dexter, C. S.; Jackson, R. F. W.; Elliott, J., *Journal of Organic Chemistry* **1999,** 64, (20), 7579-7585.
28. Ozinskas, A. J.; Rosenthal, G. A., *Journal of Organic Chemistry* **1986,** 51, (26), 5047-50.
29. Howarth, N. M.; Wakelin, L. P. G., *Journal of Organic Chemistry* **1997,** 62, (16), 5441-5450.
30. Alcon, M.; Moyano, A.; Pericas, M. A.; Riera, A., *Tetrahedron: Asymmetry* **1999,** 10, (23), 4639-4651.
31. Conti, P.; De Amici, M.; Grazioso, G.; Roda, G.; Negra, F. F. B.; Nielsen, B.; Stensbol, T. B.; Madsen, U.; Braeuner-Osborne, H.; Frydenvang, K.; De Sarro, G.; Toma, L.; De Micheli, C., *Journal of Medicinal Chemistry* **2004,** 47, (27), 6740-6748.
32. Kaul, R.; Surprenant, S.; Lubell, W. D., *Journal of Organic Chemistry* **2005,** 70, (10), 3838-3844.
33. Raju, B. G.; Patel, D. V.; Trias, J. Administration of negamycin or deoxynegamycin for the treatment of bacterial infections, and preparation thereof. 2003109583, 2003.
34. Kaur, N.; Delcros, J.-G.; Martin, B.; Phanstiel, O., *Journal of Medicinal Chemistry* **2005,** 48, (11), 3832-3839.
35. Mori, K., *European Journal of Organic Chemistry* **2005**, (10), 2040-2044.

Appendix A Electroanalytical Methods

Electroanalytical methods encompass all electrochemical techniques that are used to study the electron transfer mechanisms between an electrode and a redox active species. The most important techniques for looking at electron transfer processes require the potential of the cell to be controlled, while the current is observed.

A.1 The Potentiostat

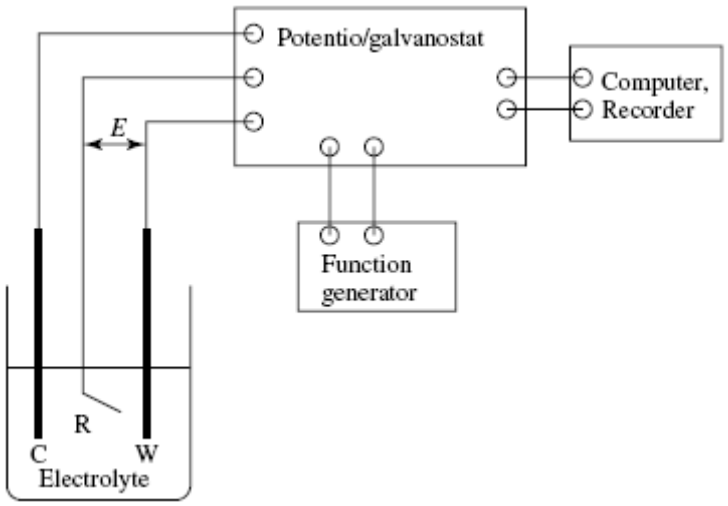

Figure A.1 A schematic diagram of the experimental setup for controlled-potential experiments. E: represents the potential difference; C: counter electrode; R: reference electrode; W: working electrode.

A potentiostat is a device that controls the voltage difference between a working electrode and a reference electrode. Both electrodes are contained in an electrochemical cell, along with a counter electrode. The voltage at the working electrode is controlled with respect to the reference electrode, by current through the counter electrode. The working electrode is often an "inert" material such as gold, platinum, or glassy carbon. In these cases, the working electrode serves as a surface on which the electrochemical reaction takes place.

A potentiostat can perform a number of important electrochemical experiments, of which there are many. The study of electron transfer in this work will focus on two techniques, which are cyclic voltammetry and chronoamperometry. The technical details of these two

techniques will be preceded by a discussion of electron transfer mechanisms at the electrode.

A.2 Electron Transfer Mechanisms at the Electrode

All electrochemical techniques involve the transfer of electrons between a surface, which is generally a metal or a semiconductor, and a redox-active species either in solution or bound to the surface. The electrode reaction can be an anodic process, where the species is oxidised by the loss of electrons to the electrode; or a cathodic process, where the species is reduced by the gain of electrons from the electrode. By convention, the current density (I) for anodic and cathodic processes are positive and negative in quantity, respectively.

The electrochemistry of organic compounds is particularly important, as nearly all organic compounds can be oxidised or reduced. Just as organic reaction mechanisms are classified for thermal reactions (such as S_N1, S_N2, etc), so are reactions that are induced by, or that include the transfer of electrons. Defining a specific electrode reaction mechanism requires that a number of parameters be determined; some of these include the potential at which the reaction proceeds, the proof of any intermediates, the electron stoichiometry, the kinetics of the various reaction steps, and the transport properties of the species involved, for processes in which diffusion to the electrode is important.

The overall process of a typical reaction of an organic species diffusing at an electrode is represented schematically in Figure A.2. In this process, the educt (≡ reactant; **E**$^{'}$), which may have undergone a chemical reaction prior to electron transfer (denoted **E**), is transported to the surface. After adsorption at the surface, electron transfer gives the product (**P**), which can then undergo further chemical reactions to form other products (denoted **P**$^{'}$).

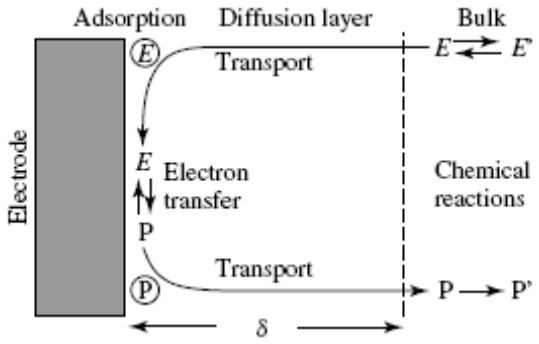

Figure A.2 Steps in a typical organic reaction. E: educt (species prior to electron transfer); P: products (species formed during or after electron transfer); circles denote adsorbed species.

If the educt and product are covalently or physiochemically adsorbed to the surface over a timescale much larger than diffusion or electron transfer, then the process is greatly simplified, and the overall reaction kinetics are different. The transport of **E** to the surface, which is largely dependant on diffusion, is often the rate-limiting step in electrochemical reactions. Therefore, if the species is immobilised on the surface, there is no diffusion event. Consequently, the overall reaction rate depends solely on the kinetics of electron transfer.

Electrochemical mechanisms can be grouped into three general types: reversible, irreversible, and quasi-reversible. Generally, for a surface phase species, the reaction can be defined as either chemically reversible or irreversible. In the latter case, electron transfer is accompanied by a chemical reaction, rendering the product structurally different to the starting material. In solution phase electrochemistry, the type of mechanism is often dependant on the kinetics of electron transfer with respect to the rate of mass transport (diffusion, migration and convection), and is therefore more complex. As this thesis deals with immobilised (non-diffusing) species, only surface species will be considered from this point forward.

A.3 The Cyclic Voltammetry Technique

Cyclic voltammetry is the most widely used electroanalytical technique, because it is a straightforward technique, and provides a wealth of mechanistic information. Voltammetry is used frequently and routinely to define the redox properties of newly

synthesized organic compounds, giving an‘electrochemical spectrum’, akin to the use of NMR to define the structural properties of compounds.

Cyclic voltammetry, a type of linear sweep voltammetry, is an electrochemical technique that monitors current as a function of potential, where the potential is continuously changed as a linear function of time. Cyclic voltammetry is differentiated from simple linear sweep voltammetry because a scan in one direction to a potential value is then reversed back to the starting potential (Figure A.3).

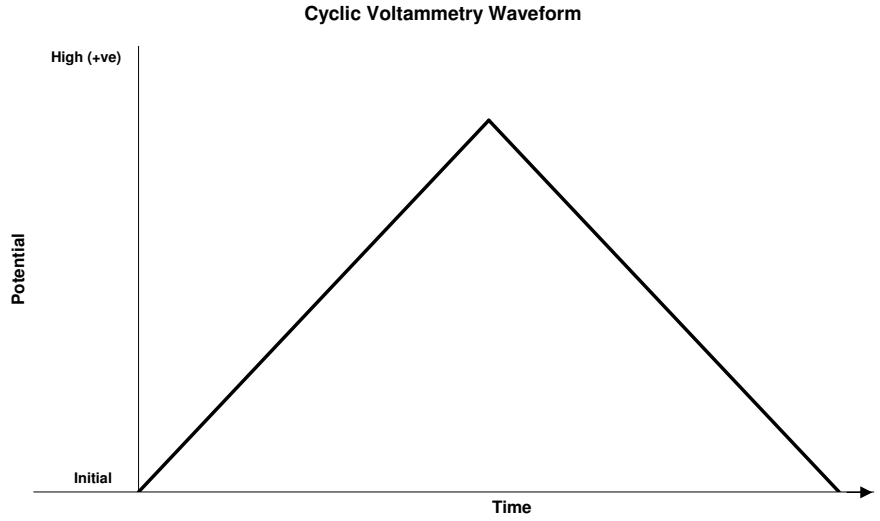

Figure A.3 Waveform of a typical cyclic voltammetry experiment for a +ve forward scan, followed by a reverse scan.

The potential range is chosen so that only the reduced (oxidised) form of the species is present at the initial potential, and only the oxidised (reduced) form at the vertex (switching) potential. The potential is scanned over time at a constant rate (scan rate), to a value where all of the redox centres are in the oxidised (reduced) form. As the species is oxidised (reduced), an anodic (cathodic) current is observed. If the reduction reaction is a chemically reversible process, then on the reverse scan (returning to the initial potential), the species reverts to the reduced (oxidised) form, generating a cathodic current.

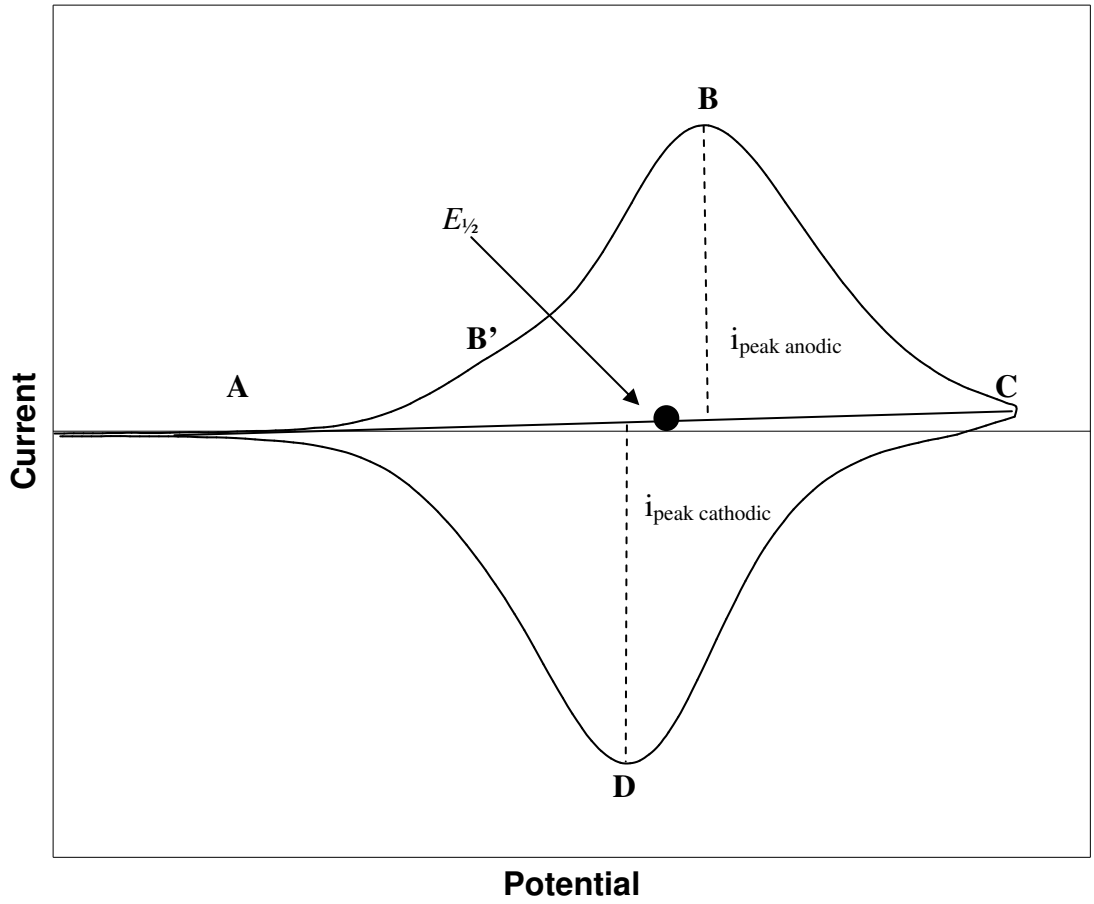

Figure A.4 Typical cyclic voltammagram of a reversible surface-confined redox process. (A) Reduced form, (B) anodic peak, (C) oxidised form and (D) cathodic peak.

Typically, voltammetry data is plotted as current response against potential, as shown in Figure A.4 for a one electron reversible process. The conversion of the redox species from the reduced form (**A**) to the oxidised form (**C**), gives an anodic current, which peaks (**B**) when the rate of oxidation is maximum. Similarly, the reverse scan cathodic current peaks (**D**) as the species is reduced to the original reduced form (**A**). Other electron transfer mechanisms give rise to cyclic voltammagrams with different appearances. A second peak (prepeak) (**B'**) due to another oxidation event can occur when surface immobilised redox groups are in different environments on the surface. The presence of a second peak is unfavourable if the electron transfer rate is to be determined.

A.4 Cyclic Voltammetry Theory

Voltammetry is diagnostic in revealing the type of electron transfer mechanism that is operating in a redox system. The potentials at which electron transfer processes occur and the effect of changing the scan rate on peak potential can tell us whether the species are in solution or surface-bound, the electron transfer reactions are reversible or irreversible, and can give information about the kinetics of the processes.

The Nernst equation describes the concentration of oxidised and reduced species at equilibrium on the surface at a given electrode potential (E), where $E^{0'}$ is the standard electrode potential pertaining to a specific redox centre, R is the universal gas constant, T is the temperature, n is the number of electrons in the half-reaction, F is the Faraday constant, and [Red] and [Ox] are the concentration of reduced and oxidised species, respectively (Equation A.1).

$$E = E^{0'} - \frac{RT}{nF} \ln \frac{[\text{Red}]}{[\text{Ox}]}$$

Equation A.1 The Nernst equation, which describes the equilibrium concentration of oxidised and reduced species on the surface, for a given electrode potential (E).

The formal potential ($E^{0'}$) may be obtained directly from the cyclic voltammagram, as it frequently corresponds to the average of the anodic and/or cathodic peak positions (irreversible mechanisms may only have an anodic peak) (Figure A.5). In an ideal reversible process, the anodic and cathodic peaks have a similar area. If no chemical steps are coupled to electron transfer at the electrode, then a 'pure electron transfer reaction' mechanism exists. The pure electron transfer reaction mechanism is fully described by $E^{0'}$ (thermodynamics), n (stoichiometry), as well as k_{et}, and α (kinetics). Visually, this mechanism is characterised by a fully developed reverse peak in the cyclic voltammagram, as shown in Figure A.4.[1]

Irreversible processes are identified as having either no reverse peak, lack of peak symmetry, or a change in peak height or position over successive scans. Surface

immobilised species exhibit irreversible behaviour if electron transfer is coupled with a chemical reaction, such as oxidation of an aldehyde to an acid, or when the rate of electron transfer is much slower than the scan rate.

Voltammetry can also distinguish between adsorbed species and solution species. Because species in solution must diffuse to the surface before electron transfer can occur, diffusion plays an important and often rate-limiting role. The relationship between peak current or area (with the units A.V) and scan rate can determine whether a species is in solution or bound at the surface. The voltammetry peak current of a solution phase species with a reversible electron transfer mechanism has an inverse squared dependence on scan rate. Conversely, with surface bound species, the relationship between peak current (or area) and scan rate is linear. The peak area for a non-diffusing system (i.e. a surface species) is directly proportional to the number of electrons transferred in the redox process. Therefore, voltammetry also yields the coverage of the redox centers in the monolayer, if the area of the electrode is known. A cyclic voltammagram with zero peak splitting (90-100 mV peak half-width) indicates a homogeneous environment around the redox centers, as the formal potential of all the redox centers are the same. This allows a means of determining the level of order within the monolayer.

Double-layer charging occurs during a scan, because of the increasing charge at the electrode surface as the potential is increased to more positive or negative values. This surface charge attracts oppositely charged ions from the solution. This is seen experimentally as a band of increased current spanning the centre of the voltammagram (Figure A.5). The anodic and cathodic peaks are additive to the double-layer capacitance current. The anodic and cathodic peak area is calculated by fitting a baseline to the peaks, using curve-fitting software, as shown in Figure A.5. This removes the double-layer capacitance contribution from the peak area.

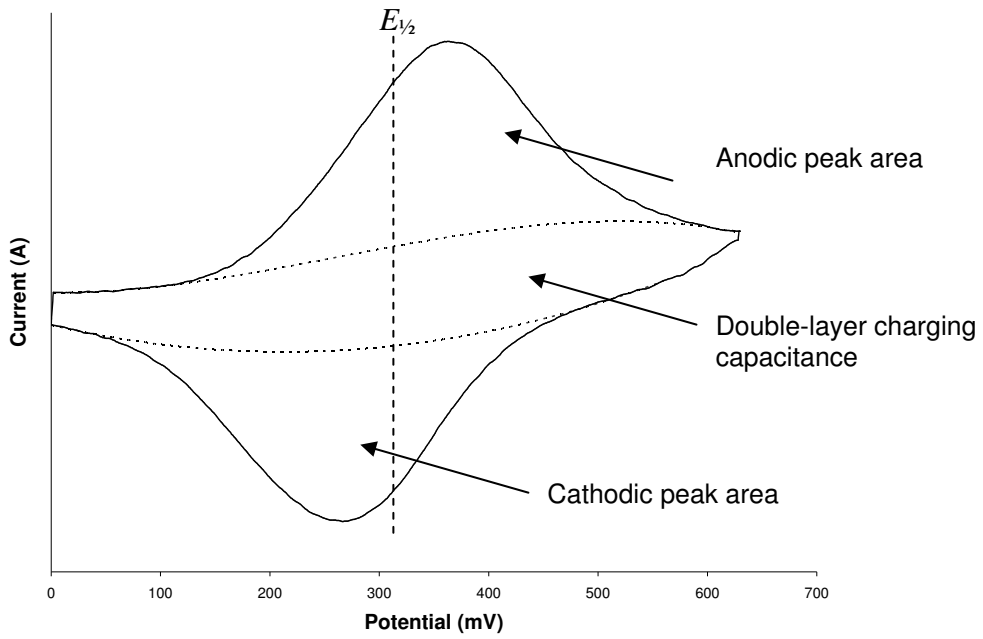

Figure A.5 A cyclic voltammagram showing siginificant double-layer charging.

The capacitance layer for well-ordered SAMs is small, and comparatively larger for those that are disordered. This is because ions can more easily permeate into the surface defects of disordered monolayers, compared with a tightly packed ordered monolayer (Figure A.6a and b).

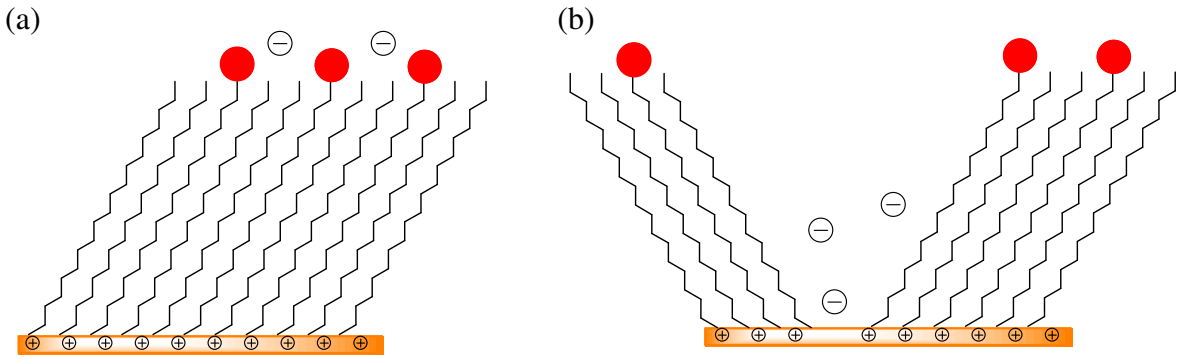

Figure A.6 Double layer charging at SAMs with (a) a well-ordered monolayer; (b) a disordered monolayer.

A.5 The Chronoamperometry Technique

Chronoamperometry (CA) is an electrochemical technique in which the potential of the working electrode is stepped and the resulting current from Faradaic processes occurring at the electrode (caused by the potential step) is monitored as a function of time. CA is a standard method for the determining the kinetics of electron transfer because because it operates on the same millisecond timescale as electron transfer and directly measures the rate of current decay across the surface species. Deducing the electron transfer kinetics from voltametric analysis is more difficult and time consuming, as it relies on modelling of the peak redox data.

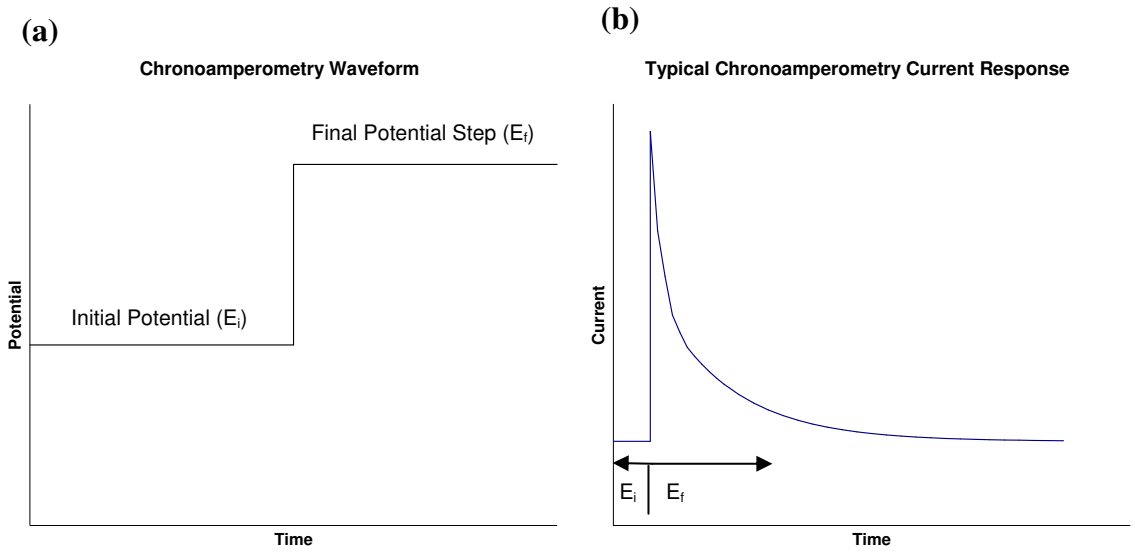

Figure A.7 (a) Waveform of the chronoamperometry technique, (b) and the typical current response.

The CA technique has a very simple potential wave form (Figure A.7a). The *initial potential* is a point where the redox species is in a single oxidation state. The potential is changed instantaneously from the *initial potential* to the *final potential step*, and is held at this value. This potential is at a value that drives the desired reaction at the electrode.

The difference between the step potential (E_f), and the formal potential ($E^{0'}$) of the species in chronoamperometry experiments is known as the overpotential (η), ($\eta = E^0 - E_f$). As the name implies, the step is to a potential different to $E^{0'}$, so that the population of the initially reduced species changes rapidly to the predominantly oxidised form (or vice versa). When the potential is changed from the initial potential to the step potential, a large current is initially observed, which decays exponentially with time (Figure A.7b), as described by the equation $i = i_0 \exp(-k_{et}t)$ where i is the current, i_0 is the initial current at t=0, and t is time.[3] Chronoamperometry data is typically collected for a number of overpotential values, so that the standard rate of electron transfer (k_{et}^0) can be determined (see section A.6).

A.6 Chronoamperometry Theory

Chronoamperometry data for surface-confined films is typically analysed by plotting the natural log of current versus time (Figure A.8b). This plot gives rate data for electron transfer (k_{et}) between the surface and the redox centre at a particular overpotential. The semilog plot contains two features: the initial steep slope of the capacitive response, followed by the moderate slope of the Faradaic response. The capacitive response (**C** in Figure A.8b) which dominates for the first 1-2 ms, is caused by charging the double-layer capacitance as the applied potential is changed.

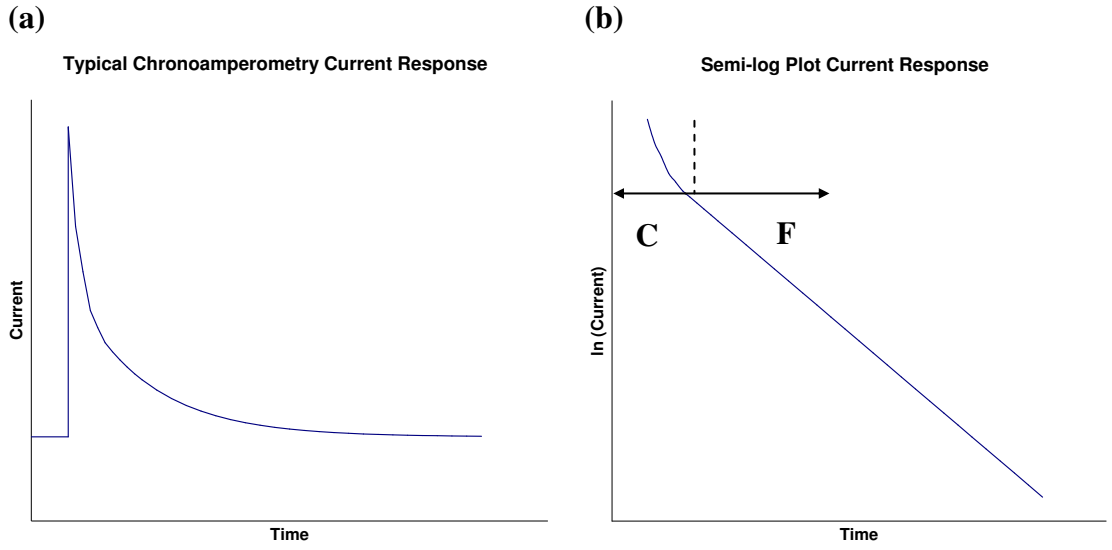

Figure A.8 (a) The current response from a potential step experiment; (b) the semi-log plot of the current response. 'C' denotes the initial capacitive response, and 'F' is the faradaic response.

The Faradaic response (**F** in Figure A.8b) occurs as a result of electron transfer between the metal and the redox probe. If the environment around the redox centres is homogeneous, then the slope (Faradaic response) will be linear with respect to time. If the environment is not homogeneous, then the slope is not linear and no rate data can be obtained. The slope of the data in the linear Faradaic portion of the plot gives the electron transfer rate constant k_{et} (s^{-1}) at that η.

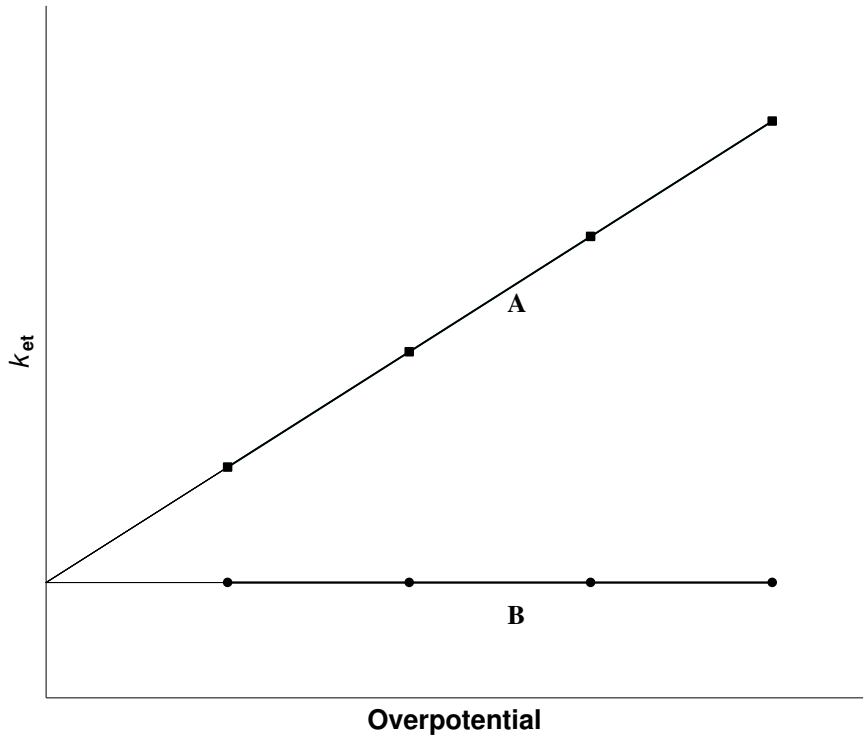

Figure A.9 A plot showing the relationship between overpotential and k_{et}. Data set A is dependant on η, which indicates that tunnelling is the dominant electron transfer. Data set B shows no dependence on η, which indicates a hopping mechanism.

To obtain useful kinetic data from surface species, a plot is constructed which contains k_{et} data for a range of η, derived from the log current/time plot. This k_{et} is plotted against overpotential, typically showing a linear relationship. Extrapolation of the data to zero overpotential gives the k_{et}^0 between the gold surface and the redox group, as described by the equation $k_{et} = k_{et}^0 \exp(-\alpha n f \eta)$, where α is the activity coefficient, n is the number of electrons transferred and f is equal to F/RT where F, R, and T are the Faraday and gas constants, and absolute temperature, respectively, and η is overpotential.[2] The dependence of k_{et} on overpotential (the slope) indicates the mode of electron transfer. The tunnelling mechanism shows a significant dependence on k_{et} while, the hopping mechanism has a low

dependence (Figure A.9, data set **A** and **B**, respectively).[3] The hopping mechanism gives fast electron transfer, so the rate-limiting step is the transfer of charge from the surface to the linker group, or the peptide to the ferrocene, rather than along the peptide backbone. A tunnelling mechanism requires the transfer of electrons through the molecular orbitals of the peptide and is distance dependent. Therefore, a greater overpotential gives a greater driving force to electron transfer. Furthermore, a larger value of k_{et}^{0} between the surface and the redox centre implies faster electron transfer. In summary, CA gives both a quantitative and qualitative measure of electron transfer in surface immobilised peptides.

Appendix B

The UV-Vis trace of peptide **4.60** at 3mM concentration in 2,2,2-trifluoroethanol is shown below.

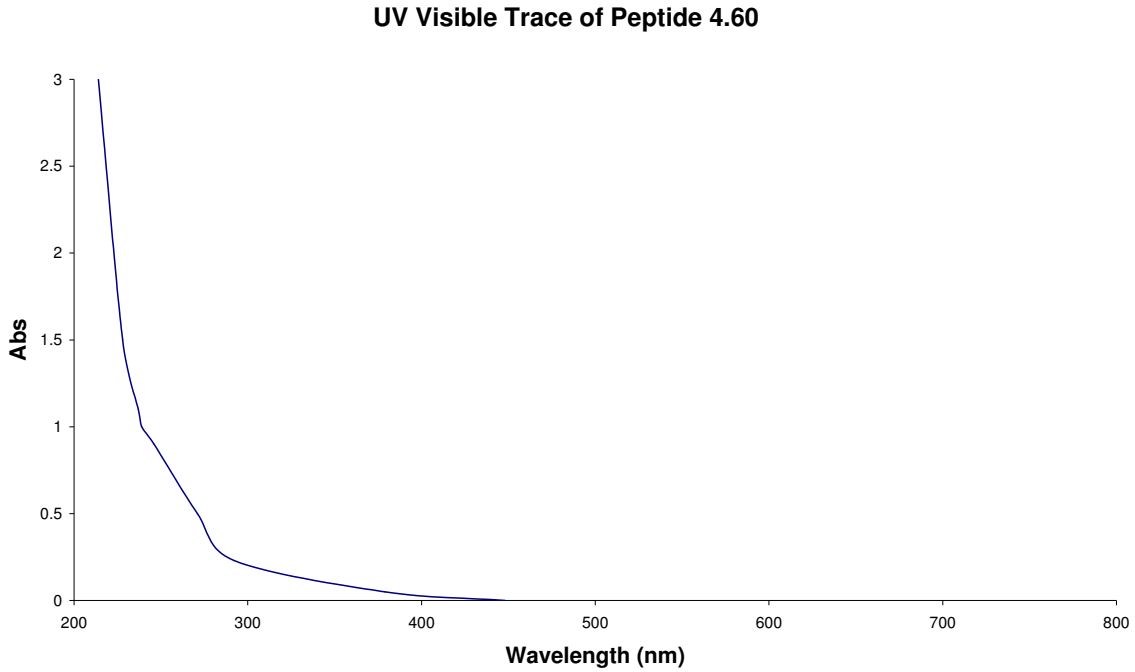

Appendix C Crystallographic Data

C.1 Crystallographic data for cycloheptene-based β-amino acid 5.63

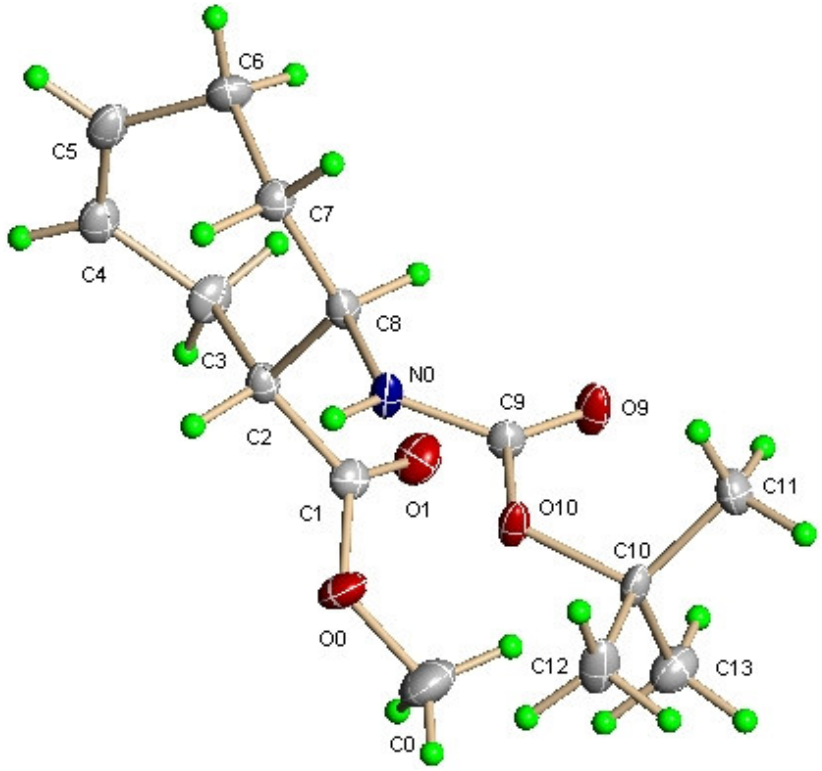

Empirical formula	$C_{14}H_{23}NO_4$	
Formula weight	269.33 g mol^{-1}	
Temperature	100 (1) K	
Wavelength	0.71073 Å (Mo-Kα radiation)	
Crystal system	Orthorhombic	
Space group	$P2_12_12_1$	
Unit cell dimensions	a = 5.1692(2) Å	α = 90 °
	b = 16.6293(7) Å	β = 90 °
	c = 16.8780(7) Å	γ = 90 °
Volume	1450.84(10) Å^3	

Z	4
Calculated density	1.233 Mgm^{-3}
Absorption coefficient	0.090 mm^{-1}
F(000)	584
Crystal size	0.43 x 0.42 x 0.35 mm
θ range for data collection	1.72 to 34.77 º
Limiting indices	$-8 \leq h \leq 7$, $-23 \leq k \leq 25$, $-26 \leq l \leq 24$
Reflections collected	28616
Independent reflections	5778 [$R_{(int)} = 0.0337$]
Completeness to theta = 25.00	100.0%
Absorption correction	Semi-empirical from equivalents
Max. and min. transmission	0.97 and 0.735
Refinement method	Full-matrix least-squares on F^2
Data / restraints / parameters	5778 / 0 / 176
Goodness-of-fit on F^2	1.093
Final R indices [I>2sigma(I)]	$R_1 = 0.0404$, $wR_2 = 0.1071$
R indices (all data)	$R_1 = 0.0484$, $wR_2 = 0.1159$
Absolute structure parameter	-0.5(6)
Largest diff. peak and hole	0.474 and -0.257 $eÅ^{-3}$

Table C.1 Atomic coordinates (x 10^4) and equivalent isotropic displacement parameters ($Å^2$ x 10^3) for **5.63**. U(eq) is defined as one third of the trace of the orthogonalized U_{ij} tensor.

Atom	x	y	z	U(eq)
C(0)	1995(3)	4898(1)	1965(1)	38(1)
N(0)	104(2)	4269(1)	4229(1)	16(1)
O(10)	1593(1)	3130(1)	3740(1)	19(1)
O(9)	4450(1)	4131(1)	4047(1)	26(1)
C(1)	948(2)	5579(1)	3133(1)	19(1)
C(2)	-913(2)	5655(1)	3824(1)	16(1)
C(3)	-1038(2)	6552(1)	4053(1)	22(1)
O(0)	197(2)	5018(1)	2608(1)	27(1)
C(4)	-3256(2)	6776(1)	4581(1)	24(1)
C(5)	-3443(2)	6523(1)	5324(1)	25(1)
C(6)	-1510(2)	5962(1)	5689(1)	24(1)
C(7)	-1426(2)	5137(1)	5276(1)	19(1)
O(1)	2909(2)	5969(1)	3055(1)	28(1)
C(8)	110(2)	5104(1)	4498(1)	15(1)
C(9)	2247(2)	3867(1)	4006(1)	16(1)
C(10)	3575(2)	2558(1)	3462(1)	18(1)

Atom	x	y	z	U(eq)
C(11)	5453(2)	2356(1)	4129(1)	22(1)
C(12)	1974(2)	1817(1)	3261(1)	26(1)
C(13)	4911(2)	2887(1)	2727(1)	26(1)

Table C.2 Bond lengths [Å] for **5.63**.

Bond	Length (Å)	Bond	Length (Å)
C(0)-O(0)	1.4432(14)	C(5)-C(6)	1.4997(16)
C(0)-H(0A)	0.96	C(5)-H(5)	0.93
C(0)-H(0B)	0.96	C(6)-C(7)	1.5387(14)
C(0)-H(0C)	0.96	C(6)-H(6A)	0.97
N(0)-C(9)	1.3476(11)	C(6)-H(6B)	0.97
N(0)-C(8)	1.4611(11)	C(7)-C(8)	1.5349(13)
N(0)-H(0)	0.86	C(7)-H(7A)	0.97
O(10)-C(9)	1.3481(11)	C(7)-H(7B)	0.97
O(10)-C(10)	1.4740(11)	C(8)-H(8)	0.98
O(9)-C(9)	1.2226(11)	C(10)-C(13)	1.5220(15)
C(1)-O(1)	1.2101(13)	C(10)-C(12)	1.5232(14)
C(1)-O(0)	1.3437(12)	C(10)-C(11)	1.5232(14)
C(1)-C(2)	1.5175(13)	C(11)-H(11A)	0.96
C(2)-C(3)	1.5422(13)	C(11)-H(11B)	0.96
C(2)-C(8)	1.5542(12)	C(11)-H(11C)	0.96
C(2)-H(2)	0.98	C(12)-H(12A)	0.96
C(3)-C(4)	1.4994(15)	C(12)-H(12B)	0.96
C(3)-H(3A)	0.97	C(12)-H(12C)	0.96
C(3)-H(3B)	0.97	C(13)-H(13A)	0.96
C(4)-C(5)	1.3273(17)	C(13)-H(13B)	0.96
C(4)-H(4)	0.93	C(13)-H(13C)	0.96

Table C.3 Bond angles [º] for **5.63**.

Atoms	Angle (º)	Atoms	Angle (º)
O(0)-C(0)-H(0A)	109.5	C(8)-C(7)-H(7A)	108.4
O(0)-C(0)-H(0B)	109.5	C(6)-C(7)-H(7A)	108.4
H(0A)-C(0)-H(0B)	109.5	C(8)-C(7)-H(7B)	108.4
O(0)-C(0)-H(0C)	109.5	C(6)-C(7)-H(7B)	108.4
H(0A)-C(0)-H(0C)	109.5	H(7A)-C(7)-H(7B)	107.4
H(0B)-C(0)-H(0C)	109.5	N(0)-C(8)-C(7)	107.38(7)
C(9)-N(0)-C(8)	123.85(7)	N(0)-C(8)-C(2)	109.39(7)
C(9)-N(0)-H(0)	118.1	C(7)-C(8)-C(2)	115.41(7)
C(8)-N(0)-H(0)	118.1	N(0)-C(8)-H(8)	108.1
C(9)-O(10)-C(10)	121.21(7)	C(7)-C(8)-H(8)	108.1
O(1)-C(1)-O(0)	122.84(10)	C(2)-C(8)-H(8)	108.1
O(1)-C(1)-C(2)	124.72(9)	O(9)-C(9)-N(0)	124.85(8)
O(0)-C(1)-C(2)	112.44(8)	O(9)-C(9)-O(10)	125.35(8)
C(1)-C(2)-C(3)	107.45(8)	N(0)-C(9)-O(10)	109.80(8)
C(1)-C(2)-C(8)	107.35(7)	O(10)-C(10)-C(13)	110.02(8)
C(3)-C(2)-C(8)	113.64(8)	O(10)-C(10)-C(12)	102.43(7)
C(1)-C(2)-H(2)	109.4	C(13)-C(10)-C(12)	110.78(9)
C(3)-C(2)-H(2)	109.4	O(10)-C(10)-C(11)	110.56(8)
C(8)-C(2)-H(2)	109.4	C(13)-C(10)-C(11)	113.11(9)
C(4)-C(3)-C(2)	114.91(8)	C(12)-C(10)-C(11)	109.42(8)
C(4)-C(3)-H(3A)	108.5	C(10)-C(11)-H(11A)	109.5
C(2)-C(3)-H(3A)	108.5	C(10)-C(11)-H(11B)	109.5
C(4)-C(3)-H(3B)	108.5	H(11A)-C(11)-H(11B)	109.5
C(2)-C(3)-H(3B)	108.5	C(10)-C(11)-H(11C)	109.5
H(3A)-C(3)-H(3B)	107.5	H(11A)-C(11)-H(11C)	109.5
C(1)-O(0)-C(0)	113.94(10)	H(11B)-C(11)-H(11C)	109.5
C(5)-C(4)-C(3)	122.61(10)	C(10)-C(12)-H(12A)	109.5
C(5)-C(4)-H(4)	118.7	C(10)-C(12)-H(12B)	109.5
C(3)-C(4)-H(4)	118.7	H(12A)-C(12)-H(12B)	109.5
C(4)-C(5)-C(6)	122.48(10)	C(10)-C(12)-H(12C)	109.5
C(4)-C(5)-H(5)	118.8	H(12A)-C(12)-H(12C)	109.5
C(6)-C(5)-H(5)	118.8	H(12B)-C(12)-H(12C)	109.5
C(5)-C(6)-C(7)	112.82(8)	C(10)-C(13)-H(13A)	109.5
C(5)-C(6)-H(6A)	109.0	C(10)-C(13)-H(13B)	109.5
C(7)-C(6)-H(6A)	109.0	H(13A)-C(13)-H(13B)	109.5
C(5)-C(6)-H(6B)	109.0	C(10)-C(13)-H(13C)	109.5
C(7)-C(6)-H(6B)	109.0	H(13A)-C(13)-H(13C)	109.5
H(6A)-C(6)-H(6B)	107.8	H(13B)-C(13)-H(13C)	109.5
C(8)-C(7)-C(6)	115.72(8)		

Table C.4 Hydrogen coordinates (x 10^4) and isotropic displacement parameters (A^2 x 10^3) for **5.63**.

	x	y	z	U (eq)
H(0A)	1875	5340	1601	57
H(0B)	1584	4407	1694	57
H(0C)	3723	4867	2171	57
H(0)	-1352	4020	4212	19
H(2)	-2634	5473	3660	19
H(3A)	563	6696	4317	26
H(3B)	-1147	6869	3571	26
H(4)	-4553	7106	4379	29
H(5)	-4824	6701	5631	30
H(6A)	-1938	5885	6243	29
H(6B)	193	6205	5663	29
H(7A)	-685	4750	5641	23
H(7B)	-3188	4970	5168	23
H(8)	1902	5258	4612	18
H(11A)	6543	2811	4232	33
H(11B)	6502	1905	3975	33
H(11C)	4499	2223	4599	33
H(12A)	1188	1611	3734	40
H(12B)	3074	1413	3033	40
H(12C)	651	1960	2887	40
H(13A)	3632	3044	2345	39
H(13B)	6003	2479	2503	39
H(13C)	5941	3345	2869	39

C.2 Crystallographic data for conjugate addition/fluorination product 5.43a

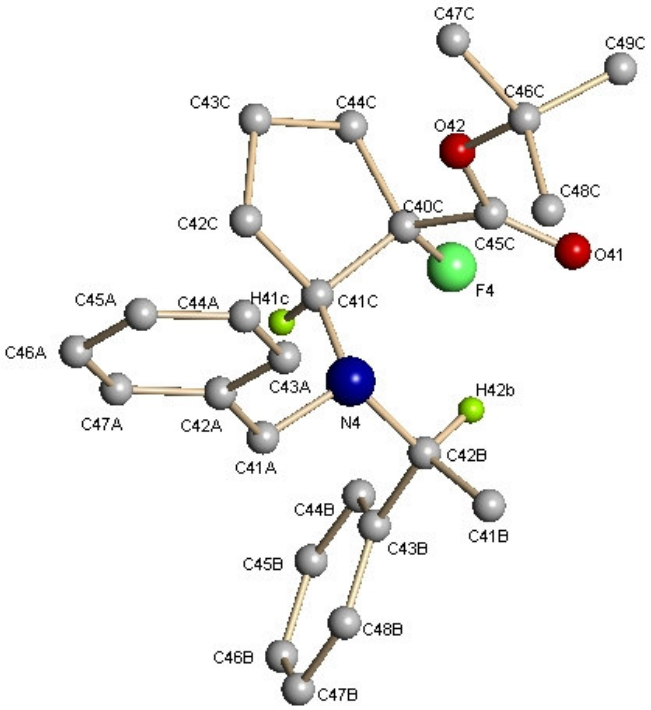

Figure C.1 Crystal structure of one of the four molecules in the asymmetric unit. The atom labelling pattern shown is consistent on all other structures, as desribed in the table below.

Atom Labels	Carbon	Nitrogen	Oxygen	Fluorine	Hydrogen*
Molecule 1	C11A-C17A C11B-C18B C10C-C19C	N1	O11 O12	F1	H(*number and letter code of attached carbon)*
Molecule 2	C21A-C27A C21B-C28B C20C-C29C	N2	O21 O22	F2	H(*number and letter code of attached carbon)*
Molecule 3	C31A-C37A C31B-C38B C30C-C39C	N3	O31 O32	F3	H(*number and letter code of attached carbon)*
Molecule 4	C41A-C47A C41B-C48B C40C-C49C	N4	O41 O42	F4	H(*number and letter code of attached carbon)*

* Only the hydrogen atoms attached to stereocentres are shown in Figure C.1

Empirical formula	$C_{25}H_{32}FNO_2$
Formula weight	397.52 $gmol^{-1}$
Temperature	293(2) K
Wavelength	0.71073 Å
Crystal system	Monoclinic
Space group	$P2_1$
Unit cell dimensions	a = 20.135(4) Å α = 90 °
	b = 8.4958(12) Å β = 92.644(5) °
	c = 26.436(5) Å γ = 90 °
Volume	4517.3(14) $Å^3$
Z	8
Density (calculated)	1.169 $Mg \cdot m^{-3}$
Absorption coefficient	0.079 mm^{-1}
F(000)	1712
Crystal size	0.97 x 0.16 x 0.11 mm^3
Theta range for data collection	0.77 to 25.05 °
Index ranges	$-22 \leq h \leq 23$, $-5 \leq k \leq 9$, $-31 \leq l \leq 16$
Reflections collected	11592
Independent reflections	8120 [$R_{(int)}$ = 0.0583]
Completeness to theta = 25.05°	94.7%
Max. and min. transmission	0.9914 and 0.9277
Refinement method	Full-matrix least-squares on F^2
Data / restraints / parameters	8120 / 1 / 1061
Goodness-of-fit on F2	0.993
Final R indices [I>2sigma(I)]	R_1 = 0.0505, wR_2 = 0.1155
R indices (all data)	R_1 = 0.0953, wR_2 = 0.1672
Absolute structure parameter	-10(10)
Largest diff. peak and hole	0.441 and -0.416 $eÅ^{-3}$

Table C.5 Atomic coordinates (x 10^4) and equivalent isotropic displacement parameters ($Å^2$ x10^3) for **5.43a**. U(eq) is defined as one third of the trace of the orthogonalized U_{ij} tensor.

	x	y	z	U(eq)		x	y	z	U(eq)
F(1)	7760(2)	1635(4)	3174(1)	28(1)	C(33B)	4840(3)	11209(8)	1309(2)	21(2)
N(1)	8429(2)	4796(6)	2742(2)	19(1)	C(34B)	4817(3)	12833(7)	1269(2)	25(2)
O(11)	9058(2)	1331(6)	3290(2)	32(1)	C(35B)	5090(4)	13611(8)	869(3)	32(2)
O(12)	9177(2)	1632(5)	2446(1)	23(1)	C(36B)	5399(4)	12768(9)	497(3)	37(2)
C(11A)	8384(3)	6285(8)	2460(2)	27(2)	C(37B)	5428(4)	11164(9)	531(3)	35(2)
C(12A)	8846(3)	6379(7)	2016(2)	23(2)	C(38B)	5149(3)	10386(8)	923(2)	26(2)
C(13A)	8663(4)	7236(9)	1588(2)	36(2)	F(4)	2068(2)	7093(5)	1520(1)	44(1)
C(14A)	9104(5)	7491(10)	1209(3)	54(2)	N(4)	2276(3)	4141(6)	807(2)	24(1)
C(15A)	9733(4)	6848(10)	1242(3)	47(2)	O(41)	1263(3)	7344(8)	717(2)	66(2)
C(16A)	9915(4)	5973(10)	1667(3)	45(2)	O(42)	2140(3)	7688(6)	225(2)	50(2)
C(17A)	9476(3)	5734(8)	2052(3)	33(2)	C(41B)	1123(3)	3143(9)	806(3)	38(2)
F(2)	3300(2)	6838(4)	4861(1)	23(1)	C(42B)	1693(3)	3820(8)	1135(2)	26(2)
N(2)	2382(2)	9941(6)	4647(2)	16(1)	C(43B)	1877(3)	2864(8)	1612(2)	25(2)
O(21)	2775(2)	6231(5)	3968(2)	28(1)	C(44B)	2113(4)	3606(9)	2053(3)	34(2)
O(22)	1746(2)	6890(5)	4202(1)	20(1)	C(45B)	2292(4)	2747(11)	2490(3)	41(2)
C(21A)	2115(3)	11389(7)	4856(2)	19(1)	C(46B)	2226(3)	1159(11)	2490(3)	39(2)
C(22A)	1371(3)	11614(7)	4760(2)	18(1)	C(47B)	1974(4)	381(9)	2063(3)	35(2)
C(23A)	1024(3)	12592(7)	5072(2)	24(2)	C(48B)	1805(3)	1253(9)	1628(2)	30(2)
C(24A)	356(4)	12974(8)	4952(3)	36(2)	C(10C)	8104(3)	1926(8)	2731(2)	22(1)
C(25A)	42(3)	12333(8)	4534(3)	32(2)	C(11C)	7950(3)	3615(7)	2545(2)	23(2)
C(26A)	378(3)	11319(8)	4232(2)	28(2)	C(12C)	7883(4)	3454(8)	1968(2)	30(2)
C(27A)	1042(3)	10966(7)	4343(2)	22(2)	C(13C)	7485(3)	1937(9)	1908(2)	36(2)
F(3)	5136(2)	6922(4)	1473(1)	27(1)	C(14C)	7816(3)	852(8)	2306(3)	30(2)
N(3)	5021(2)	10023(6)	2193(2)	16(1)	C(15C)	8832(3)	1610(7)	2869(2)	22(1)
O(31)	4086(2)	6503(6)	1993(2)	31(1)	C(16C)	9885(3)	1149(8)	2436(2)	27(2)
O(32)	4676(2)	6792(5)	2736(1)	24(1)	C(17C)	10329(3)	2258(8)	2740(3)	31(2)
C(31A)	5324(3)	11479(7)	2394(2)	22(2)	C(18C)	9951(4)	-535(8)	2632(3)	41(2)
C(32A)	5416(3)	11524(7)	2969(2)	19(1)	C(19C)	10010(3)	1213(10)	1870(3)	41(2)
C(33A)	4870(3)	11149(8)	3265(2)	24(2)	C(20C)	2604(3)	7035(7)	4825(2)	17(1)
C(34A)	4926(3)	11237(8)	3785(2)	28(2)	C(21C)	2428(3)	8676(7)	5025(2)	17(1)
C(35A)	5525(3)	11680(7)	4035(2)	25(2)	C(22C)	1782(3)	8379(7)	5296(2)	21(1)
C(36A)	6066(3)	12020(8)	3749(2)	25(1)	C(23C)	1933(3)	6820(8)	5567(2)	27(2)
C(37A)	5996(3)	11957(8)	3217(2)	26(2)	C(24C)	2284(3)	5858(7)	5175(2)	23(2)
C(41A)	2637(3)	2685(8)	704(2)	28(2)	C(25C)	2395(3)	6698(7)	4276(2)	18(1)
C(42A)	2936(3)	2620(8)	186(2)	25(2)	C(26C)	1392(3)	6373(8)	3724(2)	24(2)
C(43A)	2581(4)	3149(10)	-236(3)	40(2)	C(27C)	675(3)	6742(9)	3829(3)	40(2)
C(44A)	2859(4)	3096(11)	-707(3)	51(2)	C(28C)	1490(4)	4625(8)	3663(3)	39(2)
C(45A)	3477(4)	2453(10)	-762(3)	45(2)	C(29C)	1613(4)	7327(9)	3283(2)	38(2)
C(46A)	3829(4)	1881(9)	-342(3)	38(2)	C(30C)	5263(3)	7147(7)	1998(2)	21(1)
C(47A)	3559(3)	1984(8)	129(2)	31(2)	C(31C)	5523(3)	8811(7)	2096(2)	21(1)
C(11B)	9081(3)	5632(8)	3508(2)	28(2)	C(32C)	6052(3)	8581(8)	2520(2)	26(2)
C(12B)	8406(3)	5026(8)	3310(2)	21(1)	C(33C)	6392(3)	7069(8)	2355(2)	26(2)
C(13B)	7814(3)	5989(7)	3474(2)	18(1)	C(34C)	5816(3)	6019(8)	2182(2)	27(2)
C(14B)	7830(3)	7609(8)	3532(2)	24(2)	C(35C)	4591(3)	6778(8)	2236(2)	21(1)
C(15B)	7269(4)	8443(8)	3673(2)	27(2)	C(36C)	4109(3)	6473(7)	3073(2)	23(2)
C(16B)	6696(3)	7647(8)	3779(2)	24(2)	C(37C)	4434(3)	6662(11)	3594(2)	42(2)

	x	y	z	U(eq)		x	y	z	U(eq)
C(17B)	6667(3)	6035(7)	3731(2)	22(2)	C(38C)	3571(4)	7685(8)	2978(3)	34(2)
C(18B)	7222(3)	5225(8)	3584(2)	21(2)	C(39C)	3863(4)	4804(8)	2982(3)	38(2)
C(21B)	2826(3)	10943(8)	3865(2)	24(2)	C(40C)	2388(3)	6994(9)	1057(2)	31(2)
C(22B)	3010(3)	10214(7)	4379(2)	17(1)	C(41C)	2726(3)	5390(8)	999(2)	24(2)
C(23B)	3546(3)	11113(7)	4682(2)	18(1)	C(42C)	3298(3)	5753(8)	650(2)	26(2)
C(24B)	3611(3)	12744(8)	4656(2)	20(1)	C(43C)	3523(4)	7436(8)	795(3)	32(2)
C(25B)	4109(3)	13515(8)	4944(2)	25(2)	C(44C)	2967(4)	8174(9)	1083(3)	40(2)
C(26B)	4552(3)	12675(8)	5250(2)	24(2)	C(45C)	1837(4)	7353(8)	651(3)	38(2)
C(27B)	4496(3)	11072(8)	5277(2)	19(1)	C(46C)	1737(7)	8157(11)	-239(3)	80(4)
C(28B)	3999(3)	10279(7)	4993(2)	18(1)	C(47C)	2324(8)	8576(15)	-582(4)	118(6)
C(31B)	3914(3)	11032(8)	1937(2)	23(2)	C(48C)	1315(9)	6793(15)	-397(5)	178(9)
C(32B)	4554(3)	10304(8)	1743(2)	20(1)	C(49C)	1312(6)	9569(11)	-142(4)	81(4)

Table C.6 Bond lengths [Å] for **5.43a**.

Bond	Length (Å)	Bond	Length (Å)	Bond	Length (Å)
F(1)-C(10C)	1.409(6)	C(13B)-C(14B)	1.385(9)	C(17C)-H(17C)	0.9600
N(1)-C(11A)	1.469(8)	C(13B)-C(18B)	1.398(9)	C(17C)-H(17D)	0.9600
N(1)-C(11C)	1.470(8)	C(14B)-C(15B)	1.400(10)	C(17C)-H(17E)	0.9600
N(1)-C(12B)	1.517(7)	C(14B)-H(14B)	0.9300	C(18C)-H(18A)	0.9600
O(11)-C(15C)	1.206(7)	C(15B)-C(16B)	1.377(10)	C(18C)-H(18C)	0.9600
O(12)-C(15C)	1.343(7)	C(15B)-H(15B)	0.9300	C(18C)-H(18D)	0.9600
O(12)-C(16C)	1.484(7)	C(16B)-C(17B)	1.376(9)	C(19C)-H(19A)	0.9600
C(11A)-C(12A)	1.533(8)	C(16B)-H(16B)	0.9300	C(19C)-H(19B)	0.9600
C(11A)-H(11A)	0.9700	C(17B)-C(18B)	1.384(9)	C(19C)-H(19C)	0.9600
C(11A)-H(11B)	0.9700	C(17B)-H(17B)	0.9300	C(20C)-C(25C)	1.521(8)
C(12A)-C(13A)	1.381(9)	C(18B)-H(18B)	0.9300	C(20C)-C(24C)	1.524(8)
C(12A)-C(17A)	1.382(9)	C(21B)-C(22B)	1.524(8)	C(20C)-C(21C)	1.537(8)
C(13A)-C(14A)	1.386(10)	C(21B)-H(21C)	0.9600	C(21C)-C(22C)	1.535(8)
C(13A)-H(13A)	0.9300	C(21B)-H(21D)	0.9600	C(21C)-H(21F)	0.9800
C(14A)-C(15A)	1.379(12)	C(21B)-H(21E)	0.9600	C(22C)-C(23C)	1.530(9)
C(14A)-H(14A)	0.9300	C(22B)-C(23B)	1.519(9)	C(22C)-H(22A)	0.9700
C(15A)-C(16A)	1.384(11)	C(22B)-H(22B)	0.9800	C(22C)-H(22C)	0.9700
C(15A)-H(15A)	0.9300	C(23B)-C(24B)	1.394(8)	C(23C)-C(24C)	1.520(9)
C(16A)-C(17A)	1.392(9)	C(23B)-C(28B)	1.394(9)	C(23C)-H(23B)	0.9700
C(16A)-H(16A)	0.9300	C(24B)-C(25B)	1.394(9)	C(23C)-H(23C)	0.9700
C(17A)-H(17A)	0.9300	C(24B)-H(24B)	0.9300	C(24C)-H(24C)	0.9700
F(2)-C(20C)	1.410(6)	C(25B)-C(26B)	1.376(10)	C(24C)-H(24D)	0.9700
N(2)-C(21A)	1.460(7)	C(25B)-H(25B)	0.9300	C(26C)-C(29C)	1.503(9)
N(2)-C(21C)	1.467(8)	C(26B)-C(27B)	1.369(9)	C(26C)-C(28C)	1.508(10)
N(2)-C(22B)	1.496(7)	C(26B)-H(26B)	0.9300	C(26C)-C(27C)	1.515(9)
O(21)-C(25C)	1.209(6)	C(27B)-C(28B)	1.397(9)	C(27C)-H(27C)	0.9600
O(22)-C(25C)	1.323(7)	C(27B)-H(27B)	0.9300	C(27C)-H(27D)	0.9600
O(22)-C(26C)	1.488(7)	C(28B)-H(28B)	0.9300	C(27C)-H(27E)	0.9600
C(21A)-C(22A)	1.521(8)	C(31B)-C(32B)	1.538(8)	C(28C)-H(28A)	0.9600
C(21A)-H(21A)	0.9700	C(31B)-H(31C)	0.9600	C(28C)-H(28C)	0.9600
C(21A)-H(21B)	0.9700	C(31B)-H(31D)	0.9600	C(28C)-H(28D)	0.9600

Bond	Length (Å)	Bond	Length (Å)	Bond	Length (Å)
C(22A)-C(27A)	1.375(8)	C(31B)-H(31E)	0.9600	C(29C)-H(29A)	0.9600
C(22A)-C(23A)	1.382(8)	C(32B)-C(33B)	1.518(8)	C(29C)-H(29B)	0.9600
C(23A)-C(24A)	1.407(10)	C(32B)-H(32B)	0.9800	C(29C)-H(29C)	0.9600
C(23A)-H(23A)	0.9300	C(33B)-C(34B)	1.384(9)	C(30C)-C(31C)	1.525(9)
C(24A)-C(25A)	1.362(10)	C(33B)-C(38B)	1.405(9)	C(30C)-C(34C)	1.532(9)
C(24A)-H(24A)	0.9300	C(34B)-C(35B)	1.382(9)	C(30C)-C(35C)	1.551(8)
C(25A)-C(26A)	1.373(9)	C(34B)-H(34B)	0.9300	C(31C)-C(32C)	1.524(9)
C(25A)-H(25A)	0.9300	C(35B)-C(36B)	1.387(10)	C(31C)-H(31F)	0.9800
C(26A)-C(27A)	1.388(9)	C(35B)-H(35B)	0.9300	C(32C)-C(33C)	1.528(9)
C(26A)-H(26A)	0.9300	C(36B)-C(37B)	1.367(10)	C(32C)-H(32A)	0.9700
C(27A)-H(27A)	0.9300	C(36B)-H(36B)	0.9300	C(32C)-H(32C)	0.9700
F(3)-C(30C)	1.413(7)	C(37B)-C(38B)	1.372(9)	C(33C)-C(34C)	1.517(9)
N(3)-C(31A)	1.468(8)	C(37B)-H(37B)	0.9300	C(33C)-H(33B)	0.9700
N(3)-C(31C)	1.473(8)	C(38B)-H(38B)	0.9300	C(33C)-H(33C)	0.9700
N(3)-C(32B)	1.501(7)	F(4)-C(40C)	1.412(7)	C(34C)-H(34C)	0.9700
O(31)-C(35C)	1.201(7)	N(4)-C(41C)	1.471(8)	C(34C)-H(34D)	0.9700
O(32)-C(35C)	1.325(7)	N(4)-C(42B)	1.516(8)	C(36C)-C(37C)	1.505(9)
O(32)-C(36C)	1.505(6)	O(41)-C(45C)	1.176(9)	C(36C)-C(38C)	1.506(9)
C(31A)-C(32A)	1.524(8)	O(42)-C(45C)	1.336(9)	C(36C)-C(39C)	1.517(9)
C(31A)-H(31A)	0.9700	O(42)-C(46C)	1.494(10)	C(37C)-H(37C)	0.9600
C(31A)-H(31B)	0.9700	C(41B)-C(42B)	1.520(9)	C(37C)-H(37D)	0.9600
C(32A)-C(37A)	1.363(8)	C(41B)-H(41C)	0.9600	C(37C)-H(37E)	0.9600
C(32A)-C(33A)	1.415(8)	C(41B)-H(41D)	0.9600	C(38C)-H(38A)	0.9600
C(33A)-C(34A)	1.375(8)	C(41B)-H(41E)	0.9600	C(38C)-H(38C)	0.9600
C(33A)-H(33A)	0.9300	C(42B)-C(43B)	1.533(9)	C(38C)-H(38D)	0.9600
C(34A)-C(35A)	1.398(9)	C(42B)-H(42B)	0.9800	C(39C)-H(39A)	0.9600
C(34A)-H(34A)	0.9300	C(43B)-C(48B)	1.377(10)	C(39C)-H(39B)	0.9600
C(35A)-C(36A)	1.385(8)	C(43B)-C(44B)	1.390(10)	C(39C)-H(39C)	0.9600
C(35A)-H(35A)	0.9300	C(44B)-C(45B)	1.399(11)	C(40C)-C(41C)	1.534(10)
C(36A)-C(37A)	1.408(8)	C(44B)-H(44B)	0.9300	C(40C)-C(44C)	1.538(10)
C(36A)-H(36A)	0.9300	C(45B)-C(46B)	1.356(11)	C(40C)-C(45C)	1.539(10)
C(37A)-H(37A)	0.9300	C(45B)-H(45B)	0.9300	C(41C)-C(42C)	1.540(8)
C(41A)-N(4)	1.467(8)	C(46B)-C(47B)	1.383(11)	C(41C)-H(41F)	0.9800
C(41A)-C(42A)	1.523(8)	C(46B)-H(46B)	0.9300	C(42C)-C(43C)	1.543(9)
C(41A)-H(41A)	0.9700	C(47B)-C(48B)	1.398(10)	C(42C)-H(42A)	0.9700
C(41A)-H(41B)	0.9700	C(47B)-H(47B)	0.9300	C(42C)-H(42C)	0.9700
C(42A)-C(43A)	1.373(10)	C(48B)-H(48B)	0.9300	C(43C)-C(44C)	1.517(10)
C(42A)-C(47A)	1.380(9)	C(10C)-C(15C)	1.519(8)	C(43C)-H(43B)	0.9700
C(43A)-C(44A)	1.389(9)	C(10C)-C(14C)	1.541(9)	C(43C)-H(43C)	0.9700
C(43A)-H(43A)	0.9300	C(10C)-C(11C)	1.544(9)	C(44C)-H(44C)	0.9700
C(44A)-C(45A)	1.373(12)	C(11C)-C(12C)	1.530(9)	C(44C)-H(44D)	0.9700
C(44A)-H(44A)	0.9300	C(11C)-H(11F)	0.9800	C(46C)-C(48C)	1.486(16)
C(45A)-C(46A)	1.378(11)	C(12C)-C(13C)	1.523(10)	C(46C)-C(49C)	1.502(14)
C(45A)-H(45A)	0.9300	C(12C)-H(12A)	0.9700	C(46C)-C(47C)	1.562(17)
C(46A)-C(47A)	1.383(8)	C(12C)-H(12C)	0.9700	C(47C)-H(47C)	0.9600
C(46A)-H(46A)	0.9300	C(13C)-C(14C)	1.528(10)	C(47C)-H(47D)	0.9600
C(47A)-H(47A)	0.9300	C(13C)-H(13B)	0.9700	C(47C)-H(47E)	0.9600
C(11B)-C(12B)	1.523(9)	C(13C)-H(13C)	0.9700	C(48C)-H(48A)	0.9600
C(11B)-H(11C)	0.9600	C(14C)-H(14C)	0.9700	C(48C)-H(48C)	0.9600

Bond	Length (Å)	Bond	Length (Å)	Bond	Length (Å)
C(11B)-H(11D)	0.9600	C(14C)-H(14D)	0.9700	C(48C)-H(48D)	0.9600
C(11B)-H(11E)	0.9600	C(16C)-C(17C)	1.506(9)	C(49C)-H(49A)	0.9600
C(12B)-C(13B)	1.526(9)	C(16C)-C(18C)	1.525(10)	C(49C)-H(49B)	0.9600
C(12B)-H(12B)	0.9800	C(16C)-C(19C)	1.530(9)	C(49C)-H(49C)	0.9600

Table C.7 Bond angles [º] for **5.43a**.

Atoms	Angle (º)	Atoms	Angle (º)	Atoms	Angle (º)
C(11A)-N(1)-C(11C)	112.6(5)	C(23B)-C(24B)-H(24B)	119.7	C(24C)-C(23C)-H(23B)	111.1
C(11A)-N(1)-C(12B)	112.8(5)	C(25B)-C(24B)-H(24B)	119.7	C(22C)-C(23C)-H(23B)	111.1
C(11C)-N(1)-C(12B)	113.0(4)	C(26B)-C(25B)-C(24B)	120.5(6)	C(24C)-C(23C)-H(23C)	111.1
C(15C)-O(12)-C(16C)	123.0(5)	C(26B)-C(25B)-H(25B)	119.7	C(22C)-C(23C)-H(23C)	111.1
N(1)-C(11A)-C(12A)	114.1(5)	C(24B)-C(25B)-H(25B)	119.7	H(23B)-C(23C)-H(23C)	109.0
N(1)-C(11A)-H(11A)	108.7	C(27B)-C(26B)-C(25B)	119.6(7)	C(23C)-C(24C)-C(20C)	106.5(5)
C(12A)-C(11A)-H(11A)	108.7	C(27B)-C(26B)-H(26B)	120.2	C(23C)-C(24C)-H(24C)	110.4
N(1)-C(11A)-H(11B)	108.7	C(25B)-C(26B)-H(26B)	120.2	C(20C)-C(24C)-H(24C)	110.4
C(12A)-C(11A)-H(11B)	108.7	C(26B)-C(27B)-C(28B)	120.7(7)	C(23C)-C(24C)-H(24D)	110.4
H(11A)-C(11A)-H(11B)	107.6	C(26B)-C(27B)-H(27B)	119.6	C(20C)-C(24C)-H(24D)	110.4
C(13A)-C(12A)-C(17A)	118.4(6)	C(28B)-C(27B)-H(27B)	119.6	H(24C)-C(24C)-H(24D)	108.6
C(13A)-C(12A)-C(11A)	120.4(6)	C(23B)-C(28B)-C(27B)	120.4(6)	O(21)-C(25C)-O(22)	126.3(5)
C(17A)-C(12A)-C(11A)	120.9(6)	C(23B)-C(28B)-H(28B)	119.8	O(21)-C(25C)-C(20C)	123.4(5)
C(12A)-C(13A)-C(14A)	121.2(8)	C(27B)-C(28B)-H(28B)	119.8	O(22)-C(25C)-C(20C)	110.2(5)
C(12A)-C(13A)-H(13A)	119.4	C(32B)-C(31B)-H(31C)	109.5	O(22)-C(26C)-C(29C)	110.5(5)
C(14A)-C(13A)-H(13A)	119.4	C(32B)-C(31B)-H(31D)	109.5	O(22)-C(26C)-C(28C)	108.7(5)
C(15A)-C(14A)-C(13A)	120.7(8)	H(31C)-C(31B)-H(31D)	109.5	C(29C)-C(26C)-C(28C)	113.8(6)
C(15A)-C(14A)-H(14A)	119.6	C(32B)-C(31B)-H(31E)	109.5	O(22)-C(26C)-C(27C)	101.9(5)
C(13A)-C(14A)-H(14A)	119.6	H(31C)-C(31B)-H(31E)	109.5	C(29C)-C(26C)-C(27C)	110.5(6)
C(14A)-C(15A)-C(16A)	118.1(7)	H(31D)-C(31B)-H(31E)	109.5	C(28C)-C(26C)-C(27C)	110.7(6)
C(14A)-C(15A)-H(15A)	120.9	N(3)-C(32B)-C(33B)	115.7(5)	C(26C)-C(27C)-H(27C)	109.5
C(16A)-C(15A)-H(15A)	120.9	N(3)-C(32B)-C(31B)	107.8(4)	C(26C)-C(27C)-H(27D)	109.5
C(15A)-C(16A)-C(17A)	121.3(8)	C(33B)-C(32B)-C(31B)	113.7(5)	H(27C)-C(27C)-H(27D)	109.5
C(15A)-C(16A)-H(16A)	119.4	N(3)-C(32B)-H(32B)	106.3	C(26C)-C(27C)-H(27E)	109.5
C(17A)-C(16A)-H(16A)	119.4	C(33B)-C(32B)-H(32B)	106.3	H(27C)-C(27C)-H(27E)	109.5
C(12A)-C(17A)-C(16A)	120.2(7)	C(31B)-C(32B)-H(32B)	106.3	H(27D)-C(27C)-H(27E)	109.5
C(12A)-C(17A)-H(17A)	119.9	C(34B)-C(33B)-C(38B)	117.1(6)	C(26C)-C(28C)-H(28A)	109.5
C(16A)-C(17A)-H(17A)	119.9	C(34B)-C(33B)-C(32B)	123.3(6)	C(26C)-C(28C)-H(28C)	109.5
C(21A)-N(2)-C(21C)	111.9(4)	C(38B)-C(33B)-C(32B)	119.6(6)	H(28A)-C(28C)-H(28C)	109.5
C(21A)-N(2)-C(22B)	112.5(5)	C(35B)-C(34B)-C(33B)	121.5(6)	C(26C)-C(28C)-H(28D)	109.5
C(21C)-N(2)-C(22B)	114.0(5)	C(35B)-C(34B)-H(34B)	119.3	H(28A)-C(28C)-H(28D)	109.5
C(25C)-O(22)-C(26C)	121.4(4)	C(33B)-C(34B)-H(34B)	119.3	H(28C)-C(28C)-H(28D)	109.5
N(2)-C(21A)-C(22A)	114.8(5)	C(34B)-C(35B)-C(36B)	120.2(7)	C(26C)-C(29C)-H(29A)	109.5
N(2)-C(21A)-H(21A)	108.6	C(34B)-C(35B)-H(35B)	119.9	C(26C)-C(29C)-H(29B)	109.5
C(22A)-C(21A)-H(21A)	108.6	C(36B)-C(35B)-H(35B)	119.9	H(29A)-C(29C)-H(29B)	109.5
N(2)-C(21A)-H(21B)	108.6	C(37B)-C(36B)-C(35B)	119.2(7)	C(26C)-C(29C)-H(29C)	109.5
C(22A)-C(21A)-H(21B)	108.6	C(37B)-C(36B)-H(36B)	120.4	H(29A)-C(29C)-H(29C)	109.5
H(21A)-C(21A)-H(21B)	107.5	C(35B)-C(36B)-H(36B)	120.4	H(29B)-C(29C)-H(29C)	109.5
C(27A)-C(22A)-C(23A)	118.8(6)	C(36B)-C(37B)-C(38B)	120.8(7)	F(3)-C(30C)-C(31C)	109.7(5)

Atoms	Angle (º)	Atoms	Angle (º)	Atoms	Angle (º)
C(27A)-C(22A)-C(21A)	121.1(5)	C(36B)-C(37B)-H(37B)	119.6	F(3)-C(30C)-C(34C)	108.9(5)
C(23A)-C(22A)-C(21A)	119.8(5)	C(38B)-C(37B)-H(37B)	119.6	C(31C)-C(30C)-C(34C)	106.7(5)
C(22A)-C(23A)-C(24A)	120.5(6)	C(37B)-C(38B)-C(33B)	121.3(6)	F(3)-C(30C)-C(35C)	104.5(5)
C(22A)-C(23A)-H(23A)	119.7	C(37B)-C(38B)-H(38B)	119.4	C(31C)-C(30C)-C(35C)	114.7(5)
C(24A)-C(23A)-H(23A)	119.7	C(33B)-C(38B)-H(38B)	119.4	C(34C)-C(30C)-C(35C)	112.3(5)
C(25A)-C(24A)-C(23A)	119.7(6)	C(41A)-N(4)-C(41C)	111.7(5)	N(3)-C(31C)-C(32C)	115.0(5)
C(25A)-C(24A)-H(24A)	120.2	C(41A)-N(4)-C(42B)	111.0(5)	N(3)-C(31C)-C(30C)	116.4(5)
C(23A)-C(24A)-H(24A)	120.2	C(41C)-N(4)-C(42B)	114.4(5)	C(32C)-C(31C)-C(30C)	103.2(5)
C(24A)-C(25A)-C(26A)	119.9(7)	C(45C)-O(42)-C(46C)	119.8(7)	N(3)-C(31C)-H(31F)	107.2
C(24A)-C(25A)-H(25A)	120.0	C(42B)-C(41B)-H(41C)	109.5	C(32C)-C(31C)-H(31F)	107.2
C(26A)-C(25A)-H(25A)	120.0	C(42B)-C(41B)-H(41D)	109.5	C(30C)-C(31C)-H(31F)	107.2
C(25A)-C(26A)-C(27A)	120.7(6)	H(41C)-C(41B)-H(41D)	109.5	C(31C)-C(32C)-C(33C)	101.8(5)
C(25A)-C(26A)-H(26A)	119.7	C(42B)-C(41B)-H(41E)	109.5	C(31C)-C(32C)-H(32A)	111.4
C(27A)-C(26A)-H(26A)	119.7	H(41C)-C(41B)-H(41E)	109.5	C(33C)-C(32C)-H(32A)	111.4
C(22A)-C(27A)-C(26A)	120.3(6)	H(41D)-C(41B)-H(41E)	109.5	C(31C)-C(32C)-H(32C)	111.4
C(22A)-C(27A)-H(27A)	119.8	N(4)-C(42B)-C(41B)	109.0(5)	C(33C)-C(32C)-H(32C)	111.4
C(26A)-C(27A)-H(27A)	119.8	N(4)-C(42B)-C(43B)	113.7(5)	H(32A)-C(32C)-H(32C)	109.3
C(31A)-N(3)-C(31C)	112.1(5)	C(41B)-C(42B)-C(43B)	114.7(6)	C(34C)-C(33C)-C(32C)	103.6(5)
C(31A)-N(3)-C(32B)	112.8(5)	N(4)-C(42B)-H(42B)	106.3	C(34C)-C(33C)-H(33B)	111.0
C(31C)-N(3)-C(32B)	112.5(4)	C(41B)-C(42B)-H(42B)	106.3	C(32C)-C(33C)-H(33B)	111.0
C(35C)-O(32)-C(36C)	121.5(5)	C(43B)-C(42B)-H(42B)	106.3	C(34C)-C(33C)-H(33C)	111.0
N(3)-C(31A)-C(32A)	114.4(5)	C(48B)-C(43B)-C(44B)	117.3(7)	C(32C)-C(33C)-H(33C)	111.0
N(3)-C(31A)-H(31A)	108.7	C(48B)-C(43B)-C(42B)	121.9(6)	H(33B)-C(33C)-H(33C)	109.0
C(32A)-C(31A)-H(31A)	108.7	C(44B)-C(43B)-C(42B)	120.7(7)	C(33C)-C(34C)-C(30C)	105.2(5)
N(3)-C(31A)-H(31B)	108.7	C(43B)-C(44B)-C(45B)	121.4(7)	C(33C)-C(34C)-H(34C)	110.7
C(32A)-C(31A)-H(31B)	108.7	C(43B)-C(44B)-H(44B)	119.3	C(30C)-C(34C)-H(34C)	110.7
H(31A)-C(31A)-H(31B)	107.6	C(45B)-C(44B)-H(44B)	119.3	C(33C)-C(34C)-H(34D)	110.7
C(37A)-C(32A)-C(33A)	117.7(5)	C(46B)-C(45B)-C(44B)	119.8(8)	C(30C)-C(34C)-H(34D)	110.7
C(37A)-C(32A)-C(31A)	123.3(5)	C(46B)-C(45B)-H(45B)	120.1	H(34C)-C(34C)-H(34D)	108.8
C(33A)-C(32A)-C(31A)	119.0(5)	C(44B)-C(45B)-H(45B)	120.1	O(31)-C(35C)-O(32)	127.1(5)
C(34A)-C(33A)-C(32A)	120.6(6)	C(45B)-C(46B)-C(47B)	120.5(8)	O(31)-C(35C)-C(30C)	123.7(5)
C(34A)-C(33A)-H(33A)	119.7	C(45B)-C(46B)-H(46B)	119.8	O(32)-C(35C)-C(30C)	109.2(5)
C(32A)-C(33A)-H(33A)	119.7	C(47B)-C(46B)-H(46B)	119.8	C(37C)-C(36C)-O(32)	102.2(5)
C(33A)-C(34A)-C(35A)	121.1(6)	C(46B)-C(47B)-C(48B)	119.0(7)	C(37C)-C(36C)-C(38C)	111.0(6)
C(33A)-C(34A)-H(34A)	119.4	C(46B)-C(47B)-H(47B)	120.5	O(32)-C(36C)-C(38C)	109.7(5)
C(35A)-C(34A)-H(34A)	119.4	C(48B)-C(47B)-H(47B)	120.5	C(37C)-C(36C)-C(39C)	111.8(6)
C(36A)-C(35A)-C(34A)	118.7(5)	C(43B)-C(48B)-C(47B)	121.9(7)	O(32)-C(36C)-C(39C)	109.0(5)
C(36A)-C(35A)-H(35A)	120.6	C(43B)-C(48B)-H(48B)	119.1	C(38C)-C(36C)-C(39C)	112.7(6)
C(34A)-C(35A)-H(35A)	120.6	C(47B)-C(48B)-H(48B)	119.1	C(36C)-C(37C)-H(37C)	109.5
C(35A)-C(36A)-C(37A)	119.5(6)	F(1)-C(10C)-C(15C)	106.0(5)	C(36C)-C(37C)-H(37D)	109.5
C(35A)-C(36A)-H(36A)	120.3	F(1)-C(10C)-C(14C)	108.7(5)	H(37C)-C(37C)-H(37D)	109.5
C(37A)-C(36A)-H(36A)	120.3	C(15C)-C(10C)-C(14C)	113.4(5)	C(36C)-C(37C)-H(37E)	109.5
C(32A)-C(37A)-C(36A)	122.3(6)	F(1)-C(10C)-C(11C)	109.2(5)	H(37C)-C(37C)-H(37E)	109.5
C(32A)-C(37A)-H(37A)	118.9	C(15C)-C(10C)-C(11C)	114.7(5)	H(37D)-C(37C)-H(37E)	109.5
C(36A)-C(37A)-H(37A)	118.9	C(14C)-C(10C)-C(11C)	104.7(5)	C(36C)-C(38C)-H(38A)	109.5
N(4)-C(41A)-C(42A)	114.6(5)	N(1)-C(11C)-C(12C)	116.2(5)	C(36C)-C(38C)-H(38C)	109.5
N(4)-C(41A)-H(41A)	108.6	N(1)-C(11C)-C(10C)	113.7(5)	H(38A)-C(38C)-H(38C)	109.5
C(42A)-C(41A)-H(41A)	108.6	C(12C)-C(11C)-C(10C)	104.0(5)	C(36C)-C(38C)-H(38D)	109.5
N(4)-C(41A)-H(41B)	108.6	N(1)-C(11C)-H(11F)	107.5	H(38A)-C(38C)-H(38D)	109.5

Atoms	Angle (º)	Atoms	Angle (º)	Atoms	Angle (º)
C(42A)-C(41A)-H(41B)	108.6	C(12C)-C(11C)-H(11F)	107.5	H(38C)-C(38C)-H(38D)	109.5
H(41A)-C(41A)-H(41B)	107.6	C(10C)-C(11C)-H(11F)	107.5	C(36C)-C(39C)-H(39A)	109.5
C(43A)-C(42A)-C(47A)	118.8(6)	C(13C)-C(12C)-C(11C)	101.7(5)	C(36C)-C(39C)-H(39B)	109.5
C(43A)-C(42A)-C(41A)	120.4(6)	C(13C)-C(12C)-H(12A)	111.4	H(39A)-C(39C)-H(39B)	109.5
C(47A)-C(42A)-C(41A)	120.8(6)	C(11C)-C(12C)-H(12A)	111.4	C(36C)-C(39C)-H(39C)	109.5
C(42A)-C(43A)-C(44A)	120.1(7)	C(13C)-C(12C)-H(12C)	111.4	H(39A)-C(39C)-H(39C)	109.5
C(42A)-C(43A)-H(43A)	120.0	C(11C)-C(12C)-H(12C)	111.4	H(39B)-C(39C)-H(39C)	109.5
C(44A)-C(43A)-H(43A)	120.0	H(12A)-C(12C)-H(12C)	109.3	F(4)-C(40C)-C(41C)	111.2(5)
C(45A)-C(44A)-C(43A)	120.8(8)	C(12C)-C(13C)-C(14C)	103.1(5)	F(4)-C(40C)-C(44C)	107.4(5)
C(45A)-C(44A)-H(44A)	119.6	C(12C)-C(13C)-H(13B)	111.1	C(41C)-C(40C)-C(44C)	104.1(5)
C(43A)-C(44A)-H(44A)	119.6	C(14C)-C(13C)-H(13B)	111.1	F(4)-C(40C)-C(45C)	104.5(5)
C(44A)-C(45A)-C(46A)	119.3(7)	C(12C)-C(13C)-H(13C)	111.1	C(41C)-C(40C)-C(45C)	114.6(6)
C(44A)-C(45A)-H(45A)	120.4	C(14C)-C(13C)-H(13C)	111.1	C(44C)-C(40C)-C(45C)	115.0(6)
C(46A)-C(45A)-H(45A)	120.4	H(13B)-C(13C)-H(13C)	109.1	N(4)-C(41C)-C(40C)	113.9(5)
C(45A)-C(46A)-C(47A)	119.7(7)	C(13C)-C(14C)-C(10C)	106.4(6)	N(4)-C(41C)-C(42C)	113.7(5)
C(45A)-C(46A)-H(46A)	120.2	C(13C)-C(14C)-H(14C)	110.4	C(40C)-C(41C)-C(42C)	103.3(5)
C(47A)-C(46A)-H(46A)	120.2	C(10C)-C(14C)-H(14C)	110.4	N(4)-C(41C)-H(41F)	108.6
C(42A)-C(47A)-C(46A)	121.3(7)	C(13C)-C(14C)-H(14D)	110.4	C(40C)-C(41C)-H(41F)	108.6
C(42A)-C(47A)-H(47A)	119.4	C(10C)-C(14C)-H(14D)	110.4	C(42C)-C(41C)-H(41F)	108.6
C(46A)-C(47A)-H(47A)	119.4	H(14C)-C(14C)-H(14D)	108.6	C(41C)-C(42C)-C(43C)	104.8(5)
C(12B)-C(11B)-H(11C)	109.5	O(11)-C(15C)-O(12)	125.7(6)	C(41C)-C(42C)-H(42A)	110.8
C(12B)-C(11B)-H(11D)	109.5	O(11)-C(15C)-C(10C)	125.1(5)	C(43C)-C(42C)-H(42A)	110.8
H(11C)-C(11B)-H(11D)	109.5	O(12)-C(15C)-C(10C)	109.2(5)	C(41C)-C(42C)-H(42C)	110.8
C(12B)-C(11B)-H(11E)	109.5	O(12)-C(16C)-C(17C)	111.3(5)	C(43C)-C(42C)-H(42C)	110.8
H(11C)-C(11B)-H(11E)	109.5	O(12)-C(16C)-C(18C)	108.8(5)	H(42A)-C(42C)-H(42C)	108.9
H(11D)-C(11B)-H(11E)	109.5	C(17C)-C(16C)-C(18C)	111.4(6)	C(44C)-C(43C)-C(42C)	107.0(6)
N(1)-C(12B)-C(11B)	108.5(5)	O(12)-C(16C)-C(19C)	102.1(5)	C(44C)-C(43C)-H(43B)	110.3
N(1)-C(12B)-C(13B)	114.2(5)	C(17C)-C(16C)-C(19C)	112.3(6)	C(42C)-C(43C)-H(43B)	110.3
C(11B)-C(12B)-C(13B)	114.7(5)	C(18C)-C(16C)-C(19C)	110.5(6)	C(44C)-C(43C)-H(43C)	110.3
N(1)-C(12B)-H(12B)	106.3	C(16C)-C(17C)-H(17C)	109.5	C(42C)-C(43C)-H(43C)	110.3
C(11B)-C(12B)-H(12B)	106.3	C(16C)-C(17C)-H(17D)	109.5	H(43B)-C(43C)-H(43C)	108.6
C(13B)-C(12B)-H(12B)	106.3	H(17C)-C(17C)-H(17D)	109.5	C(43C)-C(44C)-C(40C)	106.5(6)
C(14B)-C(13B)-C(18B)	117.1(6)	C(16C)-C(17C)-H(17E)	109.5	C(43C)-C(44C)-H(44C)	110.4
C(14B)-C(13B)-C(12B)	123.3(6)	H(17C)-C(17C)-H(17E)	109.5	C(40C)-C(44C)-H(44C)	110.4
C(18B)-C(13B)-C(12B)	119.6(6)	H(17D)-C(17C)-H(17E)	109.5	C(43C)-C(44C)-H(44D)	110.4
C(13B)-C(14B)-C(15B)	121.1(7)	C(16C)-C(18C)-H(18A)	109.5	C(40C)-C(44C)-H(44D)	110.4
C(13B)-C(14B)-H(14B)	119.4	C(16C)-C(18C)-H(18C)	109.5	H(44C)-C(44C)-H(44D)	108.6
C(15B)-C(14B)-H(14B)	119.4	H(18A)-C(18C)-H(18C)	109.5	O(41)-C(45C)-O(42)	128.1(8)
C(16B)-C(15B)-C(14B)	120.0(6)	C(16C)-C(18C)-H(18D)	109.5	O(41)-C(45C)-C(40C)	125.2(7)
C(16B)-C(15B)-H(15B)	120.0	H(18A)-C(18C)-H(18D)	109.5	O(42)-C(45C)-C(40C)	106.7(6)
C(14B)-C(15B)-H(15B)	120.0	H(18C)-C(18C)-H(18D)	109.5	C(48C)-C(46C)-O(42)	107.7(7)
C(17B)-C(16B)-C(15B)	120.1(7)	C(16C)-C(19C)-H(19A)	109.5	C(48C)-C(46C)-C(49C)	110.4(12)
C(17B)-C(16B)-H(16B)	119.9	C(16C)-C(19C)-H(19B)	109.5	O(42)-C(46C)-C(49C)	111.4(7)
C(15B)-C(16B)-H(16B)	119.9	H(19A)-C(19C)-H(19B)	109.5	C(48C)-C(46C)-C(47C)	116.9(11)
C(16B)-C(17B)-C(18B)	119.3(6)	C(16C)-C(19C)-H(19C)	109.5	O(42)-C(46C)-C(47C)	98.1(9)
C(16B)-C(17B)-H(17B)	120.3	H(19A)-C(19C)-H(19C)	109.5	C(49C)-C(46C)-C(47C)	111.6(9)
C(18B)-C(17B)-H(17B)	120.3	H(19B)-C(19C)-H(19C)	109.5	C(46C)-C(47C)-H(47C)	109.5
C(17B)-C(18B)-C(13B)	122.3(6)	F(2)-C(20C)-C(25C)	105.7(4)	C(46C)-C(47C)-H(47D)	109.5
C(17B)-C(18B)-H(18B)	118.8	F(2)-C(20C)-C(24C)	109.1(5)	H(47C)-C(47C)-H(47D)	109.5

Atoms	Angle (º)	Atoms	Angle (º)	Atoms	Angle (º)
C(13B)-C(18B)-H(18B)	118.9	C(25C)-C(20C)-C(24C)	110.5(5)	C(46C)-C(47C)-H(47E)	109.5
C(22B)-C(21B)-H(21C)	109.5	F(2)-C(20C)-C(21C)	109.2(5)	H(47C)-C(47C)-H(47E)	109.5
C(22B)-C(21B)-H(21D)	109.5	C(25C)-C(20C)-C(21C)	116.2(5)	H(47D)-C(47C)-H(47E)	109.5
H(21C)-C(21B)-H(21D)	109.5	C(24C)-C(20C)-C(21C)	106.1(4)	C(46C)-C(48C)-H(48A)	109.5
C(22B)-C(21B)-H(21E)	109.5	N(2)-C(21C)-C(22C)	114.2(5)	C(46C)-C(48C)-H(48C)	109.5
H(21C)-C(21B)-H(21E)	109.5	N(2)-C(21C)-C(20C)	116.1(4)	H(48A)-C(48C)-H(48C)	109.5
H(21D)-C(21B)-H(21E)	109.5	C(22C)-C(21C)-C(20C)	103.0(5)	C(46C)-C(48C)-H(48D)	109.5
N(2)-C(22B)-C(23B)	115.1(4)	N(2)-C(21C)-H(21F)	107.7	H(48A)-C(48C)-H(48D)	109.5
N(2)-C(22B)-C(21B)	108.1(5)	C(22C)-C(21C)-H(21F)	107.7	H(48C)-C(48C)-H(48D)	109.5
C(23B)-C(22B)-C(21B)	113.7(5)	C(20C)-C(21C)-H(21F)	107.7	C(46C)-C(49C)-H(49A)	109.5
N(2)-C(22B)-H(22B)	106.5	C(23C)-C(22C)-C(21C)	102.0(5)	C(46C)-C(49C)-H(49B)	109.5
C(23B)-C(22B)-H(22B)	106.5	C(23C)-C(22C)-H(22A)	111.4	H(49A)-C(49C)-H(49B)	109.5
C(21B)-C(22B)-H(22B)	106.5	C(21C)-C(22C)-H(22A)	111.4	C(46C)-C(49C)-H(49C)	109.5
C(24B)-C(23B)-C(28B)	118.2(6)	C(23C)-C(22C)-H(22C)	111.4	H(49A)-C(49C)-H(49C)	109.5
C(24B)-C(23B)-C(22B)	122.8(6)	C(21C)-C(22C)-H(22C)	111.4	H(49B)-C(49C)-H(49C)	109.5
C(28B)-C(23B)-C(22B)	119.0(5)	H(22A)-C(22C)-H(22C)	109.2		
C(23B)-C(24B)-C(25B) 154	120.6(7)	C(24C)-C(23C)-C(22C)	103.5(5)		

Table C.8 Hydrogen coordinates (x 10^4) and isotropic displacement parameters (Å^2 x 10^3) for **5.43a.**

	x	y	z	U(eq)		x	y	z	U(eq)
H(11A)	8490	7143	2692	32	H(11F)	7512	3904	2663	27
H(11B)	7929	6429	2332	32	H(12A)	7645	4339	1815	36
H(13A)	8235	7649	1554	43	H(12C)	8314	3361	1822	36
H(14A)	8974	8102	930	65	H(13B)	7516	1505	1570	43
H(15A)	10027	6998	985	56	H(13C)	7020	2109	1974	43
H(16A)	10339	5537	1697	54	H(14C)	8167	245	2160	36
H(17A)	9608	5138	2334	39	H(14D)	7492	130	2437	36
H(21A)	2343	12277	4712	23	H(17C)	10283	3302	2604	47
H(21B)	2214	11399	5218	23	H(17D)	10782	1922	2725	47
H(23A)	1235	13001	5364	29	H(17E)	10203	2258	3086	47
H(24A)	130	13661	5157	43	H(18A)	9919	-539	2993	62
H(25A)	-400	12581	4452	38	H(18C)	10374	-954	2547	62
H(26A)	159	10863	3952	33	H(18D)	9602	-1170	2480	62
H(27A)	1266	10289	4133	26	H(19A)	9702	531	1689	62
H(31A)	5047	12362	2285	26	H(19B)	10456	875	1816	62
H(31B)	5754	11613	2250	26	H(19C)	9951	2272	1750	62
H(33A)	4469	10840	3107	29	H(21F)	2772	8972	5282	20
H(34A)	4561	10999	3973	33	H(22A)	1697	9213	5535	26
H(35A)	5558	11744	4386	30	H(22C)	1405	8282	5057	26
H(36A)	6472	12288	3907	30	H(23B)	2218	6981	5869	32
H(37A)	6359	12219	3028	31	H(23C)	1526	6306	5662	32
H(41A)	2335	1803	734	33	H(24C)	1968	5199	4985	27
H(41B)	2992	2558	962	33	H(24D)	2620	5189	5338	27
H(43A)	2154	3543	-206	48	H(27C)	532	6074	4096	60
H(44A)	2623	3502	-988	61	H(27D)	400	6562	3528	60

	x	y	z	U(eq)		x	y	z	U(eq)
H(45A)	3656	2404	-1079	54	H(27E)	639	7824	3929	60
H(46A)	4245	1429	-374	46	H(28A)	1939	4420	3576	59
H(47A)	3802	1617	413	37	H(28C)	1190	4239	3399	59
H(11C)	9418	4873	3438	42	H(28D)	1402	4103	3975	59
H(11D)	9073	5798	3867	42	H(29A)	1552	8426	3352	56
H(11E)	9178	6608	3344	42	H(29B)	1354	7040	2984	56
H(12B)	8356	3974	3456	25	H(29C)	2075	7126	3234	56
H(14B)	8221	8152	3476	28	H(31F)	5752	9139	1794	25
H(15B)	7282	9535	3695	32	H(32A)	5854	8452	2845	31
H(16B)	6328	8200	3883	29	H(32C)	6361	9457	2539	31
H(17B)	6279	5496	3797	26	H(33B)	6684	7271	2081	31
H(18B)	7202	4135	3557	25	H(33C)	6648	6597	2636	31
H(21C)	2524	10260	3679	36	H(34C)	5672	5377	2460	33
H(21D)	3221	11084	3680	36	H(34D)	5943	5332	1910	33
H(21E)	2618	11946	3913	36	H(37C)	4787	5908	3640	63
H(22B)	3195	9172	4312	20	H(37D)	4110	6492	3844	63
H(24B)	3320	13322	4446	24	H(37E)	4612	7706	3630	63
H(25B)	4143	14605	4928	29	H(38A)	3254	7610	3237	51
H(26B)	4888	13194	5438	29	H(38C)	3352	7499	2653	51
H(27B)	4792	10505	5488	23	H(38D)	3765	8717	2984	51
H(28B)	3971	9188	5011	21	H(39A)	4231	4087	3014	57
H(31C)	3723	10327	2174	35	H(39B)	3659	4726	2647	57
H(31D)	3602	11205	1656	35	H(39C)	3542	4542	3226	57
H(31E)	4016	12017	2100	35	H(41F)	2918	5066	1331	29
H(32B)	4431	9264	1609	24	H(42A)	3144	5706	297	31
H(34B)	4613	13413	1517	30	H(42C)	3659	5010	706	31
H(35B)	5066	14703	849	38	H(43B)	3930	7402	1006	38
H(36B)	5584	13288	228	44	H(43C)	3604	8044	494	38
H(37B)	5640	10593	285	42	H(44C)	2831	9166	928	48
H(38B)	5165	9292	934	31	H(44D)	3113	8369	1432	48
H(41C)	1254	2148	670	57	H(47C)	2535	9525	-461	177
H(41D)	1011	3856	534	57	H(47D)	2155	8728	-924	177
H(41E)	742	2997	1007	57	H(47E)	2641	7732	-571	177
H(42B)	1542	4849	1252	31	H(48A)	1569	5840	-357	267
H(44B)	2153	4697	2058	40	H(48C)	1168	6913	-745	267
H(45B)	2456	3264	2780	49	H(48D)	936	6744	-190	267
H(46B)	2351	588	2779	46	H(49A)	992	9304	102	122
H(47B)	1918	-705	2066	42	H(49B)	1086	9890	-453	122
H(48B)	1639	729	1340	36	H(49C)	1588	10415	-14	122

C.3 References

1. Nicholson, R. S., *Analytical Chemistry* **1966,** 38, (10), 1406.
2. Bard, A. J.; Faulkner, L. R., *Electrochemical methods : fundamentals and applications* 1st ed.; Wiley: New York, 1980; p 718.
3. Watanabe, J.; Morita, T.; Kimura, S., *Journal of Physical Chemistry B* **2005,** 109, (30), 14416-14425.